



Characterisation of circulating tumour cells in metastatic prostate cancer

Alice Elizabeth Hartley

A thesis submitted for the degree Doctor of Philosophy

September 2019

Northern Institute for Cancer Research

Faculty of Medical Sciences

Newcastle University

Abstract

In the UK, prostate cancer is the most prevalent male cancer and approximately 40% of men will have metastatic disease at diagnosis. The treatment pathway in metastatic prostate cancer is offered often without any histological or genetic knowledge of the tumour and there is currently no reliable biomarker to monitor response to treatment.

Over the past decade, there has been increasing interest in circulating tumour cells (CTCs). These cells, which have broken away from the tumour of origin and can be captured via a simple blood test, can be quantified, sequenced or examined for antigen expression. Stem cell marker expression, specifically Oct4, SOX2 and Nanog, has been found to correlate with aggressive disease when looking at solid prostate tissue. Consequently, exploring the expression of these markers in circulating tumour cells could enable the development of a new biomarker in prostate cancer.

This study had three aims. The first was to optimise an assay using flow cytometry to enable detection of the stem cell markers Oct4, SOX2 and Nanog, alongside epithelial and mesenchymal markers in CTCs from patients with metastatic prostate cancer. The second aim was to explore the prognostic role of these markers and the final aim was to culture CTCs from patients to enable downstream utilisation.

Blood was obtained from seventy-eight patients with different stages of prostate cancer and processed using two flow-cytometry based methods; one on the Imagestream, a combined flow cytometer and high-resolution microscope, and the second using conventional multi-channel FACS. Enumeration of total number of CTCs in addition to the individual marker positive cells was correlated with existing clinical data (PSA and Alkaline Phosphatase level, in addition to survival). Cells from six patients were successfully maintained in culture for up to a year. Attempts to prove the genotype of these cells included real time qPCR, SNP Array and whole exome sequencing experiments. Cells from one patient were implanted into five NSG mice and experiments to look at both chemokine expression and the Young's modulus of the cells were also performed.

No correlation was found between either CTC count or antigen expression and the clinical outcome of the patients. Unfortunately, due to a lack of good quality DNA the sequencing

experiments didn't yield any data and despite one of the mice developing a hind leg paralysis, there was no histological evidence of an engrafted tumour. The chemokine receptor and Young's modulus experiments showed promising early results and form part of some ongoing collaborative projects.

The first aim of developing an assay to detect prostate cancer CTCs was achieved, and survival data at a later time point is going to be collected to ascertain whether the markers explored in this study have a prognostic role. Whilst cells were successfully cultured, the genetic signature of these is still unclear and future plans to continue this work are currently in progress.

Acknowledgements

I would like to thank my supervisors Kenny Rankin, Craig Robson and Rakesh Heer, for giving me the ideas for the project, supporting me through the PhD process and taking a lab-novice on board. I am especially grateful to Kenny for his support following maternity leave when I was trying to juggle working with looking after two young children. Also, my sponsors, Prostate Cancer UK and The Royal College of Surgeons of England (for year 1), and Cancer Research UK (for years 2 and 3) who enabled me to undertake the research.

The Urology research team based at the Freeman Hospital (Wendy, Pete, Nic and Bernadette) have really helped me with the ethics, patient identification and sample collection, and have provided moral support throughout the entire project. Similarly, I am grateful to the Oncology consultants, Dr Asabi, Dr Frew, Dr Pedley and Dr McMEnamin, for allowing me access to their clinics to enable me to take blood samples from their patients.

Laura, Natasha, Emma and Rachel have taught me all I know regarding lab techniques, and Laura in particular has always been available for trouble shooting and helping with tricky bits of experiments, for which I am extremely grateful. Thanks also to David, Misti and Anantha who have been the stalwarts of the Imagestream team and have provided technical and moral support when the machine had a bad day. Maria and Justin were also a fantastic support in my final year, and I am very grateful to them for help with some of my experiments. I must extend my gratitude also to Adam for his statistical advice, which was incredibly helpful in the analysis of the data.

I would like to thank the team in the Flow Cytometry Core Facility, particularly Andy Filby, for all the help with the FACS assay and cell sorts, and to Helen Blair, Huw Thomas and Samir Luli for the help setting up the mouse experiments. Thanks in particular to Helen for looking after the mice and helping with the subsequent experiments. I am also grateful to the team at the Pathology Node in the RVI, who did the initial mouse immunohistochemistry, and then to Calum Kirk who sectioned and stained an entire mouse spine because I would not give up hope that there was a tumour in there!

Thanks to Daniel, Jason and Kamyra for their help with the Atomic Force Microscope and Chemokine Receptor experiments respectively. Discussions with them led to looking at things in a different way, which I hope will form the basis for future work.

Finally, I would like to thank my family. My parents John and H  l  ne, for their help looking after the boys so I could write up, and for the painstaking proof reading. My husband Simon, who has sacrificed many weekends and holidays to allow me to write, and my children Lawrence and Henry, who have put up with me on the computer for endless hours. I am also grateful to the twins, Rowan and Marianne, whose pending arrival gave me the impetus to finish writing.

Abbreviations

ADT – Androgen deprivation therapy

AF488 – Alexa Fluor 488 (fluorochrome)

AF647 – Alexa Fluor 647 (fluorochrome)

AFP – α -Fetoprotein

AFM – Atomic force microscope

AKT – Protein kinase B

ALP – Alkaline phosphatase

APC - Allophycocyanin

AR – Androgen receptor

ARv7 – Androgen receptor variant 7

BD – Becton Dickinson Ltd.

BPH – Benign prostatic hyperplasia

BRCA2 – Breast cancer type 2 gene

BSA – Bovine serum albumin

CD – Cluster of differentiation (cell surface markers)

CDX – Cell line derived xenograft

CK – Cytokeratin

CNA – Copy number aberration

COSHH – Control of substances hazardous to health

CRPC – Castrate resistant prostate cancer

CT – Computed tomography

CTC – Circulating tumour cells

ctDNA – Circulating tumour DNA

DAB – 3,3-diaminobenzidine

DAPI – 4,6-diamino-2-phenylindole

DCCs – Disseminated cancer cells

DMEM – Dulbecco's modified eagle's medium

DNA – Deoxyribonucleic acid

DPBS – Dulbecco's phosphate buffered saline

Draq5 – Deep red anthraquinone 5

EAU – European Association of Urology

ECOG – Eastern co-operative oncology group

EDTA – Ethylenediaminetetraacetic acid

EGFR – Epidermal growth factor receptor

EMT – Epithelial – mesenchymal transition

EpCAM – Epithelial cell adhesion molecule

ERG – Erythroblast transformation-specific related gene

FACS – Fluorescent activated cell sorting

FCCF – Flow cytometry core facility (Newcastle University)

FCS / FBS – Foetal calf serum / Foetal bovine serum

FDA – United States food and drug administration

FisH – Fluorescence in-situ hybridisation

FITC – Fluorescein isothiocyanate

FOXA1 – Forkhead box A1

FOXO – Forkhead box O

GAPDH – Glyceraldehyde 3-phosphate dehydrogenase

GLUT1 – Glucose transporter 1

H&E – Haematoxylin and eosin

hESC – Human embryonic stem cells

HER2 – Human epidermal growth factor receptor 2

HIF-1 α - Hypoxia inducible factor 1 alpha

HOXB13 – Homeobox protein 13

HMAB – Hormones maximum androgen blockade

HSA – Hormones single agent

HTA – Human tissue act

IGFR1 – Insulin-like growth factor receptor 1

iPS – induced pluripotent stem cells

IS – Imagestream

KLK3 – Kallikrein-3

KLF4 – Kruppel-like factor 4

LUTS – Lower urinary tract symptoms

MAB – Maximum androgen blockade

MACS – Magnetic activated cell sorting

MET – Mesenchymal – epithelial transition

MMP – Matrix Metalloproteinase

mpMRI – Multiparametric MRI

MRI – Magnetic resonance imaging

mRNA – Messenger RNA

MSC – Mesenchymal stem cell

MT1-MMP – Membrane type 1-matrix metalloproteinase

mTOR – Mechanistic target of rapamycin

MYC – Oncogene discovered from myelocytomatosis

NDM – New diagnosis metastatic

NICR – Northern Institute for Cancer Research

NkX3 – NK3 homeobox

Oct4 - octamer-binding transcription factor 4

PBS- Phosphate buffered saline

PCR – Polymerase chain reaction

PDX – Patient derived xenograft

PE – Phycoerythrin

PerCP – Peridinin chlorophyll protein

PI3K- Phosphoinositide 3-kinase

PIN – Prostate intraepithelial neoplasia

PSA – Prostate specific antigen

PSMA – prostate specific membrane antigen

PTEN – Phosphatase and tensin homolog

Ras – Rat sarcoma oncogene

RNA – Ribonucleic acid

RPMI – Roswell Park Memorial Institute medium

RT-PCR – Reverse transcriptase polymerase chain reaction

RT-qPCR – Real time quantitative polymerase chain reaction

SCNA – Somatic copy number alterations

SNP – Single nucleotide polymorphism

SOX2 – SRY (Sex determining region)-related HMG-box gene 2

SPOP – Speckle-type POZ protein

TBST – Tris-buffered saline and polysorbate 20

TGF- β – Transforming growth factor beta

TMPRSS2 – Transmembrane protease serine 2

TNM – Tumour, node and metastasis (staging system)

TP53 – Tumour protein 53

TRIS – Trisaminomethane

TURP – Trans-urethral resection of the prostate

UN3373 – United Nations Biological Substance Category B

UV – Ultra Violet

WNT – Wingless related integration site

ZEB1 – Zinc Finger E-box Binding Homeobox 1

Table of Contents

Abstract	i
Acknowledgements.....	iii
Abbreviations	v
List of Figures and Tables	xxi
Chapter 1. Introduction	1
1.1 The prostate gland	1
1.2 Prostate cancer	2
1.2.1 Background and Epidemiology	2
1.2.2 Diagnosis of prostate cancer.....	3
1.2.3 Classification and staging of prostate cancer	5
1.2.4 Treatment options and prognosis.....	7
1.3 The molecular properties of cancer cells.....	9
1.3.1 Genetic alterations – background.....	9
1.3.2 The hallmarks of cancer	10
1.4 The molecular characteristics of prostate cancer.....	12
1.4.1 Background	12
1.4.2 The androgen receptor signaling pathway	16
1.4.3 The PI3K/AkT/mTOR pathway	16
1.4.4 Transcription Factors	17
1.4.5 Oncogenes and tumour suppressor genes	18

1.5 Tumour heterogeneity and the metastatic process.....	19
1.5.1 Background.....	19
1.5.2 Heterogeneity in cancer in general	20
1.5.3 The theory of clonal evolution	21
1.5.4 The cancer stem cell theory	21
1.5.5 The role of the microenvironment.....	22
1.5.6 Metastasis and the spread of cells from the primary tumour	23
1.5.7 Epithelial to Mesenchymal Transition.....	25
1.5.8 Heterogeneity in the patient with metastatic prostate cancer	27
1.6 Biomarkers in prostate cancer and potential options for new markers.....	28
1.6.1 Background.....	28
1.6.2 PSA.....	28
1.6.3 Prostate-specific Membrane Antigen.....	29
1.6.4 Epithelial vs Mesenchymal markers	29
1.6.5 Androgen Receptor	30
1.6.6 Matrix-Metalloproteinases.....	30
1.6.7 Stem cell markers	31
1.6.8 Circulating biomarkers	32
1.7 Circulating tumour cells.....	33
1.7.1 CTCs and their role as a liquid biopsy.....	33
1.7.2 Definition	34
1.7.3 Morphology	34
1.7.4 Enumeration	34

1.7.5 Characterisation.....	36
1.7.6 Isolation methods – background	37
1.7.7 Isolation – protein-based selection	38
1.7.8 Isolation – physical properties	40
1.7.9 Isolation – direct analysis.....	41
1.7.10 Downstream analysis of CTCs for personalised medicine	41
1.8 Rationale for the project.....	43
Aims and Hypothesis.....	45
Chapter 2. Materials and Methods.....	46
2.1 General Laboratory Practice	46
2.2 Primary cell culture	46
2.2.1 Routine cell culture using cell lines.....	46
2.2.2 Cell culture of mesenchymal stem cells.....	48
2.2.3 Cell culture of iPS cells	48
2.2.4 Cell culture of circulating tumour cells	49
2.3 Collection, storage and preparation of whole blood samples to use on Imagestream and FACS.....	50
2.3.1 Patients	50
2.3.2 Collection and storage of blood.....	50
2.3.3 Red cell lysis	51
2.3.4 White cell depletion.....	51
2.3.5 Permeabilisation and addition of antibodies.....	52
2.3.6 Antibodies used for samples processed on the Imagestream and FACS	52

2.4 Processing and Analysing samples on the Imagestream ^x	54
2.4.1 The Imagestream ^x	54
2.4.2 Laser set-up to enable comparable data.....	54
2.4.3 Single colour controls	55
2.4.4 Compensation matrix	55
2.4.5 Thresholds and reduction of false positives.....	56
2.4.6 Preparation of a template and sample processing	62
2.4.7 Post-processing analysis	62
2.5 Processing and Analysing samples on the FACS Machine.....	62
2.5.1 Choice of FACS machine	62
2.5.2 Single colour controls	62
2.5.3 Processing of samples and gating strategies.....	63
2.5.4 Post processing analysis	63
2.6 Extracting CTCs from whole blood	63
2.6.1 Preparing cell lines spiked into blood.....	63
2.6.2 RosetteSep Density Centrifugation	64
2.6.3 Magnetic Separation	64
2.6.4 Physical Separation (Parsortix).....	66
2.7 DNA extraction and downstream utilisation	67
2.7.1 DNA extraction and amplification	67
2.7.2 Measuring DNA quantity	67
2.7.3 Real time quantitative PCR.....	68
2.7.4 SNP Array.....	69

2.7.5 Whole exome sequencing.....	69
2.8 Chemokine receptor experiments	69
2.8.1 Immunofluorescence	69
2.8.2 Imagestream ^x	71
2.9 Tumour growth in NSG mice.....	71
2.9.1 Permissions and basic care	71
2.9.2 Implantation of cells	71
2.9.3 Extermination, imaging and dissection.....	72
2.9.4 Immunohistochemistry	72
2.10 Measuring mechanical properties of cells using the Atomic Force Microscope	73
2.10.1 Preparation of cells	73
2.10.2 Using the Atomic Force Microscope	74
2.10.3 Post procedure analysis	75
 Chapter 3. The role of the Imagestream platform in the detection and analysis of CTCs in metastatic prostate cancer	 77
3.1 Platform choice	77
3.1.1 Background	77
3.1.2 Choice of platform based on method of CTC detection	78
3.1.3 The Veridex CellSearch	79
3.1.4 Fluorescence Activated Flow Cytometry (FACS).....	80
3.1.5 The Imagestream ^x (Merck)	80
3.2 The optimization of an assay to use on the Imagestream ^x	82
3.2.1 The choice of assay	82

3.2.2 Collection and storage of blood from patients and healthy volunteers	82
3.2.3 Fixation of whole blood and lysis of erythrocytes	83
3.2.4 White cell depletion	84
3.2.5 Permeabilisation.....	85
3.2.6 Processing of blood spiked with cell lines to determine retrieval rate on the Imagestream ^x	85
3.3 Antigen expression and choice of antibodies.....	86
3.3.1 Fluorescence and primary vs secondary conjugation	86
3.3.2 Number of channels and choice of antigens.....	86
3.3.3 The decision not to use a prostate specific antibody.....	87
3.3.4 Epithelial antigens	88
3.3.5 Stem Cell antigens	88
3.3.6 Overlap of expression.....	88
3.3.7 Heterogeneity of antigen expression within cell lines	89
3.3.8 Epithelial antigen expression in patient samples.....	92
3.3.9 Final antibody panel	93
3.4 Optimisation of antibodies	95
3.4.1 Antibody optimisation of EpCAM using cell lines.....	95
3.4.2 Antibody optimisation of Oct4, SOX2 and Nanog using cell lines.....	96
3.4.3 Antibody optimisation of CD45 and DAPI	105
3.5 Cell size as an alternative means of detection	105
3.5.1 Background.....	105
3.5.2 Cell line size	106

3.5.3 Patient samples.....	108
3.6 Final Assay and Gating Strategy.....	110
3.6.1 Sample preparation	110
3.6.2 Antibody selection	110
3.6.3 Imagestream Setup.....	110
3.6.4 Gating strategy for collection and analysis of an Imagestream file	110
3.7 Results by patient characteristic.....	111
3.8 Discussion.....	118
 Chapter 4. The role of multi-channel FACS in the detection and analysis of CTCs in metastatic prostate cancer	 120
4.1 Platform choice	120
4.1.1 Background	120
4.1.2 Choice of Platform	121
4.2 Antigen expression and choice of antibodies	122
4.2.1 Number of channels and choice of antigens	122
4.2.2 The decision not to use a prostate specific antibody	123
4.2.3 White cell markers	123
4.2.4 Epithelial antigens.....	125
4.2.5 Mesenchymal antigens	126
4.2.6 Stem cell antigens	126
4.2.7 Final antibody panel.....	126
4.2.8 Overlap of expression	127
4.3 Optimisation of antibodies	128
4.3.1 Introduction	128

4.3.2 White cell antigens	128
4.3.3 Epithelial antigens	134
4.3.4 Mesenchymal antigens.....	138
4.3.5 Stem cell antigens.....	140
4.3.6 DAPI	143
4.4 Optimisation of an assay to use on a conventional FACS machine with sorting capabilities.....	143
4.4.1 Collection and storage of blood from patients and healthy volunteers.....	143
4.4.2 Preparation of blood samples	144
4.4.3 Optimisation of cell sorting and post-sort storage	144
4.5 Controls, gating strategies and analysis	144
4.5.1 Single colour controls and laser set-up	144
4.5.2 Gating Strategies	145
4.5.3 Healthy Volunteer controls	155
4.6 Downstream analysis.....	156
4.6.1 Immunofluorescence.....	156
4.6.2 DNA extraction for PCR and sequencing	158
4.7 Results by patient characteristic	160
4.8 Discussion	166
Chapter 5. The clinical significance of CTCs detected by Imagestream and FACS	169
5.1 Clinical Data	169
5.1.1 Demographics of patients	169
5.1.2 Healthy volunteer controls.....	173
5.1.3 Clinical blood results.....	173

5.1.4 Number of deaths	184
5.2 Results of Imagestream detected CTCs	184
5.2.1 Definition of CTC data recorded	184
5.2.2 Total CTC count	185
5.2.3 CTC count and PSA	194
5.2.4 CTC count and ALP	195
5.2.5 Antigen expression.....	196
5.2.6 Antigen expression in patients that died	204
5.3 Results of FACS detected CTCs.....	205
5.3.1 Definition of CTC data recorded	205
5.3.2 Total CTC count	205
5.3.3 CTC count and PSA	214
5.3.4 CTC count and ALP	216
5.3.5 Antigen expression.....	217
5.3.6 Antigen expression in patients that died	225
5.4 Statistical comparison of Imagestream-detected and FACS-detected CTCs	226
5.5 Discussion.....	227
 Chapter 6. The use of CTCs to develop different models for target discovery	 231
6.1 Rationale for attempting to use CTCs for target discovery	231
6.2 Comparison of different techniques for CTC extraction from whole blood	231
6.2.1 Background	231
6.2.2 Density centrifugation	232
6.2.3 Magnetic Separation	234
6.2.4 Physical Properties (Parsortix)	236

6.2.5 Overall retrieval and choice of method.....	238
6.3 Optimisation of Cell Culture	243
6.3.1 Background.....	243
6.3.2 Different culture media	243
6.3.3 Normoxic versus hypoxic conditions for cell culture	244
6.3.4 Testing the media and culture conditions on cancer cell lines	244
6.3.5 Testing the media and culture conditions on white blood cells	245
6.4 Using clinical samples for CTC culture.....	247
6.4.1 The first clinical sample	247
6.4.2 Clinical samples and the lessons learnt from attempted CTC culture	249
6.5 Proving the authenticity of the cells from clinical samples in culture	250
6.5.1 Background.....	250
6.5.2 Antigen expression	250
6.5.3 Real Time qPCR.....	254
6.5.4 SNP Array.....	254
6.5.5 Whole-exome sequencing.....	255
6.6 Exploring the chemical properties of cultured CTCs	257
6.6.1 Background.....	257
6.6.2 Choice of chemokine receptors and their corresponding ligands	257
6.6.3 Demonstrating the presence of chemokine receptors in cell lines	258
6.6.4 Demonstrating the presence of chemokine receptors in CTCs.....	263
6.7 Development of an in-vivo model using NSG mice	267
6.7.1 Background.....	267

6.7.2 Pre-mortem findings	268
6.7.3 Post-mortem analysis	268
6.8 Exploring the physical properties of cultured CTCs	277
6.8.1 Background	277
6.8.2 Principles of an AFM	278
6.8.3 Results of the AFM indentation experiments.....	278
6.9 Discussion.....	282
Chapter 7. Discussion and future work.....	285
Appendix	i
Bibliography	x

List of Figures and Tables

Figure 1.1 A Flowchart to demonstrate treatment of metastatic castrate resistance prostate cancer (adapted from <i>EAU guidelines (Urology, 2018)</i>). Treatment is based on the performance status of the patient and how severe the symptoms are.	8
Figure 1.2 The eight hallmarks (1. sustaining proliferative signalling, 2. evading growth suppressors, 3. resisting cell death, 4. enabling cellular immortality, 5. inducing angiogenesis, 6. activating invasion and metastasis, 7. avoiding immune destruction and 8. reprogramming cellular energy) and two characteristics (1. tumour promoting inflammation and 2. genome instability and mutation) of cancer cells as described by Hanahan and Weinberg. (printed with permission from the authors) (Hanahan and Weinberg, 2011).....	9
Figure 1.3 A diagram to demonstrate the steps involved in the development of metastasis. Taken from <i>The pathogenesis of cancer metastasis: the seed and soil hypothesis revisited (Fidler, 2003)</i>	24
Figure 1.4 The survival curve for patients expressing Oct4/SOX2/Nanog in prostate tumours. Patients were categorised as having either high (n = 69) or low (n = 67) expression, as determined by visual assessment of immuno-histochemical staining of prostate tumours. Taken from <i>The induction of core pluripotency master regulators in cancers defines poor clinical outcomes and treatment resistance (Hepburn et al., 2019)</i>	32
Figure 2.1 Images of the synthetic speed beads displaying fluorescence of three antibodies Oct4, SOX2 and Nanog at 1:50 concentration.....	55
Figure 2.2 Graphs to show the Intensity of Fluorescence of Oct4 in Healthy Volunteer Blood Samples with no staining, stained with isotype control, stained with antibodies and compared to blood from patient samples. The results from all cells taken from twelve different healthy volunteers were combined to provide the three control graphs on the left, and then compared to cells from six patients with metastatic prostate cancer. The dotted line demonstrates the threshold above which cells would be considered to be putative CTCs.	57
Figure 2.3 Graphs to show the Intensity of Fluorescence of SOX2 in Healthy Volunteer Blood Samples with no staining, stained with isotype control, stained with antibodies and compared to blood from patient samples. . The results from all cells taken from twelve different healthy volunteers were combined to provide the three control graphs on the left, and then compared to cells from six patients with metastatic prostate cancer. The dotted line demonstrates the threshold above which cells would be considered to be putative CTCs.	58
Figure 2.4 Graphs to show the Intensity of Fluorescence of Nanog in Healthy Volunteer Blood Samples with no staining, stained with isotype control, stained with antibodies and compared to blood from patient samples. . The results from all cells taken from twelve different healthy volunteers were combined to provide the three control graphs on the left, and then compared to cells from six patients with metastatic prostate cancer. The dotted line demonstrates the threshold above which cells would be considered to be putative CTCs.	59

Figure 2.5 Imagestream images showing Oct4 expression in a possible stem cell from a healthy volunteer sample and a CTC from a patient sample.	60
Figure 2.6 Imagestream images showing SOX2 expression in a possible stem cell from a healthy volunteer sample and a CTC from a patient sample	61
Figure 2.7 Imagestream images showing Nanog expression in a possible stem cell from a healthy volunteer sample and a CTC from a patient sample	61
Figure 2.8 A diagram to show the set-up of the Atomic Force Microscope, (<i>taken from Deng et al.(Deng et al., 2018)</i>). The cell of interest would be placed on the yellow tube and indented with either a conical or spherical AFM probe on the end of a cantilever. The movement of a laser detected by a photodiode is used to create a three-dimensional image of the cell.....	75
Figure 2.9 A diagram to demonstrate the conical tip of the AFM inserting into a cell surface. The tan of the angle between the edge and the midline, and the depth of the indentation in the cell are the two variables used to calculate the Young’s modulus of the cell.	76
Figure 2.10 A diagram to demonstrate the spherical tip of the AFM being inserted into a cell surface. The radius of the tip and the depth of indentation into the cell are the two variables used to calculate the Young’s modulus of the cell.	76
Figure 3.1 Graphs to show the percentage retrieval of different numbers of two prostate cancer cell lines spiked into healthy volunteer whole blood when using the NICR assay. 20 000 or 50 000 cells of each cell line were spiked into 2mls of whole healthy volunteer blood and the NICR Imagestream assay was used to process the sample. The number of cells from each cell line at the end were identified using size and fluorescence (Vimentin for PC3 and EpCAM for LNCaP).....	86
Figure 3.2 Imagestream images to demonstrate heterogeneity of antigen expression within prostate cancer cell lines. (Images 1, 2 & 3 are LNCaP cells, Image 4 is a CWR-22-Rv1 cell and Images 5 is a PC3 cell).	90
Figure 3.3 Graphs to show the percentage of each of the combinations of antigens expressed in each cell line. All cell lines were stained with EpCAM, Cytokeratin, Vimentin and the nuclear marker DAPI. Cells were processed on the Imagestream and the number of cells displaying fluorescence corresponding to each antigen, or combination of antigens, were recorded. LNCaP cells were predominantly EpCAM+/CK-/Vimentin-, PC3 cells were predominantly EpCAM-/CK-/Vimentin+ and CWR-22Rv1 cells were predominantly EpCAM+/CK-/Vimentin-.	91
Figure 3.4 Venn Diagrams to demonstrate the combination of antigens expressed by cells detected in the blood of patients with metastatic prostate cancer. Diagram a) included all samples but diagram b) excludes sample 10 which had a very high number of cells found and could skew the data. The revised data without sample 10 shows that the majority of CTCs found in the 9 patients expressed both EpCAM and CK.	93
Figure 3.5 A graph to demonstrate the excitation (dotted line) and emission (solid block) wavelengths of the fluorochromes conjugated to the antibodies used in this assay (courtesy of BD Biosciences).	94

Figure 3.6 Graphs to demonstrate LNCaP cells unstained (yellow), stained with isotype control (orange) and with increasing levels of antibody (red). Each volume of antibody was used to determine the lowest level that could be utilised by demonstrating a shift from the negative controls (unstained cells and isotype controls).....	95
Figure 3.7 An Imagestream image demonstrating the cell membrane staining using the EpCAM antibody at a concentration of 1:200.....	96
Figure 3.8 Imagestream images to demonstrate expression of Oct4, SOX2 and Nanog in two different Mesenchymal Stem Cells. The first cell is only positive for Nanog but the second expresses all three stem cell antigens.....	96
Figure 3.9 Unlabelled iPS cells gated based on size. Cells falling within this gate were counted as whole cells so that debris and doublets did not give false readings during subsequent fluorescence optimisation.....	97
Figure 3.10 Graphs to demonstrate fluorescence in iPS cells only (black), cells with isotype control (red) and cells with Oct4 (AF488) at decreasing concentrations: a) 1:50, b) 1:100, c) 1:200 and d) 1:500. The highest concentration shows a shift in fluorescence in the majority of cells labelled with the antigen compared to the isotype and unlabelled cells but the three lower concentrations show an overlap with the negative controls.....	98
Figure 3.11 Graphs to show the percentage of iPS cells that fell inside the positive gate, which was drawn by excluding the unlabelled cells as a negative control. The graphs show the fluorescence of the iPS cells with decreasing concentrations of Oct4 (AF488) antibody: b) 1:50, c) 1:100, d) 1:200 and e) 1:500.....	100
Figure 3.12 Graphs to demonstrate fluorescence in iPS cells only (black), cells with isotype control (red) and cells with SOX2 (AF555) at decreasing concentrations: a) 1:50, b) 1:100, c) 1:200 and d) 1:500. There is a clear shift in the cells labelled with the 1:50 concentration when compared to the unlabelled cells and isotype control, but an overlap with the negative controls in the lower concentrations.	101
Figure 3.13 Graphs to show the percentage of iPS cells that fell inside the positive gate, which was drawn by excluding the unlabelled cells as a negative control. The graphs show the fluorescence of the iPS cells with decreasing concentrations of SOX2 (AF555) antibody: b) 1:50, c) 1:100, d) 1:200 and e) 1:500.....	102
Figure 3.14 Graphs to demonstrate fluorescence in iPS cells only (black), cells with isotype control (red) and cells with Nanog (PerCP Cy5.5) at decreasing concentrations: a) 1:50, b) 1:100, c) 1:200 and d) 1:500. There is a larger overlap with the negative controls, even at the highest concentration, which was thought to be due to the pluripotency of the iPS cells. ...	103
Figure 3.15 Graphs to show the percentage of iPS cells that fell inside the positive gate, which was drawn by excluding the unlabelled cells as a negative control. The graphs show the fluorescence of the iPS cells with decreasing concentrations of PerCP Cy5.5 antibody: b) 1:50, c) 1:100, d) 1:200 and e) 1:500.....	104
Figure 3.16 Images to demonstrate PC3 cells when run in whole blood on a) the Imagestream (yellow events) and b) conventional FACS (blue events). (Blood cells are black)	106

Figure 3.17 Images to demonstrate LNCaP cells when run in whole blood on a) the Imagestream (yellow events) and b) conventional FACS (blue events). (Blood cells are black).	107
Figure 3.18 Images taken from the Imagestream to demonstrate a) a PC3 cell, b) an LNCaP cell and c) a white cell.....	108
Figure 3.19 Images taken from the Imagestream to show a variation in sizes of CTCs (a-e) in comparison with a white cell (f).	109
Figure 4.1 Three dot plots to show the CD45/CD16 negative population when three cell lines were added to blood from three healthy volunteers and stained with CD45 and CD16 antibodies. The cells within the red gate are negative for both CD45 and CD16.	125
Figure 4.2 Graphs to demonstrate the excitation (dotted line) and emission (solid block) wavelengths of the fluorochromes conjugated to the antibodies used in this assay (courtesy of BD Biosciences).....	128
Figure 4.3 Graphs to show the optimisation of the CD45 antibody - unstained white cells (yellow), white cells stained with the isotype control (orange) and white cells stained with CD45 (BV786) using four different volumes of the antibody (a-d).....	129
Figure 4.4 Graphs to show the proportion of unlabelled cells in white blood cell samples stained with four different volumes of CD45 (BV786) when using 10^6 white cells.....	130
Figure 4.5 A graph to show the percentages of unlabelled white cells at different volumes of antibody for CD45 (BV786) when using 10^6 white cells.	131
Figure 4.6 Graphs to show the optimisation of the CD16 antibody using unstained white cells (yellow), white cells stained with the isotype control (orange) and white cells with CD16 (APC-H7) using four different volumes of the antibody (a-d).....	132
Figure 4.7 Graphs to show the proportion of unlabelled cells in white blood cell samples stained with CD16 (APC-H7) when using 10^6 cells.....	133
Figure 4.8 A graph to show the percentages of unlabelled white cells at different volumes of antibody for CD16 (APC-H7) when using 10^6 white cells.....	134
Figure 4.9 Graphs to show the optimisation of EpCAM (BV650) antibody using LNCaP cells. This shows unstained cells (yellow), LNCaP cells stained with the isotype control (orange) and LNCaP cells stained with EpCAM (BV650) (red) using four different volumes of the antibody (a-d).....	135
Figure 4.10 An Imagestream image of an LNCaP cell stained with EpCAM (BV650) when using $0.5\mu\text{l}$, demonstrating cell membrane staining.....	136
Figure 4.11 Graphs to show optimisation of the cytokeratin (PECy7) antibody using MCF-7 cells. These graphs show unstained MCF-7 cells (yellow), MCF-7 cells stained with the isotype control (orange) and MCF-7 cells stained with cytokeratin (PECy7) (red) using four different volumes of the antibody (a-d).	137

Figure 4.12 An Imagestream image of an MCF-7 cell stained with cytokeratin (PECy7) when using 0.5µl, demonstrating cytoplasmic staining.....	138
Figure 4.13 Graphs to show the optimisation of the vimentin (AF647) antibody using PC3 cells. These graphs show unstained cells (yellow), PC3 cells stained with the isotype control (orange) and PC3 cells stained with vimentin (AF647) (red) using four different volumes of the antibody (a-d).....	139
Figure 4.14 An Imagestream image of a PC3 cell stained with Vimentin (AF647) when using 1µl, demonstrating cytoplasmic and membrane staining	140
Figure 4.15 Graphs to show the optimisation of Oct4 (BV421) antibody using iPS cells. These show unstained cells (yellow), iPS cells stained with the isotype control (orange) and iPS cells stained with Oct4 (BV421) (red) using three different volumes of the antibody (a-c).....	141
Figure 4.16 An Imagestream image of an iPS cell stained with Oct4 (BV421) when using 2µl, demonstrating nuclear staining.....	141
Figure 4.17 Graphs to show the optimisation of SOX2 (FITC) antibody using iPS cells. These graphs show unstained cells (yellow), iPS cells stained with the isotype control (orange) and iPS cells stained with SOX2 (FITC) (red) using three different volumes of the antibody (a-c).	142
Figure 4.18 An Imagestream image of an iPS cell stained with SOX2 (FITC) when using 2µl, demonstrating nuclear staining.....	142
Figure 4.19 A compensation matrix created on the BD FACS Fusion when running each sample. Any significant overlap would show in red.	145
Figure 4.20 Graphs to show the fluorescence of a) LNCaP cells with no staining, b) staining with the isotype control, c) staining with the EpCAM antibody, d) combined data and e) the final gate used for the assay. This final gate was drawn to include any cells expressing higher fluorescence than the isotype control.	146
Figure 4.21 Graphs to show the fluorescence of MCF7 cells with a) no staining, b) staining with the isotype control, c) staining with the cytokeratin antibody, d) combined data and e) the final gate used for the assay. This final gate was drawn to include any cells expressing higher fluorescence than the isotype control.	148
Figure 4.22 Graphs to show the fluorescence of PC3 cells with a) no staining, b) staining with the isotype control, c) staining with the Vimentin antibody, d) combined data and e) the final gate used for the assay. This final gate was drawn to include any cells expressing higher fluorescence than the isotype control.	149
Figure 4.23 Graphs to show the fluorescence of PC3 cells with a) no staining, b) staining with the isotype control, c) staining with the MT1-MMP antibody, d) combined data and e) the final gate used for the assay. This final gate was drawn to include any cells expressing higher fluorescence than the isotype control.	150
Figure 4.24 Graphs to show the fluorescence of iPS cells with a) no staining, b) staining with the isotype control, c) staining with the Oct4 antibody, d) combined data and e) the final	

gate used for the assay. This final gate was drawn to include any cells expressing higher fluorescence than the isotype control.	152
Figure 4.25 Graphs to show the fluorescence of iPS cells with a) no staining, b) staining with the isotype control, c) staining with the SOX2 antibody, d) combined data and e) the final gate used for the assay. This final gate was drawn to include any cells expressing higher fluorescence than the isotype control.	153
Figure 4.26 Graphs to show the fluorescence of iPS cells with a) no staining, b) staining with the isotype control, c) staining with the Nanog antibody, d) combined data and e) the final gate used for the assay. This final gate was drawn to include any cells expressing higher fluorescence than the isotype control.	155
Figure 4.27 A graph to demonstrate the gating of whole CD45-/CD16- cells, which should contain predominantly non-white blood cells. A gate was drawn round the population that was negative for both antigens and this was the gate used to capture putative CTCs.	156
Figure 4.28 Immunofluorescence images to demonstrate three cells sorted on the BD FACS Fusion based on negative expression of CD45/CD16. These cells were cell lines spiked in healthy volunteer blood and stained with EPCAM, Cytokeratin, Vimentin, MT1-MMP. CD45 and DAPI. Cell a) was positive for EpCAM, cell b) was positive for Cytokeratin and the cells in c) were positive for Vimentin.....	157
Figure 4.29 A graph to demonstrate DNA yield from 3 different cells lines using either fixed or unfixed cells. 1000 cells from three different cell lines underwent DNA extraction and amplification, before DNA levels were measured on the Qubit. This was to determine whether fixation gave a false estimation of DNA quantity.....	159
Figure 5.1 A graph to demonstrate the breakdown of patients used in this study by stage of disease. The majority have metastatic disease, either newly diagnosed, on hormone suppression, or are on second line therapy for castrate resistant disease.	172
Figure 5.2 A graph to demonstrate the type of hormone therapy patients were on. Thirteen patients were on single hormone agents compared to sixteen patients who were on maximum androgen blockade.	172
Figure 5.3 Graphs to show a) PSA level and b) ALP level at the time of blood sampling for all patients at each stage of the disease (the bar denotes the median). Those with metastatic disease have a higher median level of PSA and ALP.	175
Figure 5.4 Graphs to show a) PSA and b) ALP at the time of sampling and at a six-month interval for patients with benign disease (the bar denotes the median) N.B. No six-month ALPs were recorded for these patients. Each coloured dot represents one patient so the corresponding value at 6 months can be seen. A black coloured dot at baseline means there was no 6-month sample recorded. The median PSA did increase only two patients had PSAs taken at six months and both had negative prostate biopsies.....	177
Figure 5.5 Graphs to show a) PSA and b) ALP at the time of sampling and after six months for patients on surveillance (the bar denotes the median). Each coloured dot represents one patient so the corresponding value at 6 months can be seen. A black coloured dot at baseline means there was no 6-month sample recorded and vice versa. There was no significant PSA	

increase at six months ($p=0.32$). As only one patient had an ALP taken at sampling time no comparison could be made. 178

Figure 5.6 Graphs to show a) PSA and b) ALP at the time of sampling and after a six-month interval for patients with newly diagnosed metastatic disease (the bar denotes the median). Each coloured dot represents one patient so the corresponding value at 6 months can be seen. A black coloured dot at baseline means there was no 6-month sample recorded. All patients showed a PSA response to treatment but this was not found to be significant ($p=0.06$). ALP increased marginally at 6 months but this was also not significant ($p=0.81$). 179

Figure 5.7 Graphs to show a) PSA and b) ALP at the time of sampling and after six months for patients on single hormonal agents (the bar denotes the median). Each coloured dot represents one patient so the corresponding value at 6 months can be seen. A black coloured dot at baseline means there was no 6-month sample recorded. The median PSA and ALP changes were not significant ($p=0.57$ and $p=0.31$ respectively)..... 180

Figure 5.8 Graphs to show a) PSA and b) ALP at the time of sampling and after six months for patients on maximum androgen blockade (the bar denotes the median). Each coloured dot represents one patient so the corresponding value at 6 months can be seen. A black coloured dot at baseline means there was no 6-month sample recorded. Both median PSA and ALP decreased but this was not significant ($p=0.08$ and 0.75 respectively). 181

Figure 5.9 Graphs to show a) PSA and b) ALP at the time of sampling and after six months for patients with castrate resistant disease (the bar denotes the median). Each coloured dot represents one patient so the corresponding value at 6 months can be seen. A black coloured dot at baseline means there was no 6-month sample recorded. Median PSA decreased but this was not significant ($p=0.36$) and median ALP rose was also not significant ($p=0.98$)..... 182

Figure 5.10 Number of prostate cancer-related deaths. There were six deaths in total and all deaths were in patients with advanced disease. 184

Figure 5.11 A graph to show the total number of putative CTCs found from patients within each treatment group, using the Imagestream. The most CTCs were found in patients with newly diagnosed metastatic prostate cancer. 185

Figure 5.12 A graph to show baseline PSA and CTC count using the Imagestream assay (the line demonstrates linear regression) $r^2 = 0.0007$ therefore there is no correlation. 194

Figure 5.13 A graph to show PSA at 6 months and CTC count using the Imagestream assay (the line demonstrates linear regression) $r^2 = 0.0035$ therefore there is no correlation. 195

Figure 5.14 A graph to show ALP at baseline and CTC count using the Imagestream assay (the line demonstrates linear regression) $r^2 = 0.11$ therefore there is no correlation..... 195

Figure 5.15 A graph to show ALP after 6 months and CTC count using the Imagestream assay (the line demonstrates linear regression) $r^2 = 0.008$ therefore there is no correlation. 196

Figure 5.16 A graph from the full patient group ($n = 78$) to show how many CTCs are expressed including each antigen combination. The most common antigens were SOX2 and Nanog..... 197

Figure 5.17 A graph to show how many CTCs expressed each antigen combination in patients with benign disease. Very few CTCs were found in this group, but the majority expressed SOX2, Nanog or a combination of Oct4 and SOX2.....	198
Figure 5.18 A graph to show how many CTCs expressed each antigen combination in patients on surveillance. CTCs from this group only expressed EpCAM, SOX2 or Nanog.....	198
Figure 5.19 A graph to show how many CTCs expressed each antigen combination in patients with newly diagnosed metastatic disease. More of the CTCs from this group expressed the three stem cell markers, either alone or in combination.....	199
Figure 5.20 A graph to show how many CTCs expressed each antigen combination in patients on a single hormonal agent. The two most common antigens expressed were Oct4 and SOX2.....	199
Figure 5.21 A graph to show how many CTCs expressed each antigen combination in patients on maximum androgen blockade. SOX2 and Nanog were again commonly expressed, and one patient had high numbers of EpCAM+ cells.....	200
Figure 5.22 A graph to show how many CTCs expressed each antigen combination in patients with castrate-resistant disease. Several patients had CTCs with each of the individual antigens, in addition to the antigens in combination, particularly Oct4/SOX2/Nanog+ cells.....	200
Figure 5.23 A graph to show the total number of CTCs found from patients within each treatment group, using FACS. This shows that those with newly diagnosed metastatic disease had the highest number of putative CTCs but there is no significant difference between the patients in different groups (p=0.36).....	206
Figure 5.24 A graph to show baseline PSA and CTC count using the FACS assay (the line demonstrates linear regression) $r^2 = 0.01$ therefore there is no correlation with CTC count and the baseline PSA.....	215
Figure 5.25 A graph to show PSA after six months and CTC count using the FACS assay (the line demonstrates linear regression) $r^2 = 0.0001$ therefore there is no correlation with CTC count and PSA at 6 months.....	215
Figure 5.26 A graph to show ALP at baseline and CTC count using the FACS assay (the line demonstrates linear regression) $r^2 = 0.02$ therefore there is no correlation between CTC count and ALP at baseline.....	216
Figure 5.27 A graph to show ALP after six months and CTC count using the FACS assay (the line demonstrates linear regression) $r^2 = 0.006$, therefore there is no correlation between CTC count and ALP at 6 months.....	217
Figure 5.28 A graph to show how many CTCs expressed each antigen using the FACS assay. MT1-MMP was expressed by the largest number of patients and all antigens were detected on CTCs.....	217
Figure 5.29 A graph to show how many CTCs expressed each antigen in the healthy volunteers. A higher than expected number of cells expressed each antigen aside from	

EpCAM. High numbers of MT1-MMP+ cells were detected. This suggests that the criteria used to determine what a positive event is was not strict enough – this could be due to gating error or have occurred during the optimisation of the antibody.218

Figure 5.30 A graph to show how many CTCs expressed each antigen in patients with benign disease. Most patients had low numbers of cells expressing each antigen but there are higher numbers of cells expressing cytokeratin and the stem cell markers than in the healthy volunteer group.218

Figure 5.31 A graph to show how many CTCs expressed each antigen in patients undergoing surveillance. Similar to the previous groups, low numbers of EpCAM+ cells and high numbers of MT1-MMP cells were detected. The median number of cells expressing the stem cell markers was higher than the previous two groups.219

Figure 5.32 A graph to show how many CTCs expressed each antigen in patients with newly diagnosed metastatic disease. Higher numbers of cells expressing all antigens were detected in this group compared to the previous three groups.219

Figure 5.33 A graph to show how many CTCs expressed each antigen in patients on single-agent hormones. There were small numbers of patients expressing multiple cells with each of the stem cell antigens but the majority of patients had low numbers of these cells.220

Figure 5.34 A graph to show how many CTCs expressed each antigen in patients on hormones – maximum androgen blockade. The median number of cells expressing Nanog was higher for this group of patients.220

Figure 5.35 A graph to show how many CTCs expressed each antigen in patients with castrate-resistant disease. This group of patients had higher median numbers of cells expressing all antigens.221

Figure 5.36 A graph to show the correlation between CTC count as detected by the Imagestream assay, and sorted cell population from the FACS assay (the line denotes linear regression) $r^2 = 0.0003$, therefore there was no correlation between the number of putative CTCs detected using the two different methods.226

Figure 6.1 A graph to show the mean number of cells retrieved ($n = 3$) when using the density centrifugation method. The cells were counted on the Imagestream^X. 1.27%, 2.20% and 0.78% of the PC3 cells were retrieved when 1000, 10 000 and 100 000 cells were spiked respectively. 0.67%, 0.70% and 0.50% of the U2OS cells were retrieved when 1000, 10 000 and 100 000 cells were spiked respectively.233

Figure 6.2 A graph to show the mean number of cells retrieved ($n = 3$) with the first magnetic separation kit (Miltenyi) using CD45 as a single marker. The cells were counted on the Imagestream^X. 1.03%, 0.25% and 1.22% of the PC3 cells were retrieved when 1000, 10 000 and 100 000 cells were spiked respectively. 2.60%, 0.85% and 2.76% of the U2OS cells were retrieved when 1000, 10 000 and 100 000 cells were spiked respectively.235

Figure 6.3 A graph to show the mean number of cells retrieved ($n = 3$) with the second magnetic separation kit (Stem Cell Technologies) using multiple white cell markers. The cells were counted on the Imagestream^X. 7.30%, 8.52% and 13.64% of the PC3 cells were retrieved when 1000, 10 000 and 100 000 cells were spiked respectively. 6.23%, 3.70% and

6.55% of the U2OS cells were retrieved when 1000, 10 000 and 100 000 cells were spiked respectively.	236
Figure 6.4 A graph to show the mean number of cells (n = 3) retrieved when using the Parsortix machine. The cells were counted on the Imagestream ^X . 2.97%, 0.99% and 0.67% of the PC3 cells were retrieved when 1000, 10 000 and 100 000 cells were spiked respectively. 0.63%, 0.29% and 0.19% of the U2OS cells were retrieved when 1000, 10 000 and 100 000 cells were spiked respectively.....	237
Figure 6.5 A graph to show the mean number of cells retrieved for each cell line, using each method when 1000 cells were spiked. (STC = Stem Cell Technologies). The Kruskal-Wallis test showed a significant difference when all four techniques were compared for the PC3 cells (p = 0.004) and U2OS cells (p = 0.03). Further analysis with the Mann-Whitney test, comparing each individual technique did not reveal a significant difference.....	239
Figure 6.6 A graph to show the mean number of cells retrieved for each cell line, using each method when 10 000 cells were spiked. (STC = Stem Cell Technologies). The Kruskal-Wallis test showed a significant difference when all four techniques were compared for the PC3 cells (p = 0.001) and U2OS cells (p = 0.006). Further analysis with the Mann-Whitney test, comparing each individual technique did not reveal a significant difference.....	240
Figure 6.7 A graph to show the mean number of cells retrieved for each cell line, using each method when 100 000 cells were spiked. (STC = Stem Cell Technologies). The Kruskal-Wallis test showed a significant difference when all four techniques were compared for the PC3 cells (p = 0.001) and U2OS cells (p = 0.006). Further analysis with the Mann-Whitney test, comparing each individual technique did not reveal a significant difference.....	241
Figure 6.8 Microscope images of the three flasks containing PC3 cells at day 16 (x40 magnification).	245
Figure 6.9 Microscope images of the three flasks containing U2OS cells at day 16 (x40 magnification).	245
Figure 6.10 Microscope images of the three flasks containing white cells at day 1 (x20 magnification).	246
Figure 6.11 Microscope images of the three flasks containing white cells at day 13 (x20 magnification).	246
Figure 6.12 Microscope images of three of the wells from patient CTC-JARO-110 at day 7 (x20 magnification). The cells were very sparse.....	247
Figure 6.13 Microscope images of three of the wells from patient CTC-JARO-110 at day 13 (x20 magnification). There was a slight increase in confluence.	247
Figure 6.14 Microscope images of three of the wells from patient CTC-JARO-110 at day 17 (x40 magnification).	248
Figure 6.15 Microscope images of three of the wells from patient CTC-JARO-110 at day 32 (x20 magnification). There was an increase in confluence from day 13.	248

Figure 6.16 A graph to show cell area against cell circularity for all cells processed during this experiment. The gate is used to identify cells that are larger than the majority of white cells are expected to be. This shows that there are several cells that are larger than the majority of white cells and these could be potential CTCs.....	251
Figure 6.17 A graph to show the intensity of CD45 for all cells processed during this experiment. There are three distinct populations of cells although population 1 is likely to be debris or cells with non-specific staining as the intensity of the CD45 expression is very low. Cells in population 2 were smaller white cells than those in population 3.	251
Figure 6.18 An Imagestream image of a typical cell seen in population 2 and population 3.	252
Figure 6.19 Imagestream images to show examples of some of the cells seen within population 1 in Figure 6.17. Cell a) expressed EpCAM and no CD45 so could be a putative CTC. Cell b) had no EpCAM, stem cell or CD45 expression so could either be a white cell that didn't express or stain positive for CD45, or a putative CTC which was negative for the markers of interest. Cell c) was a Nanog positive cell but expressed Nanog at a level higher than normal white cells, so could be a putative CTC.	252
Figure 6.20 A graph to show the intensity of Nanog for all DAPI+/CD45- cells processed during these experiments. The majority of the cells expressed Nanog at a much higher level than is normally expressed in white cells, so these could represent putative CTCs.....	253
Figure 6.21 A graph to show the area against circularity plot but with the possible CTCs (CD45-/DAPI+ cells) highlighted in yellow. There is a considerable overlap in size between those cells that were negative for CD45 and white cells expressing CD45. As Nanog expression in the CD45- cells is high, we can be reasonably confident that these cells are not white cells but that they could be putative CTCs.	254
Figure 6.22 Three immuno-fluorescent images demonstrating the 1:10 dilution of the isotype control for a) CXCR6, b) CCR7 and c) CXCR4. (As these were negative the images showing further dilutions are not shown).	259
Figure 6.23 Immuno-fluorescent images to show PC3 cells stained with increasing antibody dilutions of the chemokine receptor CXCR6 (PE). No positive staining was demonstrated..	260
Figure 6.24 Immuno-fluorescent images to show PC3 cells stained with increasing antibody dilutions of the chemokine receptor CCR7 (FITC). No positive staining was demonstrated.	261
Figure 6.25 Immuno-fluorescent images to show PC3 cells stained with increasing antibody dilutions of the chemokine receptor CXCR4 (APC). Some staining was seen at the highest concentration, but this is likely to be non-specific.....	262
Figure 6.26 Imagestream images of cells cultured from patient CTC-JACH-73 demonstrating CCR7 and CXCR4 expression on these cells.	263
Figure 6.27 Imagestream images of cells cultured from patient CTC-JARO-110 demonstrating CCR7, CXCR6 and CXCR4 expression on these cells.	264

Figure 6.28 Imagestream images of cells cultured from patient CTC-STCH-122 demonstrating CCR7 and CXCR4 expression on these cells.	265
Figure 6.29 Imagestream images of cells cultured from patient CTC-PEWA-123 demonstrating CCR7 and CXCR4 expression on these cells.	265
Figure 6.30 Imagestream images of cells cultured from patient CTC-JEWR-124 demonstrating CCR7 and CXCR4 expression on these cells.	266
Figure 6.31 X-ray images of the femurs of both mice with palpable femoral lumps. No obvious sclerotic (or lytic) lesions were seen in the femur of either mouse.	269
Figure 6.32 CT reconstructed images of the lower limbs of Both Notch. Image a) shows a left oblique-lateral view and image b) shows a right oblique-lateral view. No obvious lesions affecting the bone were identified.	269
Figure 6.33 CT reconstructions of the pelvis and spine of Both Notch. No obvious bony lesions were identified.....	270
Figure 6.34 H&E staining of a) the right femur of Both Notch and b) the right femur of a control mouse.	271
Figure 6.35 H&E staining of two sections of spine from Both Notch.	271
Figure 6.36 H&E staining of a section of spine from a control mouse. This shows a comparable histological picture to Both Notch.	271
Figure 6.37 PSA staining from the right femur of a) Both Notch and b) a control mouse. The circular sections in the top left are positive controls from human prostate tissue. No PSA staining is identified.	272
Figure 6.38 PSA staining from two sections of spine taken from Both Notch. The circular sections in the top left are positive controls from human prostate tissue. No PSA staining is identified.	272
Figure 6.39 PSA staining from the spine of the control mouse. No PSA staining is identified.	273
Figure 6.40 MT1-MMP staining from the right femur of a) Both Notch and b) the control mouse. There is non-specific background staining in both specimens.	273
Figure 6.41 MT1-MMP staining from the spine of Both Notch. There is non-specific background staining in both specimens.	274
Figure 6.42 MT1-MMP staining from the spine of the control mouse. There is non-specific background staining in both specimens.	274
Figure 6.43 Anti-mitochondrial human antibody staining of the right femur of a) Both Notch and b) the control mouse. There is non-specific staining in both specimens.	275
Figure 6.44 Anti-mitochondrial human antibody staining of the spine of Both Notch. No antibody was detected.....	275

Figure 6.45 Anti-mitochondrial human antibody staining of a second section of the spine of Both Notch. No antibody was detected.	276
Figure 6.46 Anti-mitochondrial human antibody staining of a third section of the spine of Both Notch. Non-specific staining was detected.	276
Figure 6.47 A force/distance curve showing the indentation (blue curve) and retraction (red curve) of a spherical tip into the glass coverslip. The indentation curve at close separations shows a typical elastic response (sharp vertical line increase in force) of a probe indenting into glass. This serves a control for comparison with the softer cell indentation profiles.	279
Figure 6.48 A force/separation curve showing the indentation (blue curve) and retraction (red curve) of a spherical tip into a U2OS cell. The difference between the indentation curve and the indentation curve into the glass slide (Fig 6.47) is striking. The indentation profile is curved rather than straight, a characteristic of viscoelastic materials. This is consistent with literature data for the indentation of cells.	279
Figure 6.49 A force/separation curve showing the indentation (blue curve) and retraction (red curve) of a spherical tip into a healthy volunteer white cell. This was repeated for 500 cycles. This has a characteristic indentation profile, showing a viscoelastic form.	280
Figure 6.50 A force/distance curve showing the insertion (blue curve) and retraction (red curve) of a spherical tip into a patient putative CTC. This cell came from a patient with very advanced metastatic prostate cancer that had EpCAM+ and triple marker Oct4/SOX2/Nanog positive cells when processed on the Imagestream. It is also the patient from which the cells that were implanted into the mice were taken. The fit of the Hertz indentation model at the point of indentation is shown. The CTC profile appears to show a different form to that of the cell lines and white blood cells.	280
Figure 6.51 A force/separation curve showing the indentation (blue curve) and retraction (red curve) of a conical tip into a PC3 cell demonstrating the viscoelastic characteristics typical of cell indentation experiments.	281

Table 1.1 The Tumour Node and Metastasis Staging system for Prostate Cancer (adapted from <i>Brierley et al, TNM Classification of malignant tumours</i> (Brierley J, 2017)).....	6
Table 1.2 Classification of prostate cancer according to risk (adapted from <i>EAU guidelines</i> (Urology, 2018))	6
Table 1.3 The most common genomic alterations in primary and metastatic prostate cancer affecting a) the androgen receptor signalling pathway, b) the PI-3-Kinase pathway, c) DNA repair and d) other frequent alterations. Adapted from the The Cancer Genome Atlas Network (2015)	15
Table 2.1 A table listing the cell lines used in this project, their tumour of origin and their anatomical site.....	47
Table 2.2 A table listing the antibodies, isotype controls, concentrations and manufacturers for the antibodies used in the Imagestream assay described in Chapter 3.	52
Table 2.3 A table listing the antibodies, isotype controls, concentrations used and manufacturers for the antibodies used in the FACS assay described in Chapter 4.....	53
Table 2.4 List of chosen laser settings for each laser on the Imagestream and the maximum power available.....	54
Table 2.5 A Table to show the forward and reverse primers used for the PCR experiment...	69
Table 2.6 A table listing the antibodies used in the chemokine receptor immunofluorescence experiments.	70
Table 2.7 A table listing the antibodies used for the immunohistochemistry analysis.....	73
Table 3.1 Laser wavelength and associated suggested fluorochromes for the Imagestream.	87
Table 3.2 The prevalence of each combination of antigens expressed by three different prostate cancer cell lines; LNCaP, PC3 and CWR-22Rv1. All three cell lines were labelled with the three antigens EpCAM, CK and Vimentin and the percentage of total cells expressing each combination of antigens was recorded.....	89
Table 3.3 The different combinations of antigens expressed in cells detected from the blood of patients with metastatic prostate cancer. All cells were labelled with EpCAM, CK, CD45 and Draq5. To be considered a possible CTC cells had to be CD45- and Draq5+. Different combinations of EpCAM and CK expression were seen in all ten patients. The most common combination was EpCAM+/CK-, seen in 52.9% of patients.	92
Table 3.4 A list of chosen antibodies and the associated fluorochrome and isotype control used in the assay described in this chapter.	94
Table 3.5 A Table demonstrating the percentage of iPS cells staining positive for each antibody at increasing concentrations.	105
Table 3.6 A table to show the number of cells expressing each antigen for blood taken from healthy volunteers when processed using the Imagestream assay.	112

Table 3.7 A table to show the number of cells expressing each antigen for blood taken from patients with benign disease when processed using the Imagestream assay.....	113
Table 3.8 A table to show the number of cells expressing each antigen for blood taken from patients on surveillance when processed using the Imagestream assay.	114
Table 3.9 A table to show the number of cells expressing each antigen for blood taken from patients with new diagnosis metastatic disease when processed using the Imagestream assay.	114
Table 3.10 A table to show the number of cells expressing each antigen for blood taken from patients on single agent hormones when processed using the Imagestream assay.....	115
Table 3.11 A table to show the number of cells expressing each antigen for blood taken from patients on maximum androgen blockade when processed using the Imagestream assay.	116
Table 3.12 A table to show the number of cells expressing each antigen for blood taken from patients with castrate resistant disease when processed using the Imagestream assay.....	118
Table 4.1 A Table to demonstrate the available lasers on the BD FACS Fusion at Newcastle University Medical School’s Flow Cytometry Core Facility, and the suggested fluorochromes (adapted from the Newcastle University FCCF website).....	122
Table 4.2 A table to list the antibodies, corresponding fluorochromes, and isotype controls chosen for this assay	127
Table 4.3 A table to show the number of cells expressing each antigen that were found in the blood from each healthy volunteer.....	161
Table 4.4 A table to show the number of cells expressing each antigen that were found in the blood from each patient with benign disease.....	161
Table 4.5 A table to show the number of cells expressing each antigen that were found in the blood from each patient on surveillance.	162
Table 4.6 A table to show the number of cells expressing each antigen that were found in the blood from each patient with newly diagnostic metastatic disease.....	162
Table 4.7 A table to show the number of cells expressing each antigen that were found in the blood from each patient on single agent hormones.	163
Table 4.8 A table to show the number of cells expressing each antigen that were found in the blood from each patient on maximum androgen blockade.	164
Table 4.9 A table to show the number of cells expressing each antigen that were found in the blood from each patient with castrate resistant disease.....	165
Table 5.1 A Table to show the Median and Mean PSA for patients in each disease stage category at the time of sampling. Those with metastatic disease have a higher median PSA level.....	175

Table 5.2 A Table to show the median and mean ALP for patients in each disease stage category at the time of sampling. The median for patients in all categories was within the normal range.....	176
Table 5.3 A table to demonstrate the median change in PSA and ALP values for the different treatment groups and their significance (using the Wilcoxon matched pairs signed rank test). None of the median PSA or ALP changes in any of the patient groups was statistically significant.	183
Table 5.4 A table to demonstrate the median and mean (+SD) no of CTCs detected via the Imagestream for patients at each disease stage.	186
Table 5.5 A table to show the number of cells expressing each antigen for blood taken from healthy volunteers when processed using the Imagestream assay.	187
Table 5.6 A table to show the number of cells expressing each antigen for blood taken from patients with benign disease when processed using the Imagestream assay.	188
Table 5.7 A table to show the number of cells expressing each antigen for blood taken from patients on surveillance when processed using the Imagestream assay.	189
Table 5.8 A table to show the number of cells expressing each antigen for blood taken from patients with new diagnosis metastatic disease when processed using the Imagestream assay.	189
Table 5.9 A table to show the number of cells expressing each antigen for blood taken from patients on single agent hormones when processed using the Imagestream assay.	190
Table 5.10 A table to show the number of cells expressing each antigen for blood taken from patients on maximum androgen blockade when processed using the Imagestream assay.	191
Table 5.11 A table to show the number of cells expressing each antigen for blood taken from patients with castrate resistant disease when processed using the Imagestream assay.	193
Table 5.12 A table to demonstrate the p-values when comparing CTC counts between the different disease stage groups when using the Mann Whitney test. There is a significant difference in CTC counts between the newly diagnosed metastatic group and those undergoing surveillance and on single-agent hormones. There is also a significant difference between those on single-agent hormones and those on maximum androgen blockade.....	193
Table 5.13 A table demonstrating the Kruskal-Wallace statistic which shows the significance of the number of CTCs displaying each antigen combination for the different disease groups. P > 0.05 for each antigen or antigen combination therefore there was no significant difference found.	201
Table 5.14 A table to list the number of CTCs expressing each stem cell antigen for each patient in the surveillance group.	202
Table 5.15 A table to demonstrate the number of CTCs that had Oct4 present or absent for patients in each disease group compared to the CTCs in the surveillance disease group. There is no significant difference found.	202

Table 5.16 A table to demonstrate the number of CTCs that had SOX2 present or absent for patients in each disease group compared to the CTCs in the surveillance disease group. There is no significant difference found.....	203
Table 5.17 A table to demonstrate the number of CTCs that had Nanog present or absent for patients in each disease group compared to the CTCs in the surveillance disease group. There is no significant difference found.....	204
Table 5.18 A table to demonstrate the odds ratios of each stem cell antigen being present or absent in the patients that had died in comparison to the patients still alive (using the results from the Imagestream assay). The presence of each antigen does not correlate with the survival of patients during the time frame studied.....	204
Table 5.19 A table to demonstrate the median and mean (+SD) no of CTCs detected via FACS for patients at each disease stage.	206
Table 5.20 A table to show the number of cells expressing each antigen that were found in the blood from each healthy volunteer.	207
Table 5.21 A table to show the number of cells expressing each antigen that were found in the blood from each patient with benign disease.	208
Table 5.22 A table to show the number of cells expressing each antigen that were found in the blood from each patient on surveillance.	209
Table 5.23 A table to show the number of cells expressing each antigen that were found in the blood from each patient with newly diagnostic metastatic disease.	210
Table 5.24 A table to show the number of cells expressing each antigen that were found in the blood from each patient on single agent hormones.	211
Table 5.25 A table to show the number of cells expressing each antigen that were found in the blood from each patient on maximum androgen blockade.	212
Table 5.26 A table to show the number of cells expressing each antigen that were found in the blood from each patient with castrate resistant disease.	214
Table 5.27 A table demonstrating the Kruskal-Wallace statistic which shows the significance of the number of CTCs displaying each antigen for the different disease groups. The p-value is less than 0.05 (and therefore significant) for numbers of cells expressing cytokeratin, SOX2, Nanog and MT1-MMP.....	222
Table 5.28 A table demonstrating the p-values when the Mann-Whitney test was performed to analyse the significance of the difference of numbers of cells expressing Cytokeratin between each disease group (p-values in bold denote significance).	223
Table 5.29 A table demonstrating the p-values when the Mann-Whitney test was performed to analyse the significance of the difference of numbers of cells expressing SOX2 between each disease group (p-values in bold denote significance).....	223

Table 5.30 A table demonstrating the p-values when the Mann-Whitney test was performed to analyse the significance of the difference of numbers of cells expressing Nanog between each disease group (p-values in bold denote significance). 224

Table 5.31 A table demonstrating the p-values when the Mann-Whitney test was performed to analyse the significance of the difference of numbers of cells expressing MT1-MMP between each disease group (p-values in bold denote significance). 224

Table 5.32 A table to demonstrate the odds ratios of each stem cell antigen being present or absent in the patients that had died in comparison to the patients still alive (using the results from the FACS assay). There was no significance found to the presence of each stem cell antigen and whether the patient died during the study timeframe. 225

Table 6.1 A table demonstrating the percentage of cells retrieved using each method, for each cell line at each different quantity. (M = Miltenyi and STC = Stem Cell Technologies). The Stem Cell Technologies kit enabled the highest percentage of cells to be recovered when cells were spiked in all three different quantities. 238

Table 6.2 A Table listing the DNA volume and concentrations provided from each sample, and the Exome quality control data prior to sequencing. Despite what should be have been sufficient quantities of DNA obtained (as measured by the Qubit) the M seq number was low and this meant there wasn't sufficient DNA, or that the fragments were possibly too short for analysis. 256

Table 6.3 A table to show the chosen Chemokine Receptors, the corresponding conjugated fluorochrome, the isotype control and the manufacturer from which they were supplied. 259

Table 6.4 A table listing the chemokine receptors that cells from each patient expressed, and the clinical location of their metastases. 266

Table 6.5 A table to show the cell type or material that was indented, the type of cantilever tip and the Young's Modulus of the cell wall or material (glass) that was calculated. The higher the Young's modulus, the less deformable the material. 281

Chapter 1. Introduction

1.1 The prostate gland

The prostate is an exocrine gland of the male reproductive system. It produces protein-rich secretions, which make up approximately 30% of seminal fluid (Lilja, 1993). The most abundantly expressed protein by prostatic cells is the kallikrein, prostate specific antigen (PSA) (Lilja, 1993). This serine protease, also known as KLK3, allows proteolysis of the coagulated ejaculate, which subsequently enables release and motility of the spermatozoa contained within this gel (Lilja, 1988).

The prostate is a walnut-shaped gland located in the male pelvis, anterior to the rectum, immediately inferior to the urinary bladder and surrounding the urethra (McNeal, 1968). Anatomically it can be divided into three zones: the outer peripheral zone, the medial transitional zone and the central zone (McNeal, 1988). These are bordered by an anterior stromal area containing fibroblasts and smooth muscle cells. Prostate cancers are most frequently found in the peripheral zone, which assists in diagnosis as they can be clinically palpated via the rectum.

The prostate is a highly branched gland formed of epithelial tissue (Wang et al., 2001). The ducts within the gland are lined by secretory luminal cells, above a basal layer which is understood to contain stem cells (Choi et al., 2012, Ousset et al., 2012, McNeal, 1988). Rare neuroendocrine cells can also be found within the epithelium (Wang et al., 2001). It is the androgen-dependent columnar cells of the luminal layer that secrete PSA and the androgen receptor (Lang et al., 2009).

As men age, their prostate size increases and this can lead to clinical lower urinary tract symptoms (LUTS) (Lim, 2017). The incidence of benign enlargement of the prostate, or benign prostatic hyperplasia (BPH), will vary according to the criteria used to diagnose it but increases with age and symptomatic BPH can affect as many as 80% of men in their eighties (Berry et al., 1984). Although BPH is a diagnosis that can only be made histologically, there is no difference between the clinical symptoms of BPH and prostate cancer, and any male exhibiting symptoms such as difficulty voiding, nocturnal voiding or a reduced urinary flow should be clinically assessed to rule out prostate cancer (Verhamme et al., 2002).

1.2 Prostate cancer

1.2.1 Background and Epidemiology

Prostate cancer is the most common male cancer in the UK (Cancer Research UK, 2018), accounting for 26.1% of cancers in men (Statistics, 2016), and the second most common male cancer worldwide (Siegel et al., 2012, Scosyrev et al., 2012b). Over one million men are diagnosed in the world each year and in Great Britain it accounts for the second highest cause of cancer related mortality (Cancer Research UK, 2018). In the UK in 2016 over forty thousand men were diagnosed with the disease, and the lifetime risk of developing it was 1 in 8 (Cancer Research UK, 2018, Statistics, 2016).

There has been a global increase in prevalence since the 1960s, which has been attributed both to improved diagnostics and the ageing population. Prostate cancer is a disease that predominantly affects older men (Siegel et al., 2012, Brewster et al., 2000); only 0.1% of cases occur in men under 50, compared to 85% in men over 65 (Patel and Klein, 2009). Increased access to PSA screening in America, and the increase in popularity of the Trans-urethral resection of the prostate (TURP) surgical procedure to treat bladder outflow obstruction caused by prostatic enlargement, led to a 44% increase in diagnosis of the disease in the 1990s (Brewster et al., 2000, Evans and Moller, 2003). But whilst prevalence increases with age, and post mortem studies have demonstrated evidence of prostate cancer in up to 71% of men over 79 (Bell et al., 2015), it is important to note that not all prostate cancers are classified as high risk. Given the age at which many men are diagnosed, the 84% ten year survival in the UK (Cancer Research UK, 2018) means that despite being the most prevalent male cancer, it only accounts for 7% of male cancer deaths (Statistics, 2016). The increase in detection rates has led to a rise in the number of both high and low risk prostate cancers (Potosky et al., 1995) and treatment will vary depending on this information and the age of the patient.

Whilst there are no clearly identifiable preventative risk factors, there are several features which may increase the likelihood of developing the disease. In addition to age, ethnic origin and a family history are the predominant risks. There is a threefold higher prevalence of prostate cancer amongst black men compared to Caucasians, and they are also at risk of developing it at a younger age (Kheirandish and Chingwundoh, 2011, Ben-Shlomo et al., 2008). Asian men have the lowest

incidence and despite this possibly being attributed to lower screening rates or access to healthcare, studies looking at cohorts who have migrated have found that the Asian migrant populations still have lower rates than the indigenous people (Ito, 2014, Metcalfe et al., 2008).

Environmental factors such as diet, cholesterol levels, incidence of diabetes and obesity have all been proposed to affect an individual's risk of developing prostate cancer. But without randomised studies, the evidence to enable any conclusions to be drawn about these relationships is too poor (Gomez-Acebo et al., 2017, Leitzmann and Rohrmann, 2012, Vidal et al., 2014).

Having a father or brother with the disease increases the risk by up to 3.4 times (Crawford, 2003, Johns and Houlston, 2003) and those with a family history are more likely to be diagnosed at a younger age, possibly due to increased awareness (Bratt, 2002). Mendelian inheritance is responsible for 5-10% of cases of prostate cancer and up to 40% of patients diagnosed under the age of 55 have an inherited component (Shen and Abate-Shen, 2010, Carter et al., 1992, Elo and Visakorpi, 2001). Mutations in this age group such as those affecting *BRCA2* and *HOXB13* genes are most common (Salinas et al., 2014, Lin et al., 2009).

1.2.2 Diagnosis of prostate cancer

Due to the age at which prostate cancer most commonly presents, detection and treatment is only beneficial to the patient if intervention will reduce mortality and afford an acceptable quality of life. A lack of reliable biomarkers means that there is currently no screening programme available in the UK, as PSA testing can diagnose indolent cancers, the management of which can cause more significant harm than leaving the patient untreated. PSA levels can also be elevated for reasons other than cancer, which could lead to unnecessary interventions, some with high morbidity. A Cochrane review in 2014 demonstrated that screening did increase the detection rate of prostate cancer, but that the majority of these were localised tumours, and there was no cancer-specific or overall survival benefit derived from treating such cancers (Hayes and Barry, 2014).

A study published by the American Urological Association proposed that men aged between 55 and 69 would benefit from a PSA screening programme in order to

detect a small number of high risk tumours within this group, but that more harm would occur as a result of screening men younger and older than this range (Carter et al., 2013). As a result, in 2017 the United States Representative Task Force produced a recommendation that men aged between 55 and 69 discussed the risk/benefit ratio of individual screening with their doctor so that these men could make an informed choice (Quality, 2018). In the UK, PSA testing but not screening is available on the NHS but is not offered routinely. As per European Association of Urology (EAU) guidelines it is usually only requested in men under 50 if they are of African origin, have urological symptoms or a family history (Urology, 2018).

Suspicion of prostate cancer from either a digital rectal examination or an elevated PSA will result in a prostate biopsy and/or cross-sectional or radio-isotope imaging. Because of the anatomical location of the prostate, access for biopsies is either trans-perineal or trans-rectal, which carries a moderate risk of infection. Rectal disinfection with iodine, or prophylactic antibiotics are often used as preventative measures (Aron et al., 2000) (Roberts et al., 2017). Until recently, 10-12 trans-rectal ultrasound biopsies taken under ultrasound guidance was the standard, with progression to saturation biopsies (20 or more) if suspicion was still high after a negative result. More recently, trans-perineal sampling often following MRI imaging of the prostate, has become more popular, but a meta-analysis comparing the two techniques has shown no increase in detection rate between the two methods (Xue et al., 2017). The recent PRECISION study comparing MRI-guided with ultrasound guided biopsies demonstrates a 12% higher detection rate in the former group (Kasivisvanathan et al., 2018) but access to this resource is not yet widespread.

If the disease is presumed to be organ confined at diagnosis, multiparametric MRI (mpMRI) is the imaging modality of choice (Ahmed et al., 2017a). Unlike standard MRI this technique includes functional imaging such as magnetic resonance spectroscopy, dynamic contrast enhanced imaging or diffusion-weighted imaging in addition (Ghai and Haider, 2015). This has an 80-100% success rate of detecting clinically significant tumours, depending on their volume (Bratan et al., 2013). If high risk disease is suspected, abdomino-pelvic CT and bone-scans are often used in addition to mpMRI, to detect whether metastases are present (Urology, 2018). If a patient is presumed to have metastatic disease at presentation, either based on

digital rectal examination or PSA, a bone scan is performed in preference to MRI or CT, in order to detect presence of bone metastases (Abuzallouf et al., 2004). If this is positive, the information that could be provided by cross-sectional imaging would not add anything to change the management of the patient.

1.2.3 Classification and staging of prostate cancer

For all patients, staging is performed using the Tumour, Node and Metastasis staging system (Brierley J, 2017). Assessment of the tumour for staging purposes is only possible for those patients who have undergone radical surgery and is not based on biopsy results. Histological analysis of the tissue will reveal the extent of invasion of the tumour, potentially into adjacent structures, and this information in combination with imaging to detect further spread of the disease will result in a stage which is summarised in Table 1.1. Stratifying patients according to this information helps predict outcome, and therefore treatment or suitability for clinical trials. Tissue architecture within a prostate tumour is described using the Gleason scoring system. The tissue is graded on a scale of 1-5, based on the histological pattern, and the two most common areas within the tumour are used to calculate the final score, up to a maximum of 10.

A study looking at biochemical recurrence after radical treatment (prostatectomy or external beam radiotherapy) classified prostate tumours in patients according to risk (Cooperberg et al., 2005). Tumours are classified into high, intermediate or low risk groups depending on PSA level, extent of the tumour within the pelvis, Gleason grade, and the presence or absence of metastatic disease as summarised in Table 1.2.

T –Primary Tumour	
TX	Tumour cannot be assessed
T0	No evidence of primary tumour
T1	Clinically unapparent tumour that is not palpable
	T1a Incidental finding in <5% of resected tissue
	T1b Incidental finding in >5% of resected tissue
	T1c Tumour identified by needle biopsy
T2	Tumour that is palpable and confined within the prostate
	T2a Tumour involves one half or less of one lobe
	T2b Tumour involves more than half of one lobe but not both lobes
	T2c Tumour involves both lobes
T3	Tumour invades through the prostatic capsule
	T3a Extracapsular extension including to bladder neck
	T3b Invasion of seminal vesicles
T4	Tumour is fixed or invades adjacent structures other than seminal vesicles
N –Regional Lymph Nodes	
NX	Regional lymph nodes cannot be assessed
N0	No regional lymph node metastasis
N1	Regional lymph node metastases present
M – Distant Metastases	
M0	No distant metastases
M1	Distant metastases
	M1a Non-regional lymph nodes
	M1b Bone
	M1c Other site (e.g. lung)

Table 1.1 The Tumour Node and Metastasis Staging system for Prostate Cancer (adapted from Brierley et al, *TNM Classification of malignant tumours* (Brierley J, 2017))

	Low Risk	Intermediate	High Risk	
PSA	PSA <10ng/mL	PSA 10-20ng/mL	PSA >20ng/mL	Any PSA
Gleason Grade	Gleason <7	Gleason 7	Gleason >7	Any Gleason
Pathological	cT1-2a	cT2b	cT2c	cT3-4 or cN+
	Local			Advanced

Table 1.2 Classification of prostate cancer according to risk (adapted from *EAU guidelines* (Urology, 2018))

1.2.4 Treatment options and prognosis

Treatment of prostate cancer can broadly be categorised into surveillance (with a view to treating or managing symptoms should the tumour progress), treatment with a curative intent, or life-prolonging management of the disease. Those men who present with localised disease at an advanced age or with significant co-morbidities may benefit from surveillance rather than intervention, as treatment of localised disease has been shown to only offer benefit if life expectancy is over ten years (Bruinsma et al., 2017). This surveillance management is further sub-divided into active surveillance (monitoring normally low-volume, low-risk disease with the aim of starting treatment at the first sign of disease progression) or watchful waiting (palliative management that involves only starting treatment once the patient becomes symptomatic). Both options are chosen with the aim of reducing the toxicity and side effects of treatment but would not be suitable if the patient has high risk disease.

In a younger, fit patient, or an older man with a reasonable life expectancy, and intermediate or high-risk disease, radical treatment is offered with the aim of curing the patient from the disease. This is predominantly in the form of either radical surgery, or localised or radical radiotherapy (which depending on the stage may include additional hormonal therapy) (Zelevsky et al., 2011).

Whilst radical treatment can offer curative treatment for men presenting with localised disease, approximately 20% of men in the UK present with metastases (Oakley-Girvan et al., 2003, England), 2016) and those aged over 75 account for almost half of the cases of metastatic disease at presentation (Scosyrev et al., 2012a, Scosyrev et al., 2012b). Between 16.5% and 25.6% of men who have had curative treatment will develop what is known as a biochemical recurrence (a sustained and increasing rise in PSA from an undetectable level to over 0.2ng/mL) (Boorjian et al., 2011, Antonarakis et al., 2012, Peters et al., 2018) and up to 29.8% of these men will develop metastatic disease (Antonarakis et al., 2012).

EAU guidelines recommend castration for those with metastatic disease, either by bilateral sub-capsular orchidectomy, or by starting androgen deprivation therapy (ADT) (Heidenreich A., 2013, Urology, 2018). This will help palliate symptoms and slow progression to symptomatic disease and sequelae such as spinal cord

compression (Pagliarulo et al., 2012). This leads to remission in 80-90% of patients (Hellerstedt and Pienta, 2002) until the cancer becomes androgen independent; so called castrate-resistant prostate cancer (CRPC) which occurs at a median time of 12-33 months (Denis and Murphy, 1993). Median overall survival from the time of diagnosis is 42 months and from castration resistance is approximately 18 months (James et al., 2015, Tangen et al., 2012).

Treatment of CRPC is offered according to Eastern Co-operative Oncology Group (ECOG) performance status, patient preference, co-morbidities and age and is summarised in Figure 1.1. Management of metastatic prostate cancer has changed dramatically in recent years, due to the availability of second line agents, and information gathered from large randomised trials such as STAMPEDE and LATITUDE (James et al., 2015, Fizazi et al., 2017) which has helped demonstrate survival benefits both from these new interventions as single agents and from different combinations of these therapies.

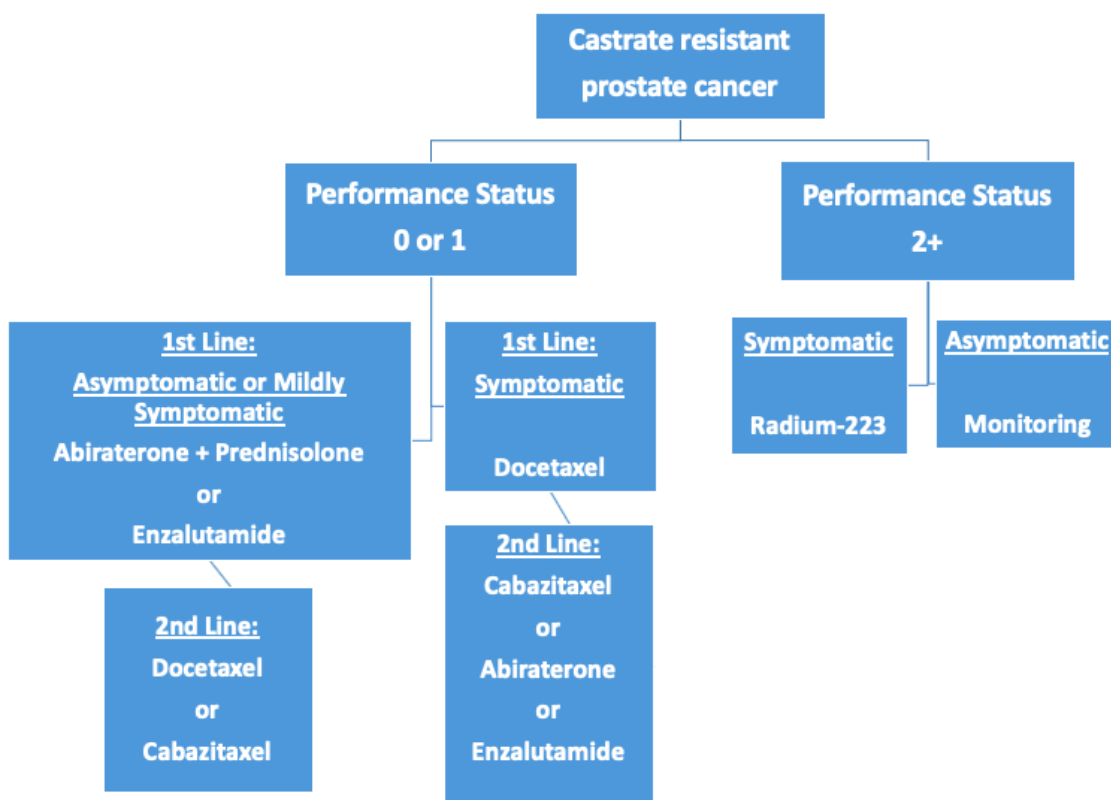


Figure 1.1 A Flowchart to demonstrate treatment of metastatic castrate resistance prostate cancer (adapted from *EAU guidelines (Urology, 2018)*). Treatment is based on the performance status of the patient and how severe the symptoms are.

1.3 The molecular properties of cancer cells

1.3.1 Genetic alterations – background

Hanahan and Weinberg's seminal paper on the hallmarks of cancer in 2000 identified six traits that cancer cells exhibit which separates them from normal healthy cells (Hanahan and Weinberg, 2000). Following the expansion of understanding of cellular interactions and regulatory pathways, they revisited these concepts in 2011. In this update they described the importance of classifying tumour cells as a complex tissue rather than an individual collection of cells, and that the interaction between the different cell types within a tumour plus the host microenvironment all play a role in tumorigenesis (Hanahan and Weinberg, 2011).

Understanding these hallmark traits and characteristics of tumour cells, and the signalling pathways involved in proliferation and metastasis is key when considering the genomic alterations known to be prevalent in prostate cancer.

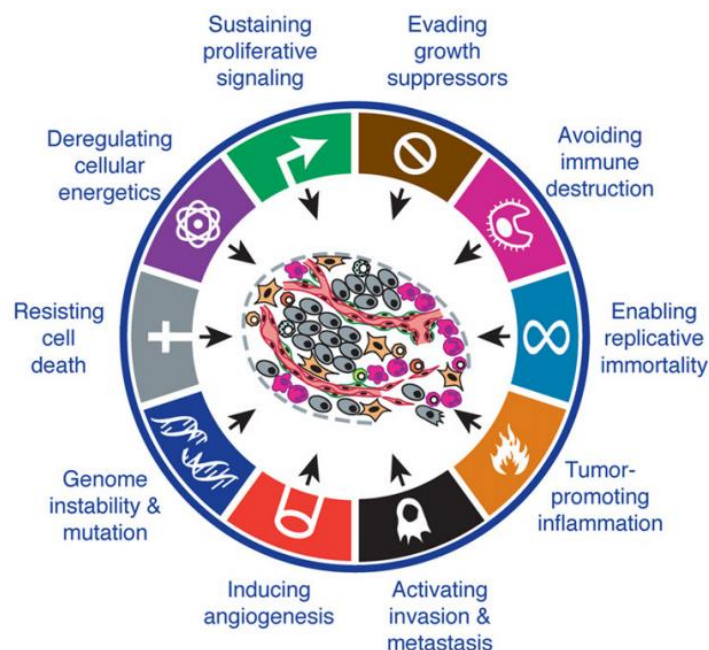


Figure 1.2 The eight hallmarks (1. sustaining proliferative signalling, 2. evading growth suppressors, 3. resisting cell death, 4. enabling cellular immortality, 5. inducing angiogenesis, 6. activating invasion and metastasis, 7. avoiding immune destruction and 8. reprogramming cellular energy) and two characteristics (1. tumour promoting inflammation and 2. genome instability and mutation) of cancer cells as described by Hanahan and Weinberg. (printed with permission from the authors) (Hanahan and Weinberg, 2011)

1.3.2 The hallmarks of cancer

The first hallmark is the ability to sustain proliferative signalling. Healthy tissue architecture is maintained by the homeostatic control of the number of cells within the tissue. Regulation of the production and release of signals that allow progression through the cell cycle is therefore necessary to limit the growth and division of cells within the tissue. Cancer cells override these regulatory pathways, resulting in a permanent 'switched on' state, and ensuing excessive cell proliferation.

The second trait is a cancer cell's ability to evade the regulatory processes that suppress cell proliferation, which would be a natural method of controlling the uninhibited proliferation outlined above. Tumour suppressor genes such as RB or TP53 act as gatekeepers to determine either progress through the cell cycle, or senescence and apoptosis. Mutations affecting these regulatory pathways can result in inactivation or inhibition of these suppressors.

The third hallmark is a cell's ability to avoid apoptosis. This mechanism of cell death is a natural sequela of physiological stresses, such as DNA damage following hyper-proliferation, or signalling imbalances from elevated levels of oncogenes.

The ability to become immortal, despite multiple replications is the fourth hallmark of a cancer cell. Normal healthy cells have a limited number of replication cycles before either reaching a crisis point and undergoing apoptosis or entering the non-proliferative state of senescence. Tumour cells can replicate an unlimited number of times, and do not appear to reach such a crisis.

Angiogenesis is an embryological phenomenon, or a temporary physiological process activated in the developed human, for example during wound healing or the female menstrual cycle. However, the need for tumours to develop their own vasculature in order to sustain growth and remove metabolic waste is enabled by an abnormal signalling process, predominantly affecting vascular endothelial cells. This 'angiogenic switch' results in ongoing vascularisation and is the fifth hallmark of cancer (Hanahan and Weinberg, 2011).

The sixth trait, which was the final feature of Hanahan and Weinberg's original description, is the ability of a cell to invade or metastasise. For a cell to leave a tumour and form a metastatic deposit in a different tissue, a series of discrete simultaneous steps are required, including shedding into the circulation, survival

within the vasculature and arrest and extravasation into a new organ (Chambers et al., 2002). This concept was first discussed by Paget when he described his 'seed and soil hypothesis' in the late nineteenth century (Fidler, 2003). This theory described the propensity for certain cancers to metastasise to pre-defined tissues, which was attributed to the relationship between the tumour cell (the seed) and the host environment (the soil). This was subsequently challenged by Ewing in the early twentieth century (Ewing, 1928) who proposed that the anatomy of the vasculature was instead responsible (e.g. in prostate cancer, Batson's venous plexus is a network of valve-less veins, connecting the deep pelvic veins with the internal vertebral veins, and thus allowing a potential direct anatomical spread of tumour cells from the prostate to the spine) (Nathoo et al., 2011). A combination of these theories in addition to other concepts such as epithelial to mesenchymal transition (EMT), the relationship between the tumour cells and the surrounding tissue, and the role that non-cancerous cells play in invasion, e.g. by secreting enzymes that degrade the extracellular matrix, has meant that metastasis is now understood to have two distinct phases. Phase one is the journey of the tumour cells from the tissue of origin to a distant site, and phase two is the adaptation of the cells to the adopted environment at this site in order to form a successful colony.

In the revised paper, Hanahan and Weinberg described two new hallmarks and two characteristics that enable the expansion of tumour cells (Hanahan and Weinberg, 2011). These characteristics are the inflammatory response that aids tumour growth, and the genetic instability of tumour cells. Inflammation can be a normal physiological response to cellular injury, but it can have the unwanted effect of providing a flood of molecules such as growth factors and enzymes. These are then utilised by the tumour cells to promote growth or encourage alterations to the tumour micro-environment e.g. extracellular matrix breakdown, turning the inflammatory response from a physiological to a pathological process. The second of these characteristics describes how tumour cells outgrow and dominate the healthy cells within a tissue. For tumour cells to display the hallmark characteristics outlined above, there must be a series of genetic alterations within these cells. These can either come about through spontaneous mutation, or impaired gene expression, e.g. inactivation of tumour suppressor genes due to the tumour cells secreting altered signals. Ultimately, DNA defects are usually identified, and the cell terminated

before expansion is enabled. For such defects to result in clonal expansion demonstrates the instability of these cells caused by an inability to respond to DNA damage.

The two new hallmarks of cancer cells are the reprogramming of energy metabolism and the evasion of immune destruction (Hanahan and Weinberg, 2011). The fact that solid tumours are more prevalent in both immuno-compromised individuals and animal models, suggests that there is an important role played by the immune system in tumour regulation. Whilst the relationship is complex - cancers in immuno-compromised individuals are often virally mediated - there is evidence of a more favourable prognosis in tumours displaying a higher proportion of cytotoxic T lymphocytes and natural killer cells, compared to those with lower numbers (Larsen et al., 2014).

The second of these new hallmarks describes the alteration of cellular energy metabolism in order to sustain the increased metabolic demands brought about by cellular expansion. The switch to glycolysis as the preferred pathway for glucose metabolism, even in aerobic conditions is found in tumour cells. Despite this resulting in lower energy yields when compared to oxidative phosphorylation, this is counteracted by upregulation of glucose transporters into the cytoplasm. Activation of oncogenes such as RAS and Myc, in addition to hypoxic conditions can upregulate glycolysis, and there are often two subpopulations found within the tumour cells – those which are glucose dependent and those which use the lactate waste product of these cells as their fuel.

1.4 The molecular characteristics of prostate cancer

1.4.1 Background

Prostate cancer genomic alterations are complex, but understanding not only where the mutations arise but also when they occur during the evolution of the prostate tumour, from localised to metastatic castrate-resistant, can help us have a better appreciation of risk, and assist drug and target discovery (Schoenborn et al., 2013, Berger et al., 2011). Combined with the knowledge of the hallmark characteristics of

tumour cells it enables an appreciation of how the common mutations found in prostate cancer cause abnormal cell growth and tumour formation. Whilst a small number of mutations are familial, the majority are somatic (Kral et al., 2011), and those most commonly seen in prostate cancer affect cell proliferation and regulation, or cause genetic instability due to prevention of DNA damage repair or impaired transcription.

Mutations can broadly be categorised into somatic copy number alterations (SCNAs) (either deletions or amplifications), structural rearrangements or point mutations (Schoenborn et al., 2013). SCNAs are very common in prostate cancer, and the increased incidence in metastatic compared to primary tumours is indicative of the increased genomic instability in advanced disease. Structural rearrangements ensue when repair of DNA breaks, occurring as a normal consequence of replication, is defective, resulting in fusion or rearrangement of chromosomes (Tomlins et al., 2005). Point mutations, where a single nucleotide base is either inserted or deleted, are often found in tumour suppressor genes, oncogenes or DNA mismatch repair enzymes in prostate cancer (Taylor et al., 2010, Kumar et al., 2011).

The most frequent genomic alterations seen in advanced prostate cancer are those affecting the androgen receptor signalling pathway, the PI3K/mTOR/AKT pathway, transcription factors, and oncogenes/tumour suppressor genes (Schoenborn et al., 2013, Shtivelman et al., 2014, Alvarez-Cubero et al., 2017, Perdomo et al., 2018). A summary of these common mutations can be seen in Table 1.3.

Name of gene	Percentage found in Primary Tumour %	Percentage found in Metastatic Tumour %	Type of alteration
AR	0	65	Amplification, Mutation
ZBTB16	4	11	Mutation, Homozygous deletion
NCOR1	3	6	Mutation, Homozygous deletion
NCOR2	2	8	Mutation, Homozygous deletion
FOXA1	4	11	Mutation
SPOP	11	8	Mutation

a) The most common genomic alterations affecting primary and metastatic prostate cancer samples related to the Androgen Receptor signalling pathway

Name of gene	Percentage found in Primary Tumour %	Percentage found in Metastatic Tumour %	Type of alteration
PTEN	17	40	Mutation, Homozygous deletion
PIK3CA	2	5	Mutation
PIK3CB	1	7	Mutation, amplification
PIK3R1	0	5	Mutation

b) The most common genomic alterations affecting primary and metastatic prostate cancer samples related to the PI-3-Kinase pathway

Name of gene	Percentage found in Primary Tumour %	Percentage found in Metastatic Tumour %	Type of alteration
<i>ATM</i>	6	5	Mutation
<i>BRCA2</i>	3	7	Mutation, Homozygous deletion
<i>CDK12</i>	2	5	Mutation
<i>FANCD2</i>	7	12	Homozygous deletion, heterozygous loss

c) The most common genomic alterations in primary and metastatic prostate cancer affecting DNA repair

Name of gene	Percentage found in Primary Tumour %	Percentage found in Metastatic Tumour %	Type of alteration
<i>TP53</i>	8	50	Mutation, homozygous del.
<i>RB1</i>	1	9	Mutation, homozygous del.
<i>KMT2C</i>	4	15	Mutation
<i>KMT2D</i>	3	12	Mutation
<i>ERG</i>	46	42	Fusion
<i>MYC</i>	7	13	Amplification

d) The most common genomic alterations in primary and metastatic prostate cancer affecting other genes.

Table 1.3 The most common genomic alterations in primary and metastatic prostate cancer affecting a) the androgen receptor signalling pathway, b) the PI-3-Kinase pathway, c) DNA repair and d) other frequent alterations. Adapted from the The Cancer Genome Atlas Network (2015)

1.4.2 The androgen receptor signaling pathway

The androgen receptor (AR) is a nuclear protein, coded for by the *AR* gene on the X chromosome (Gao et al., 2005). It is regulated by the binding of the two ligands testosterone or 5- α -dihydrotestosterone in the cytoplasm, and primarily acts as an intracellular transcription factor. It is predominantly expressed in tissues such as the prostate or epididymis (Keller et al., 1996), and as prostate cancer is androgen sensitive, blocking production of the ligands, or binding of these at the receptor site form the basis of several treatments.

In localised prostate cancer the AR has not been found to be altered, but instead there can be mutations affecting regulators or co-factors of the AR in up to 50% of these tumours (Taylor et al., 2010). In contrast in castrate-resistant disease, alterations in the AR have been found in up to 60% of tumours and activation of the AR still occurs despite castrate levels of circulating androgens (Taylor et al., 2010, Grasso et al., 2012). For the tumour to survive and continue to proliferate despite low levels of androgens mean that alternative mechanisms of AR activation have occurred in the castrate model. Gene amplification (Visakorpi et al., 1995), activation of AR mutations (Sun et al., 2006), formation of splice variants (Dehm et al., 2008, Hu et al., 2009) an increase in the expression or activation of AR regulators or co-factors e.g. *FOXA1* (Grasso et al., 2012) and increased synthesis of androgens from within the tumour (Stanbrough et al., 2006) are all potential mechanisms by which the AR can be reactivated in advanced disease.

The ligand-binding domain is the most frequent site of AR mutations and can result in truncated forms of the receptor (Alvarez-Cubero et al., 2017). ARv7 is a splice variant of the receptor that lacks a ligand binding domain and is resistant to the actions of tumour-suppressor *SPOP* (An et al., 2014). It has been the focus of attention in recent years because of the associated resistance to drugs Enzalutamide and Abiraterone (Antonarakis et al., 2014).

1.4.3 The PI3K/AKT/mTOR pathway

The PI3K/AKT/mTOR pathway is important in regulation of the cell cycle and is activated in several cancers in response to different growth factor receptors or cell

adhesion molecules (LoPiccolo et al., 2008, Yap et al., 2008). In prostate cancer, activation of this pathway is often caused by mutations in the tumour suppressor *PTEN* (Taylor et al., 2010, Berger et al., 2011) and leads to unregulated cellular proliferation. It is associated with more aggressive disease and poorer disease specific outcomes (Majumder and Sellers, 2005, Yoshimoto et al., 2007).

Activation of PI3K causes phosphorylation of the cellular phospholipid phosphoinositides, which has a key role in intracellular signalling. This causes activation of AKT, a serine/threonine kinase which also plays an important role in cell fate, affecting apoptosis, transcription and progression through the cell cycle (LoPiccolo et al., 2008). MTOR, another serine/threonine kinase, is produced as either a direct or indirect product of AKT and is important for protein translation (Schoenborn et al., 2013).

Mutations in the individual *PI3KCA*, *AKT1* and *MTOR* genes can lead to upregulation of this pathway, in addition to tumour suppressor genes as previously mentioned (Robbins et al., 2011, LoPiccolo et al., 2008). Because of the relative frequency in which mutations affecting this pathway present (up to 50% of primary tumours and 100% of metastases (Schoenborn et al., 2013, Robbins et al., 2011)), and the correlation with aggressive disease, therapeutic targets have been explored, some of which are in early clinical trials (Chang et al., 2015, Yap et al., 2008).

1.4.4 Transcription Factors

Because of their role in the regulation of gene expression, mutations affecting transcription factors will have a significant impact on the expression of key genes. In prostate cancer, mutations in the forkhead box proteins FOXA and FOXO, which are DNA binding transcription factors, affect the AR signalling pathway. Amplifications and point mutations in *FOXA1* have been demonstrated in the disease (Robbins et al., 2011, Grasso et al., 2012), and the ensuing suppression of AR signalling causes a more aggressive, de-differentiated tumour to develop (Imamura et al., 2012).

Mutations in *FOXA1* are one of the most commonly observed alterations seen in prostate cancer, and can be found in between 7 and 10% of patients (Institute, 2018, Taylor et al., 2010, Grasso et al., 2012). Conversely FOXO proteins have a tumour

suppressor role, and regulate transcription related to epithelial-mesenchymal transition. Therefore mutations causing decreased expression in FOXO will impede DNA damage repair, inhibit regulation of cell cycle progression and facilitate unregulated EMT (Katoh et al., 2013, Ma et al., 2018). Post-translational phosphorylation of FOXO proteins can occur in prostate cancer due to upregulation of AKT, which inhibits their function as transcription factors (Katoh et al., 2013). To date there are no clinically available agents directed at these forkhead box proteins, but they remain of interest as potential therapeutic targets.

1.4.5 Oncogenes and tumour suppressor genes

Alterations to proto-oncogenes, either by point mutations, chromosomal rearrangement or gene amplification result in these genes becoming activated oncogenes, and the subsequent activation of unregulated cell proliferation. Amplifications of the *MYC* oncogene are found in a third of patients with castrate-resistant prostate cancer (Shtivelman et al., 2014), and this can cause sustained signalling and immortality (Gil et al., 2005). This gene also opposes the action of *NKX3.1*, an important prostatic tumour suppressor gene, (Shtivelman et al., 2014) and when *MYC* amplification is found in conjunction with *NKX3.1* loss in primary tumours it is associated with a high risk of recurrence (Locke et al., 2012).

Oncogenic fusion products can occur as a result of chromosomal rearrangement. The most commonly seen example of this in prostate cancer is the fusion of the androgen regulated *TMPRSS2* gene with members of the ETS family (most commonly the *ERG* oncogene) resulting in the *TMPRSS2-ERG* fusion gene. This binds to and inhibits existing androgen receptors, causing DNA damage and preventing further AR expression, resulting in the development of poorly differentiated tissue. Presence of this specific mutation is therefore associated with advanced and aggressive disease and is found in at least 50% of prostate tumours (Tomlins et al., 2005, Mehra et al., 2008). Increased and impaired expression of *ERG* can also occur as a result of the *TMPRSS2-ERG* fusion gene; an example of which is a shortened ERG protein, resistant to the effects of the tumour suppressor *SPOP* (Shtivelman et al., 2014).

Mutations in the speckle-type POZ tumour suppressor *SPOP* are found in 6-10% (Institute, 2018) of prostate cancers and are associated with a poor prognosis (Barbieri et al., 2012). They occur independently of other mutations, specifically those affecting *PTEN*, *PI3K*, *TP53* and *TMPRSS2-ERG* fusion (Barbieri et al., 2012, Zhang et al., 2014). Mutations in *SPOP* are not only associated with impaired *ERG* degradation but also with inactivation of AR degradation (Adamo and Lodomery, 2016, Gan et al., 2015).

Other common tumour suppressor gene mutations include those in *TP53* and *PTEN*. *TP53* mutations can be found in 18% of prostate cancers (Institute, 2018) and prevent the normal cell cycle arrest when DNA damage is detected, thus allowing progression of cells containing altered DNA. Loss of phosphatase *PTEN*, a tumour suppressor which is a regulator of both the *PI3K/Akt/mTOR* pathway and the *G2/S* checkpoint in the cell cycle, is seen in approximately 20% of patients with organ confined disease and 50% of those with metastatic cancer (Jamaspishvili et al., 2018). The loss of one allele of *PTEN* is seen in high grade prostate intraepithelial neoplasia (PIN), a precursor of prostate cancer, but loss of both alleles is predictive of progression and a more aggressive phenotype. Increased production of glucose mediator *GLUT-1* is seen as a consequence of impaired *PTEN* regulation of the *PI3K/Akt/mTOR* pathway. This encourages increased cellular glucose uptake to fuel aerobic glycolysis which as previously discussed is one of the new hallmarks of cancer cells.

1.5 Tumour heterogeneity and the metastatic process

1.5.1 Background

Identifying mutations in these genes and pathways is important both in the discovery of a new predictive biomarker in prostate cancer but also potentially as targets for therapeutic intervention. Sequencing of tumours has provided expansion of the understanding of commonly occurring mutations, and recent studies have started teasing out the order in which these mutations occur (Wedge et al., 2018).

Personalised medicine may be able to provide an individualised prognosis and identify therapeutic options, but it can be expensive. Unless the presence or absence

of a specific gene can be linked to a defined clinical outcome, e.g. resistance to a treatment such as in breast cancer or gastrointestinal stromal tumours (Day et al., 2017, Mei et al., 2018), then it is less clinically useful. It therefore does not currently contribute to the treatment pathway outside of clinical trials in the majority of tumours (Robinson et al., 2015).

As demonstrated, mutations can develop during the progression of the disease, therefore for sequencing to be of help in guiding treatment, it must be performed on tissue that can reflect not only the previous treatment, but the most genomically altered part of the tumour (Robinson et al., 2015). As previously discussed, taking biopsies from prostate, bone or lymph nodes in the predominantly elderly population is a significantly morbid procedure, and the treatment decision based on the results would have to be considered validated enough to make the risk worthwhile.

Tissue sampling must also take into consideration the heterogeneity of the tumour, and in the case of a metastatic patient, whether the biopsy sample from a solid lesion is representative of disseminated disease. Sampling bias from solid tumours may prevent the detection of the most aggressive sub-clone.(Burrell et al., 2013) One study describes an upgrading of 54.4% of tumours following radical prostatectomy, that were thought to be Gleason 3+3 tumours at biopsy, demonstrating that even at whole cell level the inaccurate detection of the most aggressive cancer cells may occur (D'Elia et al., 2014). When subcellular expression is of interest it is vital to identify the most aggressive population to begin with.

1.5.2 Heterogeneity in cancer in general

It is well documented that inter-tumour heterogeneity exists amongst tumours of the same tissue type.(Lawrence et al., 2013, Vogelstein et al., 2013, Burrell et al., 2013). This can occur due to specific mutations affecting the signalling pathways and may affect the rate of disease progression or the response to a certain treatment e.g. hormone sensitivity in breast cancer (Burrell et al., 2013, Weigelt and Reis-Filho, 2009). Indeed the treatment that is offered, especially in cancers such as breast cancer, is often based on different biomarkers being identified between different individuals (Bedard et al., 2013).

Further to this there is evidence that within an individual tumour there are areas of heterogeneity and different sub-clone populations, and that this intra-tumour heterogeneity is clinically significant (Burrell et al., 2013, Meacham and Morrison, 2013, Greaves and Maley, 2012, Lawrence et al., 2013, Robertson-Tessi et al., 2015). There are two main theories as to how tumours develop in this way; the theory of clonal evolution and the cancer stem cell theory.

1.5.3 *The theory of clonal evolution*

The theory of clonal evolution proposed by Nowell in 1976 is based on Darwinian concepts and describes how any of the cells within a tumour could be responsible for the development of a genotypically different sub clone (Nowell, 1976). During cell division, mutations are inherited by daughter cells and with the increasing number of cell divisions, cells acquire more and more mutations. As described earlier, if these mutations affect the identification of abnormal cells or the ability to halt abnormal cell division, these cells will continue to increase in number and will result in genetic instability. Within a tumour either a clonal sweep, linear evolution or branched evolution will occur (Burrell et al., 2013). In the case of a clonal sweep, a mutated cell divides and the daughter cells outnumber and take over the entire tumour, ultimately not causing a heterogeneous pattern. However intra-tumour heterogeneity occurs as a result of linear or branched evolution due to a new clone failing to oust the existing cell population, or multiple sub clones developing simultaneously. Some of these sub clones may be eliminated by treatment but the most aggressive survive and go on to cause metastases and further sub clone formation (Nowell, 1976, Bedard et al., 2013, Klein, 2013).

Evidence to support the theory of clonal evolution is demonstrated by the progression of a benign adenoma to an adenocarcinoma which can then form metastases.

1.5.4 *The cancer stem cell theory*

In contrast to the theory of clonal evolution, the cancer stem cell theory proposes that there are only specific cells within a tumour that are responsible for tumour development (Fabian et al., 2009). These cancer stem cells behave in a similar way to normal healthy stem cells in that they are capable of self-renewal, are resistant to

apoptosis and can differentiate into numerous cell types (Gil et al., 2008). This concept was first proposed by Bonnet and Dick in the late 1990s, when they explored the expression of surface markers of cells to be transplanted for a leukaemic xenograft model (Bonnet and Dick, 1997). They discovered that much lower numbers of cells expressing a specific combination of markers caused tumour development in immuno-compromised mice, in comparison to a larger number of heterogeneous cancer cells.

Cancer stem cells give rise either to daughter stem cells or to progenitor cells, the latter of which have a limited capacity to self-renew but are fast-cycling and can differentiate following interaction with the local tissue microenvironment. It is proposed that it is these progenitor cells that are the casualties of chemotherapy, but that the slow-cycling stem cells are the reason for a period of dormancy after treatment, followed by recurrent metastases (Fabian et al., 2009, Gil et al., 2008). Normal healthy stem cells can become cancer stem cells following a series of genetic or epigenetic mutations.

Bonnet and Dick's work was pivotal in the support of this theory over Nowell's, however there are questions to consider. One of the challenges in terms of identifying these cells is that the markers on the cell surface are either no different to the other cells or stem cells within the tissue, or there is considerable variation between different stem cells and the proteins they express (Scatena et al., 2013). This makes identifying the specific population of interest very difficult. It is also possible, albeit with a much higher number of cells, to induce *in vivo* tumour formation with an un-sorted cell population. However, given the inability to identify specific cancer stem cell markers, this could be explained by a heterogeneous cancer stem cell population.

1.5.5 The role of the microenvironment

Whilst it is not clear which of these theories is correct, what is known for certain is that tumour development and heterogeneity occur as a result of both intrinsic epigenetic and genetic changes, and the extrinsic interactions of the tumour with its microenvironment (Scatena et al., 2013, Gupta and Massague, 2006, Junttila and de Sauvage, 2013, Burrell et al., 2013). As we know from Hanahan and Weinberg's work, a cell's ability to overcome apoptosis is one of the hallmarks of cancer. But the ability

of a cancer cell to interact with its host environment will not only increase its survival, but its ability to metastasise (Gupta and Massague, 2006).

Tumours undergo Gompertzian growth, displaying a prolific early phase followed by slowing of growth as the tumour increases in size (Hanin and Bunimovich-Mendrazitsky, 2014). During this, the tumour cells and the native healthy cells will compete with each other for nutrients, vascular supply and space to expand (Greaves and Maley, 2012). The surrounding tissues in a healthy subject will normally impede tumour development, but damage to these tissues, e.g. via UV light, radiotherapy or dietary variations such as an increase in adipose tissue, can promote changes. This can result in local responses such as an increase in inflammatory infiltrates or vascularisation, which could assist with tumour growth or act as a protective measure against targeted therapies (Greaves and Maley, 2012, Junttila and de Sauvage, 2013).

The plasticity of the tumour cells, as supported by the cancer stem cell theory, means that they may exhibit different phenotypes if they embed in different anatomical locations, due to the interaction with the host environment (Klein, 2013, Bedard et al., 2013). Different sub-clones may favour a specific micro-environment either in the treatment naïve patient or following pharmacological intervention (Burrell et al., 2013, Junttila and de Sauvage, 2013, Gatenby et al., 2011). Protein expression can differ between cells of different sub-populations, and this has made it possible to identify the origin of metastatic deposits from within the primary tumour or other metastases (Lawrence et al., 2013, Gudem et al., 2015).

1.5.6 Metastasis and the spread of cells from the primary tumour

Metastasis is considered to be the primary cause of disease-related death in patients with cancer (Fidler, 2003, Gupta and Massague, 2006, Pantel and Brakenhoff, 2004, Klein, 2008), accounting for up to 90% of cancer mortality (Gupta and Massague, 2006). The cells within a tumour that evolve with certain attributes such as increased motility, invasiveness and an ability to survive targeted treatments are more likely to escape from the tumour of origin (Bednarz-Knoll et al., 2012). These cells escape into the vasculature either from the primary tumour, or from existing metastatic deposits (Gudem et al., 2015) via a number of proposed mechanisms, and a proportion of

these will form distant colonies in target organs (Gupta and Massague, 2006, Kim et al., 2009, Chiang and Massague, 2008). In order for this to happen, a series of steps must occur, and failure to progress along this cascade may prevent the development of metastases (Fidler and Kripke, 2015, Fidler, 2003). These steps are outlined in Figure 1.2.

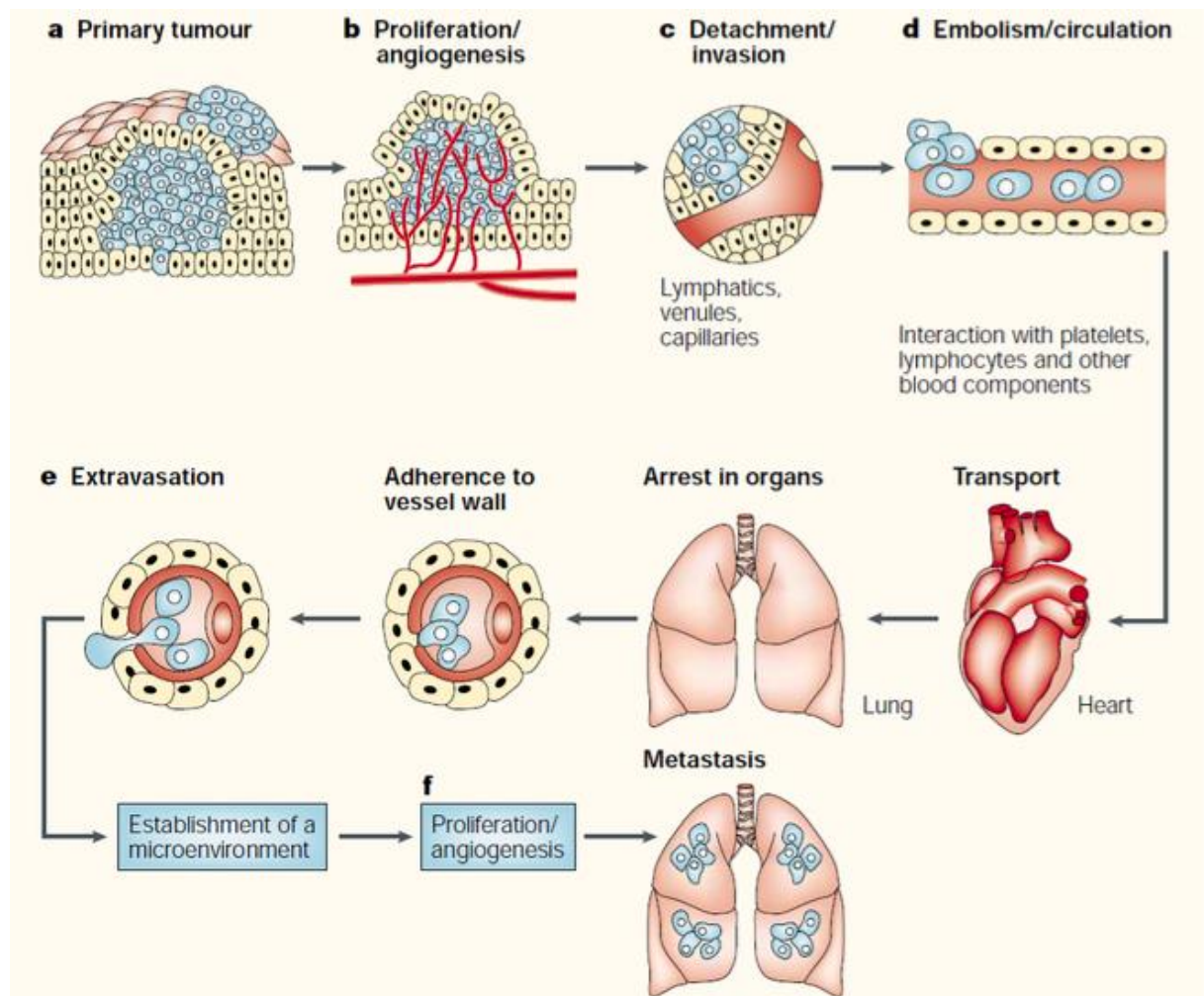


Figure 1.3 A diagram to demonstrate the steps involved in the development of metastasis. Taken from *The pathogenesis of cancer metastasis: the seed and soil hypothesis revisited* (Fidler, 2003)

It was originally thought that the formation of metastases was seen in the advanced stages of tumour progression. However it is now understood that cells can escape from the tumour at an early stage and lie dormant at distant sites until the relevant oncogenes are activated, or the host environment supports propagation (Klein, 2008). These disseminated cancer cells (DCCs) are present in the lymph nodes and bone marrow of patients with known tumours or with a previous cancer diagnosis but considered to be in remission with no clinical or radiological signs of metastases

(Klein, 2013, Bednarz-Knoll et al., 2012). Sampling of these cells has demonstrated considerable heterogeneity. Some of the patients with these DCCs will never develop metastases and therefore these cells may either die or lack the stem cell characteristics that would enable them to progress. But some of these DCCs will embed, and the combination of their genetic code and their interaction with the host environment will enable them to proliferate and develop secondary tumours sometimes many years from the initial diagnosis of the primary.

1.5.7 Epithelial to Mesenchymal Transition

In order for cells to detach from the primary tumour and escape into the adjacent vessels, they need to undergo either active or passive detachment. Passive transfer into the vasculature could occur due to physical tumour invasion, and would not require the cells to change physically (Bednarz-Knoll et al., 2012). However, it has been proposed that some undergo a phenotypic change called epithelial-mesenchymal transition (EMT) (van Denderen and Thompson, 2013, Christiansen and Rajasekaran, 2006). This process is similar to the epithelial-mesenchymal transition and subsequent mesenchymal-epithelial transition (MET) that occurs in embryos to allow movement of cells and colonisation in different anatomical locations (Christiansen and Rajasekaran, 2006) or in wound healing (Stone et al., 2016). It is unclear whether the process is a full requirement for all cells as biopsies of solid metastases have shown epithelial characteristics (Tarin et al., 2005, Christiansen and Rajasekaran, 2006). The fact that epithelial cells have been detected from blood samples in patients with metastatic disease would support the argument that not all cells need to undergo this process in order to escape from the primary tumour, or that EMT is incomplete and cells may still display epithelial characteristics (Thiery and Sleeman, 2006, Christiansen and Rajasekaran, 2006, Armstrong et al., 2011).

EMT is an evanescent and reversible process that is associated with aggressive disease, formation of metastases and resistance to chemotherapy and other drug treatments (Mani et al., 2008, May et al., 2011, Yang et al., 2004, Christiansen and Rajasekaran, 2006). Cancer stem cells often express mesenchymal markers and induction of EMT can also induce progenitor cells to develop stem cell like characteristics (Mani et al., 2008, Kong et al., 2011). Epithelial cells classically interact

with each other via close cell membrane contact along the length of the cell. They display apical-basal polarisation and have a structured cytoskeleton. Adoption of the mesenchymal phenotype results in a change in polarity and cytoskeleton and a reduction of the cell contact so that interaction with adjacent cells is much more focal. These changes result in the cells being held much more loosely together, encourage increased motility, and degradation of the extra-cellular matrix (Thiery and Sleeman, 2006, Christiansen and Rajasekaran, 2006, Bednarz-Knoll et al., 2012). E-cadherin, a transmembrane protein expressed by epithelial cells, is down-regulated during EMT in exchange for an upregulation of the mesenchymal marker N-cadherin (Bednarz-Knoll et al., 2012).

It is thought that cells undergo EMT as a result of the interaction with their local environment, and that stresses such as hypoxia or pH changes can induce the relevant signals. One of the characteristics of EMT is a resistance to apoptosis, so it is thought that a cell that undergoes this phenomenon is more likely to survive as it escapes into the bloodstream and travels through this potentially hostile environment to a distant site (Valdes et al., 2002, Barrallo-Gimeno and Nieto, 2005, Peinado et al., 2007). The induction of migratory potential in adjacent cells can also occur as a result of cytokine expression by cells undergoing EMT (Voss et al., 2011, Fernando et al., 2011). This may assist with invasion and the potential of a cell to metastasise. Protein synthesis can also be down-regulated as a result of the unfolded protein response, a feature of EMT that decreases the rigidity of the cell (Wouters and Koritzinsky, 2008).

A combination of growth factors, transcription factors and micro-RNAs are responsible for the activation of EMT (Bednarz-Knoll et al., 2012, Mani et al., 2008, Tam and Weinberg, 2013). Signals from the microenvironment induce signalling between cells, which in turn causes activation of various transcription factors including TWIST, SLUG, SNAIL and ZEB-1 (Zheng and Kang, 2014). The TGF- β and WNT signalling pathways are both responsible for the induction of EMT and result in the phosphorylation of cytoplasmic proteins which have a key role in the regulation of genes affecting cell mortality (De Craene and Berx, 2013). Higher levels of these proteins have been found in tumour cells in advanced, aggressive disease (Mani et al., 2008, May et al., 2011, Li et al., 2013).

In prostate cancer, despite being a tumour of epithelial origin, expression of EMT-related genes or mesenchymal proteins has also been associated with advanced disease. Increased N-cadherin expression and loss of E-cadherin correlates with higher Gleason score and poorer clinical outcome (Contreras et al., 2010, Gravdal et al., 2007). And in castrate resistant disease, a prevalence of genes associated with EMT has been found when compared to tumours that are still androgen sensitive (Gorges et al., 2012, Armstrong et al., 2011, Chen et al., 2013).

Proteins such as CD44, MT1-MMP, Vimentin, Twist, SNAIL, SLUG, and ZEB1 and 2 are all increased in EMT and could act as potential biomarkers for the detection of cells undergoing this process (Hernandez et al., 2015, Li et al., 2013, Raimondi et al., 2011).

1.5.8 Heterogeneity in the patient with metastatic prostate cancer

In recent years there has been a move away from the reliance on solid tissue biopsies in advanced prostate cancer. In those patients who develop metastatic disease following radical treatment, biopsies or whole prostate specimens may be many years old and basing targeted treatments on genetic information from this tissue would be suboptimal.

Prostate biopsy is a morbid procedure that is usually reserved for the aid of diagnosis in younger patients, or those with lower PSA values who are likely to receive radical treatment. Diagnosis in patients who have a clinically suspicious prostate (T3/T4) is made by a combination of PSA, digital rectal examination and bone scan or CT (Heidenreich A., 2013). With the current treatment cascade, prostate, lymph node or bone biopsy serve no additional purpose once metastatic disease has been diagnosed and carry a high morbidity. The standard treatment of androgen deprivation therapy would be initiated for all men falling into this category, and despite our knowledge of tumour heterogeneity, there is currently no way to predict which of these men would respond well, and which are likely to develop early castrate resistance.

Whilst some of the current clinical trials include serial biopsies in order to gain further understanding of the molecular changes that occur in conjunction with disease resistance, we do not have routine access to IHC specimen libraries in metastatic patients compared to those who have undergone radical surgery. This,

along with the sampling bias associated with any solid tissue biopsy because of tumour heterogeneity, has meant that response to treatment is still based on serum PSA levels, and to date, no new biomarker has been developed for use in the clinic.

A large number of the studies looking at sequencing of metastatic tumours have been performed on post-mortem samples, or as part of a clinical trial (Robinson et al., 2015). Putting the cost aside, without any solid tissue to sequence in the majority of metastatic prostate cancer patients, and no reliable biomarker, we are effectively treating these men blindly. Once castrate-resistance occurs, progression along the treatment cascade is largely reliant on PSA levels and clinical symptoms.

1.6 Biomarkers in prostate cancer and potential options for new markers

1.6.1 Background

In patients diagnosed with metastatic disease, and also those who present with it following treatment with curative intent, especially in the ageing patient, it would be prudent to predict at this diagnosis who is likely to respond well to ADT. This would allow earlier commencement of second-line agents before there is a significant decline in cardiovascular status. Monitoring of response both to ADT and other treatments such as docetaxel, enzalutamide and abiraterone is also currently suboptimal because of the lack of a reliable biomarker. In the era where personalised medicine is becoming an increasingly popular concept there is a distinct need for a new prostate cancer biomarker.

1.6.2 PSA

As discussed, PSA is the only FDA approved biomarker available for use in clinical practice in the UK, but can be elevated for reasons other than prostate cancer, and also downregulated in advanced or poorly differentiated disease (Leibovici et al., 2007). PSA values are inconsistent with tumour burden and levels at diagnosis of metastatic cancer do not correlate with the subsequent success of ADT. This makes it an ineffective tool as either a diagnostic or a predictive biomarker.

1.6.3 Prostate-specific Membrane Antigen

Prostate-specific membrane antigen (PSMA) is a type II membrane protein that acts as a glutamate-releasing carboxypeptidase (Carter et al., 1996). Although expressed in all types of prostate tissue, it has also been found in other tumours including renal, bladder, testicular and breast (Chang, 2004). Despite it being upregulated in prostate cancer when compared to benign prostate disease (Israeli et al., 1994), until recently its role as a biomarker in prostate cancer has not been utilised. Early studies showed that its expression was not significantly different in the serum of patients with benign versus malignant disease (Murphy et al., 2000).

The expression of PSMA is now known to be inversely related to the androgen levels of a tumour (Meller et al., 2015), and recent interest has increased due to the understanding that PSMA-induced glutamate release has been shown to activate the PI3K-AKT-mTOR pathway (Kaittanis et al., 2018). PSMA ligands such as ^{68}Ga -PSMA-11 have been used as an adjunct to Choline-PET scans to look for early recurrence in prostate cancer patients treated with curative intent (Afshar-Oromieh et al., 2017, Afshar-Oromieh et al., 2015). It has increased the sensitivity of these scans but it is currently only available for use as part of clinical trials.

1.6.4 Epithelial vs Mesenchymal markers

Although over 90% of solid tumours have an epithelial phenotype (Christiansen and Rajasekaran, 2006), some are mesenchymal in origin, e.g. sarcoma and melanoma. Because of the potential for cells to undergo EMT, ideally even cells from an epithelial tumour should be analysed for their expression of both epithelial and mesenchymal proteins. If this occurred in addition to a tumour specific marker they could be resolutely identified as circulating tumour cells from a specific tumour of origin. Unfortunately, this assumes an existent reliable tumour-specific biomarker, which is not available in prostate cancer.

Typical epithelial markers such as EpCAM and Cytokeratin have a higher expression in epithelial tumours when compared to normal epithelial tissue (Litvinov et al., 1994). They are the most commonly used epithelial markers when looking at epithelial cancers (Barriere et al., 2014), but other proteins involved with tissue architecture such as E-cadherin or Zona Occludens (ZO) have also been used (Gall and Frampton,

2013, Lindley and Briegel, 2010). In tissue undergoing EMT, epithelial marker expression is often downregulated and therefore not detectable.

Mesenchymal markers such as fibronectin and vimentin have been co-expressed alongside cytokeratin in patients with metastatic breast and prostate cancer (Armstrong et al., 2011). However, as prostate cancer is an epithelial and not a mesenchymal tumour, looking for markers associated with EMT rather than pure mesenchymal markers may be more useful. Proteins such as Twist1, Zeb1, Akt and PI3K (Odero-Marah et al., 2018, Barriere et al., 2012, Lo et al., 2017) have all been explored.

1.6.5 Androgen Receptor

Because of the dependence of prostate tumour growth on AR signalling, the AR has been used as a biomarker in the detection of prostate cancer for many years (Chen et al., 2004). With the discovery of up to twenty-two splice variants of the AR (Chen et al., 2004), detection of these and other genomic alterations discussed previously have been used when looking at prostate cancer (Beltran et al., 2016).

1.6.6 Matrix-Metalloproteinases

Matrix metalloproteinases (MMPs) have been studied extensively with respect to tumour biology because of their ability to degrade the extracellular matrix; a key step in the metastatic process (Seiki, 2003, Escaff et al., 2010, Fingleton, 2008). There are 28 of these zinc-dependent endopeptidases, usually expressed in cells of mesenchymal origin. Studies looking at the link between MMP expression and prostate cancer have found higher serum levels of MMP-2 and MMP-9 in patients with prostate cancer compared to healthy controls, but no difference between those with bony metastases compared to locally confined disease (Incorvaia et al., 2007, Salminen et al., 2006). Similarly levels of MMP-7 were found to be higher in patients with metastatic prostate cancer compared to healthy controls and those with focal disease (Szarvas et al., 2011). Some of the MMPs have been expressed in epithelial tumour cells and membrane type-1 matrix metalloproteinase known as MT1-MMP or MMP-14 as per the classification system has been shown to induce morphological change from the epithelial to mesenchymal phenotype in prostate cancer cells (Cao et al., 2008). Whilst it is not a prostate specific marker, due to the propensity of

prostate cancer to metastasise to bone, it could be used as a surrogate in the absence of a reliable prostate specific biomarker.

1.6.7 Stem cell markers

Many studies have looked at the cancer stem cell in prostate cancer, and the role of stem cell marker expression has been explored in relation to tumour progression (Ruscetti et al., 2015, Bae et al., 2011), metastasis (Matsika et al., 2015, Mochizuki et al., 2004, Conley-LaComb et al., 2012), and resistance to treatment (Qin et al., 2012, Hoogland et al., 2014, Kerr et al., 2015). It is unlikely that cancer stem cells are true stem cells, as their ability to divide and differentiate are different from, albeit similar to stem cells, (Valent et al., 2012), but they will express a variety of stem cell markers. This variation in expression has been one of the challenges in identifying them, as due to tumour heterogeneity there will be differences in marker expression (Deng and Tang, 2015) between tumours, which in turn need to be correlated with clinical significance. In prostate cancer, cancer stem cell markers such as CD117 (Kerr et al., 2015, Wiesner et al., 2008), CD133 (Miyazawa et al., 2014, Oktem et al., 2014), CD44 (Klarmann et al., 2009, Oktem et al., 2014), and CXCR4 (Dubrovska et al., 2012) have been explored.

Following Yamanka's seminal work looking at using embryonic stem cell makers Oct3/4, SOX2, Klf4 and c-myc to restore pluripotency in mouse (Takahashi and Yamanaka, 2006) and human fibroblasts (Takahashi et al., 2007), the expression of these four transcription factors has frequently been used to prove the stem-ness of cancer stem cells. Expression of embryonic stem cell gene signatures in breast cancer was shown to be associated with an adverse prognosis (Ben-Porath et al., 2008) and since those data in 2008, this has been replicated in other cancers such as bladder, prostate, renal and rectal (Amini et al., 2014, Hepburn et al., 2019, Rasti et al., 2018, You et al., 2018).

Work generated from prostate tissue by my group, prior to the start of this project, demonstrated that specific key regulators of the embryonic stem cell gene expression network, transcription factors Oct4, Sox2 and Nanog (OSN), are significantly up-regulated in patients that develop castrate resistant disease more rapidly, and 93% of the tumours expressed all three factors (Hepburn et al., 2019).

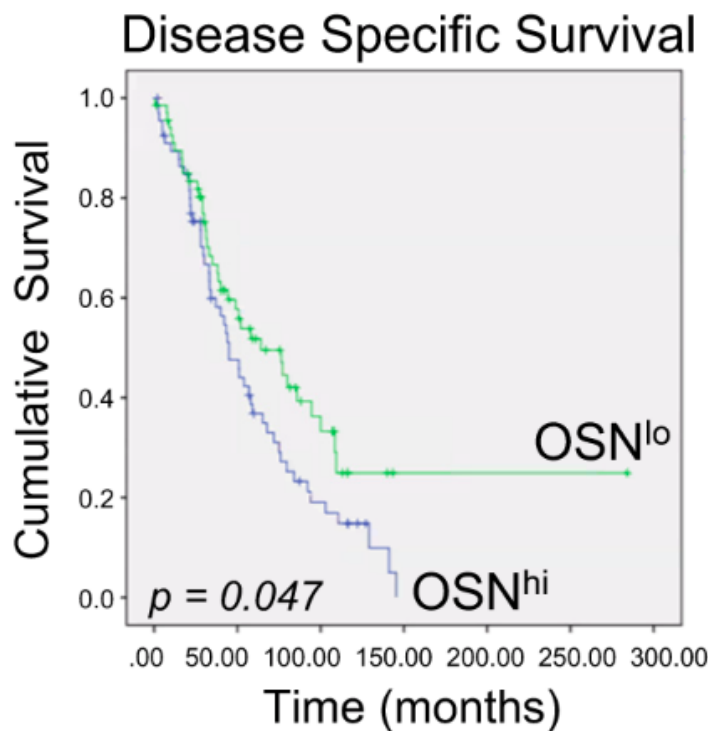


Figure 1.4 The survival curve for patients expressing Oct4/SOX2/Nanog in prostate tumours. Patients were categorised as having either high (n = 69) or low (n = 67) expression, as determined by visual assessment of immuno-histochemical staining of prostate tumours. Taken from *The induction of core pluripotency master regulators in cancers defines poor clinical outcomes and treatment resistance* (Hepburn et al., 2019).

1.6.8 Circulating biomarkers

As discussed already, the disseminated cancer cells that have broken away from the tumour to cause metastatic deposits will at some point be found in the circulation. Many researchers believe these, or a subset of these cells, to be the cancer stem cells from the original tumour (Harris and Kerr, 2017, Reya et al., 2001, Schilling et al., 2012). Over the past decade there has been increasing interest in these so-called circulating tumour cells (CTCs) and also circulating tumour DNA (ctDNA); the DNA fragments from disrupted tumour cells. Exploring the protein expression, or sequencing these cells or ctDNA to look for known mutations can provide useful clinical and prognostic information without the need for a solid tumour biopsy (Boysen et al., 2018, Chaux et al., 2012, Reid et al., 2010, Thoma, 2014, Torquato et al., 2019). Translational studies, such as the TRACER_x study (Tracking cancer evolution through therapy) have looked at sequencing ctDNA from patients with non-small cell lung cancer (Abbosh et al., 2017). By detecting single-nucleotide variants (SNVs) from the ctDNA in patients pre and post-operatively, it has been possible to

predict disease relapse. Whilst individual patient sequencing is expensive, it may help to guide who receives post-surgical chemotherapy in lung cancer patients. Currently only 5% of patients receive benefit from this treatment and 20% experience significant toxic side effects (Abbosh et al., 2017). A higher volume of ctDNA, as determined by a higher allele fraction, has also been found to be associated with more aggressive disease in both lung (Abbosh et al., 2017) and breast cancer (Garcia-Murillas et al., 2015).

Other circulating biomarkers such as messenger RNAs (mRNA) (Souza et al., 2017, Ross et al., 2012, Olmos et al., 2012) and micro RNAs (miRNA) (Matin et al., 2018, Richardsen et al., 2019) also contain genetic information about the tumour and have been investigated in patients with prostate cancer.

Whichever circulating biomarker is chosen, a simple blood sample, which carries a much lower risk to the patient than a prostate biopsy, and can be easily repeated at serial intervals, is an appealing platform for biomarker discovery.

1.7 Circulating tumour cells

1.7.1 CTCs and their role as a liquid biopsy

Although tumour cells were first identified in the circulation in the nineteenth century (Ashworth, 1869), it was not until the early 2000s that interest in them took off. Because they can be accessed via a blood sample, they offer a way of potentially accessing genetic information about the tumour to aid in diagnosis and prognosis, or provide information for therapeutic targets (Danila et al., 2011c, Bedard et al., 2013, Hu et al., 2013). Blood samples are easily obtainable, can be repeated at several time-points throughout the course of the disease and carry minimal risk to the patient. In addition, the problem arising from the changing expression of different sub-clones as a result of adaptations in the local environment from therapeutic interventions can in theory be overcome by serial blood sampling (Gatenby et al., 2011). In the patient with metastatic prostate cancer, they offer an insight into the extent of the disease which cannot reliably be ascertained by conventional diagnostics methods such as imaging or PSA sampling.

1.7.2 Definition

The FDA defines a circulating tumour cell as one with the following characteristics: positive for the epithelial membrane glycoprotein EpCAM, and the cytoskeleton protein Cytokeratin (CK) 8,9 or 19, an intracellular nucleus, negative CD45 expression (a common protein expressed by all types of leucocyte) and a cell area of more than $4 \times 4 \mu\text{m}^2$ (Attard and de Bono, 2011). A study looking at the presence of CTCs in healthy volunteers concluded that cells reaching the classification were occasionally present in the blood of patients with no known cancers. But these events were so rare and the numbers so small that a CTC count of 2 or more was classified as abnormal (Allard et al., 2004). To date the only FDA approved platform for detection of CTCs is the Veridex CellSearch, which uses the principles of positive immunomagnetic selection for EpCAM, before further analysis based on additional protein expression (Kagan et al., 2002).

1.7.3 Morphology

Studies of the physical structure of CTCs have found them to be highly pleomorphic and for there to be considerable heterogeneity in their shape (Park et al., 2014). This is perhaps unsurprising given that they represent a highly disparate population. The increased level of cytomorphological variation has been demonstrated to correlate with poor prognosis in prostate cancer (Ligthart et al., 2013). CTCs are usually larger than leucocytes, and whilst in other cancers this increase in size is discernible, prostate CTCs are smaller than those found in patients with breast or colorectal cancer (Coumans et al., 2013) in addition to being smaller to prostate cancer cell lines (Park et al., 2014, Coumans et al., 2013). They have a higher nuclear: cytoplasmic ratio due to the relative size of the nucleus in a small cell, which makes them more rigid and less deformable, an important feature when considering filtration devices for capture. The nucleus is often hyperchromatic or lobulated; also a characteristic which can assist detection (Dhar et al., 2016).

1.7.4 Enumeration

One of the main issues affecting the detection of CTCs is the ability to pick out the tumour cells from the background of millions of leucocytes and erythrocytes. Even in patients with a heavy metastatic burden, these CTCs are comparably rare events, and

on average it is thought that the ratio may be as few as one CTC per billion blood cells (Maheswaran and Haber, 2010, Ross et al., 1993). This poses a challenge for identification but recent advances in cell sorting technology have enabled low numbers of tumour cells to be identified from this background noise (Alix-Panabières and Pantel, 2014, Danila et al., 2011c).

The original studies looking at the presence of CTCs in patients with metastatic cancer reported prognostic information based on CTC count. A higher number of CTCs at diagnosis or an increase during treatment is associated with poorer overall survival, and more of these cells are seen in patients with bony metastases compared to those with M1a disease (metastases to non-regional lymph nodes) (Danila et al., 2007, Lorente et al., 2018).

Johann de Bono's seminal work looking at the number of CTCs in patients with metastatic prostate cancer and treatment with chemotherapy demonstrated an increase in overall survival of 21.7 months vs 11.5 months for those patients who had a CTC count of 5 or less per 7.5ml of blood before treatment, detected via the CellSearch platform ($p = <0.0001$) (de Bono et al., 2008). Patients whose count decreased to 5 or less following chemotherapy had a favourable prognosis compared to those who had more than 5 and it was shown that CTC count was more sensitive than PSA values in predicting survival and recurrence. This was a key factor leading to the approval of CTC count as an FDA verified research method in the assessment of metastatic prostate cancer. In both breast and colorectal cancer, the number of CTCs used as a threshold for poor prognosis is 5 and 3 respectively (Cristofanilli et al., 2004, de Bono et al., 2008, Cohen et al., 2008).

More recently, in patients treated with abiraterone acetate, a post-treatment CTC count of less than 5 per 7.5ml of blood has also been shown to correlate with a more favourable prognosis, although the study had low numbers of patients (Danila et al., 2011a). In patients with androgen sensitive disease a count of 3 or more CTCs can predict time to progression of castrate resistance (Goodman et al., 2011).

However, with the number of CTCs detected in an individual patient often being very low, even with a high capture efficiency there is a risk of classifying patients into the wrong prognostic group. Further analysis of CTC count has shown that the actual CTC number is indicative of prognosis, with higher CTC counts associated with poorer

survival (Scher et al., 2009) and a significant increase or decrease in number being more relevant than crossing the threshold of 5 cells per blood sample. CTC count now forms part of the TNM staging system for breast cancer (Lv et al., 2016) but its value with respect to changing treatment decisions is undefined.

There have also been studies demonstrating that over a third of patients with metastatic disease falling into the poor prognosis category have no CTCs in their blood (Mego et al., 2011, Riethdorf et al., 2007). This could be due to the rigid classification of what a CTC is, and because of the heterogeneity of advanced tumours; phenotypic changes such as EMT are not accounted for and cells are not detected.

As a result CTC count is not yet a constituent of clinical guidelines and does not have any bearing on treatment choice outside of clinical trials (Alix-Panabières and Pantel, 2014).

1.7.5 Characterisation

Whilst enumeration of CTCs has been shown to provide prognostic clinical information, studies are now looking at sub-cellular characterisation to enable further understanding of the biology of these cells and to provide additional prognostic information or for the development of therapeutic agents (Alix-Panabières and Pantel, 2014).

In addition to conventional flow cytometry, platforms such as the CellSearch and Imagestream not only sort the cells but allow investigation of sub-cellular characteristics by enabling the detection of additional proteins of interest using immunofluorescence microscopy. Fluorescence in situ hybridisation (FISH) has been used to look for genetic mutations and in metastatic prostate cancer studies using this technique have identified mutations in PTEN, the androgen receptor and the TMPRSS2-ERG fusion (Attard et al., 2009, Shaffer et al., 2007, Leversha et al., 2009). Reverse transcription polymerase chain reaction (RT-PCR) and reverse transcription quantitative PCR (RT-qPCR) amplify specific transcripts to allow characterisation but there is a high false positive rate and it is not possible to determine whether the read-out is sourced from a true CTC or another cell within the blood (Lowes and Allan, 2014). Micro-arrays with specific probes can be utilised to provide detailed

genetic information at an RNA or DNA level. Whilst this is a useful technique and can be used as an absolute comparison between different samples, or samples from the same patient at different stages of treatment, it provides huge amount of data and can be costly to analyse (Magbanua et al., 2012, Lowes and Allan, 2014). Sequencing techniques such as Sanger sequencing, pyrosequencing and next-generation sequencing can also be used to determine the genotype of CTCs. Using next-generation sequencing, several mutations found in CTCs from patients with colorectal cancer were identified that had originally been overlooked in the primary tissue but were found on subsequent analysis (Heitzer et al., 2013).

Functional assays such as the EPISPOT are also available but rely on cell culture so fixed or apoptotic cells would not be assessed using this method. The EPISPOT technique involves the culture of CTCs on plates containing fluorescently-conjugated antibodies against proteins of interest followed by visualisation using a fluorescence microscope (Danila et al., 2011b, Ramirez et al., 2014).

Characterisation is potentially impeded by the technique used to select the CTCs. Background noise from samples contaminated with excess white blood cells is an issue – less so if looking for the presence or absence of a gene, but potentially problematic if looking for quantitative levels of expression (Hu et al., 2013). The choice of detection platform to use will depend on the phenotype of the tumour (whether it is largely epithelial or mesenchymal), the morphology of the cells, the question needing to be answered (e.g. enumeration versus the need for downstream analysis) and the local availability and cost of processing.

1.7.6 Isolation methods – background

Several different methods such as immuno-selection, filtration techniques and translational assays have been utilised to detect CTCs. As discussed, the CellSearch platform is the only FDA validated method for detection of CTCs. This was initially validated in 2004 for the use in breast cancer (Allard et al., 2004, Cristofanilli et al., 2004, Riethdorf et al., 2007) and subsequently prostate in 2007 (Danila et al., 2007, de Bono et al., 2008) and colo-rectal cancer in 2008 (Cohen et al., 2008). An 85% capture rate is reported using this method (Allard et al., 2004).

The detection of CTCs is possible via a variety of techniques based on the principles of either positive or negative selection. Positive selection relies upon the sensitivity of the machine or procedure to identify the small number of CTCs amongst the billions of other cells. Negative selection involves the removal of red and white blood cells in order to allow the CTCs to be detected more easily. However, by depleting the other cells first to negatively select for the CTCs there is the risk of damaging the cells of interest during the sorting process.

There are two important issues to address when evaluating CTC detection platforms. The first is the reproducibility of any technique. For a biomarker to be of clinical use it needs to be robust enough to withstand inter-laboratory use and despite many methods quoting high recovery rates of CTCs in an experimental setting, they have not been reproduced by other laboratories. The second is that the definition of a CTC appears to vary and those platforms that do not use the FDA criteria may not be measuring the same cell population. It is possible that the FDA definition needs to be revised and that by being too restrictive it is not identifying the true number of CTCs. But those that use tumour specific markers in place of the standard epithelial markers cannot be directly compared to the CellSearch.

1.7.7 Isolation – protein-based selection

Cells can be sorted based on their expression of specific proteins using conventional flow cytometry or a combination of flow, immunofluorescence or magnetic selection. The majority of clinical studies use protein-based selection due to the high retrieval rates and reproducibility. Fluorescently-conjugated antibodies can be used to detect target antigens on the cells of interest and depending on the type of platform used for analysis, information on the location and level of a specific protein either on the cell surface or within a cell can be collected. If the platform contains multiple filters, it enables several proteins to be analysed simultaneously. Obtaining a visual image of the cell also helps rule out false positive results. A major disadvantage of using fluorescence is the bleed that transpires from using fluorochromes of similar wavelengths. If two fluorochromes attached to different antibodies emit similar wavelengths they could be excited by light of one wavelength and give overlapping results. There are ways of minimising this effect but care must be taken to avoid eliminating cells (Lowes and Allan, 2014). Ideally fluorochromes of very different

wavelengths would be used but most flow cytometers or light-microscopes are limited by the numbers of filters they have and when investigating multiple proteins this is not always practical. Downstream analysis is possible if a platform with a cell sorting capacity is used (Watanabe et al., 2014, Vishnoi et al., 2015, Magbanua et al., 2012, Gorner et al., 2015, Carpenter et al., 2014).

The CellSearch uses immuno-magnetic beads conjugated to the EpCAM antibody. Cells positive for EpCAM are magnetically selected and visually analysed by a trained technician to ensure they meet the FDA morphological criteria (Danila et al., 2011c). These cells are then analysed further for expression of CK, CD45 and DAPI. It is possible to use one additional tumour specific marker when using the CellSearch which allows further characterisation. This could be one of the three that have been made commercially available, HER2, EGFR and IGF-1R, or users have the option to develop their own using the remaining fluorescent channel (Lowes and Allan, 2014).

Microfluidic chips have been developed using silicon micro-pillars, embedded with EpCAM antibodies, arranged in a herringbone pattern (Nagrath et al., 2007, Gleghorn et al., 2010, Stott et al., 2010, Ozkumur et al., 2013). The herringbone structure aids micro-fluidic mixing which allows the best opportunity for antibody contact as the larger cells, most likely to be CTCs, are more likely to come into contact with the pillars.

Other methods such as nanostructured substrates and microtubes have also utilised anti-EpCAM antibodies but are not in widespread use (Wang et al., 2009, Wang et al., 2011). *In vivo* sampling has been used to detect CTCs on a real time basis in patients with lung and breast cancer (Saucedo-Zeni et al., 2012). A wire impregnated with EpCAM antibodies was inserted via a venous cannula into patients for 30 minutes and CTCs were detected in 92% of patients. Further validation studies are ongoing with respect to this technique.

Protein-based selection can not only be used for positive enrichment, but it can be also used for the negative depletion of leucocytes. Immuno-magnetic beads conjugated to the CD45 antibody can be used to deplete whole blood of white blood cells. Although this process has been shown to cause minimal effect on the retrieval rate of CTCs, it does not accomplish high purities due to residual white cells (Harouaka et al., 2014, He et al., 2008).

The Imagestream platform is a combined flow-cytometer and high resolution microscope (Zuba-Surma et al., 2007). This enables cell sorting based on size and/or protein expression which can be done either via the analysis software or visually. The majority of white cells are depleted using immuno-magnetic separation prior to processing, thus it uses principles of negative selection, with the aim of achieving a high CTC output. Five lasers are used to detect fluorescence from cells expressing proteins attached to conjugated antibodies. Recovery of CTCs is approximately 50-60% (Dent et al., 2015) so its use in clinical trials with respect to enumeration may be limited. However, it provides very detailed cellular images so its strength is in sub-cellular analysis.

1.7.8 Isolation – physical properties

There are many ways of isolating CTCs based on their physical properties. Separating CTCs from erythrocytes is possible using centrifugation, using the assumption that CTCs have a higher density than other cells within the blood. The cells can be subsequently identified using methods such as RT-PCR but most studies report a low yield, usually well below 50% (Rosenberg et al., 2002, Muller et al., 2005, Weitz et al., 1998). This method has been successfully utilised to obtain CTCs from patients with small cell lung cancer which have then been implanted into mice to create an *in vivo* model (Hodgkinson et al., 2014).

Di-electrophoresis is an alternative method that involves the application of an electric field to whole blood samples. If the field is non-uniform the cells become polarised and different populations with the same polarisation move towards one of the electrodes. So far this method is in the early stages of clinical use but retrieval rates of 70-95% have been documented in spiked cell line samples (Yang et al., 1999, Gupta et al., 2012).

Microfilters work on the principle that CTCs are larger than the majority of the cell population in blood and allow the passage of cells smaller than 8µm through specially designed pores. In theory this would allow rapid processing of whole blood samples. Several different filter systems exist, made from different materials with different shaped pores and they have been used in clinical studies of lung, liver and prostate cancer (Hofman et al., 2011, Vona et al., 2004, Chen et al., 2013). Capture rates of 89% have been reported (Zheng et al., 2007).

The Parsortix system is a platform using micro-filters that capture CTCs in cassettes assuming that they are larger and more resistant to compression (Miller et al., 2018). Cells can be processed from any bodily fluid, not just blood, which could be useful when looking at specific cancers that present with ascites or in bone marrow. When compared to the CellSearch Platform, recovery rates were no worse (Hvichia et al., 2016) and one study found that CTCs were detected in more patients when using the Parsortix as EpCAM-negative cells were identified, that subsequently stained positive for Cytokeratin (Chudziak et al., 2016).

There is a risk of missing CTCs if size criteria alone is used. Compared to erythrocytes and leucocytes, CTCs were originally assumed to be larger and less fragile (Alix-Panabières and Pantel, 2014). Erythrocytes are a-nuclear and predominantly less than 4µm in diameter. Leucocytes differ in size depending on their sub-classification but can be up to 20µm in diameter (Bergman, 1995) As the FDA definition includes nucleate cells with a diameter over 4µm, CTCs cannot be distinguished from white cells based on size alone. Filter technology could be improved by reducing pore size, but the purity would then be low and subsequent enrichment steps would need to be enhanced which may reduce the retrieval rate of the cells of interest.

1.7.9 Isolation – direct analysis

It is possible to avoid the risk of cell loss, or the error in detection that occurs with techniques using either positive or negative selection, by analysing the whole nucleated cell population within a blood sample. Following the lysis of erythrocytes, cells are seeded onto slides, frozen, and high throughput scanning devices can examine up to 25 million cells per minute (Harouaka et al., 2014). It has been utilised in some clinical studies (Werner et al., 2015, Marrinucci et al., 2012) but its use is currently not widespread.

1.7.10 Downstream analysis of CTCs for personalised medicine

Because of the ability to not only enumerate but characterise CTCs, they can now be utilised for disease screening or monitoring in response to treatment. Enumeration following specific treatments has been explored in pancreatic (Ankeny et al., 2016), breast (Smerage et al., 2014, Cristofanilli et al., 2019) and prostate cancer (Lu et al., 2013, Danila et al., 2011a). In men with prostate cancer treated with androgen

deprivation therapy, CTCs have been detected despite un-recordable PSA levels, suggesting seeding of the disease when it is apparently dormant (Thalgott et al., 2013). Trials looking at the viability of using CTC count as a cancer-related endpoint following treatment have discovered that it is a more sensitive prognostic tool than PSA decline or an increase in bone or visceral metastases (de Bono et al., 2008, Danila et al., 2007).

Prediction of response to chemotherapy has been shown to be almost 84% accurate in patients with small cell lung cancer when looking at chromosomal copy number aberrations (CNA) in CTCs (Carter et al., 2017). Similarly, mutations that develop during the course of treatment can be identified by serial sampling of CTCs, and in non-small cell lung cancer, EGFR mutations linked to drug resistance have been found after sequencing CTCs (Forde and Ettinger, 2015).

In prostate cancer, predicting failure of treatment with enzalutamide and abiraterone in metastatic disease has been shown by detecting the AR-V7 variant of the androgen receptor in CTCs (Antonarakis et al., 2014). AR mutations have also been found in other studies looking at patients with castrate resistant disease on these two treatments (Attard et al., 2009, Crespo et al., 2015, Jiang et al., 2010). AR signalling, specifically with respect to the relationship with PSA and PSMA has also been explored in CTCs (Miyamoto et al., 2012). Attempts were made to look at TMPRSS2-ERG fusion status in CTCs to see if this could predict success of abiraterone treatment (Danila et al., 2011a), but whilst CTC expression was found to correlate to the expression in solid tissue, no predictive value was determined. PTEN gene loss in solid tissue has also been shown to correlate with PTEN loss in CTCs (Punnoose et al., 2015).

Whilst these exciting advances form the basis for clinical trials, the adoption of CTC enumeration or characterisation does not yet form part of routine clinical practice. This is due to the difficulty in reproducing cell counts from the same patient (Leon-Mateos et al., 2016), the widespread variability of platforms with different recovery rates, and the difference in cancer phenotypes, rendering methods such as the CellSearch invalid for non-epithelial tumours.

The utilisation of CTCs for target discovery is an emerging field, and successful organoid creation (Drost et al., 2016) and xenograft models (Hodgkinson et al., 2014) have been developed. Propagation in culture has been achieved (Cayrefourcq et al.,

2015, Kolostova et al., 2015, Kulasinghe et al., 2016) which has enabled this heterogenous population to be explored in more detail. Although developing such models on an individual patient basis is not currently financially viable outside of the research arena, it has advanced the understanding of tumour genetics, and will hopefully continue to do so.

1.8 Rationale for the project

With a wealth of treatments available for metastatic prostate cancer, the lack of a predictive biomarker to determine the rate of disease progression is a real issue in the management of men with advanced prostate cancer. Although sequencing is now much more common following initiatives such as the 100 000 genomes project (Consortium, 2019) it is still in its early stages, and the identification of a biomarker from a simple blood sample could really benefit patients. In the predominantly elderly population that has the disease, declining cardiovascular status is inevitable, and earlier introduction of the current second line treatments may increase disease specific and overall survival.

When considering how to approach this project, the local resources and expertise were taken into account. Because colleagues within the institute had developed an assay using the Imagestream (Dent et al., 2015) to detect CTCs, it was felt that this would be a good opportunity to adapt this for use in prostate cancer. The advantage of the Imagestream is that multiple markers could be explored concurrently, which would potentially allow novel additional information to be obtained, compared to the data obtained from CellSearch experiments. Due to the number of studies looking at the frequently detected genomic alterations in prostate cancer and the size of the cohort that could be included in this study, looking purely at these alterations in CTCs was unlikely to yield anything novel. The work that colleagues in the group had undertaken looking at the embryonic stem cell signature work in solid prostate tissue provided an opportunity to explore this in CTCs (Hepburn et al., 2019). If transcription factors Oct4, SOX2 and Nanog could be detected in CTCs from patients with prostate cancer, it could be hypothesised that these patients would progress more rapidly to castrate resistant disease, which would correlate with the results from solid tissue.

In addition, exploring the role of matrix-metalloproteinases, specifically MMP-14 due to its ability to induce EMT in prostate cancer (Cao et al., 2008), would give a potentially novel way of identifying prostate cancer CTCs undergoing EMT, a phenomenon that is currently not possible to explore with the CellSearch platform.

Plans to culture CTCs would mean that downstream experiments could be performed, and this could be utilised by the drug discovery groups within the NICR.

On a personal level, my rationale for undertaking this work is to enable me to have a better understanding of the molecular mechanisms behind prostate cancer. As a practising Urologist, I see patients with advanced prostate cancer on a daily basis and understand the need for a more sensitive biomarker. My ambitions to be involved, and potentially design and lead clinical trials in this area would be supported by a more substantial knowledge of the processes involved in molecular biology research, and a greater understanding of the basic science.

Aims and Hypothesis

Aims

- 1) To optimise an assay using flow cytometry to enable detection of the stem cell markers Oct4, SOX2 and Nanog, alongside epithelial and mesenchymal markers, in circulating tumour cells from patients with metastatic prostate cancer.
- 2) To prospectively evaluate the prognostic value of Oct4, Sox2, Nanog and MT1-MMP in circulating tumour cells in metastatic prostate cancers.
- 3) To culture circulating tumour cells from patient samples for downstream utilisation.

Hypothesis

The expression of the stem cell markers Oct4, SOX2 and Nanog in circulating tumour cells (CTCs) from patients with prostate cancer is associated with more aggressive disease, and the retention of such CTCs will allow further downstream evaluation.

Chapter 2. Materials and Methods

2.1 General Laboratory Practice

All experiments were performed adhering to Newcastle University safety standards for working with chemical and biological substances. Attendance at Control of Substance Hazardous to Health (COSHH) and BioCOSHH training was mandatory during the first year of the project. Risk assessments were carried out for each type of experiment and stored in the laboratory safety file. Appropriate protective clothing, gloves or glasses were worn, and experiments were carried out in the most suitable location e.g. under fume hoods.

2.2 Primary cell culture

2.2.1 Routine cell culture using cell lines

Plates, flasks and other tissue-culture plastic-ware were sourced from Corning. Cell culture was performed using an aseptic technique in a class II BioMat-2 microbiological safety cabinet (Medical Air Technology Ltd.). Cell lines were sustained as adherent cultures in Roswell Park Memorial Institute (RPMI) media (Hepes modification) (Sigma Aldrich) with 10% foetal bovine serum (FBS) and 20mM L-glutamine (Sigma Aldrich) to make Full Media. Incubation of cells was performed at 37°C in a humidified environment in incubators with 5% CO₂ (Heraeus Equipment Ltd.). Cells were tested for mycoplasma every other month in accordance with Institute policy (MycoAlert).

The following six cell lines were used during experiments (Table 2.1). The first three (LNCaP, PC3 and CWR-22Rv1) are prostatic, the fourth (MCF7) from a breast tumour and the final two (U2OS and SJSA-1) from an osteosarcoma. In addition, mesenchymal stem cells harvested from a patient, and induced pluripotent stem (iPS) cells derived from benign prostate tissue were used.

Cell Line	Tumour origin	Anatomical site	Reference
LNCaP	Prostate	Lymph node metastasis	(Seim et al., 2017)
PC3	Prostate	Bone metastasis	(Seim et al., 2017)
CWR-22Rv1	Prostate	Mouse xenograft (prostate tumour CWR22)	(Sramkoski et al., 1999)
MCF7	Breast	Pleural effusion	(Comsa et al., 2015)
U2OS	Osteosarcoma	Bone primary	(Niforou et al., 2008)
SJSA-1	Osteosarcoma	Bone primary	(Research, 2019)

Table 2.1 A table listing the cell lines used in this project, their tumour of origin and their anatomical site.

Cells under passage 30 were used at all times. Thawing occurred at room temperature and the thawed cells were then mixed with 10ml of RPMI Full Media before transfer to a 25cm³ flask containing 20ml of media. Culture was performed until they had reached 75% confluency and they were then split into a 75cm³ or 175cm³ flask, depending on requirements for subsequent experiments.

Phosphate Buffered Saline (PBS) (137 mM NaCl, 83 mM KCl, 10 mM Na₂HPO₄) was prepared for mass laboratory use using PBS tablets in sterilised de-ionised water. Trypsin was prepared using stocks of Trypsin (Sigma Aldrich) diluted to 10% with PBS.

Cells were passaged by aspirating the media from the flask and washing the adherent layer with PBS. 10% Trypsin was added to lift the cells off the flask, and the flask was incubated for five minutes at 37°C. Media was then added (volume dependent on flask size) and the cell/media/trypsin suspension was transferred to a universal container. This was then spun at 400g for five minutes in a bench-top centrifuge. The supernatant was aspirated, and media was added to re-suspend the cell pellet. The required volume of cell suspension was then transferred to a fresh flask containing full media and the cells were incubated until required. If passage was not required after three days then cells were washed with PBS and fresh full media added.

2.2.2 Cell culture of mesenchymal stem cells

Cells were obtained from the bone marrow of a paediatric patient and selected using FACS (with thanks to Kenny Rankin and Daniel Hipps). Ethical approval for this was granted by the NRES Committee North East – Newcastle and North Tyneside 1 Ethics Committee, (July 2018, REC Number 17-NE-0361, IRAS Reference Number 233551, ethics form in Appendix). The Mesenchymal Stem Cell Phenotyping kit (Miltenyi Biotec) was used to identify Mesenchymal Stem Cells by labelling the bone marrow cells with a cocktail of the following fluorescently conjugated antibodies: CD14(PerCP), CD20(PerCP), CD34(PerCP), CD45(PerCP), CD73(APC), CD90(FITC) and CD105(PE). The Mesenchymal Stem Cells expressing CD73, CD90 and CD105 were sorted from the remaining cells and expanded in culture. Incubation was performed at 37°C in humidified conditions with 5% CO₂. Dulbecco's Modified Eagle's Medium (DMEM) (Sigma Aldrich) was used as the basal media, to which 2.5mls/l of Penicillin/Streptomycin, 0.5mls/l of Gentamicin, 4.5g/l of glucose, 5ml/L of FBS and 2mM of Glutamine were added to make full media.

Media was changed every 48 hours and cells were passaged using Trypsin (as above) when they reached 75% confluency.

2.2.3 Cell culture of iPS cells

Cells were obtained from benign prostate tissue from patients at the Freeman Hospital, to generate iPS cells (with thanks to Emma Curry). Ethical approval for this was granted by the NRES Committee North East – Newcastle and North Tyneside 1 Ethics Committee, (July 2018, REC Number 17-NE-0361, IRAS Reference Number 233551, ethics form in Appendix). The iPS cells were cultured at 37°C in the incubators described above using mTESR1 medium (Stem Cell Technologies) on hESC-qualified Matrigel coated plates (Corning). Full mTESR1 medium was made by adding 100ml of the 5x mTESR1 supplement (Stem Cell Technologies) to 400ml of mTESR1 basal medium (Stem Cell Technologies). Aliquots of 50ml were kept at –20°C and when thawed were used within two weeks. Matrigel plates were prepared by mixing thawed hESC-qualified Matrigel (Corning) and DMEM/F12 (Sigma Aldrich) which had been kept at 4°C (quantities were dependent on plate size). Sufficient Matrigel/DMEM/F12 mixture to cover the base of the plate was added and left at room temperature for one hour to set. The plates could be used straight away or could be covered with parafilm and kept in sterile

conditions at 4°C for up to one week. Prior to passage, plates were prepared by removing the Matrigel and adding mTESR1 full media.

Cells were closely observed for colony formation, and media was replaced at a maximum of every 48 hours. To passage iPS cells, fresh plates were prepared as above, media was aspirated, and the adherent layer of cells washed with Dulbecco's PBS (Gibco). (This contains no calcium or magnesium). 1mg/ml of Dispase (Stem Cell Technologies) was added to each well / plate and the plate then incubated for five minutes at 37°C. The Dispase was aspirated and cells washed with DPBS. Cells required manual dissection and colony selection, which was performed using sterile pipettes in a fume hood containing a dissection microscope (Nikon SMZ1000). Each colony was transferred to a new plate or well that had been prepared prior to passage, and incubated at 37°C.

To create a suspension of iPS cells from adherent colonies, media was aspirated and cells were washed as above with DPBS. A volume of Gentle Cell Dissociation Reagent (Stem Cell Technologies) (volume dependent on plate size but enough to cover the adherent cells) was added to each plate. Following a ten-minute incubation at 37°C, manual disturbance of the cell colonies was achieved by pipetting the solution, and the cells/reagent pipetted into a universal container. DMEM/F12 media (Sigma Aldrich) was used to wash the plate and obtain any residual cells. A matched volume of DMEM/F12 was added to the universal before centrifugation on a bench-top centrifuge at 300g for five minutes. The supernatant was then aspirated, and cells re-suspended in DMEM/F12 for downstream use.

2.2.4 Cell culture of circulating tumour cells

Twelve-well plates (Corning) were prepared with 2ml of Mesenchymal Stem Cell Growth Medium (Lonza) in each well. This full media was made from the constituents of the Mesenchymal Stem Cell Growth Medium Bullet-kit (Lonza), which contains the basal media, set volumes of L-glutamine and antibiotics, and a pre-determined cocktail of growth supplements. All the constituent parts were combined, kept at 4°C and used within six months. After infections in initial experiments, additional Nystatin (ThermoFisher Scientific) was added to the Full Media at a dilution of 1:100.

4mls of patient blood (ethics form in Appendix) was processed using the Easy Sep CTC Human enrichment kit (Stem Cell Technologies) described in section 2.6.2. The resulting cell suspension (in a 15ml Falcon tube, (Corning)) was very gelatinous so centrifugation at 400g

for ten minutes on a bench-top centrifuge was performed. The supernatant was discarded, apart from a very small volume at the bottom of the Falcon tube (no pellet was visible due to low cell numbers). 2.4mls of Full Mesenchymal Stem Cell Growth Media was used to resuspend the cells and this was divided equally between the twelve wells. Media was changed every 48 hours.

To passage these cells, media was aspirated and each well of the cells washed with 2mls of DPBS. 2mls of Gentle Cell Dissociation Reagent (Stem Cell Technologies) was added to each well prior to incubation at 37°C for ten minutes. Manual disturbance of the remaining adherent cells was performed using a sterile pipette, and the cell/reagent suspension was transferred to a Falcon tube containing 1ml of media. Bench-top centrifugation was performed at 400g for ten minutes and the supernatant aspirated. Fresh media was added to the pellet to resuspend, and the cell suspension was then divided into plates or flasks containing fresh Full Mesenchymal Stem Cell Media.

2.3 Collection, storage and preparation of whole blood samples to use on Imagestream and FACS

2.3.1 Patients

Blood was collected from patients at the Freeman Hospital, Newcastle-upon-Tyne, using consent forms accepted by the NRES Committee North East – Newcastle and North Tyneside 1 Ethics Committee, who approved the use of patient blood for this study (October 2012, REC Number 12-NE-0256, ethics form in Appendix). All patients attended Urology or Uro-oncology clinics and were either diagnosed, or were new patients, with suspected prostate cancer. Patients with different stages of the disease were targeted to try and obtain representative samples. Samples taken from new patients whose investigations subsequently showed no evidence of prostate cancer were used as the benign cohort.

2.3.2 Collection and storage of blood

Vacutainers (BD Biosciences) were used to obtain the samples to ensure sterility, and blood was collected in tubes containing potassium ethylene-diaminetetraacetic acid (K₂EDTA) (BD Biosciences). Samples were put into plastic bags and transported back to the NICR at room

temperature in a second bag clearly marked with the UN 3373 label (used for diagnostic human specimens). All specimens were processed within four hours of sampling. Samples were logged using the Achiever Medical sampling tracking system, which was updated once processing had occurred.

Any whole cells remaining after processing were kept at -80°C in a locked freezer designated for specimens that were covered by the HTA. HTA training was undertaken within the first year of the project and renewed after three years.

2.3.3 Red cell lysis

For each 2ml of blood to be processed, a 50ml Falcon tube was prepared. 5mls of 10% MACS BSA solution (Miltenyi Biotec) was added to each Falcon tube and put on to a bench-top tube roller for twenty minutes to ensure coating of the entire tube. The MACS was then aspirated to leave an empty, coated tube. A 1:5 dilution of PhosFlow Fix/Lyse buffer (BD Biosciences) and distilled water was made, and 40ml of this solution was added to each Falcon tube. Tubes were warmed in a water bath for one hour at 37°C prior to the addition of whole blood.

200 μl of FcR blocking agent (Miltenyi Biotec) was added to each original 4ml blood tube and mixed by gently pipetting. 2mls of blood was then pipetted into the prepared Falcon tube containing 40mls of the diluted Fix/Lyse buffer. Tubes were inverted six times to ensure full mixing and then replaced in the water bath for a further 20 minutes. The tubes were then transferred to a bench-top centrifuge and spun at 500g for eight minutes. The supernatant was aspirated and the remaining pellet (containing white cells and potential CTCs) was resuspended in 500 μl of Robosep buffer (Stem Cell Technologies) and transferred to a 15ml Falcon tube. Each 50ml Falcon tube was washed with 1ml of Robosep to capture any remaining cells, and this was added to the 15ml Falcon tube from the same sample.

2.3.4 White cell depletion

Each 15ml Falcon tube was spun on a bench-top centrifuge at 500g for eight minutes at room temperature. The supernatant was aspirated, and the cell pellet was resuspended in a further 500 μl of Robosep buffer. 50 $\mu\text{l}/\text{ml}$ of the EasySep Human CD45 Depletion cocktail (Stem Cell Technologies) was added and mixed via gentle pipetting. The tube was then left at room temperature for 15 minutes. 100 $\mu\text{l}/\text{ml}$ of EasySep Dextran RapidSpheres (Stem Cell

Technologies) was added to the tube, gently mixed via pipetting and left at room temperature for ten minutes. 4.5mls of Robosep buffer was added to the Falcon tube and gently pipetted. 10µl was then aspirated onto a haemocytometer to count the cells.

The tube was inserted (with cap off) into the EasySep magnet, The Big Easy, (Stem Cell Technologies) for ten minutes at room temperature. Following this, the tube with magnet still attached was inverted into a clean 15ml Falcon tube. A further 10µl was aspirated onto the haemocytometer and cells counted, to enable the depletion to be calculated. The contents of the tube were then spun at 500g for eight minutes on a bench-top centrifuge, and the supernatant discarded.

2.3.5 Permeabilisation and addition of antibodies

A permeabilisation agent was made using the 10x PermWash (containing Saponin and FBS) (BD Biosciences) diluted into distilled water at a 1:10 ratio. 1ml of the 1:10 solution was added to each 15ml Falcon tube and the re-suspended cells were transferred to an Eppendorf. Cells were Incubated in the permeabilisation agent for one hour at room temperature or overnight at 4°C. Eppendorfs were spun in a bench-top Eppendorf centrifuge at 400g for five minutes and the supernatant discarded. Cells were re-suspended in 100µl of 1:10 PermWash prior to the addition of antibodies.

2.3.6 Antibodies used for samples processed on the Imagestream and FACS

Antibodies used for the Imagestream and FACS assays described in Chapters 3 and 4 respectively are listed in Tables 2.2 and 2.3. Optimisation is discussed in these chapters.

Antibody	Fluorochrome	Isotype control	Concentration	Manufacturer
EpCAM	PE-Vio615	REA(S)	1:200	Miltenyi Biotec
Oct4	AF488	IgG1κ	1:50	BD Biosciences
SOX2	AF555	IgG2a	1:50	BD Biosciences
Nanog	Per-CP Cy5.5	IgG1κ	1:50	BD Biosciences
CD45	PECy7	IgG1κ	1:50	BioLegend
DAPI	-	-	1:500	BioLegend

Table 2.2 A table listing the antibodies, isotype controls, concentrations and manufacturers for the antibodies used in the Imagestream assay described in Chapter 3.

Antibody	Fluorochrome	Isotype control	Concentration	Manufacturer
EpCAM	BV650	IgG1 λ	1:200	BD Biosciences
Cytokeratin	PE Cy7	IgG1	1:200	2BScientific
Vimentin	AF647	IgG1	1:100	Santa Cruz
MT1-MMP	PE	IgG1 κ	(3 μ l:10 ⁴ cells)	Merck Millipore
Oct4	BV421	IgG1 κ	1:50	BD Biosciences
SOX2	FITC	REA 320	1:50	Miltenyi
Nanog	PerCP Cy5.5	IgG1 κ	1:50	BD Biosciences
CD45	BV786	IgG1 κ	(7.5 μ l:10 ⁶ white cells)	BD Biosciences
CD16	APC H7	IgG1 κ	(7.5 μ l:10 ⁶ white cells)	BD Biosciences

Table 2.3 A table listing the antibodies, isotype controls, concentrations used and manufacturers for the antibodies used in the FACS assay described in Chapter 4.

All antibodies were added to the Eppendorfs containing the cells suspended in the 100 μ l of 1:10 PermWash at the concentrations listed above. For the MT1-MMP, CD45 and CD16 in the FACS assay, 10 μ l of the suspension was aspirated onto a haemocytometer so that the volume of antibody could be applied per volume of cells. This is because these three antibodies are expressed by white cells and the number of white cells would vary between patients.

Following incubation for one hour at room temperature, Eppendorfs were spun at 400g for five minutes on a bench-top centrifuge and the supernatant discarded. Cells were then resuspended in 200 μ l of Robosep (remaining in the Eppendorf) if for processing on the Imagestream, or 500 μ l of Robosep (and transferred to a FACS tube) if for processing on the FACS machine.

2.4 Processing and Analysing samples on the Imagestream^x

2.4.1 The Imagestream^x

The Imagestream^x Mark II (Merck) is a combined high-resolution microscope and flow cytometer which allows the user to view the image of any event displayed on the dot plot. It is described in detail in Chapter 3.

2.4.2 Laser set-up to enable comparable data

In order to compare results between clinical samples, laser settings must be kept the same. The laser settings are initially determined by running a sample containing cells expressing each antigen of interest and adjusting the strength of each laser so that the lowest power is used whilst still being able to visualise the cell. In this case a combination of cell types is required as no one cell will display all antigens. If the lasers are all run on high power there will be significant fluorescence bleed into adjacent channels which will result in false positives. The antithesis of this is the risk of not detecting cells that only weakly express the antigen. As with antibody optimisation, the laser set-up needs to be performed using cell lines or synthetic beads rather than the clinical samples, so there is always a risk that the laser settings may be too low for detecting expression in the clinical samples. A compromise needs to be reached and acceptance of under-detection was chosen over the risk of collecting data with large numbers of false positives (Table 2.4).

Laser (nm)	Power used (mW)	Maximum Power Available (mW)
405	50	150
488	30	200
561	40	200
642	85	150

Table 2.4 List of chosen laser settings for each laser on the Imagestream and the maximum power available.

2.4.3 Single colour controls

Cell lines or Ultracomp ebeads (ThermoFisher Scientific) were used as single colour controls for the Imagestream experiments. 100 000 cells or 1 drop of ebeads were stained with each individual antibody that was used in the experiment and suspended in 100µl of Robosep. The Brightfield camera was turned off and the laser strength was set initially on maximum and then decreased to the lowest level possible that still enabled good visualisation of the cell/bead. This was repeated for cells/beads expressing each antibody in turn until settings for all lasers had been determined. A suspension of cells containing cells/beads expressing all antibodies was run to ascertain whether the final laser settings permitted adequate visualisation and the laser settings were fixed and recorded. 500-1000 cells/beads for each individual antibody were then captured and this data was used to prepare a compensation matrix. This matrix calculated the spectral overlap of each fluorophore. Single colour controls were repeated every four weeks or if a new vial of antibody was purchased.



Figure 2.1 Images of the synthetic speed beads displaying fluorescence of three antibodies Oct4, SOX2 and Nanog at 1:50 concentration.

2.4.4 Compensation matrix

The fluorescence in the channel of each sample from the single colour control is plotted against the fluorescence in the adjacent channel in order to determine what true fluorescence is and what is bleed. The best fit linear regression for each fluorochrome is determined and this data then contributes to a compensation matrix. This shows the proportion of overlap of each fluorochrome into adjacent channels. Overlap of <0.1 (10%) is considered acceptable by the manufacturer but the smaller the overlap the more accurate the data. If a value of more than 10% is observed, a graph of the fluorescence in the channel plotted against the channel into which it bleeds can be plotted. This can help identify outliers (e.g. doublets or debris that is very bright). Gating this out will help identify true positives and the matrix can be recalculated.

Once the clinical sample has been run, the completed matrix is then applied to the raw image data file to create a data analysis file. Cell populations can then be analysed according to a number of variables, including size (area), shape and intensity of the attached fluorochrome.

2.4.5 Thresholds and reduction of false positives

Due to the presence of mesenchymal stem cells in healthy blood, performing the assay on patients without prostate cancer would identify any circulating, non-cancer Oct4, SOX2 and Nanog positive cells. It is therefore necessary to perform the assay on healthy volunteers and compare the results with those cells detected in patients with known metastatic prostate cancer in order to determine thresholds of significance.

Blood samples were obtained from twelve healthy male volunteers and processed using the NICR assay. They were divided into three; one third were processed as cells only, one third were labelled with the isotype controls of Oct4, SOX2, Nanog and CD45, and also with DAPI, and the final third with the antibodies themselves in addition to DAPI. Blood from six patients with advanced disease was also prepared using the same assay and stained with the antibodies and DAPI. These were used as the positive control (Figures 2.2, 2.3 and 2.4).

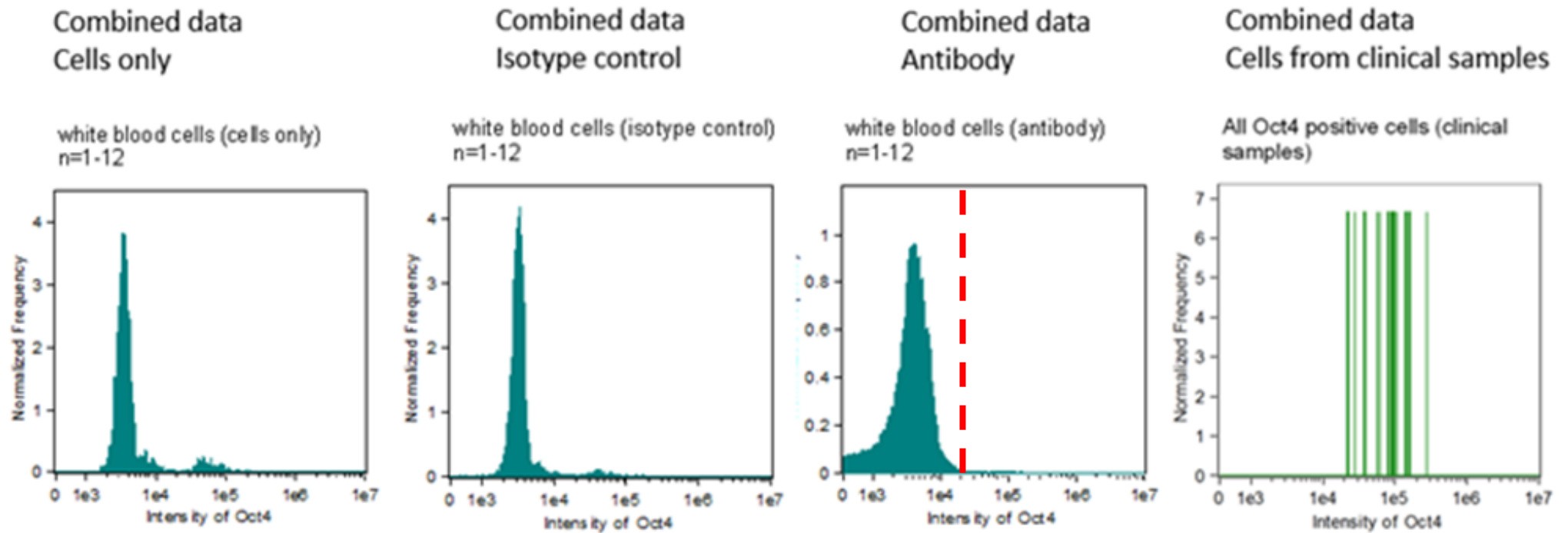


Figure 2.2 Graphs to show the Intensity of Fluorescence of Oct4 in Healthy Volunteer Blood Samples with no staining, stained with isotype control, stained with antibodies and compared to blood from patient samples. The results from all cells taken from twelve different healthy volunteers were combined to provide the three control graphs on the left, and then compared to cells from six patients with metastatic prostate cancer. The dotted line demonstrates the threshold above which cells would be considered to be putative CTCs.

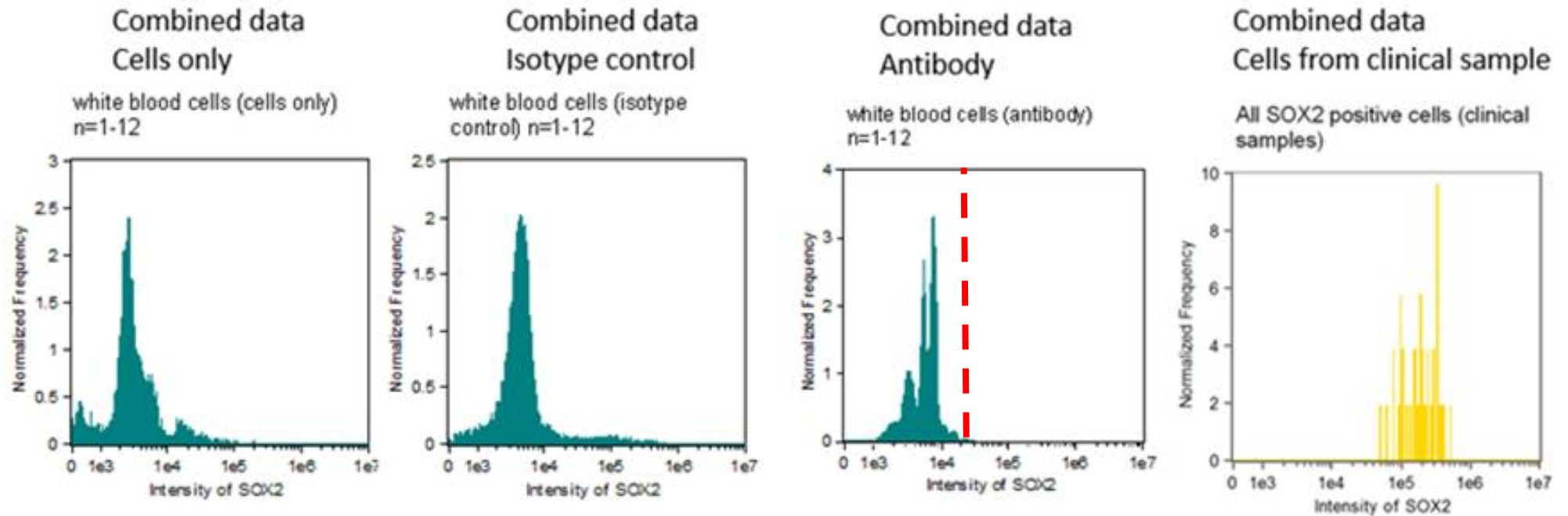


Figure 2.3 Graphs to show the Intensity of Fluorescence of SOX2 in Healthy Volunteer Blood Samples with no staining, stained with isotype control, stained with antibodies and compared to blood from patient samples. . The results from all cells taken from twelve different healthy volunteers were combined to provide the three control graphs on the left, and then compared to cells from six patients with metastatic prostate cancer. The dotted line demonstrates the threshold above which cells would be considered to be putative CTCs.

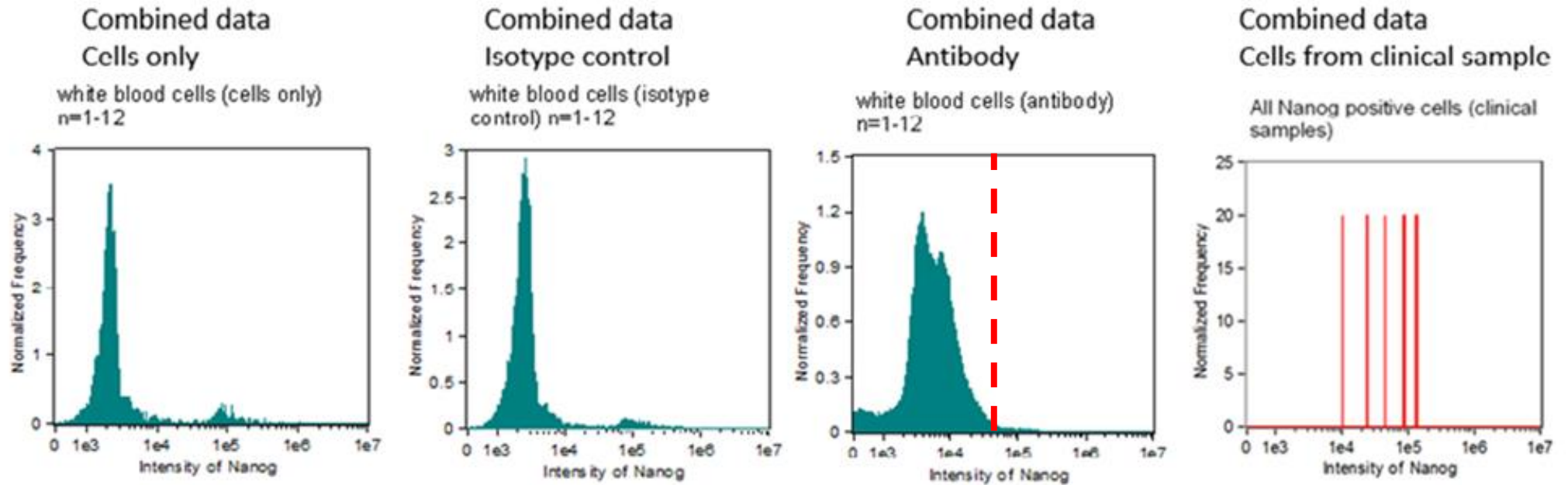


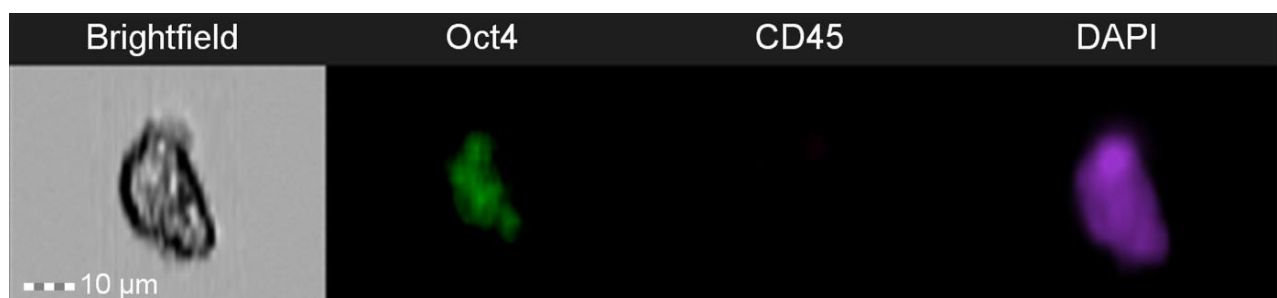
Figure 2.4 Graphs to show the Intensity of Fluorescence of Nanog in Healthy Volunteer Blood Samples with no staining, stained with isotype control, stained with antibodies and compared to blood from patient samples. . The results from all cells taken from twelve different healthy volunteers were combined to provide the three control graphs on the left, and then compared to cells from six patients with metastatic prostate cancer. The dotted line demonstrates the threshold above which cells would be considered to be putative CTCs.

Despite graphical evidence of expression of Oct4, SOX2 and Nanog in healthy white blood cells, there was a log shift increase in expression of Oct4 and SOX2 in the cells from clinical samples. This would suggest that cells gated below the $1.4e4$ level of intensity should be excluded as non-significant. When looking at Nanog, some of the cells in the clinical sample did overlap from the intensity of $1e4$. Only small numbers of Nanog positive cells were found at an intensity lower than $1.6e4$ so this was considered the threshold and it was accepted that there would be a possibility that Nanog positive cells below this would be missed. It was felt this would be more accurate than including possible false positives.

The Imagestream enables direct observation of the cells, and the majority of whole cells from the healthy volunteer samples that expressed the stem-cell markers, also expressed CD45, which would additionally enable exclusion of these cells. Mesenchymal stem cells have been shown to display haematopoietic markers (Maleki et al., 2014), therefore this experiment not only demonstrates the increased fluorescence in the patient samples, but also highlights the relevance of using the Imagestream, to visually exclude false positives (Figures 2.5, 2.6 and 2.7).

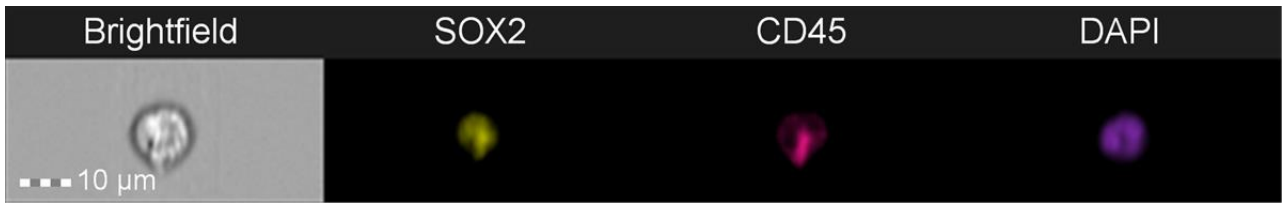


a) Oct4 / CD45 positive cell

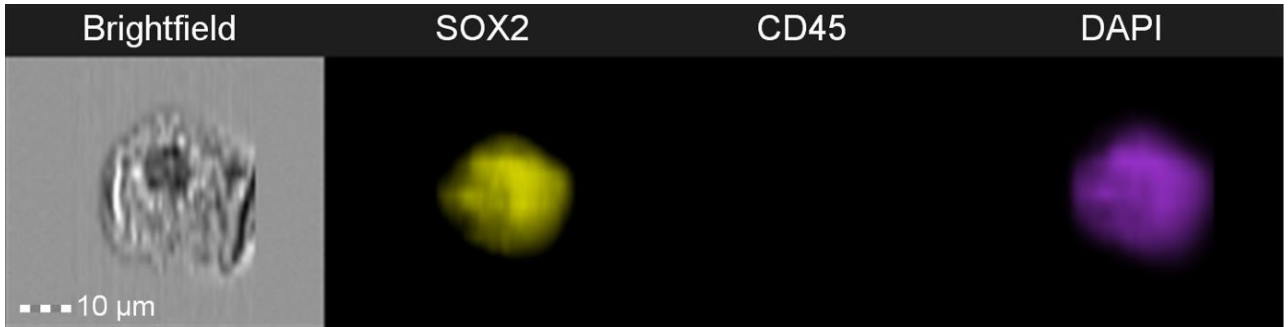


b) Oct4 positive CTC

Figure 2.5 Imagestream images showing Oct4 expression in a possible stem cell from a healthy volunteer sample and a CTC from a patient sample.



a) SOX2 / CD45 positive cell



b) SOX2 positive CTC

Figure 2.6 Imagestream images showing SOX2 expression in a possible stem cell from a healthy volunteer sample and a CTC from a patient sample



a) Nanog / CD45 positive cell



b) Nanog positive CTC

Figure 2.7 Imagestream images showing Nanog expression in a possible stem cell from a healthy volunteer sample and a CTC from a patient sample

2.4.6 Preparation of a template and sample processing

Unlike conventional FACS, not all data could be collected as file size would be too big to open. Therefore, various gating strategies based on fluorescence, size or nuclear content were used to collect data. For clinical samples, cells were gated based on DAPI signal (cells with no signal were assumed to be fragments) and then negative expression for CD45 (to exclude white cells). Further selection was felt to be too restrictive at this data collection stage. All Eppendorfs were covered with foil to prevent degradation of fluorescence and the whole sample was processed until the Eppendorf was empty.

2.4.7 Post-processing analysis

Each raw image file (rif) was combined with the appropriate compensation matrix (cif) to create a data analysis file (daf). Cells could be analysed based on various factors including size, fluorescence and nuclear content using the associated Imagestream analysis software, IDEAS. Fluorescence thresholds for positive identification of CTCs using stem cell markers are described in Chapter 3. Cell counts for each clinical sample were recorded and statistical analysis was performed using Prism GraphPad (version 8) and MedCalc.net (for odds ratios).

2.5 Processing and Analysing samples on the FACS Machine

2.5.1 Choice of FACS machine

The BD FACS Fusion (BD Biosciences) was used for this study. It has cell sorting capabilities and is described in more detail in Chapter 4.

2.5.2 Single colour controls

Cell lines or Ultracomp ebeads (ThermoFisher Scientific) were also used as single colour controls for the FACS experiments. 100 000 cells or 1 drop of ebeads were stained with each individual antibody that was used in the experiment and suspended in 500µl of Robosep in a FACS tube. Cells/beads with individual fluorescently-conjugated antibodies were run in the same way, initially on maximum laser setting and then decreased to the lowest level possible that still enabled excitation to a level above the paired isotype control. Cells with no staining

and cells with the isotype of each antibody were used to determine the positive expression of the beads or cells with antibody. Again, this was repeated for cells/beads expressing each antibody in turn until settings for all lasers had been determined.

A suspension of cells containing cells/beads expressing all antibodies was run to check the final laser settings, which were then fixed and recorded. Single colour controls were repeated every four weeks or if a new vial of antibody was purchased.

2.5.3 Processing of samples and gating strategies

FACS tubes were covered in foil to prevent degradation of fluorescence. When each tube was nearly empty, additional Robosep buffer was added so that as many cells as possible were processed. All data was captured but cells were sorted based on cell size (to exclude debris) and negative expression of both CD45 and CD16. The gates were set using spiked whole blood and the same template applied to all clinical samples.

2.5.4 Post processing analysis

All data was analysed using the gate templates for the fluorescence of each individual antibody described during optimization in Chapter 4. Analysis was conducted initially using the FACS programme FlowJo (Version 10.6.1), and subsequently with FCS Express (Version 6). Statistical analysis was again performed using Prism GraphPad (version 8) and MedCalc.net (for odds ratios).

2.6 Extracting CTCs from whole blood

2.6.1 Preparing cell lines spiked into blood

All of the experiments in this section were initially performed using cell lines (PC3 or U2OS) and healthy volunteer blood. Blood was collected using a vacutainer (BD Biosciences) in an EDTA tube (4mls) (BD Biosciences) from colleagues in the NICR under the ethical conditions outlined by the institution. Cells were harvested using trypsin as described in section 2.2.1 and when resuspended in media following the centrifugation, 10 μ l was transferred to a

haemocytometer to enable cells to be counted. The required number was calculated per volume of the cell suspension and pipetted into the vial of blood.

After each method was tested recovered cells were then stained with either DAPI and Vimentin (PC3 cells) or DAPI and CD44 (U2OS cells) prior to processing on the Imagestream. Single colour controls were run and laser settings were established prior to processing, and the same template used for all arms of this experiment. All experiments were conducted in a hood under sterile conditions.

2.6.2 RosetteSep Density Centrifugation

The RosetteSep CTC Enrichment cocktail containing Anti-CD36 (Stem Cell Technologies) was used. 50µl of the cocktail /ml of blood was mixed in a Falcon tube by gently pipetting and left to incubate at room temperature for 20 minutes. An equal volume (2mls) of Dulbecco's PBS (DPBS) with 2% FBS (Stem Cell Technologies) was then added to the blood and mixed gently. 2ml of Lymphoprep Density Gradient Medium (Stem Cell Technologies) was added to a fresh Falcon tube and the blood/PBS mixture from the first tube was carefully pipetted onto the density medium in the second tube, with care taken to avoid mixing. Centrifugation in a bench-top centrifuge was then performed at 1200g for 20 minutes, at room temperature with the brake off. The top third of the top layer (plasma) was discarded and the layer beneath at the plasma/density medium interchange was carefully pipetted into a fresh Falcon tube. A matched volume of DPBS was added to this tube and centrifuged at 300g for ten minutes with the brake on low. The supernatant was discarded, and the previous step repeated. The second supernatant was discarded, and the recovered cells transferred to an Eppendorf in Robosep for the addition of antibodies.

2.6.3 Magnetic Separation

Single marker selection

The *Straight from Whole Blood CD45 Microbeads (human)* kit was used for this experiment (Miltenyi Biotec). This contains MACS Whole Blood Columns and the Microbead cocktail. Separation buffer is made using a 1:20 dilution of MACS BSA solution with autoMACS Rinsing solution (both Miltenyi Biotec). This is kept at 4°C throughout the experiment. A 30µm nylon mesh filter can be purchased additionally to filter blood into a single cell suspension and remove clots. A MACS magnet and stand is also required for the experiment (Miltenyi).

Blood was passed through the filter into a Falcon tube and 50µl of the microbeads from the kit per ml of blood were added and mixed via gentle pipetting before incubation at 4°C for 15 minutes. Whole Blood Columns were placed in the magnetic stand and attached to the MACS magnet (Miltenyi Biotec). (Each column had capacity for 7.5ml of blood). 3ml of separation buffer from the kit was inserted into the column to wash the column through. Once drained, a fresh Falcon tube was inserted underneath the column and the 2ml of blood with microbeads was then carefully pipetted into the column. 500µl of separation buffer was used to wash out the blood tube and was then pipetted into the column. A further 2 x 2ml of separation buffer was inserted into the column to wash through any remaining cells. Red blood cell lysis of the erythrocytes in the recovered cell population was performed by preparing a 1:10 dilution of the Red Blood Cell Lysis Solution 10x (Miltenyi Biotec) with distilled water. An equal volume of the lysis solution was added to the cell solution, vortexed for five seconds and incubated for ten minutes at room temperature. The tube was then centrifuged at 300g for five minutes and the supernatant discarded. The residual cells were resuspended in 100µl of Robosep and transferred to an Eppendorf for addition of antibodies.

Multiple marker selection

The EasySep Direct Human CTC Enrichment kit (Stem Cell Technologies) was used for this experiment. This contains the Direct Human CTC Enrichment Cocktail and EasySep Direct RapidSpheres. Medium is PBS free from calcium and magnesium (DPBS), containing 2% FBS and 2mM EDTA (either purchased as the EasySep buffer (Stem Cell Technologies) or made from the constituent parts. The Big Easy magnet used in section 2.3.3 is also required for this experiment.

The blood was transferred from its collection tube to a 15ml Falcon tube and 50µl of the enrichment cocktail per ml of blood was mixed via gentle pipetting and incubated at room temperature for five minutes. The RapidSpheres were vortexed for ten seconds and 50µl of these per ml of blood was added. An equal volume of the medium was added and gently mixed, before the Falcon tube was placed in the magnet for ten minutes (with lid off). The tube with magnet still attached was inverted into a fresh 15ml Falcon tube and a further 50µl of RapidSpheres per ml of original blood sample was added to the fresh sample. This was then placed immediately into the magnet again for ten minutes and the tube and magnet inverted into a fresh Falcon. The remaining cells were then centrifuged at 400g for five minutes and the supernatant discarded. 100µl of Robosep was added and cells

transferred to an Eppendorf for antibody labelling, or for the clinical samples, 2.4ml of Mesenchymal Stem Cell Media (Lonza) was added prior to plating out in twelve-well plates.

2.6.4 Physical Separation (Parsortix)

The Parsortix PR1 Cell Separation System (Angle) comprises the machine, a buffer, and disposable cassettes that are used to capture the cells. Standard PBS (as described in section 2.2.1) is used as the buffer for priming and processing. In the NICR the machine is on a laboratory bench and therefore not in a sterile environment. Each stage of the process is listed as a specific programme on the instrument and the user follows the protocol and start each programme in turn.

The machine was put through a wash protocol prior to starting (about ninety minutes) using a cleaning cassette (replaced once a month) and a new cassette was loaded into the cassette holder. Priming was then performed when selecting programme PX2_P. Blood processing was then started by priming the line that drew blood into the machine, using programme PX2_S99F. The blood tube containing blood at room temperature was then attached to the machine with the line inside, and the blood was drawn up into the machine. The tube was inverted when it was almost empty, to ensure as much blood was drawn up as possible. To harvest the cells, which were now inside the cassette, programme PX2_H was selected and a clean 15ml Falcon tube inserted under the harvest line. The harvest valve was turned anti-clockwise to position HAR and the cells in 200µl of buffer were eluted into the Falcon tube. The option of flushing the lines and cassette with a further 1ml was utilised and this was added to the Falcon tube, which was then spun at 400g for five minutes, the supernatant discarded and 100µl of Robosep used to suspend the pellet prior to transfer to an Eppendorf for antibody staining.

Programme PTX2_CT was then selected to allow cleaning of the instrument prior to the next sample.

2.7 DNA extraction and downstream utilisation

2.7.1 DNA extraction and amplification

The Repli-g Mini kit (Qiagen) was used for these experiments. This contained nuclease free water, REPLI-g Mini DNA Polymerase, REPLI-g Mini reaction buffer, DLB buffer and stop solution. Microcentrifuge tubes were purchased separately (Qiagen). Cells were passaged from culture, washed carefully with DPBS (Stem Cell Technologies) and resuspended in 5µl of nuclease-free water.

A buffer (D1) was created by mixing 9µl of DLB buffer with 32µl of nuclease-free water. A second buffer (N1) was created by mixing 12µl of stop solution with 68µl of nuclease-free water. Both were vortexed and kept on ice prior to use. A master mix was created by mixing 10µl of nuclease-free water, 29µl of the Mini-reaction buffer and 1µl of the DNA Polymerase. 5µl of cell suspension was pipetted into a microcentrifuge tube and 5µl of buffer D1 was added and vortexed for five seconds and centrifuged briefly. This was followed by incubation at room temperature for five minutes. 10µl of buffer N1 was added to the tube, vortexed and centrifuged briefly. 30µl of the master mix was then added to the tube and incubated at 30°C for 16 hours. The sample was then heated for three minutes at 65°C to inactivate the DNA Polymerase.

The amplified DNA quantity was then measured using the Qubit as described in section 2.7.2. For the sequencing experiments (SNP Array and Whole Exome Sequencing) the amplified DNA was kept at -20°C and for the PCR experiments it was diluted 1:20 with nuclease-free water and 3µl of the diluted sample was used for each PCR experiment.

2.7.2 Measuring DNA quantity

The quantity of DNA recovered following the extraction and amplification in the previous step was measured using the Qubit (ThermoFisher Scientific). This platform consists of the machine (a benchtop fluorometer), a Qubit assay kit and 500µl polypropylene PCR tubes. The assay kit contained Qubit Reagent, Qubit Buffer and two separate standard solutions for calibration (standard 1 and standard 2).

Each sample from section 2.7.1 was run in a separate tube and labelled prior to the start. A master mix of 1:200 Qubit Reagent: Qubit Buffer was created; 200µl of this was prepared

per sample as the master mix. 190µl of the master mix was added to the tubes used for standards, and 10µl of each standard was added to this and vortexed. The assay type was selected (dsDNA high sensitivity) and the two tubes containing the standards were inserted consecutively to enable a fluorescence vs concentration calibration graph to be drawn. 190µl of the master mix was added to 10µl of each clinical sample. Each sample was then inserted into the machine and the DNA quantity recorded.

2.7.3 Real time quantitative PCR

In order to ascertain the DNA copy number of three genes (PSA, AR-V7 and TMPRSS2) real time qPCR was performed using the diluted DNA from samples in section 2.7.1. 384-well plates were used with each well containing 9µl of a master mix. This master mix comprised 5µl of the double-stranded DNA binding dye SYBR Green, 3.2µl of sterile distilled water, and 0.4µl of each of the forward and reverse primers listed in Table 2.4 (Sigma Aldrich). A control housekeeping gene (GAPDH) was run in parallel and a negative control containing DNA-free water was also used.

Plates were run on the Applied Biosystems 7900HT Platform (ThermoFisher Scientific) initially at 50°C for two minutes, followed by two minutes at 95°C and 40 cycles of 15 seconds at 95°C before one minute at 60°C. Dissociation curves were checked to ensure a single peak (quality control) and because this was not the case, further analysis was not attempted.

Gene	Forward Primer	Reverse Primer
PSA	CCCACTGCATCAGGAACAAA	GAGCGGGTGTGGGAAGCT
ARV7	CCATCTTGTCGTCTTCGGAAATGT	TGAATGAGGCAAGTCAGCCTTTCT
TMPRSS2	CACGGACTGGATTTATCGACAA	CGTCAAGGACGAAGACCATGT
GAPDH	CGACCACTTTGTCAAGCTCA	GGGTCTTACTCCTTGGAGGC

Table 2.5 A Table to show the forward and reverse primers used for the PCR experiment.

2.7.4 SNP Array

A Single-Nucleotide Polymorphism (SNP) Array was attempted using the amplified DNA from section 2.7.1. This was used as a method because detecting specific amplifications and deletions that were known to be present in prostate cancer would prove the cells were prostatic in origin, rather than white blood cells. DNA was transferred on ice to the Northern Genetics Service at the Centre for Life, Newcastle University, for this to be performed (with thanks to Dr Chris Lowe).

2.7.5 Whole exome sequencing

Whole exome sequencing was attempted by using the amplified DNA from section 2.7.1. This method was used as a way of attempting to identify any prostate cancer specific mutations, rather than specifically targeting certain genes. DNA was transferred on ice to the Centre for Life at Newcastle University for this to be performed (with thanks to Dr Chris Lowe).

2.8 Chemokine receptor experiments

2.8.1 Immunofluorescence

Cells were trypsinised, spun and resuspended in media. 10µl of the cell suspension was put on a haemocytometer and the volume of media containing 200 000 cells was calculated. A master mix of cells was made, containing 200 000 cells multiplied by the number of samples required. Six-well plates were labelled for each antibody and corresponding isotype control.

A microscope coverslip was dipped into methanol for sterilisation, left to air-dry and placed into each well of the plate required for a different concentration of the antibody. 2ml of RPMI media (Sigma Aldrich) was added to each well and the volume of media containing 200 000 cells was pipetted into each well.

Plates were cultured in the incubator overnight at 37°C. The following day, media was aspirated from each well and 1ml of PBS was pipetted in carefully to wash the cells. The PBS was aspirated and 1ml of 4% paraformaldehyde (Sigma Aldrich) was added to each well (this was performed in a fume hood). The plates were left at room temperature for twenty minutes to allow fixation. Following this, the paraformaldehyde was discarded, and the cells washed twice with 1ml of PBS. 1ml of 0.1% Triton (ThermoFisher Scientific) was applied to each well to enable permeabilisation, and they were then incubated at room temperature for ten minutes. 4% BSA solution was made by dissolving 4g of BSA powder (Sigma Aldrich) in 100ml of PBS. 1ml of 4% BSA solution was pipetted into each well as a block, and they were then incubated for thirty minutes at room temperature.

Parafilm was taped to an ice-box lid and 50µl of each antibody or isotype control (Table 2.5) at each concentration was pipetted as a spot onto the parafilm. Each coverslip was then placed face down on the spot and incubated for one hour at room temperature. Three PBS washes were carefully applied to each coverslip to wash off excess antibody. Drops of DAPI mounting media (Vector Laboratories) were spotted onto microscope slides and the coverslips placed face down on the spots. Slides were placed into slide holders and kept in the cold room overnight, for analysis the following day.

Chemokine Receptor	Fluorescent conjugate	Isotype control	Manufacturer
CXCR6	PE	REA (S)	Miltenyi Biotec
CCR7	FITC	REA (S)	Miltenyi Biotec
CXCR4	APC	REA (S)	Miltenyi Biotec

Table 2.6 A table listing the antibodies used in the chemokine receptor immunofluorescence experiments.

Slides were then analysed using fluorescent microscopy on the Leica DMR microscope.

2.8.2 Imagestream^x

Gentle Cell Dissociation agent (Stem Cell Technologies) was used to lift the cells off the plates, and the cell/media/dissociation agent was centrifuged at 400g for five minutes. The supernatant was discarded, and cells were resuspended in 100µl of PermWash (BD Biosciences). Antibodies were added at a concentration of 1:50 and left to incubate for one hour at room temperature. Cells were spun in a bench-top centrifuge at 400g for five minutes and the supernatant discarded. Due to low cell numbers, a washing step was not performed but the cells were resuspended in 200µl of Robosep and processed on the Imagestream.

2.9 Tumour growth in NSG mice

2.9.1 Permissions and basic care

Five NOD/LtSz-*scid* *IL2R_γ* null (NSG) mice (four male and one female) were used for this study. Permission was granted under Home Office License number PPL70/8769, granted to Dr Huw Thomas. The mice were kept in the same cage and examined and weighed at least once a week. They were observed on a daily basis for signs of ill health.

2.9.2 Implantation of cells

The cells from patient CTC-JARO-110 were harvested from culture (passage 2) and using a haemocytometer it was estimated that there were approximately 2000 cells. They were transported at room temperature to the Comparative Biology Centre (CBC) within the university.

The mice were weighed and taken in the cage to a laminar flow hood where anaesthesia was induced using isoflurane. The depth of anaesthesia was maintained throughout the implantation. Once anaesthetised, the knee area was shaved, and disinfectant was rubbed into the skin. The knee was held flexed and the cells (divided equally between all five mice) were injected into the distal femur using a 29G needle and insulin syringe. The mice were then monitored and given a subcutaneous injection of 5mg/kg of Carprofen prior to waking, for analgesia.

2.9.3 Extermination, imaging and dissection

All mice were anaesthetised using isoflurane and once a sufficient depth of anaesthesia achieved a syringe was injected into their heart to withdraw the circulating blood volume. Once their heart had stopped beating, an anterior midline incision was made along the length of the mouse and dissection was performed. Spine, femurs and liver were dissected out and put into formalin pots for fixation and subsequent immunohistochemistry. For the two mice who had X-rays of their femur, they were transferred to the X-ray room prior to dissection but after death. X-rays were taken by a qualified vet. For the mouse who underwent a CT scan, it was taken to the CT room after death and CT images were performed by Dr Samir Luli. Individual CT slice images were reconstructed using the micro-CT software (Bruker).

2.9.4 Immunohistochemistry

The mouse organs were embedded in paraffin blocks following fixation and 3mm slides were cut. They were de-waxed by immersion for five minutes in xylene and hydrated through a 100% to 50% ethanol gradient. Following this they were rinsed with water and placed in a decloaking chamber with a citrate buffer (pH6) to enable antigen retrieval. To reduce the incidence of non-specific background staining due to endogenous peroxidase, slides were blocked for ten minutes at room temperature with 3% hydrogen peroxide solution.

A wash of the slides with TBST-T was performed. TBS-T was made by adding 26g of TRIS and 320g of sodium chloride to 1.5L of distilled water and placing on a stirrer. To prevent non-specific binding of the antibodies, 2.5% horse serum was used to block the slides for twenty minutes, and then a further wash in TBST-T was performed before addition of the primary antibody. The antibodies used for this experiment are listed in Table 2.6 and were prepared using 4% BSA (made by dissolving 2g of BSA (Sigma Aldrich) in 50ml of PBS). The antibodies were applied to the slide, ensuring full coverage, and left to incubate at room temperature for one hour. Following this, a further TBS-T wash was performed and a Mouse-on-Mouse detection kit (Vector Laboratories) was applied for fifteen minutes to reduce the background staining initially seen, caused by using an antibody raised in a mouse, on mouse tissue.

Antibody	Host species	Concentration	Manufacturer
Anti-human mitochondria	Mouse	1:200	AbCAM
PSA	Rabbit	1:200	Roche
MT1-MMP	Rabbit	1:200	Merck

Table 2.7 A table listing the antibodies used for the immunohistochemistry analysis.

A five-minute incubation with 3,3-diaminobenzidine (DAB) solution (Vector Laboratories) was then performed before the slides were rinsed in running water for five minutes. Slides were counter-stained in haematoxylin for five seconds before dehydration through an ethanol gradient of 50% - 100%. Following this they were immersed in xylene before mounting onto coverslips. The slides were then scanned into the Aperio system (Leica) for imaging purposes.

2.10 Measuring mechanical properties of cells using the Atomic Force Microscope

2.10.1 Preparation of cells

Cell lines (PC3 and U2OS), white cells from healthy volunteers and the cells cultured from four patients were cultured onto cover slips. As with the start of the immunofluorescence protocol, cell lines were trypsinised, spun and resuspended in media. 10µl of the cell suspension was put on a haemocytometer and the volume of media containing 200 000 cells was calculated. A master mix of cells was made, containing 200 000 cells multiplied by the number of samples required. Six-well plates were labelled for each antibody and corresponding isotype control. A microscope coverslip was dipped into methanol for sterilisation, left to air-dry and placed into each well of the plate required for a different concentration of the antibody. 2ml of RPMI media (Sigma Aldrich) was added to each well and the volume of media containing 200 000 cells was pipetted into each well.

The white cells were obtained from two separate blood samples from healthy volunteers in the NICR. 1ml of healthy volunteer blood was mixed in a Falcon tube with PharmLyse buffer (BD Biosciences) which lyses the red cells without fixation. After incubating at room temperature for 15 minutes, the tube was spun at 400g for ten minutes and the supernatant

discarded. The resultant cell pellet was resuspended in 2ml of the Lonza Mesenchymal Stem Cell media and 50 μ l of the cell/media suspension was added to a six-well plate containing 2ml of the media and sterile coverslips.

For the patient cells, Gentle Dissociation Agent (Stem Cell Technologies) was used to lift the cells off the plate and the cell/media/dissociation agent was centrifuged at 400g for five minutes. The supernatant was discarded, and cells were resuspended in 4.8mls of Mesenchymal Stem Cell Media (Lonza). Half of the suspension was used for ongoing culture of the cells and half was transferred and divided between the wells of a six-well plate containing sterile coverslips. Each well contained 2ml of the media.

Both the cell lines, white cells and the patient cells were cultured in the incubation conditions described earlier in the chapter. Cell lines were ready the following day but patient cells took approximately twelve weeks until there was enough growth to proceed with the experiments. Media was changed every 48 hours.

Once confluent, plates were sealed with parafilm and transported to the School of Engineering, Newcastle University, to proceed with the experiment.

2.10.2 Using the Atomic Force Microscope

The Atomic Force Microscope was set up as shown in Figure 2.1. The tip of the probe on the cantilever can either be spherical or conical. Because of the experimental nature of this work the conical tip was used for the PC3 cells, and the spherical tip was used for the U2OS cells, white cells, patient cells and glass coverslip (as a control).

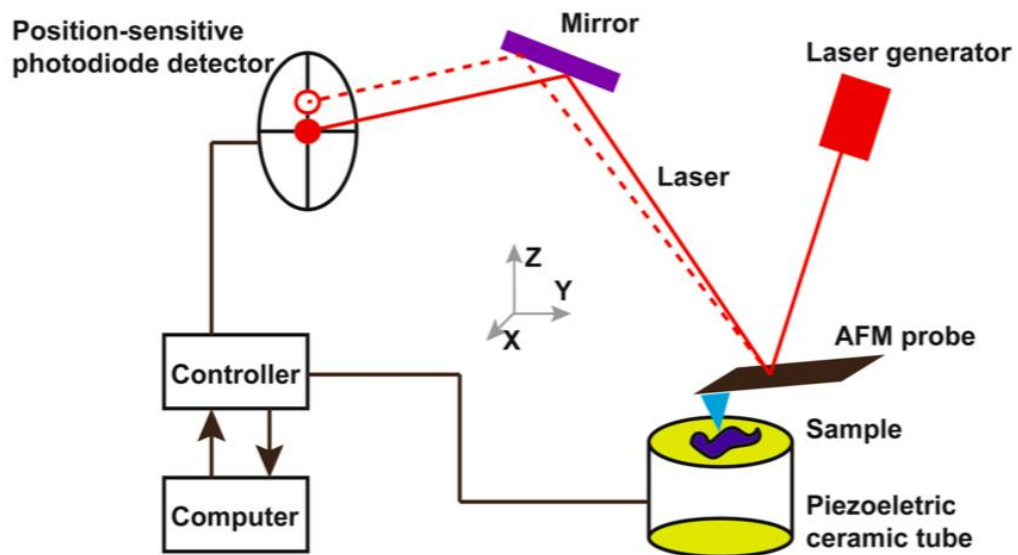


Figure 2.8 A diagram to show the set-up of the Atomic Force Microscope, (taken from Deng et al.(Deng et al., 2018)). The cell of interest would be placed on the yellow tube and indented with either a conical or spherical AFM probe on the end of a cantilever. The movement of a laser detected by a photodiode is used to create a three-dimensional image of the cell.

A coverslip from each six-well plate was placed cell side up on the ceramic tube and the probe began the approach towards the cells. The repulsive or attractive force between the tip and the cell would change once the tip was on the surface of the cell, and the surface underneath the tip was then scanned. An image was generated of the immediate area around the probe tip, which allowed the movement of the cantilever to ensure centralization on a cell. Once confident of position, the tip was readjusted to the cell surface and the probe was inserted into the cell to cause deformation.

The force required to indent the cell, and the distance between the cell surface and maximum indentation, was then used to plot force-distance curves (both approach and retraction). From this, the Young's modulus of the cell wall was calculated.

2.10.3 Post procedure analysis

Determination of the Young's modulus is dependent on the type of probe tip used. For the conical tip, the Sneddon model is used. This assumes no adhesion between the cell surface and the probe, no visco-elasticity and that the Young's modulus of the material forming the tip is much higher than the Young's modulus of the cell wall. Figure 2.2 demonstrates the conical tip inserting into a cell surface.

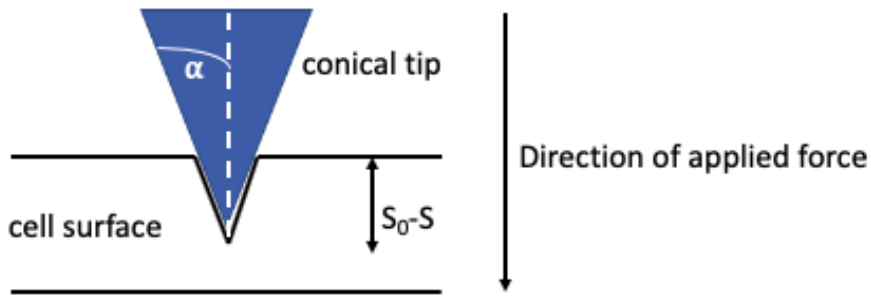


Figure 2.9 A diagram to demonstrate the conical tip of the AFM inserting into a cell surface. The tan of the angle between the edge and the midline, and the depth of the indentation in the cell are the two variables used to calculate the Young's modulus of the cell.

The following equation was used to determine the Young's modulus of the cell where $E_{surface}$ is the Young's modulus of the cell, $\nu_{surface}$ is the Poisson's ratio of the cell surface, and $S_0 - S$ is the indentation on the surface: $F_{Sneddon} = \frac{2}{\pi} \frac{E_{surface}}{(1-\nu_{surface}^2)} \tan \alpha (S_0 - S)^2$.

For cells indented with the spherical tip, the Hertz model is used. The same assumptions apply. Figure 2.3 demonstrates the spherical tip inserting into the cell surface.

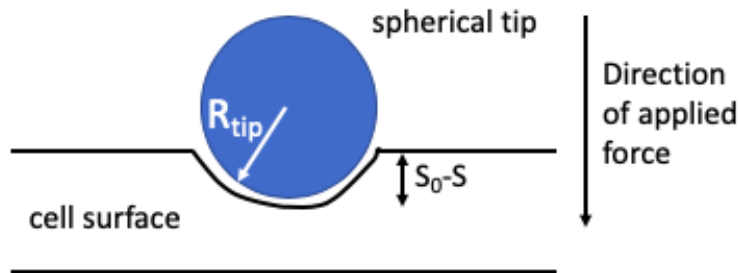


Figure 2.10 A diagram to demonstrate the spherical tip of the AFM being inserted into a cell surface. The radius of the tip and the depth of indentation into the cell are the two variables used to calculate the Young's modulus of the cell.

The following equation was used to determine the Young's modulus of the cell. R_{tip} is the radius of the spherical tip: $F_{Hertz} = \frac{4}{3} \frac{E_{surface}}{(1-\nu_{surface}^2)} \sqrt{R_{tip}} (S_0 - S)^{3/2}$.

Chapter 3. The role of the Imagestream platform in the detection and analysis of CTCs in metastatic prostate cancer

Chapter Summary

This chapter discusses the reason for choosing the platforms used during the main part of this project for the detection and analysis of CTCs. This novel assay development, using a combination of epithelial and stem cell markers on the Imagestream is described. This includes the choice of antibodies used, cell line optimisation and thresholds used for determining true positives, based on results obtained from healthy volunteer blood samples, including the spiking of prostate cancer cells into the healthy blood. Because the FDA definition of a CTC does not include cells that express Oct4, SOX2 and Nanog, any cells described in this chapter that are EpCAM positive and/or express any of these three stem cell antigens are deemed putative CTCs.

3.1 Platform choice

3.1.1 Background

The decision on which platform to use in this project to detect CTCs is dependent on a number of factors. Cost per sample, and availability are important. The funding for this project is finite and whilst there are other groups within the institution working on similar projects in other cancers, it would not be feasible to buy an entirely new machine. The options are therefore restricted to what is already available at Newcastle, or within easy geographical reach if considering collaboration with another centre. If thinking of using a platform outside of the university, access to the machine must tie in with when the samples are obtained, and transport +/- processing costs (if using technical staff in this centre) must be factored in.

Speed of use is also key. The time between obtaining the blood from the patient to the start of processing, and also the length of time taken to run the assay should both be kept to a minimum to ensure accuracy and consistency. Newcastle Hospitals has one of the largest Urology departments in Europe, and due to the high numbers of patients presenting with metastatic prostate cancer, sufficient samples could be obtained during this study from patients solely within the Newcastle area. This would help keep the time from sampling to processing to a minimum, and as constant as possible to enable comparison of results.

A lengthy processing assay using unfixed blood could also potentially alter results. Fixing the blood immediately after sampling would minimise this problem, and there are also blood collection tubes available that contain a preservative cocktail to allow conservation of a blood sample up to 96 hours at room temperature. (This will be discussed later in this chapter). Downstream applications such as genomic sequencing could however be limited if using small numbers of fixed cells, so forward planning is important. Laborious assays would also restrict the number of samples possible to process during this project, which would reduce the power of any study.

Replication of results is also imperative, especially if considering utilisation in the clinic in the future. A complicated assay with multiple steps would have the potential to introduce user error or restrict the number of technical staff who would be available to process samples. Whilst this latter point is not relevant for this project as all the sample processing will be performed by the author of this study, it is something to consider when planning the potential future transfer of any successful assay into the clinical environment. If an assay uses a rare and expensive piece of equipment, it will limit the number of centres in which samples can be processed which will in itself increase the cost per sample, along with issues surrounding transport and time between sampling and processing.

3.1.2 Choice of platform based on method of CTC detection

As discussed already, options for detection of CTCs are broadly categorised into those reliant on protein expression, physical characteristics or those involving direct analysis. Because of the lack of an available high throughput scanning device, the latter method was discounted for this study. Cell sorting based on physical properties may overlook cells expressing the proteins of interest which happen to have a different morphology. Therefore, because the aim of this study is to explore protein expression, it would be logical to use a method of detection that depends on this.

Given that the study design relies on processing whole blood, any modality used to detect CTCs has to possess the ability to allow processing of a large number of cells. Whilst the majority of the components of the blood are not of interest (e.g. leucocytes and erythrocytes) any assay would either need to allow quick processing of whole blood and accurate subsequent identification of CTCs (positive selection), or would include steps to deplete the superfluous cells (negative selection). Both have their limitations – positive selection can result in an inaccurate identification rate due to the low percentage of cells of

interest being recovered. To combat this, high volumes of antibody could be used to avoid dilution in a large volume, but this in turn could lead to inappropriate binding and false positives. Negative selection can cause accidental depletion of the target population.

3.1.3 The Veridex CellSearch

As discussed previously, the only FDA-approved technique for identifying CTCs is the Veridex CellSearch (Cohen et al., 2008, Cristofanilli et al., 2004, de Bono et al., 2008). This is still only validated for *non-clinical* work, but has been used as an additional outcome measure in several high profile clinical trials in patients with breast cancer, prostate cancer and colorectal cancer (Hayes et al., 2006, de Bono et al., 2008) . This method involves a density centrifugation step, followed by exposure to magnetically bound EpCAM antibodies. The sample is then processed through a magnetic field, which is then used to positively select the antibody-bound CTCs. Because of the reliance on epithelial antibodies, there is the potential to miss detection of CTCs that are of a different phenotype, or those that do not attach to the magnetic particles, either due to heterogeneity or inadequate binding. Given the findings from some studies showing that up to a third of patients with metastatic breast cancer do not have any detectable CTCs (Riethdorf et al., 2007) (which could be due to detection error), and to address the issue of epithelial to mesenchymal transition, this platform does have its limitations. However, it must be acknowledged that the CellSearch is still the only FDA-approved platform, and it has maintained that status since 2008 despite the introduction and availability of numerous other CTC detection platforms.

Newcastle University does not have a CellSearch platform, but although collaboration with other centres would potentially have enabled the use of one for this project, particularly for platform comparisons, the decision was made to use alternatives. Because the aim of this study is to investigate the role of mesenchymal and stem cell markers, in addition to epithelial markers, selecting purely based on epithelial markers could mean overlooking cells of interest and would therefore not be the most appropriate tool for this study. Whilst any other platform will not be FDA-approved, to explore and potentially advance the understanding of stem cell marker expression in CTCs, because of the requirement to use epithelial antibodies, it was felt that the CellSearch would be too restrictive.

3.1.4 Fluorescence Activated Flow Cytometry (FACS)

The availability of conventional flow cytometers, and their use for processing high cell numbers, such as those found in whole blood, makes them an obvious choice for a technique that would be both accessible and theoretically cheap to run. Most universities with molecular or cell biology laboratories, or indeed hospital laboratories, will have their own flow cytometry machines and therefore processing samples using an assay developed for this platform would be easily reproducible.

FACS for detecting low cell numbers is not however without its limitations. Gates used to include or exclude cells must be applied to all samples to ensure consistency, and when using fluorescence thresholds, events counted as exceeding the minimum threshold must also be gated according to size and cellular complexity (forward and side scatter) to ensure they don't represent debris (O'Connor et al., 2001). Due to the fact that CTCs are rare events, and statistically many of the samples will not contain these cells, reliance on the absolute value of fluorescence expressed, without any imaging of the cells to substantiate this, lends itself to a high false positive rate. In addition, false positives due to erroneous antibody binding will be hard to determine, although if using the same panel of antibodies, this rate should be consistent throughout all samples, still allowing comparison.

One method to overcome not knowing the exact nature of the cells that reach the positive threshold is to sort these cells before analysing them further using techniques such as conventional immunofluorescence (Miyamoto et al., 2012), Fluorescence in situ Hybridisation (FISH) (Punnoose et al., 2015) or by extracting DNA or RNA for PCR or sequencing (Steinestel et al., 2019, Miyamoto et al., 2015). Even if ultimately the basic FACS assay without additional sorting was accurate enough to lead to the use of this test in clinical practice, sorting the cells to provide information about their validity is important to do during the development of the assay. Meticulous scrutiny of any potential positive cell would enable accurate calculation of the false positive rate.

The use of FACS with cell sorting and downstream analysis was one of the techniques used in this study and is discussed in Chapter 4.

3.1.5 The Imagestream^X (Merck)

An alternative technique that can be used to overcome the issue of whether or not an event is truly positive or not is to use a platform that provides the phenotypical information obtained through FACS with simultaneous imaging of each cellular event. The Imagestream^X

(Merck) is a combined high resolution microscope and flow cytometer (Zuba-Surma et al., 2007), which allows the user to view the image of any event displayed on the dot plot. This platform was already *in situ* within the institution and an assay for CTC detection using this modality had recently been developed by a Newcastle group (Dent et al., 2015). For this reason, and because it would provide detailed data to satisfy the aims of the study, the Imagestream^X was chosen.

The machine is available with up to six lasers, which excite fluorochromes, conjugated to antibodies, emitting light at specified wavelengths. Whilst the company cites that the use of up to twelve fluorochromes simultaneously is achievable, there would be a considerable degree of laser overlap in practice. This would either manifest as false positives, or if strict compensation was employed then cells which only weakly expressed an antigen would be missed. Due to the expected heterogeneity of the clinical samples in this study, using fluorochromes with the minimum overlap possible would enable detection of weakly positive cells whilst being confident that they were true positives. The Newcastle Imagestream machine has four lasers, therefore a maximum of seven antigens with separate fluorochromes could be reliably used for any panel.

Similar to conventional FACS, cells must be labelled with a panel of antibodies in advance of processing and, when comparing samples, laser settings and antibody concentrations must be consistent. Cell sorting is possible based on physical characteristics and/or protein expression and analysis can be achieved either by using the analysis software, or, somewhat laboriously, through individual visual inspection of events. One major advantage of this platform is that it does not select the cells solely based on EpCAM, thus allowing exploration of the presence of non-epithelial cells of interest. Erythrocytes and the majority of white cells are depleted using a combination of red cell lysis and immuno-magnetic separation prior to processing, thus it uses principles of both positive and negative selection. Recovery of CTCs is approximately 50-60% (Dent et al., 2015) so its use with respect to enumeration may be limited. However, it provides very detailed cellular images, so its strength is in phenotypic analysis.

Unlike conventional FACS where the user would keep diluting the sample as the contents of the FACS tube diminishes (so as to avoid ingestion of air), the Imagestream processes the entire contents of the sample Eppendorf. This allows a more accurate comparison of the true number of CTCs found between samples. However, the files collected by the Imagestream are very large because each event has an image associated with it. This means

that in order to collect usable data, it would be optimal to deplete as many of the unwanted cells (in this case erythrocytes and leucocytes). Despite aiming to deplete these extra cells, some gating still has to be employed during the running of the Imagestream samples so that the files are of a manageable size to use. This is unlike conventional FACS where all data is stored and gates can be applied afterwards during the analysis stage. Samples with higher concentrations of cells can be run but will need to be divided into multiple Eppendorfs. As each Eppendorf tube with a volume of 200µl containing a maximum concentration of 2×10^7 cells/ml can take 60-80 minutes to process, running time could be impractical if samples contain excessive numbers of superfluous cells.

3.2 The optimization of an assay to use on the Imagestream^x

3.2.1 The choice of assay

The protocol developed by colleagues within the NICR for CTC detection (NICR assay) was used as the assay to process blood in preparation to run on the Imagestream for this project (Dent et al., 2015). Because this protocol had been developed in detail and various reagents had been tested before the final protocol optimized, it was felt unnecessary to spend further time on optimization. Other documented assays use the same principles of erythrocyte lysis followed by immuno-magnetic depletion of white cells (Lopez-Riquelme et al., 2013, Zuba-Surma et al., 2007, Zuba-Surma and Ratajczak, 2011). The remaining cells (remaining leucocytes and CTCs) are then permeabilised with detergent before the antibodies are applied. The cells are then resuspended in a buffer in an Eppendorf which can be directly placed into the Imagestream.

3.2.2 Collection and storage of blood from patients and healthy volunteers

Blood was obtained from Urology and Uro-oncology clinics at the Freeman Hospital, or from healthy volunteers from within the NICR. Ethical consent permitted up to 12ml of blood to be taken from each patient. For the purposes of this project, 4ml was used for the assay described in this chapter, 4ml was used for FACS analysis (Chapter 4) and in some patients a further 4ml was used for culturing of CTCs (Chapter 6). Although the seminal papers on CTCs discuss the number of CTCs per 7.5ml of blood, a smaller volume was chosen because it would allow a higher number of assays to be performed for each patient.

Blood tubes containing potassium ethylene-diaminetetraacetic acid (K₂EDTA) were chosen, a compound which prevents clotting whilst preserving cell morphology. Tubes were filled to capacity as high concentrations of EDTA: blood can alter the binding of metallic ions which could in turn affect antibody binding sites in downstream assays (Bowen and Adcock, 2016). Cellular degeneration will occur if the storage temperature and time to processing is not optimized (Adcock et al., 2016). For this reason, blood was transported and stored at room temperature and processed within four hours of sampling. Preliminary experiments were conducted by a colleague to compare cell retrieval when using EDTA tubes compared to CellSave (CellSearch) tubes. The CellSave tubes are reported to stabilize the blood for up to 96 hours by containing an undisclosed cell preservative in addition to EDTA (Qin et al., 2014, Kang et al., 2016). Despite this, work performed by colleagues demonstrated a decline in cell retrieval after 36 hours. Because these results raise concern over the efficiency of CTC recovery from delayed samples and also the cost of the CellSave tubes is much higher, the decision was made to process the blood immediately, following collection in EDTA tubes.

3.2.3 Fixation of whole blood and lysis of erythrocytes

The NICR assay takes a minimum of 24 hours after blood collection before the sample is ready to run (including incubation times). As the Imagestream does not enable cell sorting for further downstream processing, the decision was made to fix the cells at the earliest stage possible. This meant that sample collection could be performed during a morning clinic, the blood transported back to the lab and fixation and erythrocyte lysis could be done within a four-hour window. White cell depletion could then be performed before overnight permeabilisation, followed by antibody staining the following morning prior to running. Density centrifugation has traditionally been used to separate the various components of whole blood but lysing agents have become more popular over the past twenty years, due to the lower mechanical stresses placed on the cells, greater reproducibility and the ability to work with smaller blood volumes (Bossuyt et al., 1997, Pinto et al., 2005). Cell lysis of erythrocytes can be performed in combination with fixation of the remaining leucocytes to limit the number of steps used to deplete unwanted cells and therefore reduce the cell loss associated with a multi-step assay.

Lysis relies on cells being exposed to hypotonic solutions so that water is transported into the cell, causing it to rupture. Additionally, chemicals can stimulate cell wall breakdown. It occurs in three stages in erythrocytes; firstly, spherisation of the usually bi-concave cells

takes place, during which time the cell surface area remains the same. This is followed by an increase in cellular volume before eventually the membrane tension exceeds a critical value and the cell ruptures (Evans et al., 2008). Organic solvents, detergents and chelating agents are frequently used as lysis agents.

Cellular fixation prevents any decay or further biochemical reactions within the cell with the aim of preserving the cell for subsequent analysis. Cross-linking fixatives, such as aldehydes and precipitating fixatives such as alcohols are two of the most commonly used types in cellular biology and the choice of agent may depend of whether secondary or tertiary protein structure is the most important feature to be subsequently examined.

The PhosFlow Lyse-Fix buffer (BD) contains both methanol and formaldehyde and allows fixation of the blood and lysis of the erythrocytes in one step. Although several commercial combined lysis and fixative agents are available, this one had been utilized and optimized by the NICR team.

3.2.4 White cell depletion

Leucocytes contain molecules within their cell surface called cluster of differentiation (CD) markers. These antigens can be targeted with specific antibodies, which have been developed following collaborative work by the Human Cell Differentiation Molecules Committee (HCDM). This group has identified over 350 leucocyte antigens, which will be expressed by different types of white cell (Molecules, 2019). Identifying leucocytes en masse is feasible if using a common leucocyte antigen such as CD45, which is expressed by all haematopoietic cells except erythrocytes (Nakano et al., 1990). The method used to deplete white cells in this assay used a CD45 antibody which was then bound to magnetic beads to enable immunomagnetic separation through a magnetic field (Dent et al., 2015). This had consistently yielded a depletion rate of 95% during optimization by the NICR team. Because there are on average $4-11 \times 10^6$ leucocytes per ml of blood, and 4mls was analysed per patient, even a 95% depletion would result in $8-22 \times 10^5$ cells remaining. When on average there are 1-10 CTCs per ml of blood in a patient with metastatic disease (Alvarez Cubero et al., 2017), even with a high depletion rate, the CTCs are incredibly rare events within the sample ($<1 \times 10^6$).

3.2.5 Permeabilisation

Although the CellSearch detects cells based on epithelial (cell surface) antigens, the Imagestream will not allow downstream processing. Therefore, any cells of interest must be labelled with the appropriate fluorescently conjugated antibody prior to processing. If the antigens are intracellular then adequate permeabilisation must be performed. Detergents and organic solvents are the two most commonly used types of permeabilising agents (Jamur and Oliver, 2010). Solvents such as methanol or acetone can also be used as fixative agents due to their coagulative effect on proteins, and work by dissolving the lipids within cell membranes so they can be more easily penetrated by the antibodies. Detergents cause physical disruption (which can be reversible) to the membrane resulting in small holes through which antibodies can pass. In this assay, permeabilisation at the same time as fixing was not considered optimal as this could affect the leucocyte depletion. Using a reversible detergent such as Saponin would mean that cells could be permeabilised to allow staining for intracellular antigens, but not fragment, as only whole cells would be considered as positive events. The BD PermWash was therefore the chosen agent following optimisation by the NICR team.

3.2.6 Processing of blood spiked with cell lines to determine retrieval rate on the Imagestream^x

Retrieval rates using the Imagestream^x are reported between 55% and 65% (Dent et al., 2015) depending on the cell type and number of cells spiked into blood. To ensure that comparable results could be achieved using prostate cancer cells, the NICR assay was used to assess retrieval rate using two different prostate cancer cell lines spiked into healthy volunteer blood. Cell quantities of 20 000 and 50 000 PC3 and LNCaP cell lines were spiked into 2mls of blood and repeated three times (Figure 3.1). Size and fluorescence were used to count the numbers of cells retrieved. Vimentin, DAPI and CD45 were used for the PC3 experiment and EpCAM, DAPI and CD45 were used for the LNCaP arm. This is due to the high EpCAM / low Vimentin expression in LNCaP cells, but low EpCAM / high Vimentin expression in the PC3 cells (Ni et al., 2013). Cells were counted as positive if CD45 negative and either EpCAM or Vimentin positive.

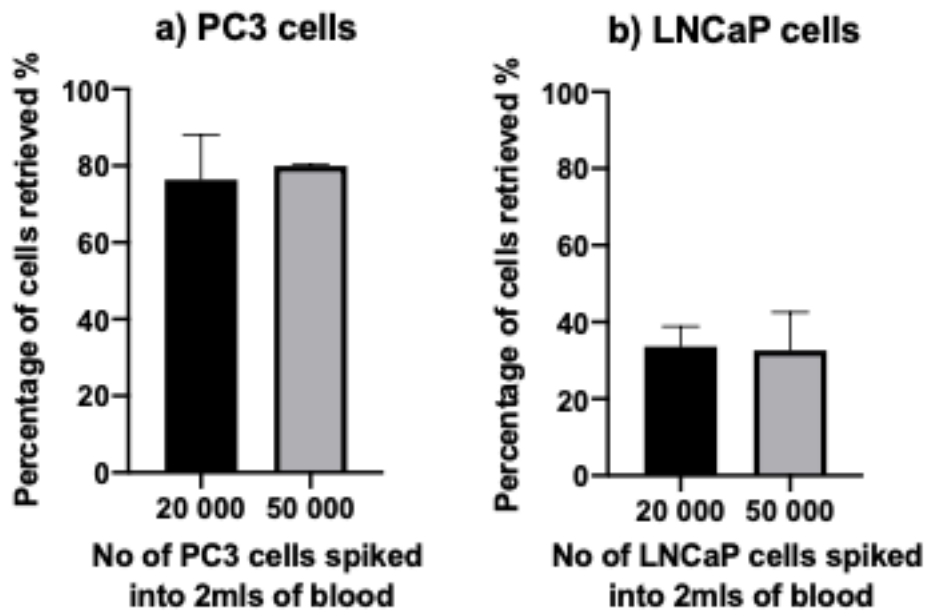


Figure 3.1 Graphs to show the percentage retrieval of different numbers of two prostate cancer cell lines spiked into healthy volunteer whole blood when using the NICR assay. 20 000 or 50 000 cells of each cell line were spiked into 2mls of whole healthy volunteer blood and the NICR Imagestream assay was used to process the sample. The number of cells from each cell line at the end were identified using size and fluorescence (Vimentin for PC3 and EpCAM for LNCaP).

This experiment demonstrates a mean retrieval rate of 76.3% and 79.9% for the 20 000 and 50 000 cell experiments for PC3, and 33.6% and 32.6% for the LNCaP arm.

3.3 Antigen expression and choice of antibodies

3.3.1 Fluorescence and primary vs secondary conjugation

Before the final decision was made on which antigens to research for this study, the concept of using antibodies that were directly conjugated to fluorochromes versus a two-step primary and secondary application was explored. Whilst using unconjugated antibodies is cheaper, there is lack of quality control, and when faced with sampling tiny populations of cells the decision was made to use commercially conjugated antibodies where possible.

3.3.2 Number of channels and choice of antigens

As previously mentioned, the Imagestream has twelve channels in which to display images, and four lasers. Two of these channels display a brightfield image which can be used to assess cell morphology and gate based on whole cell or nuclear size criteria. Out of the remaining ten channels, six different fluorescently conjugated antibodies could be reliably used to identify different antigens as any more would risk significant spectral overlap. At

least one white cell marker would be necessary, in order to assist with gating strategy and elimination of leucocytes. A nuclear marker is also important as the FDA definition of a CTC clearly specifies criteria that identifies whole cells. This leaves the option of exploring a further four antigens. Whatever the combination of antibodies that makes up the final panel, it has to identify cells with the expected epithelial phenotype in addition to any new markers that are to be explored. In order to get robust data the choice was made not to explore a mesenchymal marker in this assay. Whilst it would be useful to ascertain how many cells had undergone EMT, adding an additional marker may compromise the data due to spectral overlap, and therefore this will be explored in chapter 4. A combination of antibodies that identifies the maximum number of phenotypically different cells whilst simultaneously being able to confidently exclude leucocytes is the ideal. The lasers available for use on the Imagestream in the NICR and a list of possible fluorochromes are listed in Table 3.1.

	Laser			
	405nm	488nm	561nm	642nm
Example Dyes	DAPI	FITC	PE	APC
	AF405	AF488	AF546	APC-Cy5.5
	AF430	AF500	AF555	DyLight 649
	Pacific Orange	AF514	PE-Texas Red	AF647
	Marina Blue	PE-Texas Red	Spectrum Orange	AF660
	Pacific Blue	PerCP	PE-AF 647	AF680
	Cascade Blue	PerCP-Cy5.5	PE-AF 680	Draq5
	DyLight 405	Draq5	Nile Blue	Cy5
	Qdot 525 - 800	PI	Calcium Orange	APC-Cy7

Table 3.1 Laser wavelength and associated suggested fluorochromes for the Imagestream.

3.3.3 The decision not to use a prostate specific antibody

As discussed, the main reason for this project is to identify a new biomarker that could be used in metastatic disease. PSA is unreliable and would not add any additional information to the level obtained during serum sampling (bloods obtained for this study were taken at the same time as bloods required for clinical review, and therefore matched PSA results were obtained). Given that not all prostate cancers express PSA and those that do may not do so at a level that represents disease burden, PSA was excluded from the antibody panel. It was felt that whilst the presence of PSA could confirm a cell as a CTC, absence could not reliably exclude it. Because of the variance in expression of PSMA, and the mutations found

in the Androgen Receptor which would require using a number of different AR antibodies, these were also felt to be unhelpful.

Due to the limited number of antigens that could be used in the panel, in the absence of having a prostate specific marker that could be used to positively identify the majority of prostate cells it was felt that using a prostate marker would not add to the understanding of cell phenotype and would restrict additional information that could be identified.

3.3.4 Epithelial antigens

The seminal papers in prostate cancer CTCs describe using EpCAM and CK as epithelial markers. Whilst EpCAM is a cell surface molecule, cytokeratins are cytoskeletal proteins. As the assay includes a permeabilisation step, this should not preclude the use of either.

Cytokeratins do however vary between different tumours, and whilst prostate tumours should theoretically contain the same combination, there will undoubtedly be heterogeneity. Choosing a cytokeratin antibody which recognizes multiple cytokeratin epitopes would be optimal.

3.3.5 Stem Cell antigens

The need to identify somatic stem cells or differentiated progenitor cells as potentially the most lethal subpopulation of tumour cells has been discussed. Whilst there are several markers to be considered, the preliminary data showing survival outcomes related to Oct4, SOX2 and Nanog expression in prostate tissue is interesting (Hepburn et al., 2019), and it would be useful to look at individual expression and compare with combined expression of all three. For this reason, this combination of stem cell markers was used for this study.

3.3.6 Overlap of expression

The presence of mesenchymal stem cells in healthy adults to enable tissue repair must be acknowledged. These cells will be in the circulation and will therefore be detected when using stem cell antibodies. An increased number of these cells will potentially be released in response to cellular destruction caused by metastatic infiltration, so whilst they will not be CTCs per se, they may be clinically significant. Completely excluding these cells in the count is therefore not sensible and would also negate the use of stem cell antibodies. Therefore, a threshold must be considered either in terms of number of cells or fluorescence, so that

comparisons between stem cell expression in healthy blood and blood from patients with metastatic prostate cancer can be made. This is outlined during the next section.

3.3.7 Heterogeneity of antigen expression within cell lines

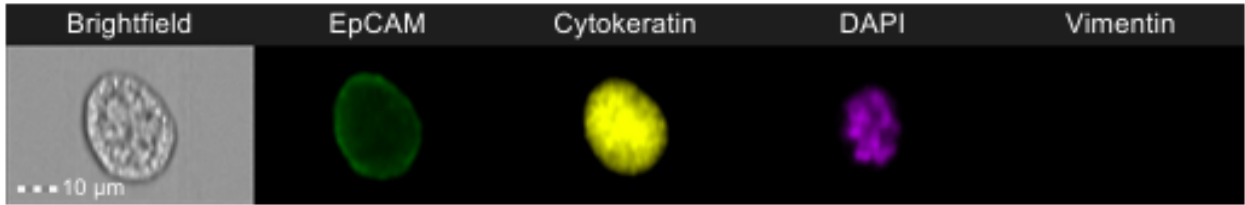
If looking for expression of proteins within a clinical sample, it must be anticipated that there will be phenotypical heterogeneity. Even within cell lines of an early passage it is likely that heterogeneity will exist, and the incidence of this would increase with the higher passage number of the cells. It is important to appreciate this when optimizing antibody concentrations and also in the interpretation of results. Similarly, distribution of cells throughout the cell cycle can influence expression of individual proteins.

In order to demonstrate this, 10 000 cells from three prostate cancer cell lines were fixed, permeabilised and stained with a combination of epithelial and mesenchymal antibodies in addition to a nuclear marker. Cells were stained with EpCAM (conjugated to AF488), a pan-Cytokeratin (conjugated to PE), Vimentin (conjugated to AF647) and DAPI as the nuclear marker and run through the Imagestream. This was repeated three times and a mean of the number was calculated (Table 3.2 and Figures 3.2 and 3.3).

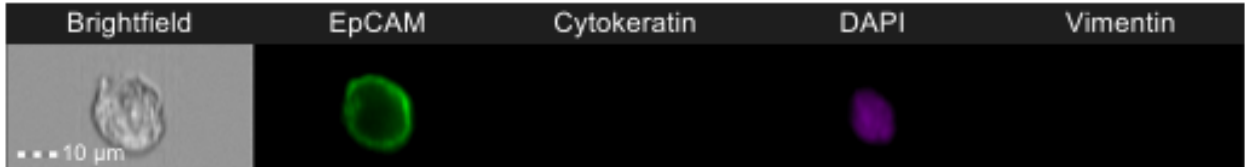
Combination of antigens	Mean percentage of each cell type for each cell line		
	LNCaP	PC3	CWR-22Rv1
1. EpCAM+/CK+/Vim-	1.58	0.38	0.72
2. EpCAM+/CK-/Vim-	97.04	0	96.86
3. EpCAM+/CK-/Vim+	0.12	0.08	0.60
4. EpCAM-/CK+/Vim-	0.70	0.04	0.16
5. EpCAM-/CK-/Vim+	0.56	99.5	2.10

Table 3.2 The prevalence of each combination of antigens expressed by three different prostate cancer cell lines; LNCaP, PC3 and CWR-22Rv1. All three cell lines were labelled with the three antigens EpCAM, CK and Vimentin and the percentage of total cells expressing each combination of antigens was recorded.

1: EpCAM+ / CK+ / Vimentin -



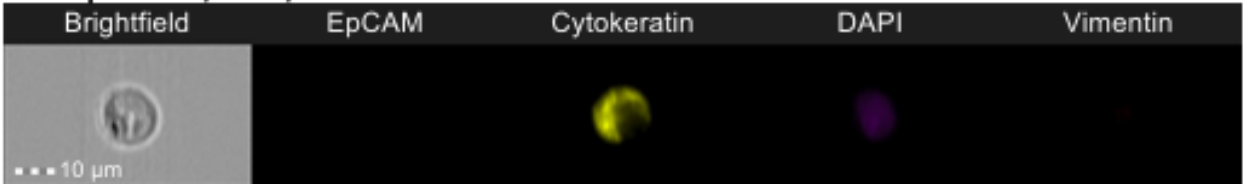
2. EpCAM+ / CK- / Vimentin -



3. EpCAM+ / CK- / Vimentin +



4. EpCAM- / CK+ / Vimentin-



5. EpCAM- / CK- / Vimentin +



Figure 3.2 Imagestream images to demonstrate heterogeneity of antigen expression within prostate cancer cell lines. (Images 1, 2 & 3 are LNCaP cells, Image 4 is a CWR-22-Rv1 cell and Images 5 is a PC3 cell).

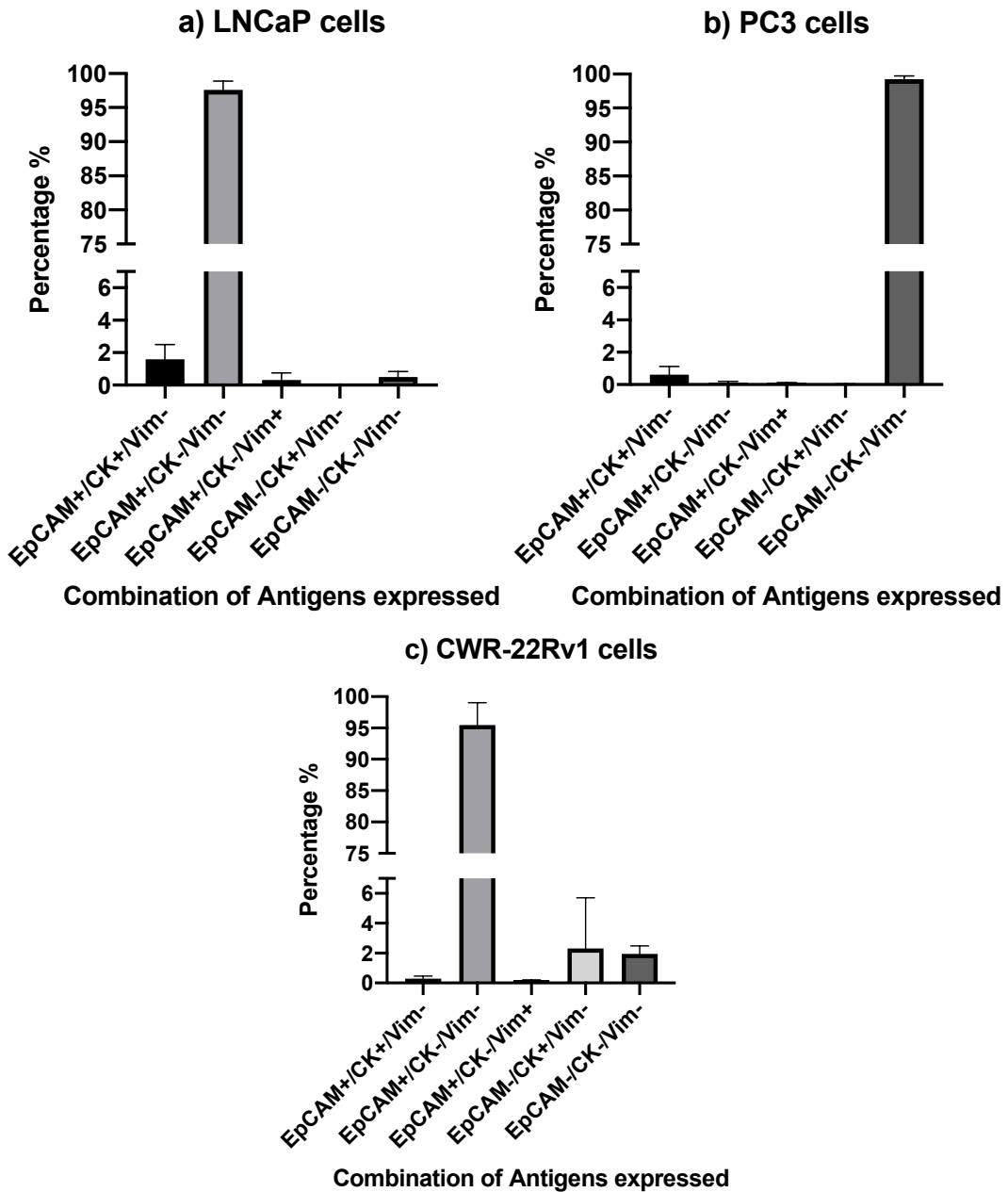


Figure 3.3 Graphs to show the percentage of each of the combinations of antigens expressed in each cell line. All cell lines were stained with EpCAM, Cytokeratin, Vimentin and the nuclear marker DAPI. Cells were processed on the Imagestream and the number of cells displaying fluorescence corresponding to each antigen, or combination of antigens, were recorded. LNCaP cells were predominantly EpCAM+/CK-/Vimentin-, PC3 cells were predominantly EpCAM-/CK-/Vimentin+ and CWR-22Rv1 cells were predominantly EpCAM+/CK-/Vimentin-.

This experiment clearly demonstrates the heterogeneity between different prostate cancer cell lines. EpCAM+/CK-/Vimentin- cells are most prevalent in both LNCaP and CWR-22Rv1 cell lines, whilst PC3 cells are predominantly EpCAM-/CK-/Vimentin+. This highlights the importance of looking for non-epithelial in addition to epithelial markers in any assay used to detect prostate cancer CTCs. Heterogeneity in clinical samples is explored further in the next section.

3.3.8 Epithelial antigen expression in patient samples

Before the final antibody panel was chosen, ten clinical samples were obtained from patients with end-stage prostate cancer (defined as being castrate resistant and on second line chemotherapy). Patients with such advanced disease were chosen due to the higher chance of having larger numbers of CTCs in their blood. These samples were processed using the NICR assay and stained with EpCAM (AF488), CK(PE), CD45 (PECy7) and Draq5 (nuclear stain). The aim of this experiment was to assess whether EpCAM or CK could be used independently as the sole epithelial marker. This would enable use of the three stem cell markers in combination, with one epithelial antigen as the fourth variable.

Out of the 10 samples, 4185 cells in total were identified as potential CTCs (CD45- and Draq5+). 849 (20.2%) of these cells did not express either of the epithelial markers EpCAM or CK but were included in this count because they were CD45 negative (Table 3.3).

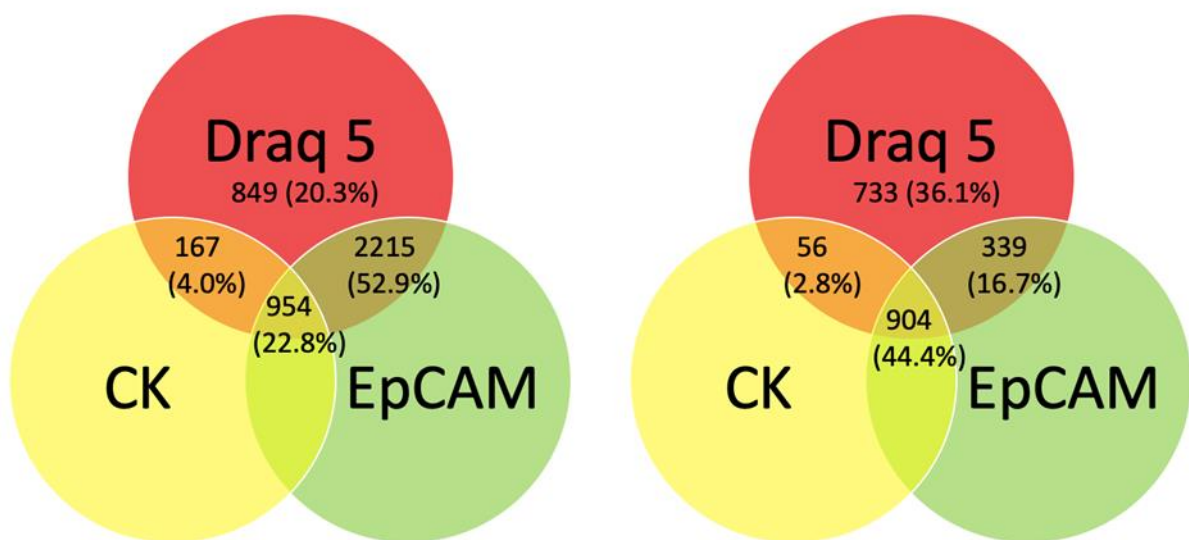
Patient No.	EpCAM+/CK+/CD45-/Draq5+	EpCAM+/CK-/CD45-/Draq5+	EpCAM-/CK+/CD45-/Draq5+	EpCAM-/CK-/CD45-/Draq5+
1	0	22	0	0
2	0	0	0	5
3	0	0	0	0
4	111	1	2	381
5	552	0	0	0
6	107	0	0	330
7	77	0	49	7
8	44	1	5	0
9	13	315	0	10
10	50	1876	111	116
Total	954 (22.9%)	2215 (52.9%)	167 (4.0%)	849 (20.2%)

Table 3.3 The different combinations of antigens expressed in cells detected from the blood of patients with metastatic prostate cancer. All cells were labelled with EpCAM, CK, CD45 and Draq5. To be considered a possible CTC cells had to be CD45- and Draq5+. Different combinations of EpCAM and CK expression were seen in all ten patients. The most common combination was EpCAM+/CK-, seen in 52.9% of patients.

The following diagrams in Figure 3.4 demonstrate the combination of antigens from table 3.3. Only 22.9% of cells can be defined as CTCs if using the FDA definition. EpCAM+ only cells were found in 5 of the samples compared to CK+ only cells in 4. These EpCAM+ only cells account for over half of the potential CTCs identified. Although there are a significantly higher number of EpCAM+ cells in total, this is skewed by one sample containing 84.5% of the total number of EpCAM cells. If this sample is removed and the remaining 9 samples are analysed, then the EpCAM+ only cells account for only 16.7% of the total population.

In this revised analysis almost double the proportion of cells are FDA-defined CTCs but there is also a higher proportion of non-epithelial cells (or at least, cells not expressing one or both of the two epithelial markers used in this experiment) compared to the first analysis. Whilst a proportion of these cells could be white cells that have not bound to the CD45 antibody, this should not account for 20-36% of the sample. This gives further evidence to support the theory that there is a significant proportion of cells without an epithelial phenotype, circulating in the blood of a patient with an epithelial tumour and these numbers are comparable with those found in the literature (Mego et al., 2011).

Interestingly, the proportion of cells expressing CK only is at most 4%. Therefore, choosing to use EpCAM as the sole epithelial antibody would only result in the failed detection of a small percentage of cells. Due to heterogeneity between samples this number would vary but it is possible that cells that would have expressed CK may be detected by the presence of one or more of the stem cell markers.



a) Combinations of antigens expressed in all ten clinical samples

b) Combinations of antigens expressed in samples 1-9

Figure 3.4 Venn Diagrams to demonstrate the combination of antigens expressed by cells detected in the blood of patients with metastatic prostate cancer. Diagram a) included all samples but diagram b) excludes sample 10 which had a very high number of cells found and could skew the data. The revised data without sample 10 shows that the majority of CTCs found in the 9 patients expressed both EpCAM and CK.

3.3.9 Final antibody panel

The final antibody combination has to be a compromise between what is commercially available, cost and avoiding spectral overlap. Despite using a pan-cytokeratin antibody which

should identify cytokeratins 4, 5, 6, 8, 10, 13 and 18 during the cell line and clinical experiments, EpCAM was found to be far more prevalent in the prostate cancer cell lines and the clinical samples compared to CKs and was therefore chosen as the epithelial marker. Inevitably there will be a proportion of prostate cancer cells in the samples that will evade detection due to antibody choice, but this is one of the limitations of any CTC work. The final list of antibodies and associated fluorochromes is outlined in Table 3.4.

Antibody	Fluorochrome	Isotype Control	Manufacturer
EpCAM	PE-Vio615	REA(S)	Miltenyi Biotec
Oct4	AF488	IgG1 κ	BD Biosciences
SOX2	AF555	IgG2a	BD Biosciences
Nanog	Per-CP Cy5.5	IgG1 κ	BD Biosciences
CD45	PECy7	IgG1 κ	BioLegend
DAPI	-	-	BioLegend

Table 3.4 A list of chosen antibodies and the associated fluorochrome and isotype control used in the assay described in this chapter.

The emission and excitation of the fluorochromes of the final panel of antibodies is demonstrated below in Figure 3.5. Some degree of spectral overlap will occur, but this will be minimised by careful compensation, using single colour controls. This will be explored in section 3.5.

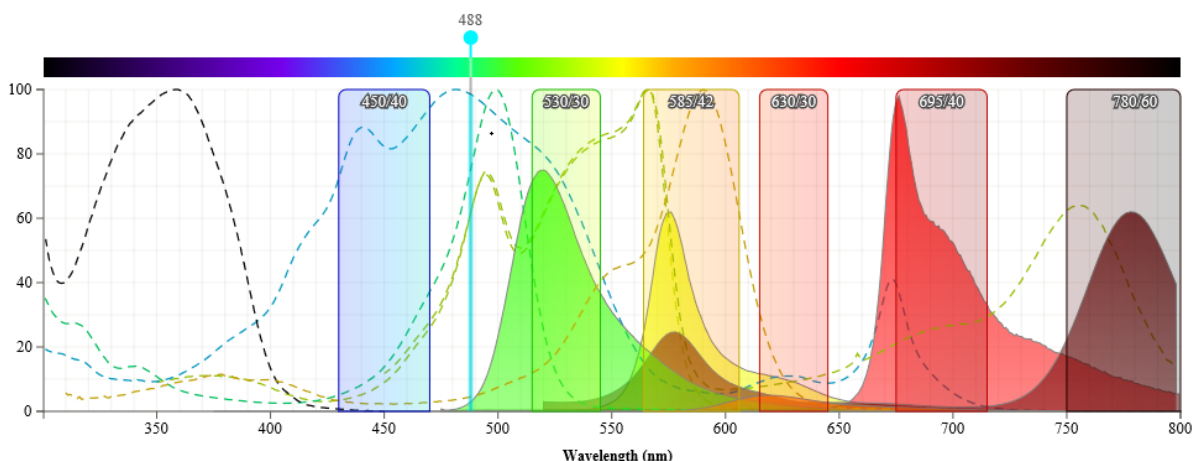


Figure 3.5 A graph to demonstrate the excitation (dotted line) and emission (solid block) wavelengths of the fluorochromes conjugated to the antibodies used in this assay (courtesy of BD Biosciences).

3.4 Optimisation of antibodies

3.4.1 Antibody optimisation of EpCAM using cell lines

Each optimisation concentration was repeated three times using 100 000 cells. Eppendorfs or FACS tubes contained the cells in 100µl of suspension. Therefore concentrations discussed are 1:500 (0.2µl), 1:200 (0.5µl), 1:100 (1µl), 1:75 (1.5µl) and 1:50 (2µl).

EpCAM (PE-Vio615) was optimised using LNCaP cells (Figure 3.6). 100 000 cells were stained with increasing concentrations of antibody and compared to the same concentration of the isotype control, and unstained cells.

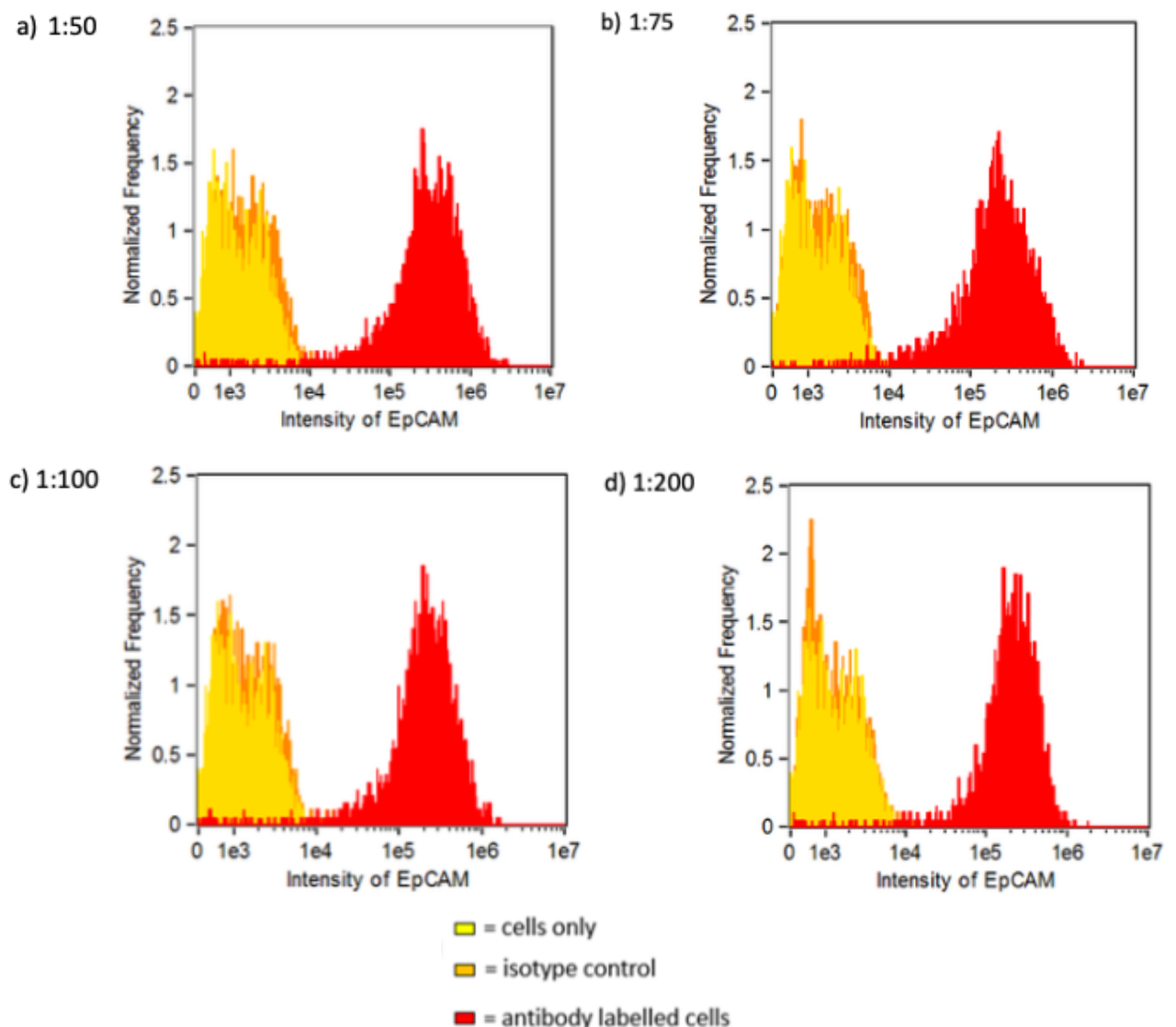


Figure 3.6 Graphs to demonstrate LNCaP cells unstained (yellow), stained with isotype control (orange) and with increasing levels of antibody (red). Each volume of antibody was used to determine the lowest level that could be utilised by demonstrating a shift from the negative controls (unstained cells and isotype controls).

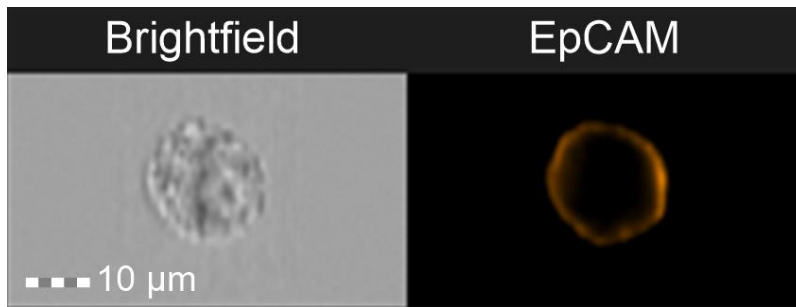


Figure 3.7 An Imagestream image demonstrating the cell membrane staining using the EpCAM antibody at a concentration of 1:200.

There was no increased shift in fluorescence when using increasing concentrations, and the images obtained demonstrated appropriate staining (Figure 3.7). Therefore the EpCAM antibody was used at a concentration of 1:200.

3.4.2 Antibody optimisation of Oct4, SOX2 and Nanog using cell lines

Expression of Oct4, SOX2 and Nanog was much more difficult to ascertain as conventional cell lines did not express the stem cell antigens in sufficient, predictable quantities.

Optimisation experiments were performed on cell lines LNCaP, PC3, SEM, TC71 and Y201 all without success. Mesenchymal stem cells were obtained from bone marrow (under ethical approval from North-East Newcastle and North Tyneside 1 Research Ethics Committee, REC no 17/NE/0361, Feb 2018) - please see appendix for ethics form) and whilst they did express the antigens (Figure 3.8), we were unable to culture them in sufficient quantities to perform reliable optimisation tests.

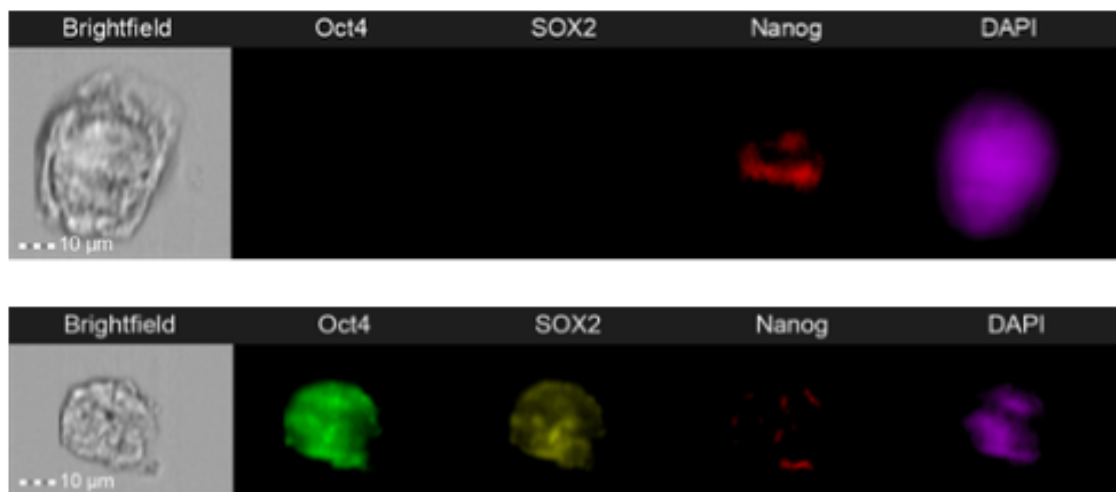


Figure 3.8 Imagestream images to demonstrate expression of Oct4, SOX2 and Nanog in two different Mesenchymal Stem Cells. The first cell is only positive for Nanog but the second expresses all three stem cell antigens.

Optimisation for Oct4, SOX2 and Nanog was therefore performed using induced pluripotent stem (iPS) cells, (obtained from benign prostate tissue). This optimisation was conducted during a period of two months when the Imagestream was undergoing repair, and therefore conventional FACS was used to examine different antibody dilutions applied to iPS cells (Figure 3.9, unlabelled iPS cells; Figure 3.10 and 3.11, Oct4 antibody-labelled cells; Figure 3.12 and 3.13, SOX2 antibody- labelled cells and Figure 3.14 and 3.15, Nanog antibody- labelled cells).

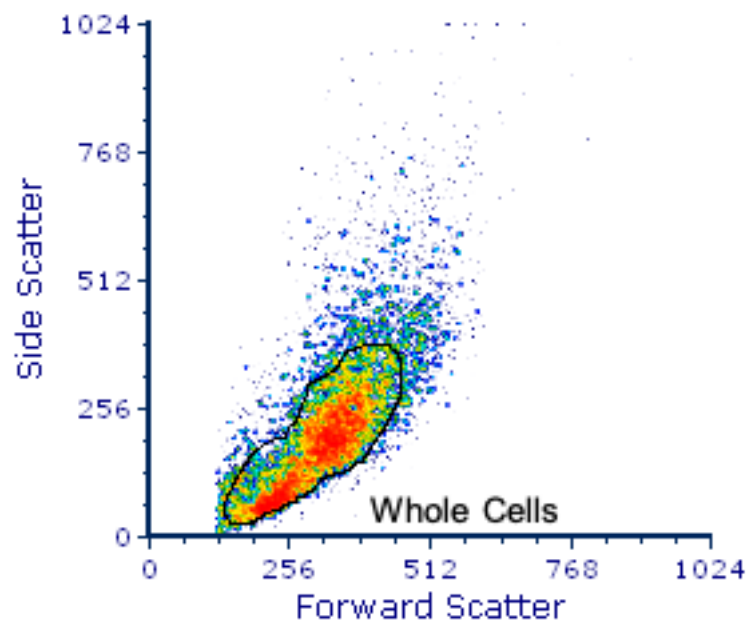
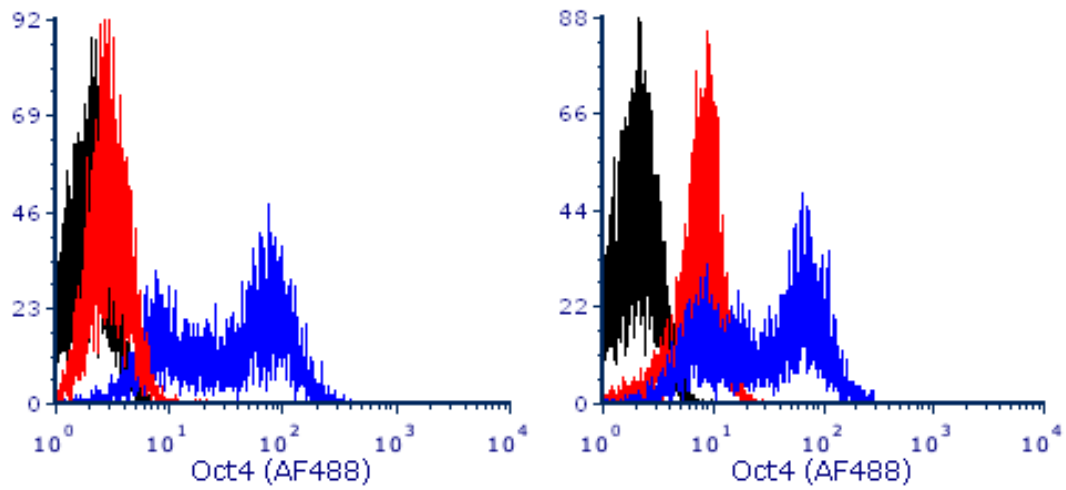
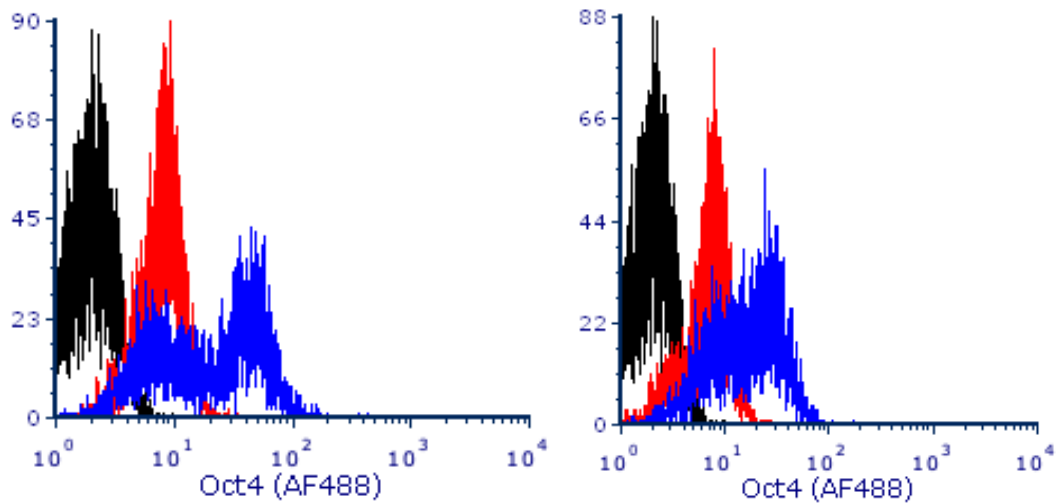


Figure 3.9 Unlabelled iPS cells gated based on size. Cells falling within this gate were counted as whole cells so that debris and doublets did not give false readings during subsequent fluorescence optimisation.



a) 1:50

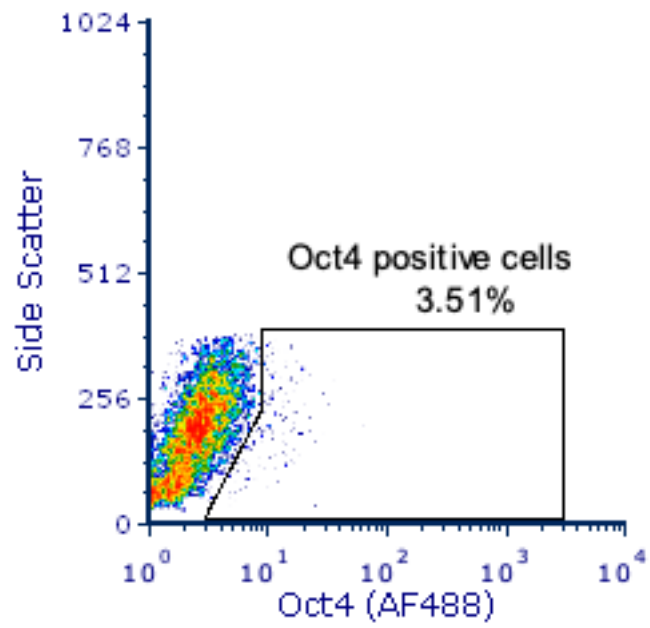
b) 1:100



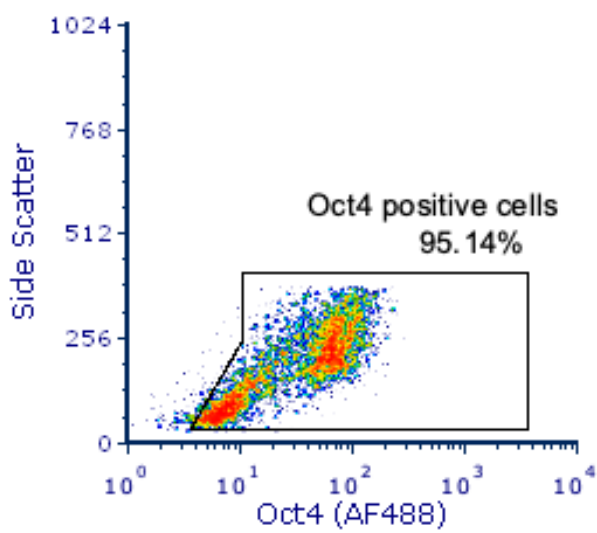
c) 1:200

d) 1:500

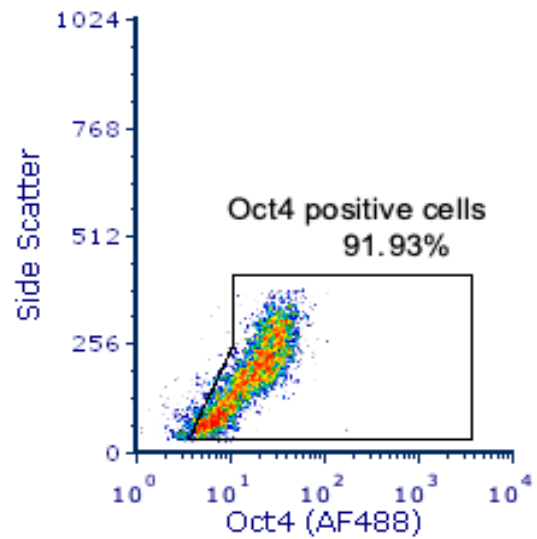
Figure 3.10 Graphs to demonstrate fluorescence in iPS cells only (black), cells with isotype control (red) and cells with Oct4 (AF488) at decreasing concentrations: a) 1:50, b) 1:100, c) 1:200 and d) 1:500. The highest concentration shows a shift in fluorescence in the majority of cells labelled with the antigen compared to the isotype and unlabelled cells but the three lower concentrations show an overlap with the negative controls.



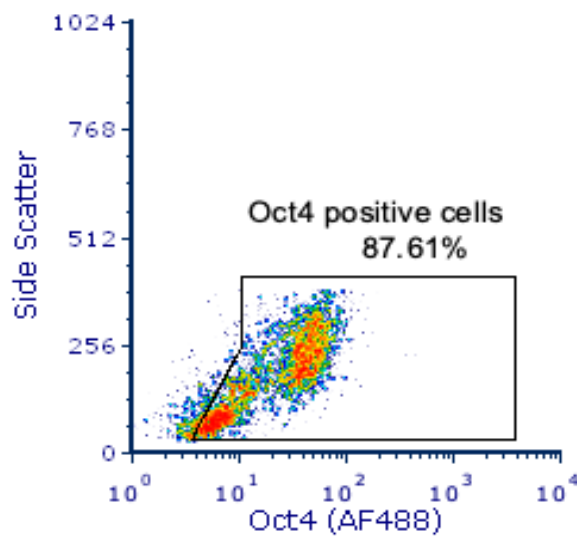
a) Cells only



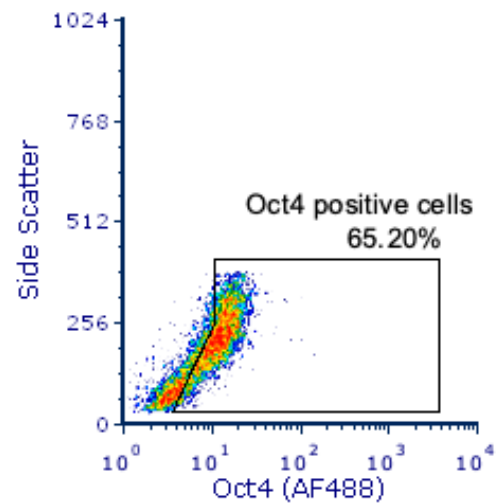
b) 1:50



c) 1:100

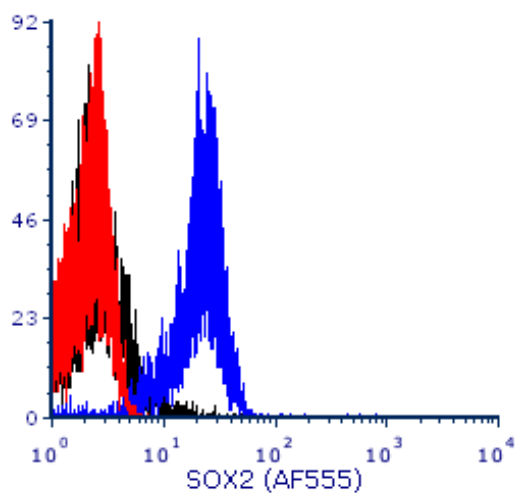


d) 1:200

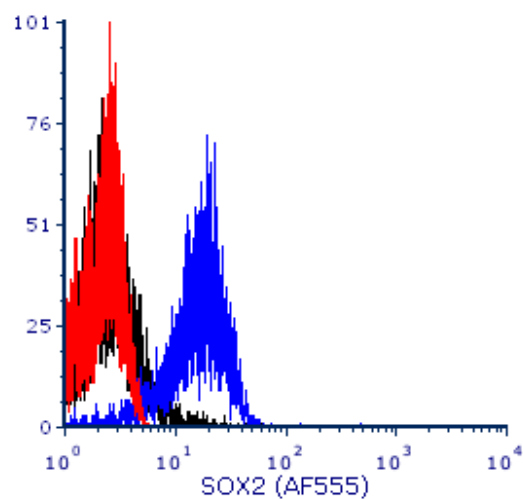


e) 1:500

Figure 3.11 Graphs to show the percentage of iPS cells that fell inside the positive gate, which was drawn by excluding the unlabelled cells as a negative control. The graphs show the fluorescence of the iPS cells with decreasing concentrations of Oct4 (AF488) antibody: b) 1:50, c) 1:100, d) 1:200 and e) 1:500.



a) 1:50



b) 1:100

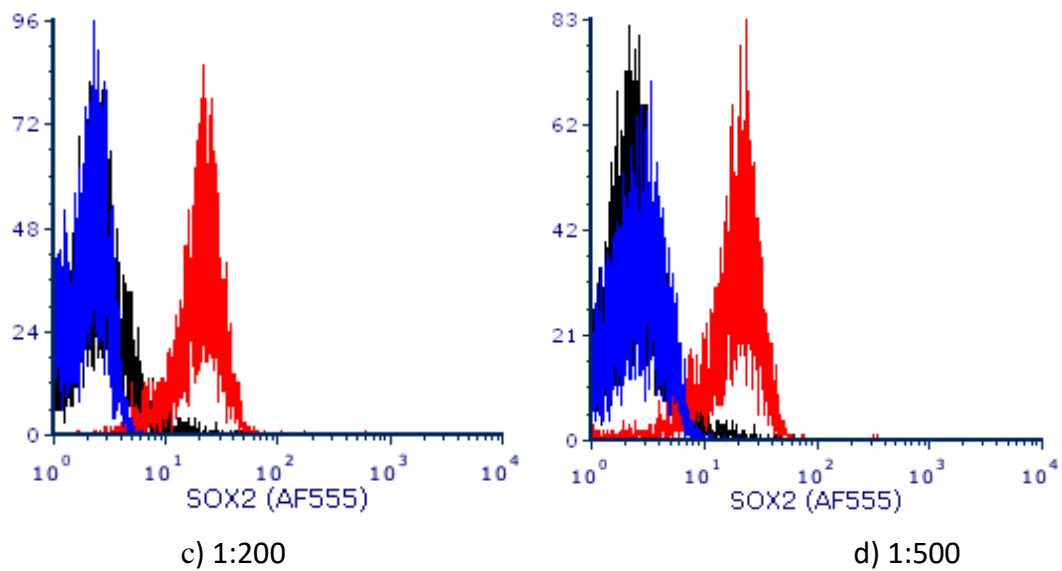
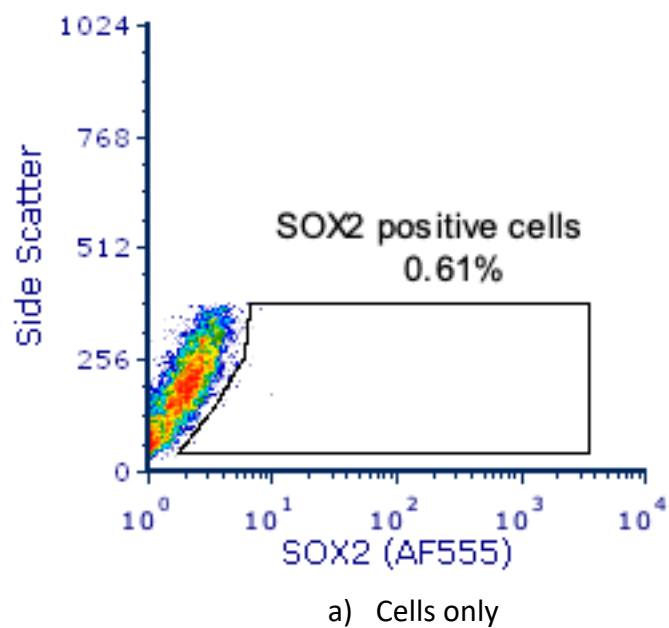
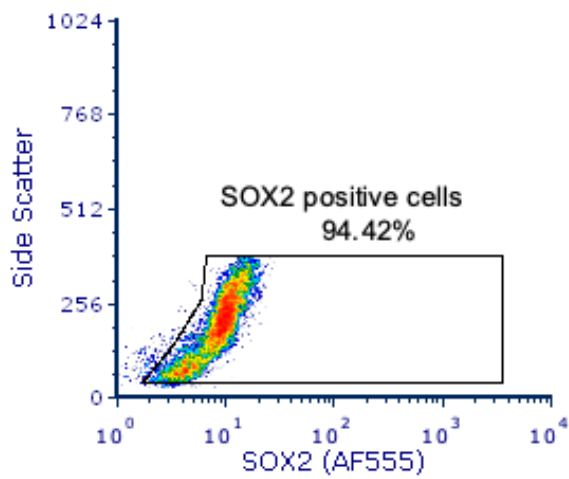
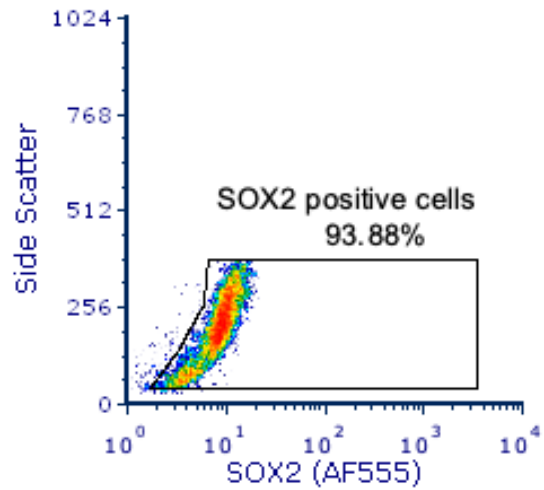


Figure 3.12 Graphs to demonstrate fluorescence in iPS cells only (black), cells with isotype control (red) and cells with SOX2 (AF555) at decreasing concentrations: a) 1:50, b) 1:100, c) 1:200 and d) 1:500. There is a clear shift in the cells labelled with the 1:50 concentration when compared to the unlabelled cells and isotype control, but an overlap with the negative controls in the lower concentrations.

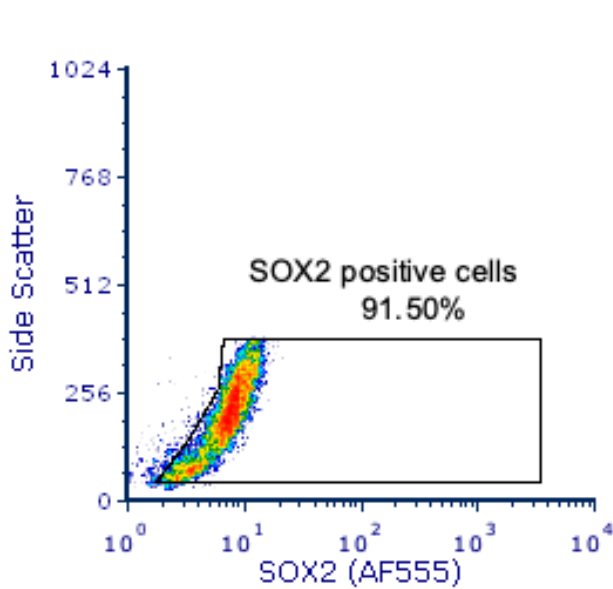




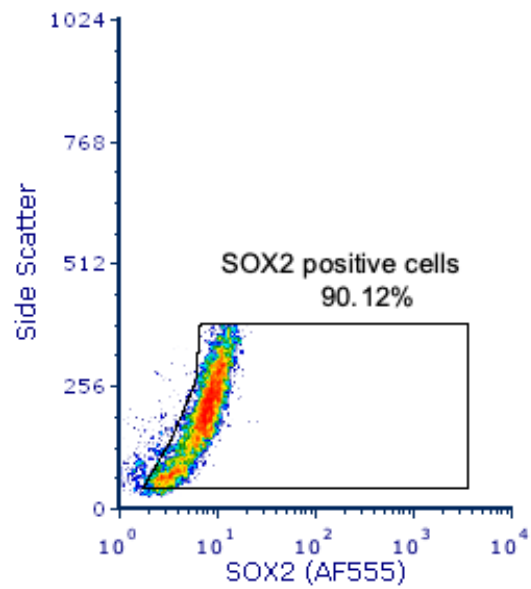
b) 1:50



c) 1:100

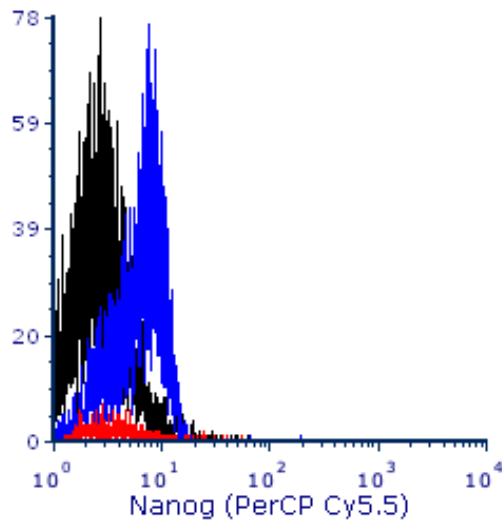


d) 1:200

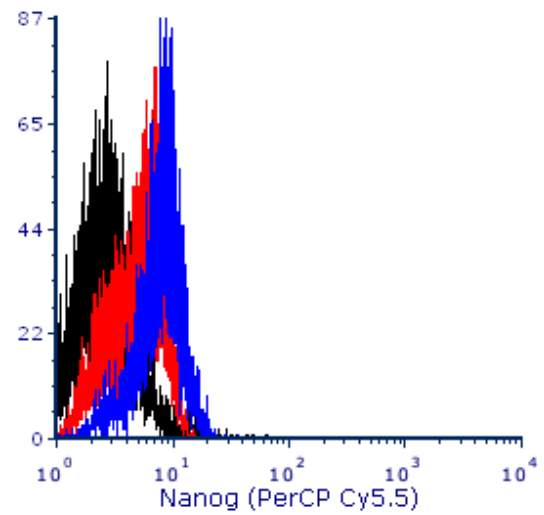


e) 1:500

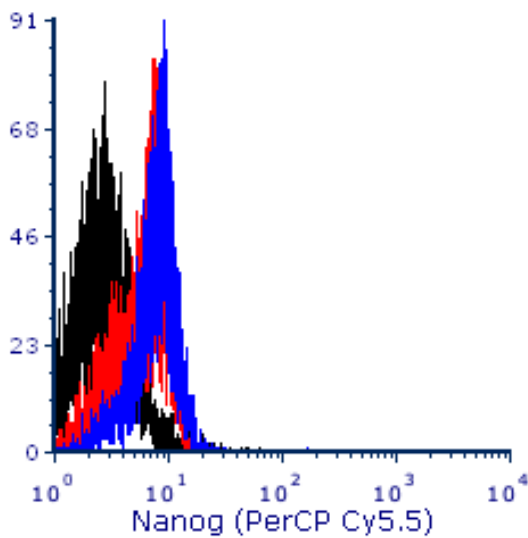
Figure 3.13 Graphs to show the percentage of iPS cells that fell inside the positive gate, which was drawn by excluding the unlabelled cells as a negative control. The graphs show the fluorescence of the iPS cells with decreasing concentrations of SOX2 (AF555) antibody: b) 1:50, c) 1:100, d) 1:200 and e) 1:500.



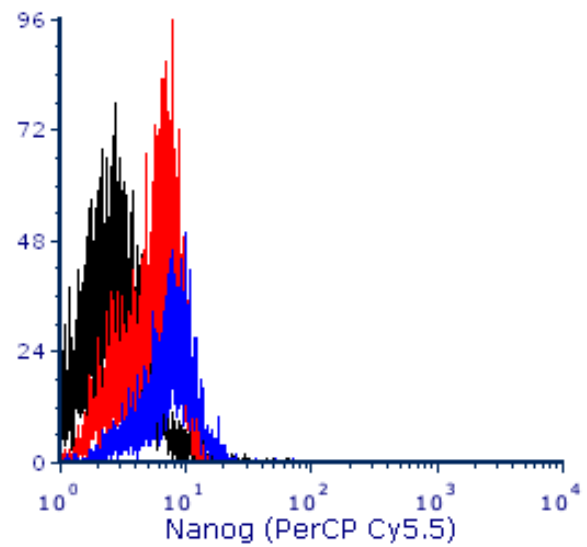
a) 1:50



b) 1:100

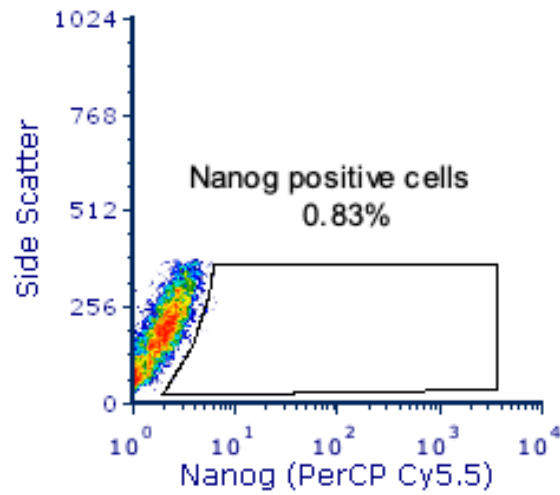


c) 1:200

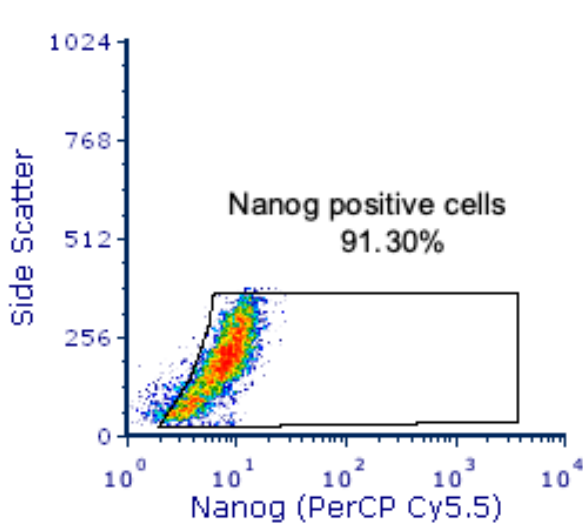


d) 1:500

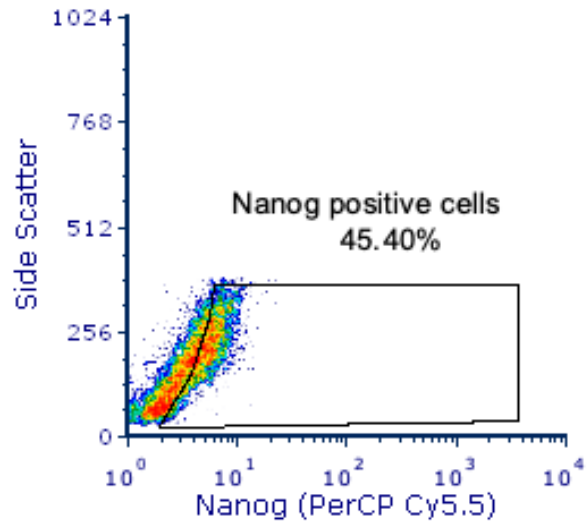
Figure 3.14 Graphs to demonstrate fluorescence in iPS cells only (black), cells with isotype control (red) and cells with Nanog (PerCP Cy5.5) at decreasing concentrations: a) 1:50, b) 1:100, c) 1:200 and d) 1:500. There is a larger overlap with the negative controls, even at the highest concentration, which was thought to be due to the pluripotency of the iPS cells.



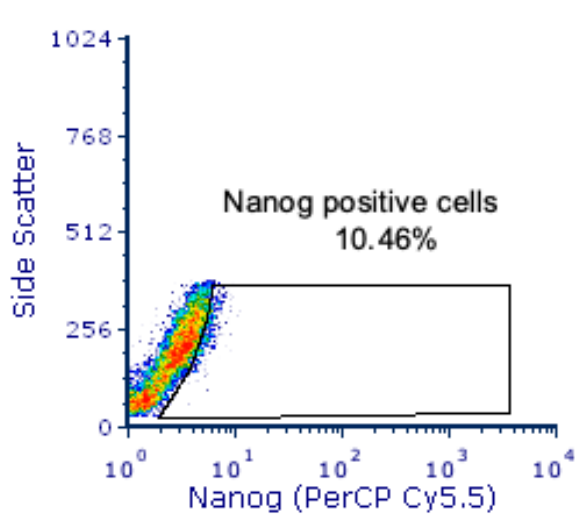
a) Cells only



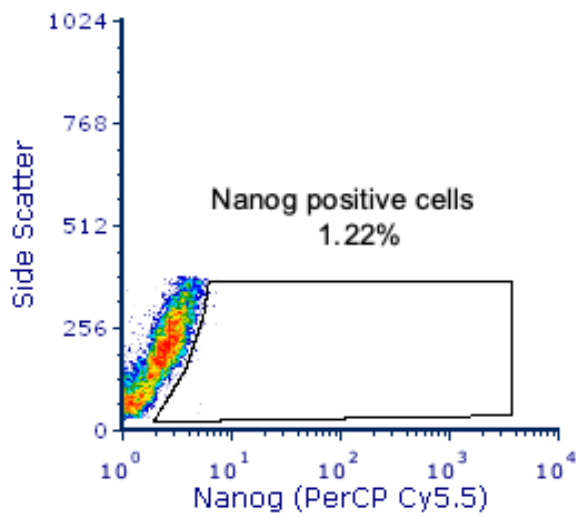
b) 1:50



c) 1:100



d) 1:200



e) 1:500

Figure 3.15 Graphs to show the percentage of iPS cells that fell inside the positive gate, which was drawn by excluding the unlabelled cells as a negative control. The graphs show

the fluorescence of the iPS cells with decreasing concentrations of PerCP Cy5.5 antibody: b) 1:50, c) 1:100, d) 1:200 and e) 1:500.

Concentration	Percentage of iPS cells staining positive at each concentration (%)		
	Oct4	SOX2	Nanog
1:50	95.14	94.42	91.30
1:100	91.93	93.88	45.40
1:200	87.61	91.50	10.46
1:500	65.20	90.12	1.22

Table 3.5 A Table demonstrating the percentage of iPS cells staining positive for each antibody at increasing concentrations.

There was a significant drop in the number of cells expressing both Oct4 and Nanog at lower concentrations of the antibody (Table 3.5). This could potentially be explained by the heterogeneity of the iPS cells, despite early passage. When looking at the Nanog experiment, there was evidence of a significant degree of overlap when using the isotype control at all concentrations (less so in the 1:50 concentration for which the opposite would be expected, but the number of cells seem to be lower which is an error of the experiment). A compromise needs to be reached and the benefit of ultimately using the Imagestream^X is that each positive image can be scrutinised visually, to ensure that the location of the positive stain is appropriate (in this case it should be nuclear).

Based on these experiments, a concentration of 1:50 (2µl) was used for each of the antibodies Oct4, SOX2 and Nanog.

3.4.3 Antibody optimisation of CD45 and DAPI

DAPI and CD45 (PECy7) had been optimised by the NICR team and the concentrations of these were kept the same; 1:500 for DAPI and 1:50 for CD45.

3.5 Cell size as an alternative means of detection

3.5.1 Background

As previously discussed, detection of CTCs based on size alone is difficult due to the size similarity between larger haematopoietic cells. Assuming CTCs are large means those becoming smaller whilst undergoing EMT may be missed (Yu et al., 2011). Selection methods using size-based criteria alone typically lead to a yield of less than 10% (Hao et al., 2018). The

NICR team who had done previous CTC work had used a gating strategy to capture cells based initially on size and then on fluorescence, to reduce the number of captured events and decrease file size. This was felt to be inappropriate in this assay as there is evidence from studies looking at cell size in different stages of prostate cancer that CTCs in patients with very advanced metastatic disease can be much smaller (Chen et al., 2015a). Despite cell lines being considerably larger than white blood cells, early experiments on the Imagestream using clinical samples detected a variation in size of possible prostate CTCs.

3.5.2 Cell line size

To identify prostate cell line cell size in comparison with white blood cells, 100 000 PC3 cells were spiked into 2mls of healthy volunteer blood. Two samples were prepared using the NICR Imagestream assay and the sample stained with Vimentin, CD45 and DAPI. Each sample was then run for ten minutes on either the Imagestream or conventional FACS. Fluorescence of Vimentin was used to identify true PC3 cells and these cells were then plotted with the white cells based on size (Figure 3.23).

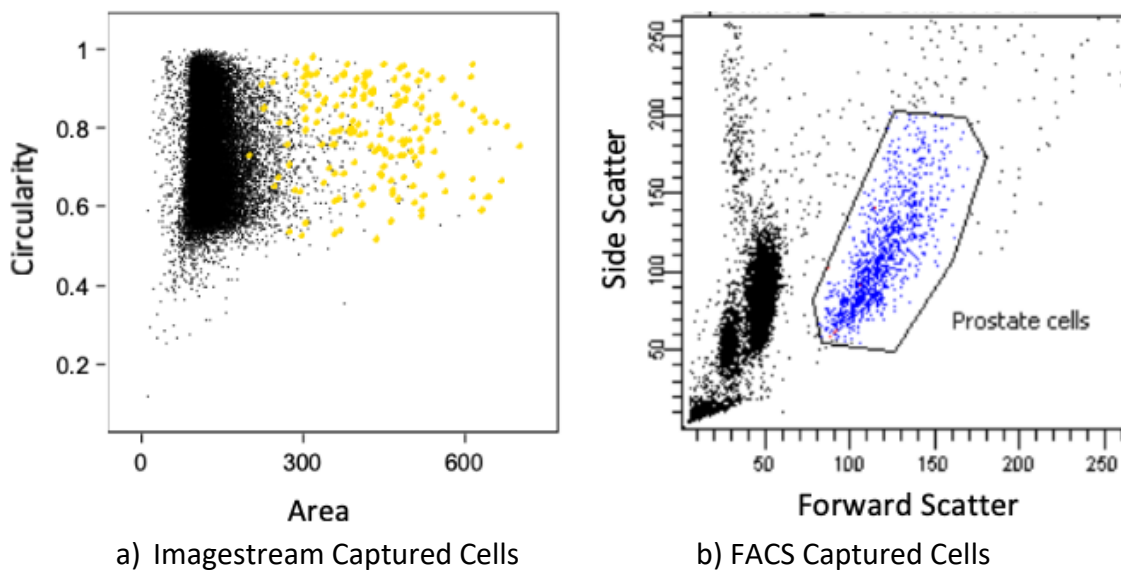
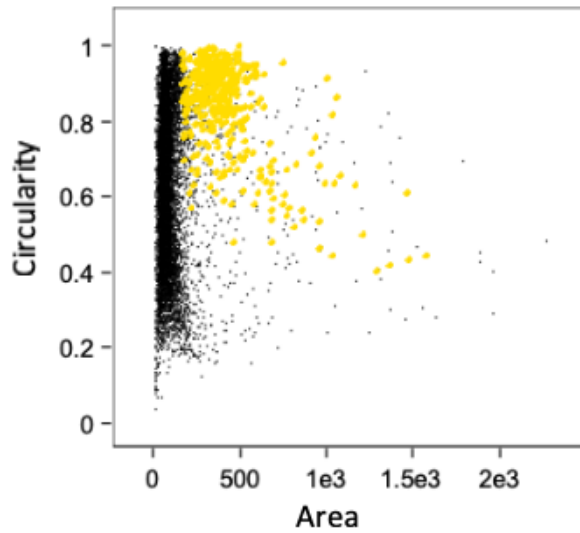
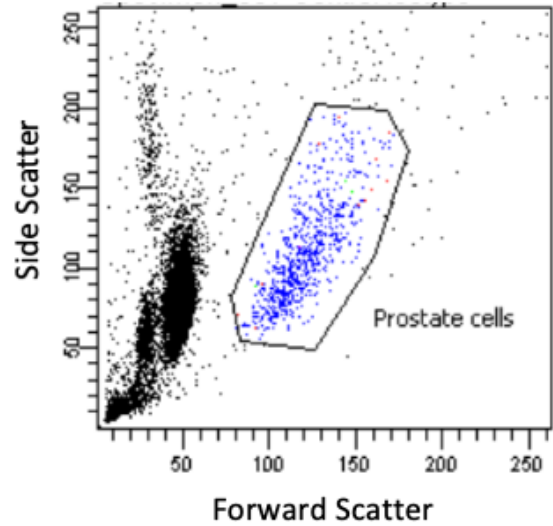


Figure 3.16 Images to demonstrate PC3 cells when run in whole blood on a) the Imagestream (yellow events) and b) conventional FACS (blue events). (Blood cells are black)

This experiment was then repeated with LNCaP cells, using EpCAM instead of Vimentin to identify the cell line (Figure 3.24).



a) Imagestream Captured Cells

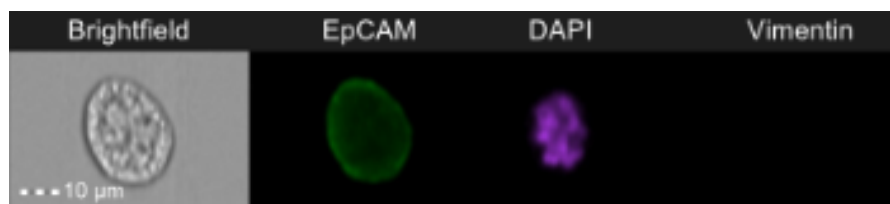


b) FACS Captured Cells

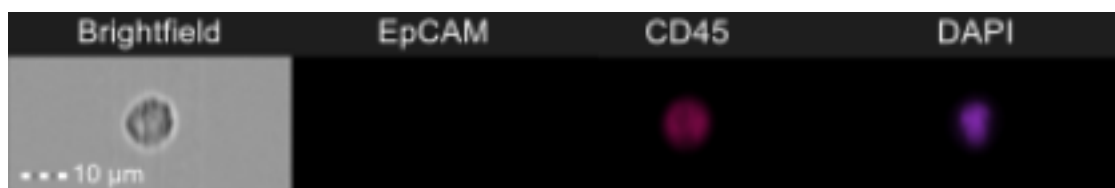
Figure 3.17 Images to demonstrate LNCaP cells when run in whole blood on a) the Imagestream (yellow events) and b) conventional FACS (blue events). (Blood cells are black).



a) a PC3 cell from the Imagestream, demonstrating that it is negative for EpCAM and positive for Vimentin



b) an LNCaP cell from the Imagestream, demonstrating that it is positive for EpCAM and negative for Vimentin



c) a CD45+ white cell

Figure 3.18 Images taken from the Imagestream to demonstrate a) a PC3 cell, b) an LNCaP cell and c) a white cell

From these graphs (Figures 3.23, 3.24) and images (Figure 3.25), it is clear that both PC3 and LNCaP cells are larger than the white blood cells. However, even with these cell lines there is a variation in size and some of the smaller cells were closer in size to the larger white cells. Gating based on size from this experiment could be appropriate, although careful re-experimentation should be performed to calculate the percentage loss of cells if considering this method, and due to low numbers of expected CTCs in clinical samples it would have to be expected that smaller cells may get missed. In order to establish whether this would be a feasible strategy in the final Imagestream assay, CTC size in clinical samples must also be explored.

3.5.3 Patient samples

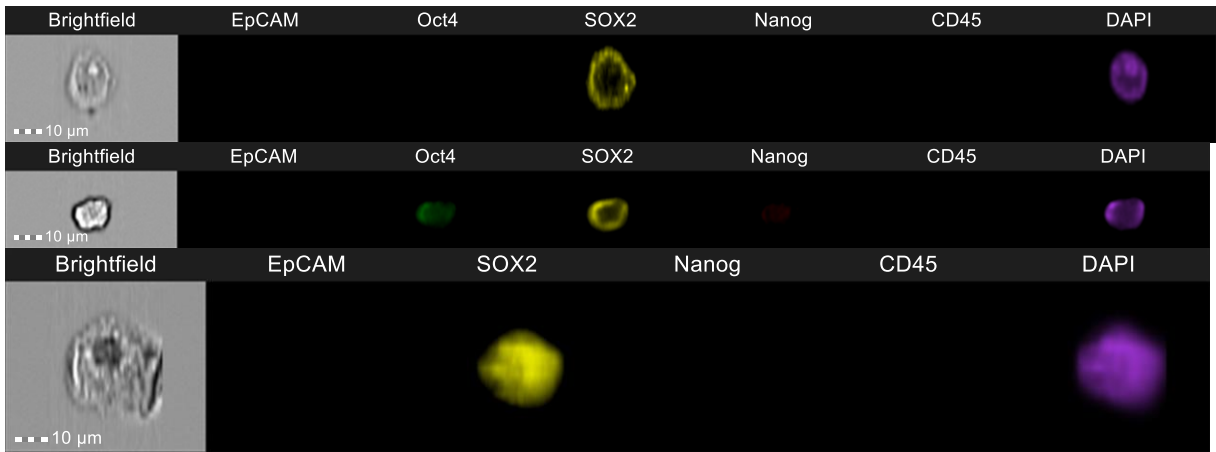
As patient samples are likely to be more heterogenous than cell lines, an observational experiment was performed on ten clinical samples that had been used at different stages during the optimization of the assay. Because these samples were run with different combinations of antibodies it was not possible to combine the data to look at overall size in graphical form. The following images were captured and show a representative variation in sizes of CTCs (Figure 3.26).



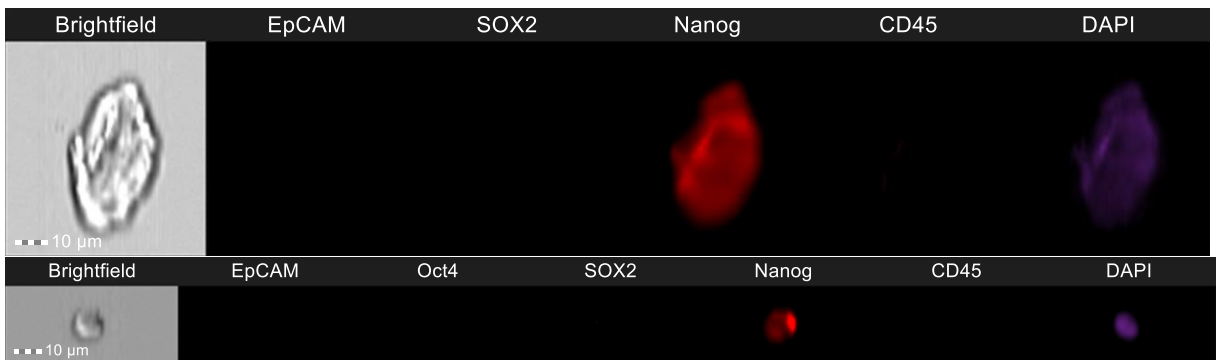
a) Two EpCAM positive cells



b) an Oct4 positive cell



c) three SOX2 positive cells



d) two Nanog positive cells



e) an Oct4 / SOX2 / Nanog positive cell



f) a white cell

Figure 3.19 Images taken from the Imagestream to show a variation in sizes of CTCs (a-e) in comparison with a white cell (f).

Because the potential number of CTCs in clinical samples is so small, it was concluded that the variation in size of CTCs found in these ten samples precluded any elimination by gating based on size. Some of the CTCs found were smaller than the white cells, and whilst there were some larger cells, a significant population could be missed.

3.6 Final Assay and Gating Strategy

3.6.1 Sample preparation

The samples were collected from patients in EDTA blood tubes and processed within four hours. A combined fixation and lysis stage was performed followed by a white cell immunomagnetic depletion. Samples were then permeabilised before the addition of antibodies.

3.6.2 Antibody selection

The following antibodies were used for this assay:

EpCAM (PE-Vio615) 1:200

Oct4 (AF488) 1:50

SOX2 (AF555) 1:50

Nanog (PerCP-Cy5.5) 1:50

CD45 (PECy7) 1:50

DAPI (1:500)

3.6.3 Imagestream Setup

Laser settings were confirmed as per table 3.6 and single colour controls were processed at the start of each week to ensure accuracy and consistent staining of antibodies.

3.6.4 Gating strategy for collection and analysis of an Imagestream file

Samples were collected using a gate to exclude CD45 positive cells and events that were DAPI negative (presumed to be debris). The gates used were set up as a template and this was applied to all clinical samples processed.

When analysing cells, all DAPI positive, EpCAM positive cells were visually inspected and included as positive events if staining was appropriate (cell membrane). DAPI positive cells displaying a threshold above $1.4e4$ (Oct4 and SOX2) and $1.6e4$ (Nanog) were also visually inspected and included if staining was appropriate (nuclear or cytoplasmic). Overall CTC count was recorded for each sample, in addition to the number of each combination of marker positive cells.

3.7 Results by patient characteristic

The following tables (Tables 3.6-3.12) show a summary of the number of cells detected by the assay described in this chapter, according to patient characteristics. Each cell expressing the combination of antigens expressed is recorded for each patient.

Patient No	Age	Treatment	PSA	EpCAM+	Oct4+	SOX2+	Nanog+	EpCAM / Oct4+ / SOX2+ / Nanog+	Oct4+ / SOX2+ / Nanog+	Epcam+ / Oct4+	Oct4+ / Nanog+	Oct4+ / SOX2+	SOX2+ / Nanog+	EpCAM+ / Nanog+	EpCAM+ / SOX2+	TOTAL
1	48	Healthy Volunteer	N/A	0	0	0	0	0	0	0	0	0	0	0	0	0
2	41	Healthy Volunteer	N/A	0	0	0	0	0	0	0	0	0	0	0	0	0
3	43	Healthy Volunteer	N/A	0	0	0	0	0	0	0	0	0	0	0	0	0
4	52	Healthy Volunteer	N/A	0	0	0	0	0	0	0	0	0	0	0	0	0
5	38	Healthy Volunteer	N/A	0	0	0	0	0	0	0	0	0	0	0	0	0

Table 3.6 A table to show the number of cells expressing each antigen for blood taken from healthy volunteers when processed using the Imagestream assay.

Patient No	Age	Treatment	PSA	EpCAM+	Oct4+	SOX2+	Nanog+	EpCAM / Oct4+ / SOX2+ / Nanog+	Oct4+ / SOX2+ / Nanog+	Epcam+ / Oct4+	Oct4+ / Nanog+	Oct4+ / SOX2+	SOX2+ / Nanog+	EpCAM+ / Nanog+	EpCAM+ / SOX2+	TOTAL
1	73	New patient – negative biopsy	9.9	0	0	5	0	0	0	0	1	0	0	0	0	5
2	79	New patient – negative biopsy	9.5	0	1	7	0	0	2	0	1	5	0	0	0	16
3	67	New patient – negative biopsy	5.6	0	0	0	0	0	0	0	0	0	0	0	0	0
4	68	New patient – negative biopsy	7.9	0	0	0	0	0	0	0	0	0	0	0	0	0
5	67	New patient – negative biopsy	7.2	0	0	0	50	0	0	0	0	0	0	0	0	50
6	70	New patient – negative biopsy	4.4	0	0	0	0	0	0	0	0	0	0	0	0	0

Table 3.7 A table to show the number of cells expressing each antigen for blood taken from patients with benign disease when processed using the Imagestream assay.

Patient No	Age	Treatment	PSA	EpCAM+	Oct4+	SOX2+	Nanog+	EpCAM / Oct4+ / SOX2+ / Nanog+	Oct4+ / SOX2+ / Nanog+	Epcam+ / Oct4+	Oct4+ / Nanog+	Oct4+ / SOX2+	SOX2+ / Nanog+	EpCAM+ / Nanog+	EpCAM+ / SOX2+	TOTAL
1	68	AS	5.3	0	0	0	0	0	0	0	0	0	0	0	0	0
2	72	AS	6.1	0	0	0	14	0	0	0	0	0	0	0	0	14
3	76	WW	27.1	0	0	0	0	0	0	0	0	0	0	0	0	0
4	84	WW	18.1	0	0	3	0	0	0	0	0	0	0	0	0	3
5	87	WW	86.0	1	0	0	1	0	0	0	0	0	0	0	0	2
6	76	AS	37.4	0	0	1	0	0	0	0	0	0	0	0	0	1

Table 3.8 A table to show the number of cells expressing each antigen for blood taken from patients on surveillance when processed using the Imagestream assay.

Patient No	Age	Treatment	PSA	EpCAM+	Oct4+	SOX2+	Nanog+	EpCAM / Oct4+ / SOX2+ / Nanog+	Oct4+ / SOX2+ / Nanog+	Epcam+ / Oct4+	Oct4+ / Nanog+	Oct4+ / SOX2+	SOX2+ / Nanog+	EpCAM+ / Nanog+	EpCAM+ / SOX2+	TOTAL
1	77	New Diag	5.2	0	0	0	303	0	0	0	1	1	1	0	0	306
2	68	New Diag	33.5	0	0	2	4	0	3	0	0	0	0	0	0	9
3	65	New Diag	18.3	0	0	1	8	0	0	0	0	0	1	0	0	10
4	74	New Diag	140.0	0	0	2	8	0	0	0	1	0	0	0	0	11
5	68	New Diag	308.0	0	1	0	6	0	1	0	12	1	0	0	0	21
6	62	New Diag	22.0	0	0	7	0	0	0	0	0	13	0	0	0	20
7	68	New Diag	47.0	0	0	1	0	0	1	0	0	0	0	0	0	2
8	69	New Diag	3.2	0	12	0	2	0	6	0	50	64	2	0	0	136

Table 3.9 A table to show the number of cells expressing each antigen for blood taken from patients with new diagnosis metastatic disease when processed using the Imagestream assay.

Pt	Age	Treatment	PSA	EpCAM+	Oct4+	SOX2+	Nanog+	EpCAM / Oct4+ / SOX2+ / Nanog+	Oct4+ / SOX2+ / Nanog+	Epcam+ / Oct4+	Oct4+ / Nanog+	Oct4+ / SOX2+	SOX2+ / Nanog+	EpCAM+ / Nanog+	EpCAM+ / SOX2+	T O T A L
1	69	Single agent	31.4	0	0	1	0	0	0	0	0	1	0	0	0	2
2	82	Single agent	1.8	0	0	0	0	0	0	0	0	0	0	0	0	0
3	71	Single agent	2.9	0	4	4	1	0	0	0	0	2	0	0	0	11
4	92	Single agent	0.2	0	0	1	0	0	0	0	1	0	1	0	0	3
5	91	Single agent	0.2	0	0	0	0	0	0	0	0	0	0	0	0	0
6	82	Single agent	50.9	0	0	0	0	0	0	0	0	0	0	0	0	0
7	87	Single agent	4.5	0	0	0	0	0	0	0	0	0	0	0	0	0
8	66	Single agent	0.1	0	0	6	0	0	0	0	0	0	0	0	0	6
9	71	Single agent	2020	0	0	34	3	0	3	0	3	0	1	1	0	45
10	77	Single agent	0.1	0	0	0	0	0	0	0	0	0	0	0	0	0
11	59	Single agent	4.5	0	0	11	1	0	0	0	0	0	0	0	0	0
12	63	Single agent	81.9	0	3	2	1	0	2	0	0	0	0	0	0	8
13	67	Single agent	3.0	0	11	0	3	0	0	0	1	3	0	0	0	18

Table 3.10 A table to show the number of cells expressing each antigen for blood taken from patients on single agent hormones when processed using the Imagestream assay.

Patient No	Age	Treatment	PSA	EpCAM+	Oct4+	SOX2+	Nanog+	EpCAM / Oct4+ / SOX2+ / Nanog+	Oct4+ / SOX2+ / Nanog+	Epcam+ / Oct4+	Oct4+ / Nanog+	Oct4+ / SOX2+	SOX2+ / Nanog+	EpCAM+ / Nanog+	EpCAM+ / SOX2+	TOTAL
1	86	MAB	245.6	84	2	0	2	0	1	0	0	1	0	0	0	90
2	84	MAB	61.4	1	0	0	1	0	0	0	0	2	0	0	0	4
3	79	MAB	1.5	0	0	0	0	0	0	0	0	0	0	0	0	0
4	87	MAB	3.1	0	0	0	185	0	0	0	0	0	0	0	0	185
5	82	MAB	24.0	0	2	5	0	0	0	0	0	1	0	0	0	8
6	77	MAB	101.0	0	1	1	11	0	0	0	1	1	0	0	0	15
7	78	MAB	1.5	0	0	0	0	0	0	0	0	0	2	0	0	2
8	69	MAB	1.8	0	0	1	0	0	0	0	0	0	0	0	0	1
9	86	MAB	12.6	0	0	2	0	0	0	0	0	0	0	0	0	2
10	83	MAB	0.1	0	0	1	0	0	0	0	0	0	0	0	0	1
11	83	MAB	23.4	0	1	0	2	0	0	0	0	0	0	0	0	3
12	74	MAB	2.0	0	0	25	36	0	1	0	0	0	0	0	0	62
13	96	MAB	34.6	0	2	57	0	1	0	0	0	0	2	0	0	62
14	80	MAB	1.7	0	0	7	0	0	0	0	0	0	0	0	0	7
15	73	MAB	5.5	0	0	40	1	0	0	0	0	0	0	0	0	41
16	65	MAB	30.6	0	0	0	4	0	0	0	6	1	0	0	0	11

Table 3.11 A table to show the number of cells expressing each antigen for blood taken from patients on maximum androgen blockade when processed using the Imagestream assay.

Pt No	Age	Treatment	PSA	EpCAM+	Oct4+	SOX2+	Nanog+	EpCAM / O/S/N	O/S/N	Epcam+ / Oct4+	Oct4+ / Nanog+	Oct4+ / SOX2+	SOX2+ / Nanog+	EpCAM+ / Nanog+	EpCAM+ / SOX2+	Total
1	77	Enzalutamide	1875	4	0	2	0	0	8	0	0	0	0	1	0	15
2	68	Docetaxel	0.8	0	0	0	14	0	0	0	0	0	0	0	0	14
3	85	Dexamethasone	55.0	0	8	9	22	0	0	0	0	0	0	0	0	39
4	69	Enzalutamide	380	11	0	1	3	0	0	0	1	3	0	0	0	19
5	77	Dexamethasone	18.0	0	0	3	12	0	0	0	3	0	0	0	0	18
6	61	Abiraterone	51.2	0	0	0	3	0	0	0	1	0	0	0	0	4
7	60	Enzalutamide	0.7	0	1	0	68	0	0	0	9	0	0	0	0	78
8	74	Dexamethasone	0.7	0	0	0	6	0	5	0	3	0	0	0	0	14
9	73	Dexamethasone	23.0	0	0	5	4	0	0	0	3	0	0	1	0	13
10	77	Docetaxel	433	0	2	66	5	0	0	0	0	0	0	0	0	73
11	58	Enzalutamide	12.4	2	5	0	1	0	3	1	4	2	0	0	0	18
12	87	Cabazitaxel	5.6	20	2	3	0	0	2	0	0	1	0	0	0	28
13	70	Dexamethasone	228	0	0	3	12	0	0	0	3	0	0	0	0	18
14	82	Enzalutamide	72.4	0	1	0	0	0	0	0	0	1	0	0	0	2
15	74	Abiraterone	16.3	0	1	0	2	0	0	0	0	1	0	0	0	4
16	74	Docetaxel	8.0	0	0	49	0	0	22	0	0	4	0	0	0	75
17	72	Enzalutamide	586	20	1	0	0	0	1	0	1	0	0	0	0	23
18	69	Radium 223	202	0	0	0	0	0	0	0	0	2	0	0	0	2
19	80	Enzalutamide	2.2	0	0	2	10	0	0	0	0	0	0	0	0	12
20	74	Enzalutamide	1.3	6	12	41	6	0	2	0	0	2	0	0	0	69
21	76	Dexamethasone	0.8	0	0	5	0	0	0	0	0	0	0	0	0	5
22	51	Enzalutamide	434	0	0	3	0	0	2	0	0	2	0	0	0	7
23	58	Docetaxel	100	0	8	3	0	0	6	0	2	2	0	0	0	21
24	76	Enzalutamide	4611	0	4	0	0	0	0	0	0	0	0	0	0	4
25	77	Radium 223	29.2	2	0	10	0	0	2	1	0	10	0	0	0	25
26	66	Enzalutamide	21.0	0	0	0	0	0	0	0	0	0	0	0	0	0
27	72	Enzalutamide	532	0	0	0	2	0	0	0	0	0	0	0	0	2
28	81	Radium 223	96.1	0	2	0	0	0	0	0	0	0	0	0	0	2
29	78	Dexamethasone	10.5	0	0	0	0	0	0	0	0	0	0	0	0	0

Table 3.12 A table to show the number of cells expressing each antigen for blood taken from patients with castrate resistant disease when processed using the Imagestream assay.

3.8 Discussion

The Imagestream offers a unique opportunity to sort cells using conventional FACS techniques in addition to visualising individual cell images, which gives it a unique advantage when testing the validity of a new assay. The ability to use up to six different fluorochromes has enabled a novel assay to be developed, looking at a combination of epithelial and stem cell markers, which has not been previously been conducted in prostate cancer CTCs.

The decision not to include a prostate specific marker was made as it was not felt it could reliably identify prostate cancer cells. An alternative method would have been to have split each sample and run a different combination of epithelial, stem cell and prostate specific markers. This was considered but due to processing and analysis time it was felt that this would compromise the overall number of samples that could be obtained and processed, and could ultimately reduce the impact of any findings. The experiment looking at epithelial marker expression demonstrated that in up to 36% of the samples there were cells that were epithelial marker negative, which strengthens the argument for looking at alternative antigens. Although a mesenchymal marker could not be added in addition to the chosen combination, this will be explored in Chapter 4 and will address the population of cells that could be undergoing EMT.

The cell line retrieval experiment to test the assay developed by the NICR team identified a considerable difference in retrieval between the two different cell lines. Whilst the PC3 retrieval rate is higher than the mean rate for the previously tested cancer cells tested using the NICR assay (oesophageal, hepatocellular, ovarian and thyroid), the LNCaP numbers are lower. Cell fragility could account for the variation. Whilst cell lines are useful in assay development, heterogeneity between cell lines and clinical samples, and between each clinical sample will mean the actual retrieval rate of each clinical sample will be unknown. This would actually be the case for any assay using clinical samples on any platform, and as this study is not looking at enumeration but presence or absence of expression of markers, the results of this experiment are reassuring enough for this assay to be used for this study. The antibody optimisation was performed using cell lines to ensure reproducibility. As with any optimisation, the actual cells of interest in the clinical samples will express the antigens

differently compared to the cell lines or synthetic beads used during optimisation. This needs to be acknowledged but even if multiple cell lines are used and an average taken, this still won't negate this, and indeed there is likely to be heterogeneity within the cell population of interest in the clinical sample. When looking at the presence of stem cell markers in healthy blood, there was an overlap between some of the CD45 negative / Nanog positive cells (presumed to be CTCs). This may mean a loss of potential CTCs if setting a threshold to exclude any white cells. Although a lower threshold could be used, and then cells could be visually inspected, because of the number of cells, this would be impractical. Setting the threshold at the decided level for Nanog is a limitation of this assay but a high number of false positives was felt to be worse than potentially missing a small number of cells.

The Nanog results could also be affected by the Nanog optimisation. Even at the 1:50 concentration, only 86% of the cell line was positive. Although this had been attributed to iPS cell heterogeneity, it could be that the antibody needed to be at a higher concentration. However, a 1:25 experiment was performed (results not shown) and there was too much overlap between the isotype control and antibody experiments. Therefore a compromise was reached, and ultimately it is hoped that only a small subset of CTCs are missed as a result of this.

The gating strategy is important as whilst ideally as many cells as possible would be captured when running the experiments, the file size needs to be manageable. A small number of early experiments was lost due to the inability to open the file after an inappropriate gating strategy was employed. Visual inspection of cells not captured by the gates, or close to the threshold was performed prior to the final gate template being applied to ensure accuracy. This assay has been developed from an existing protocol used by colleagues looking at different cancers. Experiments looking at the pros and cons of different antibody combinations were used before deciding on the ultimate panel. Rigorous antibody optimisation and a personalised Imagestream set-up including careful fluorochrome choice, controls and gating have ensured that this new assay will detect as many CTCs as possible in clinical samples from patients with metastatic prostate cancer.

Chapter 4. The role of multi-channel FACS in the detection and analysis of CTCs in metastatic prostate cancer

Chapter Summary

This chapter discusses the reason for exploring the role of a multi-channel FACS assay in the detection of CTCs from patients with metastatic prostate cancer. This novel assay development, using a combination of epithelial, mesenchymal and stem cell markers on the BD FACS Fusion is described. This includes the choice of antibodies used, cell line optimisation, gating strategies and options for downstream analysis. The pros and cons of this assay are also discussed, and the final assay outlined prior to the results, which can be found in Chapter 5. Because the FDA definition of a CTC does not include cells that express Oct4, SOX2 and Nanog, any cells described in this chapter that are EpCAM positive and/or express any of these three stem cell antigens are deemed putative CTCs.

4.1 Platform choice

4.1.1 Background

Whilst the Imagestream offers the ability to visualise cells that have been sorted fluorescently, it does have limitations. The benefits of being able to visualise cells to ensure appropriate staining are huge, especially when developing a new assay. However, the number of lasers (4) limits the number of antigens that can be investigated, the running time of the sample is relatively long and laborious, file size means cells need to be gated before capture so the whole sample can't be analysed, and the analysis itself is very time consuming. Samples are not retrievable so downstream analysis is not possible and when exploring the potential of a new assay to be used in clinical settings, few institutions will possess an Imagestream.

In contrast, conventional FACS is a well-established method of cell sorting and most large institutions will have access to a machine, either in a hospital setting or related academic establishment. Processing and analysis of samples is relatively quick, and file size is not a limitation, so all data can be saved, with subsequent analysis used to eliminate unrequired information. The downside of FACS is the potential to have false positives. Debris or cells

that have stuck to the wrong fluorochrome can be included in gates that would give a disproportionately high number of positive events. Whilst it is possible to reduce this error to some degree (e.g. gating out doublets using size-based criteria) when looking at a small population of cells such as CTCs, this could lead to a significant over-estimation. One way to circumvent this is to use FACS cell sorting and downstream analysis on the cells. The population of interest could then undergo DNA or RNA extraction for sequencing, or be put onto a slide for conventional immuno-fluorescence. Whilst this would mean a considerable volume of work, during the development of the assay it would ensure validation, and a margin of error could be calculated for the over-estimation of CTC count. If acceptable, this downstream analysis could subsequently be negated.

4.1.2 Choice of Platform

Again, from a logistical perspective one of the available platforms at Newcastle University was chosen. The BD FACS Fusion has five lasers (UV 355 nm, Violet 405nm, Blue 488nm, Yellow/Green 561nm and Red 635 nm) which would comfortably allow ten fluorochromes to be used simultaneously, without any concern about significant overlap (Table 4.1). It has the option to sort into Eppendorfs, multi-well plates or onto slides. This was the chosen platform for development of this assay.

	Laser				
	UV 355nm	405nm	488nm	561nm	642nm
Example	BUV 395	BV421	FITC	PE	APC
Dyes	DAPI	V450	AF488	PE-Dazzle	APC-Cy7
	Hoechst Blue	DAPI	Brilliant Blue 515	AF555	APC-H7
	BUV 737	Pacific Blue	GFP	PE-Cy7	AF647
		BV510	YFP	PE-Cy5.5	AF700
		BV605	Zombie Green		Draq5
		BV650	PerCP-Cy5.5		
		BV711			
		BV786			

Table 4.1 A Table to demonstrate the available lasers on the BD FACS Fusion at Newcastle University Medical School's Flow Cytometry Core Facility, and the suggested fluorochromes (adapted from the Newcastle University FCCF website).

4.2 Antigen expression and choice of antibodies

4.2.1 Number of channels and choice of antigens

Unlike in the Imagestream assay when the number of antigens was limited to six, the extra laser and lack of brightfield images gives the option for including an additional four antibodies. Choosing an antibody panel must take into account overlap of fluorescence, what is commercially available and the use of reliable fluorochromes where possible. Despite the antibody options in Table 4.1, not all fluorochromes give a consistent emission and are therefore less reliable than others.

Some of the more common antigens are commercially available directly conjugated to a range of fluorochromes yet some of the rarer antigens are only available either unconjugated or conjugated to a limited number of fluorochrome types. Buying directly conjugated antibodies not only ensures consistency but reduces the error that could be introduced by adding a secondary fluorochrome. Although laser settings and antibodies should be routinely tested at regular intervals to ensure no fluorescent decay, when buying the antibody and fluorochrome to conjugate, the combined product must also be tested to

ensure consistency in fluorescence. This can be improved upon by using a conjugation kit, so that a stock of the combined antibody/fluorochrome can be made at any one time, but this can be expensive.

The optimal final antibody panel was decided upon by finding directly conjugated antibodies for the rare antigens first, then choosing fluorochromes with minimal overlap for the more common antigens. Only one antibody (MT1-MMP) was not available as a commercial conjugate.

4.2.2 The decision not to use a prostate specific antibody

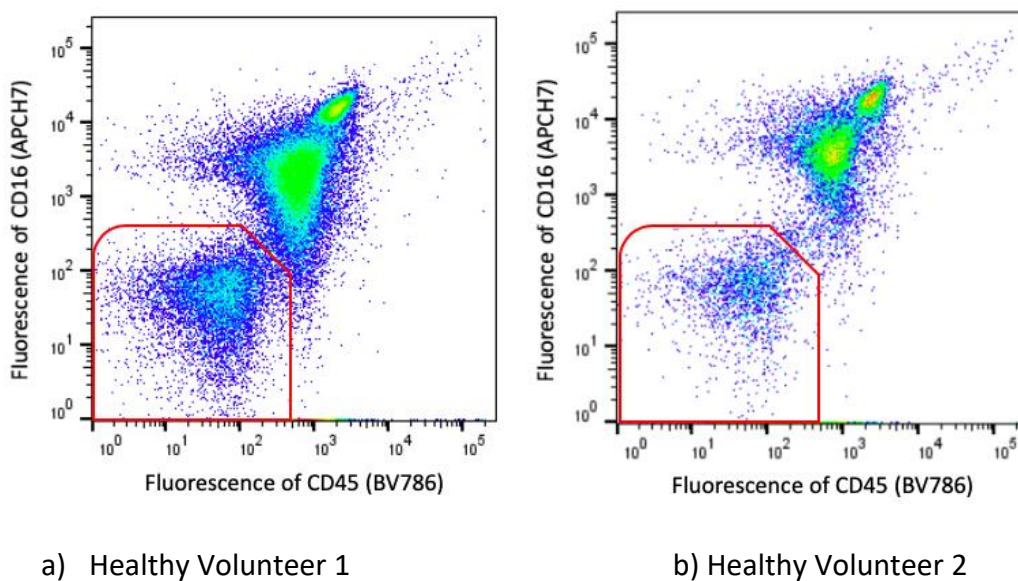
Although four extra channels were available to use in this assay compared to the previous assay on the Imagestream, again the decision was made not to include a prostate specific antibody. The reasons for this were the same as previously, in that heterogeneity of PSA and the Androgen Receptor (the most obvious choices to use as markers) in patients with advanced disease would not enable reliable identification of prostate cancer cells. Both EpCAM and Cytokeratin were included, so that the small proportion of EpCAM- epithelial cells could be correctly identified (and cells could therefore meet the FDA definition for a CTC). In addition to this, exploration of mesenchymal markers was desired and inclusion of Vimentin and MT1-MMP in this assay, the latter of which can induce epithelial to mesenchymal transition in prostate cancer cells, allowed a novel combination of epithelial, mesenchymal and stem cell markers to be studied; this had not been performed previously in metastatic prostate cancer.

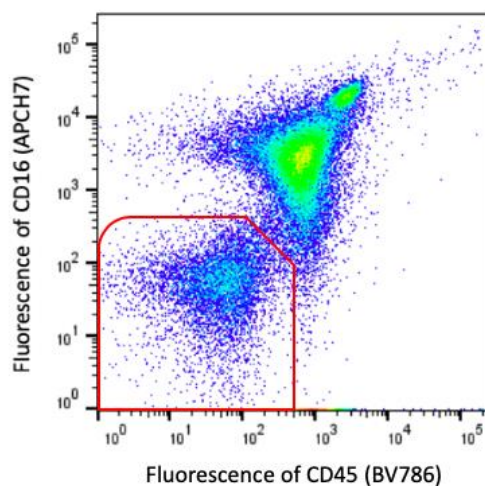
4.2.3 White cell markers

The final additional channel was used for a second white cell marker. In the Imagestream assay, the thresholds for Oct4, SOX2 and Nanog in haematopoietic cells were found to be lower than in CTCs. Because visual inspection of these cells to confirm whether the 'positive' population are CTCs is not possible using this assay, it would not be possible to reliably repeat this experiment, and so a second white cell marker was chosen. Whilst the majority of haematopoietic cells would be positive for both markers, the use of a second marker would hopefully identify a small population of cells that didn't bind to one of the white cell antibodies. Labelling as many cells as possible to exclude them as CTCs would make the assay more robust.

CD16 was chosen as the second white cell marker, used in addition to CD45. Whilst CD45 is also known as the common leucocyte antigen and is expressed on all human white cells (Altin and Sloan, 1997) CD16 is a surface marker found on macrophages, monocytes, neutrophils and natural killer cells (Janeaway, 2001). It would appear from looking at other studies in the literature, CD16 is often used as a second white cell marker to CD45 as combining the two antibodies will detect the highest number of white cells (Fujimoto et al., 2000, Kahng et al., 2015).

An experiment was performed to identify how distinct the white cell population using these two markers. 500 000 cells from each of three different cell lines (PC3, MCF7 and LNCaP) were added to 2mls of Healthy Volunteer Blood. Prior experimentation proved that none of these cell lines expressed CD45 or CD16. The blood then underwent lysis, fixation, permeabilisation and the following antibodies added: CD45 (BV786), CD16 (APC-H7), Pan-cytokeratin (PECy7), EpCAM (BV650) and Vimentin (AF647). All antibodies were directly conjugated to the fluorochromes described. This was repeated three times and all three samples were then processed on the FACS Fusion (a-c) (Figure 4.1).





c) Healthy Volunteer 3

Figure 4.1 Three dot plots to show the CD45/CD16 negative population when three cell lines were added to blood from three healthy volunteers and stained with CD45 and CD16 antibodies. The cells within the red gate are negative for both CD45 and CD16.

From these graphs it is clear that the majority of the white cells are positive for both markers but that there are tails within the population, indicating that some white cells are only positive for one or the other. This demonstrates the importance of having two white cell markers. Exact proportions of unlabelled cells will be explored in the next section during the antibody optimisation.

Although the cells within the gate are the negative population (PC3, LNCaP and MCF7 cells) there is a degree of overlap between these cells and the white cell population. Because each cell in this and the final assay will be exposed to a combination of antibodies it should be possible to determine if the cells here are white cells or not by looking at their fluorescence. However, this will be a limitation of the final assay as it will not be able to determine the difference between white cells that haven't attached to either antibody, or CTCs that are negative for all the chosen markers. Because of the variation and number of different antibodies used it is hoped that this population will be very small. This will be explored in the next section.

4.2.4 Epithelial antigens

As already mentioned, because of the availability of additional channels, Cytokeratin was included in addition to EpCAM, so that cells displaying only one of these markers could still be detected, but also because those fulfilling full FDA criteria (EpCAM+/CK+/CD45- and

nucleated cells) could be counted. This would allow comparison of this assay with those in the literature.

4.2.5 Mesenchymal antigens

Whilst prostate cancer is of epithelial origin, the use of a mesenchymal antibody could help detect cells which have undergone epithelial to mesenchymal transition. There is the option of choosing an established mesenchymal marker such as N-cadherin or Vimentin (Armstrong et al., 2011, Satelli et al., 2017, Gravdal et al., 2007), or a marker more specific to EMT such as Twist1 or Zeb1 (Kong et al., 2011, Thiery and Sleeman, 2006, Christiansen and Rajasekaran, 2006). Given the propensity of prostate cancer to metastasize to bone, using a more unconventional marker such as membrane type-1 matrix metalloproteinase (MT1-MMP) could potentially provide a greater understanding of disease pattern (Bonfil et al., 2007) (Trudel et al., 2008). As the cellular results will be correlated with clinical data on disease progression, using this as a mesenchymal marker may provide new information. MT1-MMP has therefore been chosen as the mesenchymal marker so that its role as a potential biomarker in metastatic prostate cancer can be explored.

4.2.6 Stem cell antigens

The same three stem cell antigens that were used in the Imagestream assay were chosen for use in this FACS assay. This would enable comparison of the presence or absence of these markers using the two assays but would also hopefully identify a population of cells that might be both negative for epithelial and mesenchymal markers.

4.2.7 Final antibody panel

The following antibodies (Table 4.2) were chosen. All were directly conjugated to the associated fluorochrome except MT1-MMP. This was conjugated in the lab using a kit, and a stock solution made. The fluorescence of this was tested each time by both FACS and Imagestream to ensure consistency.

Antibody	Laser	Fluorochrome	Isotype Control	Manufacturer
EpCAM	405 670/30	BV650	IgG1 λ	BD Biosciences
Cytokeratin	561 586/15	PE Cy7	IgG1	2BScientific
Vimentin	640 670/30	AF647	IgG1	Santa Cruz
MT1-MMP	561 586/15	PE	IgG1 κ	Merck Millipore
Oct4	405 450/50	BV421	IgG1 κ	BD Biosciences
SOX2	488 530/30	FITC	REA 320	Miltenyi
Nanog	488 530/30	PerCP Cy5.5	IgG1 κ	BD Biosciences
CD45	405 780/60	BV786	IgG1 κ	BD Biosciences
CD16	640 780/60	APC H7	IgG1 κ	BD Biosciences

Table 4.2 A table to list the antibodies, corresponding fluorochromes, and isotype controls chosen for this assay

4.2.8 Overlap of expression

Care was taken to ensure that the chosen fluorochromes had minimal overlap (Figure 4.2). By using the five lasers, and ensuring careful compensation, overlap or bleed between channels was reduced to a minimum. This ensured that the results could be as accurate as possible.

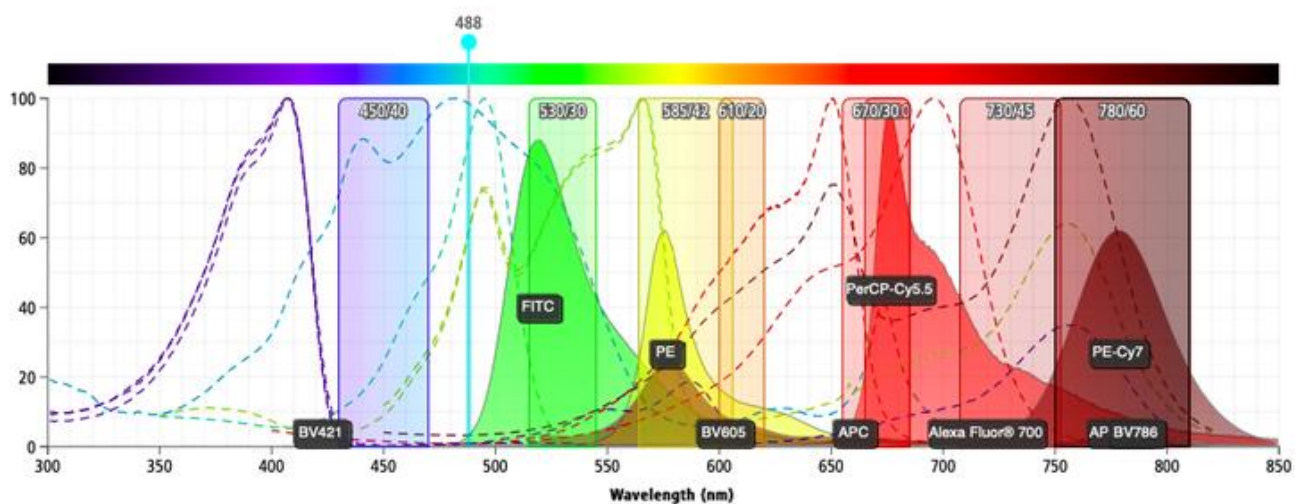


Figure 4.2 Graphs to demonstrate the excitation (dotted line) and emission (solid block) wavelengths of the fluorochromes conjugated to the antibodies used in this assay (courtesy of BD Biosciences)

4.3 Optimisation of antibodies

4.3.1 Introduction

All concentrations of antibodies were optimized based on concentrations recommended by the manufacturer. Set numbers of cells were used, and as the optimisation was performed on the Imagestream all cells were permeabilised in 100µl of PermWash or suspended in 100µl of flow buffer if the antigen was on the cell membrane. They were then washed and resuspended in 200µl of flow buffer and all processed on the Imagestream.

4.3.2 White cell antigens

The optimisation of the white cell antigens (CD45 and CD16) must be done per volume of cells rather than volume of blood, to account for the variability of the number of white cells in a patient's blood. This is particularly relevant when considering patients who are immunocompromised, or those who may have an immune response (leucocytosis) to tumour growth or a specific treatment.

Blood was obtained from three healthy volunteers and fixation and red cell lysis was performed. 10^6 cells were counted using the haemocytometer. Four separate volumes of the antibody were added to a standardised volume of cells in solution, and matching concentrations of the isotype control were added to matching blood samples. Cells with no

staining, cells with the isotype and cells with the antibody were then processed on the Imagestream. Results from all three samples were combined in the following graphs (Figure 4.3).

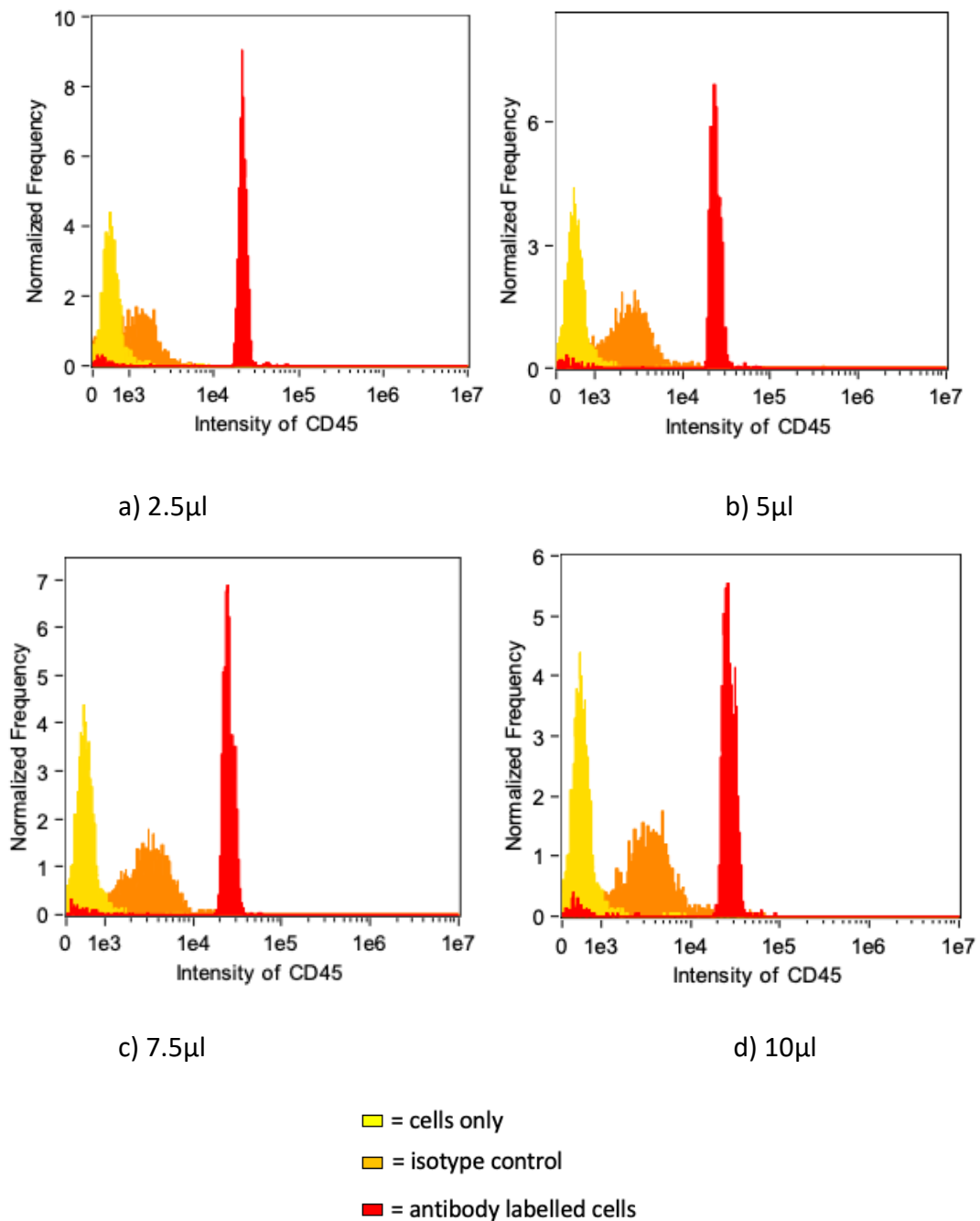


Figure 4.3 Graphs to show the optimisation of the CD45 antibody - unstained white cells (yellow), white cells stained with the isotype control (orange) and white cells stained with CD45 (BV786) using four different volumes of the antibody (a-d).

There is a distinct shift in fluorescence between the isotype control and the cells stained with the antibody, even at the lowest concentration. Based on this, the lowest concentration could be used, but this was explored in more detail when looking at the proportion of unlabelled cells (cells that did not pick up the antibody). To look at the proportion of unlabelled cells in the sample with the antibody, gates were drawn over the negative population. Cells within this gate were counted and the percentage of unlabelled cells at each concentration can be seen in Figure 4.4 and Figure 4.5. Based on these results, a volume of 7.5 μ l was used per 10⁶ white cells.

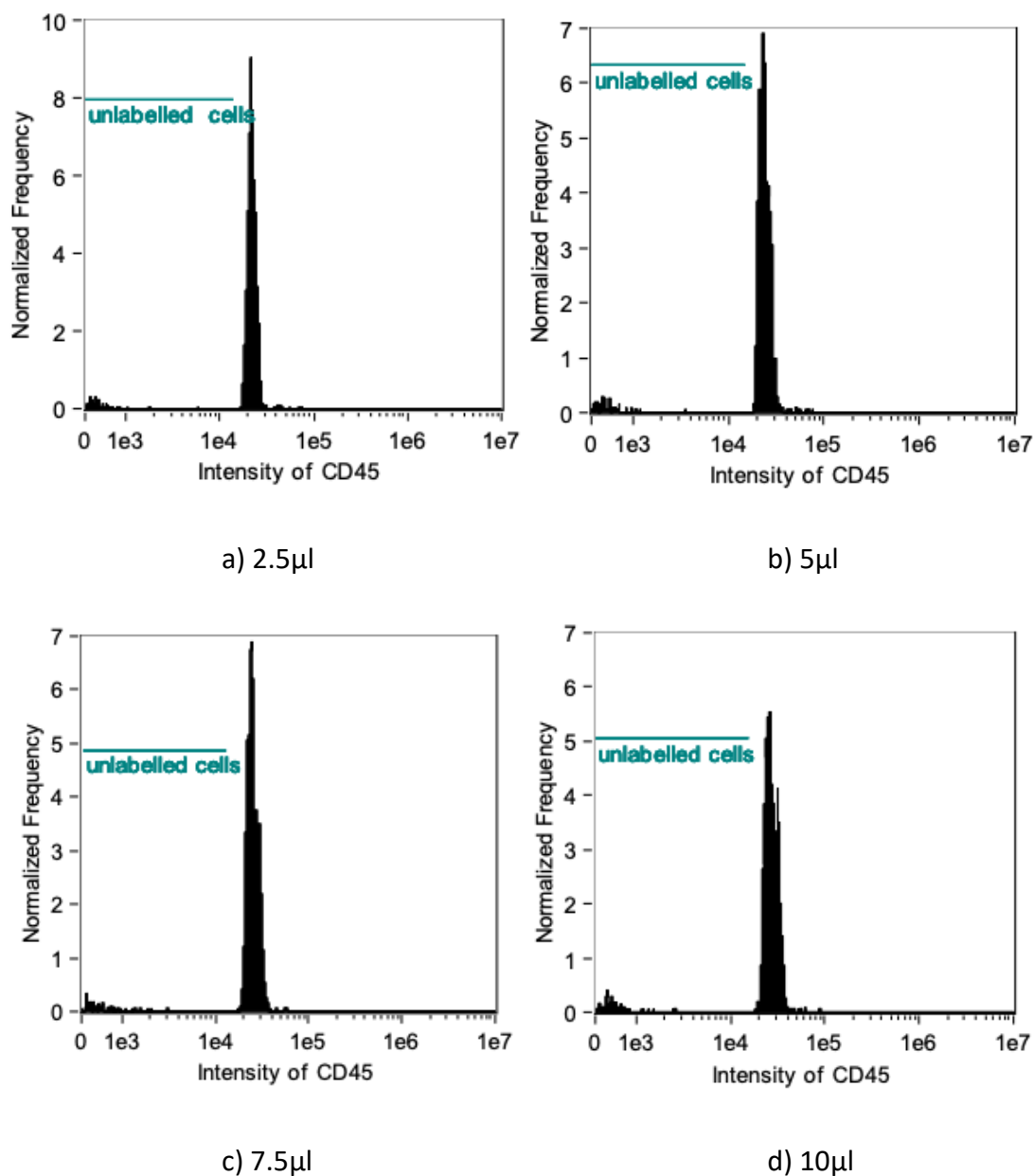


Figure 4.4 Graphs to show the proportion of unlabelled cells in white blood cell samples stained with four different volumes of CD45 (BV786) when using 10⁶ white cells.

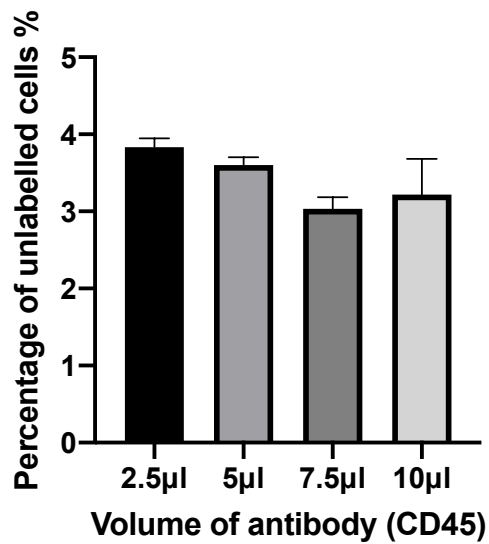
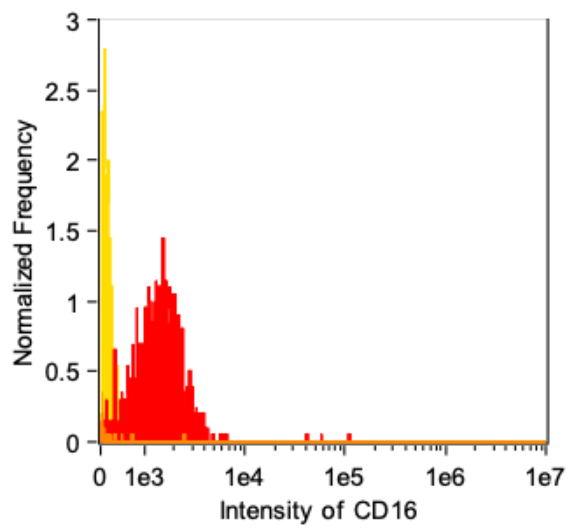
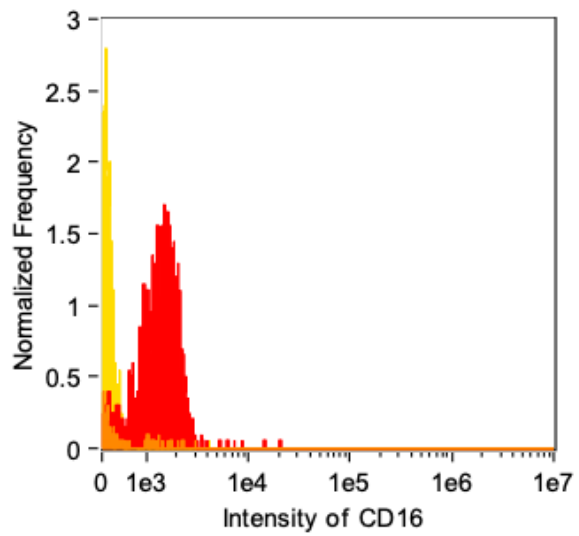


Figure 4.5 A graph to show the percentages of unlabelled white cells at different volumes of antibody for CD45 (BV786) when using 10^6 white cells.

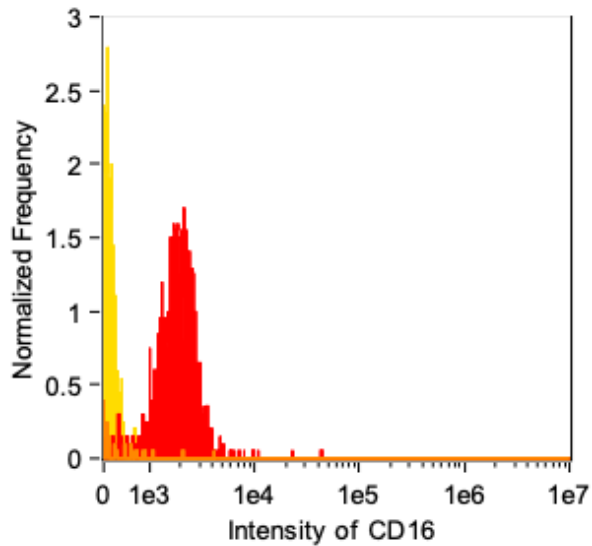
The same protocol was repeated for optimisation of CD16. Cells obtained from healthy volunteers were prepared and 10^6 cells were counted prior to addition of either the antibody or isotype control. The cells were then processed on the Imagestream and the experiment repeated three times. The combined results are displayed in the following graphs (Figure 4.6).



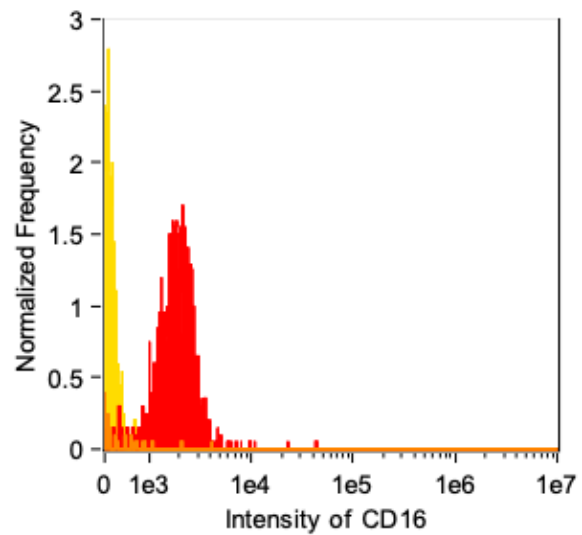
a) 1µl



b) 2.5µl



c) 5µl



d) 7.5µl

- █ = cells only
- █ = isotype control
- █ = antibody labelled cells

Figure 4.6 Graphs to show the optimisation of the CD16 antibody using unstained white cells (yellow), white cells stained with the isotype control (orange) and white cells with CD16 (APC-H7) using four different volumes of the antibody (a-d).

There is not such a significant shift from the isotype control, and whilst present it appears that there is a higher proportion of unlabelled cells. This was explored in the same way as for the CD45 labelled cells. The following graphs (Figure 4.7) demonstrate the population of unlabelled cells in the arm of the experiment where CD16 (APC-H7) was added to the cells at different concentrations, which is further tabulated in Figure 4.8.

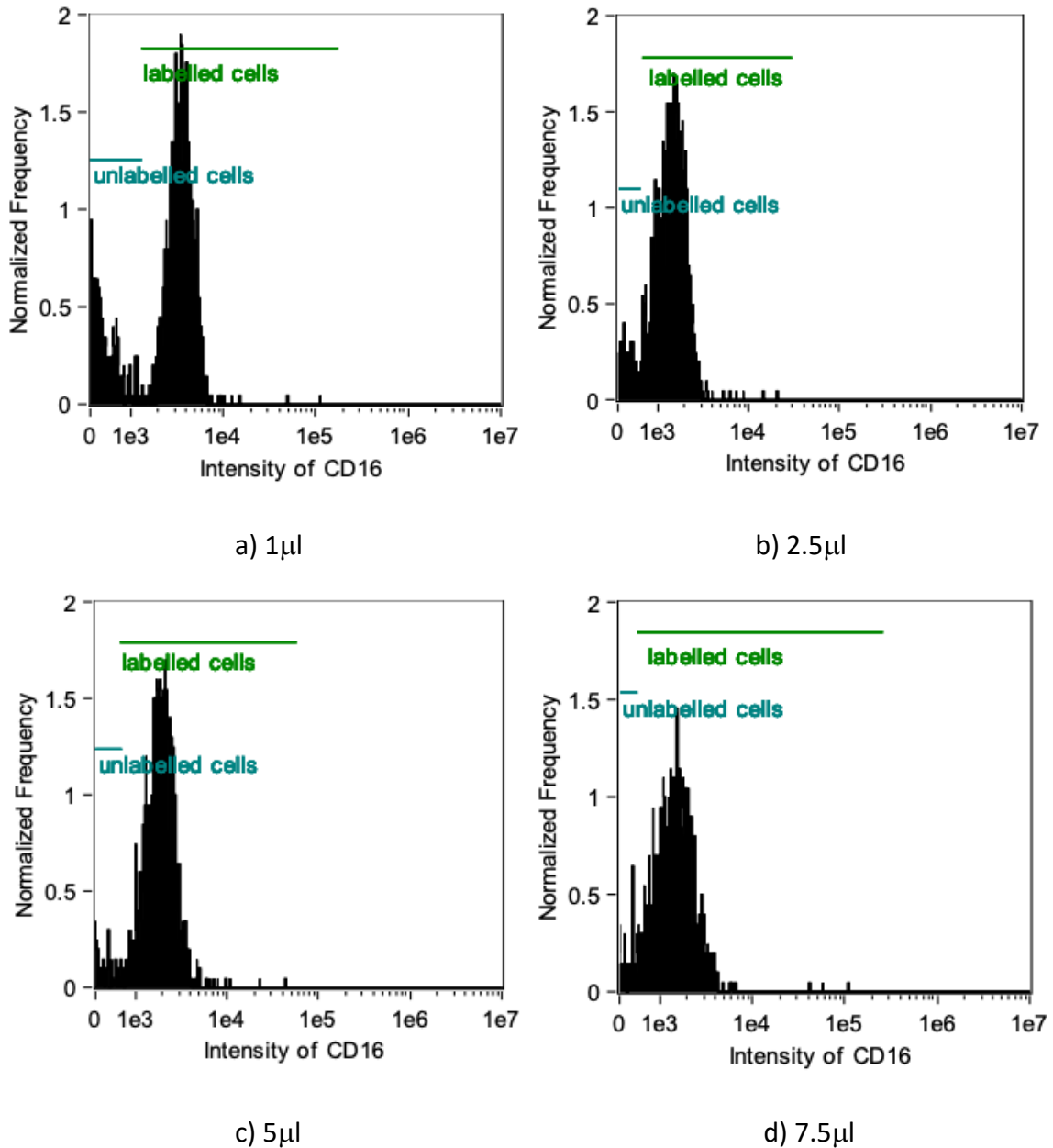


Figure 4.7 Graphs to show the proportion of unlabelled cells in white blood cell samples stained with CD16 (APC-H7) when using 10^6 cells.

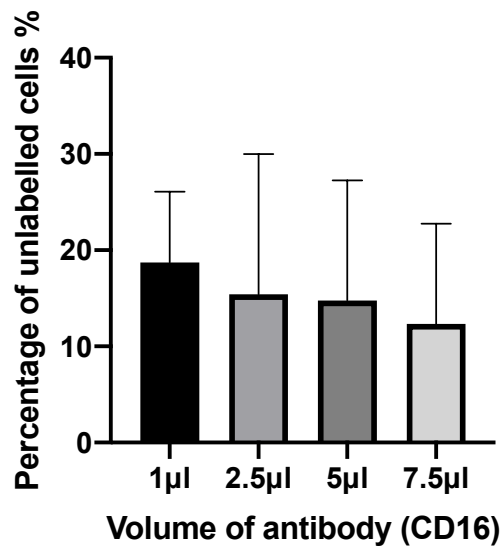


Figure 4.8 A graph to show the percentages of unlabelled white cells at different volumes of antibody for CD16 (APC-H7) when using 10^6 white cells.

In comparison to CD45, there are higher proportions of unlabelled white cells when using CD16. This is to be expected as not all white cells express the CD16 antigen. Using these results, 7.5µl of the CD16 antibody per 10^6 white cells was chosen as the volume of antibody for this assay. This means 12.4% of cells will be unlabelled if using CD16 only. However only 3.1% of cells are unlabelled from using the CD45 antigen alone. Whilst the experiment counting the total number of unlabelled white cells was not performed, it is hoped that a proportion of the 3.1% unlabelled cells will be detected by the addition of the CD16 antibody, so that a gate such as the one used in Figure 4.1 can be used to select all non-white cells, prior to further fluorescent analysis.

4.3.3 Epithelial antigens

The EpCAM antibody chosen for this assay is conjugated to a different fluorochrome (BV650) to that used in the Imagestream assay in Chapter 3, to fit into the final chosen panel.

Optimisation therefore must be performed, and the chosen cell line was LNCaP. 100 000 LNCaP cells were fixed, washed and resuspended in flow buffer. Four different volumes of the EpCAM (BV650) antibody were added to the cells, and the same volumes of the isotype controls were added to matched samples. Cells with no staining and the samples were then processed on the Imagestream. This was repeated three times and the results are displayed in the following graphs (Figure 4.9).

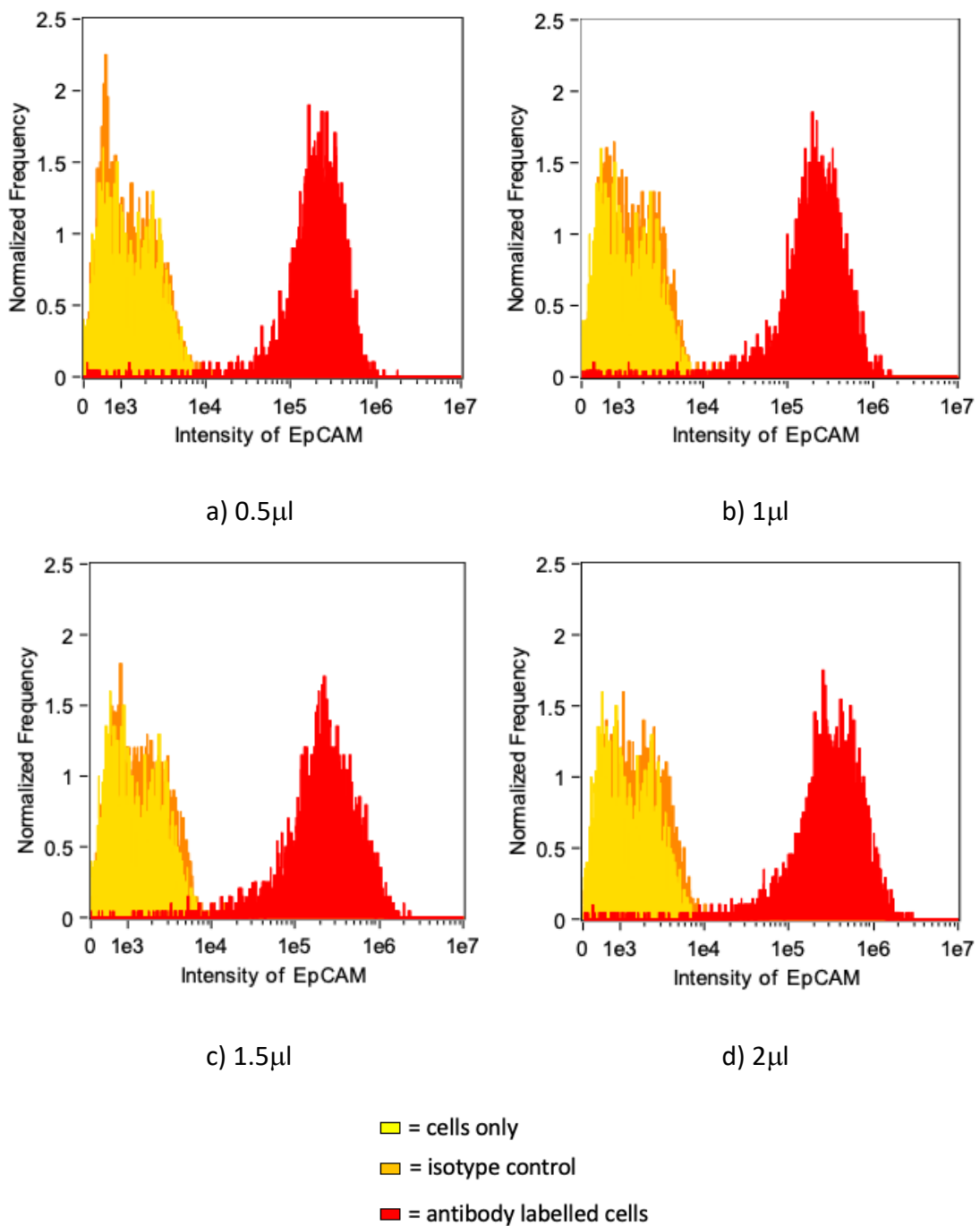


Figure 4.9 Graphs to show the optimisation of EpCAM (BV650) antibody using LNCaP cells. This shows unstained cells (yellow), LNCaP cells stained with the isotype control (orange) and LNCaP cells stained with EpCAM (BV650) (red) using four different volumes of the antibody (a-d).

There is a distinct shift in fluorescence between the unstained cells, isotype control and the cells stained with the antibody, even at the lowest concentration (Figure 4.9). Therefore the 0.5 μ l volume was chosen. An Imagestream image of a cell stained using this antibody concentration is seen in Figure 4.10.

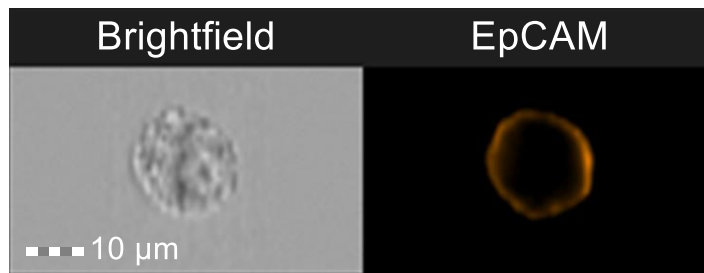


Figure 4.10 An Imagestream image of an LNCaP cell stained with EpCAM (BV650) when using 0.5 μ l, demonstrating cell membrane staining.

The pan-cytokeratin antibody chosen for this assay is conjugated to PECy7 and was optimised using the MCF-7 cell line. Whilst this is a breast cancer cell line, over 99% of MCF-7 cells express cytokeratin. 100 000 cells were fixed, permeabilised and stained with four increasing volumes of the cytokeratin (PECy7) antibody before being resuspended in 200 μ l of flow buffer and processed on the Imagestream. Matched samples for cells only and cells stained with the isotype control were also run and each repeated three times. The results are displayed in the following graphs (Figure 4.11).

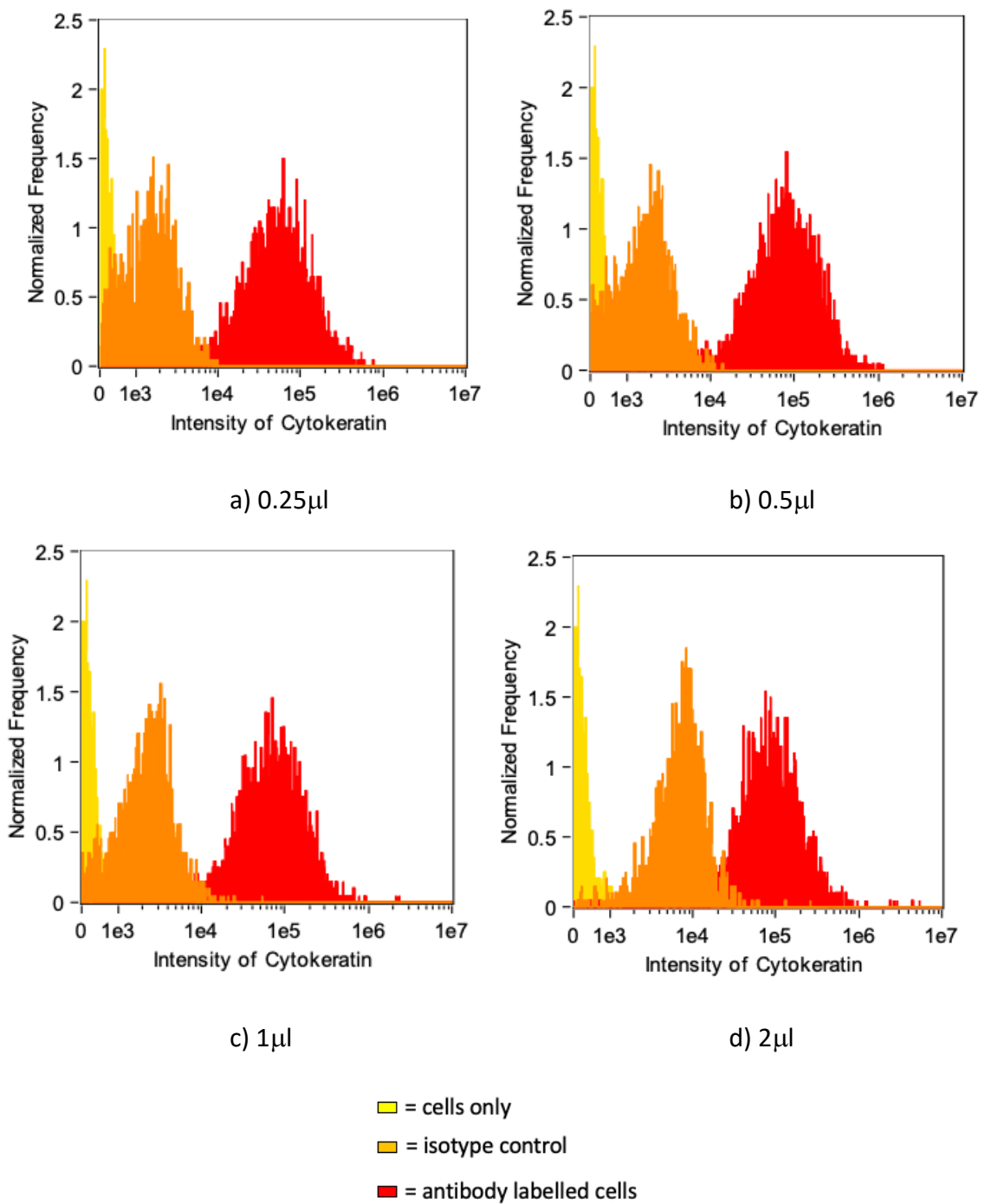


Figure 4.11 Graphs to show optimisation of the cytokeratin (PECy7) antibody using MCF-7 cells. These graphs show unstained MCF-7 cells (yellow), MCF-7 cells stained with the isotype control (orange) and MCF-7 cells stained with cytokeratin (PECy7) (red) using four different volumes of the antibody (a-d).

When using higher volumes of the antibody (1 μ l and 2 μ l) the isotype control appears to overlap with the cells stained with the antibodies. This could be because it becomes sticky at higher concentrations but as a result the 0.5 μ l volume of antibody was chosen for the final assay (Figure 4.12).

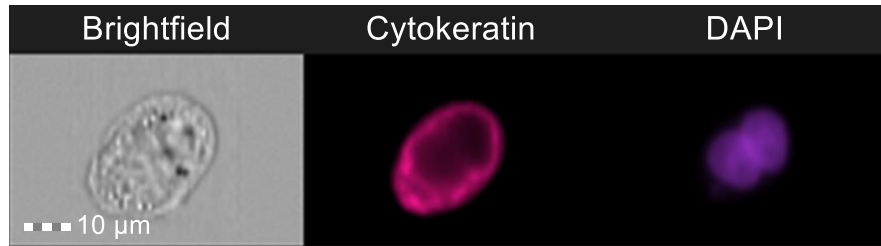


Figure 4.12 An Imagestream image of an MCF-7 cell stained with cytokeratin (PECy7) when using 0.5 μ l, demonstrating cytoplasmic staining.

4.3.4 Mesenchymal antigens

The MT1-MMP antibody, conjugated to PE, had already been optimised by colleagues in the group for another workstream. 3 μ l of antibody per 100 000 cells was used and this was the concentration used for this assay.

Vimentin conjugated to AF647 was optimised using 100 000 PC3 cells. The cells were fixed and permeabilised followed by the addition of four different volumes of the antibodies. Cells were then resuspended in flow buffer and processed on the Imagestream, alongside matched samples with the Isotype control and PC3 cells only. This was repeated three times and the combined results are displayed in the following graphs (Figure 4.13).

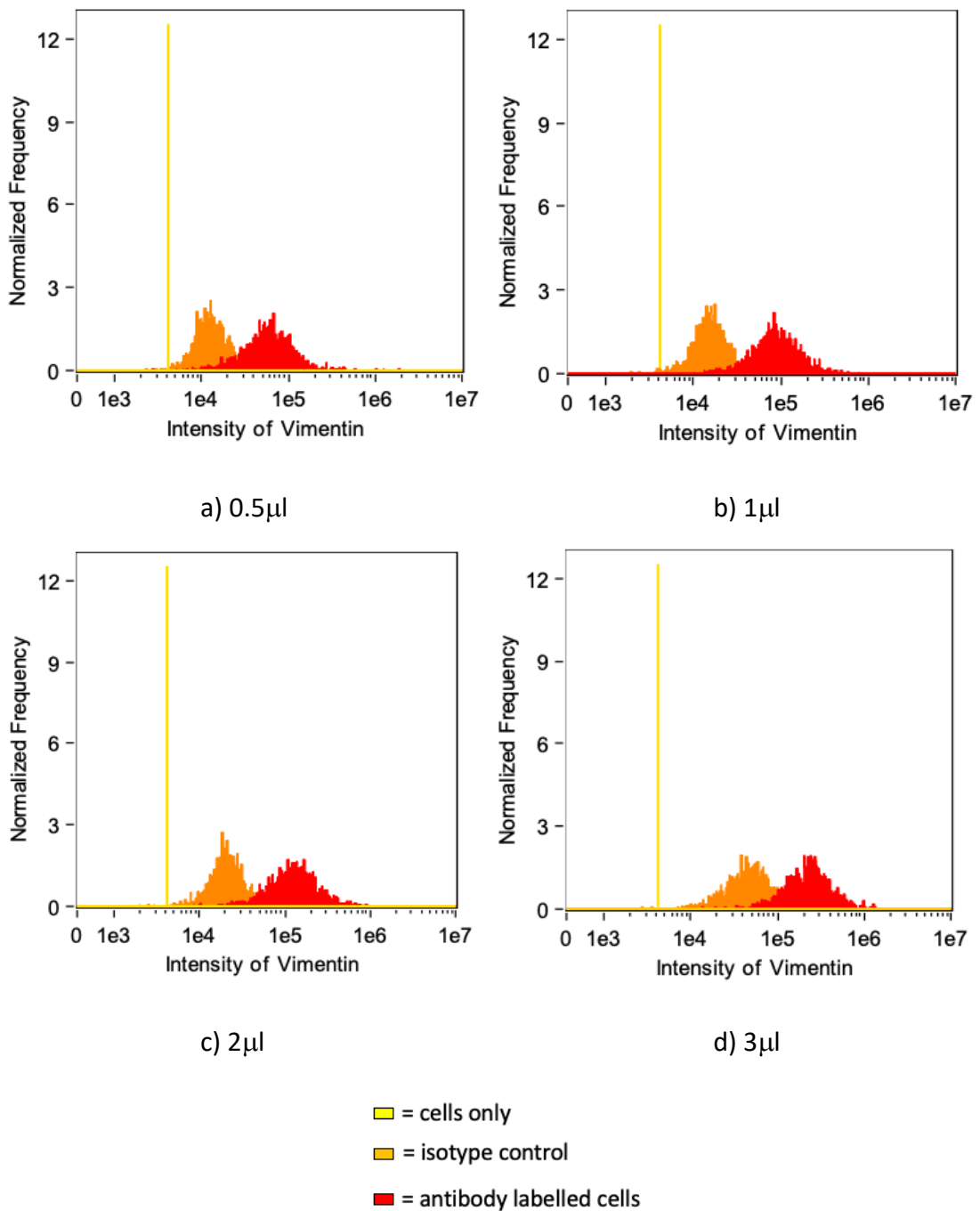


Figure 4.13 Graphs to show the optimisation of the vimentin (AF647) antibody using PC3 cells. These graphs show unstained cells (yellow), PC3 cells stained with the isotype control (orange) and PC3 cells stained with vimentin (AF647) (red) using four different volumes of the antibody (a-d).

Similar to the cytokeratin antibody, at higher volumes there was an overlap between the isotype and antibody stained cells. Again, this could be due to the isotype being sticky at higher concentrations. The volume chosen for the final assay was 1 μ l based on the results demonstrated in Figure 4.13. A cell stained with this concentration of antibody can be seen in Figure 4.14.



Figure 4.14 An Imagestream image of a PC3 cell stained with Vimentin (AF647) when using 1 μ l, demonstrating cytoplasmic and membrane staining

4.3.5 Stem cell antigens

The Stem Cell antigens needed to be optimised on iPS cells, as similar to before, because the mesenchymal stem cells harvested from bone marrow did not grow in sufficient quantities. Despite trials on several cell lines, positive staining was not seen. The same Nanog antibody that was used in the Imagestream assay was used in this assay, so optimisation was only necessary for Oct4 (BV421) and SOX2 (FITC). 100 000 iPS cells were fixed, permeabilised and stained with three increasing volumes of the two antibodies. Matched samples were stained with the paired isotype control for each antibody and the samples were all re-suspended in 200 μ l of flow buffer and processed on the Imagestream, alongside samples with unstained cells. The results can be seen in the following graphs (Figures 4.15, 4.16, 4.17 and 4.18).

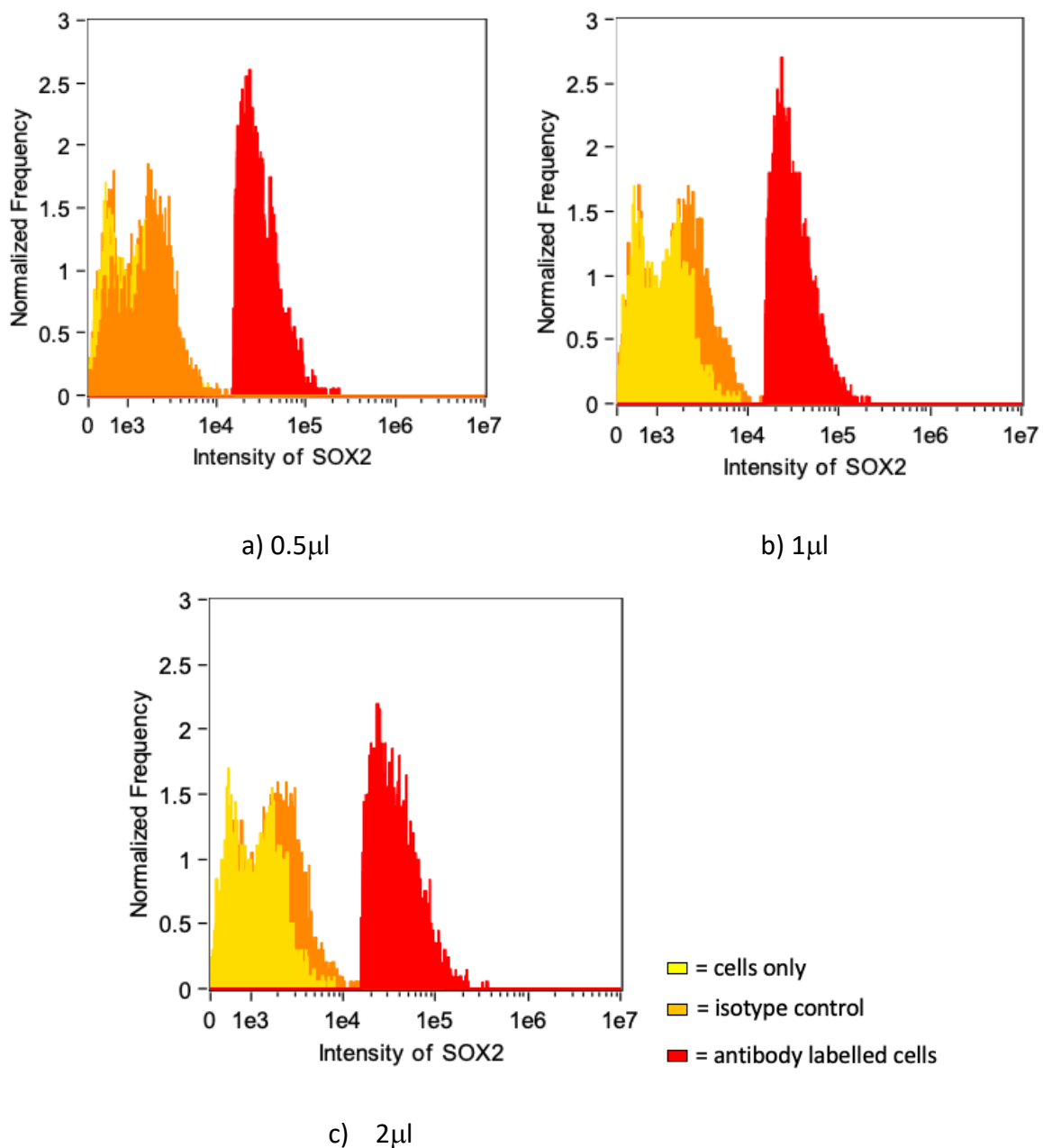


Figure 4.17 Graphs to show the optimisation of SOX2 (FITC) antibody using iPS cells. These graphs show unstained cells (yellow), iPS cells stained with the isotype control (orange) and iPS cells stained with SOX2 (FITC) (red) using three different volumes of the antibody (a-c).

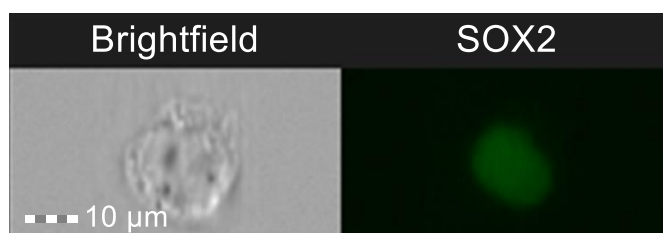


Figure 4.18 An Imagestream image of an iPS cell stained with SOX2 (FITC) when using 2 μl, demonstrating nuclear staining.

iPS cells can differentiate into any cell type depending on their culture environment so it is critical to use early passage cells if stem-like properties are still to be observed. By the nature of the way they are cultured and how often they have to be split, using cells in sufficient quantity meant that some cells are likely to have differentiated prior to the optimisation experiment. This could account for the overlap between the isotype control and the antibody stained cells during the Oct4 optimisation. There was a logarithmic increase in fluorescence using the 2µl quantity yet the tail overlapped with the isotype staining. These cells could be cells that have lost their stem cell properties, or only weakly express them. The overlap could also be due to the stickiness of the isotype at higher concentrations. There wasn't much change in isotype fluorescence between the 0.5µl and 1µl volume but when using the 2µl volume the cells stained with the isotype showed a higher fluorescence. For these two reasons, a higher volume of antibody was not chosen and 2µl of both Oct4 (BV421) and SOX2 (FITC) were used for this assay (Figures 4.15 and 4.17, respectively).

4.3.6 DAPI

DAPI concentration was kept the same as for the Imagestream assay in chapter 3 at 1:500 (or 0.2µl).

4.4 Optimisation of an assay to use on a conventional FACS machine with sorting capabilities

4.4.1 Collection and storage of blood from patients and healthy volunteers

4 ml of blood collected in K₂EDTA tubes from the patients described in Chapter 3 was used for this assay. Consent was obtained from all patients and blood was transported from the hospital to the lab at room temperature in a Biohazard UN3373 marked container. Because I performed the collection and processing for both assays, and the first stage needed to be performed within four hours from blood harvest, the decision was made to use the same blood preparation protocol as per the Imagestream assay.

4.4.2 Preparation of blood samples

The BD PhosFlow FixLyse Buffer was immediately applied to the blood to allow cellular fixation and lysis of erythrocytes. Immunomagnetic white cell depletion was performed prior to permeabilisation. Antibody staining with the antibodies described in the previous section was then applied, before washing and resuspension in FACS tubes using 200µl of flow buffer. Samples were processed the same day on the BD FACS Fusion, to ensure no degradation of fluorescence.

4.4.3 Optimisation of cell sorting and post-sort storage

A gating strategy was optimised based first on forward and side scatter, to eliminate cell debris and doublets, and then on negative fluorescence for both CD16 and CD45 as per Figure 4.1. Cells within the gate shown in this figure were assumed to be the potential CTC population and were collected in a sterile Eppendorf, suspended in two drops of flow buffer.

The sorted cell population was then frozen in a -80°C freezer, which is kept locked under HTA guidelines. All flow data was saved (including the non-sorted population) for analysis.

4.5 Controls, gating strategies and analysis

4.5.1 Single colour controls and laser set-up

As per the Imagestream assay in Chapter 3, in order to determine the laser settings to enable minimal bleed but detect cells expressing each fluorochrome, flow cytometry compensation beads (Ultracomp ebeads, ThermoFisher Scientific) were stained with each antibody (LNCaP cells were used for DAPI). Beads with no staining were run using each laser, and then the beads stained with each antibody were processed. If a high level of bleed was detected between one laser and another, the laser setting was reduced. All samples were run initially to determine rough laser settings, and then processed again using final settings once adjustments had been made.

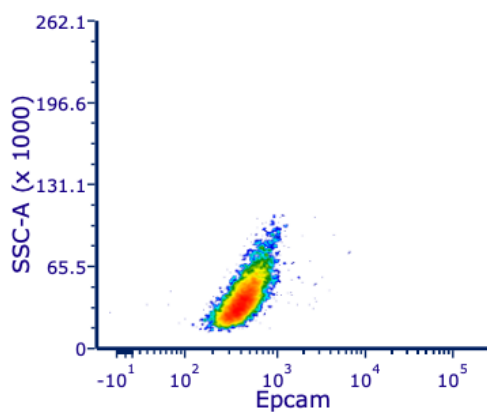
These laser settings were then used each time the experiment was run to ensure comparable data (Figure 4.19). Single colour controls were repeated every four weeks or every time a new antibody vial was purchased, to minimise variation.

Source	Target									
	561 582/15-A	561 780/60-A	488 530/30-A	488 710/50-A	405 450/50-A	405 670/30-A	405 780/60-A	355 450/50-A	640 670/30-A	640 780/60-A
561 582/15-A	1.0024	-0.01008	-0.01256	-0.06789	0.00051	-0.00109	0.00482	-0.00006	-0.00177	0.00606
561 780/60-A	-0.23718	1.02147	-0.02803	-0.01377	-0.01856	-0.00092	-0.04665	-0.00034	-0.00136	-0.0354
488 530/30-A	-0.00029	0.00132	1.00021	-0.0145	-0.00689	-0.00015	0.00069	-0.00015	0.0006	0.00068
488 710/50-A	0.0233	-0.10152	-0.011	1.005	0.01044	-0.20885	-0.06092	-0.00016	-0.02976	-0.05302
405 450/50-A	-0.0006	-0.00005	-0.00329	-0.00023	1.00016	-0.00221	-0.00023	-0.00288	0.00000	0.00012
405 670/30-A	0.0019	-0.0217	-0.00605	-0.01104	-0.04515	1.00383	-0.0728	0.00000	-0.05198	0.01835
405 780/60-A	-0.00589	0.02704	-0.00114	-0.003	-0.08425	-0.00681	1.01621	0.00005	0.00092	-0.19876
355 450/50-A	0.0	0.0	0.0	0.0	0.0	0.0	0.0	1.0	0.0	0.0
640 670/30-A	-0.02799	0.12451	-0.00253	-0.01836	-0.00828	-0.00921	0.03606	-0.00006	1.00447	-0.49818
640 780/60-A	0.08641	-0.38966	-0.00474	0.00499	0.0049	-0.00278	-0.06803	-0.00007	-0.00648	1.03368

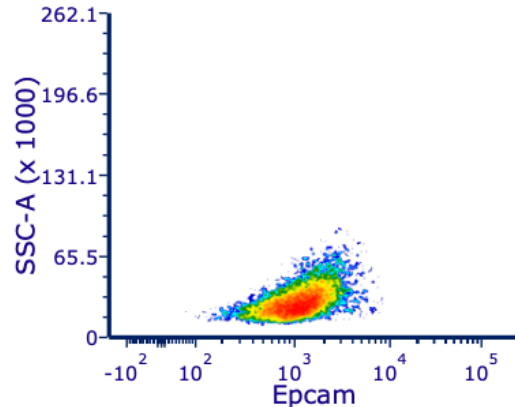
Figure 4.19 A compensation matrix created on the BD FACS Fusion when running each sample. Any significant overlap would show in red.

4.5.2 Gating Strategies

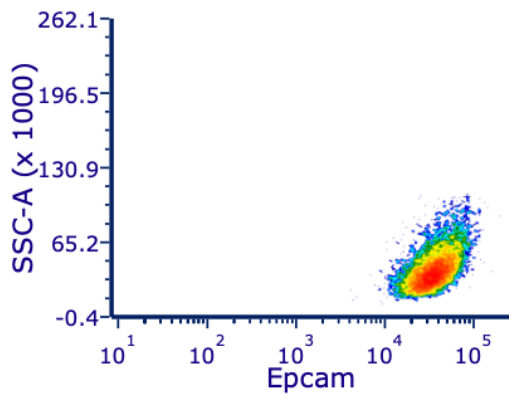
For each antibody, cells expressing the antigen were stained with the antibody in question and processed alongside cells with the isotype control and cells with no staining. Gates were first drawn based on forward and side scatter to exclude debris and doublets, and then drawn to enable inclusion of cells that had a higher fluorescence than the cells with the isotype (Figures 4.20 – 4.26).



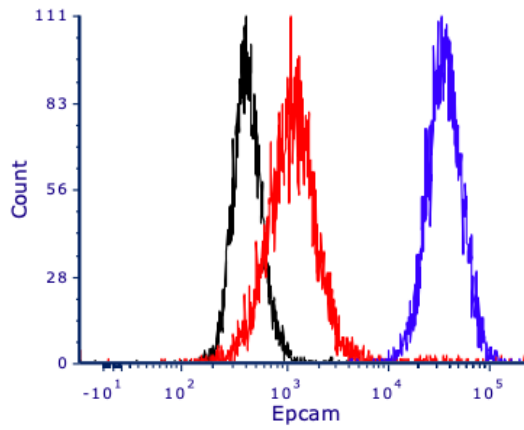
a) LNCaP unstained cells



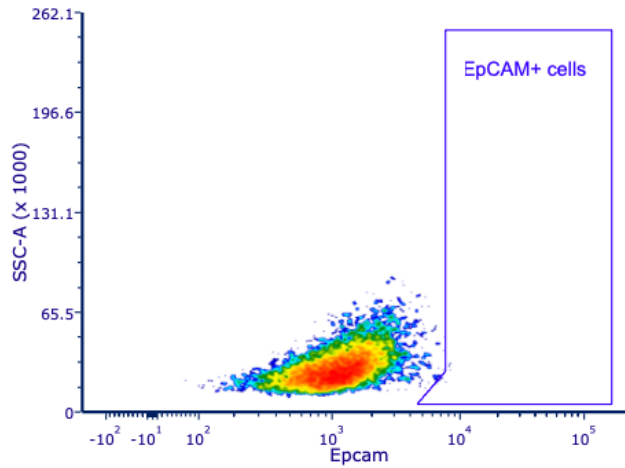
b) LNCaP cells with isotype control



c) LNCaP cells with EpCAM (BV421)

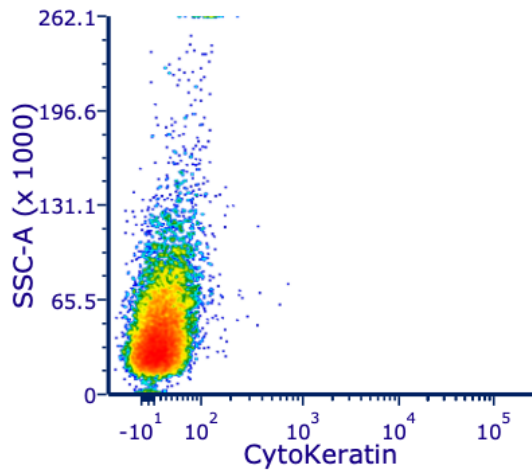


d) Fluorescence on LNCaP unstained cells (black), cells with isotype control (red) and cells and cells with EpCAM (BV421) (blue).

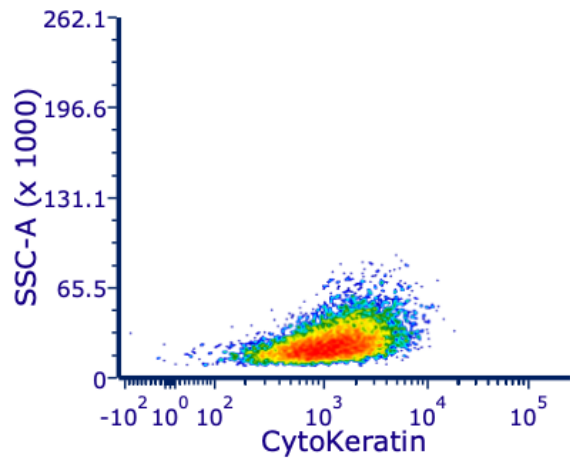


e) Gate used to identify EpCAM positive CTCs

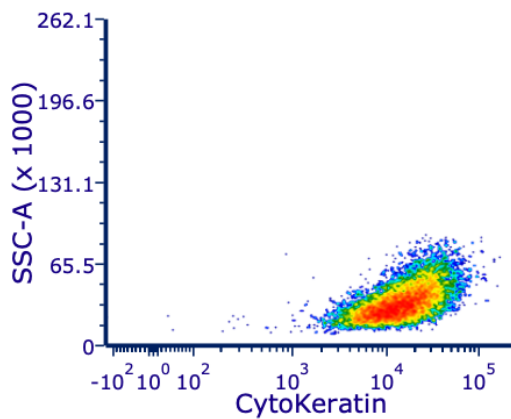
Figure 4.20 Graphs to show the fluorescence of a) LNCaP cells with no staining, b) staining with the isotype control, c) staining with the EpCAM antibody, d) combined data and e) the final gate used for the assay. This final gate was drawn to include any cells expressing higher fluorescence than the isotype control.



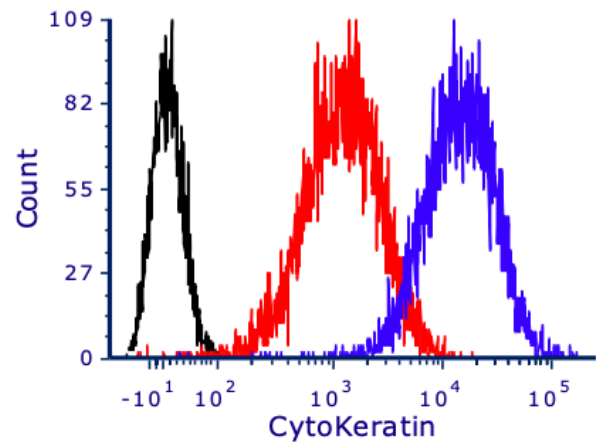
a) MCF-7 cells only



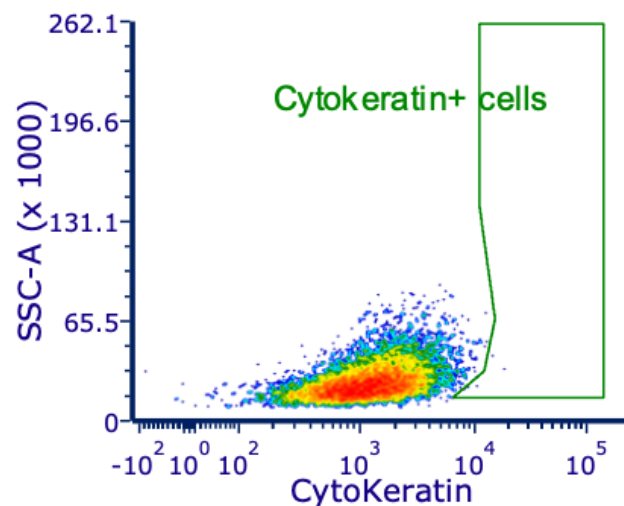
b) MCF-7 cells with Isotype control



c) MCF-7 cells with CK (PECy7)

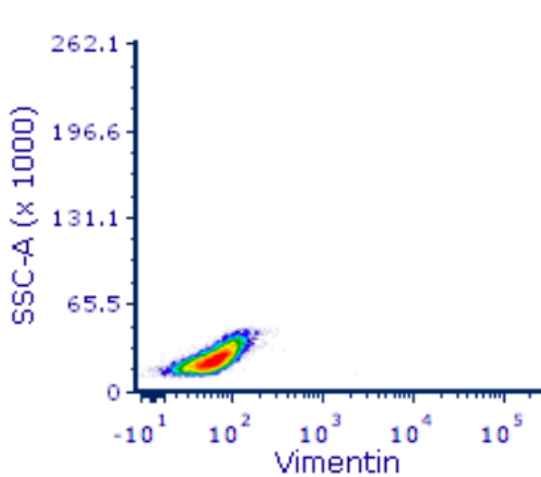


d) Fluorescence on MCF-7 unstained cells (black), cells with isotype control (red) and cells with CK (PECy7) (blue).

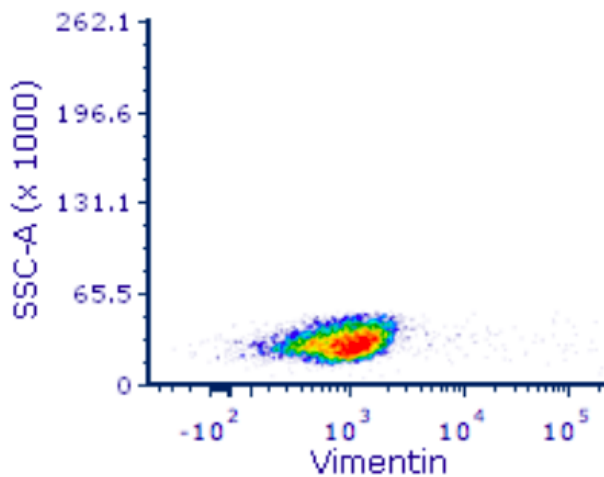


e) Gate used to identify Cytokeratin positive CTCs

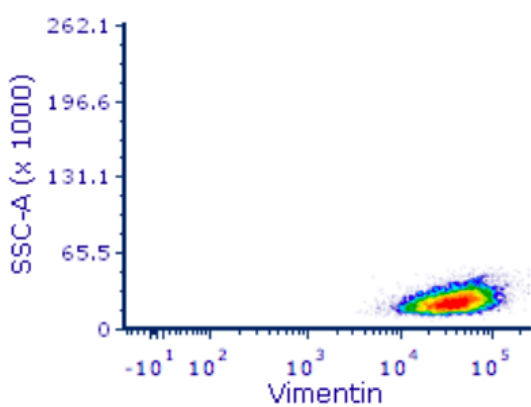
Figure 4.21 Graphs to show the fluorescence of MCF7 cells with a) no staining, b) staining with the isotype control, c) staining with the cytokeratin antibody, d) combined data and e) the final gate used for the assay. This final gate was drawn to include any cells expressing higher fluorescence than the isotype control.



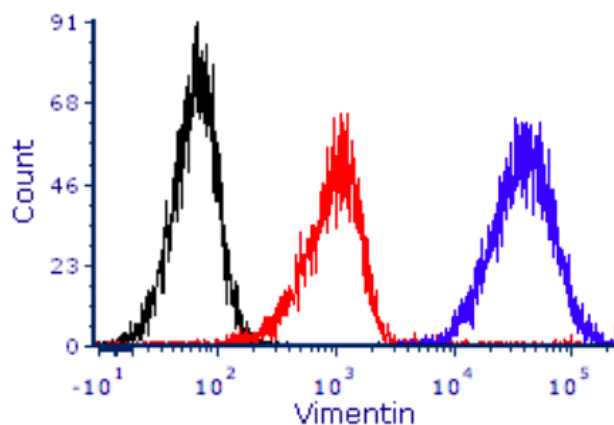
a) PC3 cells only



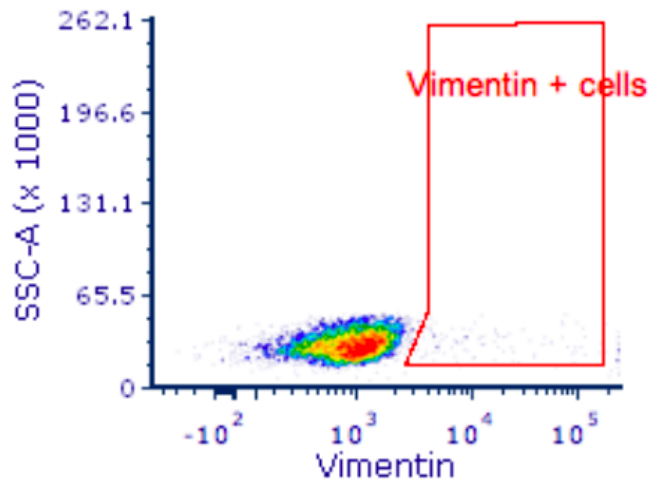
b) PC3 cells with Isotype control



c) PC3 cells with Vimentin (AF647)

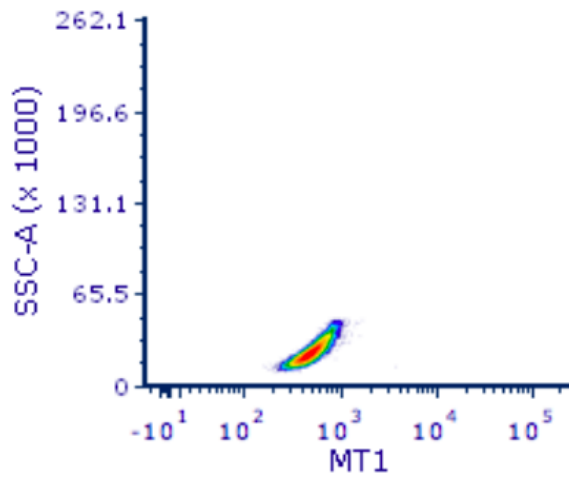


d) Fluorescence on PC3 cells only (black), cells with isotype control (red) and cells with Vimentin (AF647) (blue).

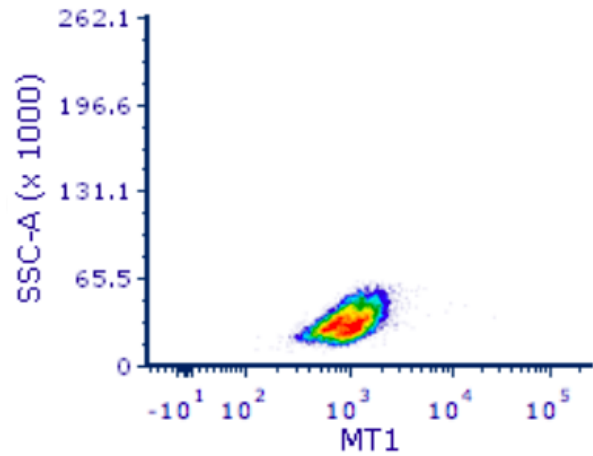


e) Gate used to identify Vimentin positive CTCs

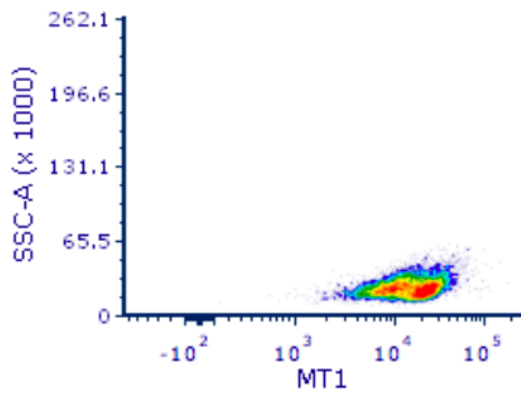
Figure 4.22 Graphs to show the fluorescence of PC3 cells with a) no staining, b) staining with the isotype control, c) staining with the Vimentin antibody, d) combined data and e) the final gate used for the assay. This final gate was drawn to include any cells expressing higher fluorescence than the isotype control.



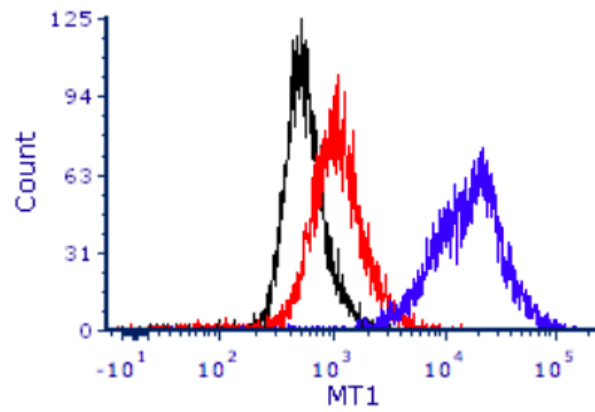
a) PC3 cells only



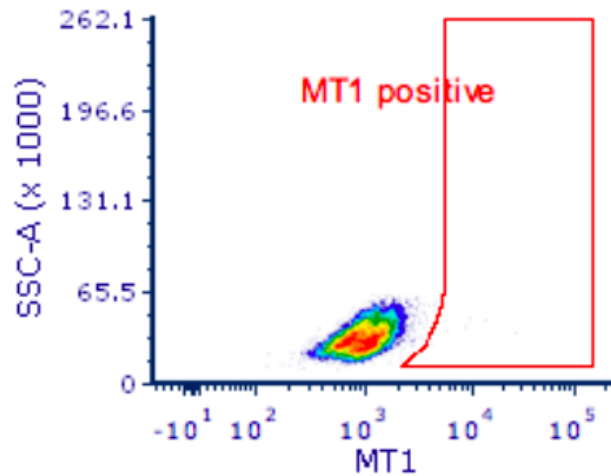
b) PC3 cells with Isotype control



c) PC3 cells with MT1-MMP (PE)

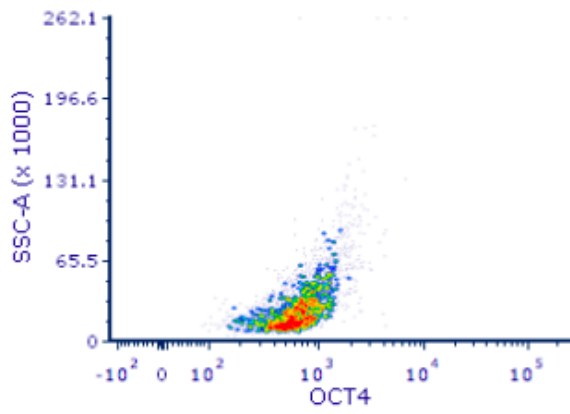


d) Fluorescence on PC3 cells only (black), cells with isotype control (red) and cells with MT1-MMP (PE) (blue).

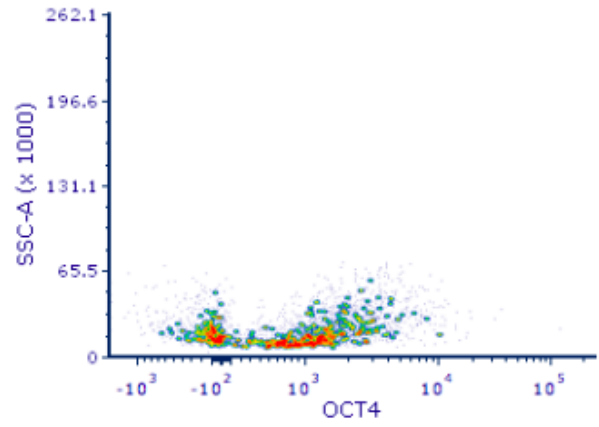


e) Gate used to identify MT1-MMP positive CTCs

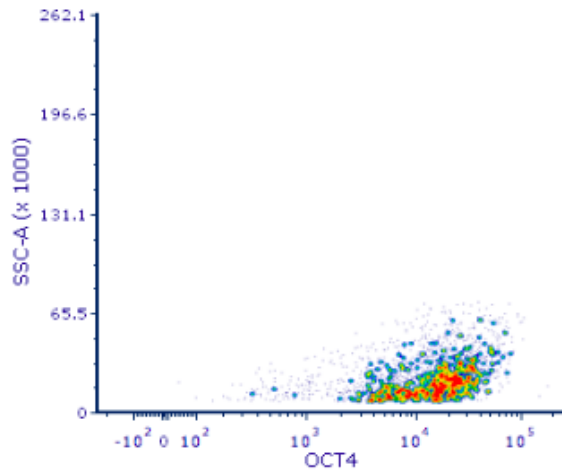
Figure 4.23 Graphs to show the fluorescence of PC3 cells with a) no staining, b) staining with the isotype control, c) staining with the MT1-MMP antibody, d) combined data and e) the final gate used for the assay. This final gate was drawn to include any cells expressing higher fluorescence than the isotype control.



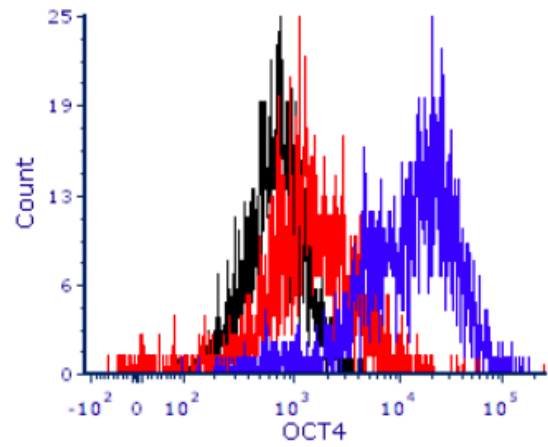
a) iPS cells only



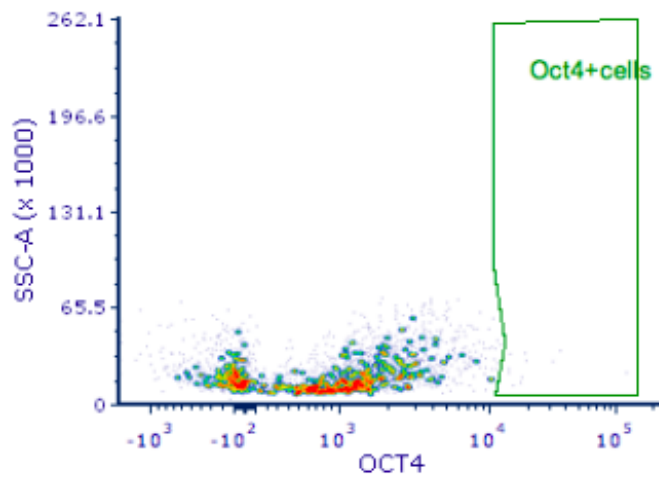
b) iPS cells with isotype control



c) iPS cells with Oct4 (BV421)

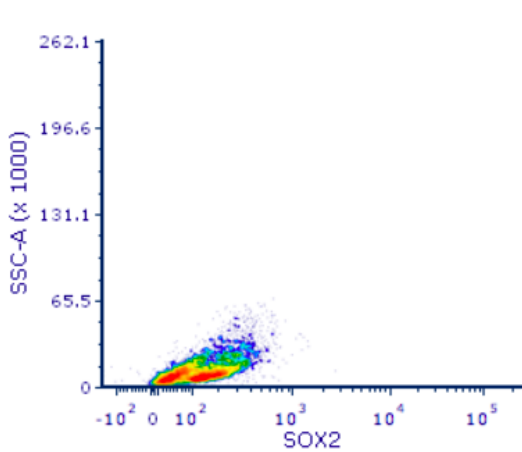


d) Fluorescence on iPS unstained cells (black), cells with isotype control (red) and cells with cells with Oct4 (BV421) (blue).

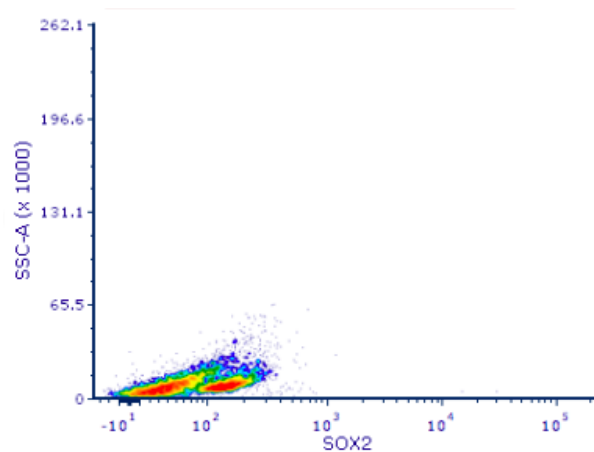


e) Gate used to identify Oct4 positive CTCs

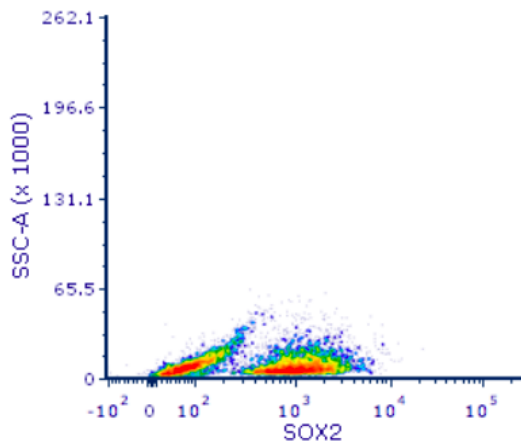
Figure 4.24 Graphs to show the fluorescence of iPS cells with a) no staining, b) staining with the isotype control, c) staining with the Oct4 antibody, d) combined data and e) the final gate used for the assay. This final gate was drawn to include any cells expressing higher fluorescence than the isotype control.



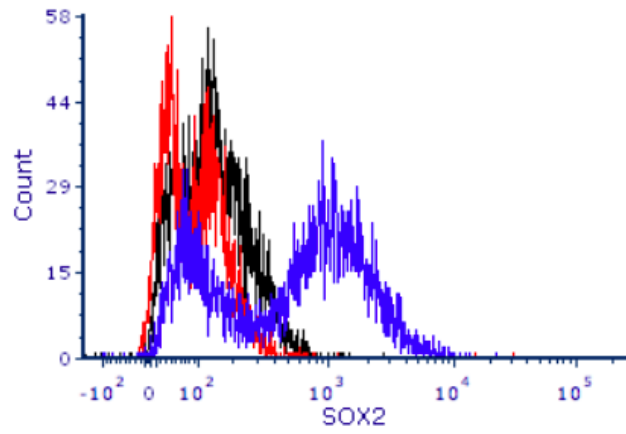
a) iPS cells only



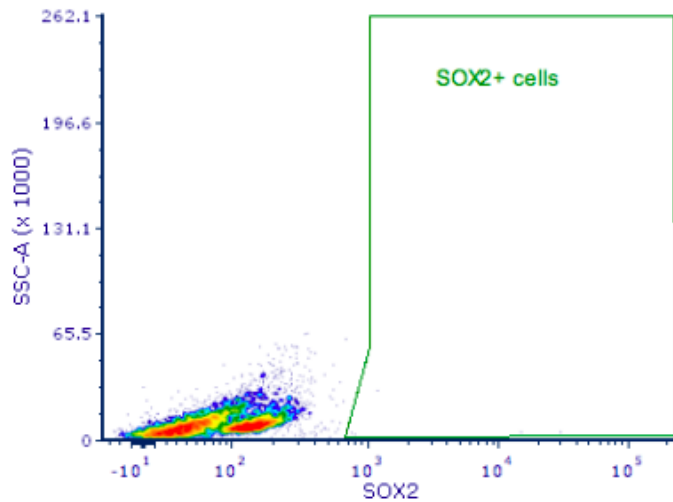
b) iPS cells with Isotype control



c) iPS cells with SOX2 (FITC)

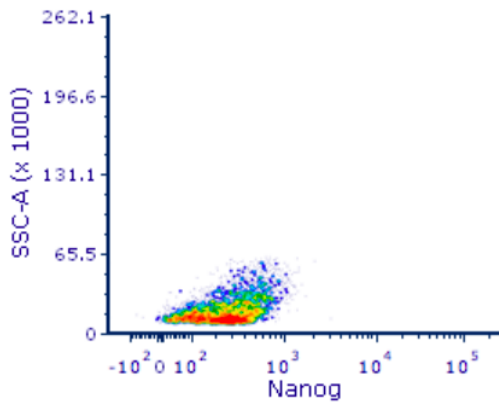


d) Fluorescence on iPS cells only (black), cells with isotype control (red) and cells with SOX2 (FITC) (blue).

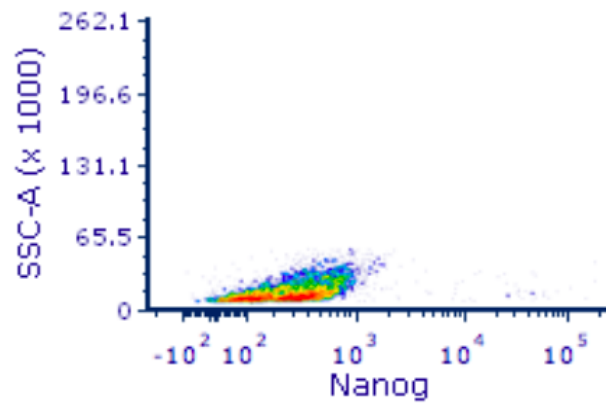


e) Gate used to identify SOX2 positive CTCs

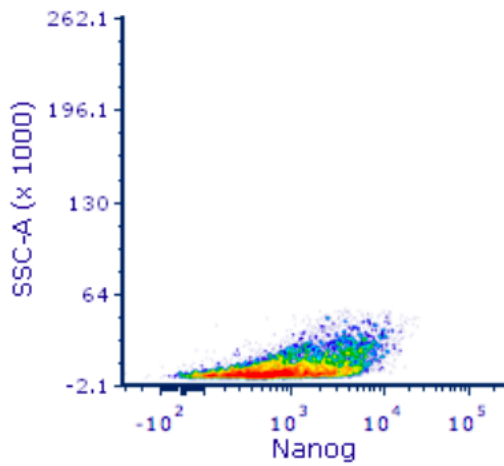
Figure 4.25 Graphs to show the fluorescence of iPS cells with a) no staining, b) staining with the isotype control, c) staining with the SOX2 antibody, d) combined data and e) the final gate used for the assay. This final gate was drawn to include any cells expressing higher fluorescence than the isotype control.



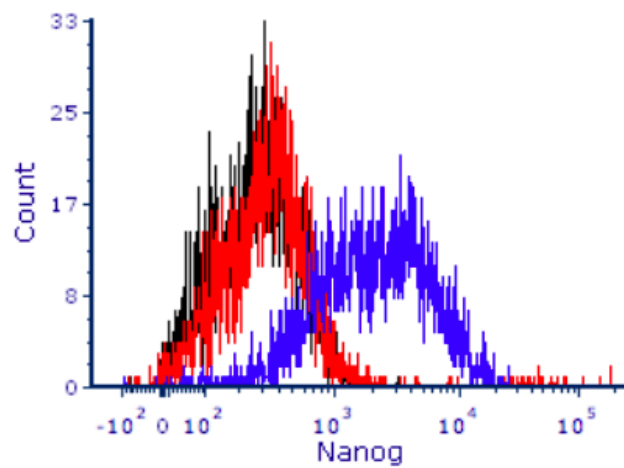
a) iPS cells only



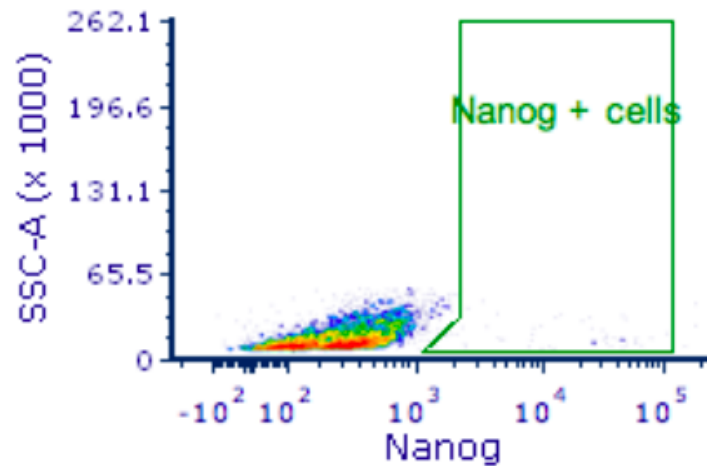
b) iPS cells with Isotype control



c) iPS cells with Nanog (PerCP Cy5.5)



d) Fluorescence on iPS unstained cells (black), cells with isotype control (red) and cells with Nanog (PerCP Cy5.5) (blue).



e) Gate used to identify Nanog positive CTCs

Figure 4.26 Graphs to show the fluorescence of iPS cells with a) no staining, b) staining with the isotype control, c) staining with the Nanog antibody, d) combined data and e) the final gate used for the assay. This final gate was drawn to include any cells expressing higher fluorescence than the isotype control.

4.5.3 Healthy Volunteer controls

Blood from five male healthy volunteers was processed as part of this assay. Because the volunteers were from the lab staff, age-matched controls were not possible. The possibility of obtaining blood from age-matched patients with no history of prostate cancer, or any other cancer (e.g. from a non-oncology clinic) was explored, but the original ethical approval did not allow this.

In order to exclude potential white blood cells expressing Oct4, SOX2 and Nanog, additional gates were used to identify whole cells and the CD45/CD16 negative population first, and then the gates in Figures 4.24 - 4.26 were applied (Figure 4.27).

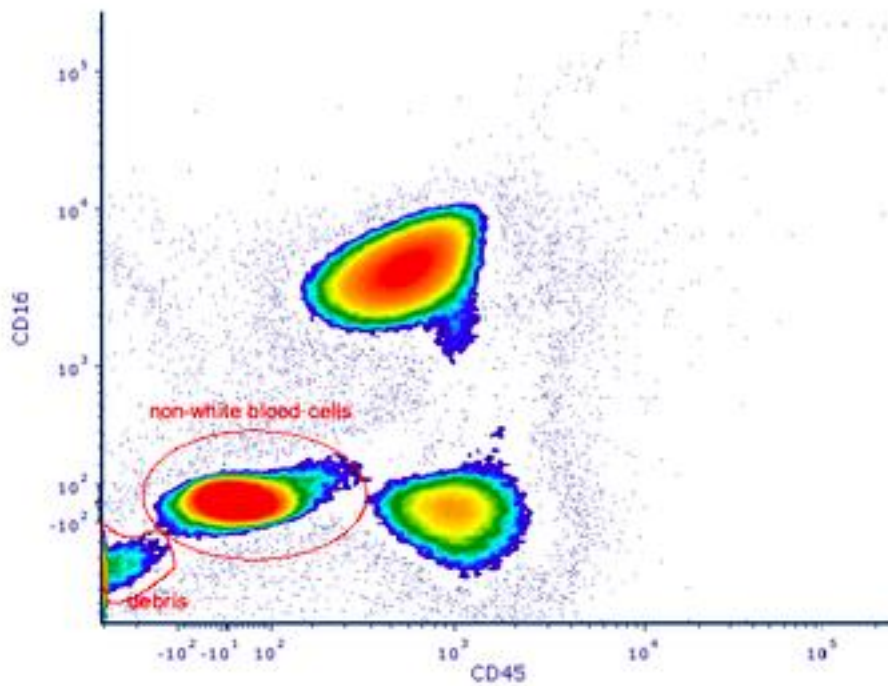


Figure 4.27 A graph to demonstrate the gating of whole CD45-/CD16- cells, which should contain predominantly non-white blood cells. A gate was drawn round the population that was negative for both antigens and this was the gate used to capture putative CTCs.

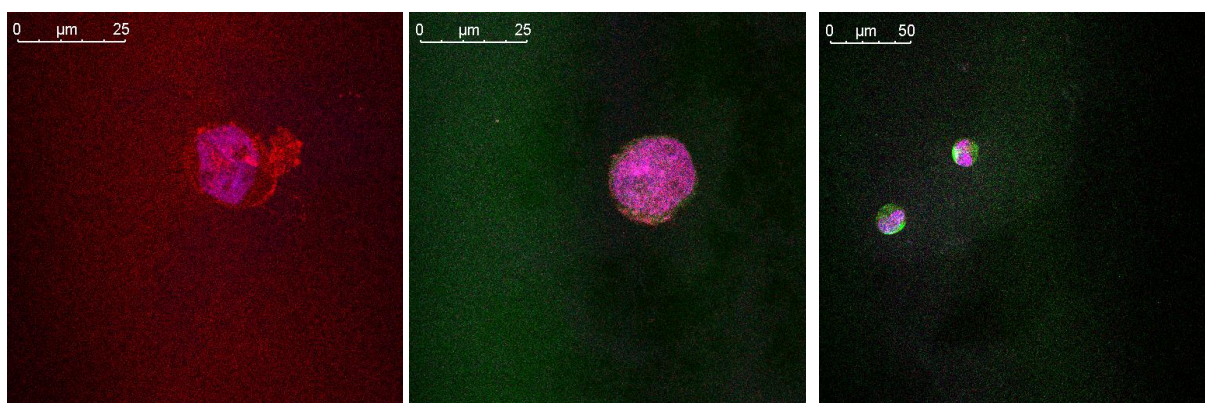
Further thresholds for Oct4, SOX2 and Nanog based on expression in the healthy volunteer bloods were not applied as without imaging or further cell characterization it was not possible to accurately determine which cells were definitely white blood cells. Expression of all antigens but particularly Oct4, SOX2 and Nanog in these healthy volunteer samples was noted and will be discussed in Chapter 5.

4.6 Downstream analysis

4.6.1 Immunofluorescence

Unlike with the Imagestream where any population of interest could be visualised, the validity of the sorted population needed to be tested to ensure that the cells within this population are indeed what they are supposed to be. One method of doing this would be to sort directly onto a microscope slide and use standard immunofluorescence to visualise the cells. This would require a microscope with the same lasers as the FACS machine, because the cells are already stained with conjugated antibodies, so the antigen binding sites would be blocked.

In order to test this concept, 100 000 of each of LNCaP, PC3 and MCF-7 cells were spiked into 2mls of healthy volunteer blood. The cells were processed using the assay described in section 4.4 but because the microscope available did not have the same laser configuration, iPS cells were not included and the antibodies used were EpCAM, Cytokeratin, Vimentin, MT1-MMP, CD45 and DAPI. Cells were sorted based first on size (using forward and side scatter to remove doublets and debris) and then by the population that was negative for both CD45 and CD16. For technical reasons, cells were not sorted directly onto microscope slides and instead were collected into three different Eppendorfs: i) EpCAM+ only, ii) EpCAM+/CK+ and iii) Vimentin+/MT1-MMP+. This was based on the presumption that cells in i) were LNCaPs, cells in ii) MCF-7s and cells in iii) PC3s. The cells were then mounted on microscope slides using DAPI mounting media. Due to the potential of fluorescence degradation, the cell sort was performed in the dark, as was the mounting of cells onto the slides. Cells were imaged in the Bioimaging facility at Newcastle University using the Nikon AR1 confocal microscope with the following lasers: 405nm, 488nm, 561nm, 647nm (Figure 4.28).



a) EpCAM+/DAPI+

b) CK+/DAPI+

c) Vimentin+/DAPI+

Figure 4.28 Immunofluorescence images to demonstrate three cells sorted on the BD FACS Fusion based on negative expression of CD45/CD16. These cells were cell lines spiked in healthy volunteer blood and stained with EPCAM, Cytokeratin, Vimentin, MT1-MMP. CD45 and DAPI. Cell a) was positive for EpCAM, cell b) was positive for Cytokeratin and the cells in c) were positive for Vimentin.

As Figure 4.28 demonstrates, it was possible to detect some of the sorted cells. However, the cells were very sparse and this was despite spiking with 100 000 of each cell of the three cell lines, with the potential of 300 000 cells to sort. In a clinical sample, the expected CTC population would be much lower, so the feasibility of this option is limited. It was time-

consuming to set up each slide with the lasers, and during the setting-up there was the risk of bleaching the samples. Though the process was repeated three times it was only possible to image one set of slides because of these time constraints, and because the experiment yielded a poor number. The decision was made not to repeat this experiment as it was felt unlikely to be possible to replicate it using clinical samples. Cells expressing MT1-MMP were also not imaged due to the laser overlap with the cells expressing Cytokeratin. Reassuringly, there were no white cells detected, which for this one experiment demonstrated a pure sort. However, if considering this method as an option, the purity of the sort would need to be investigated in more detail.

4.6.2 DNA extraction for PCR and sequencing

Because imaging the sorted cells proved difficult, the decision was made to sort the cells and use a DNA amplification kit to get enough DNA from the small sorted cell population. This would enable a PCR to be performed to look for prostate specific mutations, or to send the cells directly for sequencing. The anticipated sorted cell population in the clinical assay would have fewer than 1000 cells, so the REPLI-g Mini kit (Qiagen) was chosen for this purpose. Due to time constraints this assay was not tested prior to the collection of clinical samples. The clinical samples were sorted and frozen at -80°C for analysis following the collection of all samples.

Approximately halfway through the collection of clinical samples, it became apparent that using this (or similar products) on fixed cells would give a falsely elevated reading of DNA. To test this theory, 1000 cells from three different cell lines underwent DNA extraction and amplification using this kit. Each cell line had two arms; fixed and unfixed. DNA levels were then measured for both using the Qubit (ThermoFisher Scientific). The results are displayed in the following graph (Figure 4.29).

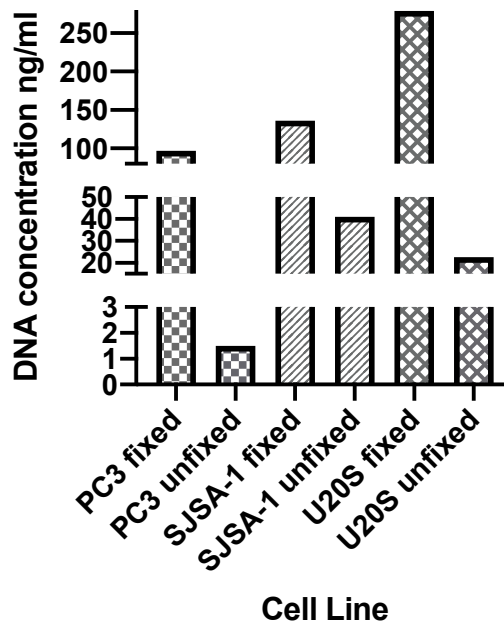


Figure 4.29 A graph to demonstrate DNA yield from 3 different cells lines using either fixed or unfixed cells. 1000 cells from three different cell lines underwent DNA extraction and amplification, before DNA levels were measured on the Qubit. This was to determine whether fixation gave a false estimation of DNA quantity.

In all three cell lines, higher values of DNA were obtained in the fixed samples compared to the unfixed samples. Because the fixative used was paraformaldehyde (similar to the fixative in the FixLyse buffer used in the final assay) this causes protein crosslinking, which would need to be reversed in order to obtain accurate results. This can be possible e.g. when looking at tissue sections, but the temperatures required to do this are very high and tissue sections will contain a much greater number of cells. The high temperatures risk damaging the cells, and when faced with a very low number to start with the risk of cell loss is very high. Fixation using coagulants such as methanol or ethanol would not cause this problem, but because over half of the clinical samples had been collected and processed by this stage it was felt that such a significant change to the assay could alter retrieval rates and therefore results.

Cells from the clinical samples were therefore sorted using the assay as described in section 1.4 but no post-sort analysis has been performed. Data obtained from this experiment must therefore be validated by comparing the results from clinical samples with the results from healthy volunteer controls. The sorted cells have been kept for all patients and controls and could in future be analysed if an appropriate method became available.

4.7 Results by patient characteristic

The following tables (Tables 4.3-4.9) show a summary of the number of cells detected by the assay described in this chapter, according to patient characteristics. Each cell expressing the different antigens expressed is recorded for each patient. Combinations of antigens were not recorded as without visual inspection of the cells, as in the Imagestream assay, it was not possible to rule out counting cells twice.

Patient No	Age	Treatment	PSA	EpCAM	CK	Oct4	SOX2	Nanog	Vimentin	MT1-MMP	Total
1	48	Healthy Volunteer	N/A	2	11	1	7	10	21	838	890
2	41	Healthy Volunteer	N/A	0	9	8	6	9	15	1082	1129
3	43	Healthy Volunteer	N/A	0	6	6	0	3	1	943	959
4	52	Healthy Volunteer	N/A	2	8	7	3	4	21	900	945
5	38	Healthy Volunteer	N/A	1	2	0	3	3	7	423	439

Table 4.3 A table to show the number of cells expressing each antigen that were found in the blood from each healthy volunteer.

Patient No	Age	Treatment	PSA	EpCAM	CK	Oct4	SOX2	Nanog	Vimentin	MT1-MMP	Total
1	73	New patient – negative biopsy	9.9	1	0	0	16	159	5	18	199
2	79	New patient – negative biopsy	9.5	8	0	1	4	225	2	0	240
3	67	New patient – negative biopsy	5.6	1	25	25	0	13	4	399	1047
4	68	New patient – negative biopsy	7.9	1	30	30	2	6	452	1434	1925
5	67	New patient – negative biopsy	7.2	1	64	64	89	17	11	112	318
6	70	New patient – negative biopsy	4.4	0	17	17	122	22	29	203	393

Table 4.4 A table to show the number of cells expressing each antigen that were found in the blood from each patient with benign disease.

Patient No	Age	Treatment	PSA	EpCAM	CK	Oct4	SOX2	Nanog	Vimentin	MT1-MMP	Total
1	68	AS	5.3	3	191	47	5320	152	13	7	5732
2	72	AS	6.1	5	0	1	5888	153	53	3	6103
3	76	WW	27.1	0	31	25	0	21	132	170	379
4	84	WW	18.1	0	30	0	2	61	42	790	925
5	87	WW	86.0	4	0	3	321	15	130	745	1218
6	76	AS	37.4	2	0	16	0	329	0	813	347

Table 4.5 A table to show the number of cells expressing each antigen that were found in the blood from each patient on surveillance.

Patient No	Age	Treatment	PSA	EpCAM	CK	Oct4	SOX2	Nanog	Vimentin	MT1-MMP	Total
1	77	New Diag	5.2	1	0	8	25	157	12	0	203
2	68	New Diag	33.5	0	0	0	24	174	3	1	202
3	65	New Diag	18.3	29	0	19	2	117	54	269	490
4	74	New Diag	140.0	0	2	2	45	0	73	3213	3335
5	68	New Diag	308.0	1	4	4	42	13	33	4085	4182
6	62	New Diag	22.0	1	117	8	1687	3	1	396	2213
7	68	New Diag	47.0	3	51	7	82	1	0	365	509
8	69	New Diag	3.2	2	244	0	254	53	7	1641	2201

Table 4.6 A table to show the number of cells expressing each antigen that were found in the blood from each patient with newly diagnostic metastatic disease.

Pt	Age	Treatment	PSA	EpCAM	CK	Oct4	SOX2	Nanog	Vimentin	MT1-MMP	Total
1	69	Single agent	31.4	2	16	1	27	36	0	8	90
2	82	Single agent	1.8	0	11	13	46	166	43	2	281
3	71	Single agent	2.9	0	0	0	6	118	6	0	130
4	92	Single agent	0.2	0	0	3	17	158	15	6	199
5	91	Single agent	0.2	0	30	3	0	8	22	122	185
6	82	Single agent	50.9	0	97	2	1	13	302	921	1336
7	87	Single agent	4.5	8	12	3	251	62	8	179	523
8	66	Single agent	0.1	2	4	0	87	9	12	74	188
9	71	Single agent	2020	5	8	14	11	0	6	450	494
10	77	Single agent	0.1	17	11	2	4	58	1	7	100
11	59	Single agent	4.5	22	15	4	2	21	195	864	1123
12	63	Single agent	81.9	199	1515	2	9	7	0	8245	9977
13	67	Single agent	3.0	2	28	1813	904	1	14	116	2878

Table 4.7 A table to show the number of cells expressing each antigen that were found in the blood from each patient on single agent hormones.

Patient No	Age	Treatment	PSA	EpCAM	CK	Oct4	SOX2	Nanog	Vimentin	MT1-MMP	Total
1	86	MAB	245.6	88	2	1	151	118	8	44	412
2	84	MAB	61.4	11	0	1	777	16	16	0	821
3	79	MAB	1.5	0	3	26	152	160	26	0	367
4	87	MAB	3.1	0	616	13	389	160	25	12	1215
5	82	MAB	24.0	1	1	6	36	119	5	1	169
6	77	MAB	101.0	1	0	0	19	123	8	1	152
7	78	MAB	1.5	0	7	5	21	117	6	0	156
8	69	MAB	1.8	0	0	2	19	434	3	24	482
9	86	MAB	12.6	15	0	4	9	172	23	1	224
10	83	MAB	0.1	1	0	0	3	90	1	1	96
11	83	MAB	23.4	0	13	1	2	10	22	164	212
12	74	MAB	2.0	16	1	5	982	0	0	80	1084
13	96	MAB	34.6	18	10	2	3	44	180	475	732
14	80	MAB	1.7	7	10	9	1	29	20	54	130
15	73	MAB	5.5	12	1	4	4	30	63	245	359
16	65	MAB	30.6	0	6	1	44	3	21	588	663

Table 4.8 A table to show the number of cells expressing each antigen that were found in the blood from each patient on maximum androgen blockade.

Pt No	Age	Treatment	PSA	EpCAM	CK	Oct4	SOX2	Nanog	Vimentin	MT1-MMP	Total
1	77	Enzalutamide	1875	8	417	13	94	62	5	2243	2842
2	68	Docetaxel	0.8	0	0	0	353	164	1	56	574
3	85	Dexamethasone	55.0	2	18	6	360	116	42	1	545
4	69	Enzalutamide	380	109	10	6	13	1	162	532	833
5	77	Dexamethasone	18.0	17	2	5	4	492	307	639	1466
6	61	Abiraterone	51.2	0	2	4	83	3	36	1247	1375
7	60	Enzalutamide	0.7	0	2	3	52	231	0	3001	3289
8	74	Dexamethasone	0.7	0	2	2	368	18	8	1352	1750
9	73	Dexamethasone	23.0	858	1176	25	19	4	58	9339	11479
10	77	Docetaxel	433	555	697	1	3	1	114	3583	4954
11	58	Enzalutamide	12.4	0	83	14	490	7	178	547	1319
12	87	Cabazitaxel	5.6	1	44	6	224	8	0	384	667
13	70	Dexamethasone	228	3	126	10	483	18	0	1059	1699
14	82	Enzalutamide	72.4	10	211	24	610	5	1	1336	2197
15	74	Abiraterone	16.3	0	122	5	22	13	21	3763	3946
16	74	Docetaxel	8.0	0	331	7	18	7	16	4751	5130
17	72	Enzalutamide	586	9	326	13	22	7	6	4482	4865
18	69	Radium 223	202	43	395	0	10	0	21	1528	1997
19	80	Enzalutamide	2.2	2	6382	1	15	3	4	3326	9733
20	74	Enzalutamide	1.3	5	207	2	6	4	2	3597	3823
21	76	Dexamethasone	0.8	1	0	0	1	0	0	187	189
22	51	Enzalutamide	434	5	721	0	5	0	15	6278	7024
23	58	Docetaxel	100	3	138	3	134	1	14	2602	2895
24	76	Enzalutamide	4611	5	6142	0	70	124	0	6697	13038
25	77	Radium 223	29.2	2	131	0	159	62	2	2059	2415
26	66	Enzalutamide	21.0	43	60	28	196	2	5	4593	4927
27	72	Enzalutamide	532	3	231	8	303	2	14	774	1335
28	81	Radium 223	96.1	4	28	5	187	0	156	1543	1923
29	78	Dexamethasone	10.5	3	47	5	232	0	340	1381	2008

Table 4.9 A table to show the number of cells expressing each antigen that were found in the blood from each patient with castrate resistant disease.

4.8 Discussion

Unfortunately, despite careful panel planning, there was too much overlap between DAPI and Oct4 (BV421). The decision was made to exclude DAPI from the panel and rely on forward and side scatter to identify whole cells rather than debris. Although this meant that the FDA criteria for a CTC could not be fulfilled using this assay, it was decided that re-arranging the panel and undergoing further optimisation of antibodies conjugated to new fluorochromes would delay the collection of clinical samples and the ability to test the assay. Although this is a flaw of this assay, the identification of cell-sized, marker positive cells was felt to be sufficient.

When using gates to include or exclude populations found on FACS these will rarely be 100% pure. There is always likely to be a slight overlap in fluorescence and this can be explained in part by cellular heterogeneity – some cells will only weakly express an antigen in comparison to others. The gate used to determine the negative white cell population in the optimisation experiment (Figure 4.1) could be made bigger and could include more cells as there is an overlap between that and the white cell population. This gate was manipulated many times in order to include as many potential CTCs as possible, without the need to study an unnecessarily large population. The experiment described in section 4.3.2 to determine the percentage of white cells not detected by each antibody demonstrated that only 3.1% of white cells were not detected by the CD45 antibody, and 12.4% by the CD16 antibody. The experiment looking at the number not detected by either was not performed, but by looking at Figure 4.1 there are cells that are positive for each antibody but not for both, so a proportion of the 3.1% not detected by CD45 will have been excluded by being positive for CD16. It will never be possible to get 100% purity; using additional white cell markers would help but would be at the expense of one of the markers of interest, but even then, there would never be 100% antigen binding. It is hoped that the use of these two white cell markers will identify a practical proportion of white cells, to eliminate them from the potential CTC population.

The optimisation experiments for the epithelial, mesenchymal and stem cell markers all used 100 000 cells. This number was chosen so that a reliable number of cells would be stained, but a number far greater than the potential number of CTCs in the samples would be used. This would ensure that any antibody quantity would be more than enough to bind with antigens expressed by CTCs.

As discussed, the overlap between the iPS cells stained with the isotype and those stained with the antibody could be due to the iPS cells losing their stem-cell properties as they start to differentiate, despite lowest passage cells being used at all times. However, on a few of the other antibodies (Vimentin, Cytokeratin) there was overlap of the isotype and antibody stained cells, particularly at higher concentrations. This could be because the isotype becomes stickier when more is used.

The gates used in section 4.5 are again not 100% discriminatory and when compared to the isotype stained cells in optimisation, most do include very small proportions of the isotype stained cells. This could mean false positives in the final assay. Despite meticulous optimisation and choosing antibody concentrations that stain the maximum number of cells without providing excess that could bind inappropriately, this is inevitable. In all cases except that of Vimentin, less than 1% of the isotype-stained cells could be found in the gate used to identify the antibody stained population, and 1.55% of the Vimentin isotype-stained cells were in this gate. It is hoped that this leaves an acceptable degree of uncertainty.

A major flaw of this assay was the inability to test its validity using downstream analysis and was in part due to trying to process samples for both this and the Imagestream assay simultaneously. Because on average four or five blood samples were collected at each clinic, processing time was high, and using the same fix/lyse process meant simultaneous processing could occur more quickly. Fixing the cells was important due to the length of the protocol. It would not have been possible to perform red cell lysis, white cell depletion, incubate with the antibodies and run the samples on the FACS sorter on the same day as collection, due to the clinic timings and time taken to obtain the samples. Fewer samples could have been obtained but the impact of any observational study would be reduced by a lower sample number. This however has to be balanced against the need for reliable data – there is little point having a large study if the data is meaningless.

The concern about using FACS is the purity and sensitivity of detecting small cell populations, such as CTCs. As the Imagestream has demonstrated, even when using size-based criteria to eliminate debris, some cell shaped events (possibly dead cells or larger debris) can bind to antibodies inappropriately and until they are further scrutinised (e.g. by imaging) they would appear as a false positive. In the assay described in this chapter the inability to use DAPI, and therefore identify whole cells, in addition to the inability to perform downstream analysis has further added to this concern. But when reviewing the literature, multiple studies do use

flow cytometry for the detection of CTCs and report detection rates as sensitive as 3 cells in 2mls of blood (Lu et al., 2015) or 1 in a million cells (Carpenter et al., 2014, Gorner et al., 2015). In this assay the use of two white cell markers in addition to the prior immunomagnetic depleting of white cells are both important ways of identifying a purer population, and using male controls to compare results against is also a strength. In addition to this, because the FACS assay is being run in parallel to the Imagestream assay, data obtained from both can be compared up to a point. Although the FACS assay uses additional markers, the stem cell markers are explored in both, and so any marked differences in detection would potentially be a sign of the FACS assay being inaccurate.

Creating a new assay involves many processes, and the development of this one was more challenging than first anticipated, in part due to the number of markers that were being investigated. The benefit of using FACS for CTC detection is the fact that most clinicians considering such an assay for a clinical trial would have access to a platform, which would increase the uptake of any trial participation. Whilst FACS sorting is relatively expensive, straight-forward FACS processing is inexpensive, and these are both important factors to consider when thinking about a new assay for clinical use. Rigorous optimisation was adopted during the development and whilst downstream analysis was not performed to test the validity, it is hoped that the process was scrupulous enough that the data obtained, as presented in Chapter 5, could be used to develop a future clinical trial.

Chapter 5. The clinical significance of CTCs detected by Imagestream and FACS

Chapter Summary

This chapter contains the results of the patient blood samples that were processed using both the Imagestream and FACS assays, described in Chapters 3 and 4 respectively. Patients have been grouped according to the treatment they were on at the time of blood sampling, and clinical data for PSA and ALP was recorded. Statistical analysis has been performed to determine whether significant differences in CTC count and antigen expression are demonstrated and whether there was any correlation shown between CTC count and the clinical parameters. Any cell described as a CTC in this chapter is a putative CTC as expression of Vimentin, MT1-MMP, Oct4, SOX2 and Nanog is not included in the FDA definition of a CTC.

5.1 Clinical Data

5.1.1 Demographics of patients

Blood was obtained from 88 male patients at the Freeman Hospital, Newcastle upon Tyne between August 2017 and April 2018. Six samples were lost when the Imagestream crashed during processing and there were problems with two different samples during FACS processing. For two further patients it was not possible to obtain any clinical data. In total therefore there are 78 patients who had blood processed on both platforms with matched clinical data. Age range was from 58-96 with a median age of 75 and a mean of 74. Men with different stages of prostate cancer were subjects for this study, ranging from those referred with a suspicion of prostate cancer but who subsequently were found to have benign prostate conditions, to those with castrate resistant disease (Figure 5.1). The latter was defined by the need for a second line agent following a rising PSA, or increase in radiological burden of disease despite maximum androgen blockade. Because not all patients had up-to-date imaging at the time of blood sampling and there were often no pathology results, classification by stage of disease was chosen but this should not be confused with TNM staging.

The original aim of the study was to identify a biomarker to predict who would respond to androgen deprivation therapy and who would benefit from initial treatment with what are known as second line agents (e.g. abiraterone or enzalutamide). Because of this, ideally patients with a new diagnosis of metastatic disease before the commencement of any treatment would be chosen. However, patients were chosen with different stages of diseases so that CTCs would be more likely to be detected. Not all patients with early metastatic disease would have high levels of CTCs in their blood, which would make commenting on the significance of the presence or absence of specific markers in their blood difficult. At this stage of the study, patients with a high metastatic burden were chosen in addition to those with early metastatic disease, so that a comparison could be made. If the findings were found to be significant then further studies recruiting larger numbers of untreated patients with metastatic disease could be performed.

The patients with benign prostatic disease were included as an age-matched control comparison.

Although patients on active surveillance are deemed curative and those on watchful waiting are considered palliative, they were classified together for the purpose of this study as the patients are not on treatment. The decision for patients to decline treatment is made on an individual basis with the aim of reducing treatment associated toxicity (Heidenreich A., 2013). Those on active surveillance have a defined investigation schedule (including biopsy, imaging and PSA testing) whereas those on watchful waiting will have an individualised schedule based on symptoms. Treatment for patients in either group can be started once progression is identified. In theory the patients in both of these groups should have stable disease and the assumption has been made that any CTCs present should not express markers associated with aggressive disease. In terms of overall CTC count, those on watchful waiting could have metastatic disease and therefore could have a higher CTC count, but because numbers of patients sampled in each category were small, they were classified together.

It is not possible to say until several months after their blood was taken whether their disease was static at the time of the sampling for this study, as subsequent PSA results may indicate disease progression. Presence of CTCs and certain markers expressed by those CTCs may be more sensitive than PSA rises. This will be explored in more detail when comparing

the interval PSAs of patients in each treatment group, but in comparison to the patients with end-stage disease, it would be expected that patients on active surveillance and watchful waiting would have both a lower CTC number and a lower number of markers associated with aggressive disease. Figure 5.1 outlines the number of patients at each stage of disease.

Seven patients who had a new diagnosis of metastatic disease but who were completely treatment naïve were included in this study. Six of these had radiological evidence of metastatic spread to either lymph nodes or bones, and the seventh was treated as a presumed metastatic diagnosis due to his PSA and the clinical examination of his prostate, despite no confirmed radiological evidence of spread.

Those patients on androgen deprivation therapy could be further divided into those on single hormonal agents, or those on maximum androgen blockade, as demonstrated in Figure 5.2. The latter consists of the addition of an anti-androgen following previous medical or surgical castration. Those on maximum androgen blockade could have well controlled, static disease. But again, subsequent clinical follow-up would identify those who had disease that quickly progressed after the time of sampling, and this will be demonstrated in more detail later in this chapter. One of the patients on maximum androgen blockade and four of the patients on single hormonal therapy had received up-front chemotherapy at the time of starting hormonal therapy, due to recent changes in the guidelines (Heidenreich A., 2013).

Patients classified for the purpose of this study as having castrate resistant disease were all on a second line agent (e.g. dexamethasone, enzalutamide, abiraterone). Because clinical trials such as STAMPEDE (2019) have changed the order of treatment in recent years, further stratification into specific treatment groups was not performed.

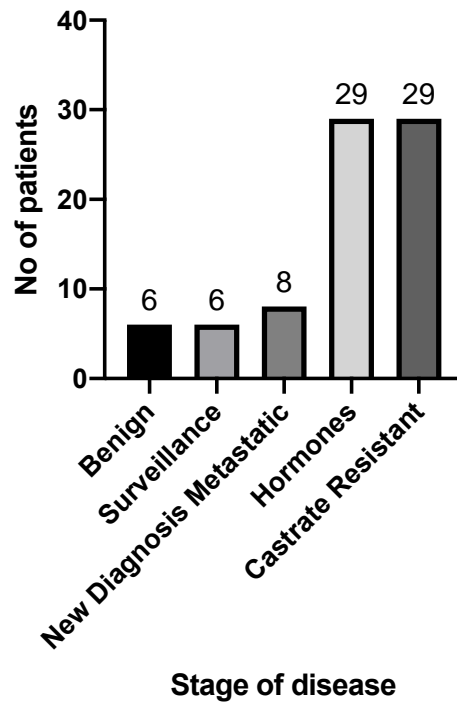


Figure 5.1 A graph to demonstrate the breakdown of patients used in this study by stage of disease. The majority have metastatic disease, either newly diagnosed, on hormone suppression, or are on second line therapy for castrate resistant disease.

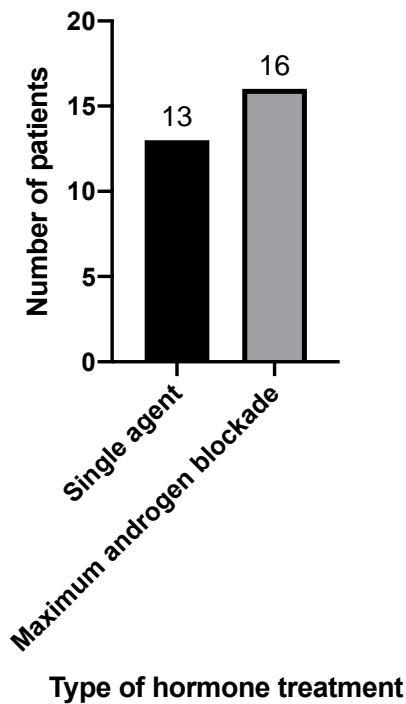


Figure 5.2 A graph to demonstrate the type of hormone therapy patients were on. Thirteen patients were on single hormone agents compared to sixteen patients who were on maximum androgen blockade.

5.1.2 Healthy volunteer controls

Five male healthy volunteers from the NICR donated blood to process on the Imagestream and FACS. There is no matched clinical data for these volunteers as ethical approval for this was not obtained, but the CTC results can be compared with the patient samples as none of the patients were known to have any existing malignancies. It was felt necessary to have some controls with no known prostate disease, as although prostate cancer has not been diagnosed in the benign patient cohort, there may be small foci of cancer that have not been detected by the existing methods.

5.1.3 Clinical blood results

For the purpose of this study, the 'time of sampling' is used to describe the time that blood was sampled from the patient for the Imagestream and FACS assays. Ethical approval had been obtained prior to starting the project and did not permit serial sampling for lab work, or any additional clinical blood tests that were not required for clinical purposes. Bloods obtained for routine clinical use could however be used so data was collected from patients at both the time of obtaining blood for the assays described in Chapters 3 and 4, and six months later.

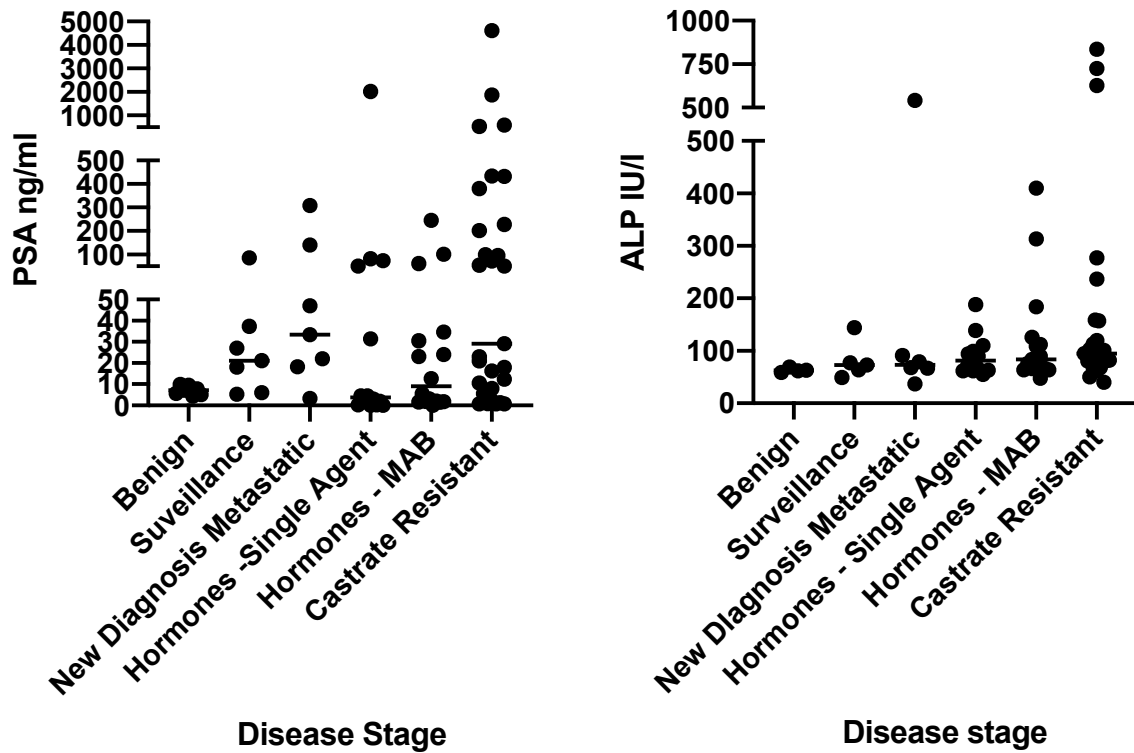
All patients attending prostate cancer clinics in the UK currently undergo interval PSA testing. As previously discussed, despite its flaws, this is the most reliable biomarker currently available and monitoring the PSA of an individual can usually indicate the response to different treatments. Actual PSA value is not usually helpful but a trend for an individual patient is more indicative of disease progression.

PSA alone is not sufficiently reliable for disease monitoring, especially in castrate resistant disease (Payne and Cornford, 2011) due to evidence of metastatic disease spread despite a stable PSA (Pezaro et al., 2014). For this reason, regular imaging (CT and/or bone scan) and repeat blood tests including a Full Blood Count, ALP and Liver profile are recommended even if the patient has no symptoms. Frequency of these investigations will vary between units, but evidence suggests this should be every 6 months for metastatic disease (Gillesen et al., 2016).

Alkaline Phosphatase (ALP) monitoring can be useful because abnormal bone tissue formation, which can occur when bone metastases are present, can lead to elevated ALP

production. This membrane-bound glycoprotein is predominantly produced in the liver but can also be produced by other organs such as bone, pancreas and kidney (Sharma et al., 2014). An increase in ALP might therefore indicate to the clinician that bone metastases are forming, or increasing in burden, and may warrant earlier radiological imaging and a possible change of treatment. A normal ALP will vary between labs but at the Freeman Hospital the normal value is 30-130 IU/l.

Because the patients have all had a variety of follow-up tests and scans, and data was collected at a relatively early time-point for follow-up, the decision was made to note PSA and ALP for each patient at the time of sampling and after a six-month interval as these provided the most complete data sets. Although this is only a crude measure, it would be expected that patients with benign disease would have a lower PSA and ALP than those with castrate resistant disease. In addition, those with treatment-controlled disease (e.g. those on hormones) would be expected to have a lower PSA and ALP than those with newly diagnosed metastatic disease, or those on treatment who are becoming resistant. These results can then be compared to CTC count and antigens expressed in the next sections, as a method of correlating the CTC results with disease severity. Figure 5.3 shows the number of patients at each disease stage and their PSA and ALP at the time of blood sampling.



a) PSA

b) ALP

Figure 5.3 Graphs to show a) PSA level and b) ALP level at the time of blood sampling for all patients at each stage of the disease (the bar denotes the median). Those with metastatic disease have a higher median level of PSA and ALP.

Disease Stage	Median PSA at sampling	Mean PSA at sampling (+SD)	Range
Benign	7.2	7.1 (2.2)	4.4-10.0
Surveillance	21.1	28.7 (27.7)	5.3-86.0
New diagnosis metastatic	33.5	81.7 (109.5)	3.2-308.0
Hormones – single agent	3.8	162.5 (535.4)	0.02-2020.0
Hormones – MAB	9.1	34.3 (62.3)	0.02-245.6
Castrate resistant	29.2	338.2 (901.1)	0.7-4611

Table 5.1 A Table to show the Median and Mean PSA for patients in each disease stage category at the time of sampling. Those with metastatic disease have a higher median PSA level.

Disease Stage	Median ALP at sampling	Mean ALP at sampling (+SD)	Range
Benign	62.5	63.3 (4.2)	59-69
Surveillance	73.0	81.4 (36.6)	49-144
New diagnosis metastatic	73.5	147.2 (193.8)	37-541
Hormones – single agent	81.5	91.2 (39.1)	55-188
Hormones – MAB	84	123.2 (100.1)	48-410
Castrate resistant	95	180.5 (215.8)	50-835

Table 5.2 A Table to show the median and mean ALP for patients in each disease stage category at the time of sampling. The median for patients in all categories was within the normal range.

As expected, the graphs in Figure 5.3, and the data in Tables 5.1 and 5.2 depict the generalized pattern that both PSA and ALP are higher as disease is more advanced. From the standard deviation it is clear that there is a greater variation in PSA results in those patients with newly diagnosed metastatic disease, single-agent hormones and castrate-resistant disease compared to those with benign disease, undergoing surveillance and on maximum androgen blockade.

In order to demonstrate this more closely, PSA and ALP at both sampling time and six-month interval were plotted for each group (Figures 5.4 – 5.8). These data were limited by the fact that not all patients had PSA measured at six months (e.g. those in the benign and surveillance groups – due to clinical need this may be monitored at 9 or 12 months) and ALP was not measured for every patient (e.g. no patient in the benign group had ALP measured at six months)(Figure 5.4).

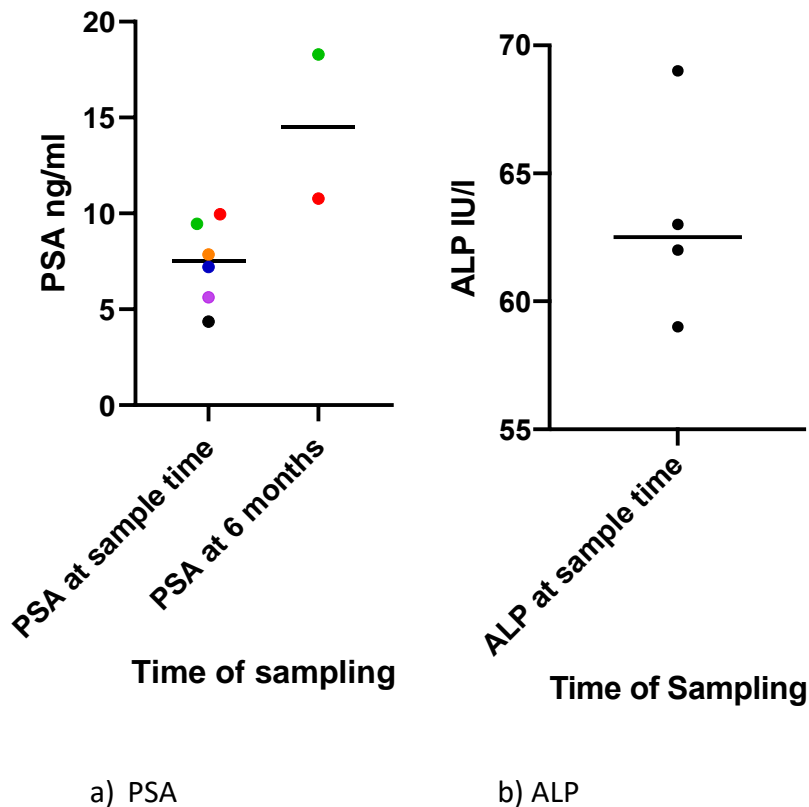


Figure 5.4 Graphs to show a) PSA and b) ALP at the time of sampling and at a six-month interval for patients with benign disease (the bar denotes the median) N.B. No six-month ALPs were recorded for these patients. Each coloured dot represents one patient so the corresponding value at 6 months can be seen. A black coloured dot at baseline means there was no 6-month sample recorded. The median PSA did increase only two patients had PSAs taken at six months and both had negative prostate biopsies.

Only two patients in this group had PSA taken at six months, and none had ALP measured. The ALP for all patients was within the normal range at the time of sampling. A modest rise in PSA was seen for the two patients with serial PSA samples but biopsies of both of these patients were negative, so it can be assumed that all patients within this category had benign disease.

It was not possible to perform statistical evaluation on the PSA or ALP progression due to lack of PSA and ALP data at six months for these patients.

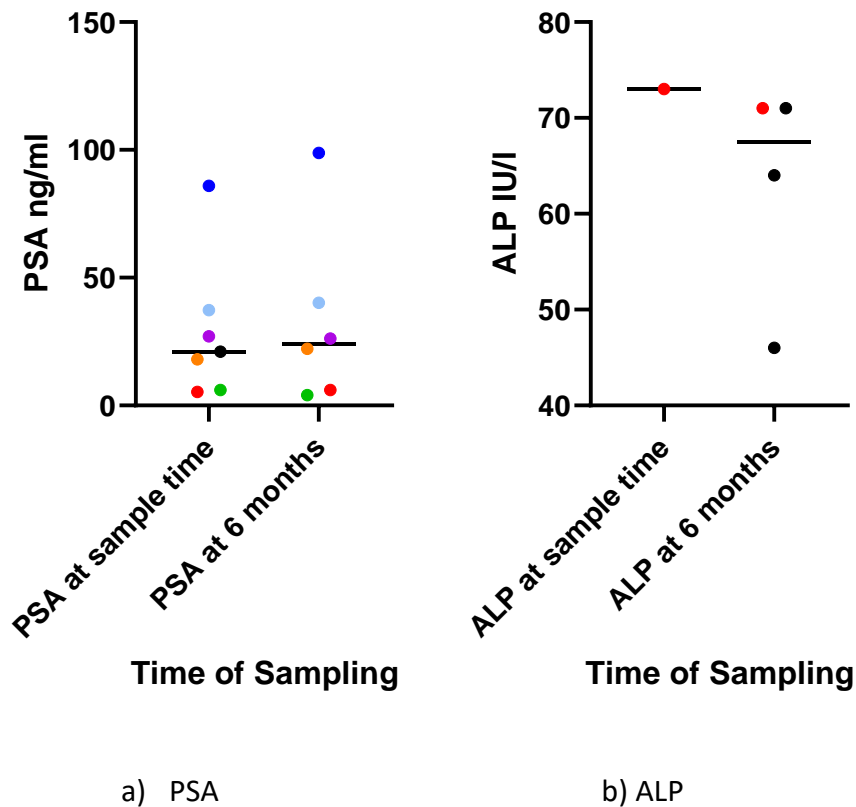


Figure 5.5 Graphs to show a) PSA and b) ALP at the time of sampling and after six months for patients on surveillance (the bar denotes the median). Each coloured dot represents one patient so the corresponding value at 6 months can be seen. A black coloured dot at baseline means there was no 6-month sample recorded and vice versa. There was no significant PSA increase at six months ($p=0.32$). As only one patient had an ALP taken at sampling time no comparison could be made.

All patients within the Surveillance group had ALPs within the normal range. The median PSAs at sampling time and at six months are very similar (Figure 5.5).

The Wilcoxon matched pairs signed rank test was used to identify whether any significant change in PSA occurred over 6 months. This showed a p-value of 0.32 which demonstrates no significant change. It was not possible to do this for the ALP due to only having one value at the time of sampling.

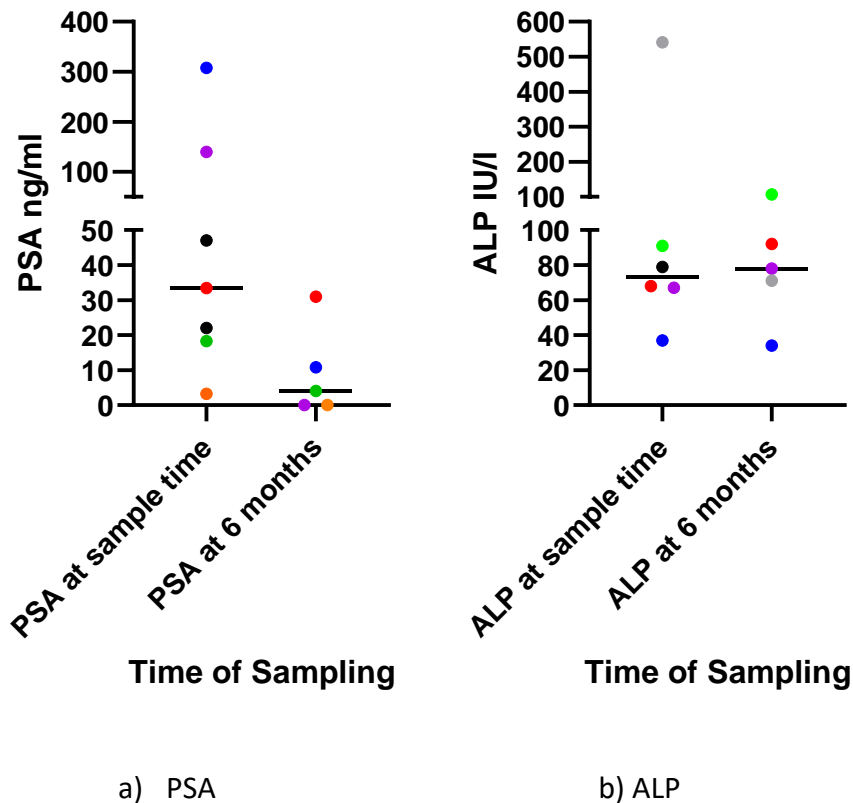


Figure 5.6 Graphs to show a) PSA and b) ALP at the time of sampling and after a six-month interval for patients with newly diagnosed metastatic disease (the bar denotes the median). Each coloured dot represents one patient so the corresponding value at 6 months can be seen. A black coloured dot at baseline means there was no 6-month sample recorded. All patients showed a PSA response to treatment but this was not found to be significant ($p=0.06$). ALP increased marginally at 6 months but this was also not significant ($p=0.81$).

The patients within the Newly Diagnosed Metastatic Disease group are of particular interest because they presented with metastatic disease and at the time of sampling were treatment naïve. Interestingly the patient with the lowest PSA had the highest ALP and had a significant bony burden of metastatic disease. All patients showed a PSA response to treatment (i.e. PSA decreased at 6 months) but the median ALP increased by 11.0IU/l (Figure 5.6). This was not found to be a statistically significant increase when the Wilcoxon matched pairs signed rank test was used ($p = 0.81$). The same test was used to determine a significant difference in PSA change which was also not found to be significant ($p = 0.06$) despite a median decrease of 14.28ng/ml over 6 months.

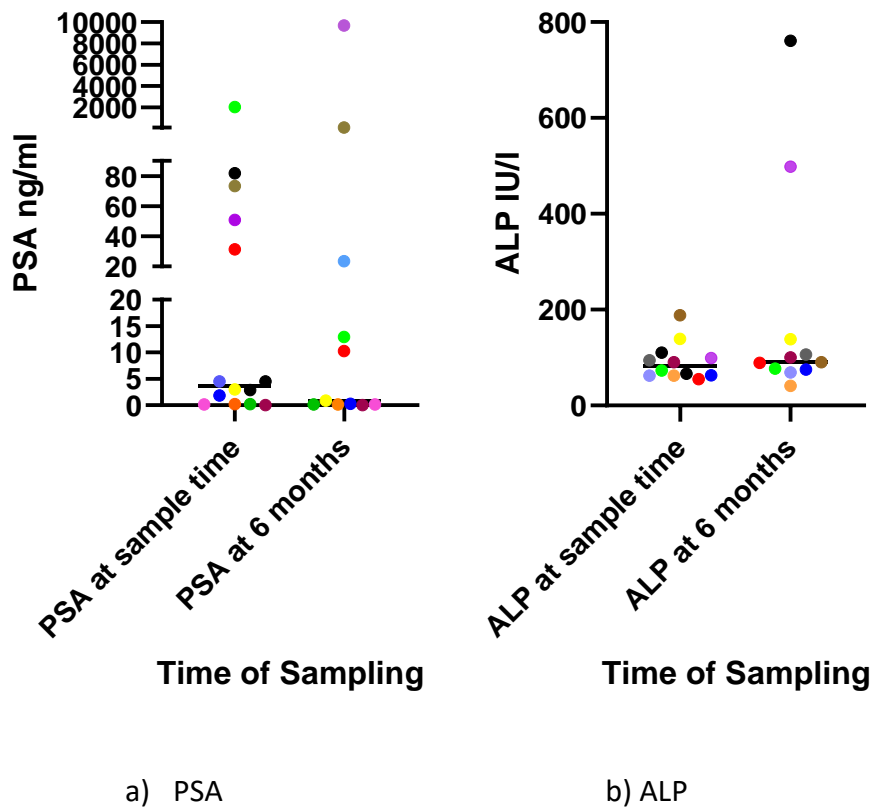


Figure 5.7 Graphs to show a) PSA and b) ALP at the time of sampling and after six months for patients on single hormonal agents (the bar denotes the median). Each coloured dot represents one patient so the corresponding value at 6 months can be seen. A black coloured dot at baseline means there was no 6-month sample recorded. The median PSA and ALP changes were not significant ($p=0.57$ and $p=0.31$ respectively).

The median PSA for patients in the Single Hormonal Agent group decreased by 0.04ng/ml but this was not found to be significant (Wilcoxon matched pairs signed rank test $p = 0.57$). Median ALP rose by 8.5IU/l but this was also not significant ($p = 0.31$) (Figure 5.7).

One patient was a particular outlier whose PSA and ALP rose dramatically during the six-month period. Despite then being started on a second line agent at six months, he died shortly afterwards. There was also one death in this group during the six months, but from a non-prostate cancer related cause.

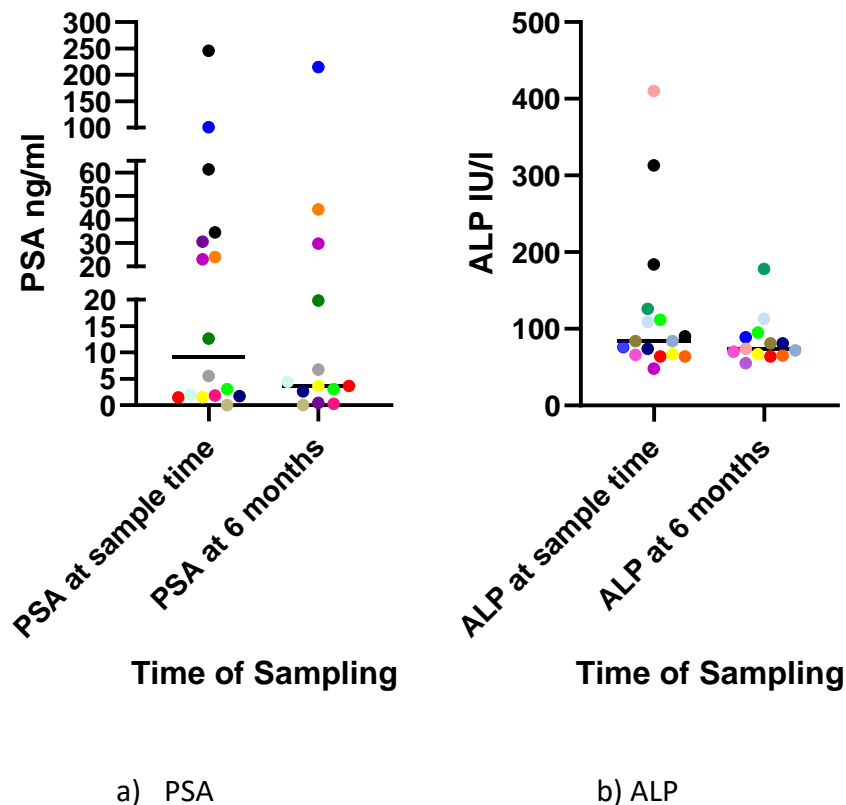


Figure 5.8 Graphs to show a) PSA and b) ALP at the time of sampling and after six months for patients on maximum androgen blockade (the bar denotes the median). Each coloured dot represents one patient so the corresponding value at 6 months can be seen. A black coloured dot at baseline means there was no 6-month sample recorded. Both median PSA and ALP decreased but this was not significant ($p=0.08$ and 0.75 respectively).

The data for the Maximum Androgen Blockade group was slightly skewed as two of the patients with higher PSA and ALP results at sampling time had died from the disease by the six-month point, and therefore no blood results were available. They account for the two highest ALP results at sampling (Figure 5.8). Of the surviving fourteen patients, four had a PSA that almost doubled during the six months, indicating that their disease could now be castrate resistant.

Median PSA decreased by 2.11ng/ml which was not found to be significant ($p = 0.08$) and median ALP change was also not significant ($p = 0.75$).

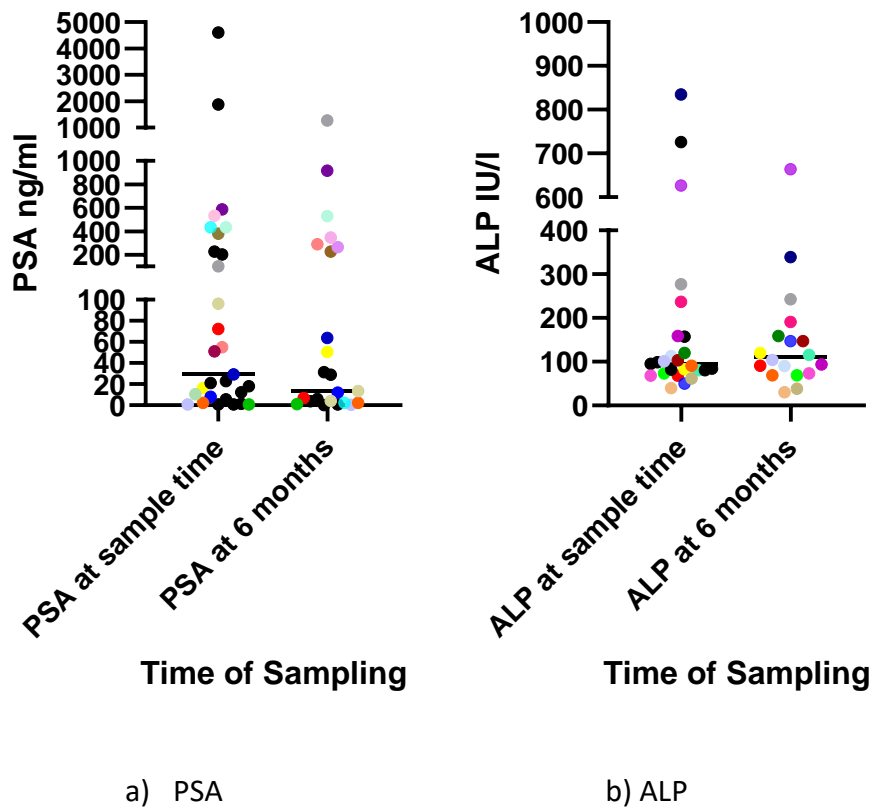


Figure 5.9 Graphs to show a) PSA and b) ALP at the time of sampling and after six months for patients with castrate resistant disease (the bar denotes the median). Each coloured dot represents one patient so the corresponding value at 6 months can be seen. A black coloured dot at baseline means there was no 6-month sample recorded. Median PSA decreased but this was not significant ($p=0.36$) and median ALP rose was also not significant ($p=0.98$).

PSA level in the Castrate Resistant Disease group was both on average higher and with a greater range, indicating that some of the patients in this group had end stage disease (no further treatment options). The two patients with the highest PSA results at time of sampling had died by the six-month point, and a further death occurred within this group, all from prostate cancer related causes.

Median PSA decreased by 0.43ng/ml which was not significant ($p = 0.36$) and median ALP increased by 3IU/l which was also not significant ($p = 0.98$) (Figure 5.9).

None of the different groups showed a significant increase or decrease in PSA or ALP during the six-month period, as demonstrated in Table 5.3. This could be due to low numbers in each group, a short follow-up time or alternatively because PSA and ALP are unreliable biomarkers.

Disease stage	p-value for change in PSA over 6 months	Median of difference in PSA (range)	p-value for change in ALP over 6 months	Median of difference in ALP over 6 months (range)
Benign	-	-	-	-
Surveillance	0.32	+1.87 (-21.1- +12.8)	-	-
Newly diagnosed metastatic	0.06	-14.28 (-297.2 – +2.4)	0.81	+11.0 (-470.0 – +24.0)
Hormones – single agent	0.57	-0.04 _-245.6 - +113.7)	0.31	+8.5 (-336.0 - +52.0)
Hormones – MAB	0.08	-2.11 (-2007.1 - +9619.1)	0.75	+1.0 (-110.0 - +399.0)
Castrate resistant disease	0.36	-0.43 (-431.6 - +1174.8)	0.98	-3.0 (-726- +496)

Table 5.3 A table to demonstrate the median change in PSA and ALP values for the different treatment groups and their significance (using the Wilcoxon matched pairs signed rank test).

None of the median PSA or ALP changes in any of the patient groups was statistically significant.

5.1.4 Number of deaths

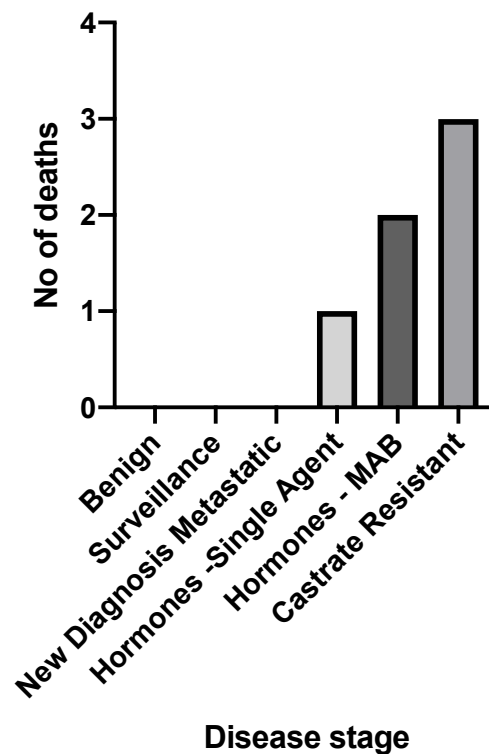


Figure 5.10 Number of prostate cancer-related deaths. There were six deaths in total and all deaths were in patients with advanced disease.

During the first six months after sampling, six patients died from prostate cancer-related causes, and one further patient from a non-associated cause (Figure 5.10). These patients all had metastatic disease at the time of their death, so their CTC antigen expression was analysed with both the FACS and Imagestream techniques.

5.2 Results of Imagestream detected CTCs

5.2.1 Definition of CTC data recorded

The total number of CTCs for each patient was recorded, in addition to the different combinations of antigens expressed by each CTC. For the purpose of this study a CTC was counted as a CD45 negative cell that expressed one or more of the following markers: EpCAM, Oct4, SOX2 and/or Nanog. The fluorescence thresholds described in Chapter 3 for Oct 4, SOX2 and Nanog were applied and only cells that expressed Oct4, SOX2 and Nanog over this threshold were included.

Disease stage (n=)	Median CTC count	Mean CTC count (+SD)	Range
Healthy volunteers (5)	0	0	0
Benign (6)	3	12 (19.7)	0-50
Surveillance (6)	2	3 (5.4)	0-14
New diagnosis metastatic (8)	16	64 (106.6)	2-305
Hormones – single agent (13)	2	7 (12.6)	0-45
Hormones – MAB (16)	8	31 (49.6)	0-185
Castrate resistant (29)	14	21 (23.5)	0-75

Table 5.4 A table to demonstrate the median and mean (+SD) no of CTCs detected via the Imagestream for patients at each disease stage.

Tables 5.5 – 5.11 list the total number of putative CTCs expressing each antigen detected on the Imagestream, according to patient characteristic.

Patient No	Age	Treatment	PSA	EpCAM+	Oct4+	SOX2+	Nanog+	EpCAM / Oct4+ / SOX2+ / Nanog+	Oct4+ / SOX2+ / Nanog+	Epcam+ / Oct4+	Oct4+ / Nanog+	Oct4+ / SOX2+	SOX2+ / Nanog+	EpCAM+ / Nanog+	EpCAM+ / SOX2+	TOTAL
1	48	Healthy Volunteer	N/A	0	0	0	0	0	0	0	0	0	0	0	0	0
2	41	Healthy Volunteer	N/A	0	0	0	0	0	0	0	0	0	0	0	0	0
3	43	Healthy Volunteer	N/A	0	0	0	0	0	0	0	0	0	0	0	0	0
4	52	Healthy Volunteer	N/A	0	0	0	0	0	0	0	0	0	0	0	0	0
5	38	Healthy Volunteer	N/A	0	0	0	0	0	0	0	0	0	0	0	0	0

Table 5.5 A table to show the number of cells expressing each antigen for blood taken from healthy volunteers when processed using the Imagestream assay.

Patient No	Age	Treatment	PSA	EpCAM+	Oct4+	SOX2+	Nanog+	EpCAM / Oct4+ / SOX2+ / Nanog+	Oct4+ / SOX2+ / Nanog+	Epcam+ / Oct4+	Oct4+ / Nanog+	Oct4+ / SOX2+	SOX2+ / Nanog+	EpCAM+ / Nanog+	EpCAM+ / SOX2+	TOTAL
1	73	New patient – negative biopsy	9.9	0	0	5	0	0	0	0	1	0	0	0	0	5
2	79	New patient – negative biopsy	9.5	0	1	7	0	0	2	0	1	5	0	0	0	16
3	67	New patient – negative biopsy	5.6	0	0	0	0	0	0	0	0	0	0	0	0	0
4	68	New patient – negative biopsy	7.9	0	0	0	0	0	0	0	0	0	0	0	0	0
5	67	New patient – negative biopsy	7.2	0	0	0	50	0	0	0	0	0	0	0	0	50
6	70	New patient – negative biopsy	4.4	0	0	0	0	0	0	0	0	0	0	0	0	0

Table 5.6 A table to show the number of cells expressing each antigen for blood taken from patients with benign disease when processed using the Imagestream assay.

Patient No	Age	Treatment	PSA	EpCAM+	Oct4+	SOX2+	Nanog+	EpCAM / Oct4+ / SOX2+ / Nanog+	Oct4+ / SOX2+ / Nanog+	Epcam+ / Oct4+	Oct4+ / Nanog+	Oct4+ / SOX2+	SOX2+ / Nanog+	EpCAM+ / Nanog+	EpCAM+ / SOX2+	TOTAL	
1	68	AS	5.3	0	0	0	0	0	0	0	0	0	0	0	0	0	0
2	72	AS	6.1	0	0	0	14	0	0	0	0	0	0	0	0	0	14
3	76	WW	27.1	0	0	0	0	0	0	0	0	0	0	0	0	0	0
4	84	WW	18.1	0	0	3	0	0	0	0	0	0	0	0	0	0	3
5	87	WW	86.0	1	0	0	1	0	0	0	0	0	0	0	0	0	2
6	76	AS	37.4	0	0	1	0	0	0	0	0	0	0	0	0	0	1

Table 5.7 A table to show the number of cells expressing each antigen for blood taken from patients on surveillance when processed using the Imagestream assay.

Patient No	Age	Treatment	PSA	EpCAM+	Oct4+	SOX2+	Nanog+	EpCAM / Oct4+ / SOX2+ / Nanog+	Oct4+ / SOX2+ / Nanog+	Epcam+ / Oct4+	Oct4+ / Nanog+	Oct4+ / SOX2+	SOX2+ / Nanog+	EpCAM+ / Nanog+	EpCAM+ / SOX2+	TOTAL
1	77	New Diag	5.2	0	0	0	303	0	0	0	1	1	1	0	0	306
2	68	New Diag	33.5	0	0	2	4	0	3	0	0	0	0	0	0	9
3	65	New Diag	18.3	0	0	1	8	0	0	0	0	0	1	0	0	10
4	74	New Diag	140.0	0	0	2	8	0	0	0	1	0	0	0	0	11
5	68	New Diag	308.0	0	1	0	6	0	1	0	12	1	0	0	0	21
6	62	New Diag	22.0	0	0	7	0	0	0	0	0	13	0	0	0	20
7	68	New Diag	47.0	0	0	1	0	0	1	0	0	0	0	0	0	2
8	69	New Diag	3.2	0	12	0	2	0	6	0	50	64	2	0	0	136

Table 5.8 A table to show the number of cells expressing each antigen for blood taken from patients with new diagnosis metastatic disease when processed using the Imagestream assay.

Pt	Age	Treatment	PSA	EpCAM+	Oct4+	SOX2+	Nanog+	EpCAM / Oct4+ / SOX2+ / Nanog+	Oct4+ / SOX2+ / Nanog+	Epcam+ / Oct4+	Oct4+ / Nanog+	Oct4+ / SOX2+	SOX2+ / Nanog+	EpCAM+ / Nanog+	EpCAM+ / SOX2+	T O T A L
1	69	Single agent	31.4	0	0	1	0	0	0	0	0	1	0	0	0	2
2	82	Single agent	1.8	0	0	0	0	0	0	0	0	0	0	0	0	0
3	71	Single agent	2.9	0	4	4	1	0	0	0	0	2	0	0	0	11
4	92	Single agent	0.2	0	0	1	0	0	0	0	1	0	1	0	0	3
5	91	Single agent	0.2	0	0	0	0	0	0	0	0	0	0	0	0	0
6	82	Single agent	50.9	0	0	0	0	0	0	0	0	0	0	0	0	0
7	87	Single agent	4.5	0	0	0	0	0	0	0	0	0	0	0	0	0
8	66	Single agent	0.1	0	0	6	0	0	0	0	0	0	0	0	0	6
9	71	Single agent	2020	0	0	34	3	0	3	0	3	0	1	1	0	45
10	77	Single agent	0.1	0	0	0	0	0	0	0	0	0	0	0	0	0
11	59	Single agent	4.5	0	0	11	1	0	0	0	0	0	0	0	0	0
12	63	Single agent	81.9	0	3	2	1	0	2	0	0	0	0	0	0	8
13	67	Single agent	3.0	0	11	0	3	0	0	0	1	3	0	0	0	18

Table 5.9 A table to show the number of cells expressing each antigen for blood taken from patients on single agent hormones when processed using the Imagestream assay.

Patient No	Age	Treatment	PSA	EpCAM+	Oct4+	SOX2+	Nanog+	EpCAM / Oct4+ / SOX2+ / Nanog+	Oct4+ / SOX2+ / Nanog+	Epcam+ / Oct4+	Oct4+ / Nanog+	Oct4+ / SOX2+	SOX2+ / Nanog+	EpCAM+ / Nanog+	EpCAM+ / SOX2+	TOTAL
1	86	MAB	245.6	84	2	0	2	0	1	0	0	1	0	0	0	90
2	84	MAB	61.4	1	0	0	1	0	0	0	0	2	0	0	0	4
3	79	MAB	1.5	0	0	0	0	0	0	0	0	0	0	0	0	0
4	87	MAB	3.1	0	0	0	185	0	0	0	0	0	0	0	0	185
5	82	MAB	24.0	0	2	5	0	0	0	0	0	1	0	0	0	8
6	77	MAB	101.0	0	1	1	11	0	0	0	1	1	0	0	0	15
7	78	MAB	1.5	0	0	0	0	0	0	0	0	0	2	0	0	2
8	69	MAB	1.8	0	0	1	0	0	0	0	0	0	0	0	0	1
9	86	MAB	12.6	0	0	2	0	0	0	0	0	0	0	0	0	2
10	83	MAB	0.1	0	0	1	0	0	0	0	0	0	0	0	0	1
11	83	MAB	23.4	0	1	0	2	0	0	0	0	0	0	0	0	3
12	74	MAB	2.0	0	0	25	36	0	1	0	0	0	0	0	0	62
13	96	MAB	34.6	0	2	57	0	1	0	0	0	0	2	0	0	62
14	80	MAB	1.7	0	0	7	0	0	0	0	0	0	0	0	0	7
15	73	MAB	5.5	0	0	40	1	0	0	0	0	0	0	0	0	41
16	65	MAB	30.6	0	0	0	4	0	0	0	6	1	0	0	0	11

Table 5.10 A table to show the number of cells expressing each antigen for blood taken from patients on maximum androgen blockade when processed using the Imagestream assay.

Pt No	Age	Treatment	PSA	EpCAM+	Oct4+	SOX2+	Nanog+	EpCAM / O/S/N	O/S/N	Epcam+ / Oct4+	Oct4+ / Nanog+	Oct4+ / SOX2+	SOX2+ / Nanog+	EpCAM+ / Nanog+	EpCAM+ / SOX2+	Total
1	77	Enzalutamide	1875	4	0	2	0	0	8	0	0	0	0	1	0	15
2	68	Docetaxel	0.8	0	0	0	14	0	0	0	0	0	0	0	0	14
3	85	Dexamethasone	55.0	0	8	9	22	0	0	0	0	0	0	0	0	39
4	69	Enzalutamide	380	11	0	1	3	0	0	0	1	3	0	0	0	19
5	77	Dexamethasone	18.0	0	0	3	12	0	0	0	3	0	0	0	0	18
6	61	Abiraterone	51.2	0	0	0	3	0	0	0	1	0	0	0	0	4
7	60	Enzalutamide	0.7	0	1	0	68	0	0	0	9	0	0	0	0	78
8	74	Dexamethasone	0.7	0	0	0	6	0	5	0	3	0	0	0	0	14
9	73	Dexamethasone	23.0	0	0	5	4	0	0	0	3	0	0	1	0	13
10	77	Docetaxel	433	0	2	66	5	0	0	0	0	0	0	0	0	73
11	58	Enzalutamide	12.4	2	5	0	1	0	3	1	4	2	0	0	0	18
12	87	Cabazitaxel	5.6	20	2	3	0	0	2	0	0	1	0	0	0	28
13	70	Dexamethasone	228	0	0	3	12	0	0	0	3	0	0	0	0	18
14	82	Enzalutamide	72.4	0	1	0	0	0	0	0	0	1	0	0	0	2
15	74	Abiraterone	16.3	0	1	0	2	0	0	0	0	1	0	0	0	4
16	74	Docetaxel	8.0	0	0	49	0	0	22	0	0	4	0	0	0	75
17	72	Enzalutamide	586	20	1	0	0	0	1	0	1	0	0	0	0	23
18	69	Radium 223	202	0	0	0	0	0	0	0	0	2	0	0	0	2
19	80	Enzalutamide	2.2	0	0	2	10	0	0	0	0	0	0	0	0	12
20	74	Enzalutamide	1.3	6	12	41	6	0	2	0	0	2	0	0	0	69
21	76	Dexamethasone	0.8	0	0	5	0	0	0	0	0	0	0	0	0	5
22	51	Enzalutamide	434	0	0	3	0	0	2	0	0	2	0	0	0	7
23	58	Docetaxel	100	0	8	3	0	0	6	0	2	2	0	0	0	21
24	76	Enzalutamide	4611	0	4	0	0	0	0	0	0	0	0	0	0	4
25	77	Radium 223	29.2	2	0	10	0	0	2	1	0	10	0	0	0	25
26	66	Enzalutamide	21.0	0	0	0	0	0	0	0	0	0	0	0	0	0
27	72	Enzalutamide	532	0	0	0	2	0	0	0	0	0	0	0	0	2
28	81	Radium 223	96.1	0	2	0	0	0	0	0	0	0	0	0	0	2
29	78	Dexamethasone	10.5	0	0	0	0	0	0	0	0	0	0	0	0	0

Table 5.11 A table to show the number of cells expressing each antigen for blood taken from patients with castrate resistant disease when processed using the Imagestream assay.

The Welch’s ANOVA test was performed to determine whether there was a significant difference in number of CTCs detected between patients in each disease stage ($p = 0.02$). The Mann Whitney test was then performed between the different groups to see which CTC counts were significantly different based on disease stage. The p-values from this test are displayed in Table 5.12.

Disease stage groups	Benign	Surv	NDM	HSA	HMAB	CR
Benign	-	0.81	0.09	0.89	0.23	0.15
Surveillance	0.81	-	0.01	0.87	0.06	0.07
Newly diagnosed metastatic	0.09	0.01	-	0.01	0.22	0.48
Hormones – single agent	0.89	0.87	0.01	-	0.05	0.06
Hormones – MAB	0.23	0.06	0.22	0.05	-	0.57
Castrate resistant	0.15	0.07	0.48	0.06	0.57	-

Table 5.12 A table to demonstrate the p-values when comparing CTC counts between the different disease stage groups when using the Mann Whitney test. There is a significant difference in CTC counts between the newly diagnosed metastatic group and those undergoing surveillance and on single-agent hormones. There is also a significant difference between those on single-agent hormones and those on maximum androgen blockade.

These results show that there is a significant difference between CTC counts from the Imagestream assay between patients in the following disease stages:

- 1) Newly diagnosed metastatic and a) surveillance, and b) hormones – single agent
- 2) Hormones – single agent, and hormones – maximum androgen blockade

These results would suggest that those on surveillance and single-agent hormones had more stable disease than those who had newly diagnosed metastatic disease and also those on maximum androgen blockade. This is unsurprising from a clinical perspective but reassuring that the assay confirms what would be predicted.

The p-values were very close to being significant between those on surveillance and those with castrate resistant disease and those on maximum androgen blockade. This may have become significant if using higher numbers of patients in each group.

5.2.3 CTC count and PSA

Although we know PSA is not a reliable predictor of disease progression, CTC count obtained from the Imagestream assay was plotted against PSA for patients in all groups, to determine whether there was a correlation, both at baseline (Figure 5.12) and six-month interval (Figure 5.13).

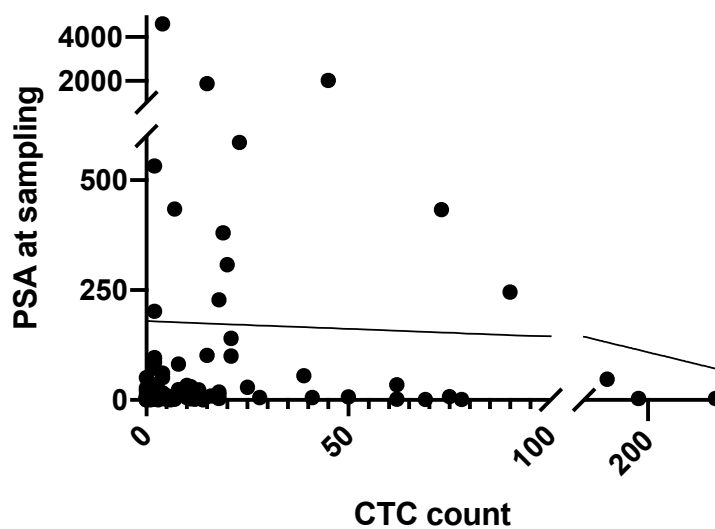


Figure 5.12 A graph to show baseline PSA and CTC count using the Imagestream assay (the line demonstrates linear regression) $r^2 = 0.0007$ therefore there is no correlation.

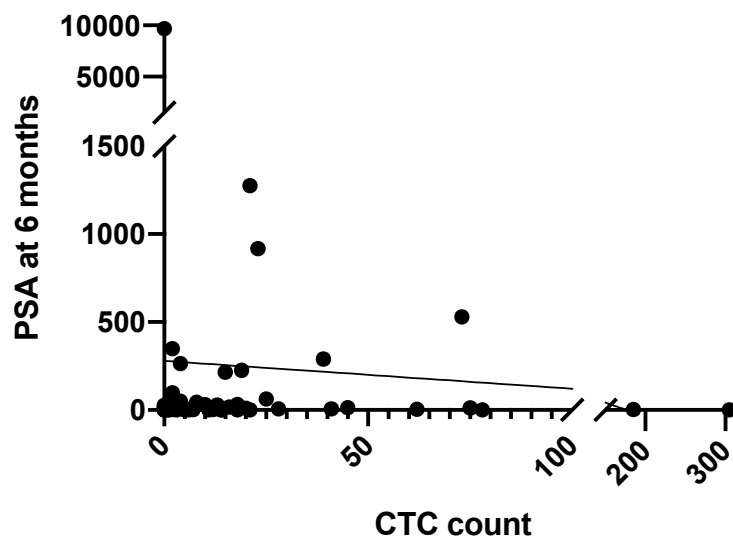


Figure 5.13 A graph to show PSA at 6 months and CTC count using the Imagestream assay (the line demonstrates linear regression) $r^2 = 0.0035$ therefore there is no correlation.

The r^2 values for the correlation between baseline PSA and CTC count is 0.007 and 0.0035 for PSA after 6 months, which suggests no correlation.

5.2.4 CTC count and ALP

Whilst ALP is not a standardised biomarker in prostate cancer, it is recommended to check ALP at intervals as discussed earlier in this chapter. ALP at baseline (Figure 5.14) and also after 6 months was correlated to CTC count for all patients (Figure 5.15).

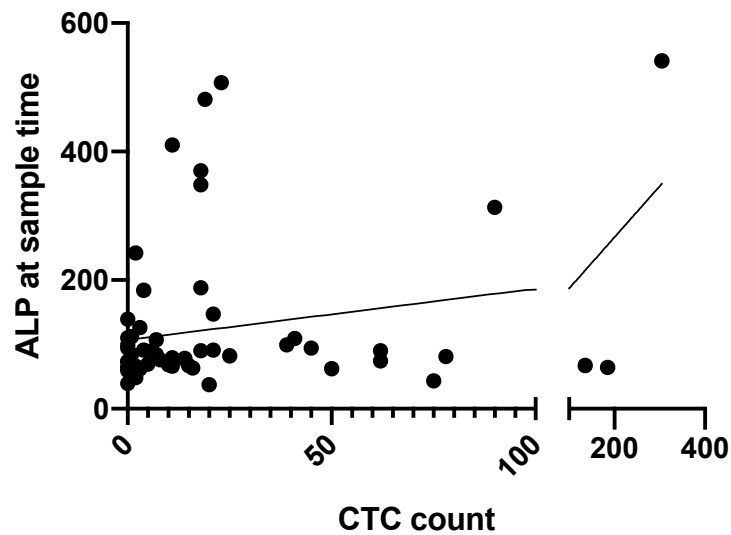


Figure 5.14 A graph to show ALP at baseline and CTC count using the Imagestream assay (the line demonstrates linear regression) $r^2 = 0.11$ therefore there is no correlation.

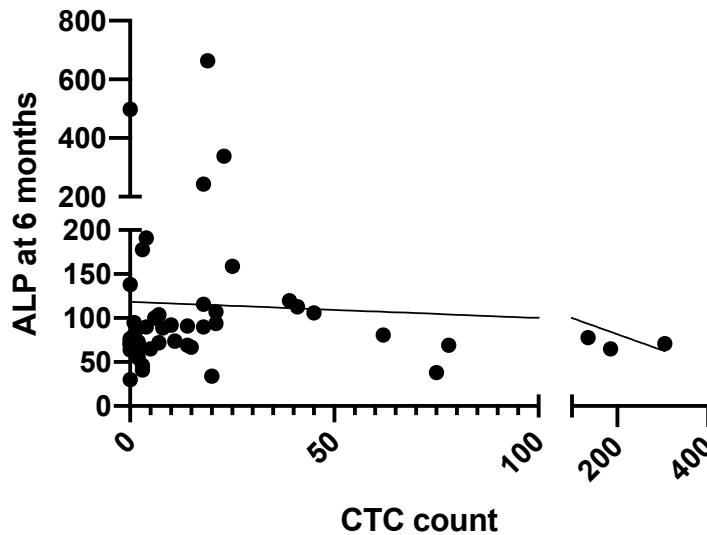


Figure 5.15 A graph to show ALP after 6 months and CTC count using the Imagestream assay (the line demonstrates linear regression) $r^2 = 0.008$ therefore there is no correlation.

The r^2 values for the correlation between CTC count and ALP at baseline and after 6 months are 0.11 and 0.008 respectively which means there is no correlation at either time-point.

5.2.5 Antigen expression

Cells were examined for the expression of antigens and all combinations were recorded. Figure 5.16 illustrates the frequency of expression of each combination. Each dot represents one patient.

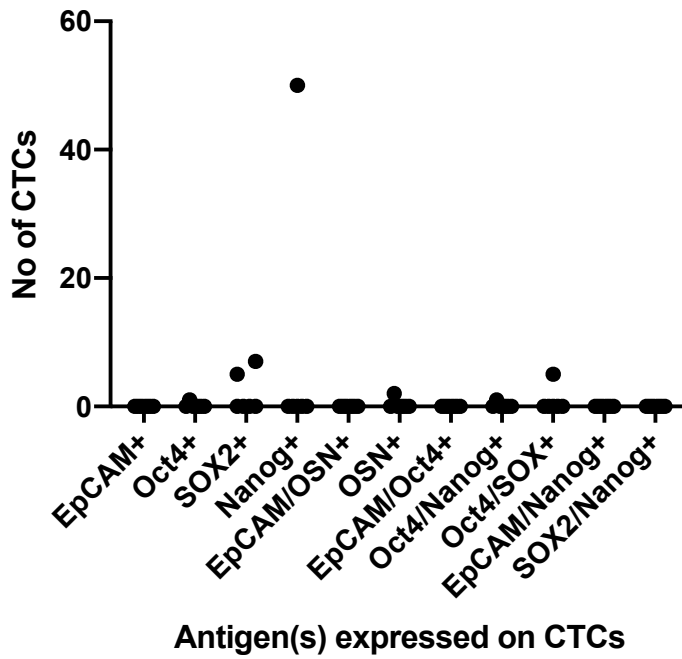


Figure 5.17 A graph to show how many CTCs expressed each antigen combination in patients with benign disease. Very few CTCs were found in this group, but the majority expressed SOX2, Nanog or a combination of Oct4 and SOX2.

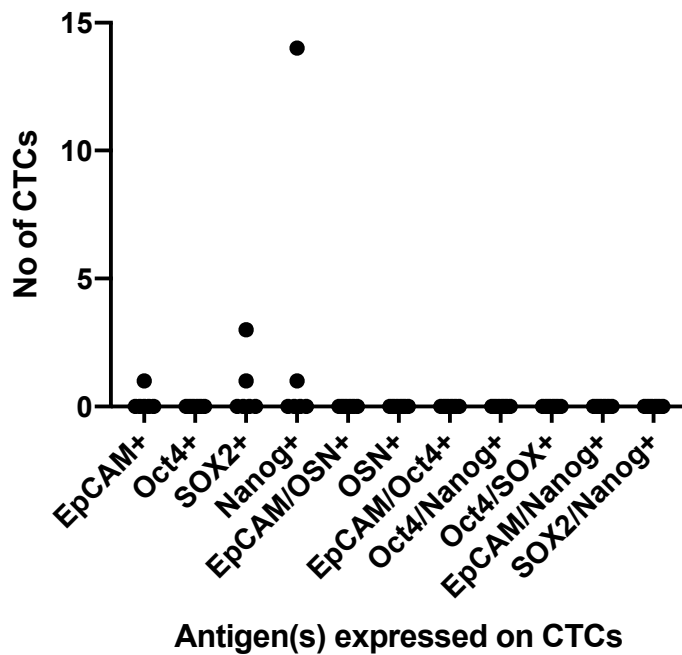


Figure 5.18 A graph to show how many CTCs expressed each antigen combination in patients on surveillance. CTCs from this group only expressed EpCAM, SOX2 or Nanog.

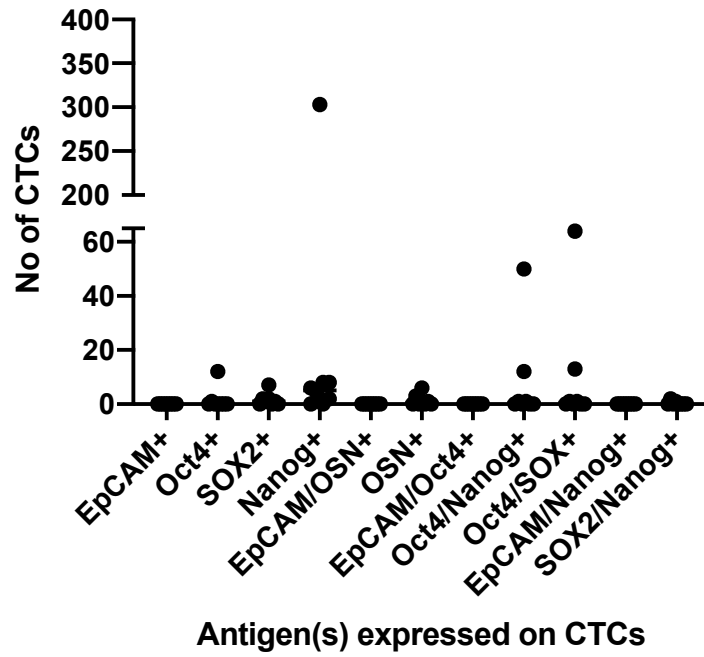


Figure 5.19 A graph to show how many CTCs expressed each antigen combination in patients with newly diagnosed metastatic disease. More of the CTCs from this group expressed the three stem cell markers, either alone or in combination.

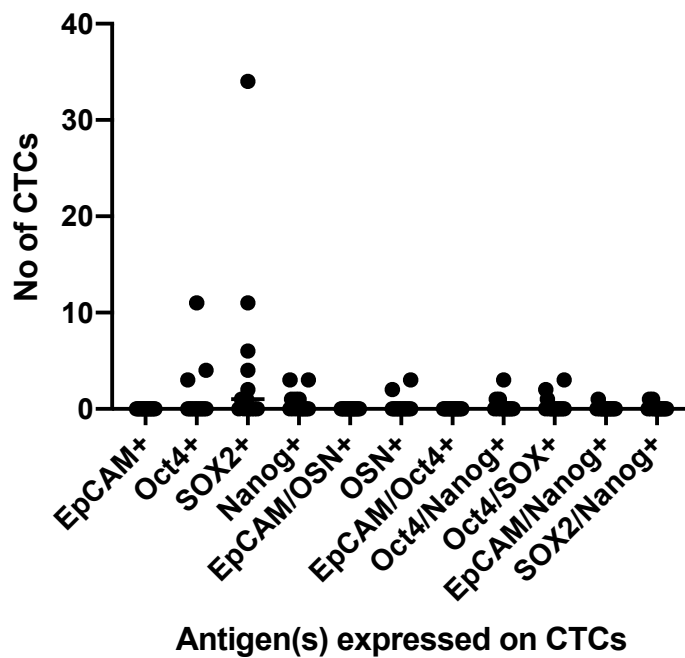


Figure 5.20 A graph to show how many CTCs expressed each antigen combination in patients on a single hormonal agent. The two most common antigens expressed were Oct4 and SOX2.

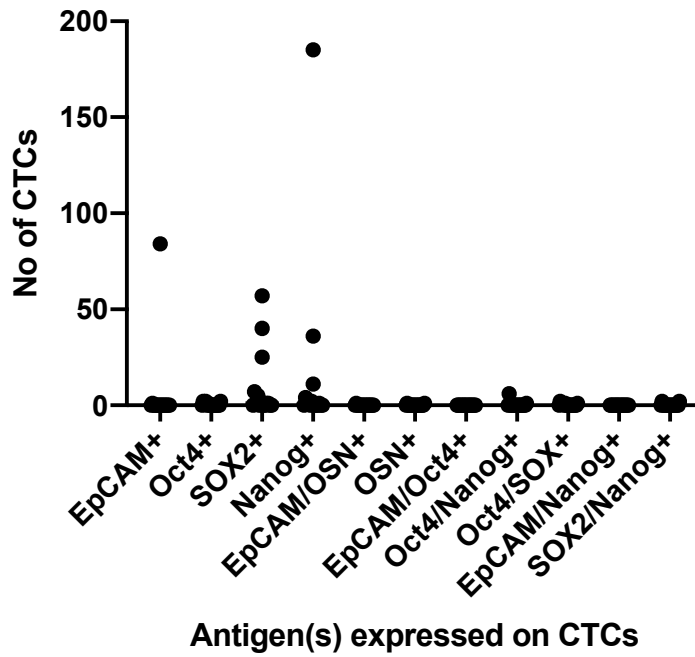


Figure 5.21 A graph to show how many CTCs expressed each antigen combination in patients on maximum androgen blockade. SOX2 and Nanog were again commonly expressed, and one patient had high numbers of EpCAM+ cells.

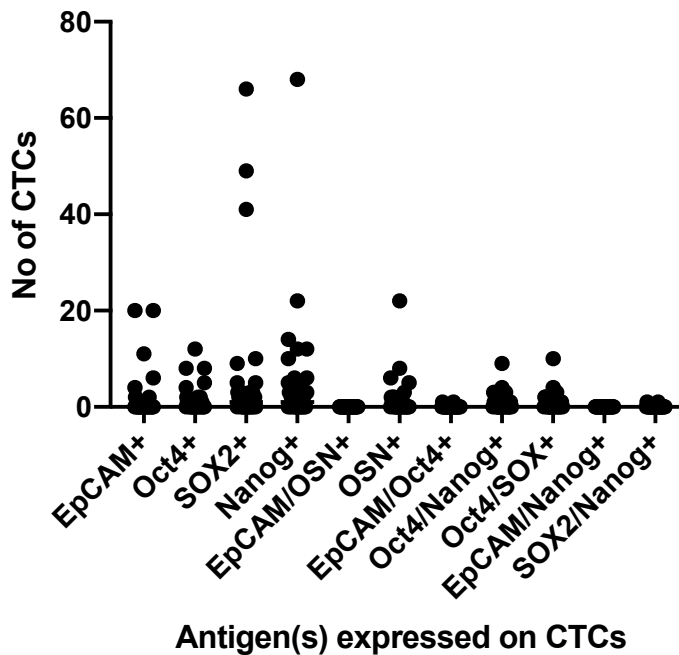


Figure 5.22 A graph to show how many CTCs expressed each antigen combination in patients with castrate-resistant disease. Several patients had CTCs with each of the individual antigens, in addition to the antigens in combination, particularly Oct4/SOX2/Nanog+ cells.

In order to examine the significance of different antigen expression between patients in each group, the Kruskal-Wallis test was performed. This compared the numbers of CTCs expressing each antigen combination for each disease stage. The results are displayed in Table 5.13.

Antigen(s)	Kruskal-Wallis statistic	p-value
EpCAM	7.52	0.28
Oct4	6.94	0.33
SOX2	6.26	0.40
Nanog	11.12	0.08
EpCAM/Oct4/Sox2/Nanog	4.19	0.65
Oct4/SOX2/Nanog	10.70	0.09
EpCAM/Oct4	3.78	0.71
Oct4/Nanog	9.95	0.13
Oct4/SOX2	8.05	0.23
EpCAM/Nanog	5.39	0.50
SOX2/Nanog	4.93	0.55

Table 5.13 A table demonstrating the Kruskal-Wallis statistic which shows the significance of the number of CTCs displaying each antigen combination for the different disease groups. $P > 0.05$ for each antigen or antigen combination therefore there was no significant difference found.

These results show that the actual number of CTCs expressing each antigen combination is not significant between patients at the different disease stages. (If there had been significance, then a t-test would have been used to determine the disease stages between which there was a significant difference.)

In order to look at this data in a different way, the odds ratio of whether the three stem cell antigens were present or absent in different groups was explored. The patients in the surveillance group were chosen as the comparison group (Table 5.14) because aside from one patient with 14 Nanog positive cells, there were minimal numbers of each of the antigens present. The healthy volunteer or benign groups were not chosen as the comparator group as none of the former had any Oct4 / SOX2 /Nanog cells, and the latter had only one patient with any. This would mean the statistical test would require

adjustment, which would make it less accurate, especially when dealing with low numbers of patients in each group.

Patient	Oct4	SOX2	Nanog
1	0	0	0
2	0	0	14
3	0	0	0
4	0	3	0
5	0	0	1
6	0	1	0

Table 5.14 A table to list the number of CTCs expressing each stem cell antigen for each patient in the surveillance group.

When looking at Oct4 (Table 5.15), although the odds ratios are all greater than 1 apart from the healthy volunteer group, this cannot be interpreted as a positive association as none of the p-values show significance. All categories have lower numbers of Oct4 positive cells present than absent, so the odds ratios are confusing. Low numbers could account for this.

a) Oct4

Disease Stage	Present	Absent	Odds Ratio	p-value	z statistic
<i>Surveillance</i>	0	6	-	-	-
Healthy volunteer	0	5	0.16	0.28	1.08
Benign	1	5	3.55	0.46	0.73
New diagnosis metastatic	2	6	5.00	0.33	0.98
Hormones – single agent	3	10	4.33	0.36	0.92
Hormones – MAB	5	11	6.21	0.24	1.18
Castrate resistant	12	16	9.84	0.13	1.51

Table 5.15 A table to demonstrate the number of CTCs that had Oct4 present or absent for patients in each disease group compared to the CTCs in the surveillance disease group. There is no significant difference found.

For SOX2 (Table 5.16), there are low odds ratios for the healthy volunteer and benign disease groups, which would imply that the presence of the antigen is not likely in these groups when compared to the surveillance group. This would be expected, although in both cases, the p-value does not show significance. Again, this could be explained by a small

number of patients in these groups and the significance might be proven with a larger sample size. All of the other groups have odds ratios greater than 1, which would suggest that presence of SOX2 is more likely in these groups compared to the surveillance group, but the p-values are not significant.

b) SOX2

Disease Stage	Present	Absent	Odds Ratio	p-value	z statistic
<i>Surveillance</i>	2	4	-	-	-
Healthy volunteer	0	5	0.16	0.28	1.08
Benign	0	5	0.16	0.28	1.08
New diagnosis metastatic	5	3	3.33	0.29	1.06
Hormones – single agent	7	6	2.33	0.41	0.82
Hormones – MAB	9	7	2.57	0.35	0.94
Castrate resistant	15	14	2.14	0.41	0.81

Table 5.16 A table to demonstrate the number of CTCs that had SOX2 present or absent for patients in each disease group compared to the CTCs in the surveillance disease group. There is no significant difference found.

When looking at Nanog (Table 5.17), there are also odds ratios of less than 1 for the healthy volunteer and benign groups, but both have p-values greater than 0.05. All other groups have odds ratios greater than 1, the highest of which is for the newly diagnostic metastatic group. Six patients in this group had cells that expressed Nanog compared to two of the surveillance group, in comparison to Nanog-absent cells in two of the newly diagnostic metastatic group and four in the surveillance group. Although the p-value is 0.13 and therefore not significant, a larger sample size may alter this outcome.

c) Nanog

Disease Stage	Present	Absent	Odds Ratio	p-value	z statistic
<i>Surveillance</i>	2	4	-	-	-
Healthy volunteer	0	5	0.16	0.28	1.08
Benign	1	5	0.40	0.51	0.66
New diagnosis metastatic	6	2	6.0	0.13	1.55
Hormones – single agent	5	8	1.25	0.83	0.22
Hormones – MAB	8	8	2.00	0.49	0.69
Castrate resistant	15	14	2.14	0.42	0.81

Table 5.17 A table to demonstrate the number of CTCs that had Nanog present or absent for patients in each disease group compared to the CTCs in the surveillance disease group. There is no significant difference found.

5.2.6 Antigen expression in patients that died

Whilst the follow-up for this study is so far at a relatively early stage, the expression of antigens in patients that had died during this time would also be of interest. The odds ratios for presence or absence of stem cell antigen expression in those patients who had died compared to those who were still alive at six months is demonstrated in the Table 5.18.

Antigen / Alive vs Dead	Present	Absent	Odds Ratio	p-value	z statistic
<i>Oct4 Alive</i>	21	51	-	-	-
Oct 4 Dead	2	4	1.21	0.83	0.22
<i>SOX2 Alive</i>	38	34	-	-	-
SOX2 Dead	1	5	0.18	0.12	0.54
<i>Nanog Alive</i>	35	37	-	-	-
Nanog Dead	2	4	0.53	0.48	0.71

Table 5.18 A table to demonstrate the odds ratios of each stem cell antigen being present or absent in the patients that had died in comparison to the patients still alive (using the results from the Imagestream assay). The presence of each antigen does not correlate with the survival of patients during the time frame studied.

Unfortunately, none of these odds ratios is significant. The value obtained for the Oct4 antigen is confusing because it is greater than 1 despite there being fewer Oct4-positive patients who died compare to Oct4-negative patients. With such a high p-value this isn't

significant anyway. Because only six patients had died within the timeframe, these results do not necessarily mean that there is no association, and it would be valuable to repeat this analysis in future, once more patients have died from prostate-related causes.

5.3 Results of FACS detected CTCs

5.3.1 Definition of CTC data recorded

Without the additional validation of a downstream assay to identify the FACS sorted population, it is not known whether the CD45-/CD16- population that were sorted are all CTCs. It is likely that they contain some white cells (debris based on size was gated out). Although there is antigen data which could be used in conjunction, cells were not examined for dual expression of antigens (due to the large number of antigens examined). For example, a cell expressing EpCAM might also express CK and therefore counting the number of cells expressing each antigen for each patient might result in counting the same cell more than once.

Therefore, for the purpose of this study, the CTC count for the FACS assay describes those cells which are CD45-CD16 negative.

5.3.2 Total CTC count

The total numbers of CTCs detected using FACS are displayed in the following graph (Figure 5.23), and the median and mean are displayed in Table 5.19. The patients with benign disease had a higher median number of CTCs than the patients with castrate-resistant disease, which is somewhat surprising and could indicate white cell contamination.

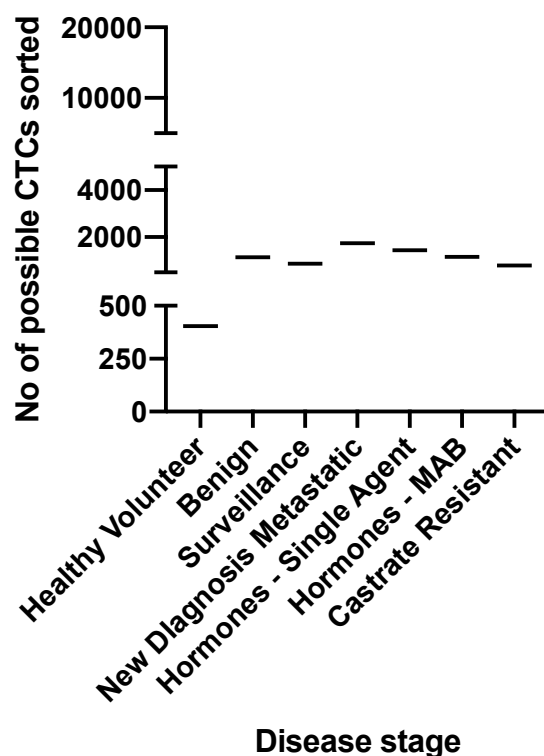


Figure 5.23 A graph to show the total number of CTCs found from patients within each treatment group, using FACS. This shows that those with newly diagnosed metastatic disease had the highest number of putative CTCs but there is no significant difference between the patients in different groups ($p=0.36$).

Disease Stage	Median CTC sort no	Mean CTC sort no (+SD)	Range
Healthy volunteers	404	413 (195.6)	172-677
Benign	1152	1243 (737.1)	481-2363
Surveillance	873	2181 (2313.1)	467-5500
New diagnosis metastatic	1747	1903 (1911.0)	168-6059
Hormones – single agent	1448	1542 (1120.1)	111-3389
Hormones – MAB	1163	3019 (4857.0)	72-20000
Castrate resistant	799	1267 (1309)	128-5286

Table 5.19 A table to demonstrate the median and mean (+SD) no of CTCs detected via FACS for patients at each disease stage.

Tables 5.20 – 5.26 list the total number of putative CTCs expressing each antigen detected on the FACS, according to patient characteristic.

Patient No	Age	Treatment	PSA	EpCAM	CK	Oct4	SOX2	Nanog	Vimentin	MT1-MMP	Total
1	48	Healthy Volunteer	N/A	2	11	1	7	10	21	838	890
2	41	Healthy Volunteer	N/A	0	9	8	6	9	15	1082	1129
3	43	Healthy Volunteer	N/A	0	6	6	0	3	1	943	959
4	52	Healthy Volunteer	N/A	2	8	7	3	4	21	900	945
5	38	Healthy Volunteer	N/A	1	2	0	3	3	7	423	439

Table 5.20 A table to show the number of cells expressing each antigen that were found in the blood from each healthy volunteer.

Patient No	Age	Treatment	PSA	EpCAM	CK	Oct4	SOX2	Nanog	Vimentin	MT1-MMP	Total
1	73	New patient – negative biopsy	9.9	1	0	0	16	159	5	18	199
2	79	New patient – negative biopsy	9.5	8	0	1	4	225	2	0	240
3	67	New patient – negative biopsy	5.6	1	25	25	0	13	4	399	1047
4	68	New patient – negative biopsy	7.9	1	30	30	2	6	452	1434	1925
5	67	New patient – negative biopsy	7.2	1	64	64	89	17	11	112	318
6	70	New patient – negative biopsy	4.4	0	17	17	122	22	29	203	393

Table 5.21 A table to show the number of cells expressing each antigen that were found in the blood from each patient with benign disease.

Patient No	Age	Treatment	PSA	EpCAM	CK	Oct4	SOX2	Nanog	Vimentin	MT1-MMP	Total
1	68	AS	5.3	3	191	47	5320	152	13	7	5732
2	72	AS	6.1	5	0	1	5888	153	53	3	6103
3	76	WW	27.1	0	31	25	0	21	132	170	379
4	84	WW	18.1	0	30	0	2	61	42	790	925
5	87	WW	86.0	4	0	3	321	15	130	745	1218
6	76	AS	37.4	2	0	16	0	329	0	813	347

Table 5.22 A table to show the number of cells expressing each antigen that were found in the blood from each patient on surveillance.

Patient No	Age	Treatment	PSA	EpCAM	CK	Oct4	SOX2	Nanog	Vimentin	MT1-MMP	Total
1	77	New Diag	5.2	1	0	8	25	157	12	0	203
2	68	New Diag	33.5	0	0	0	24	174	3	1	202
3	65	New Diag	18.3	29	0	19	2	117	54	269	490
4	74	New Diag	140.0	0	2	2	45	0	73	3213	3335
5	68	New Diag	308.0	1	4	4	42	13	33	4085	4182
6	62	New Diag	22.0	1	117	8	1687	3	1	396	2213
7	68	New Diag	47.0	3	51	7	82	1	0	365	509
8	69	New Diag	3.2	2	244	0	254	53	7	1641	2201

Table 5.23 A table to show the number of cells expressing each antigen that were found in the blood from each patient with newly diagnostic metastatic disease.

Pt	Age	Treatment	PSA	EpCAM	CK	Oct4	SOX2	Nanog	Vimentin	MT1-MMP	Total
1	69	Single agent	31.4	2	16	1	27	36	0	8	90
2	82	Single agent	1.8	0	11	13	46	166	43	2	281
3	71	Single agent	2.9	0	0	0	6	118	6	0	130
4	92	Single agent	0.2	0	0	3	17	158	15	6	199
5	91	Single agent	0.2	0	30	3	0	8	22	122	185
6	82	Single agent	50.9	0	97	2	1	13	302	921	1336
7	87	Single agent	4.5	8	12	3	251	62	8	179	523
8	66	Single agent	0.1	2	4	0	87	9	12	74	188
9	71	Single agent	2020	5	8	14	11	0	6	450	494
10	77	Single agent	0.1	17	11	2	4	58	1	7	100
11	59	Single agent	4.5	22	15	4	2	21	195	864	1123
12	63	Single agent	81.9	199	1515	2	9	7	0	8245	9977
13	67	Single agent	3.0	2	28	1813	904	1	14	116	2878

Table 5.24 A table to show the number of cells expressing each antigen that were found in the blood from each patient on single agent hormones.

Patient No	Age	Treatment	PSA	EpCAM	CK	Oct4	SOX2	Nanog	Vimentin	MT1-MMP	Total
1	86	MAB	245.6	88	2	1	151	118	8	44	412
2	84	MAB	61.4	11	0	1	777	16	16	0	821
3	79	MAB	1.5	0	3	26	152	160	26	0	367
4	87	MAB	3.1	0	616	13	389	160	25	12	1215
5	82	MAB	24.0	1	1	6	36	119	5	1	169
6	77	MAB	101.0	1	0	0	19	123	8	1	152
7	78	MAB	1.5	0	7	5	21	117	6	0	156
8	69	MAB	1.8	0	0	2	19	434	3	24	482
9	86	MAB	12.6	15	0	4	9	172	23	1	224
10	83	MAB	0.1	1	0	0	3	90	1	1	96
11	83	MAB	23.4	0	13	1	2	10	22	164	212
12	74	MAB	2.0	16	1	5	982	0	0	80	1084
13	96	MAB	34.6	18	10	2	3	44	180	475	732
14	80	MAB	1.7	7	10	9	1	29	20	54	130
15	73	MAB	5.5	12	1	4	4	30	63	245	359
16	65	MAB	30.6	0	6	1	44	3	21	588	663

Table 5.25 A table to show the number of cells expressing each antigen that were found in the blood from each patient on maximum androgen blockade.

Pt No	Age	Treatment	PSA	EpCAM	CK	Oct4	SOX2	Nanog	Vimentin	MT1-MMP	Total
1	77	Enzalutamide	1875	8	417	13	94	62	5	2243	2842
2	68	Docetaxel	0.8	0	0	0	353	164	1	56	574
3	85	Dexamethasone	55.0	2	18	6	360	116	42	1	545
4	69	Enzalutamide	380	109	10	6	13	1	162	532	833
5	77	Dexamethasone	18.0	17	2	5	4	492	307	639	1466
6	61	Abiraterone	51.2	0	2	4	83	3	36	1247	1375
7	60	Enzalutamide	0.7	0	2	3	52	231	0	3001	3289
8	74	Dexamethasone	0.7	0	2	2	368	18	8	1352	1750
9	73	Dexamethasone	23.0	858	1176	25	19	4	58	9339	11479
10	77	Docetaxel	433	555	697	1	3	1	114	3583	4954
11	58	Enzalutamide	12.4	0	83	14	490	7	178	547	1319
12	87	Cabazitaxel	5.6	1	44	6	224	8	0	384	667
13	70	Dexamethasone	228	3	126	10	483	18	0	1059	1699
14	82	Enzalutamide	72.4	10	211	24	610	5	1	1336	2197
15	74	Abiraterone	16.3	0	122	5	22	13	21	3763	3946
16	74	Docetaxel	8.0	0	331	7	18	7	16	4751	5130
17	72	Enzalutamide	586	9	326	13	22	7	6	4482	4865
18	69	Radium 223	202	43	395	0	10	0	21	1528	1997
19	80	Enzalutamide	2.2	2	6382	1	15	3	4	3326	9733
20	74	Enzalutamide	1.3	5	207	2	6	4	2	3597	3823

21	76	Dexamethasone	0.8	1	0	0	1	0	0	187	189
22	51	Enzalutamide	434	5	721	0	5	0	15	6278	7024
23	58	Docetaxel	100	3	138	3	134	1	14	2602	2895
24	76	Enzalutamide	4611	5	6142	0	70	124	0	6697	13038
25	77	Radium 223	29.2	2	131	0	159	62	2	2059	2415
26	66	Enzalutamide	21.0	43	60	28	196	2	5	4593	4927
27	72	Enzalutamide	532	3	231	8	303	2	14	774	1335
28	81	Radium 223	96.1	4	28	5	187	0	156	1543	1923
29	78	Dexamethasone	10.5	3	47	5	232	0	340	1381	2008

Table 5.26 A table to show the number of cells expressing each antigen that were found in the blood from each patient with castrate resistant disease.

The Kruskal-Wallis test was performed to ascertain whether there was a significant difference in the number of CTCs detected for patients with each disease stage. The Kruskal-Wallis statistic was 6.67 and the p-value was 0.36, demonstrating no significant difference in CTC count using the FACS assay, for patients at different disease stages.

5.3.3 CTC count and PSA

Although the CTC count data from this FACS assay appears to be unreliable, CTC count and PSA, both at baseline and after six months, were correlated for all patients, regardless of disease stage (Figures 5.24 and 5.25).

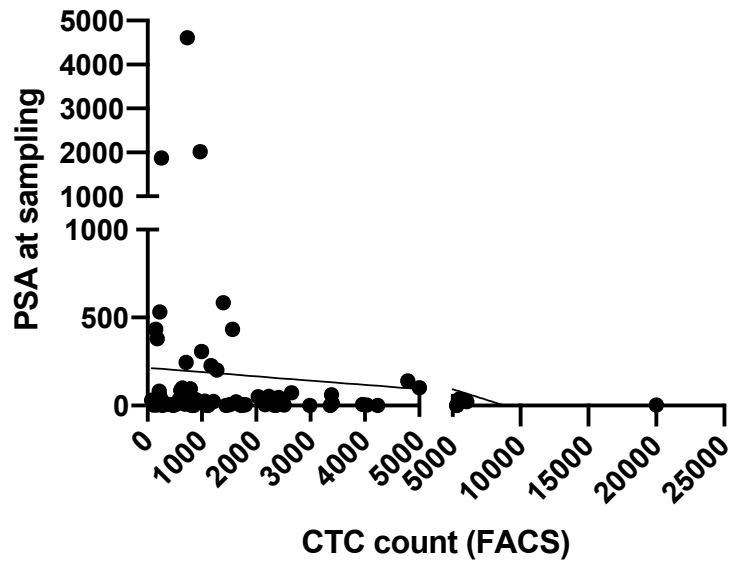


Figure 5.24 A graph to show baseline PSA and CTC count using the FACS assay (the line demonstrates linear regression) $r^2 = 0.01$ therefore there is no correlation with CTC count and the baseline PSA.

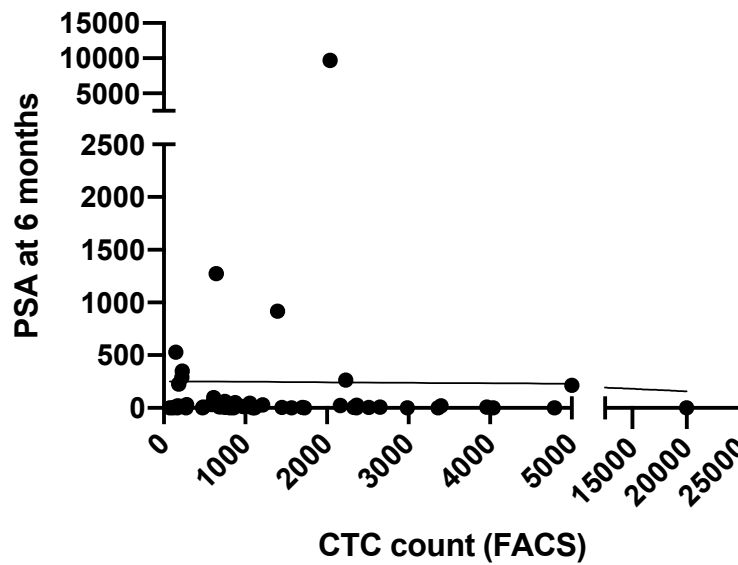


Figure 5.25 A graph to show PSA after six months and CTC count using the FACS assay (the line demonstrates linear regression) $r^2 = 0.0001$ therefore there is no correlation with CTC count and PSA at 6 months.

The r^2 values for both time-points were 0.01 and 0.0001 respectively, indicating no correlation with PSA.

5.3.4 CTC count and ALP

The same was done for CTC count and ALP, both at baseline and after six months, and the results are displayed in the following graphs (Figures 5.26 and 5.27).

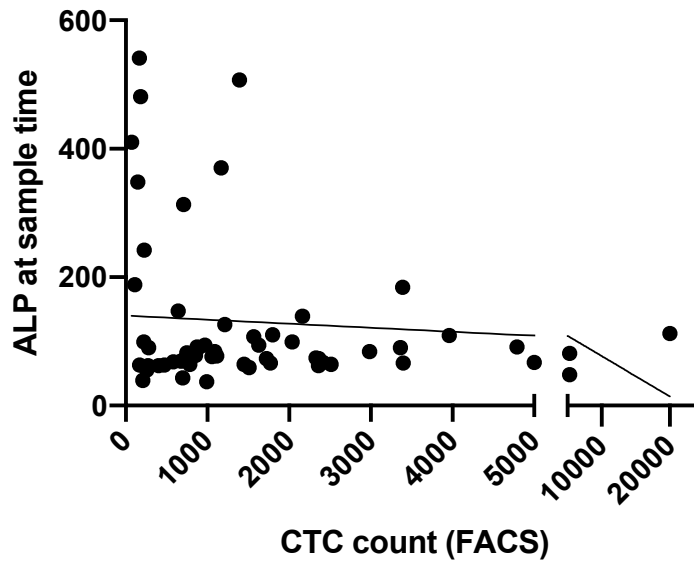


Figure 5.26 A graph to show ALP at baseline and CTC count using the FACS assay (the line demonstrates linear regression) $r^2 = 0.02$ therefore there is no correlation between CTC count and ALP at baseline.

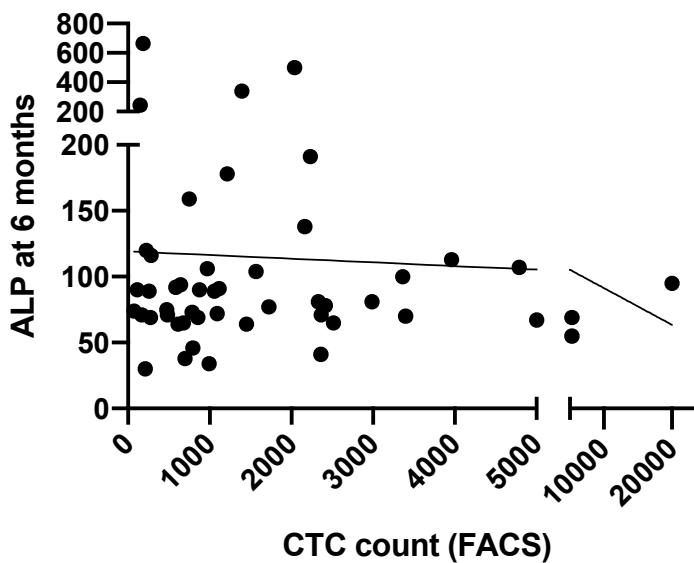


Figure 5.27 A graph to show ALP after six months and CTC count using the FACS assay (the line demonstrates linear regression) $r^2 = 0.006$, therefore there is no correlation between CTC count and ALP at 6 months.

No correlation was seen between CTC count and ALP at either baseline or after six months, demonstrated by the r^2 values of 0.02 and 0.006 respectively.

5.3.5 Antigen expression

Cells were examined for the expression of antigens. Unlike for the Imagestream results, combinations of antigens were not recorded due to the risk of counting cells twice. Figure 5.28 illustrates the frequency of expression of each antigen. Each dot represents one patient.

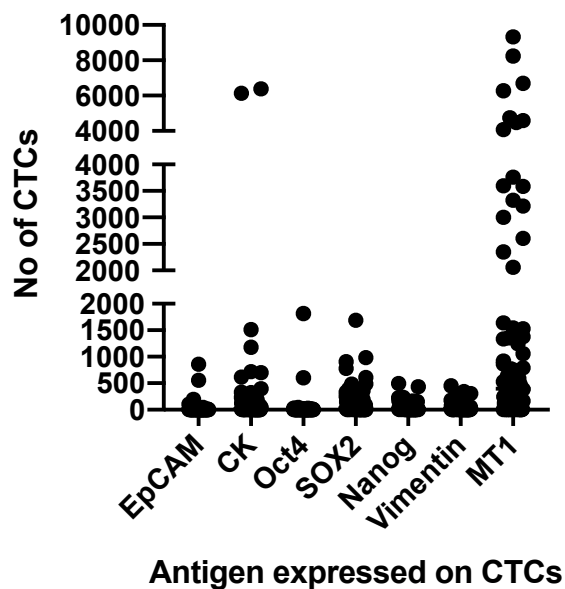


Figure 5.28 A graph to show how many CTCs expressed each antigen using the FACS assay. MT1-MMP was expressed by the largest number of patients and all antigens were detected on CTCs.

To look at this in more detail, this data was then broken down into treatment type (Figures 5.29 – 5.35).

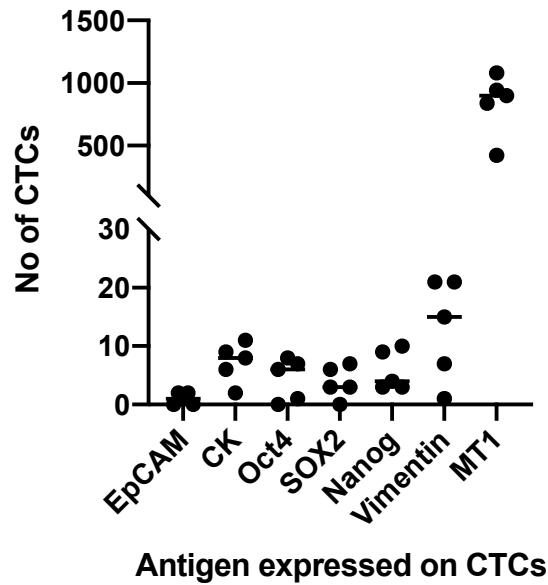
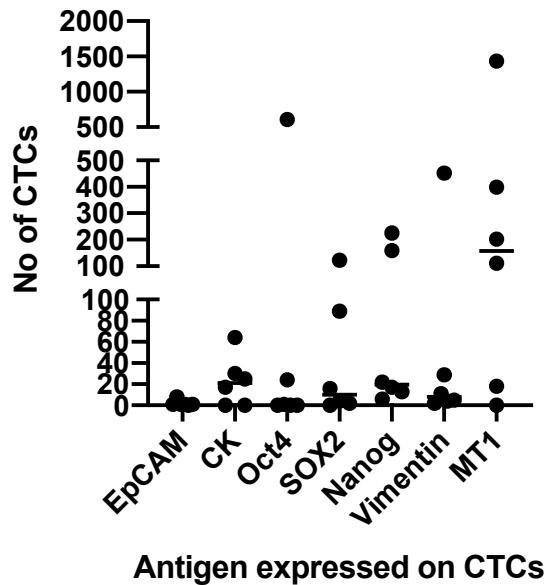


Figure 5.29 A graph to show how many CTCs expressed each antigen in the healthy volunteers. A higher than expected number of cells expressed each antigen aside from EpCAM. High numbers of MT1-MMP+ cells were detected. This suggests that the criteria used to determine what a positive event is was not strict enough – this could be due to gating error or have occurred during the optimisation of the antibody.



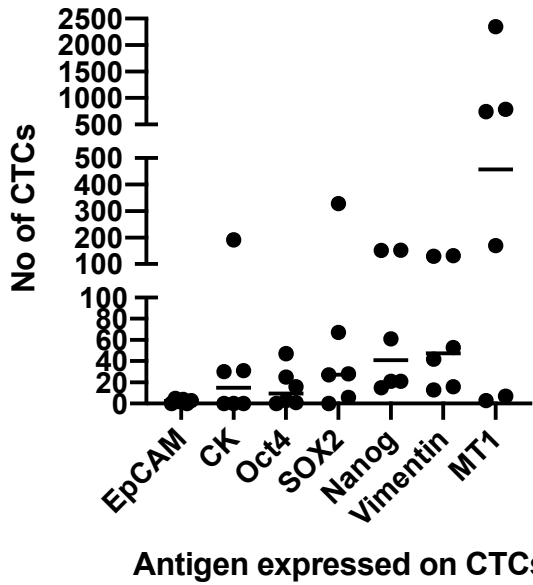


Figure 5.31 A graph to show how many CTCs expressed each antigen in patients undergoing surveillance. Similar to the previous groups, low numbers of EpCAM+ cells and high numbers of MT1-MMP cells were detected. The median number of cells expressing the stem cell markers was higher than the previous two groups.

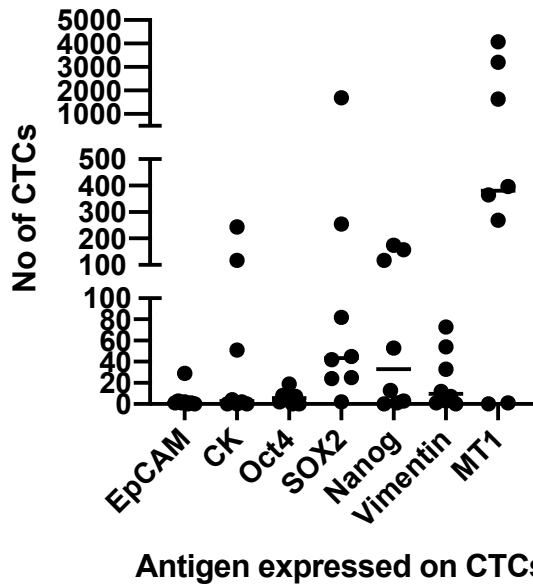


Figure 5.32 A graph to show how many CTCs expressed each antigen in patients with newly diagnosed metastatic disease. Higher numbers of cells expressing all antigens were detected in this group compared to the previous three groups.

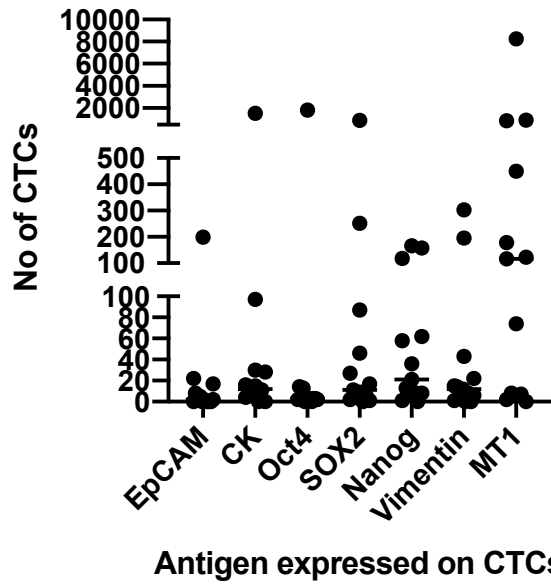


Figure 5.33 A graph to show how many CTCs expressed each antigen in patients on single-agent hormones. There were small numbers of patients expressing multiple cells with each of the stem cell antigens but the majority of patients had low numbers of these cells.

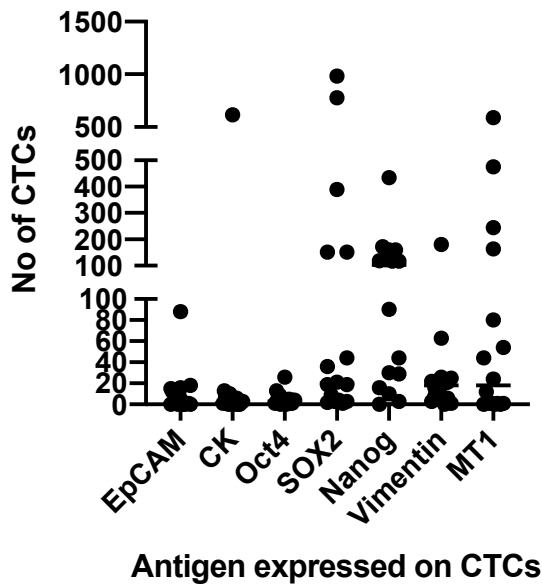


Figure 5.34 A graph to show how many CTCs expressed each antigen in patients on hormones – maximum androgen blockade. The median number of cells expressing Nanog was higher for this group of patients.

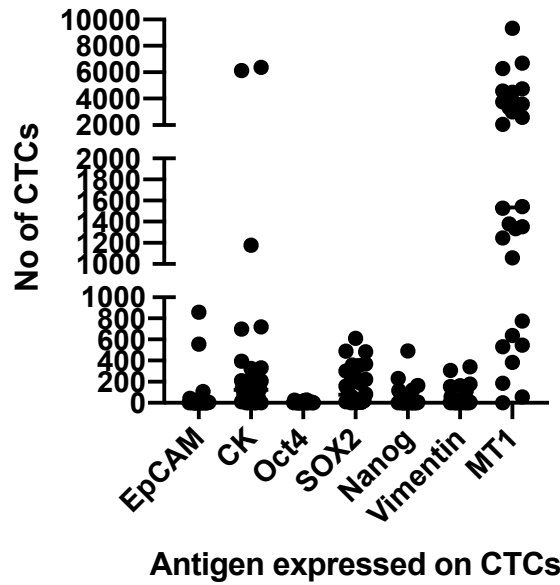


Figure 5.35 A graph to show how many CTCs expressed each antigen in patients with castrate-resistant disease. This group of patients had higher median numbers of cells expressing all antigens.

From these graphs, what is most concerning is the high numbers of 'CTCs' in the healthy volunteers and patients with benign disease, particularly the no of cells expressing MT1-MMP. This could indicate a problem with the MT1-MMP antibody leading to a lot of false positives, or detection of white cells expressing MT1-MMP.

In order to examine the significance of different antigen expression between patients in each group, the Kruskal-Wallis test was performed. This compared the numbers of CTCs expressing each antigen for each disease stage. The results are displayed in table 5.27.

Antigen(s)	Kruskal-Wallace statistic	p-value
EpCAM	4.11	0.66
Cytokeratin	19.87	0.03
Oct4	1.85	0.93
SOX2	12.58	0.05
Nanog	15.85	0.01
Vimentin	0.65	0.22
MT1-MMP	34.64	<0.001

Table 5.27 A table demonstrating the Kruskal-Wallace statistic which shows the significance of the number of CTCs displaying each antigen for the different disease groups. The p-value is less than 0.05 (and therefore significant) for numbers of cells expressing cytokeratin, SOX2, Nanog and MT1-MMP.

Unlike in the Imagestream assay, there was a significant difference found in the number of antigens expressed for four of the antigens (Cytokeratin, SOX2, Nanog and MT1-MMP). Although the MT1-MMP results should be interpreted with a high level of suspicion, instead of odds ratios, Mann-Whitney tests were performed between the different disease groups for each of the four antigens to show which groups showed significant differences (Tables 5.28 – 5.31).

a) Cytokeratin

Disease stage groups	HV	Benign	Surv	NDM	HSA	HMAB	CR
Healthy volunteer	-	0.40	>0.99	0.65	0.15	0.17	0.04
Benign	0.40	-	0.98	>0.99	0.85	0.22	0.04
Surveillance	>0.99	0.98	-	0.77	0.85	0.75	0.04
Newly diagnosed metastatic	0.65	>0.99	0.77	-	0.51	0.68	0.04
Hormones – single agent	0.15	0.85	0.85	0.51	-	0.01	0.03
Hormones – MAB	0.17	0.22	0.75	0.68	0.01	-	0.002
Castrate resistant	0.04	0.04	0.04	0.04	0.03	0.002	-

Table 5.28 A table demonstrating the p-values when the Mann-Whitney test was performed to analyse the significance of the difference of numbers of cells expressing Cytokeratin between each disease group (p-values in bold denote significance).

b) SOX2

Disease stage groups	HV	Benign	Surv	NDM	HSA	HMAB	CR
Healthy volunteer	-	0.45	0.12	0.02	0.11	0.05	0.01
Benign	0.45	-	0.62	0.24	0.78	0.32	0.05
Surveillance	0.12	0.62	-	0.57	0.65	0.95	0.37
Newly diagnosed metastatic	0.02	0.24	0.57	-	0.17	0.33	>0.99
Hormones – single agent	0.11	0.78	0.65	0.17	-	0.50	0.06
Hormones – MAB	0.05	0.32	0.95	0.33	0.50	-	0.27
Castrate resistant	0.01	0.05	0.37	>0.99	0.06	0.27	-

Table 5.29 A table demonstrating the p-values when the Mann-Whitney test was performed to analyse the significance of the difference of numbers of cells expressing SOX2 between each disease group (p-values in bold denote significance).

c) Nanog

Disease stage groups	HV	Benign	Surv	NDM	HSA	HMAB	CR
Healthy volunteer	-	0.02	0.01	0.43	0.10	0.01	0.90
Benign	0.02	-	0.78	0.51	0.59	0.58	0.05
Surveillance	0.01	0.78	-	0.55	0.37	0.68	0.02
Newly diagnosed metastatic	0.43	0.51	0.55	-	0.98	0.36	0.36
Hormones – single agent	0.10	0.59	0.37	0.98	-	0.14	0.07
Hormones – MAB	0.01	0.58	0.68	0.36	0.14	-	0.01
Castrate resistant	0.90	0.05	0.02	0.36	0.07	0.01	-

Table 5.30 A table demonstrating the p-values when the Mann-Whitney test was performed to analyse the significance of the difference of numbers of cells expressing Nanog between each disease group (p-values in bold denote significance).

d) MT1-MMP

Disease stage groups	HV	Benign	Surv	NDM	HSA	HMAB	CR
Healthy volunteer	-	0.08	0.18	0.52	0.04	0.01	0.10
Benign	0.08	-	0.70	0.36	0.84	0.24	0.01
Surveillance	0.18	0.70	-	0.85	0.59	0.05	0.03
Newly diagnosed metastatic	0.52	0.36	0.85	-	0.38	0.05	0.08
Hormones – single agent	0.04	0.84	0.59	0.38	-	0.12	0.01
Hormones – MAB	0.01	0.24	0.05	0.05	0.12	-	<0.001
Castrate resistant	0.10	0.01	0.03	0.08	0.01	<0.001	-

Table 5.31 A table demonstrating the p-values when the Mann-Whitney test was performed to analyse the significance of the difference of numbers of cells expressing MT1-MMP between each disease group (p-values in bold denote significance).

In order to consider the results of the FACS assay as reliable, there should be a significant difference found between the number of cells expressing each antigen in the healthy volunteer group and all other patients. Unfortunately, the Cytokeratin results only show a

significant difference between one of the patient groups, SOX2 and Nanog between three of the six patient groups, and MT1-MMP between two patient groups. This means that the healthy volunteers, who have no known prostate cancer, are just as likely to have the same number of cells expressing the different antigens as those in the patient groups. Although there are some significant differences between patient groups for each of these four antigens, these results are meaningless if the control group is also testing positive.

This could in part be due to low numbers of healthy volunteers in particular, but also low numbers in the treatment groups, but it could also be a reflection of the inaccuracy of the assay.

5.3.6 Antigen expression in patients that died

Similar to the Imagestream assay, the expression of antigens in patients that had died during the study time was explored. The odds ratios for presence or absence of stem cell antigen expression in the six patients who had died compared to those who were still alive at six months is demonstrated in Table 5.32.

Antigen / Alive vs Dead	Present	Absent	Odds ratio	p-value	z statistic
<i>Oct4 alive</i>	59	13	-	-	-
Oct 4 dead	3	3	0.22	0.08	1.73
<i>SOX2 alive</i>	68	4	-	-	-
SOX2 dead	6	0	0.85	0.92	0.10
<i>Nanog alive</i>	65	7	-	-	-
Nanog dead	5	1	0.54	0.60	0.53

Table 5.32 A table to demonstrate the odds ratios of each stem cell antigen being present or absent in the patients that had died in comparison to the patients still alive (using the results from the FACS assay). There was no significance found to the presence of each stem cell antigen and whether the patient died during the study timeframe.

Although all of the odds ratios are less than 1, suggesting that the presence of each antigen is not associated with death, none of these odds ratios are significant. Again, this could be because only six patients had died within the timeframe, and it would be valuable to repeat this analysis in future, once more patients have died from prostate cancer related causes.

5.4 Statistical comparison of Imagestream-detected and FACS-detected CTCs

Comparison of the two techniques is not really possible in terms of antigen expression, as different antigen combinations were used for both techniques. Because the same amount of blood was used for both assays from matching patients, and the samples were prepared in the same way, CTC count from the Imagestream, and the sorted cell population (which although not verified as pure CTCs are the closest comparable numbers of CTCs) from the FACS assay should show a correlation (Figure 5.36).

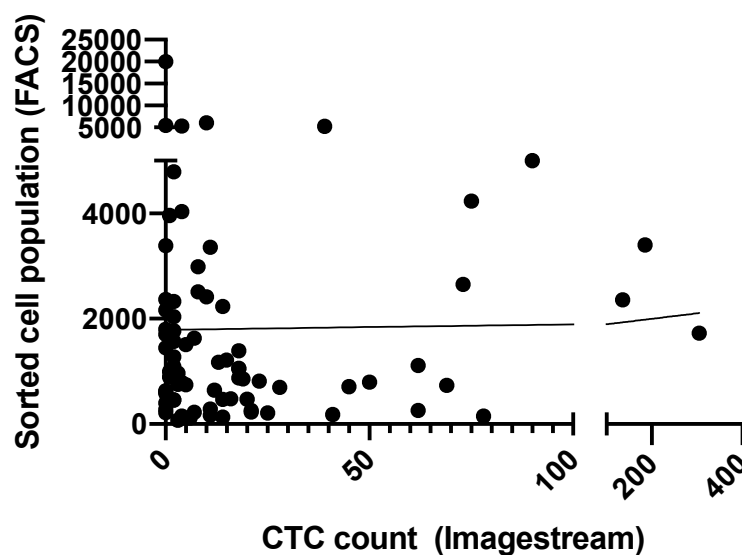


Figure 5.36 A graph to show the correlation between CTC count as detected by the Imagestream assay, and sorted cell population from the FACS assay (the line denotes linear regression) $r^2 = 0.0003$, therefore there was no correlation between the number of putative CTCs detected using the two different methods.

This graph shows that the cell numbers identified as CTCs by the Imagestream, and the CD45-/CD16- population sorted via FACS do not correlate. It would be expected that the FACS sorted population would be less pure and contain white cells that have not picked up the antibody, but this error should affect all samples and therefore be negated. Because there was no significant difference between CTC counts for patients in the different disease groups using the FACS assay, whereas there were using the Imagestream assay, this suggests that the FACS assay is likely to be the method which is the more unreliable of the two, possible due to the detection of false positives.

5.5 Discussion

This work is an observational study, rather than a clinical trial, which means that only a limited number of conclusions can be drawn. Because patients were not randomised to different treatment types, they have all received slightly different treatments or had them at different time-points. Due to the relatively fast-changing treatment regimes, a consequence of the findings of existing clinical trials, patients will not have necessarily received medications in the same order, and some with more recent diagnoses may have had completely new treatments.

Ethical approval was already obtained prior to the start of this study, and it was only once the collection of patient samples commenced that it became clear that additions to this approval would have been useful. Serial blood samples for CTC counts would have been beneficial so that a change in both count and antigen expression could be correlated with clinical findings. However, in reality this would have meant ongoing work beyond the time that was funded for this study and would have meant a further funding application. Whilst this is still possible now, it might be more useful to reflect on what has been learnt from this data and design a more optimal investigation, with a new ethics application, as this is likely to provide more useful information than continuing to add to the existing data.

Categorising the patients into the different disease stages / treatment groups was done based on the assumption that patients in these categories would have different expected CTC findings. If a larger cohort had been studied, or longer timeframes explored, this may not be necessary, and disease progression could be correlated with CTC findings and extrapolated back to look at treatments. There are many ways to analyse this data but for the purpose of this study it was felt this might be useful.

Because the blood sampling, consent, transportation, processing and analysis were performed by a single person, this limited the number of patients that could be included in the study. The collection and processing phase lasted approximately six months and it took this long to obtain blood from 88 patients. No more than five patients could be targeted from any clinic due to the time taken to consent and sample the blood. Depending on the day of the clinic only five samples could be run per week due to the FACS assay requiring staff from the facility to run the sort (during working hours only). If blood was obtained on a

Monday, a second clinic could be targeted on a Wednesday or Thursday but clinics on Fridays could not be utilised.

Clinic lists were obtained prior to the day the patient attended, and notes were accessed to see which patients would be appropriate. Some patients declined consent, for a small number it was not possible to obtain blood due to vascular access, and some patients were not approached when it was clear that they were unwell, or their disease had progressed to the terminal phase. Therefore, despite best intentions and careful planning, on some occasions only two patients were consented from a clinic. Working as part of a bigger team and being able to access multiple clinics a week would help mitigate some of these factors and would enable more patients to be included in the study within the same time frame.

The decision to correlate CTC count for both assays with PSA and ALP was made because of limited other means of predicting disease progression. As discussed in Chapter 1, it is known that PSA is not a reliable marker of advancing disease (Lucia et al., 2008, Thompson et al., 2004), hence the need for a new biomarker, and there was incomplete data for ALP. But in the short time-frame there were not enough patients with radiological investigations to use those as a marker of progression. The fact that there was no median change in PSA or ALP in any of the groups between the baseline level and the levels six months later could be due to the short time frame, the low number of patients in each group or the fact that they are both unreliable biomarkers. As further time has now passed, it would be possible to obtain PSA and ALP results for all patients a year after their original samples and it would be interesting to see if this longer time frame would produce a more significant outcome. Percentage change of PSA and ALP might be more relevant than the actual change in the values. Another option would be to wait a little longer (e.g. two years) and collect death data to allow the Kaplan-Meier estimator to be calculated. As the original study on which this work was based looked at survival based on Oct4/SOX2/Nanog expression in prostate tissue this would be a useful comparison. This work is planned once the relevant time period has elapsed.

When looking at the data from the two assays, the Imagestream data appears to be more reliable as none of the healthy volunteers had CTCs detected. Because cells could be examined visually once gating had been used to sort into different populations it is

unsurprising that this method was more likely to be accurate than the FACS assay for looking at small cell populations such as CTCs.

For the Imagestream results, the patients in the benign group had a higher median and mean number of CTCs than the surveillance group, which is unexpected. It is possible that these patients might have had small foci of cancer that had not been detected, and longer-term follow-up, including data on disease progression would be interesting. With such low numbers though, the significance of this difference is questionable. In the original seminal papers on CTCs a count of >2 CTCs was considered diagnostic, meaning that 1-2 CTCs could be found in healthy volunteers (possibly contaminants or false positives) (Allard et al., 2004). The mean number of putative CTCs found in the benign patients on Imagestream was affected by one particular sample in which there was a high number of Nanog positive cells. It is possible that these were false positives and that each of the other samples contained a small number of cells that, allowing for a small margin of error, should be ignored.

A significant difference in overall CTC count was found between the newly diagnosed metastatic patients and those on both surveillance and single-agent hormones, and between those on single agent hormones and maximum androgen blockade. Significance was not found but the p-value was close to 0.05 for patients undergoing surveillance in comparison to those with both castrate-resistant disease and on maximum androgen blockade, and larger numbers in the groups may have led to this becoming significant. Whilst these results do not prove anything new, they do help to validate the results obtained using this assay and mean that the antigen data can be interpreted with some reassurance of accuracy.

Unfortunately, the antigen expression on CTCs from patients in each group was not statistically significantly different when comparing each group all together, or when looking at the odds ratio of the antigens being present or absent. This lack of difference in antigen expression is surprising given that the counts are significantly different between the groups, but could be explained by the relatively low numbers of CTCs to start with, that means each antigen or combination of antigens is expressed in even lower numbers. The odds ratio could be worked out between all of the groups, but given that the surveillance group had the lowest number of CTCs (while still having counts greater than 0) a difference is unlikely to be shown. There was also no difference when looking at the odds ratio of the three stem cell antigens being present in patients who were alive versus those who were dead. Looking at

this odds ratio over a longer time period may be helpful as a higher number of patients will have died, and this work is planned alongside the Kaplan-Meier work.

When looking at the FACS results, the CTC count itself is likely to have a higher degree of error, in that rather than looking at antigen positive cells, all CD45-/CD16- cells were counted. As explained, it was felt that this was most accurate, given the inability to validate the cells further. But what is concerning, and means the results for the antigen expression for this assay must be interpreted with caution, is that there is no significant difference in CTC counts between any of the groups, including the healthy volunteers.

A difference in antigen expression for the FACS assay was found to be significant for four of the antigens, but the majority were not significantly different to the healthy volunteer control group. This data should therefore be interpreted with a high index of suspicion. Odds ratios for the different antigens were not calculated for the FACS assay but given the relatively high number of cells expressing antigens, and the low numbers of patients in each group, it is unlikely to have yielded any significant differences.

The odds ratios looking at the presence or absence of the three stem cell antigens were also not found to show an association in those patients who were dead or alive. Whilst low numbers of early deaths could be blamed, given the other findings from this assay it is more likely to be due to unreliable data.

The results from the Imagestream assay are disappointing in that antigen expression on CTCs at this stage does not appear to be significant. However the data may yet predict survival if correlated to prostate cancer related deaths and/or disease progression over a longer time-frame. The FACS assay appears to have a high degree of error and the results at this stage indicate that reliable data is unlikely to be generated from this arm of the work. Some groups have had success isolating CTCs using conventional FACS such as the one in this assay. But given the availability of FACS machines and the relative ease at which high throughput of samples can be processed, the fact that the literature is not full of studies recommending this method may indicate that many groups have had similar experiences.

Chapter 6. The use of CTCs to develop different models for target discovery

Chapter Summary

This chapter explores the potential use of CTCs once they have been extracted and cultured. Different models are explored based on the physical and chemical properties of the CTCs. These include experiments looking at the stiffness of different cells, their chemokine expression, and a CDX mouse model, the latter two of which have not been previously investigated in prostate cancer. (It should be noted that where the term CTC is used that these cells are deemed putative CTCs as they do not fulfil the criteria set by the FDA).

6.1 Rationale for attempting to use CTCs for target discovery

During the process of optimising the FACS and Imagestream assays, review of the literature revealed that there had been successful attempts to culture CTCs (Hwang et al., 2017, Cayrefourcq et al., 2015, Zhang et al., 2013, Hamilton et al., 2016, Kolostova et al., 2014, Kolostova et al., 2015, Kulasinghe et al., 2016), albeit at extremely low frequency of success. Some of these cells were then used for downstream models, such as circulating tumour cell derived xenograft (CDX) mouse models (Hodgkinson et al., 2014, Morrow et al., 2016). Discussion with colleagues within the Institute working in different fields (pharmacy, drug discovery and bio-engineering) led to the ideas described in this chapter regarding different uses for CTCs. Because of the high numbers of samples collected for the FACS and Imagestream assays, an attempt at culturing was made. The following experiments were conducted, in order to explore the possibility of utilising CTCs in a different way for clinical benefit such a drug discovery.

6.2 Comparison of different techniques for CTC extraction from whole blood

6.2.1 Background

The methods used to extract CTCs for the Imagestream and FACS assays had used an initial fixation step. Whilst this worked well for the Imagestream assay and would have worked for the FACS assay had there not been the issue with the sorted population, it would not enable

cell culture. Different methods of CTC extraction were already in existence or became commercially available during the course of this project. These were compared using cell lines spiked in blood to see which yielded the highest retrieval count.

Three different experiments were performed using increasing numbers of spiked cells (1000, 10 000 and 100 000 cells) in 2mls of blood. Each was repeated three times and performed for two different cell lines, PC3 and U2OS. Cell lines were harvested and counted using a haemocytometer before being added to the blood. Blood containing spiked cells was then processed using each method and cell retrieval was measured by running the cells on the Imagestream. This was to ensure that white cells were not falsely increasing retrieval numbers and, although there would have been a degree of cell loss, as this method was applied to all arms of the experiment it was felt that this would not affect the comparative numbers. The cells of interest were resuspended in Robosep buffer and stained with CD45(PECy7), Vimentin (AF647) and DAPI (for PC3s) or CD45(PECy7), CD44(FITC) and DAPI (for U2OS).

For this experiment I am grateful to Maria Georgiou (technician in the Rankin group) for her assistance in preparing and running some of the samples.

6.2.2 Density centrifugation

The Stem Cell Technologies Rosette-Sep Anti-CD36 CTC Enrichment kit was chosen for this experiment. This particular preparation was used due to its use in the successful retrieval and subsequent CDX mouse model created from a patient with small cell lung cancer that was discussed in the seminal paper on CTC CDX models (Hodgkinson et al., 2014).

Density centrifugation is one of the most basic cell separation techniques available and can be performed on a bench-top centrifuge using standard Falcon tubes (Kitz et al., 2018). It works on the assumption that CTCs will have a density lower than 1.077g/ml (Alunni-Fabbroni and Sandri, 2010). In its most basic form, this method can be performed solely using a density gradient medium, which will cause cells with different densities to separate into different layers when the tube is spun in a high-speed centrifuge. The top layer is usually plasma, followed by the CTC layer, and then the layer containing the white cells, leaving the red cells at the bottom of the flask (Lowe and Allan, 2014). The plasma layer can be carefully pipetted off and discarded, revealing the CTC layer. An obvious weakness of this technique is cell contamination between the layers, either due to inadequate separation

during the centrifugation stage, or manual mixing at the pipetting stage. It assumes CTC cell density will be universally different to cells found in the blood, which although is true of larger CTCs, smaller ones can often be denser (van der Toom et al., 2016). One strength of the method is that it does not rely on carcinoma cell markers, and the CTC antigen heterogeneity will not matter. Various kits are commercially available that include antibodies targeted at white cells, to reduce the contamination between the white cell layer and the CTCs.

The Rosette-Sep kit contains a cocktail of antibodies that targets the white cell population (CD2, CD16, CD19, CD36, CD38, CD45 and CD66b) in addition to glycophorin A on red blood cells. Blood is incubated with this cocktail at room temperature and then mixed with the Lymphoprep density gradient medium prior to centrifugation. The results of the density centrifugation experiment for the two different cell lines using the three different cell numbers spiked in 2ml of blood are shown in Figure 6.1. A prostate and osteosarcoma cell were used to complement work conducted by other members of the group, looking into CTC extraction from patients with osteosarcoma.

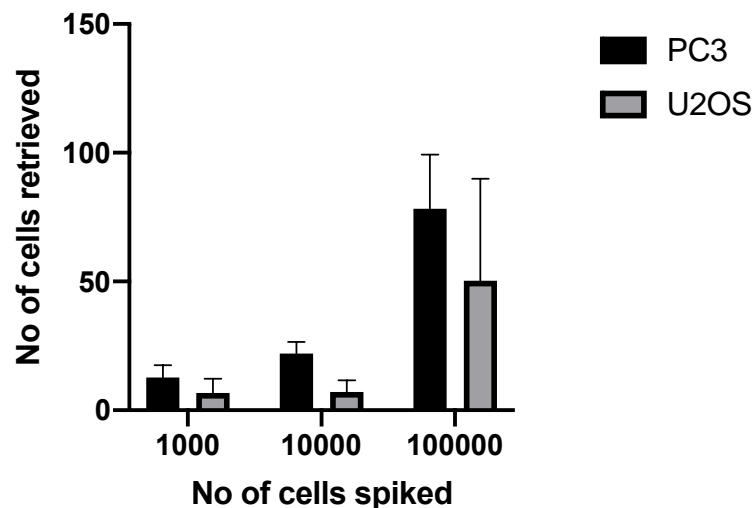


Figure 6.1 A graph to show the mean number of cells retrieved ($n = 3$) when using the density centrifugation method. The cells were counted on the Imagestream^X. 1.27%, 2.20% and 0.78% of the PC3 cells were retrieved when 1000, 10 000 and 100 000 cells were spiked respectively. 0.67%, 0.70% and 0.50% of the U2OS cells were retrieved when 1000, 10 000 and 100 000 cells were spiked respectively.

As expected, increasing numbers are retrieved when higher numbers are spiked into the blood, although the variability, demonstrated by the standard deviation, is much higher in the 100 000-cell arm of the experiment. PC3 retrieval is slightly better, possibly because the cells are less fragile compared to the U2OS.

6.2.3 Magnetic Separation

This principle uses magnetically conjugated antibodies against either white cell antigens or CTC antigens which are commercially available in cocktails that are mixed directly with whole blood, followed by magnetic beads which bind to the relevant antibodies. The blood is then processed through a magnet for either negative or positive selection. For positive selection (e.g. antigen that will be positive on the CTC population) the cells that are magnetically selected are retained in the tube for further analysis whereas for negative selection (e.g. white cell antigens) the magnetically selected cells are discarded.

Two different commercial kits were used, which both use the same principle of negative selection. The first of these was a single white cell marker kit (CD45) from Miltenyi Biotec and the second was the Stem Cell Technologies Easy Sep CTC Human enrichment kit which contains antibodies to multiple white cell markers. This method also included an initial red cell lysis step using density centrifugation prior to the application of the magnetically labelled micro-beads. The micro-bead cocktail was then combined with the remaining blood components and incubated prior to being passed through magnetic filters.

The results of this first magnetic separation experiment for the two different cell lines using the three different cell numbers spiked in 2ml of blood are shown in Figure 6.2.

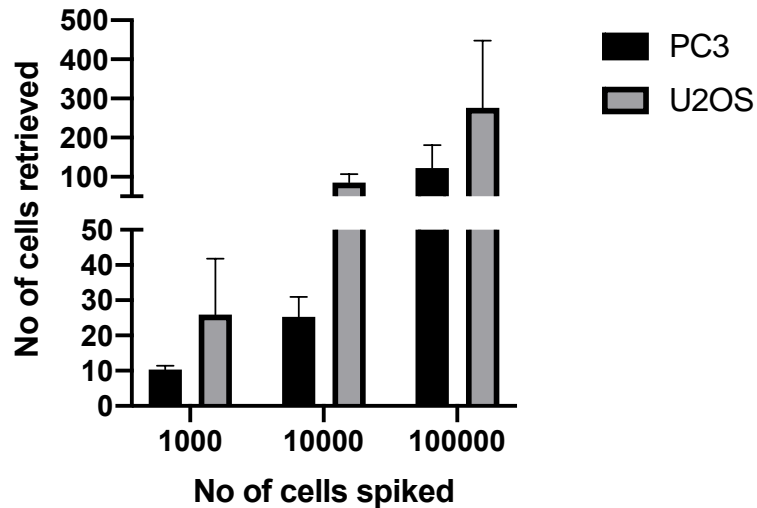


Figure 6.2 A graph to show the mean number of cells retrieved (n = 3) with the first magnetic separation kit (Miltenyi) using CD45 as a single marker. The cells were counted on the Imagestream^X. 1.03%, 0.25% and 1.22% of the PC3 cells were retrieved when 1000, 10 000 and 100 000 cells were spiked respectively. 2.60%, 0.85% and 2.76% of the U2OS cells were retrieved when 1000, 10 000 and 100 000 cells were spiked respectively.

This experiment needed repeating several times to get accurate results as the red cell lysis did not work particularly well. Even when running the sample through the Imagestream there was clear evidence of remaining erythrocytes. This was the only method in which there was a higher retrieval rate of U2OS compared to PC3 cells, and there was not a proportionally higher number retrieved in the 100 000 spiked-cell arm.

The second magnetic separation method used a multiple white cell marker cocktail. The Stem Cell Technologies Easy Sep CTC Human enrichment kit contains a combination of anti-white cell antibodies (CD2, CD14, CD16, CD19, CD45, CD61, CD66b) and Glycophorin A to target erythrocytes. There is no initial red cell lysis or density centrifugation step and the cocktail is applied to whole blood.

The results of this second magnetic separation experiment for the two different cell lines using the three different cell numbers spiked in 2ml of blood are shown in Figure 6.3.

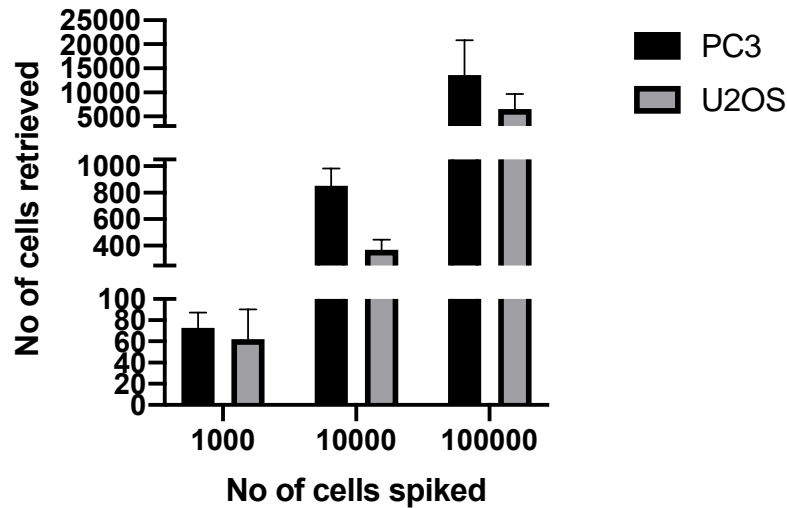


Figure 6.3 A graph to show the mean number of cells retrieved (n = 3) with the second magnetic separation kit (Stem Cell Technologies) using multiple white cell markers. The cells were counted on the Imagestream^X. 7.30%, 8.52% and 13.64% of the PC3 cells were retrieved when 1000, 10 000 and 100 000 cells were spiked respectively. 6.23%, 3.70% and 6.55% of the U2OS cells were retrieved when 1000, 10 000 and 100 000 cells were spiked respectively.

Because a higher number of white cell antibodies was used in this cocktail, it might be expected that a lower number of cells would be retrieved due to cell line cells possibly adhering to more of the white cells remaining on the magnet. However, a higher proportion of cells were retrieved from both cell lines at all three concentrations, when compared to the previous two methods.

6.2.4 Physical Properties (Parsortix)

The final method chosen for this experiment was retrieval based on physical properties. The NICR has a Parsortix machine which works by passing whole blood through a cassette containing multiple filters at a constant pressure of 99bar (Miller et al., 2018). It assumes that CTCs will be both bigger and less deformable (due to a higher nuclear: cytoplasmic ratio) than the leucocytes and erythrocytes (Kitz et al., 2018, Miller et al., 2018). By using a combination of buffers and priming fluids, the blood is drawn through the machine and the cassette is used to filter out unwanted cells. The CTCs are then collected in an Eppendorf. This method had been used successfully to separate CTCs from whole blood in patients with metastatic prostate cancer (El-Heliebi et al., 2018).

Benefits of this method include the lack of antigen labelling and the consequent potential for heterogeneous CTC populations to be identified. Small CTCs might be missed however, and the filters can clog easily.

The results of this physical separation experiment for the two different cell lines using the three different cell numbers spiked in 2ml of blood are demonstrated in Figure 6.4.

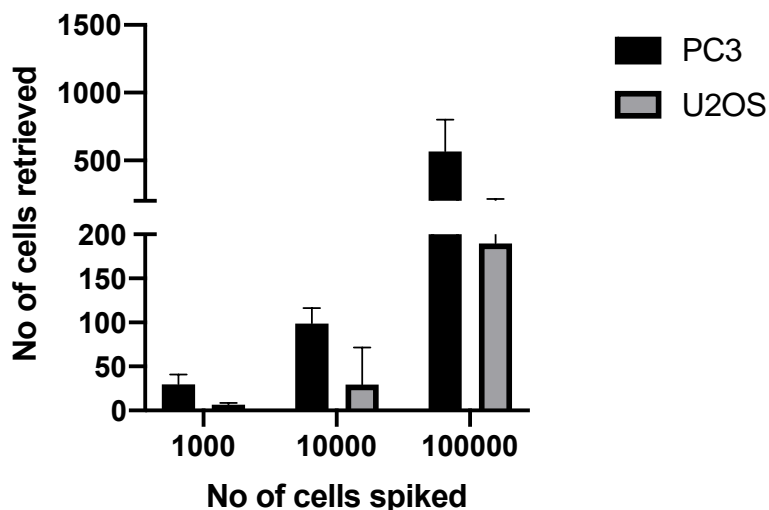


Figure 6.4 A graph to show the mean number of cells ($n = 3$) retrieved when using the Parsortix machine. The cells were counted on the Imagestream^x. 2.97%, 0.99% and 0.67% of the PC3 cells were retrieved when 1000, 10 000 and 100 000 cells were spiked respectively. 0.63%, 0.29% and 0.19% of the U2OS cells were retrieved when 1000, 10 000 and 100 000 cells were spiked respectively.

The actual numbers of cells retrieved were comparable to the density centrifugation method and the magnetic separation method using the Miltenyi kit. There were issues with filter clogging during a couple of the experiments and this meant eight repeats were required in order to get a full set of results. Again, the U2OS retrieval is lower in comparison to the PC3 cells, which could be due to cell fragility.

6.2.5 Overall retrieval and choice of method

In order to compare the numbers of cells retrieved some basic statistics were performed to compare the methods. The following table (Table 6.1) and graph (Figure 6.5) outline the mean number of cells retrieved using each method, for each cell line and at each quantity.

No of cells spiked	Percentage recovery					
	1000		10 000		100 000	
Cell line	PC3	U2OS	PC3	U2OS	PC3	U2OS
Density centrifugation	1.27	0.67	2.20	0.70	0.78	0.50
Magnetic sep'n (M kit)	1.03	2.60	0.25	0.85	1.22	2.76
Magnetic sep'n (STC kit)	7.30	6.23	8.52	3.70	13.64	6.55
Physical (Parsortix)	2.97	0.63	0.99	0.29	0.67	0.19

Table 6.1 A table demonstrating the percentage of cells retrieved using each method, for each cell line at each different quantity. (M = Miltenyi and STC = Stem Cell Technologies). The Stem Cell Technologies kit enabled the highest percentage of cells to be recovered when cells were spiked in all three different quantities.

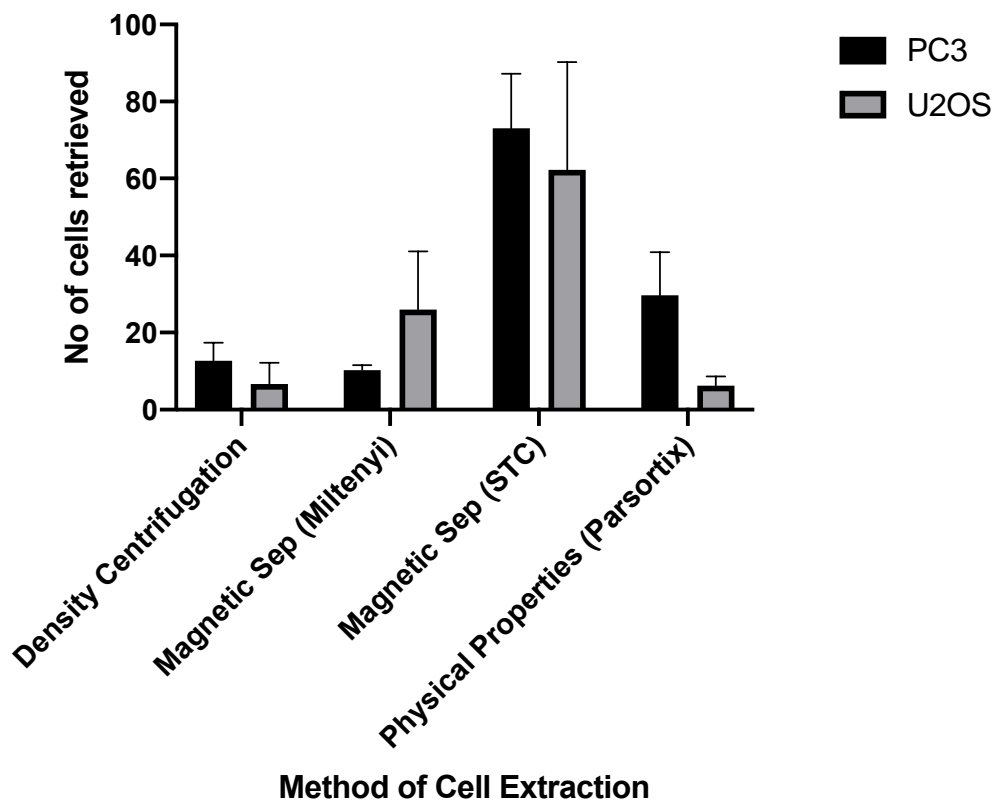


Figure 6.5 A graph to show the mean number of cells retrieved for each cell line, using each method when 1000 cells were spiked. (STC = Stem Cell Technologies). The Kruskal-Wallis test showed a significant difference when all four techniques were compared for the PC3 cells ($p = 0.004$) and U2OS cells ($p = 0.03$). Further analysis with the Mann-Whitney test, comparing each individual technique did not reveal a significant difference.

The Kruskal-Wallis test was performed which showed a significant difference when comparing all four methods for both PC3 ($p = 0.004$, Kruskal-Wallis statistic = 9.0) and U2OS ($p = 0.03$, Kruskal-Wallis statistic = 9.1) for the 1000 cell experiment. The Mann-Whitney test was then performed to demonstrate whether there was a significant difference between each of the individual values (performed separately for each different cell line) but this did not reveal any significant differences between methods.

Although the Stem Cell Technologies kit appears to produce a higher retrieval rate, the Mann-Whitney test shows that the numbers retrieved are not significantly different from any of the other methods. This could be due to low numbers of repeats, and overall low cell numbers too.

The Kruskal-Wallis test was repeated to compare the retrieval rate of all four methods for the 10 000-cell experiments. For the PC3 arm the p -value was 0.001 (Kruskal-Wallis statistic = 9.6) and for the U2OS arm the p -value was 0.006 (Kruskal-Wallis statistic = 8.7). The mean

number of cells retrieved using each method for the 10 000-cell experiment is shown in the following graph (Figure 6.6).

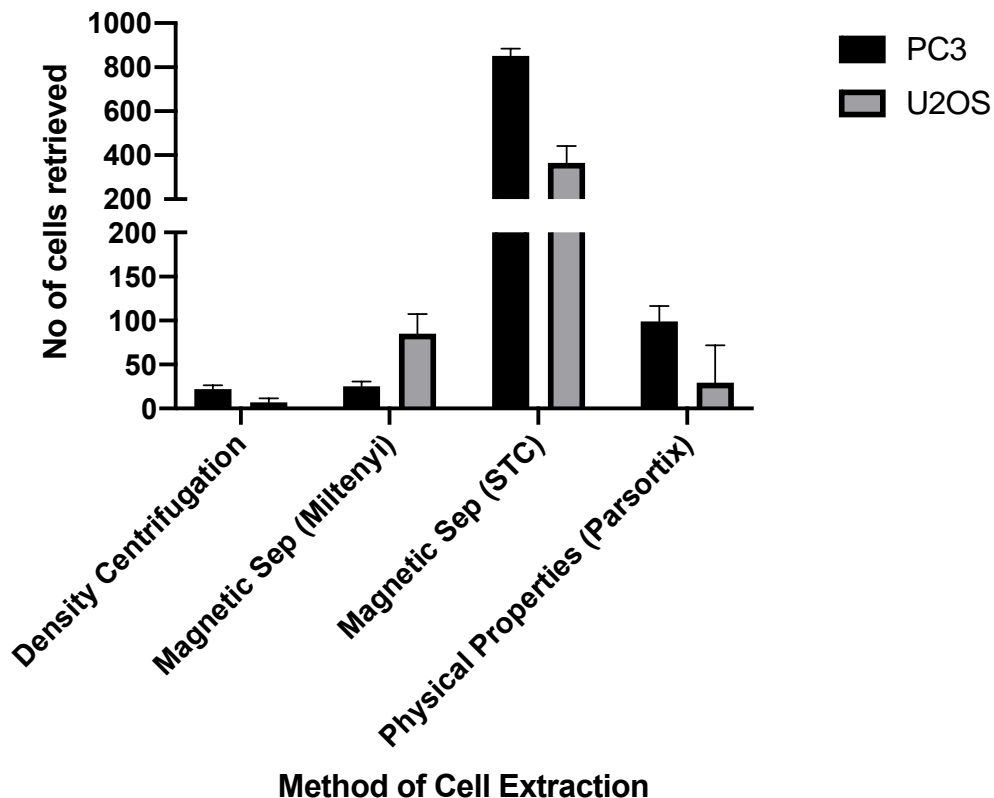


Figure 6.6 A graph to show the mean number of cells retrieved for each cell line, using each method when 10 000 cells were spiked. (STC = Stem Cell Technologies). The Kruskal-Wallis test showed a significant difference when all four techniques were compared for the PC3 cells ($p = 0.001$) and U2OS cells ($p = 0.006$). Further analysis with the Mann-Whitney test, comparing each individual technique did not reveal a significant difference.

The Mann-Whitney test was then performed to demonstrate whether there was a significant difference between each of the individual values (performed separately for each different cell line) but despite the results shown in Figure 6.6 showing a higher retrieval rate for the Stem Cell Technologies kit, these figures are not significant and there were no significant differences between methods.

For the final arm of the experiment (100 000 spiked cells) the Kruskal-Wallis test was performed for each cell line separately, to investigate whether there were significant differences between the four methods. For the PC3 cells, the p-value was 0.001 (Kruskal-Wallis statistic = 9.5) and for the U2OS cells the p-value was 0.006 (Kruskal-Wallis statistic =

8.7). The mean number of cells retrieved using each method for the 100 000-cell experiment is shown in the following graph (Figure 6.7).

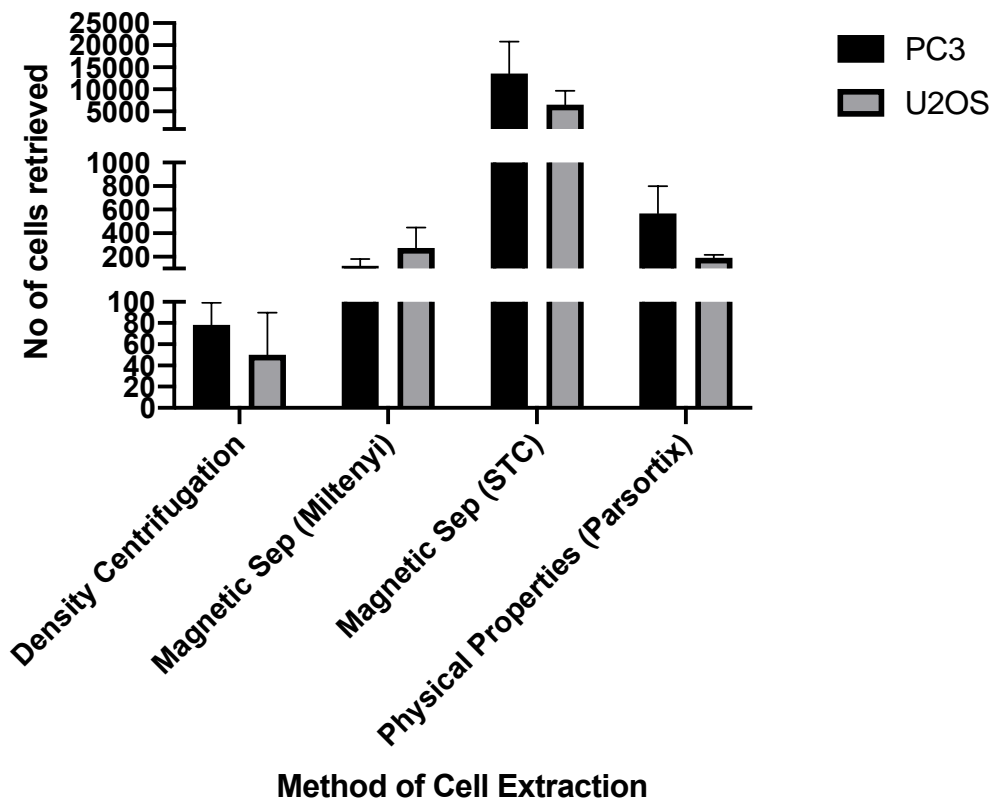


Figure 6.7 A graph to show the mean number of cells retrieved for each cell line, using each method when 100 000 cells were spiked. (STC = Stem Cell Technologies). The Kruskal-Wallis test showed a significant difference when all four techniques were compared for the PC3 cells ($p = 0.001$) and U2OS cells ($p = 0.006$). Further analysis with the Mann-Whitney test, comparing each individual technique did not reveal a significant difference.

None of the individual methods for the 100 000-cell spiked experiment showed a significant difference in retrieval rate when the Mann-Whitney test was performed, despite there being higher overall numbers retrieved. Again, this could be due to only repeating each method three times.

Although the statistical analyses do not demonstrate a significant difference in retrieval rate, the multiple magnetic marker kit from Stem Cell Technologies was chosen as the method of choice for extracting CTCs from clinical samples.

The Density Centrifugation method had been used before by different groups to obtain viable CTCs that could then be cultured and successfully transplanted into mice for a CDX

model (Hodgkinson et al., 2014). However, when this method was attempted here, there were technical difficulties preventing contamination of cells from other layers while obtaining the purified enriched cell layer. This is likely to have improved with use but as overall numbers were lower than with the magnetic kit from STC, the decision was made not to use this method.

There were often issues with the red cell lysis using the Miltenyi kit, and this arm of the experiment had to be repeated eight times in order to obtain the ultimate sample free of red cells. It also only used one white cell marker to extract white cells from the cell pellet, and there were many more white cells seen on the subsequent Imagestream analysis. As discussed later in section 6.3.2, white cells grow prolifically in culture and could potentially starve CTCs of nutrients. For this experiment the white cells were gated out of the analysis, but if the cells of interest were being transferred straight to a culture medium, not only could they be deprived of nutrients but it would be more difficult to discern which cells were CTCs and which were white cells when planning ongoing CTC specific experiments.

The Parsortix was discounted as the machine itself was situated in non-sterile conditions in the NICR. This meant that subsequent attempts at culture ended up in infection. Preliminary discussions were made about transferring the machine into a tissue culture hood, but lack of resources and the fact that others using this machine did not require sterile conditions meant that this did not occur. In addition, the two cell lines used for the spiking experiment both have cells much larger than white blood cells. If these cell lines still didn't result in significantly higher retrieval numbers compared to other methods, it raises concern that small CTCs from clinical samples may be completely missed.

Because the Stem Cell Technologies kit uses multiple magnetic markers against white cells, it would be expected to have potentially one of the lower yields of CTCs. However, possibly because it did not involve a separate red cell lysis phase (which could have fragmented some of the cells), the cell retrieval was higher, even if not significant. It was a much purer sample too, with very few white cells seen on the Imagestream.

This chosen method resulted in cells within a gelatinous-looking suspension. This was spun down and whilst no visible pellet was seen, the majority of the gelatinous material was discarded (presumed to be plasma and platelets) and media was used to resuspend any cells that remained, before transfer to a 24-well plate for incubation.

6.3 Optimisation of Cell Culture

6.3.1 Background

In order to perform downstream experiments that could be repeated, CTCs obtained would ideally need to be expanded by growing in culture. Harvested numbers from each patient are likely to be small and, although concern about differentiation must be considered, even one or two cell passages are likely to increase cell numbers to the required amount. Ideally, sequencing at every passage would be performed to look at differentiation but for logistic and financial reasons this would not always be possible.

6.3.2 Different culture media

On reviewing the literature, there were several groups who had successfully managed to culture CTCs but very few who had managed to keep these cells alive beyond 14 days. For those with longer term success, media choice varied between specific stem cell media (Hwang et al., 2017) and basic RPMI (Kolostova et al., 2014, Kolostova et al., 2015, Hamilton et al., 2016, Yu et al., 2014) or DMEM (Zhang et al., 2013, Cayrefourcq et al., 2015, Kulasinghe et al., 2016). Some added varying quantities of insulin (Cayrefourcq et al., 2015, Zhang et al., 2013), antibiotics (Drost et al., 2016, Hamilton et al., 2016, Zhang et al., 2013) and steroids (Drost et al., 2016, Zhang et al., 2013) and all used different quantities of growth factors and foetal bovine serum (Cayrefourcq et al., 2015, Drost et al., 2016, Hamilton et al., 2016, Kolostova et al., 2014, Kolostova et al., 2015, Kulasinghe et al., 2016, Yu et al., 2014, Zhang et al., 2013).

Due to the stage of the project, there was limited time to set up experiments to try and compare the different media and additives. Because of this, and to reduce the risk of introducing infection by adding several individual components, the Lonza Mesenchymal Stem Cell Growth Medium Bulletkit was chosen. This contains a basal media that is specifically designed to promote stem cell growth without encouraging differentiation. It also contains a pre-determined cocktail of growth supplements and set volumes of L-glutamine and antibiotics. Once combined, the full media can be stored at 4°C for up to six months.

6.3.3 Normoxic versus hypoxic conditions for cell culture

Some of the studies that looked at successful CTC culture described maintaining cell culture under hypoxic conditions (Cayrefourcq et al., 2015, Kulasinghe et al., 2016). These groups varied the oxygen tension and found that the CTCs proliferated more quickly under hypoxic conditions. It is established that under hypoxic conditions, hypoxia inducible factor 1 alpha (HIF-1 α) is induced (Liao et al., 2007). In turn this targets pro-metastatic genes such as GLUT1 and LOX, which promote tumour growth and metastasis (Semenza et al., 1996, Sowter et al., 2001).

A hypoxic incubator and tissue culture hood are available in the NICR, but at the time of the planned experiments they were undergoing repair and were not available for a period of two months. Cells obtained from patient samples were therefore kept under normoxic conditions for the purposes of this experiment.

6.3.4 Testing the media and culture conditions on cancer cell lines

Before using precious clinical samples, two cancer cell lines were spiked into whole blood, selected using the Stem Cell Technologies multiple-magnetic white cell marker kit described in section 6.2 and maintained in the Lonza Mesenchymal Stem Cell culture described in section 6.3.2. This was to ascertain whether the method of cell retrieval would be viable to use on clinical samples (in terms of incidence of infection and other practical logistics). 1000 PC3 or U2OS cells were spiked in to 2ml of healthy volunteer blood and the kit was used as described earlier. The resultant cell suspension was spun down, and cells resuspended in 2ml of the Lonza media. This cell suspension was then divided into six and added to a six-well plate with each well containing 2ml of the media. Each cell line experiment was repeated three times. The incubation procedure followed the method described for cell line culture in Chapter 2 and media was changed every third day. After six days they were sufficiently confluent to transfer to T75 flasks and after sixteen days they were still viable and had required two further 1:20 passages. The following images (Figures 6.8 and 6.9) were taken at sixteen days.

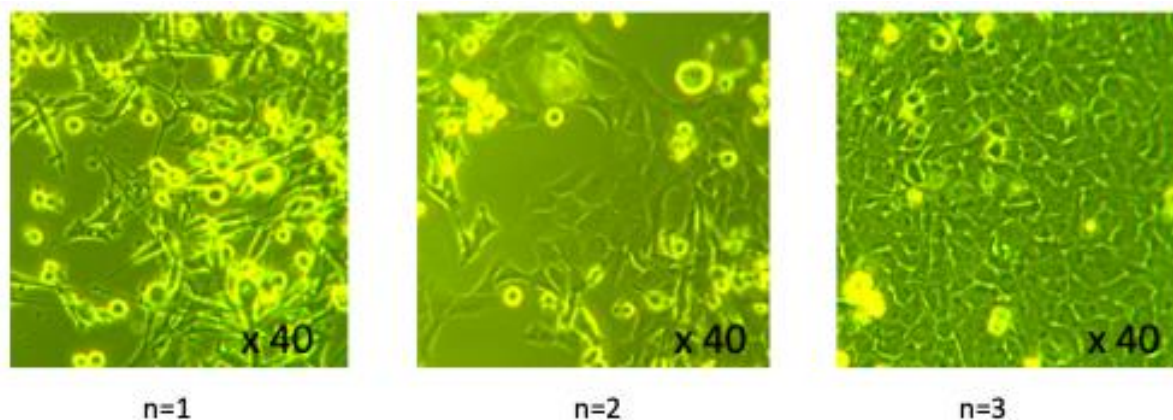


Figure 6.8 Microscope images of the three flasks containing PC3 cells at day 16 (x40 magnification).

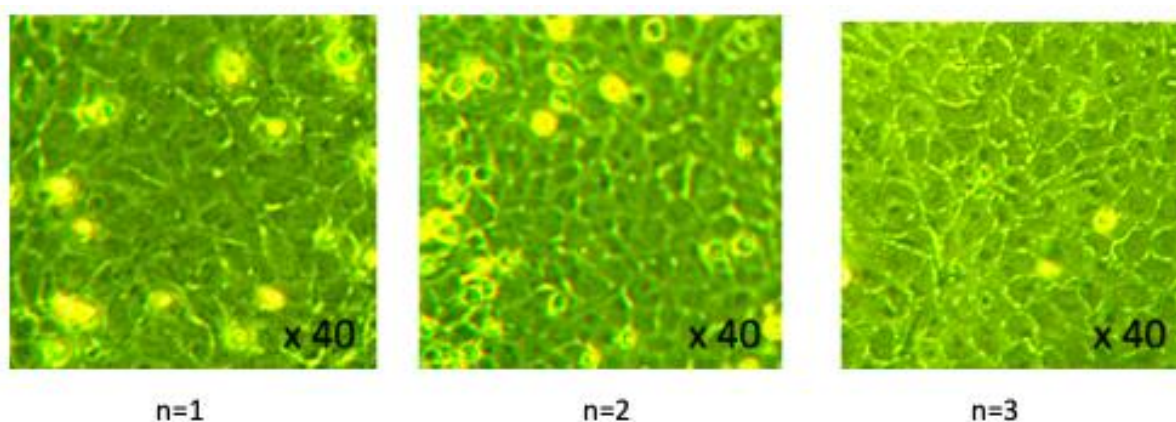


Figure 6.9 Microscope images of the three flasks containing U2OS cells at day 16 (x40 magnification).

This experiment demonstrates that the CTC selection kit and media are both suitable for the selection and maintenance of cancer cell lines in culture. Whilst anticipated CTC numbers will often be much lower, and CTC proliferation may not be as successful in these conditions, there were no significant difficulties encountered, and the morphology of the cells showed that they were the cell lines and not white cells. It was therefore felt that this method would be suitable to use with clinical blood samples.

6.3.5 Testing the media and culture conditions on white blood cells

Low numbers of CTCs were anticipated from the selection method in the clinical samples, and therefore retrieved cells were put directly into culture, rather than sorting them further via another method such as FACS. Because the sample was unlikely to be 100% pure and was likely to contain some white cells, an experiment to determine whether or not white blood cells would survive in the culture conditions was performed. This was done to ascertain a)

whether they would survive and b) their proliferation rate. If they died under these conditions then we could be confident that any surviving cells were a pure CTC population, and similarly if they proliferated quickly, the slow growth of any cells from the clinical samples is more likely to indicate CTCs rather than white cells.

Images were taken at day 1 (Figure 6.10) and day 13 (Figure 6.11).

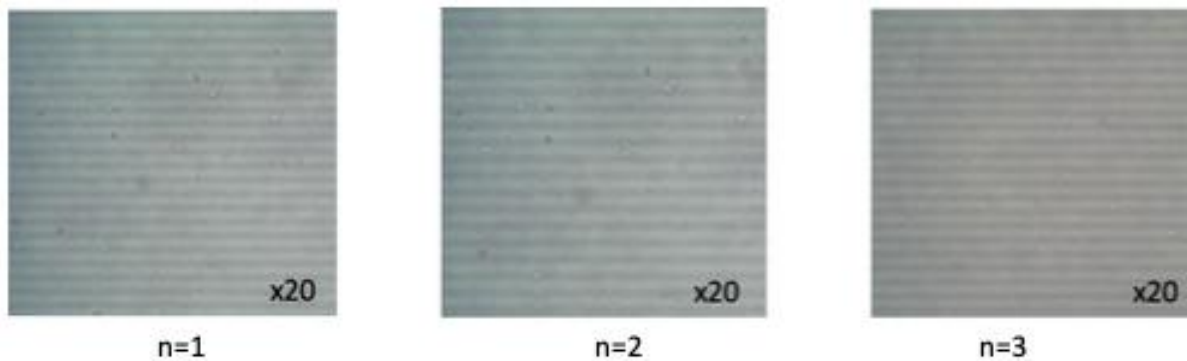


Figure 6.10 Microscope images of the three flasks containing white cells at day 1 (x20 magnification).

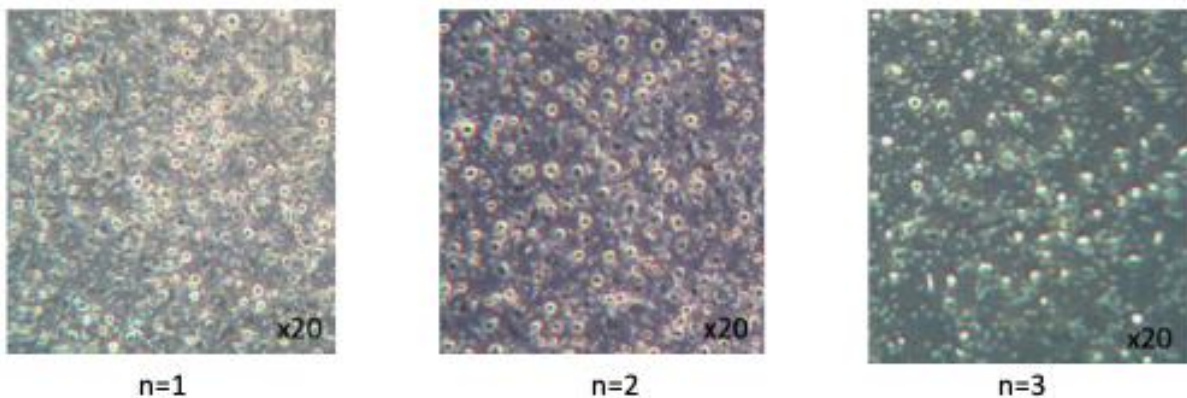


Figure 6.11 Microscope images of the three flasks containing white cells at day 13 (x20 magnification).

Despite the white cells being sparsely distributed in the original well, by day 10 they would have been confluent enough to transfer to a T75 flask, and at day 13 they were clearly over confluent. This experiment proves that white cells do survive in the culture environment and that they proliferate very quickly. By using the multiple-white cell antibody cocktail in the Stem Cell Technologies CTC kit it is hoped that very few white cells will be present in the cell suspension that is ultimately put into culture.

6.4 Using clinical samples for CTC culture

6.4.1 The first clinical sample

4ml of blood was obtained from a patient with end stage castrate resistant prostate cancer. The patient had multiple bony and lymph node metastases and had received treatment for both a spinal cord compression and pathological fractures. The blood was processed under sterile conditions using the Stem Cell Technologies Mesenchymal Stem Cell kit and incubated in the Lonza Mesenchymal Stem Cell media in a 12-well plate under the standard incubation conditions described in Chapter 2. Media was changed every second day and images taken at day 7 (Figure 6.12), day 13 (Figure 6.13), day 17 (Figure 6.14) and day 32 (Figure 6.15).

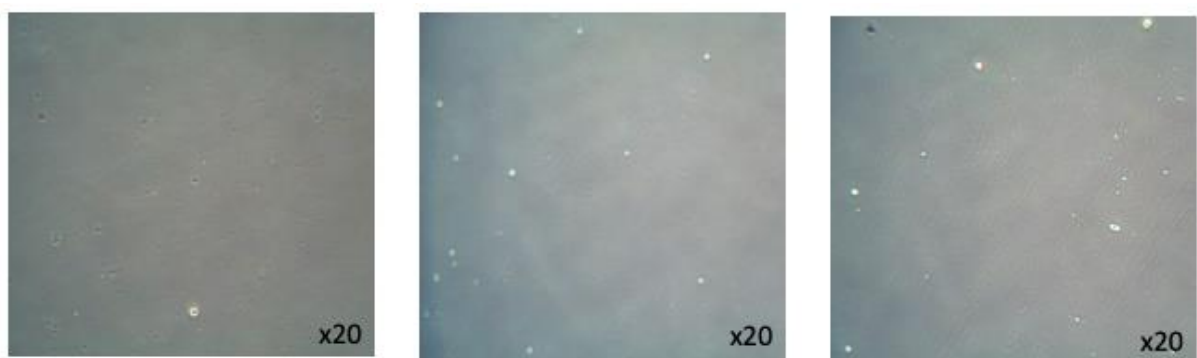


Figure 6.12 Microscope images of three of the wells from patient CTC-JARO-110 at day 7 (x20 magnification). The cells were very sparse.

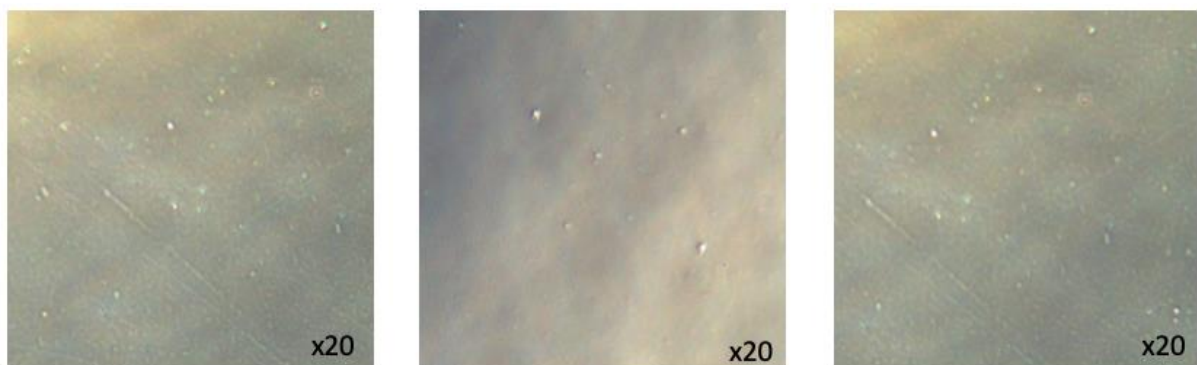


Figure 6.13 Microscope images of three of the wells from patient CTC-JARO-110 at day 13 (x20 magnification). There was a slight increase in confluence.

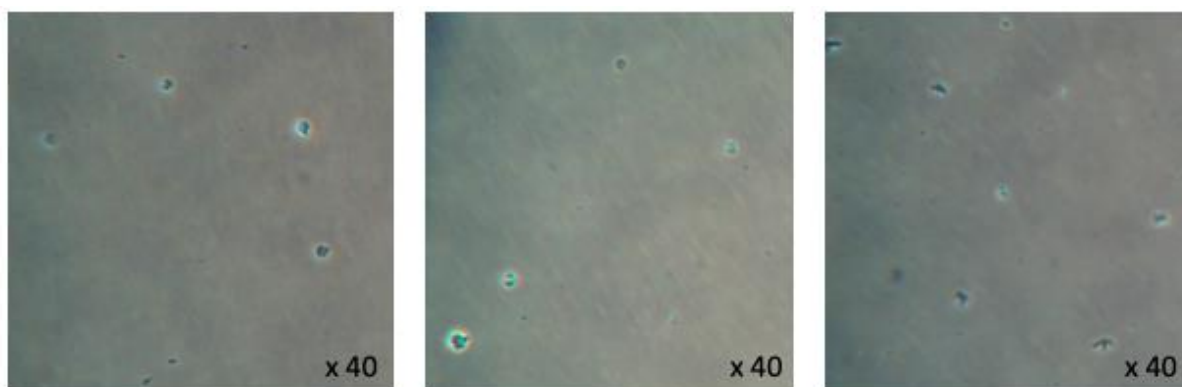


Figure 6.14 Microscope images of three of the wells from patient CTC-JARO-110 at day 17 (x40 magnification).

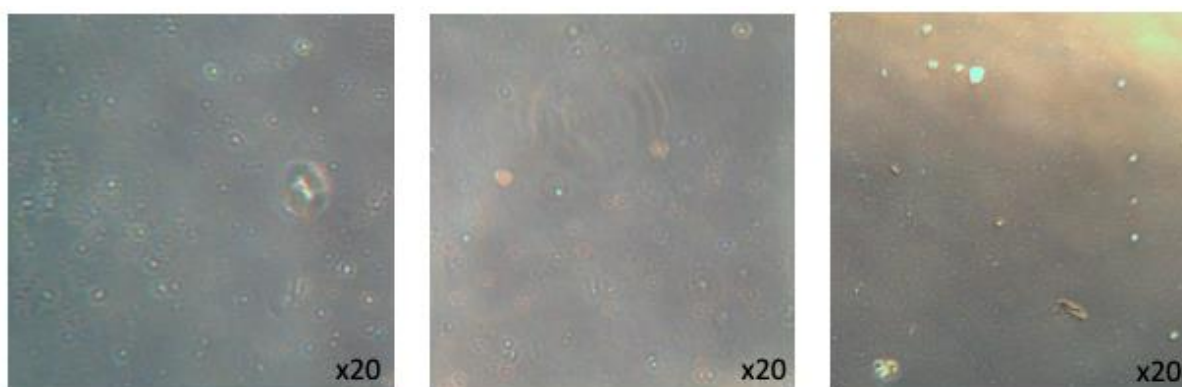


Figure 6.15 Microscope images of three of the wells from patient CTC-JARO-110 at day 32 (x20 magnification). There was an increase in confluence from day 13.

The different magnifications were used to demonstrate the overall confluence in the well and the individual cell morphologies.

Because the cells had not proliferated as quickly as the white cells in the experiment in section 6.3.5 but had grown in number, it was assumed that these cells were CTCs. The cells were trypsinised on day 33 and half were put back into fresh media for ongoing culture whilst the other half was processed on the Imagestream. The results of this experiment are discussed in section 6.5.2.

Due to the relatively long time that it takes to expand these cells in culture, at this stage the decision was made to obtain further clinical samples for this purpose to enable potential CTCs to grow for use in further experiments.

6.4.2 Clinical samples and the lessons learnt from attempted CTC culture

Blood from twenty-five patients with castrate resistant prostate cancer was obtained using the same method as with the first sample. Media was changed every second day but, despite performing this in sterile conditions and using vacutainers rather than needles to harvest the blood, by the end of week four, sixteen samples had to be discarded due to infection. Some of these infections were obviously bacterial but some were likely to be fungal (due to spores seen under microscopic examination). The media already contained an antibiotic combination of penicillin and streptomycin, so nystatin was added to the full media. Four further samples succumbed to infection over the next six weeks, which meant that there were six remaining, including the original patient's. These were maintained in culture for the next six months, and due to slow growth only required passage approximately every two months.

During the harvest process from the initial CTC selection kit, the resultant cell suspension was very gelatinous. Initially, because no cell pellet was seen and there was concern about fragmenting the low numbers of cells had centrifugation been performed, this gelatinous material containing the potential CTCs was put directly into media. This was contrary to what was performed in the cell-line experiment, but there had been a visible cell pellet in that. Unfortunately, this then formed a jelly-like substance in the wells of the plate. Although some cells could be seen adhering to the bottom of the plate, there were also some cells within this jelly-like material. This material could not be aspirated and instead had to be manually removed using a pipette and sterile forceps in order to change the media. After this happened to the first six samples (all but one of which succumbed to infection) the decision was made to spin the collection tube from the CTC kit, and discard the majority of the supernatant before resuspending.

Because so many of the samples were lost to infection, it was not possible to determine whether all contained cells that could have been CTCs. However, patients with the highest clinical burden of disease were targeted, and paired samples on the Imagestream showed all had CTCs detected via the method described in Chapter 3.

6.5 Proving the authenticity of the cells from clinical samples in culture

6.5.1 Background

Although the cells grown in culture were growing very slowly, and this is contrary to the white cells that grew much more rapidly, it cannot be assumed that this feature alone means that they are CTCs. Sequencing the cells would be the gold standard but this is technically difficult and expensive (involving DNA extraction from a small cell number followed by transporting the cells to a different institute). In addition, because of the slow growth of the cells in culture, when passaging them any cells taken out for analysis will mean a lower number of cells remaining for further culture and expansion.

The following methods of cell analysis were attempted in order to determine what the cells actually were.

6.5.2 Antigen expression

For the first patient sample that was cultured (CTC-JARO-110), the cells were trypsinised on day 33 (the day after the image in Figure 6.15 was taken). One third of the cells were put back into culture, a third were used for the experiment described in section 6.8 and a third were prepared to run on the Imagestream. The latter sample was spun at 400g and resuspended in 4% Paraformaldehyde for twenty minutes for fixation. The paraformaldehyde was then washed off and the cells were permeabilised and stained with the following antibodies, in line with the Imagestream method described in Chapter 3: CD45 (PECy7), EpCAM (PE-Vio 615), Oct4 (AF488), SOX2 (AF555), Nanog (PerCP-Cy5.5) and DAPI. All cells were subsequently resuspended in 200µl of Robosep buffer and run through the Imagestream.

A basic plot looking at cell size was performed and the results are shown in Figure 6.16. This shows a small number of much larger cells than would be expected if white cells only were present in the sample.

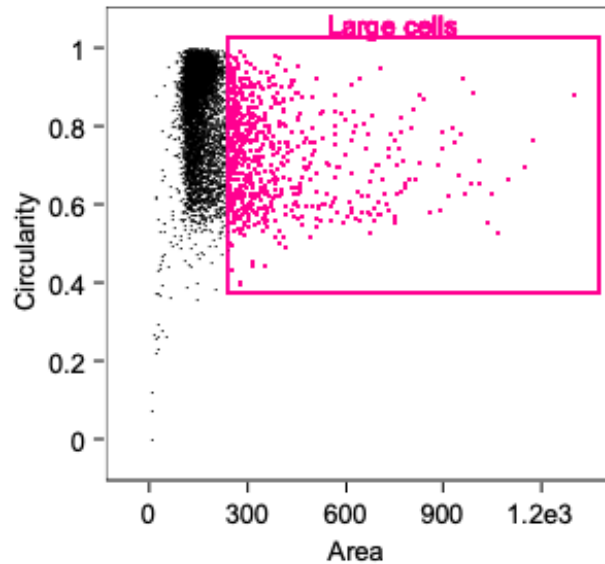


Figure 6.16 A graph to show cell area against cell circularity for all cells processed during this experiment. The gate is used to identify cells that are larger than the majority of white cells are expected to be. This shows that there are several cells that are larger than the majority of white cells and these could be potential CTCs.

To identify cells that were not white cells, the intensity of CD45 for all cells was plotted. This revealed three distinct populations (Figure 6.17).

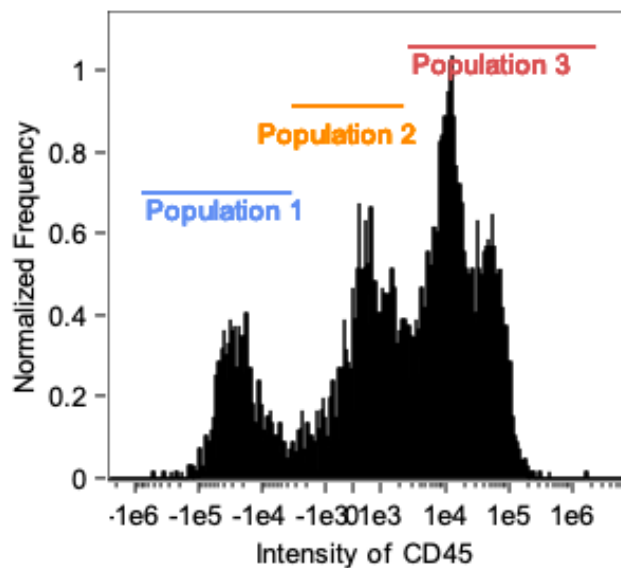


Figure 6.17 A graph to show the intensity of CD45 for all cells processed during this experiment. There are three distinct populations of cells although population 1 is likely to be debris or cells with non-specific staining as the intensity of the CD45 expression is very low. Cells in population 2 were smaller white cells than those in population 3.

When the individual cells in each of these populations were looked at more closely, cells within population 2 and population 3 were predominantly white cells that stained positive for CD45 (Figure 6.18). The variation in intensity between population 2 and population 3 was broadly explained by the size of the white cell.



Figure 6.18 An Imagestream image of a typical cell seen in population 2 and population 3.

The cells within population 1 were a mixture of large cells with large nuclei, very few of which were positive for the other antigens, and a large number of small, Nanog+ cells (Figure 6.19).



a) An EpCAM+/DAPI+ cell



b) A DAPI+ cell



c) A small Nanog+/DAPI+ cell

Figure 6.19 Imagestream images to show examples of some of the cells seen within population 1 in Figure 6.17. Cell a) expressed EpCAM and no CD45 so could be a putative CTC. Cell b) had no EpCAM, stem cell or CD45 expression so could either be a white cell that didn't express or stain positive for CD45, or a putative CTC which was negative for the markers of interest. Cell c) was a Nanog positive cell but expressed Nanog at a level higher than normal white cells, so could be a putative CTC.

All of the cells from the whole population that were DAPI+/CD45- were counted as potential CTCs. An intensity plot of Nanog for all of these cells was then performed (Figure 6.20). This was to establish whether the Nanog+ cells expressed Nanog at an intensity over the

threshold set in Chapter 3, which was higher than the intensity at which white cells expressed it.

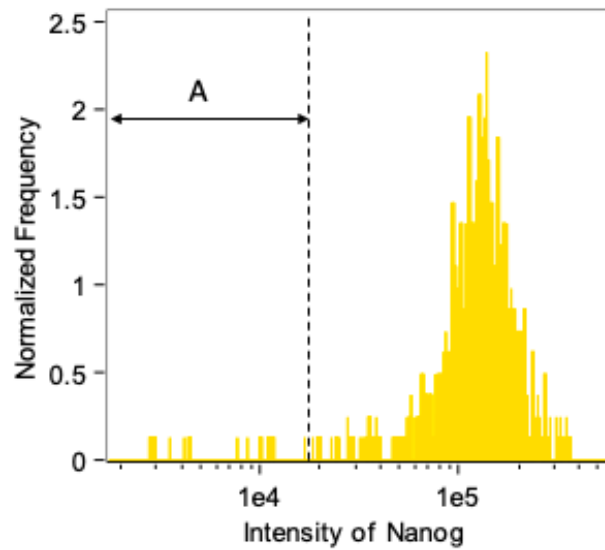


Figure 6.20 A graph to show the intensity of Nanog for all DAPI+/CD45- cells processed during these experiments. The majority of the cells expressed Nanog at a much higher level than is normally expressed in white cells, so these could represent putative CTCs.

From this graph, the majority of the possible CTCs expressed Nanog at a level much higher than is normally expressed in white cells. The cells in gate A when visualised appeared much larger than the Nanog+ cells in Figure 6.19c. Additionally, they did not obviously visually express Nanog. An example of one of these cells is seen in Figure 6.19b. This result means that we can say with some degree of confidence that the small cells seen in Figure 6.19c are not white cells, with the inference that they are CTCs. All CD45-/DAPI+ cells were highlighted on the original plot of cell size (Figure 6.21).

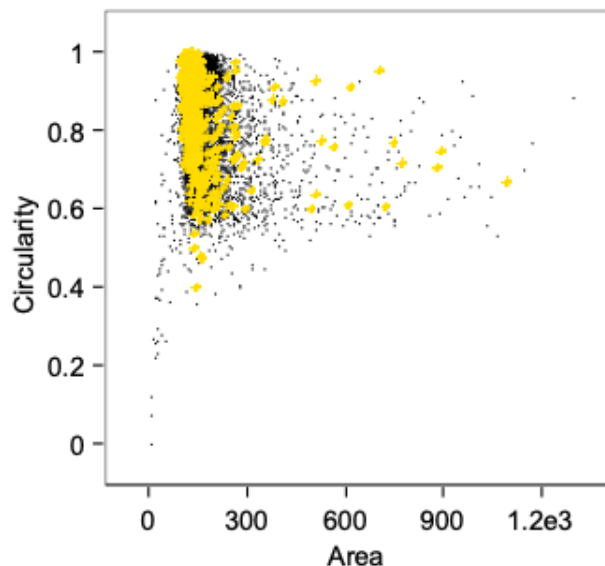


Figure 6.21 A graph to show the area against circularity plot but with the possible CTCs (CD45-/DAPI+ cells) highlighted in yellow. There is a considerable overlap in size between those cells that were negative for CD45 and white cells expressing CD45. As Nanog expression in the CD45- cells is high, we can be reasonably confident that these cells are not white cells but that they could be putative CTCs.

This graph demonstrates that whilst some of the larger cells do appear to be CTCs, some were bits of debris that did not contain nuclei. What is particularly fascinating about this plot is that the majority of the CD45-/DAPI+ cells were of a similar size compared to white cells. Because we have looked at Nanog expression in these cells we can be reasonably confident that they are not just white cells that have lost CD45 expression but could be small CTCs. In total there were 818 possible CTCs out of a total of 6680 events (cells/debris).

Whilst this data is reassuring, it is not conclusive and so other methods were conducted.

6.5.3 Real Time qPCR

A real-time quantitative PCR experiment was attempted to look at gene copy number of PSA, ARV7 and TMPRSS2 in the DNA from cells from five of the patients with cells in culture. The cells were trypsinised and DNA extraction and amplification were performed using the Qiagen Repli-g Mini kit. PC3 cells were also used as a control for this experiment. DNA quantity was measured using the Qubit (ThermoFisher Scientific) and was sufficient to proceed with the experiment. Unfortunately, the dissociation curves for all three genes at all concentrations showed multiple peaks. The housekeeper gene did amplify successfully so there may have been a problem with the primers for the three genes of interest. This happened again when the experiment was repeated, but because the cells were so slow to grow it was not possible to obtain further cells at this stage for analysis using this method.

6.5.4 SNP Array

A different approach was attempted; a SNP Array to detect single nucleotide polymorphisms that commonly occur in prostate cancer within the cells in culture. This was initially performed on cells belonging to three of the patients, and subsequently for the remaining three patients. PC3 cells were used as a control on both occasions. DNA was extracted and amplified using the Repli-g Mini kit (Qiagen) and measured using the Qubit to ensure adequate quantities. The DNA was then transferred on ice to a different department within the university for the SNP Array to be performed.

Unfortunately, in the first instance, despite the Qubit measuring adequate levels of DNA in all but one of the samples (>500µg), the SNP wasn't possible as they couldn't detect sufficient quantities of DNA. For the second set of patients, the flasks containing the cells were transferred directly to the department for the DNA extraction to be performed there. Unfortunately, again not enough DNA was extracted; the SNP was run anyway but failed.

6.5.5 Whole-exome sequencing

As a final attempt to determine the validity of the cells in culture, DNA was extracted from the cells of three patients and one cell line control and sent for whole-exome sequencing. Instead of extracting the DNA from cells in culture, it was performed on thawed samples that were frozen when passaged (passage 3 for CTC-JACH-73, passage 4 for CTC-JEWR-124 and passage 5 for CTC-JARO-110). This was done purely for time reasons as the cells take so long to grow in culture. The DNA extraction and amplification were performed by my colleague, Justin Englebert, using the Repli-G mini kit (Qiagen). Cells were transported in suspension on ice to another institution within the university. I am grateful to Justin Englebert, (technician in the Rankin group) for his help with the DNA extraction.

The DNA quantities and exome quality control data from the samples are shown in Table 6.2. A lower percentage of duplications (% dups) is preferable as higher numbers suggest an enrichment bias. Although we were advised by the sequencing team that an M seq number above 20 is preferable they were confident that they had enough DNA. However, when they attempted interpretation of the sequencing there had not been enough DNA from the patient samples. There was sufficient DNA from the two cell lines (U2OS cells were also sent as a positive control for some osteosarcoma patient cells) so the issue here may have been short DNA fragments from the patient samples, rather than an overall lack of DNA.

Unfortunately, this meant again we did not have any conclusive results from this experiment.

Sample	Sample provided				Exome quality control		
	Qubit conc (ng/μl)	Total DNA (ng)	Volume (μl)	Conc (ng/μl)	% Dups	%GC	M seqs
CTC-JACH-73	8.96	896	15	59.73	76.5–79	57.00	6.9–7.1
CTC-JARO-110	18.1	1810	15	120.67	56.0–57.9	45	23.1–23.7
CTC-JEWR-124	4.92	492	15	32.80	75.1–77.4	54.00	7.2–7.3
PC3 (control)	4.44	444	15	29.60	13.5–14.1	48	19.5–19.9

Table 6.2 A Table listing the DNA volume and concentrations provided from each sample, and the Exome quality control data prior to sequencing. Despite what should have been sufficient quantities of DNA obtained (as measured by the Qubit) the M seq number was low and this meant there wasn't sufficient DNA, or that the fragments were possibly too short for analysis.

6.6 Exploring the chemical properties of cultured CTCs

6.6.1 Background

One potential use of CTCs would be to explore their chemokine receptor expression. Chemokines are cytokines secreted by cells in order to enable motility towards cells with their corresponding ligands (Salazar et al., 2013, Ahmed et al., 2017b). Whilst chemokine mediated activity is not necessarily pathological (e.g. white cell infiltration as part of the inflammatory response (Wong et al., 2010)), there is increasing evidence that tumour cells may express chemokines that assist in the metastatic process (Engl et al., 2006, Singh and Lokeshwar, 2011, Singh et al., 2004, Kakinuma and Hwang, 2006, Ben-Baruch, 2008, Zlotnik et al., 2011).

Knowing which chemokines are secreted by particular cell types means that if tumour cells have a chemokine receptor that would bind with this protein, a prediction could be made on where that cell might metastasise to. This could help target specific treatments; e.g. early use of radium-223 in prostate cancer for men who have CTCs that are likely to spread to bone, or the interactions could be utilised for future drug discovery.

Evidence from an assay where chemokines are placed in agarose gel spots, in a dish containing cells in media, has shown that migration of these cells towards the gel spot occurs if the cells contain the corresponding ligand (Ahmed et al., 2017b). Collaboration with the authors of this study led to the design of an experiment where a similar agarose spot assay would be performed using the cells grown in culture from patients.

6.6.2 Choice of chemokine receptors and their corresponding ligands

Before setting up the Agarose Spot assay, a decision had to be made about which chemokine receptors on potential prostate cells would be most useful to look at, and therefore which ligands to put in the gel spots. The published study (Ahmed et al., 2017b) used two cell lines: PC3 cells which express CXCR4 and CCR7, and SW480 cells which express CXCR4. They had used the chemokines CXCL12, CCL19 and CCL21 in the gels; the former would attract cells expressing CXCR4 and the latter two would attract those expressing CCR7 (Ahmed et al., 2017b). Rather than just repeat the experiment, the literature was studied to find which chemokine receptors are most likely to be expressed on prostate cancer cells.

CXCR6 interacts with the ligand CXCL16, and expression in prostate cancer tissue correlates with a more aggressive phenotype, with earlier progression to metastatic disease (Richardson et al., 2015, Wang et al., 2008). Matrix-metalloproteinases (specifically MMP1, MMP9 and MMP13) are activated by CXCR6 expression (Singh et al., 2016) which increases cell invasiveness by promoting degradation of the basement membrane and extracellular matrix (Curran and Murray, 2000). Additionally, the interaction between CXCR6 and its ligand CXCL16 affects cell motility by affecting the actin binding potential of the cell cytoskeleton to the extracellular matrix (Singh et al., 2016).

The ligands of CCR7 (CCL19 and CCL21) are predominantly secreted by lymphocytes (particularly B-cells, T-cells and natural killer cells) and high levels have been found in the lymph node metastases of various cancers (Cassier et al., 2011, Du et al., 2017). Upregulation of CCR7 in both prostate and gallbladder cancer has been shown to be mediated by TNF- α via the ERK pathway (Maolake et al., 2018, Hong et al., 2016b, Hong et al., 2016a).

The ligand CXCL12 is secreted by numerous cell types including osteoblasts and skeletal muscle cells (Ratajczak et al., 2003, Ponomarev et al., 2000) and interacts with the receptor CXCR4. Levels increase after damage to tissues, promoting haematopoietic invasion as a response to injury (Wang et al., 2006). In prostate cancer specifically, the CXCR4/CXCL12 interaction encourages adherence of the tumour cells to bone marrow endothelium via $\alpha_v\beta_3$ integrin upregulation and activation of CD164 (Sun et al., 2007).

Choosing chemokine receptors CXCR6, CCR7 and CXCR4 would potentially provide information about the aggressiveness of the tumour, and whether it is likely to metastasise to bone and/or lymph nodes. As a result, these three chemokine receptors were used for this experiment, with the aim of using the ligands CXCL16, CCL19, CCL21 and CXCL12.

6.6.3 Demonstrating the presence of chemokine receptors in cell lines

Before setting up the agarose spot assay, expression of the three receptors was explored using immuno-fluorescence on both cell lines and the cells from patients in culture. Table 6.3 lists the purchased antibody and fluorescent conjugate.

Chemokine Receptor	Fluorescent conjugate	Isotype control	Manufacturer
CXCR6	PE	REA (S)	Miltenyi Biotec
CCR7	FITC	REA (S)	Miltenyi Biotec
CXCR4	APC	REA (S)	Miltenyi Biotec

Table 6.3 A table to show the chosen Chemokine Receptors, the corresponding conjugated fluorochrome, the isotype control and the manufacturer from which they were supplied.

PC3 cells were used and the antibody was diluted at increasing amounts and run in parallel with the isotype control (Figures 6.22-6.25).

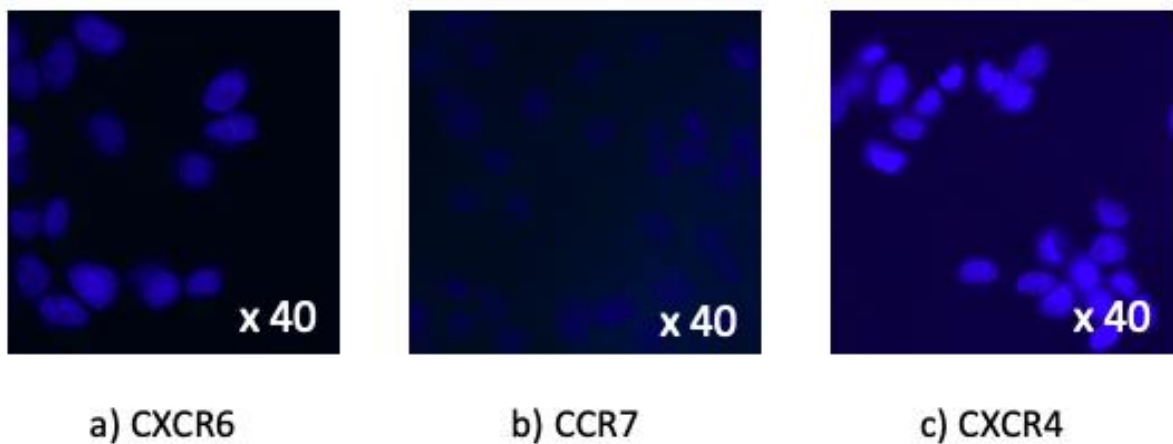


Figure 6.22 Three immuno-fluorescent images demonstrating the 1:10 dilution of the isotype control for a) CXCR6, b) CCR7 and c) CXCR4. (As these were negative the images showing further dilutions are not shown).

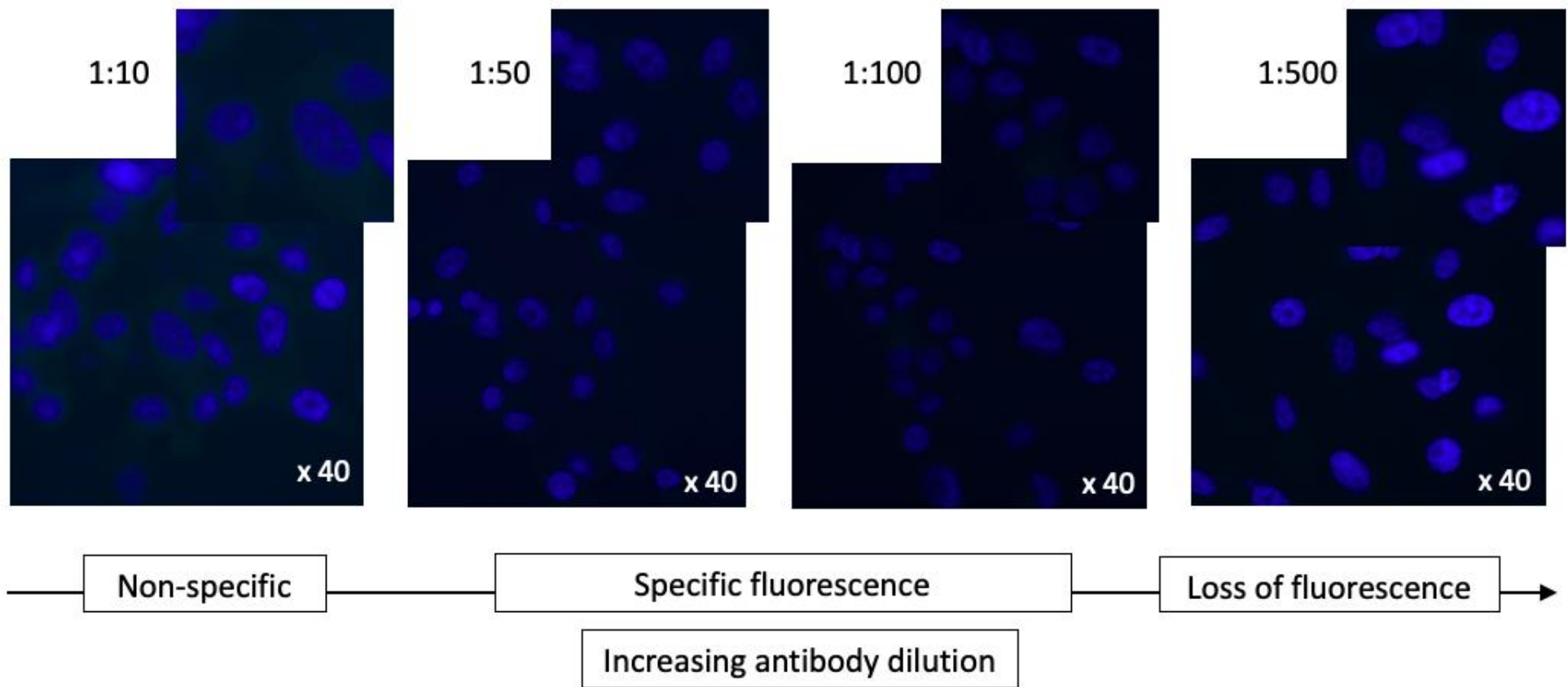


Figure 6.23 Immuno-fluorescent images to show PC3 cells stained with increasing antibody dilutions of the chemokine receptor CXCR6 (PE). No positive staining was demonstrated.

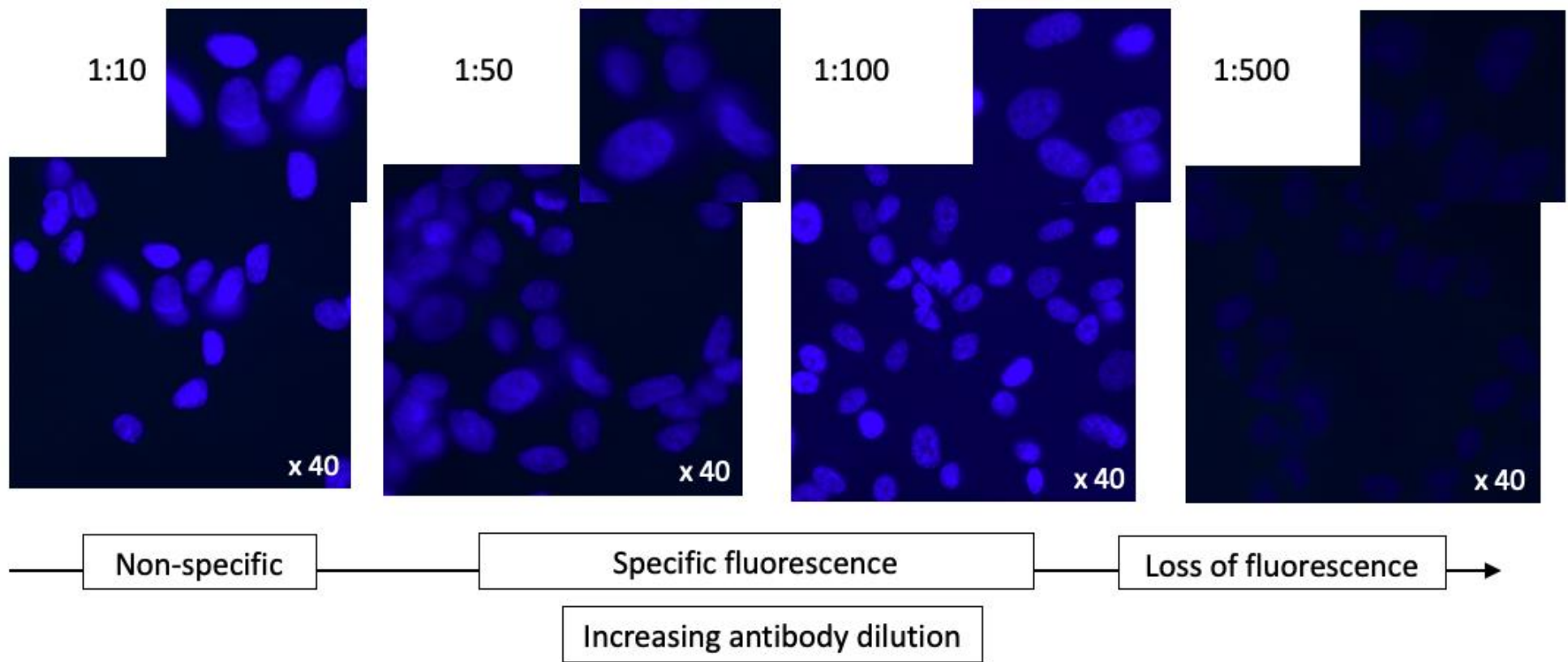


Figure 6.24 Immuno-fluorescent images to show PC3 cells stained with increasing antibody dilutions of the chemokine receptor CCR7 (FITC). No positive staining was demonstrated.

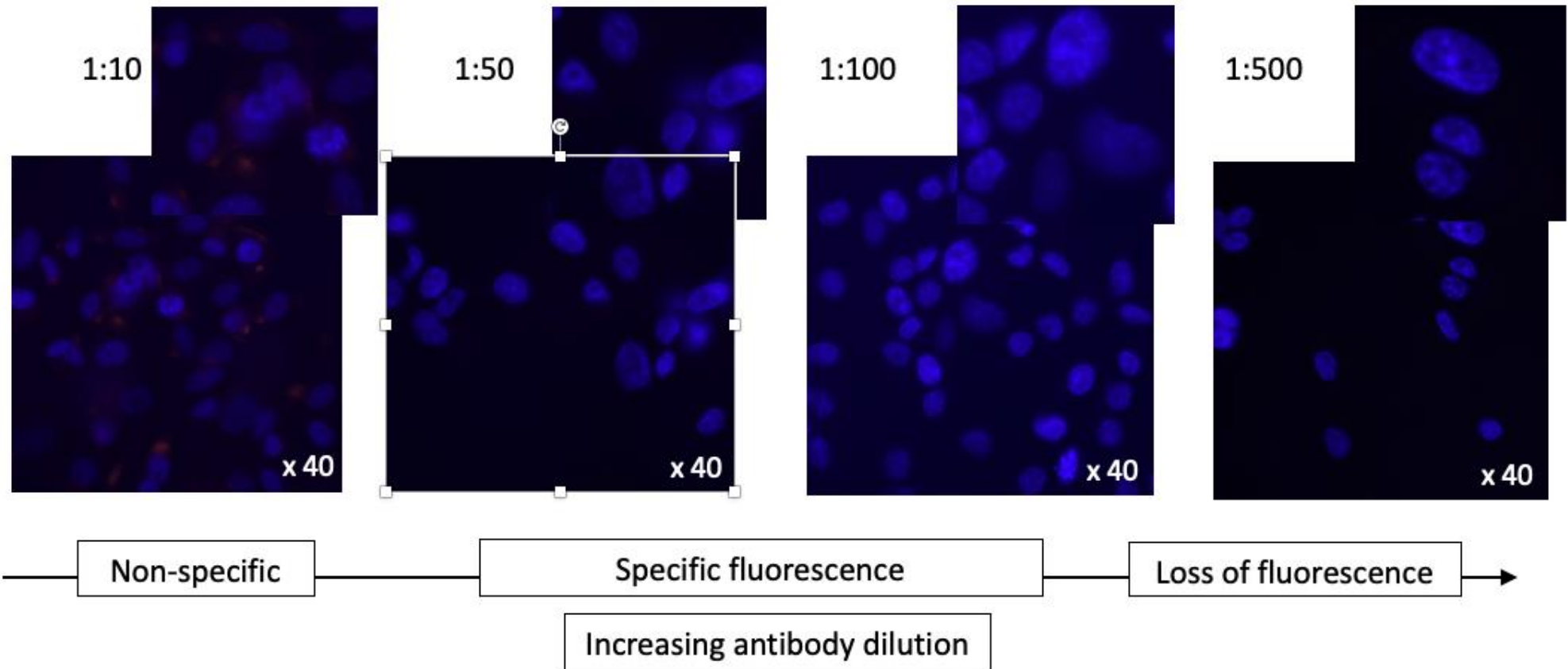


Figure 6.25 Immuno-fluorescent images to show PC3 cells stained with increasing antibody dilutions of the chemokine receptor CXCR4 (APC). Some staining was seen at the highest concentration, but this is likely to be non-specific.

Aside from what is likely to be non-specific fluorescence when using the CXCR4 antibody, none of the three chemokine receptors were detected on PC3 cells, despite using low passage cells. Although most studies in the literature describe expression of these three chemokine receptors on PC3 cells, a small number have not found any expression (Darash-Yahana et al., 2004, Heresi et al., 2005). Despite this, attempts were made at looking for chemokine receptor expression in the cultured CTCs.

6.6.4 Demonstrating the presence of chemokine receptors in CTCs

Cells from five patients were plated out for the immuno-fluorescence protocol used for the cell lines. But despite culture over several weeks, the cells were so sparse that when the antibodies were added there were not enough cells on the coverslips to give meaningful results.

Instead, the cells from each patient were stained in suspension and processed using the Imagestream. Figures 6.26 - 6.30 show some example cells from each patient and the chemokine receptors they expressed.

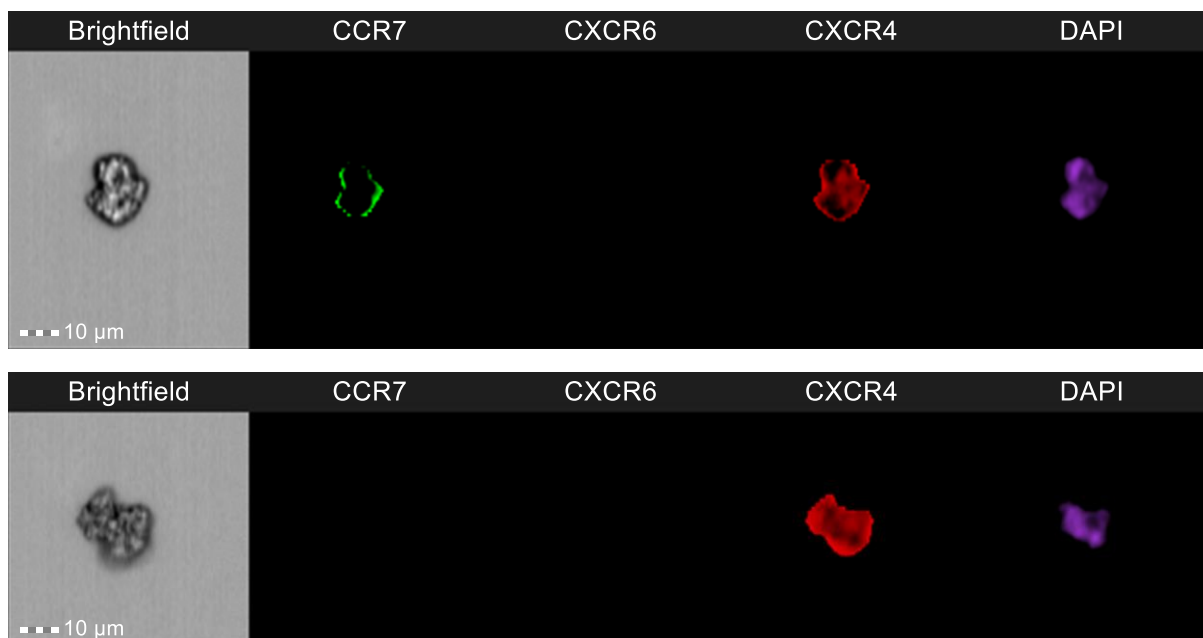


Figure 6.26 Imagestream images of cells cultured from patient CTC-JACH-73 demonstrating CCR7 and CXCR4 expression on these cells.

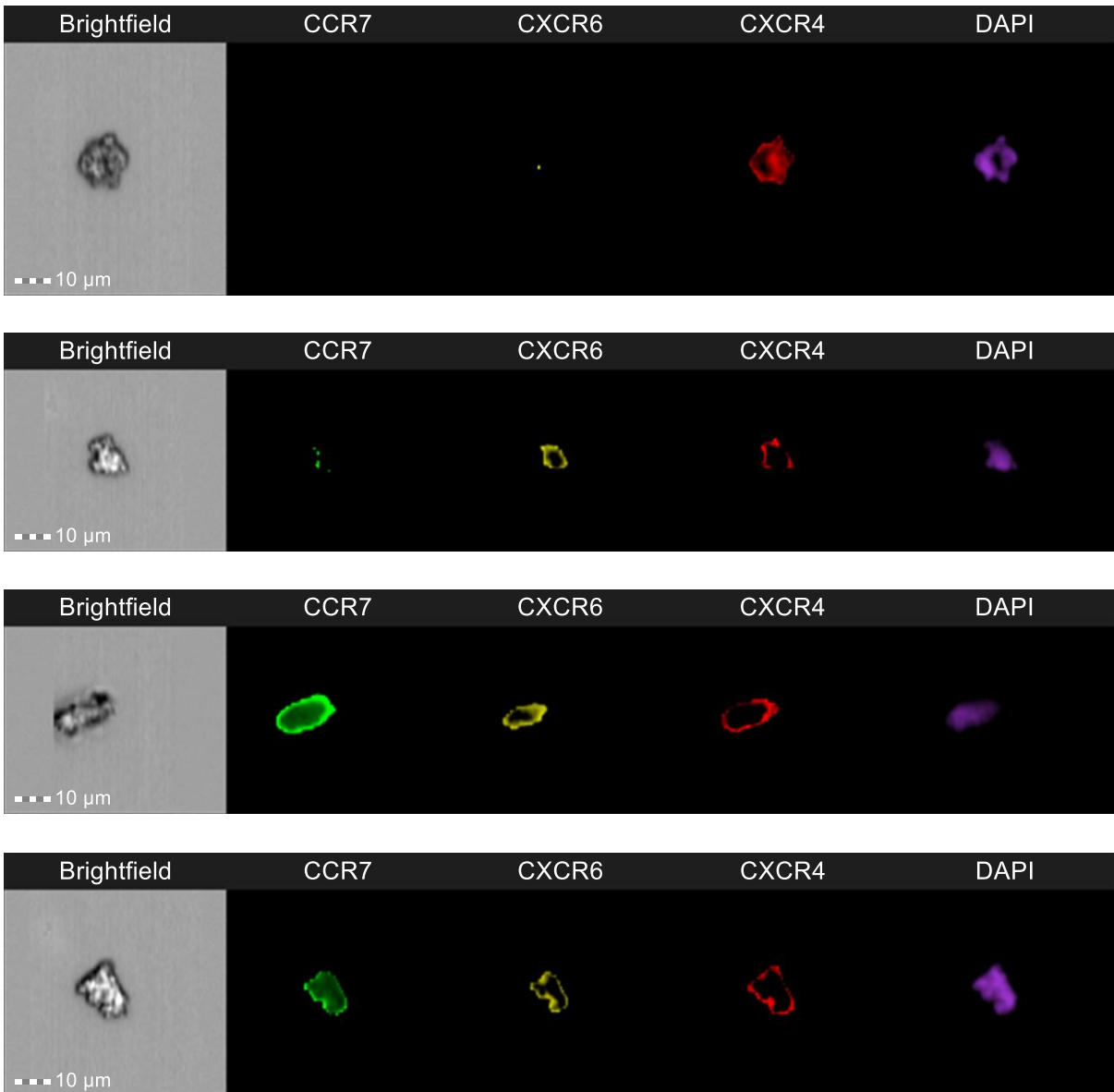


Figure 6.27 Imagestream images of cells cultured from patient CTC-JARO-110 demonstrating CCR7, CXCR6 and CXCR4 expression on these cells.



Figure 6.28 Imagestream images of cells cultured from patient CTC-STCH-122 demonstrating CCR7 and CXCR4 expression on these cells.

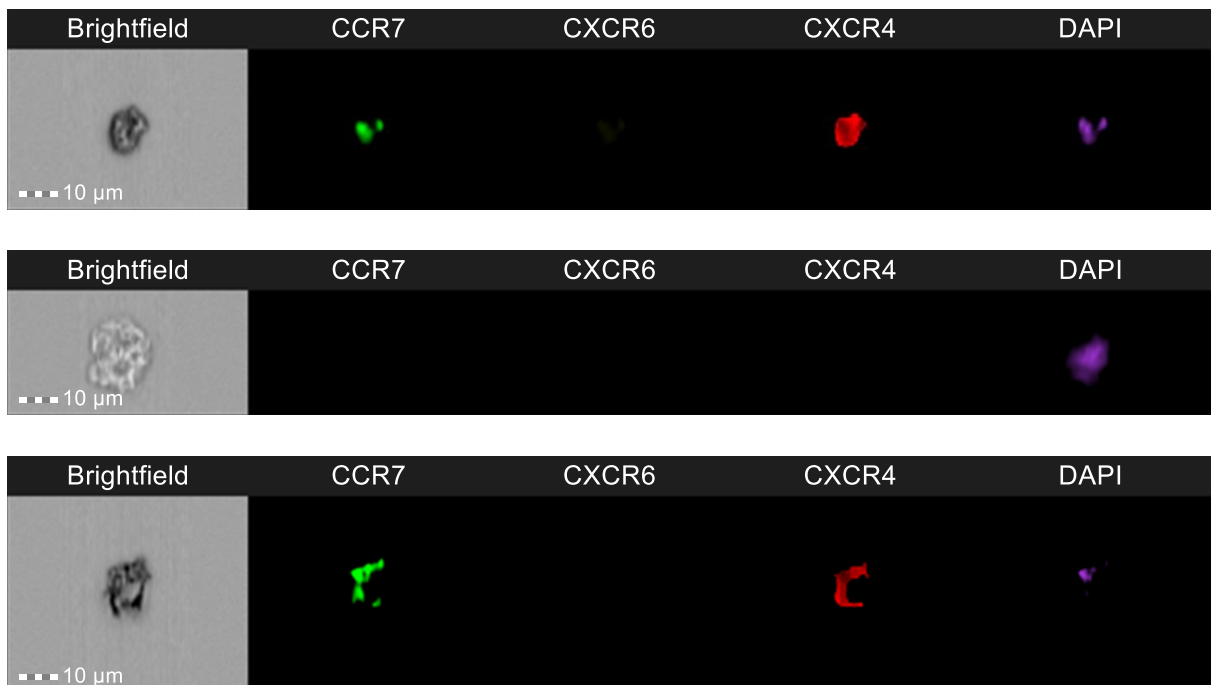


Figure 6.29 Imagestream images of cells cultured from patient CTC-PEWA-123 demonstrating CCR7 and CXCR4 expression on these cells.

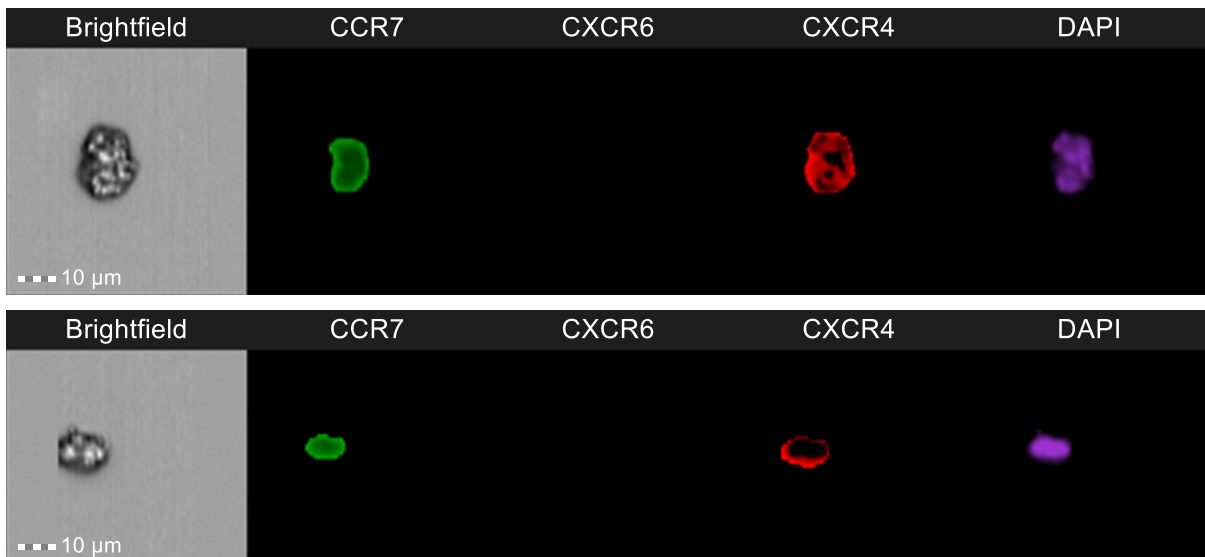


Figure 6.30 Imagestream images of cells cultured from patient CTC-JEWR-124 demonstrating CCR7 and CXCR4 expression on these cells.

These images show that there is some heterogeneity between cells from the same patient, which is to be expected. Table 6.4 tabulates the chemokine receptors found on cells from each patient.

Patient	Chemokine Receptor			Location of metastases
	CXCR6	CCR7	CXCR4	
CTC-JACH-73		+	+	Bone, Lymph Nodes
CTC-JARO-110	+	+	+	Bone, Lymph Nodes
CTC-STCH-122		+	+	Bone
CTC-PEWA-123		+	+	Lymph Nodes
CTC-JEWR-124		+	+	Bone, Lymph Nodes

Table 6.4 A table listing the chemokine receptors that cells from each patient expressed, and the clinical location of their metastases.

These results are encouraging when considering the authenticity of the cells. If they are CTCs they only provide a glimpse of the heterogeneous population of tumour cells that were present at the time of sampling, but correlation to clinical presentation is significant. The only patient with cells expressing all three receptors (CTC-JARO-110) had a very aggressive form of the disease and died within a month of his blood being taken. Patient CTC-JACH-73

had a small number of lymph node metastases but predominantly bony disease and not all of his cells expressed CCR7. Patients CTC-STCH-122 and CTC-JEWR-124 expressed both CCR7 and CXCR4 in all cells despite no obvious lymph node metastases in CTC-STCH-122, and patient CTC-PEWA-123 had cells with no expression at all, despite lymph node metastases.

Whilst this data alone is insufficient to draw any meaningful conclusions, progression to the agarose spot assay was planned. Unfortunately, during the culturing process (which took several months) the cells became infected and had to be discarded. As this was the end of the project there was insufficient time to repeat the culture, so the agarose spot assay was not performed. Frozen cells from earlier passages are still available and future plans to proceed with the assay are in formation.

6.7 Development of an *in-vivo* model using NSG mice

6.7.1 Background

The CDX mouse model created from CTCs in patients with small-cell lung cancer (Hodgkinson et al., 2014) resulted in tumour development in mice. These subsequently responded to chemotherapeutic agents in the same way as tumours in the corresponding patients, and therefore provided a relevant *in vivo* model for target discovery. To date, no such model exists in prostate cancer as all previous *in vivo* prostate cancer models have been created by using either prostate cancer cell lines, organoids or cells from solid tumours (Karthaus et al., 2014, Chua et al., 2014, Clevers, 2016). Organoids have been created from CTCs in advanced prostate cancer by a group that have experience with creating *in-vivo* organoid models (Gao et al., 2014, Gao and Chen, 2015), currently these have not been implanted in mice, nor have any CDX models have been directly created from CTCs. Because prostate biopsies are rarely taken in advanced disease, and also because sampling bias can overlook tumour heterogeneity, using CTCs in prostate cancer to create a CDX model could offer a clinically relevant tissue model for target discovery. Therefore, an attempt was made to create a CDX mouse model in prostate cancer, using the cells cultured from patients.

Due to timing and financial constraints only one patient's cells were used (CTC-JARO-110) but implanted into five NOD/LtSz-*scid* *IL2R_γ* null (NSG) mice. These mice were chosen due to their immune-deficiency and because other members of the institution had successfully created PDX models using these mice. Because of the low numbers of cells, the decision was made to implant them intrafemorally, rather than subcutaneously or via the tail vein as it

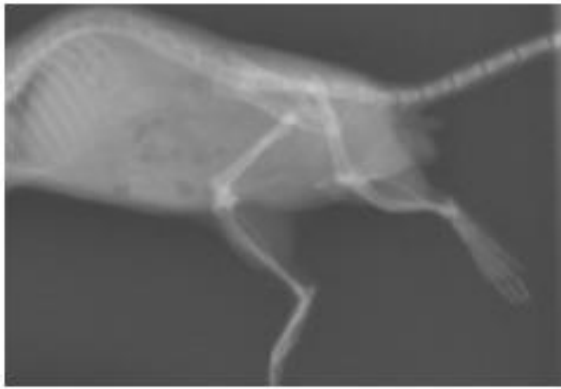
was felt that this would be a more protective environment that could encourage tumour growth. Additionally, as the patient from which the cells were derived had multiple bony metastases, a bone environment was felt most likely to be successful for the cells to engraft.

6.7.2 Pre-mortem findings

The mice showed no significant changes for the first four months. During the fifth month, one (Left Notch) developed a palpable lump at the femoral injection site and a second (Right Notch) developed this three weeks later. These were not usual following intra-femoral injections, but due to both maintaining their weights and showing no obvious signs of distress, observation continued. During the sixth month, a third mouse (Both Notch) developed sudden onset hind leg paralysis, consistent with spinal cord compression, and was culled humanely. Shortly afterwards, the two mice with the femoral lumps started to look scruffy and started shallow breathing. The remaining four mice were culled at this stage.

6.7.3 Post-mortem analysis

Post-mortem X-ray images of the two mice with femoral lumps were obtained (Figure 6.31), and a CT scan (Figures 6.32 and 6.33) was performed on the spine and lower limbs of Both Notch, to ascertain if there was an obvious spinal cord compression. No obvious lesions were seen on the X-rays. The CT showed possible sclerosis in the pelvis and femura but unfortunately the scan did not show the entire lumbar spine or any of the thoracic spine and so a cord compression could not be confirmed. This was because of the sudden onset of symptoms from that mouse – the CT scanner had been installed only the previous day and it was unknown how long scanning would take. The first set of images was taken but the operator was then unable to scan for further images (lumbar/thoracic spine) due to time constraints.



a) Left Notch



b) Right Notch

Figure 6.31 X-ray images of the femurs of both mice with palpable femoral lumps. No obvious sclerotic (or lytic) lesions were seen in the femur of either mouse.



a) Left oblique lateral view



b) Right oblique lateral view

Figure 6.32 CT reconstructed images of the lower limbs of Both Notch. Image a) shows a left oblique-lateral view and image b) shows a right oblique-lateral view. No obvious lesions affecting the bone were identified.

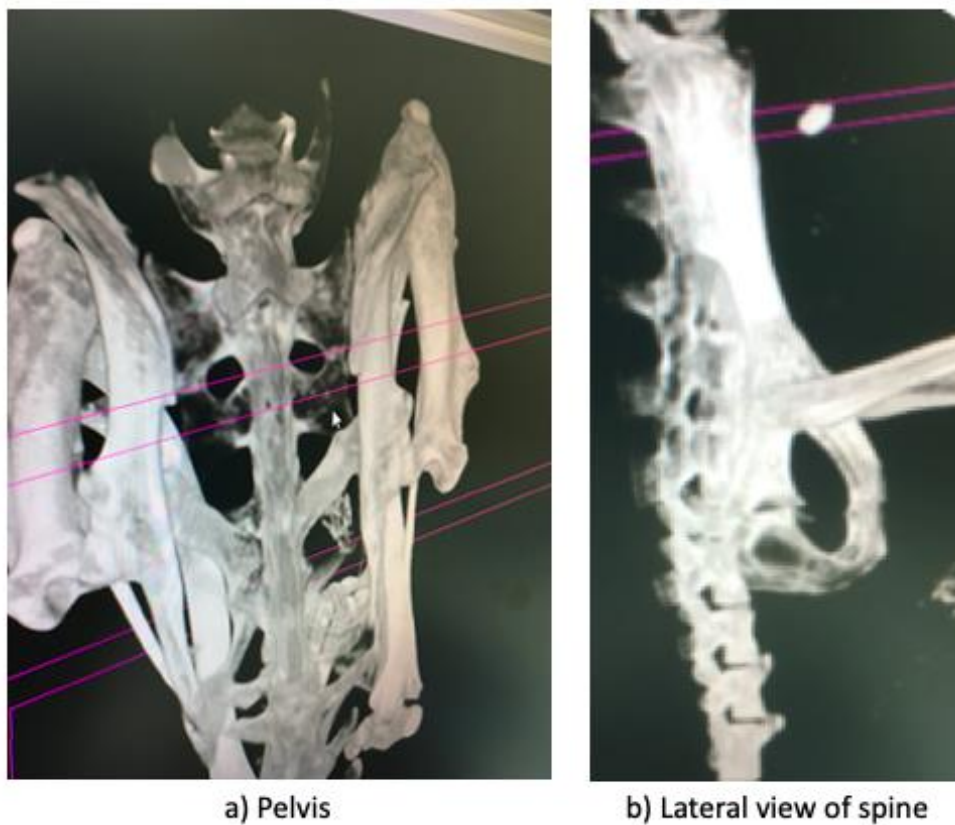


Figure 6.33 CT reconstructions of the pelvis and spine of Both Notch. No obvious bony lesions were identified

Whilst the CT results were inconclusive, attempts to perform immuno-histochemical staining on the mouse with the presumed cord compression (Both Notch) were made. The spine and right femur (injection site) were sectioned and stained with Haematoxylin and Eosin (H&E), and for PSA and MT1-MMP expression. This was performed by the pathology department within the Royal Victoria Infirmary, Newcastle-upon-Tyne. A control mouse of the same age and species without cells implanted was also sectioned, and staining was performed simultaneously as a negative control.

The H&E staining of the femur (Figure 6.34) and spine (Figures 6.35 and 6.36) of Both Notch and a control mouse can be seen below.



a) Both Notch R Femur

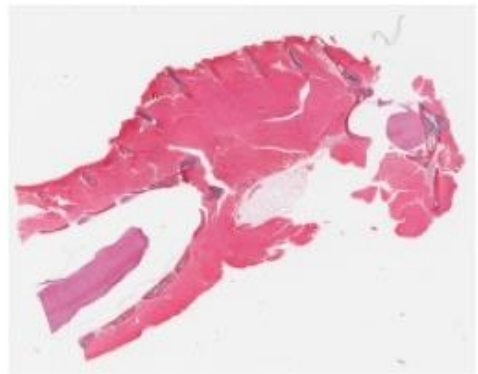


b) Control R Femur

Figure 6.34 H&E staining of a) the right femur of Both Notch and b) the right femur of a control mouse.



a) Both Notch Spine



b) Both Notch Spine

Figure 6.35 H&E staining of two sections of spine from Both Notch.

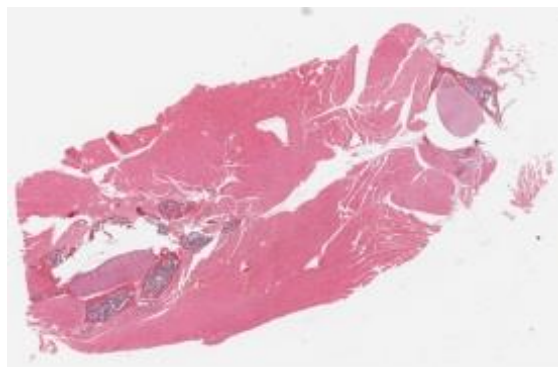


Figure 6.36 H&E staining of a section of spine from a control mouse. This shows a comparable histological picture to Both Notch.

Despite the clinical findings, the H&E staining did not detect any obvious spinal cord lesions or tumour cells that were recognisably prostatic in origin. Further staining with PSA was therefore attempted (Figures 6.37-6.39). Control tissue from prostate tumour can be seen in Figures 6.37 and 6.38 to demonstrate the validity of the antibody.

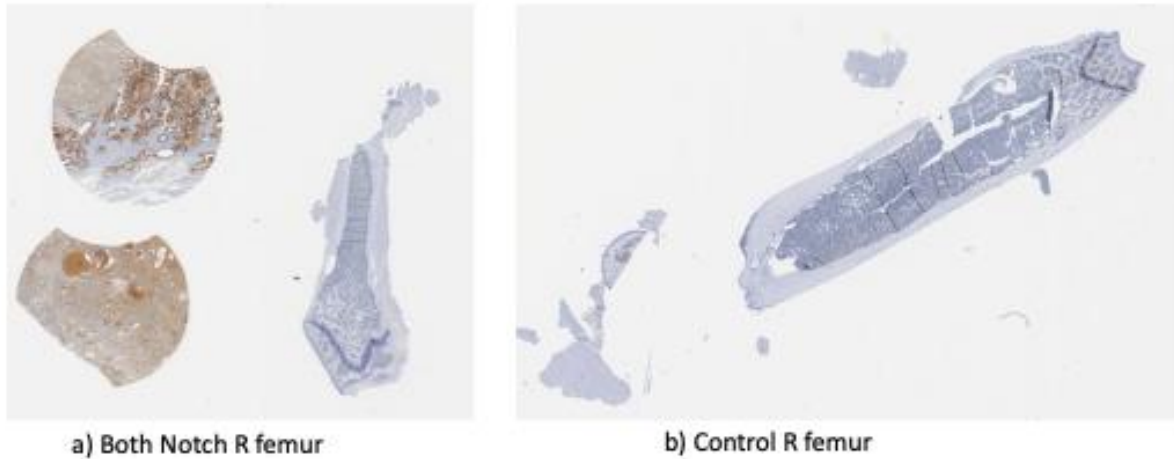


Figure 6.37 PSA staining from the right femur of a) Both Notch and b) a control mouse. The circular sections in the top left are positive controls from human prostate tissue. No PSA staining is identified.

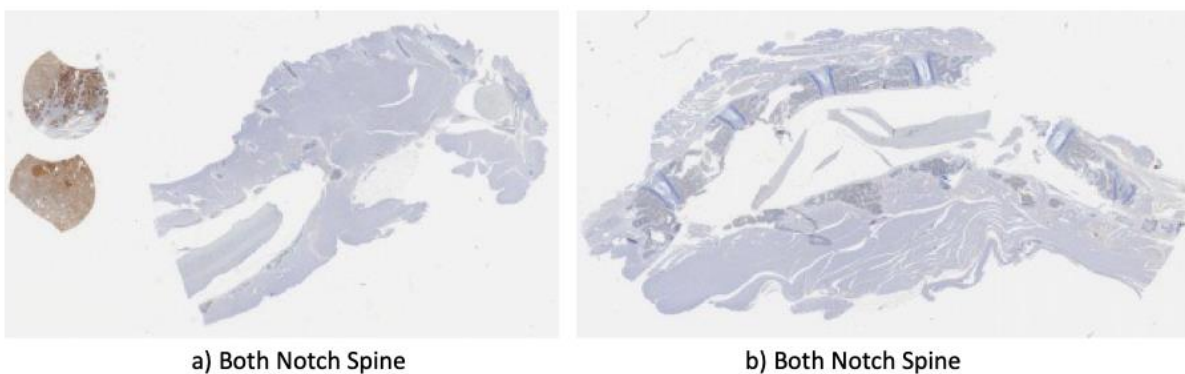
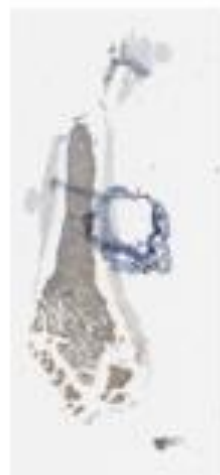


Figure 6.38 PSA staining from two sections of spine taken from Both Notch. The circular sections in the top left are positive controls from human prostate tissue. No PSA staining is identified.

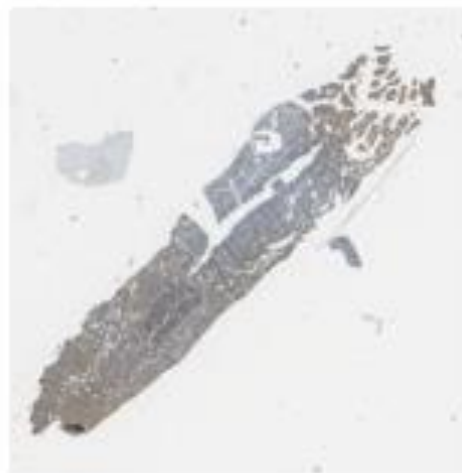


Figure 6.39 PSA staining from the spine of the control mouse. No PSA staining is identified.

None of the PSA staining was positive from the right femur or spine of Both Notch. Further staining with MT1-MMP was attempted (Figures 6.40-6.42) as the patient from which the cells were taken had MT1-MMP positive bone lesions when he presented with a pathological fracture.



a) Both Notch R Femur



b) Control R femur

Figure 6.40 MT1-MMP staining from the right femur of a) Both Notch and b) the control mouse. There is non-specific background staining in both specimens.

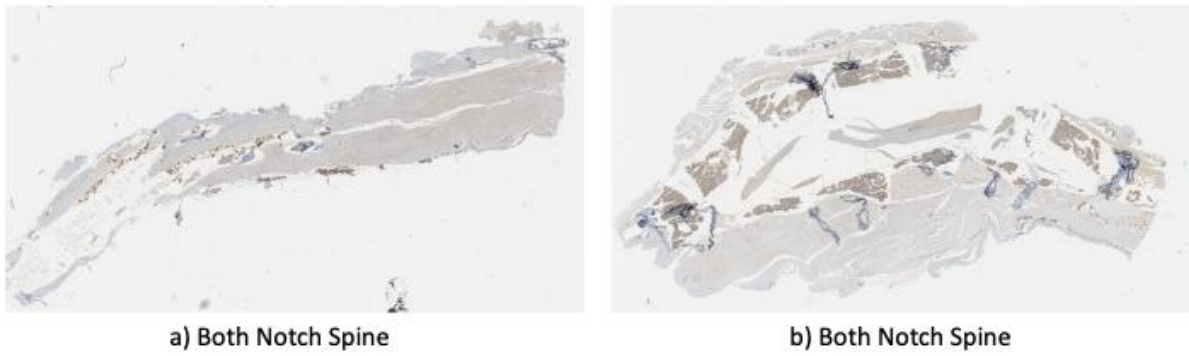


Figure 6.41 MT1-MMP staining from the spine of Both Notch. There is non-specific background staining in both specimens.

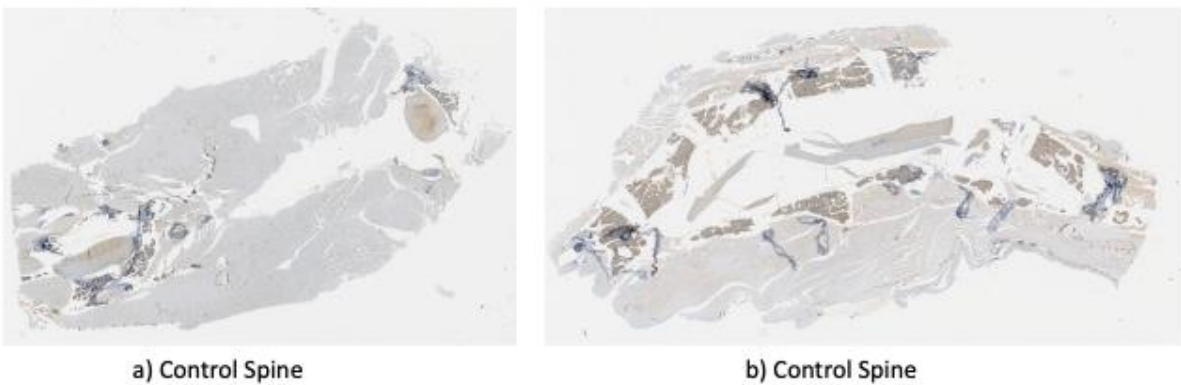
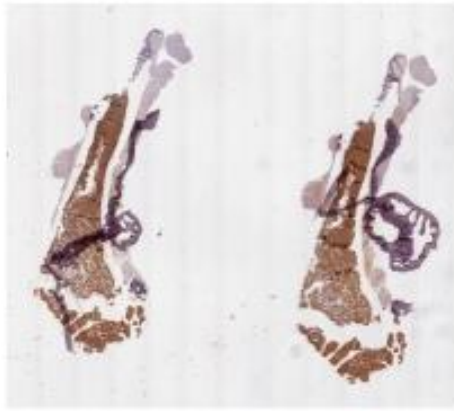


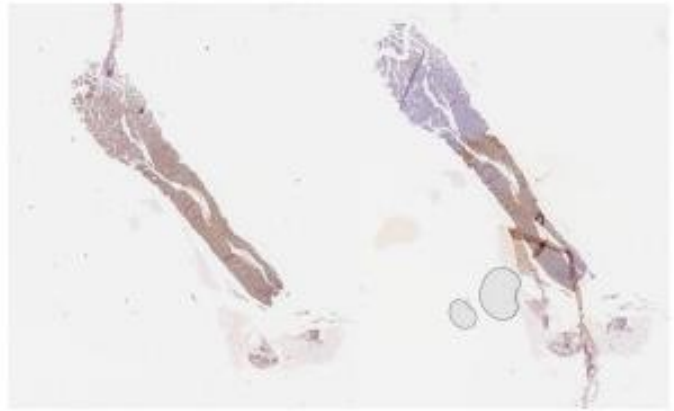
Figure 6.42 MT1-MMP staining from the spine of the control mouse. There is non-specific background staining in both specimens.

Although initially this appeared positive, there is no difference between the staining in Both Notch and the control mouse, and a Consultant Pathologist confirmed that they were negative. Therefore, the conclusion was made that there was no evidence of PSA+ or MT1-MMP+ cells in the femur or spine of the mouse with the suspected spinal cord compression.

Because the clinical findings led to suspicions of positive pathology, attempts were made to look for any human cells within this mouse, in case cell differentiation had occurred. An anti-human-mitochondrial antibody was used for this purpose, which should detect any human cell, regardless of whether the cell was prostatic or had differentiated (Figures 6.43-6.46). I am very grateful to Dr Calum Kirk for performing the immuno-histochemical staining on these sections.



a) Both Notch R Femur



b) Control R Femur

Figure 6.43 Anti-mitochondrial human antibody staining of the right femur of a) Both Notch and b) the control mouse. There is non-specific staining in both specimens.

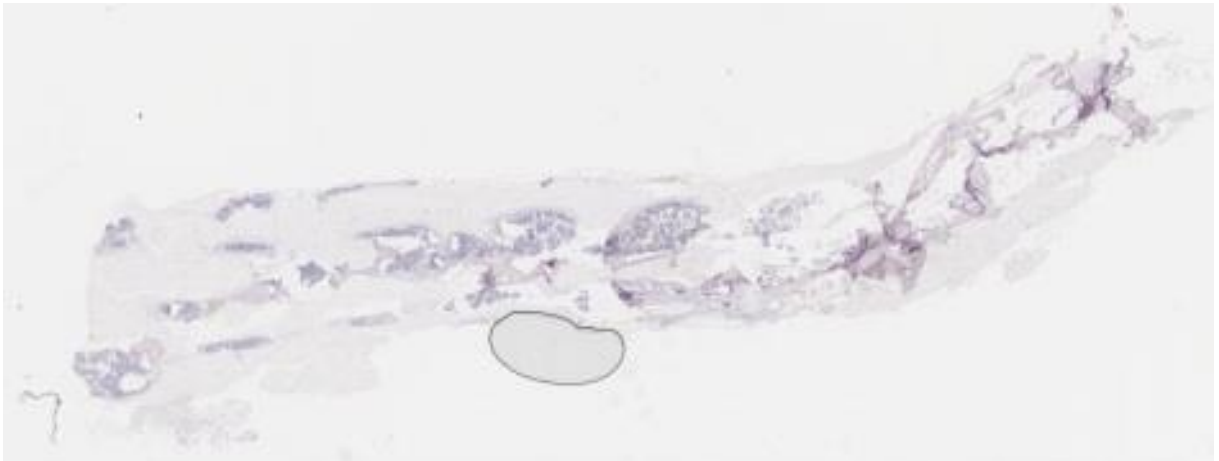


Figure 6.44 Anti-mitochondrial human antibody staining of the spine of Both Notch. No antibody was detected.



Figure 6.45 Anti-mitochondrial human antibody staining of a second section of the spine of Both Notch. No antibody was detected.

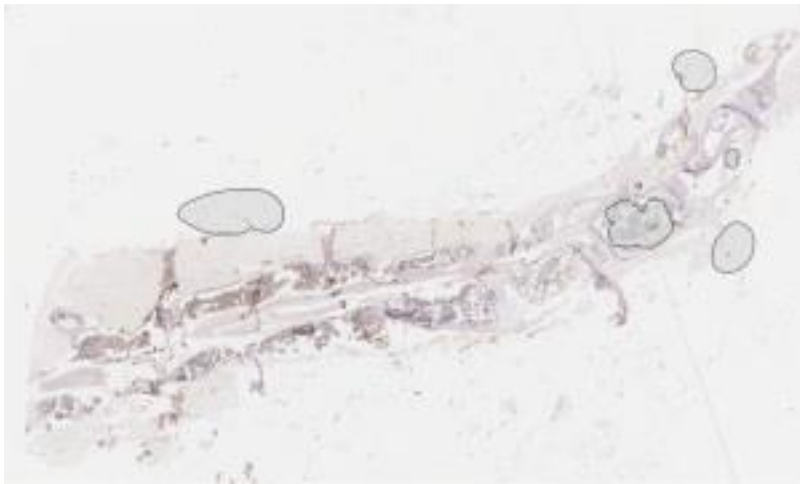


Figure 6.46 Anti-mitochondrial human antibody staining of a third section of the spine of Both Notch. Non-specific staining was detected.

Despite sectioning the entire spine and right femur of Both Notch, no obvious spinal cord lesion or cells positive for the anti-mitochondrial antibody were found. Some non-specific femoral staining was seen in the femur of both the control and Both Notch, despite using the mouse-on-mouse (MOM) kit. This was used to reduce endogenous mouse immunoglobulin staining caused by using an antibody raised in a mouse. The clinical sign of hind-leg paralysis is very unusual in the NSG mice without underlying pathology, but although efforts were made to find a lesion, nothing was confirmed. The conclusion must therefore be drawn that the cells that were implanted into the mice did not engraft and a CDX model was not achieved.

6.8 Exploring the physical properties of cultured CTCs

6.8.1 Background

CTCs can also provide us with information about the mechanical properties of tumour cells that may be more relevant than the cells obtained from solid tissue. They are likely to be the most clinically relevant cells from a tumour, and if cultured, the cells will still be living and therefore their structure not affected by a fixation process. Thus, information about their physical structure could help with the design of new drug treatments, particularly those aimed at cell wall degradation or rupture. Experiments using an Atomic Force Microscope (AFM) have demonstrated that changes in cell stiffness can be an indication of underlying pathology such as cancer (Guck et al., 2005, Lekka and Laidler, 2009) and the stiffness of cells can indicate how likely a cell is to metastasise (Luo et al., 2016, Cross et al., 2007, Cross et al., 2008). Comparisons in the Young's Modulus of malignant and non-malignant cells using breast cancer cell lines have shown a lower value in the former group (Li et al., 2008).

In prostate cancer there have been several studies to measure the Young's modulus of the cell of prostate cancer cell lines (Faria et al., 2008, Raudenska et al., 2019, Murphy et al., 2013) and tissue (Chen et al., 2015b), and a study using PC3 cells looking at cytoskeletal changes in response to different drug treatments showed corresponding changes in the Young's modulus of the cell membrane (Ren et al., 2015). There has been one study looking at prostate CTCs, which found that cells from patients with castrate-resistant disease were three times less stiff than those with castrate-sensitive disease (Osmulski et al., 2014). This study identified CTCs using EpCAM staining following a filtration process, which may have excluded cells undergoing EMT, or those not expressing EpCAM. Although other techniques for measuring the mechanical properties of cells exist, such as optical or acoustic tweezers, electrical field stimulation or parallel plate flow, the AFM is the most commonly used in cancer research (Rodriguez, 2013). With this in mind, some preliminary experiments were conducted on the patient cells in culture, some white cells and two different cell lines to look at cell stiffness using an AFM. I am very grateful to Dr Daniel Frankel for his help and guidance with this experiment.

6.8.2 Principles of an AFM

An AFM uses a tip (either spherical or conical) on the end of a flexible cantilever to indent a cell. The attractive or repulsive force between the cell and the tip of the cantilever is measured, and using the value of the force, and the distance between the cell surface and the tip, a force-separation curve can be plotted (Kuznetsova et al., 2007). Analysis of this force-separation curve can be used to estimate the Young's modulus of a cell, (Puricelli et al., 2015) using either the Sneddon model for a conical tip, or the Hertz model for a spherical tip. The smaller the value of the Young's modulus, the more deformable the cell (Deng et al., 2018). The cantilever tip is repeatedly inserted and retracted into the cell numerous times, to allow an average force to be calculated. These models assume elastic deformation (the cell is viscoelastic) but are valid for small indentations into the surface. Thus the model is fitted to the first part of the indentation curve whereby viscoelastic effects are minimal.

In addition, the movement of a laser aimed at the cantilever is detected by a photodiode and used to create a three-dimensional image of the cell surface (Mozafari et al., 2005). The resolution of the AFM is much higher than electron or light microscopes (Deng et al., 2018) therefore enabling the precise indentation of the cantilever tip into a cell.

6.8.3 Results of the AFM indentation experiments

Cells were cultured onto glass coverslips and transported in media to the School of Engineering at Newcastle University. Each coverslip was placed separately inside the AFM liquid cell, buffer exchanged to PBS (600 ul) and then loaded into the Agilent 5500 AFM. Indentation measurements for conical probes were taken using silicon cantilevers (PPP-CONTR, Nanosensors, Switzerland) and borosilicate spherical probes 5 μm in diameter (NovaScan Technologies). After laser alignment on the back of the cantilever and calibration of the photodetector, the optical microscope was used to identify the cells of interest. Repeated indentations and retractions were then undertaken (approximately 500 cycles) was recorded. The software, SPIP version 6.3.3 (Image Metrology, Lyngby, Denmark) was then used to process the force/separation curves and fit the indentation model to the approach curve allowing the Young's modulus of the cell to be calculated. Below are the force/separation curves obtained from indenting into the glass coverslip with no cells (Figure 6.47) and different cell types (Figures 6.48 – 6.51).

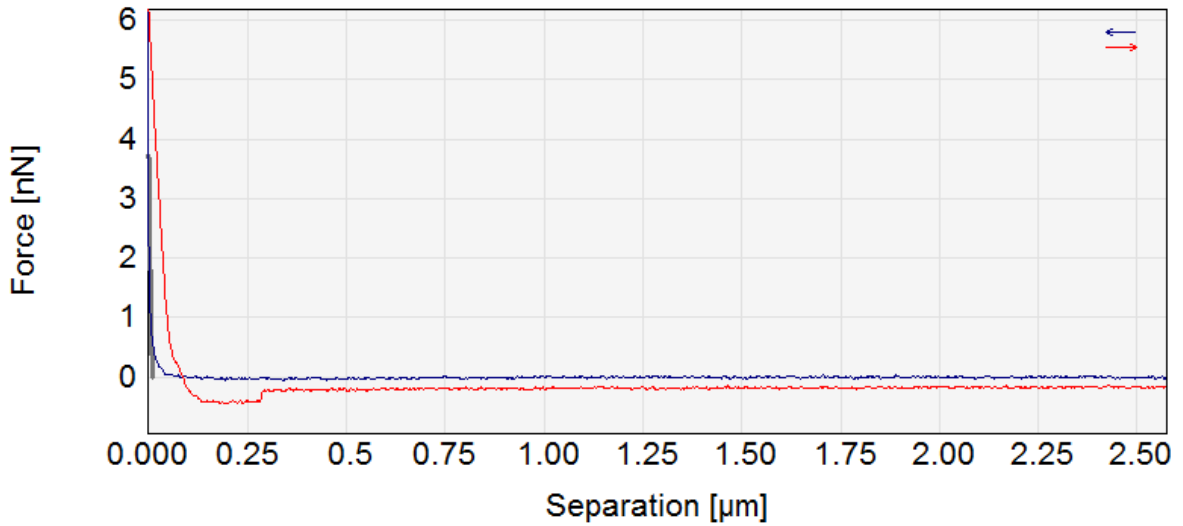


Figure 6.47 A force/distance curve showing the indentation (blue curve) and retraction (red curve) of a spherical tip into the glass coverslip. The indentation curve at close separations shows a typical elastic response (sharp vertical line increase in force) of a probe indenting into glass. This serves a control for comparison with the softer cell indentation profiles.

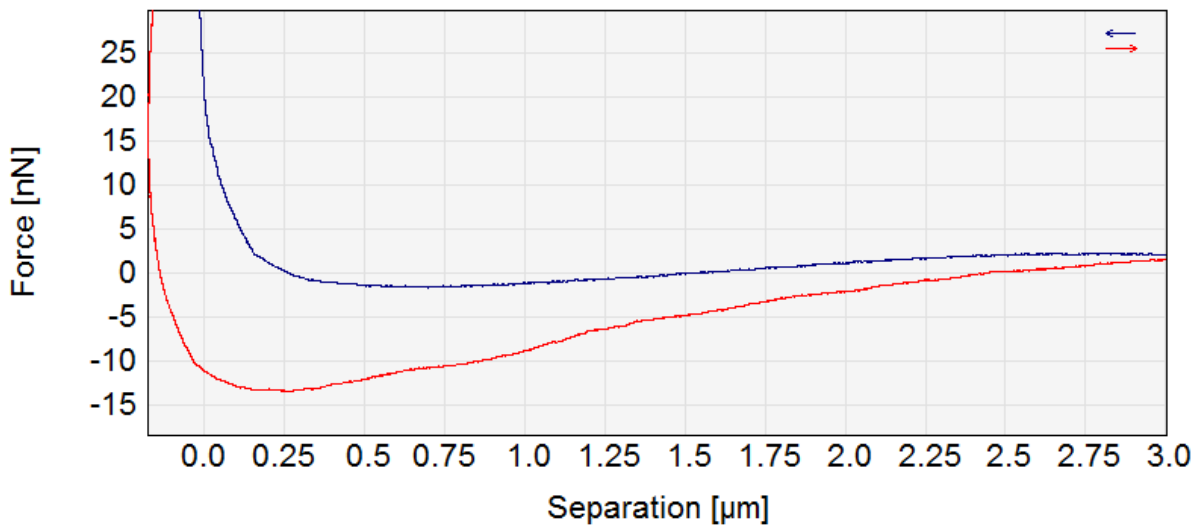


Figure 6.48 A force/separation curve showing the indentation (blue curve) and retraction (red curve) of a spherical tip into a U2OS cell. The difference between the indentation curve and the indentation curve into the glass slide (Fig 6.47) is striking. The indentation profile is curved rather than straight, a characteristic of viscoelastic materials. This is consistent with literature data for the indentation of cells.

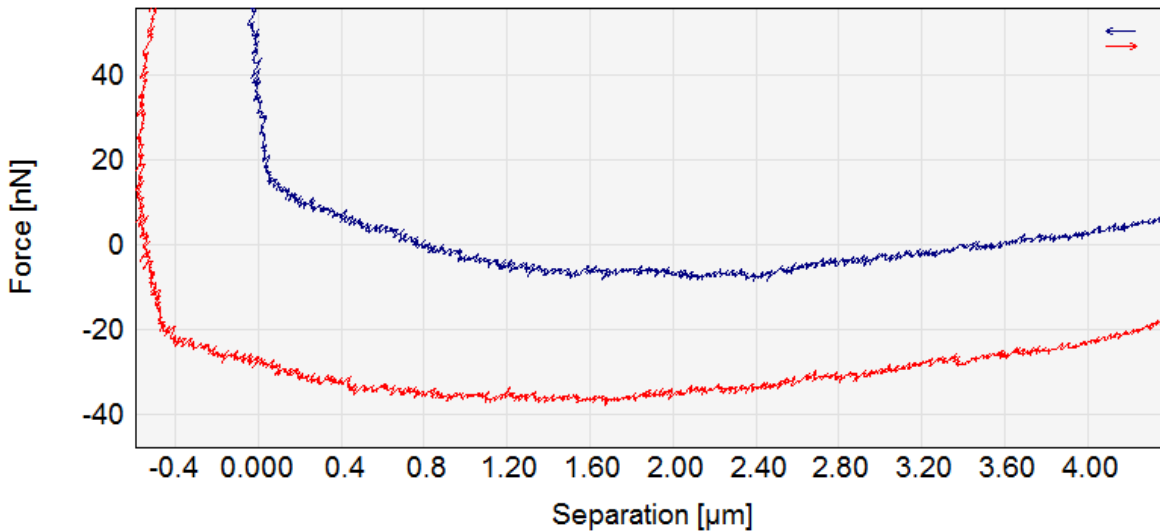


Figure 6.49 A force/separation curve showing the indentation (blue curve) and retraction (red curve) of a spherical tip into a healthy volunteer white cell. This was repeated for 500 cycles. This has a characteristic indentation profile, showing a viscoelastic form.

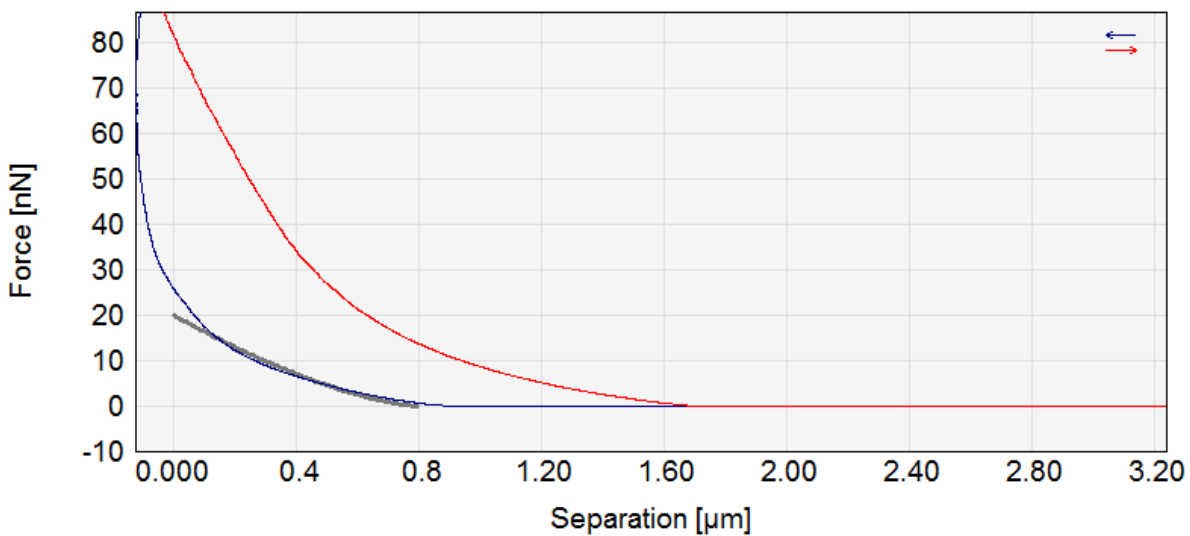


Figure 6.50 A force/distance curve showing the insertion (blue curve) and retraction (red curve) of a spherical tip into a patient putative CTC. This cell came from a patient with very advanced metastatic prostate cancer that had EpCAM+ and triple marker Oct4/SOX2/Nanog positive cells when processed on the Imagestream. It is also the patient from which the cells that were implanted into the mice were taken. The fit of the Hertz indentation model at the point of indentation is shown. The CTC profile appears to show a different form to that of the cell lines and white blood cells.

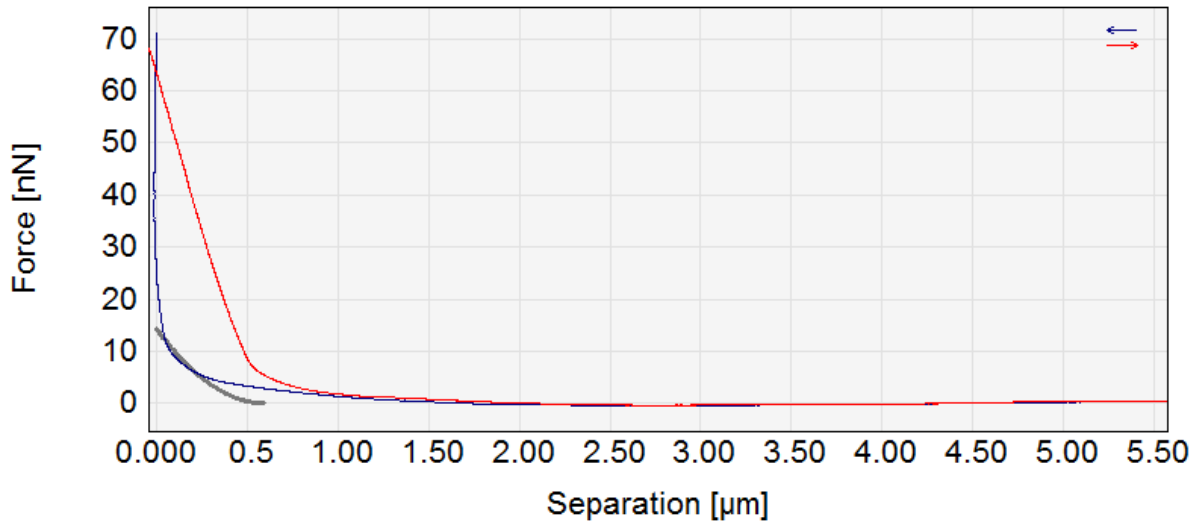


Figure 6.51 A force/separation curve showing the indentation (blue curve) and retraction (red curve) of a conical tip into a PC3 cell demonstrating the viscoelastic characteristics typical of cell indentation experiments.

Table 6.5 outlines the type of cell or material, the tip used to make the indentations and the calculated Young's Modulus of the cell (or glass).

Cell Type / Material	Tip (Spherical / Conical)	Young's Modulus of cell (kPa)
Glass slide	Spherical	1300
U2OS cell (cell line)	Spherical	13.3
White cell	Spherical	30.4
Patient cell	Spherical	10.0
PC3 cell (cell line)	Conical	183

Table 6.5 A table to show the cell type or material that was indented, the type of cantilever tip and the Young's Modulus of the cell wall or material (glass) that was calculated. The higher the Young's modulus, the less deformable the material.

6.9 Discussion

The work conducted in this chapter was not planned at the outset of the project but developed during the course of the three years. Collaboration with colleagues led to some interesting opportunities but lack of time and financial resources meant that some experiments could not be completed or repeated. This work will hopefully form the basis for future projects, some of which are currently underway.

The four separation techniques that were chosen were not the only techniques available but were used either due to what had been successful in other studies (e.g. the Rosette-Sep) or what was readily available in the lab (e.g. the Parsortix). All had the benefit of sorting the CTCs either by physical properties or negative selection, meaning that downstream analysis would not be affected should further antibodies need to be used in experiments. Some methods (e.g. the Rosette-Sep) were probably more affected by user error than others, and further attempts at spiked cell retrieval would be performed if this work was to be continued. Those based on separation by physical properties (the Rosette-Sep and the Parsortix) may have a higher loss of the more fragile CTCs due to cell disruption, and it is possible that the density-separation technique may not detect the smaller, denser CTCs at all. Although the cell retrieval was not statistically different for any of the methods for each of the three spiked cell amounts, spiking with 10 000 or 100 000 cells may not be that representative as any clinical samples are unlikely to contain this many CTCs. Part of the reason for doing this was to increase the chances of finding the spiked cells, and also due to the fact that cell lines were counted using a manual haemocytometer, which would introduce a higher proportional error when using lower numbers. Using an automated haemocytometer could improve this in future experiments.

For future experiments looking at optimum media and culture conditions, comparing growth rates using different media would be attempted. Culturing under hypoxic conditions would also be useful, to see if this made any difference to the rate of growth. Using the Imagestream or conventional FACS could also be used to confirm that there were no white cells in the experiment described in section 6.3.

The inability to prove the phenotype of the cells from patients in culture was a huge drawback to this work, but one that is probably inevitable at this early stage. With such low numbers of cells in culture, extracting DNA, even when using a kit that is specifically designed for low cell numbers, was always going to be challenging in inexperienced hands.

The cells growing in culture did appear to adhere strongly to the plates, and so even with gentle trypsin agents it was difficult to harvest all of the cells that were growing. Planning future work where culture conditions are investigated and a more optimal rate of growth established could help increase cell number, which would in turn increase the chances of getting DNA in sufficient quantities, and hopefully higher quality, to sequence. User inexperience was likely to have contributed to the failure of the RT-qPCR experiment as it was not a technique that was familiar.

The chemokine receptor experiment shows promising early results, but without corresponding sequencing data it would be difficult to prove the cell phenotype using this method alone. Further experiments looking at the chemokine expression in white cells from the same patient would be useful, in addition to looking at the expression in cells from more patients, particularly those with early metastatic disease. Discussions are underway to develop this work in the near future.

The attempted CDX model was ambitious given the resources but the clinical findings were encouraging. Unfortunately, the subsequent inability to confirm engraftment, either at the implantation site or the spine, was frustrating and means that the clinical symptoms were unlikely to be related to the implanted cells. Repeating this experiment would be possible but sequencing the cells prior to implantation would be preferable.

The AFM work is only very preliminary, and in order to make statistical comparisons of the Young's Modulus of the cell walls of different cells, much larger numbers of cells would need to be included in the experiment. What is interesting is the shape of the curves; the most rigid material (the glass coverslip) has a very different shape, consistent with an elastic material, compared to the gentle curve of the patient cell which is more viscoelastic. As the PC3 cell and the U2OS cell were indented with different shaped tips the curves can't be directly compared, but the PC3 data was included to show proof of principle. Both the U2OS cell and the patient cell have much gentler curves compared to the white cell, and a lower Young's modulus, which would indicate that the cancer cells are more deformable. This is consistent with findings in the literature (Cross et al., 2007, Cross et al., 2008, Luo et al., 2016) but due to heterogeneity of individual cancer cells and the pure lack of numbers of cells, it is not possible to draw any conclusions from this experiment. However the concept has been tested and if further work confirms that the patient cells in culture are CTCs, ongoing experiments in this field could easily be replicated in sufficient quantities to allow

statistical analysis. This could potentially lead to work with a clinical impact, and as such, this data has been included in a grant application in order to further the work.

Chapter 7. Discussion and future work

With respect to the original aims of the project, the first aim of optimising an assay to enable detection of embryonic stem cell markers in combination with epithelial and mesenchymal markers has partially been achieved. Whilst these cells are not CTCs as defined by the FDA, they are putative CTCs and for the purpose of this study will be referred to as CTCs. The Imagestream assay was robust and white cells could be confidently excluded, in addition to cells expressing either epithelial and stem cell markers being positively identified. The healthy volunteers had no CTCs detected, and the patients with metastatic disease had the most CTCs. This is consistent with what is found in the literature both in relative terms but also absolute numbers. It is not possible to directly compare CTCs numbers as the ones detected in this assay are putative due to the non-FDA approved antigen combination, and the fact that 4mls of blood was sampled compared to 7.5ml. But the order of magnitude is comparable and I am therefore confident that this demonstrates the reliability of the assay.

The downsides of this assay were the fact that it was relatively laborious compared to conventional FACS assays, and gating strategies had to be adopted prior to saving data. As CD45 positive cells were chosen to be excluded, potential CTCs that were adherent to white cells may have been overlooked by using this method. There are lots of different ways to approach the gating, and whilst colleagues within the institute had gated on size, saving data from cells over a certain size threshold, because of the fact that many prostate CTCs are smaller than CTCs from other tumours (Park et al., 2014), the decision had been made not to use size as a criteria. The lack of ability to capture the cells at the end of the process for any downstream analysis was also a flaw, but one that was accepted prior to choosing the platform for this study.

Not having a prostate specific marker to identify prostate cells was another downside to this assay. As explained already the lack of channels to use different fluorochromes meant that using a prostate marker in addition to epithelial and stem cell markers would not have been possible. One way to circumvent this in future would be to divide the blood samples from each patient and run different combinations of markers, e.g. have a prostate specific marker, two stem cell markers and an epithelial marker, and then a second panel with the remaining stem cell marker in conjunction with the prostate marker and epithelial marker. Perhaps if this was done, a third panel with the combination described in Chapter 3 should still be used

as the study from which this work was based on looked at expression of all three embryonic stem cell antigens and found that prognosis and disease specific survival was worst when all three were expressed (Hepburn et al., 2019). Whilst this would make the assay even more laborious, if fewer clinical samples were obtained then work could be focused, or if this was explored as part of a trial then utilising more than one member of staff would help with processing time.

The FACS assay was carefully optimised but despite this, DAPI could not be used due to fluorescent overlap. This was addressed by using forward and side scatter to identify whole cells, and if the cell sort issue could be overcome then DAPI or another nuclear identifier could be used when downstream analysis was undertaken. This issue with the cell sort was really unfortunate and could have easily been overcome by using a non-fixative lysing agent if the implications had been realised when designing the assay. For future work, changing this first step in the protocol would be very straightforward as the antibody panel could remain the same. All the samples from the cell sort are still in storage under HTA approved conditions, so if a product becomes available that would enable DNA or RNA extraction from low cell numbers then these samples could still be utilised. The main benefit of the FACS assay was the ability to explore multiple markers simultaneously, in addition to the fact that most centres will have access to a FACS platform, making it accessible for use in a clinical trial.

In terms of the second aim of the project, Oct4, SOX2 and Nanog expression in CTCs has not been shown to correlate with prognosis. However, it is possible that it is too early to demonstrate a relationship. Correlating CTC results with PSA and ALP levels was probably not going to yield a positive relationship, as neither of these is a substantial predictor of disease progression, and there was such limited clinical data (with respect to length of follow-up). The original work looked at time to castrate resistance and disease specific mortality in patients who had had radical prostatectomies (Hepburn et al., 2019). With respect to castrate resistance, it would only be possible to look at some of the patients included in this project, as many were on hormone treatment already. Disease progression could be used instead and looking at the incidence of radiologically defined metastatic disease would be one option but would need to be looked at over a much longer time period. Survival data would be very interesting and a correlation with the embryonic stem cell marker expression alone or in combination could easily be performed, again over a

longer time period. This work is already in progress as clinical data is being recorded at regular intervals. It is likely that the data from only the Imagestream assay could be used for this purpose as without the confirmation of the cells captured, falsely high numbers of Oct4, SOX2 and Nanog positive cells may be included.

Because MT1-MMP can also be expressed by haematopoietic cells (Nishida et al., 2012), the high levels of MT1-MMP expression even in the healthy control samples meant that for the FACS assay, the results for this antigen couldn't really be interpreted. If MT1-MMP was added to the Imagestream panel then this could be overcome by visual exclusion after CD45 gating, or if the FACS sort was possible then downstream processing could include a step to determine which cells were haematopoietic and which were true mesenchymal tumour cells.

As a result of the issues described above, the hypothesis for this project cannot be proven, although it is hoped that once longer-term clinical data becomes available that this may change. If doing the project again I would ensure that ethical permission was granted to allow serial samples to be obtained from patients. This would enable CTC detection at different time points so rather than comparing CTC count to clinical information, progression in terms of an increase or decrease in CTC number, or CTC expression could be explored.

In terms of the final aim of the project, cells obtained from patients were successfully cultured *in-vitro* for up to a year, but the genetic signature of these cells is still unclear. Whilst there were undoubtedly some white cells, the morphology, stem cell expression and cell stiffness suggested that there were some other cells within the population. Whether these were tumour cells it is not possible to say due to the unsuccessful attempts to sequence them. But these findings are promising and form the basis for future planned work. The results of the experiments using the Atomic Force Microscope have already been included in a grant application for some further work looking at the stiffness of tumour cells, and cells from five patients at various different passages (up to passage five) are still in frozen storage. One grant application for further work by the author of this study has been unsuccessful but if further funds did become available, ongoing work to culture cells from patients would be undertaken, in order to progress the work in Chapter 6.

To conclude, the assay developed for the Imagestream has allowed me to detect putative CTCs and I intend to publish this as a methods paper. By collecting survival data at the two-

year point, I hope to see whether there is a correlation between putative CTC count and/or expression and publish these results from the Imagestream assay too. The cells obtained from patients that were maintained in culture are currently in frozen storage, and if funding becomes available to do further experimentation on them to determine their genotype then this will be pursued. And if the grant application for the Atomic Force Microscope work is approved then that experiment will be expanded to look at multiple different types of cells and multiple cells from each patient.

Appendix

1) Ethical permission for the harvest of solid tissue (prostate and bone marrow):

REC Number 17-NE-0361, IRAS Reference Number 233551, July 2018

2) Ethical permission for the harvest of blood for CTC work:

REC Number 12-NE-0256, October 2012



Health Research Authority
North East – Newcastle & North Tyneside 1 Research Ethics Committee

HRA Newcastle
Newcastle Blood Donor Centre
Holland Drive
Newcastle upon Tyne
NE2 4NQ

Telephone: 0207 1048084

20 July 2018

Dr Christopher M Morris
Newcastle University
Medical Toxicology Centre
Wolfson Building
Claremont Place
Newcastle upon Tyne
NE2 4AA

Dear Dr Morris

Title of the Research Tissue Bank: Newcastle Biobank
REC reference: 17/NE/0361
Designated Individual: Dr Christopher M Morris
IRAS project ID: 233551

Thank you for your letter of 9 July 2018, responding to the Committee's request for further information on the above research tissue bank and submitting revised documentation.

The further information was considered at the meeting of the Sub-Committee of the REC in correspondence. A list of the members who were present at the meeting is attached.

We plan to publish your research summary wording for the Research Tissue Bank on the HRA website, together with your contact details. Publication will be no earlier than three months from the date of this favourable opinion letter. The expectation is that this information will be published for all Research Tissue Banks that receive an ethical opinion but should you wish to provide a substitute contact point, wish to make a request to defer, or require further information, please contact hra.studyregistration@nhs.net outlining the reasons for your request. Under very limited circumstances (e.g. for student research which has received an unfavourable opinion), it may be possible to grant an exemption to the publication of the Research Tissue Bank.

Confirmation of ethical opinion

On behalf of the Committee, I am pleased to confirm a **Favourable** ethical opinion of the above research tissue bank on the basis described in the application form and supporting documentation as revised.

The Committee has also confirmed that the favourable ethical opinion applies to all research projects conducted in the UK using tissue or data supplied by the tissue bank, provided that the release of tissue or data complies with the attached conditions. It will not be necessary for these researchers to make project-based applications for ethical approval. They will be deemed to have ethical approval from this committee. You should provide the researcher with a copy of this letter as confirmation of this. The Committee should be notified of all projects receiving tissue and data from this tissue bank by means of an annual report.

This application was for the renewal of a Research Tissue Bank application. The previous REC Reference number for this application was 12/NE/0395.

Duration of ethical opinion

The favourable opinion is given for a period of five years from the date of this letter and provided that you comply with the standard conditions of ethical approval for Research Tissue Banks set out in the attached document. You are advised to study the conditions carefully. The opinion may be renewed for a further period of up to five years on receipt of a fresh application. It is suggested that the fresh application is made 3-6 months before the 5 years expires, to ensure continuous approval for the research tissue bank.

Research Tissue Bank Renewals

The Research Tissue Bank has been renewed for a further five years from the end of the previous five year period. The previous five year period ran from 07/01/2013 to 06/01/2018. This Research Tissue Bank may be renewed for further periods of five years at a time by following the process described in the above paragraph.

Approved documents

The documents reviewed and approved at

<i>Document</i>	<i>Version</i>	<i>Date</i>
Covering letter on headed paper [Further info or clarification (17_NE_0361)]	N/A	11 December 2017
Human Tissue Authority licence [The Medical School Licence_Ref. 12534]	N/A	22 September 2009
Other [Institute of Genetic Medicine Licence_Ref. 12534]	N/A	22 June 2011
Other [Centre of Ageing & Vitality Licence_Ref. 12534]	N/A	22 June 2011
Other [Freeman Hospital Licence_Ref. 12534]	N/A	22 September 2009
Other [School of Agriculture Licence_Ref. 12534]	N/A	22 September 2009
Other [NIHR Nat Biosample Centre (Milton Keynes)_HTA License]	N/A	12 November 2014
Other [CV 1 Page CMM]	N/A	
Other [Tissue donation information pack_v1.0_18Dec17]	1.0	18 December 2017
Participant consent form [assent_11-15_v1.0 (tracked)]	1	10 October 2017
Participant consent form [Newcastle Biobank Consent V7.0 (tracked)]	7.0	10 October 2017
Participant consent form [assent_11-15_v1.0 (clean)]	1.0	10 October 2017
Participant consent form [Newcastle Biobank Consent V7.0 (final)]	7.0	10 October 2017
Participant consent form [Newcastle Biobank Consent_V7.1_12Dec17_(tracked)]	7.1	12 December 2017
Participant consent form [Consent Form (private)_V1.0_12Dec17]	1.0	12 December 2017
Participant information sheet (PIS) [PIL 6-10_V1.1_12Dec17_(tracked)]	1.1	12 December 2017
Participant information sheet (PIS) [PIL 11-15_V1.1_12Dec17_(tracked)]	1.1	12 December 2017
Participant information sheet (PIS) [NBB PIL_V5.2_01Feb18_(tracked)]	5.2	01 February 2018
Participant information sheet (PIS) [NBB PIL_V5.2_01Feb18_(clean)]	5.2	01 February 2018
Participant information sheet (PIS) [PIL (Private)_V1.1_01Feb18_(tracked)]	1.1	01 February 2018
Participant information sheet (PIS) [PIL (Private)_V1.1_01Feb18_(clean)]	1.1	01 February 2018
Protocol for management of the tissue bank [Newcastle Biobank Protocol v7.1]	7.1	19 December 2017
REC Application Form [RTB_Form_02112017]		02 November 2017
Relative consent form [consent_parent_v3.0 (clean)]	3.0	10 October 2017

Relative consent form [consent_parent_v3.1_12Dec17_(tracked)]	3.1	12 December 2017
Relative information sheet [Parent Info Leaflet_V1.1_01Feb18_(tracked)]	1.1	01 February 2018
Relative information sheet [Parent Info Leaflet_V1.1_01Feb18_(clean)]	1.1	01 February 2018
Response to Request for Further Information		09 July 2018
Summary of research programme(s) [NBB Access Policy V4.0 tracked]	4	10 October 2017
Summary of research programme(s) [NBB Access Policy V4.0 (clean)]	4.0	10 October 2017

Licence from the Human Tissue Authority

Thank you for providing a copy of the above licence.

Research governance

Under the Research Governance Framework (RGF), there is no requirement for NHS research permission for the establishment of research tissue banks in the NHS. Applications to NHS R&D offices through IRAS are not required as all NHS organisations are expected to have included management review in the process of establishing the research tissue bank.

Research permission is also not required by collaborators at tissue collection centres (TCCs) who provide tissue or data under the terms of a supply agreement between the organisation and the research tissue bank. TCCs are not research sites for the purposes of the RGF.

Research tissue bank managers are advised to provide R&D offices at all TCCs with a copy of the REC application for information, together with a copy of the favourable opinion letter when available. All TCCs should be listed in Part C of the REC application.

NHS researchers undertaking specific research projects using tissue or data supplied by a research tissue bank must apply for permission to R&D offices at all organisations where the research is conducted, whether or not the research tissue bank has ethical approval.

Site-specific assessment (SSA) is not a requirement for ethical review of research tissue banks.

Registration of Research Tissue Banks

It is a condition of the ethical approval that all Research Tissue Banks are registered on the UK Clinical Research Collaboration (UKCRC) Tissue Directory. The Research Tissue Bank should be registered no later than 6 weeks after the date of this favourable ethical opinion letter or 6 weeks after the Research Tissue Bank holds tissue with the intention to provide for research purposes. Please use the following link to register the Research Tissue Bank on the UKCRC Directory: <https://directory.biobankinguk.org/Register/Biobank> Registration is defined as having added details of the types of tissue samples held in the tissue bank.

There is no requirement to separately notify the REC but you should do so at the earliest opportunity e.g. when submitting an amendment or annual progress report form. We will monitor the registration details as part of the annual progress reporting process.

Statement of compliance

The Committee is constituted in accordance with the Governance Arrangements for Research Ethics Committees and complies fully with the Standard Operating Procedures for Research Ethics Committees in the UK.

After ethical review

Reporting requirements

The attached standard conditions give detailed guidance on reporting requirements for research tissue banks with a favourable opinion, including:

- Notifying substantial amendments
- Submitting Annual Progress reports.

The HRA website also provides guidance on these topics, which is updated in the light of changes in reporting requirements or procedures.

User Feedback

The Health Research Authority is continually striving to provide a high quality service to all applicants and sponsors. You are invited to give your view of the service you have received and the application procedure. If you wish to make your views known please use the feedback form available on the HRA website: <http://www.hra.nhs.uk/about-the-hra/governance/quality-assurance/>

HRA Training

We are pleased to welcome researchers and R&D staff at our training days – see details at <http://www.hra.nhs.uk/hra-training/>

17/NE/0361

Please quote this number on all correspondence

Yours sincerely

pp



Mr Paddy Stevenson
Chair

E-mail: nrescommittee.northeast-newcastleandnorthtyneside1@nhs.net

Enclosures: List of names and professions of members who were present at the meeting and those who submitted written comments

Standard approval conditions SL-AC3

Copy to: Dr Timothy Peakman – UK Biocentre

North East - Newcastle & North Tyneside 1 Research Ethics Committee

Attendance at Sub-Committee of the REC meeting in correspondence

Committee Members:

<i>Name</i>	<i>Profession</i>	<i>Present</i>	<i>Notes</i>
Dr Liz Baker	Clinical Research Scientist	Yes	
Reverend Nigel Goodfellow	Head of Chaplaincy	Yes	
Mr Paddy Stevenson (Chair)	Research Operations Manager	Yes	

Also in attendance:

<i>Name</i>	<i>Position (or reason for attending)</i>
Ms Gillian Mayer	REC Manager



Health Research Authority

NRES Committee North East - Newcastle & North Tyneside 1

TEDCO Business Centre
Room 002
Rolling Mill Road
Jarrow
NE32 3DT

Telephone: 0191 428 3387
Facsimile: 0191 428 3432

01 October 2012

Dr Zoe Davison
The Northern Institute for Cancer Research
Paul O'Gorman Building
Framlington Place
Newcastle-Upon-Tyne
NE2 4HH

Dear Dr Davison

Title of the Research Tissue Bank: The Newcastle Biomedicine Cancer Biobank
REC reference: 12/NE/0256
Designated Individual: Professor Andrew Hall

Thank you for your letter of 19 September 2012, responding to the Committee's request for further information on the above research tissue bank and submitting revised documentation.

The further information has been considered on behalf of the Committee by the Chair.

Confirmation of ethical opinion

On behalf of the Committee, I am pleased to confirm a favourable ethical opinion of the above research tissue bank on the basis described in the application form and supporting documentation as revised.

The Committee has also confirmed that the favourable ethical opinion applies to all research projects conducted in the UK using tissue or data supplied by the tissue bank, provided that the release of tissue or data complies with the attached conditions. It will not be necessary for these researchers to make project-based applications for ethical approval. They will be deemed to have ethical approval from this committee. You should provide the researcher with a copy of this letter as confirmation of this. The Committee should be notified of all projects receiving tissue and data from this tissue bank by means of an annual report.

Duration of ethical opinion

The favourable opinion is given for a period of five years from the date of this letter and provided that you comply with the standard conditions of ethical approval for Research Tissue Banks set out in the attached document. You are advised to study the conditions carefully. The opinion may be renewed for a further period of up to five years on receipt of a fresh application. It is suggested that the fresh application is made 3-6 months before the 5 years expires, to ensure continuous approval for the research tissue bank.

Additional conditions of approval

In addition to the standard conditions attached, ethical approval is subject to the following:

A Research Ethics Committee established by the Health Research Authority

Amendment of the Participant Information Sheet to reflect the correct committee name - Newcastle and North Tyneside 1.

Approved documents

The documents reviewed and approved at the meeting were:

<i>Document</i>	<i>Version</i>	<i>Date</i>
Covering Letter	Zoe Davison (Newcastle University)	19 June 2012
Human Tissue Authority Licence	Licence Number 12534	22 September 2009
Other: Investigator CV	Zoe Davison BSc PhD	
Other: Standard Procedure for Obtaining Consent	Revision 1	26 September 2012
Other: Standard Procedure for Documenting Consent	Revision 4	26 September 2012
Other: Standard Procedure for Sample Anonymisation	Revision 2	26 September 2012
Other: Request for Samples	1	18 June 2012
Participant Consent Form	2.0 (Tracked and Clean Copies)	03 September 2012
Participant Information Sheet	2.0 (Tracked and Clean Copies)	03 September 2012
Protocol for Management of the Tissue Bank	Version 1.0	18 June 2012
Protocol for Management of the Tissue Bank	Access Policy Version 2.0 (Tracked and Clean Copies)	13 September 2012
REC application	IRAS Version 3.4 61782/335083/3/539	22 June 2012
Response to Request for Further Information	Zoe Davison	19 September 2012

Licence from the Human Tissue Authority

Thank you for providing a copy of the above licence.

Research governance

Under the Research Governance Framework (RGF), there is no requirement for NHS research permission for the establishment of research tissue banks in the NHS. Applications to NHS R&D offices through IRAS are not required as all NHS organisations are expected to have included management review in the process of establishing the research tissue bank.

Research permission is also not required by collaborators at tissue collection centres (TCCs) who provide tissue or data under the terms of a supply agreement between the organisation and the research tissue bank. TCCs are not research sites for the purposes of the RGF.

Research tissue bank managers are advised to provide R&D offices at all TCCs with a copy of the REC application for information, together with a copy of the favourable opinion letter when available. All TCCs should be listed in Part C of the REC application.

NHS researchers undertaking specific research projects using tissue or data supplied by a research tissue bank must apply for permission to R&D offices at all organisations where the research is conducted, whether or not the research tissue bank has ethical approval.

Site-specific assessment (SSA) is not a requirement for ethical review of research tissue banks. There is no need to inform Local Research Ethics Committees.

Statement of compliance

The Committee is constituted in accordance with the Governance Arrangements for Research Ethics Committees and complies fully with the Standard Operating Procedures for Research Ethics Committees in the UK.

After ethical review

Now that you have completed the application process please visit the National Research Ethics Service website > After Review

Here you will find links to the following:

- a) Providing feedback. You are invited to give your view of the service that you have received from the National Research Ethics Service and the application procedure. If you wish to make your views known please use the feedback form available on the website.
- b) Annual Reports. Please refer to the attached conditions of approval.
- c) Amendments. Please refer to the attached conditions of approval.

12/NE/0256

Please quote this number on all correspondence

Yours sincerely



pp

Mr Chris Turnock
Chair

E-mail: nrescommittee.northeast-newcastleandnorthtyneside1@nhs.net

Enclosures: Standard approval conditions SL-AC3

Copy to: Professor Andrew Hall, Newcastle University

Bibliography

2015. The Molecular Taxonomy of Primary Prostate Cancer. *Cell*, 163, 1011-25.
2019. <http://www.stampededtrial.org/participants/about-stampede/>: MRC Clinical Trials Unit, UCL. [Accessed].
- ABBOSH, C., BIRKBAK, N. J., WILSON, G. A., JAMAL-HANJANI, M., CONSTANTIN, T., SALARI, R., LE QUESNE, J., MOORE, D. A., VEERIAH, S., ROSENTHAL, R., MARAFIOTI, T., KIRKIZLAR, E., WATKINS, T. B. K., MCGRANAHAN, N., WARD, S., MARTINSON, L., RILEY, J., FRAIOLI, F., AL BAKIR, M., GRONROOS, E., ZAMBRANA, F., ENDOZO, R., BI, W. L., FENNESSY, F. M., SPONER, N., JOHNSON, D., LAYCOCK, J., SHAFI, S., CZYZEWSKA-KHAN, J., ROWAN, A., CHAMBERS, T., MATTHEWS, N., TURAJLIC, S., HILEY, C., LEE, S. M., FORSTER, M. D., AHMAD, T., FALZON, M., BORG, E., LAWRENCE, D., HAYWARD, M., KOLVEKAR, S., PANAGIOTOPOULOS, N., JANES, S. M., THAKRAR, R., AHMED, A., BLACKHALL, F., SUMMERS, Y., HAFEZ, D., NAIK, A., GANGULY, A., KAREHT, S., SHAH, R., JOSEPH, L., MARIE QUINN, A., CROSBIE, P. A., NAIDU, B., MIDDLETON, G., LANGMAN, G., TROTTER, S., NICOLSON, M., REMMEN, H., KERR, K., CHETTY, M., GOMERSALL, L., FENNELL, D. A., NAKAS, A., RATHINAM, S., ANAND, G., KHAN, S., RUSSELL, P., EZHIL, V., ISMAIL, B., IRVIN-SELLERS, M., PRAKASH, V., LESTER, J. F., KORNASZEWSKA, M., ATTANOOS, R., ADAMS, H., DAVIES, H., OUKRIF, D., AKARCA, A. U., HARTLEY, J. A., LOWE, H. L., LOCK, S., ILES, N., BELL, H., NGAI, Y., ELGAR, G., SZALLASI, Z., SCHWARZ, R. F., HERRERO, J., STEWART, A., QUEZADA, S. A., PEGGS, K. S., VAN LOO, P., DIVE, C., LIN, C. J., RABINOWITZ, M., AERTS, H., et al. 2017. Phylogenetic ctDNA analysis depicts early-stage lung cancer evolution. *Nature*, 545, 446-451.
- ABUZALLOUF, S., DAYES, I. & LUKKA, H. 2004. Baseline staging of newly diagnosed prostate cancer: a summary of the literature. *J Urol*, 171, 2122-7.
- ADAMO, P. & LADOMERY, M. R. 2016. The oncogene ERG: a key factor in prostate cancer. *Oncogene*, 35, 403-14.
- ADCOCK, D. M., FAVALORO, E. J. & LIPPI, G. 2016. Critical pre-examination variables in the hemostasis laboratory and their quality indicators. *Clin Biochem*, 49, 1315-1320.
- AFSHAR-OROMIEH, A., AVTZI, E., GIESEL, F. L., HOLLAND-LETZ, T., LINHART, H. G., EDER, M., EISENHUT, M., BOXLER, S., HADASCHIK, B. A., KRATOCHWIL, C., WEICHERT, W., KOPKA, K., DEBUS, J. & HABERKORN, U. 2015. The diagnostic value of PET/CT imaging with the (68)Ga-labelled PSMA ligand HBED-CC in the diagnosis of recurrent prostate cancer. *Eur J Nucl Med Mol Imaging*, 42, 197-209.
- AFSHAR-OROMIEH, A., HOLLAND-LETZ, T., GIESEL, F. L., KRATOCHWIL, C., MIER, W., HAUFE, S., DEBUS, N., EDER, M., EISENHUT, M., SCHAFFER, M., NEELS, O., HOHENFELLNER, M., KOPKA, K., KAUCZOR, H. U., DEBUS, J. & HABERKORN, U. 2017. Diagnostic performance of (68)Ga-PSMA-11 (HBED-CC) PET/CT in patients with recurrent prostate cancer: evaluation in 1007 patients. *Eur J Nucl Med Mol Imaging*, 44, 1258-1268.
- AHMED, H. U., EL-SHATER BOSAILY, A., BROWN, L. C., GABE, R., KAPLAN, R., PARMAR, M. K., COLLACO-MORAES, Y., WARD, K., HINDLEY, R. G., FREEMAN, A., KIRKHAM, A. P., OLDROYD, R., PARKER, C. & EMBERTON, M. 2017a. Diagnostic accuracy of multi-parametric MRI and TRUS biopsy in prostate cancer (PROMIS): a paired validating confirmatory study. *Lancet*, 389, 815-822.
- AHMED, M., BASHEER, H. A., AYUSO, J. M., AHMET, D., MAZZINI, M., PATEL, R., SHNYDER, S. D., VINADER, V. & AFARINKIA, K. 2017b. Agarose Spot as a Comparative Method for

- in situ Analysis of Simultaneous Chemotactic Responses to Multiple Chemokines. *Sci Rep*, 7, 1075.
- ALIX-PANABIÈRES, C. & PANTEL, K. 2014. Challenges in circulating tumour cell research. *Nature Reviews Cancer*, 14, 623-631.
- ALLARD, W. J., MATERA, J., MILLER, M. C., REPOLLET, M., CONNELLY, M. C., RAO, C., TIBBE, A. G., UHR, J. W. & TERSTAPPEN, L. W. 2004. Tumor cells circulate in the peripheral blood of all major carcinomas but not in healthy subjects or patients with nonmalignant diseases. *Clin Cancer Res*, 10, 6897-904.
- ALTIN, J. G. & SLOAN, E. K. 1997. The role of CD45 and CD45-associated molecules in T cell activation. *Immunol Cell Biol*, 75, 430-45.
- ALUNNI-FABBRONI, M. & SANDRI, M. T. 2010. Circulating tumour cells in clinical practice: Methods of detection and possible characterization. *Methods*, 50, 289-97.
- ALVAREZ-CUBERO, M. J., MARTINEZ-GONZALEZ, L. J., ROBLES-FERNANDEZ, I., MARTINEZ-HERRERA, J., GARCIA-RODRIGUEZ, G., PASCUAL-GELER, M., COZAR, J. M. & LORENTE, J. A. 2017. Somatic Mutations in Prostate Cancer: Closer to Personalized Medicine. *Mol Diagn Ther*, 21, 167-178.
- ALVAREZ CUBERO, M. J., LORENTE, J. A., ROBLES-FERNANDEZ, I., RODRIGUEZ-MARTINEZ, A., PUCHE, J. L. & SERRANO, M. J. 2017. Circulating Tumor Cells: Markers and Methodologies for Enrichment and Detection. *Methods Mol Biol*, 1634, 283-303.
- AMINI, S., FATHI, F., MOBALEGI, J., SOFIMAJIDPOUR, H. & GHADIMI, T. 2014. The expressions of stem cell markers: Oct4, Nanog, Sox2, nucleostemin, Bmi, Zfx, Tcl1, Tbx3, Dppa4, and Esrrb in bladder, colon, and prostate cancer, and certain cancer cell lines. *Anat Cell Biol*, 47, 1-11.
- AN, J., WANG, C., DENG, Y., YU, L. & HUANG, H. 2014. Destruction of full-length androgen receptor by wild-type SPOP, but not prostate-cancer-associated mutants. *Cell Rep*, 6, 657-69.
- ANKENY, J. S., COURT, C. M., HOU, S., LI, Q., SONG, M., WU, D., CHEN, J. F., LEE, T., LIN, M., SHO, S., ROCHEFORT, M. M., GIRGIS, M. D., YAO, J., WAINBERG, Z. A., MUTHUSAMY, V. R., WATSON, R. R., DONAHUE, T. R., HINES, O. J., REBER, H. A., GRAEBER, T. G., TSENG, H. R. & TOMLINSON, J. S. 2016. Circulating tumour cells as a biomarker for diagnosis and staging in pancreatic cancer. *Br J Cancer*, 114, 1367-75.
- ANTONARAKIS, E. S., FENG, Z., TROCK, B. J., HUMPHREYS, E. B., CARDUCCI, M. A., PARTIN, A. W., WALSH, P. C. & EISENBERGER, M. A. 2012. The natural history of metastatic progression in men with prostate-specific antigen recurrence after radical prostatectomy: long-term follow-up. *BJU Int*, 109, 32-9.
- ANTONARAKIS, E. S., LU, C., WANG, H., LUBER, B., NAKAZAWA, M., ROESER, J. C., CHEN, Y., MOHAMMAD, T. A., CHEN, Y., FEDOR, H. L., LOTAN, T. L., ZHENG, Q., DE MARZO, A. M., ISAACS, J. T., ISAACS, W. B., NADAL, R., PALLER, C. J., DENMEADE, S. R., CARDUCCI, M. A., EISENBERGER, M. A. & LUO, J. 2014. AR-V7 and resistance to enzalutamide and abiraterone in prostate cancer. *N Engl J Med*, 371, 1028-38.
- ARMSTRONG, A. J., MARENCO, M. S., OLTEAN, S., KEMENY, G., BITTING, R. L., TURNBULL, J. D., HEROLD, C. I., MARCOM, P. K., GEORGE, D. J. & GARCIA-BLANCO, M. A. 2011. Circulating tumor cells from patients with advanced prostate and breast cancer display both epithelial and mesenchymal markers. *Mol Cancer Res*, 9, 997-1007.
- ARON, M., RAJEEV, T. P. & GUPTA, N. P. 2000. Antibiotic prophylaxis for transrectal needle biopsy of the prostate: a randomized controlled study. *BJU Int*, 85, 682-5.
- ASHWORTH, T. 1869. A case of cancer in which cells similar to those in the tumours were seen in the blood after death. *Australasian Medical Journal*, 14, 146-149.

- ATTARD, G. & DE BONO, J. S. 2011. Utilizing circulating tumor cells: challenges and pitfalls. *Curr Opin Genet Dev*, 21, 50-8.
- ATTARD, G., SWENNENHUIS, J. F., OLMOS, D., REID, A. H., VICKERS, E., A'HERN, R., LEVINK, R., COUMANS, F., MOREIRA, J., RIISNAES, R., OOMMEN, N. B., HAWCHE, G., JAMESON, C., THOMPSON, E., SIPKEMA, R., CARDEN, C. P., PARKER, C., DEARNALEY, D., KAYE, S. B., COOPER, C. S., MOLINA, A., COX, M. E., TERSTAPPEN, L. W. & DE BONO, J. S. 2009. Characterization of ERG, AR and PTEN gene status in circulating tumor cells from patients with castration-resistant prostate cancer. *Cancer Res*, 69, 2912-8.
- BAE, K. M., PARKER, N. N., DAI, Y., VIEWEG, J. & SIEMANN, D. W. 2011. E-cadherin plasticity in prostate cancer stem cell invasion. *Am J Cancer Res*, 1, 71-84.
- BARBIERI, C. E., BACA, S. C., LAWRENCE, M. S., DEMICHELIS, F., BLATTNER, M., THEURILLAT, J. P., WHITE, T. A., STOJANOV, P., VAN ALLEN, E., STRANSKY, N., NICKERSON, E., CHAE, S. S., BOYSEN, G., AUCLAIR, D., ONOFRIO, R. C., PARK, K., KITABAYASHI, N., MACDONALD, T. Y., SHEIKH, K., VUONG, T., GUIDUCCI, C., CIBULSKIS, K., SIVACHENKO, A., CARTER, S. L., SAKSENA, G., VOET, D., HUSSAIN, W. M., RAMOS, A. H., WINCKLER, W., REDMAN, M. C., ARDLIE, K., TEWARI, A. K., MOSQUERA, J. M., RUPP, N., WILD, P. J., MOCH, H., MORRISSEY, C., NELSON, P. S., KANTOFF, P. W., GABRIEL, S. B., GOLUB, T. R., MEYERSON, M., LANDER, E. S., GETZ, G., RUBIN, M. A. & GARRAWAY, L. A. 2012. Exome sequencing identifies recurrent SPOP, FOXA1 and MED12 mutations in prostate cancer. *Nat Genet*, 44, 685-9.
- BARRALLO-GIMENO, A. & NIETO, M. A. 2005. The Snail genes as inducers of cell movement and survival: implications in development and cancer. *Development*, 132, 3151-61.
- BARRIERE, G., FICI, P., GALLERANI, G., FABBRI, F., ZOLI, W. & RIGAUD, M. 2014. Circulating tumor cells and epithelial, mesenchymal and stemness markers: characterization of cell subpopulations. *Ann Transl Med*, 2, 109.
- BARRIERE, G., RIOUALLON, A., RENAUDIE, J., TARTARY, M. & RIGAUD, M. 2012. Mesenchymal and stemness circulating tumor cells in early breast cancer diagnosis. *BMC Cancer*, 12, 114.
- BEDARD, P. L., HANSEN, A. R., RATAIN, M. J. & SIU, L. L. 2013. Tumour heterogeneity in the clinic. *Nature*, 501, 355-64.
- BEDNARZ-KNOLL, N., ALIX-PANABIERES, C. & PANTEL, K. 2012. Plasticity of disseminating cancer cells in patients with epithelial malignancies. *Cancer Metastasis Rev*, 31, 673-87.
- BELL, K. J., DEL MAR, C., WRIGHT, G., DICKINSON, J. & GLASZIOU, P. 2015. Prevalence of incidental prostate cancer: A systematic review of autopsy studies. *Int J Cancer*, 137, 1749-57.
- BELTRAN, H., ANTONARAKIS, E. S., MORRIS, M. J. & ATTARD, G. 2016. Emerging Molecular Biomarkers in Advanced Prostate Cancer: Translation to the Clinic. *Am Soc Clin Oncol Educ Book*, 35, 131-41.
- BEN-BARUCH, A. 2008. Organ selectivity in metastasis: regulation by chemokines and their receptors. *Clin Exp Metastasis*, 25, 345-56.
- BEN-PORATH, I., THOMSON, M. W., CAREY, V. J., GE, R., BELL, G. W., REGEV, A. & WEINBERG, R. A. 2008. An embryonic stem cell-like gene expression signature in poorly differentiated aggressive human tumors. *Nat Genet*, 40, 499-507.
- BEN-SHLOMO, Y., EVANS, S., IBRAHIM, F., PATEL, B., ANSON, K., CHINEGWUNDOH, F., CORBISHLEY, C., DORLING, D., THOMAS, B., GILLATT, D., KIRBY, R., MUIR, G., NARGUND, V., POPERT, R., METCALFE, C. & PERSAD, R. 2008. The risk of prostate

- cancer amongst black men in the United Kingdom: the PROCESS cohort study. *Eur Urol*, 53, 99-105.
- BERGER, M. F., LAWRENCE, M. S., DEMICHELIS, F., DRIER, Y., CIBULSKIS, K., SIVACHENKO, A. Y., SBONER, A., ESGUEVA, R., PFLUEGER, D., SOUGNEZ, C., ONOFRIO, R., CARTER, S. L., PARK, K., HABEGGER, L., AMBROGIO, L., FENNELL, T., PARKIN, M., SAKSENA, G., VOET, D., RAMOS, A. H., PUGH, T. J., WILKINSON, J., FISHER, S., WINCKLER, W., MAHAN, S., ARDLIE, K., BALDWIN, J., SIMONS, J. W., KITABAYASHI, N., MACDONALD, T. Y., KANTOFF, P. W., CHIN, L., GABRIEL, S. B., GERSTEIN, M. B., GOLUB, T. R., MEYERSON, M., TEWARI, A., LANDER, E. S., GETZ, G., RUBIN, M. A. & GARRAWAY, L. A. 2011. The genomic complexity of primary human prostate cancer. *Nature*, 470, 214-20.
- BERGMAN, R. A., AFFIFI, A.K., HEIDGER, P.M., 1995. *Section 4: Blood* [Online]. Available: <http://www.anatomyatlases.org/MicroscopicAnatomy/Section04/Section04.shtml> [Accessed 2015].
- BERRY, S. J., COFFEY, D. S., WALSH, P. C. & EWING, L. L. 1984. The development of human benign prostatic hyperplasia with age. *J Urol*, 132, 474-9.
- BONFIL, R. D., DONG, Z., TRINDADE FILHO, J. C., SABBOTA, A., OSENKOWSKI, P., NABHA, S., YAMAMOTO, H., CHINNI, S. R., ZHAO, H., MOBASHERY, S., VESSELLA, R. L., FRIDMAN, R. & CHER, M. L. 2007. Prostate cancer-associated membrane type 1-matrix metalloproteinase: a pivotal role in bone response and intraosseous tumor growth. *Am J Pathol*, 170, 2100-11.
- BONNET, D. & DICK, J. E. 1997. Human acute myeloid leukemia is organized as a hierarchy that originates from a primitive hematopoietic cell. *Nat Med*, 3, 730-7.
- BOORJIAN, S. A., THOMPSON, R. H., TOLLEFSON, M. K., RANGEL, L. J., BERGSTRALH, E. J., BLUTE, M. L. & KARNES, R. J. 2011. Long-term risk of clinical progression after biochemical recurrence following radical prostatectomy: the impact of time from surgery to recurrence. *Eur Urol*, 59, 893-9.
- BOSSUYT, X., MARTI, G. E. & FLEISHER, T. A. 1997. Comparative analysis of whole blood lysis methods for flow cytometry. *Cytometry*, 30, 124-33.
- BOWEN, R. A. & ADCOCK, D. M. 2016. Blood collection tubes as medical devices: The potential to affect assays and proposed verification and validation processes for the clinical laboratory. *Clin Biochem*, 49, 1321-1330.
- BOYSEN, G., NAVA RODRIGUES, D., RESCIGNO, P., SEED, G., DOLLING, D. I., RIISNAES, R., CRESPO, M., ZAFEIRIOU, Z., SUMANASURIYA, S., BIANCHINI, D., HUNT, J., MOLONEY, D., PEREZ-LOPEZ, R., TUNARIU, N., MIRANDA, S., FIGUEIREDO, I., FERREIRA, A., CHRISTOVA, R., GIL, V., AZIZ, S., BERTAN, C., DE OLIVEIRA, F. M., ATKIN, M., CLARKE, M., GOODALL, J., SHARP, A., MACDONALD, T. Y., RUBIN, M. A., YUAN, W., BARBIERI, C. E., CARREIRA, S., MATEO, J. & DE BONO, J. S. 2018. SPOP mutated/ CHD1 deleted lethal prostate cancer and abiraterone sensitivity. *Clin Cancer Res*.
- BRATAN, F., NIAF, E., MELODELIMA, C., CHESNAIS, A. L., SOUCHON, R., MEGE-LECHEVALLIER, F., COLOMBEL, M. & ROUVIERE, O. 2013. Influence of imaging and histological factors on prostate cancer detection and localisation on multiparametric MRI: a prospective study. *Eur Radiol*, 23, 2019-29.
- BRATT, O. 2002. Hereditary prostate cancer: clinical aspects. *J Urol*, 168, 906-13.
- BREWSTER, D. H., FRASER, L. A., HARRIS, V. & BLACK, R. J. 2000. Rising incidence of prostate cancer in Scotland: increased risk or increased detection? *BJU Int*, 85, 463-72; discussion 472-3.
- BRIERLEY J, G. M., WITTAKIND C 2017. TNM Classification of Malignant Tumours. Union for International Cancer Control.

- BRUINSMA, S. M., ROOBOL, M. J., CARROLL, P. R., KLOTZ, L., PICKLES, T., MOORE, C. M., GNANAPRAGASAM, V. J., VILLERS, A., RANNIKKO, A., VALDAGNI, R., FRYDENBERG, M., KAKEHI, Y., FILSON, C. P. & BANGMA, C. H. 2017. Expert consensus document: Semantics in active surveillance for men with localized prostate cancer - results of a modified Delphi consensus procedure. *Nat Rev Urol*, 14, 312-322.
- BURRELL, R. A., MCGRANAHAN, N., BARTEK, J. & SWANTON, C. 2013. The causes and consequences of genetic heterogeneity in cancer evolution. *Nature*, 501, 338-45.
- CANCER RESEARCH UK. 2018. *Prostate cancer incidence statistics* [Online]. Cancer Research UK. Available: <http://www.cancerresearchuk.org/health-professional/cancer-statistics/statistics-by-cancer-type/prostate-cancer> [Accessed 2018].
- CAO, J., CHIARELLI, C., RICHMAN, O., ZARRABI, K., KOZAREKAR, P. & ZUCKER, S. 2008. Membrane type 1 matrix metalloproteinase induces epithelial-to-mesenchymal transition in prostate cancer. *J Biol Chem*, 283, 6232-40.
- CARPENTER, E. L., RADER, J., RUDEN, J., RAPPAPORT, E. F., HUNTER, K. N., HALLBERG, P. L., KRYTSKA, K., O'DWYER, P. J. & MOSSE, Y. P. 2014. Dielectrophoretic capture and genetic analysis of single neuroblastoma tumor cells. *Front Oncol*, 4, 201.
- CARTER, B. S., BEATY, T. H., STEINBERG, G. D., CHILDS, B. & WALSH, P. C. 1992. Mendelian inheritance of familial prostate cancer. *Proc Natl Acad Sci U S A*, 89, 3367-71.
- CARTER, H. B., ALBERTSEN, P. C., BARRY, M. J., ETZIONI, R., FREEDLAND, S. J., GREENE, K. L., HOLMBERG, L., KANTOFF, P., KONETY, B. R., MURAD, M. H., PENSON, D. F. & ZIETMAN, A. L. 2013. Early detection of prostate cancer: AUA Guideline. *J Urol*, 190, 419-26.
- CARTER, L., ROTHWELL, D. G., MESQUITA, B., SMOWTON, C., LEONG, H. S., FERNANDEZ-GUTIERREZ, F., LI, Y., BURT, D. J., ANTONELLO, J., MORROW, C. J., HODGKINSON, C. L., MORRIS, K., PRIEST, L., CARTER, M., MILLER, C., HUGHES, A., BLACKHALL, F., DIVE, C. & BRADY, G. 2017. Molecular analysis of circulating tumor cells identifies distinct copy-number profiles in patients with chemosensitive and chemorefractory small-cell lung cancer. *Nat Med*, 23, 114-119.
- CARTER, R. E., FELDMAN, A. R. & COYLE, J. T. 1996. Prostate-specific membrane antigen is a hydrolase with substrate and pharmacologic characteristics of a neuropeptidase. *Proc Natl Acad Sci U S A*, 93, 749-53.
- CASSIER, P. A., TREILLEUX, I., BACHELOT, T., RAY-COQUARD, I., BENDRISS-VERMARE, N., MENETRIER-CAUX, C., TREDAN, O., GODDARD-LEON, S., PIN, J. J., MIGNOTTE, H., BATHELEMY-DUBOIS, C., CAUX, C., LEBECQUE, S. & BLAY, J. Y. 2011. Prognostic value of the expression of C-Chemokine Receptor 6 and 7 and their ligands in non-metastatic breast cancer. *BMC Cancer*, 11, 213.
- CAYREFOURCQ, L., MAZARD, T., JOOSSE, S., SOLASSOL, J., RAMOS, J., ASSENAT, E., SCHUMACHER, U., COSTES, V., MAUDELONDE, T., PANTEL, K. & ALIX-PANABIÈRES, C. 2015. Establishment and characterization of a cell line from human circulating colon cancer cells. *Cancer Res*, 75, 892-901.
- CHAMBERS, A. F., GROOM, A. C. & MACDONALD, I. C. 2002. Dissemination and growth of cancer cells in metastatic sites. *Nat Rev Cancer*, 2, 563-72.
- CHANG, L., GRAHAM, P. H., NI, J., HAO, J., BUCCI, J., COZZI, P. J. & LI, Y. 2015. Targeting PI3K/Akt/mTOR signaling pathway in the treatment of prostate cancer radioresistance. *Crit Rev Oncol Hematol*, 96, 507-17.
- CHANG, S. S. 2004. Overview of Prostate-Specific Membrane Antigen. *Reviews in Urology*, 6, S13-S18.
- CHAUX, A., PESKOE, S. B., GONZALEZ-ROIBON, N., SCHULTZ, L., ALBADINE, R., HICKS, J., DE MARZO, A. M., PLATZ, E. A. & NETTO, G. J. 2012. Loss of PTEN expression is

- associated with increased risk of recurrence after prostatectomy for clinically localized prostate cancer. *Mod Pathol*, 25, 1543-9.
- CHEN, C. D., WELSBIE, D. S., TRAN, C., BAEK, S. H., CHEN, R., VESSELLA, R., ROSENFELD, M. G. & SAWYERS, C. L. 2004. Molecular determinants of resistance to antiandrogen therapy. *Nat Med*, 10, 33-9.
- CHEN, C. L., MAHALINGAM, D., OSMULSKI, P., JADHAV, R. R., WANG, C. M., LEACH, R. J., CHANG, T. C., WEITMAN, S. D., KUMAR, A. P., SUN, L., GACZYNSKA, M. E., THOMPSON, I. M. & HUANG, T. H. 2013. Single-cell analysis of circulating tumor cells identifies cumulative expression patterns of EMT-related genes in metastatic prostate cancer. *Prostate*, 73, 813-26.
- CHEN, J. F., HO, H., LICHTERMAN, J., LU, Y. T., ZHANG, Y., GARCIA, M. A., CHEN, S. F., LIANG, A. J., HODARA, E., ZHAU, H. E., HOU, S., AHMED, R. S., LUTHRINGER, D. J., HUANG, J., LI, K. C., CHUNG, L. W., KE, Z., TSENG, H. R. & POSADAS, E. M. 2015a. Subclassification of prostate cancer circulating tumor cells by nuclear size reveals very small nuclear circulating tumor cells in patients with visceral metastases. *Cancer*, 121, 3240-51.
- CHEN, W., BRANDES, Z., ROY, R., CHEKMAREVA, M., PANDYA, H. J., DESAI, J. P. & FORAN, D. J. 2015b. Robot-Guided Atomic Force Microscopy for Mechano-Visual Phenotyping of Cancer Specimens. *Microsc Microanal*, 21, 1224-35.
- CHIANG, A. C. & MASSAGUE, J. 2008. Molecular basis of metastasis. *N Engl J Med*, 359, 2814-23.
- CHOI, N., ZHANG, B., ZHANG, L., ITTMANN, M. & XIN, L. 2012. Adult murine prostate basal and luminal cells are self-sustained lineages that can both serve as targets for prostate cancer initiation. *Cancer Cell*, 21, 253-65.
- CHRISTIANSEN, J. J. & RAJASEKARAN, A. K. 2006. Reassessing epithelial to mesenchymal transition as a prerequisite for carcinoma invasion and metastasis. *Cancer Res*, 66, 8319-26.
- CHUA, C. W., SHIBATA, M., LEI, M., TOIVANEN, R., BARLOW, L. J., BERGREN, S. K., BADANI, K. K., MCKIERNAN, J. M., BENSON, M. C., HIBSHOOSH, H. & SHEN, M. M. 2014. Single luminal epithelial progenitors can generate prostate organoids in culture. *Nat Cell Biol*, 16, 951-61, 1-4.
- CHUDZIAK, J., BURT, D. J., MOHAN, S., ROTHWELL, D. G., MESQUITA, B., ANTONELLO, J., DALBY, S., AYUB, M., PRIEST, L., CARTER, L., KREBS, M. G., BLACKHALL, F., DIVE, C. & BRADY, G. 2016. Clinical evaluation of a novel microfluidic device for epitope-independent enrichment of circulating tumour cells in patients with small cell lung cancer. *Analyst*, 141, 669-78.
- CLEVERS, H. 2016. Modeling Development and Disease with Organoids. *Cell*, 165, 1586-1597.
- COHEN, S. J., PUNT, C. J., IANNOTTI, N., SAIDMAN, B. H., SABBATH, K. D., GABRAIL, N. Y., PICUS, J., MORSE, M., MITCHELL, E., MILLER, M. C., DOYLE, G. V., TISSING, H., TERSTAPPEN, L. W. & MEROPOL, N. J. 2008. Relationship of circulating tumor cells to tumor response, progression-free survival, and overall survival in patients with metastatic colorectal cancer. *J Clin Oncol*, 26, 3213-21.
- COMSA, S., CIMPEAN, A. M. & RAICA, M. 2015. The Story of MCF-7 Breast Cancer Cell Line: 40 years of Experience in Research. *Anticancer Res*, 35, 3147-54.
- CONLEY-LACOMB, M. K., HUANG, W., WANG, S., SHI, D., JUNG, Y. S., NAJY, A., FRIDMAN, R., BONFIL, R. D., CHER, M. L., CHEN, Y. Q. & KIM, H. R. 2012. PTEN regulates PDGF ligand switch for beta-PDGFR signaling in prostate cancer. *Am J Pathol*, 180, 1017-27.
- CONSORTIUM, G. E. R. 2019. *100 000 Genomes Project* [Online]. Available: <https://genomicsengland.co.uk> [Accessed].

- CONTRERAS, H. R., LEDEZMA, R. A., VERGARA, J., CIFUENTES, F., BARRA, C., CABELLO, P., GALLEGOS, I., MORALES, B., HUIDOBRO, C. & CASTELLON, E. A. 2010. The expression of syndecan-1 and -2 is associated with Gleason score and epithelial-mesenchymal transition markers, E-cadherin and beta-catenin, in prostate cancer. *Urol Oncol*, 28, 534-40.
- COOPERBERG, M. R., PASTA, D. J., ELKIN, E. P., LITWIN, M. S., LATINI, D. M., DU CHANE, J. & CARROLL, P. R. 2005. The University of California, San Francisco Cancer of the Prostate Risk Assessment score: a straightforward and reliable preoperative predictor of disease recurrence after radical prostatectomy. *J Urol*, 173, 1938-42.
- COUMANS, F. A., VAN DALUM, G., BECK, M. & TERSTAPPEN, L. W. 2013. Filter characteristics influencing circulating tumor cell enrichment from whole blood. *PLoS One*, 8, e61770.
- CRAWFORD, E. D. 2003. Epidemiology of prostate cancer. *Urology*, 62, 3-12.
- CRESPO, M., VAN DALUM, G., FERRALDESCHI, R., ZAFEIRIOU, Z., SIDERIS, S., LORENTE, D., BIANCHINI, D., RODRIGUES, D. N., RIISNAES, R., MIRANDA, S., FIGUEIREDO, I., FLOHR, P., NOWAKOWSKA, K., DE BONO, J. S., TERSTAPPEN, L. W. & ATTARD, G. 2015. Androgen receptor expression in circulating tumour cells from castration-resistant prostate cancer patients treated with novel endocrine agents. *Br J Cancer*, 112, 1166-74.
- CRISTOFANILLI, M., BUDD, G. T., ELLIS, M. J., STOPECK, A., MATERA, J., MILLER, M. C., REUBEN, J. M., DOYLE, G. V., ALLARD, W. J., TERSTAPPEN, L. W. & HAYES, D. F. 2004. Circulating tumor cells, disease progression, and survival in metastatic breast cancer. *N Engl J Med*, 351, 781-91.
- CRISTOFANILLI, M., PIERGA, J. Y., REUBEN, J., RADEMAKER, A., DAVIS, A. A., PEETERS, D. J., FEHM, T., NOLE, F., GISBERT-CRIADO, R., MAVROUDIS, D., GRISANTI, S., GIULIANO, M., GARCIA-SAENZ, J. A., STEBBING, J., CALDAS, C., GAZZANIGA, P., MANSO, L., ZAMARCHI, R., DE LASCOITI, A. F., DE MATTOS-ARRUDA, L., IGNATIADIS, M., CABEL, L., VAN LAERE, S. J., MEIER-STIEGEN, F., SANDRI, M. T., VIDAL-MARTINEZ, J., POLITAKI, E., CONSOLI, F., GENERALI, D., CAPPELLETTI, M. R., DIAZ-RUBIO, E., KRELL, J., DAWSON, S. J., RAIMONDI, C., RUTTEN, A., JANNI, W., MUNZONE, E., CARANANA, V., AGELAKI, S., ALMICI, C., DIRIX, L., SOLOMAYER, E. F., ZORZINO, L., DARRIGUES, L., REIS-FILHO, J. S., GERRATANA, L., MICHIELS, S., BIDARD, F. C. & PANTEL, K. 2019. The clinical use of circulating tumor cells (CTCs) enumeration for staging of metastatic breast cancer (MBC): International expert consensus paper. *Crit Rev Oncol Hematol*, 134, 39-45.
- CROSS, S. E., JIN, Y. S., RAO, J. & GIMZEWSKI, J. K. 2007. Nanomechanical analysis of cells from cancer patients. *Nat Nanotechnol*, 2, 780-3.
- CROSS, S. E., JIN, Y. S., TONDRE, J., WONG, R., RAO, J. & GIMZEWSKI, J. K. 2008. AFM-based analysis of human metastatic cancer cells. *Nanotechnology*, 19, 384003.
- CURRAN, S. & MURRAY, G. I. 2000. Matrix metalloproteinases: molecular aspects of their roles in tumour invasion and metastasis. *Eur J Cancer*, 36, 1621-30.
- D'ELIA, C., CERRUTO, M. A., CIOFFI, A., NOVELLA, G., CAVALLERI, S. & ARTIBANI, W. 2014. Upgrading and upstaging in prostate cancer: From prostate biopsy to radical prostatectomy. *Mol Clin Oncol*, 2, 1145-1149.
- DANILA, D. C., ANAND, A., SUNG, C. C., HELLER, G., LEVERSHA, M. A., CAO, L., LILJA, H., MOLINA, A., SAWYERS, C. L., FLEISHER, M. & SCHER, H. I. 2011a. TMPRSS2-ERG status in circulating tumor cells as a predictive biomarker of sensitivity in castration-resistant prostate cancer patients treated with abiraterone acetate. *Eur Urol*, 60, 897-904.

- DANILA, D. C., FLEISHER, M. & SCHER, H. I. 2011b. Circulating tumor cells as biomarkers in prostate cancer. *Clin Cancer Res*, 17, 3903-12.
- DANILA, D. C., HELLER, G., GIGNAC, G. A., GONZALEZ-ESPINOZA, R., ANAND, A., TANAKA, E., LILJA, H., SCHWARTZ, L., LARSON, S., FLEISHER, M. & SCHER, H. I. 2007. Circulating tumor cell number and prognosis in progressive castration-resistant prostate cancer. *Clin Cancer Res*, 13, 7053-8.
- DANILA, D. C., PANTEL, K., FLEISHER, M. & SCHER, H. I. 2011c. Circulating tumors cells as biomarkers: progress toward biomarker qualification. *Cancer J*, 17, 438-50.
- DARASH-YAHANA, M., PIKARSKY, E., ABRAMOVITCH, R., ZEIRA, E., PAL, B., KARPLUS, R., BEIDER, K., AVNIEL, S., KASEM, S., GALUN, E. & PELED, A. 2004. Role of high expression levels of CXCR4 in tumor growth, vascularization, and metastasis. *Faseb j*, 18, 1240-2.
- DAY, S., COOMBES, R. C., MCGRATH-LONE, L., SCHOENBORN, C. & WARD, H. 2017. Stratified, precision or personalised medicine? Cancer services in the 'real world' of a London hospital. *Social Health Illn*, 39, 143-158.
- DE BONO, J. S., SCHER, H. I., MONTGOMERY, R. B., PARKER, C., MILLER, M. C., TISSING, H., DOYLE, G. V., TERSTAPPEN, L. W., PIENTA, K. J. & RAGHAVAN, D. 2008. Circulating tumor cells predict survival benefit from treatment in metastatic castration-resistant prostate cancer. *Clin Cancer Res*, 14, 6302-9.
- DE CRAENE, B. & BERX, G. 2013. Regulatory networks defining EMT during cancer initiation and progression. *Nat Rev Cancer*, 13, 97-110.
- DEHM, S. M., SCHMIDT, L. J., HEEMERS, H. V., VESSELLA, R. L. & TINDALL, D. J. 2008. Splicing of a novel androgen receptor exon generates a constitutively active androgen receptor that mediates prostate cancer therapy resistance. *Cancer Res*, 68, 5469-77.
- DENG, Q. & TANG, D. G. 2015. Androgen receptor and prostate cancer stem cells: biological mechanisms and clinical implications. *Endocr Relat Cancer*, 22, T209-20.
- DENG, X., XIONG, F., LI, X., XIANG, B., LI, Z., WU, X., GUO, C., LI, X., LI, Y., LI, G., XIONG, W. & ZENG, Z. 2018. Application of atomic force microscopy in cancer research. *J Nanobiotechnology*, 16, 102.
- DENIS, L. & MURPHY, G. P. 1993. Overview of phase III trials on combined androgen treatment in patients with metastatic prostate cancer. *Cancer*, 72, 3888-95.
- DENT, B. M., OGLE, L. F., O'DONNELL, R. L., HAYES, N., MALIK, U., CURTIN, N. J., BODDY, A. V., PLUMMER, E. R., EDMONDSON, R. J., REEVES, H. L., MAY, F. E. & JAMIESON, D. 2015. High-resolution imaging for the detection and characterisation of circulating tumour cells from patients with oesophageal, hepatocellular, thyroid and ovarian cancers. *Int J Cancer*.
- DHAR, M., PAO, E., RENIER, C., GO, D. E., CHE, J., MONTOYA, R., CONRAD, R., MATSUMOTO, M., HEIRICH, K., TRIBOULET, M., RAO, J., JEFFREY, S. S., GARON, E. B., GOLDMAN, J., RAO, N. P., KULKARNI, R., SOLLIER-CHRISTEN, E. & DI CARLO, D. 2016. Label-free enumeration, collection and downstream cytological and cytogenetic analysis of circulating tumor cells. *Sci Rep*, 6, 35474.
- DROST, J., KARTHAUS, W. R., GAO, D., DRIEHUIS, E., SAWYERS, C. L., CHEN, Y. & CLEVERS, H. 2016. Organoid culture systems for prostate epithelial and cancer tissue. *Nat Protoc*, 11, 347-58.
- DU, P., LIU, Y., REN, H., ZHAO, J., ZHANG, X., PATEL, R., HU, C., GAN, J. & HUANG, G. 2017. Expression of chemokine receptor CCR7 is a negative prognostic factor for patients with gastric cancer: a meta-analysis. *Gastric Cancer*, 20, 235-245.
- DUBROVSKA, A., ELLIOTT, J., SALAMONE, R. J., TELEGEEV, G. D., STAKHOVSKY, A. E., SCHEPOTIN, I. B., YAN, F., WANG, Y., BOUCHEZ, L. C., KULARATNE, S. A., WATSON, J.,

- TRUSSELL, C., REDDY, V. A., CHO, C. Y. & SCHULTZ, P. G. 2012. CXCR4 expression in prostate cancer progenitor cells. *PLoS One*, 7, e31226.
- EL-HELIEBI, A., HILLE, C., LAXMAN, N., SVEDLUND, J., HAUDUM, C., ERCAN, E., KRONEIS, T., CHEN, S., SMOLLE, M., ROSSMANN, C., KRZYWKOWSKI, T., AHLFORD, A., DARAI, E., VON AMSBERG, G., ALSDORF, W., KONIG, F., LOHR, M., DE KRUIJFF, I., RIETHDORF, S., GORGES, T. M., PANTEL, K., BAUERNHOFER, T., NILSSON, M. & SEDLMAYR, P. 2018. In Situ Detection and Quantification of AR-V7, AR-FL, PSA, and KRAS Point Mutations in Circulating Tumor Cells. *Clin Chem*, 64, 536-546.
- ELO, J. P. & VISAKORPI, T. 2001. Molecular genetics of prostate cancer. *Ann Med*, 33, 130-41.
- ENGL, T., RELJA, B., BLUMENBERG, C., MULLER, I., RINGEL, E. M., BEECKEN, W. D., JONAS, D. & BLAHETA, R. A. 2006. Prostate tumor CXC-chemokine profile correlates with cell adhesion to endothelium and extracellular matrix. *Life Sci*, 78, 1784-93.
- ENGLAND), N. C. R. A. A. S. P. H. 2016. *Survival by Stage - Cancer statistics England 2016* [Online]. Available: http://www.ncin.org.uk/publications/survival_by_stage [Accessed].
- ESCAFF, S., FERNANDEZ, J. M., GONZALEZ, L. O., SUAREZ, A., GONZALEZ-REYES, S., GONZALEZ, J. M. & VIZOSO, F. J. 2010. Study of matrix metalloproteinases and their inhibitors in prostate cancer. *Br J Cancer*, 102, 922-9.
- EVANS, H. S. & MOLLER, H. 2003. Recent trends in prostate cancer incidence and mortality in southeast England. *Eur Urol*, 43, 337-41.
- EVANS, J., GRATZER, W., MOHANDAS, N., PARKER, K. & SLEEP, J. 2008. Fluctuations of the red blood cell membrane: relation to mechanical properties and lack of ATP dependence. *Biophys J*, 94, 4134-44.
- EWING, J. 1928. Neoplastic diseases. A treatise on tumors. *American Journal of Medical Sciences*, 176.
- FABIAN, A., BAROK, M., VEREB, G. & SZOLLOSI, J. 2009. Die hard: are cancer stem cells the Bruce Willises of tumor biology? *Cytometry A*, 75, 67-74.
- FARIA, E. C., MA, N., GAZI, E., GARDNER, P., BROWN, M., CLARKE, N. W. & SNOOK, R. D. 2008. Measurement of elastic properties of prostate cancer cells using AFM. *Analyst*, 133, 1498-500.
- FERNANDO, R. I., CASTILLO, M. D., LITZINGER, M., HAMILTON, D. H. & PALENA, C. 2011. IL-8 signaling plays a critical role in the epithelial-mesenchymal transition of human carcinoma cells. *Cancer Res*, 71, 5296-306.
- FIDLER, I. J. 2003. The pathogenesis of cancer metastasis: the 'seed and soil' hypothesis revisited. *Nat Rev Cancer*, 3, 453-8.
- FIDLER, I. J. & KRIPKE, M. L. 2015. The challenge of targeting metastasis. *Cancer Metastasis Rev*, 34, 635-41.
- FINGLETON, B. 2008. MMPs as therapeutic targets--still a viable option? *Semin Cell Dev Biol*, 19, 61-8.
- FIZAZI, K., TRAN, N., FEIN, L., MATSUBARA, N., RODRIGUEZ-ANTOLIN, A., ALEKSEEV, B. Y., OZGUROGLU, M., YE, D., FEYERABEND, S., PROTHEROE, A., DE PORRE, P., KHEOH, T., PARK, Y. C., TODD, M. B. & CHI, K. N. 2017. Abiraterone plus Prednisone in Metastatic, Castration-Sensitive Prostate Cancer. *N Engl J Med*, 377, 352-360.
- FORDE, P. M. & ETTINGER, D. S. 2015. Managing acquired resistance in EGFR-mutated non-small cell lung cancer. *Clin Adv Hematol Oncol*, 13, 528-32.
- FUJIMOTO, H., SAKATA, T., HAMAGUCHI, Y., SHIGA, S., TOHYAMA, K., ICHIYAMA, S., WANG, F. S. & HOUWEN, B. 2000. Flow cytometric method for enumeration and classification of reactive immature granulocyte populations. *Cytometry*, 42, 371-8.

- GALL, T. M. & FRAMPTON, A. E. 2013. Gene of the month: E-cadherin (CDH1). *J Clin Pathol*, 66, 928-32.
- GAN, W., DAI, X., LUNARDI, A., LI, Z., INUZUKA, H., LIU, P., VARMEH, S., ZHANG, J., CHENG, L., SUN, Y., ASARA, J. M., BECK, A. H., HUANG, J., PANDOLFI, P. P. & WEI, W. 2015. SPOP Promotes Ubiquitination and Degradation of the ERG Oncoprotein to Suppress Prostate Cancer Progression. *Mol Cell*, 59, 917-30.
- GAO, D. & CHEN, Y. 2015. Organoid development in cancer genome discovery. *Curr Opin Genet Dev*, 30, 42-8.
- GAO, D., VELA, I., SBONER, A., IAQUINTA, P. J., KARTHAUS, W. R., GOPALAN, A., DOWLING, C., WANJALA, J. N., UNDVALL, E. A., ARORA, V. K., WONGVIPAT, J., KOSSAI, M., RAMAZANOGLU, S., BARBOZA, L. P., DI, W., CAO, Z., ZHANG, Q. F., SIROTA, I., RAN, L., MACDONALD, T. Y., BELTRAN, H., MOSQUERA, J. M., TOUIJER, K. A., SCARDINO, P. T., LAUDONE, V. P., CURTIS, K. R., RATHKOPF, D. E., MORRIS, M. J., DANILA, D. C., SLOVIN, S. F., SOLOMON, S. B., EASTHAM, J. A., CHI, P., CARVER, B., RUBIN, M. A., SCHER, H. I., CLEVERS, H., SAWYERS, C. L. & CHEN, Y. 2014. Organoid cultures derived from patients with advanced prostate cancer. *Cell*, 159, 176-187.
- GAO, W., BOHL, C. E. & DALTON, J. T. 2005. Chemistry and structural biology of androgen receptor. *Chem Rev*, 105, 3352-70.
- GARCIA-MURILLAS, I., SCHIAVON, G., WEIGELT, B., NG, C., HREBIEN, S., CUTTS, R. J., CHEANG, M., OSIN, P., NERURKAR, A., KOZAREWA, I., GARRIDO, J. A., DOWSETT, M., REIS-FILHO, J. S., SMITH, I. E. & TURNER, N. C. 2015. Mutation tracking in circulating tumor DNA predicts relapse in early breast cancer. *Sci Transl Med*, 7, 302ra133.
- GATENBY, R. A., GILLIES, R. J. & BROWN, J. S. 2011. Of cancer and cave fish. *Nat Rev Cancer*, 11, 237-8.
- GHAI, S. & HAIDER, M. A. 2015. Multiparametric-MRI in diagnosis of prostate cancer. *Indian J Urol*, 31, 194-201.
- GIL, J., KERAI, P., LLEONART, M., BERNARD, D., CIGUDOSA, J. C., PETERS, G., CARNERO, A. & BEACH, D. 2005. Immortalization of primary human prostate epithelial cells by c-Myc. *Cancer Res*, 65, 2179-85.
- GIL, J., STEMBALSKA, A., PESZ, K. A. & SASIADEK, M. M. 2008. Cancer stem cells: the theory and perspectives in cancer therapy. *J Appl Genet*, 49, 193-9.
- GILLESSEN, S., OMLIN, A., ATTARD, G., DE BONO, J. S., EFSTATHIOU, E., FIZAZI, K., HALABI, S., NELSON, P. S., SARTOR, O., SMITH, M. R., SOULE, H. R., AKAZA, H., BEER, T. M., BELTRAN, H., CHINNAIYAN, A. M., DAUGAARD, G., DAVIS, I. D., DE SANTIS, M., DRAKE, C. G., EELES, R. A., FANTI, S., GLEAVE, M. E., HEIDENREICH, A., HUSSAIN, M., JAMES, N. D., LECOUVET, F. E., LOGOTHETIS, C. J., MASTRIS, K., NILSSON, S., OH, W. K., OLMOS, D., PADHANI, A. R., PARKER, C., RUBIN, M. A., SCHALKEN, J. A., SCHER, H. I., SELLA, A., SHORE, N. D., SMALL, E. J., STERNBERG, C. N., SUZUKI, H., SWEENEY, C. J., TANNOCK, I. F. & TOMBAL, B. 2016. Management of patients with advanced prostate cancer: recommendations of the St Gallen Advanced Prostate Cancer Consensus Conference (APCCC) 2015. *Ann Oncol*.
- GLEGHORN, J. P., PRATT, E. D., DENNING, D., LIU, H., BANDER, N. H., TAGAWA, S. T., NANUS, D. M., GIANNAKAKOU, P. A. & KIRBY, B. J. 2010. Capture of circulating tumor cells from whole blood of prostate cancer patients using geometrically enhanced differential immunocapture (GEDI) and a prostate-specific antibody. *Lab Chip*, 10, 27-9.
- GOMEZ-ACEBO, I., DIERSSEN-SOTOS, T., FERNANDEZ-NAVARRO, P., PALAZUELOS, C., MORENO, V., ARAGONES, N., CASTANO-VINYALS, G., JIMENEZ-MONLEON, J. J., RUIZ-CERDA, J. L., PEREZ-GOMEZ, B., RUIZ-DOMINGUEZ, J. M., MOLERO, J. A., POLLAN, M.,

- KOGEVINAS, M. & LLORCA, J. 2017. Risk Model for Prostate Cancer Using Environmental and Genetic Factors in the Spanish Multi-Case-Control (MCC) Study. *Sci Rep*, 7, 8994.
- GOODMAN, O. B., JR., SYMANOWSKI, J. T., LOUDYI, A., FINK, L. M., WARD, D. C. & VOGELZANG, N. J. 2011. Circulating tumor cells as a predictive biomarker in patients with hormone-sensitive prostate cancer. *Clin Genitourin Cancer*, 9, 31-8.
- GORGES, T. M., TINHOFER, I., DROSCHE, M., ROSE, L., ZOLLNER, T. M., KRAHN, T. & VON AHSEN, O. 2012. Circulating tumour cells escape from EpCAM-based detection due to epithelial-to-mesenchymal transition. *BMC Cancer*, 12, 178.
- GORNER, K., BACHMANN, J., HOLZHAUER, C., KIRCHNER, R., RABA, K., FISCHER, J. C., MARTIGNONI, M. E., SCHIEMANN, M. & ALUNNI-FABBRONI, M. 2015. Genetic analysis of circulating tumor cells in pancreatic cancer patients: A pilot study. *Genomics*, 106, 7-14.
- GRASSO, C. S., WU, Y. M., ROBINSON, D. R., CAO, X., DHANASEKARAN, S. M., KHAN, A. P., QUIST, M. J., JING, X., LONIGRO, R. J., BRENNER, J. C., ASANGANI, I. A., ATEEQ, B., CHUN, S. Y., SIDDIQUI, J., SAM, L., ANSTETT, M., MEHRA, R., PRENSNER, J. R., PALANISAMY, N., RYSLIK, G. A., VANDIN, F., RAPHAEL, B. J., KUNJU, L. P., RHODES, D. R., PIENTA, K. J., CHINNAIYAN, A. M. & TOMLINS, S. A. 2012. The mutational landscape of lethal castration-resistant prostate cancer. *Nature*, 487, 239-43.
- GRAVDAL, K., HALVORSEN, O. J., HAUKAAS, S. A. & AKSLEN, L. A. 2007. A switch from E-cadherin to N-cadherin expression indicates epithelial to mesenchymal transition and is of strong and independent importance for the progress of prostate cancer. *Clin Cancer Res*, 13, 7003-11.
- GREAVES, M. & MALEY, C. C. 2012. Clonal evolution in cancer. *Nature*, 481, 306-13.
- GUCK, J., SCHINKINGER, S., LINCOLN, B., WOTTAWAH, F., EBERT, S., ROMEYKE, M., LENZ, D., ERICKSON, H. M., ANANTHAKRISHNAN, R., MITCHELL, D., KAS, J., ULVICK, S. & BILBY, C. 2005. Optical deformability as an inherent cell marker for testing malignant transformation and metastatic competence. *Biophys J*, 88, 3689-98.
- GUNDEM, G., VAN LOO, P., KREMEYER, B., ALEXANDROV, L. B., TUBIO, J. M., PAPAEMMANUIL, E., BREWER, D. S., KALLIO, H. M., HOGNAS, G., ANNALA, M., KIVINUMMI, K., GOODY, V., LATIMER, C., O'MEARA, S., DAWSON, K. J., ISAACS, W., EMMERT-BUCK, M. R., NYKTER, M., FOSTER, C., KOTE-JARAI, Z., EASTON, D., WHITAKER, H. C., NEAL, D. E., COOPER, C. S., EELES, R. A., VISAKORPI, T., CAMPBELL, P. J., MCDERMOTT, U., WEDGE, D. C. & BOVA, G. S. 2015. The evolutionary history of lethal metastatic prostate cancer. *Nature*, 520, 353-7.
- GUPTA, G. P. & MASSAGUE, J. 2006. Cancer metastasis: building a framework. *Cell*, 127, 679-95.
- GUPTA, V., JAFFERJI, I., GARZA, M., MELNIKOVA, V. O., HASEGAWA, D. K., PETHIG, R. & DAVIS, D. W. 2012. ApoStream(), a new dielectrophoretic device for antibody independent isolation and recovery of viable cancer cells from blood. *Biomicrofluidics*, 6, 24133.
- HAMILTON, G., RATH, B., KLAMETH, L. & HOCHMAIR, M. J. 2016. Small cell lung cancer: Recruitment of macrophages by circulating tumor cells. *Oncoimmunology*, 5, e1093277.
- HANAHAH, D. & WEINBERG, R. A. 2000. The hallmarks of cancer. *Cell*, 100, 57-70.
- HANAHAH, D. & WEINBERG, R. A. 2011. Hallmarks of cancer: the next generation. *Cell*, 144, 646-74.

- HANIN, L. & BUNIMOVICH-MENDRAZITSKY, S. 2014. Reconstruction of the natural history of metastatic cancer and assessment of the effects of surgery: Gompertzian growth of the primary tumor. *Math Biosci*, 247, 47-58.
- HAO, S. J., WAN, Y., XIA, Y. Q., ZOU, X. & ZHENG, S. Y. 2018. Size-based separation methods of circulating tumor cells. *Adv Drug Deliv Rev*, 125, 3-20.
- HAROUAKA, R., KANG, Z., ZHENG, S. Y. & CAO, L. 2014. Circulating tumor cells: Advances in isolation and analysis, and challenges for clinical applications. *Pharmacology and Therapeutics*, 141, 209-221.
- HARRIS, K. S. & KERR, B. A. 2017. Prostate Cancer Stem Cell Markers Drive Progression, Therapeutic Resistance, and Bone Metastasis. *Stem Cells Int*, 2017, 8629234.
- HAYES, D. F., CRISTOFANILLI, M., BUDD, G. T., ELLIS, M. J., STOPECK, A., MILLER, M. C., MATERA, J., ALLARD, W. J., DOYLE, G. V. & TERSTAPPEN, L. W. 2006. Circulating tumor cells at each follow-up time point during therapy of metastatic breast cancer patients predict progression-free and overall survival. *Clin Cancer Res*, 12, 4218-24.
- HAYES, J. H. & BARRY, M. J. 2014. Screening for prostate cancer with the prostate-specific antigen test: a review of current evidence. *Jama*, 311, 1143-9.
- HE, W., KULARATNE, S. A., KALLI, K. R., PRENDERGAST, F. G., AMATO, R. J., KLEE, G. G., HARTMANN, L. C. & LOW, P. S. 2008. Quantitation of circulating tumor cells in blood samples from ovarian and prostate cancer patients using tumor-specific fluorescent ligands. *Int J Cancer*, 123, 1968-73.
- HEIDENREICH A., B. P. J., BELLMUNT J., BOLLA M., JONIAU S., MASON M.D., MATVEEV V., MOTTET N., VAN DER KWAST T.H., WEIGEL T., ZATTONI F. 2013. European Association of Urology Guidelines on Prostate Cancer. *In: UROLOGY*, E. A. O. (ed.). EAU Website.
- HEITZER, E., AUER, M., GASCH, C., PICHLER, M., ULZ, P., HOFFMANN, E. M., LAX, S., WALDISPUEHL-GEIGL, J., MAUERMANN, O., LACKNER, C., HOFER, G., EISNER, F., SILL, H., SAMONIGG, H., PANTEL, K., RIETHDORF, S., BAUERNHOFER, T., GEIGL, J. B. & SPEICHER, M. R. 2013. Complex tumor genomes inferred from single circulating tumor cells by array-CGH and next-generation sequencing. *Cancer Res*, 73, 2965-75.
- HELLERSTEDT, B. A. & PIENTA, K. J. 2002. The current state of hormonal therapy for prostate cancer. *CA Cancer J Clin*, 52, 154-79.
- HEPBURN, A. C., STEELE, R. E., VEERATTERAPILLAY, R., WILSON, L., KOUNATIDOU, E. E., BARNARD, A., BERRY, P., CASSIDY, J. R., MOAD, M., EL-SHERIF, A., GAUGHAN, L., MILLS, I. G., ROBSON, C. N. & HEER, R. 2019. The induction of core pluripotency master regulators in cancers defines poor clinical outcomes and treatment resistance. *Oncogene*, 38, 4412-4424.
- HERESI, G. A., WANG, J., TAICHMAN, R., CHIRINOS, J. A., REGALADO, J. J., LICHTSTEIN, D. M. & ROSENBLATT, J. D. 2005. Expression of the chemokine receptor CCR7 in prostate cancer presenting with generalized lymphadenopathy: report of a case, review of the literature, and analysis of chemokine receptor expression. *Urol Oncol*, 23, 261-7.
- HERNANDEZ, J. R., KIM, J. J., VERDONE, J. E., LIU, X., TORGA, G., PIENTA, K. J. & MOONEY, S. M. 2015. Alternative CD44 splicing identifies epithelial prostate cancer cells from the mesenchymal counterparts. *Med Oncol*, 32, 159.
- HODGKINSON, C. L., MORROW, C. J., LI, Y., METCALF, R. L., ROTHWELL, D. G., TRAPANI, F., POLANSKI, R., BURT, D. J., SIMPSON, K. L., MORRIS, K., PEPPER, S. D., NONAKA, D., GREYSTOKE, A., KELLY, P., BOLA, B., KREBS, M. G., ANTONELLO, J., AYUB, M., FAULKNER, S., PRIEST, L., CARTER, L., TATE, C., MILLER, C. J., BLACKHALL, F., BRADY, G. & DIVE, C. 2014. Tumorigenicity and genetic profiling of circulating tumor cells in small-cell lung cancer. *Nat Med*, 20, 897-903.

- HOFMAN, V., BONNETAUD, C., ILIE, M. I., VIELH, P., VIGNAUD, J. M., FLEJOU, J. F., LANTUEJOL, S., PIATON, E., MOURAD, N., BUTORI, C., SELVA, E., POUDEX, M., SIBON, S., KELHEF, S., VENISSAC, N., JAIS, J. P., MOURoux, J., MOLINA, T. J. & HOFMAN, P. 2011. Preoperative circulating tumor cell detection using the isolation by size of epithelial tumor cell method for patients with lung cancer is a new prognostic biomarker. *Clin Cancer Res*, 17, 827-35.
- HONG, H., HE, C., ZHU, S., ZHANG, Y., WANG, X., SHE, F. & CHEN, Y. 2016a. CCR7 mediates the TNF-alpha-induced lymphatic metastasis of gallbladder cancer through the "ERK1/2 - AP-1" and "JNK - AP-1" pathways. *J Exp Clin Cancer Res*, 35, 51.
- HONG, H., JIANG, L., LIN, Y., HE, C., ZHU, G., DU, Q., WANG, X., SHE, F. & CHEN, Y. 2016b. TNF-alpha promotes lymphangiogenesis and lymphatic metastasis of gallbladder cancer through the ERK1/2/AP-1/VEGF-D pathway. *BMC Cancer*, 16, 240.
- HOOGLAND, A. M., VERHOEF, E. I., ROOBOL, M. J., SCHRODER, F. H., WILDHAGEN, M. F., VAN DER KWAST, T. H., JENSTER, G. & VAN LEENDERS, G. J. 2014. Validation of stem cell markers in clinical prostate cancer: alpha6-integrin is predictive for non-aggressive disease. *Prostate*, 74, 488-96.
- HU, B., ROCHEFORT, H. & GOLDKORN, A. 2013. Circulating tumor cells in prostate cancer. *Cancers (Basel)*, 5, 1676-90.
- HU, R., DUNN, T. A., WEI, S., ISHARWAL, S., VELTRI, R. W., HUMPHREYS, E., HAN, M., PARTIN, A. W., VESSELLA, R. L., ISAACS, W. B., BOVA, G. S. & LUO, J. 2009. Ligand-independent androgen receptor variants derived from splicing of cryptic exons signify hormone-refractory prostate cancer. *Cancer Res*, 69, 16-22.
- HVICHIA, G. E., PARVEEN, Z., WAGNER, C., JANNING, M., QUIDDE, J., STEIN, A., MULLER, V., LOGES, S., NEVES, R. P., STOECKLEIN, N. H., WIKMAN, H., RIETHDORF, S., PANTEL, K. & GORGES, T. M. 2016. A novel microfluidic platform for size and deformability based separation and the subsequent molecular characterization of viable circulating tumor cells. *Int J Cancer*, 138, 2894-904.
- HWANG, E., UH, J. H., LEE, H. S., LEE, C. H., LEE, S. J., AHN, S. H., SON, B. H., LEE, J. W., YU, J. H., KWON, N. J., LEE, W. C., YANG, K. S., CHOI, S. H., KIM, M. S., LEE, J. & JEON, B. H. 2017. Cancer gene panel analysis of cultured circulating tumor cells and primary tumor tissue from patients with breast cancer. *Oncol Lett*, 13, 4627-4632.
- IMAMURA, Y., SAKAMOTO, S., ENDO, T., UTSUMI, T., FUSE, M., SUYAMA, T., KAWAMURA, K., IMAMOTO, T., YANO, K., UZAWA, K., NIHEI, N., SUZUKI, H., MIZOKAMI, A., UEDA, T., SEKI, N., TANZAWA, H. & ICHIKAWA, T. 2012. FOXA1 promotes tumor progression in prostate cancer via the insulin-like growth factor binding protein 3 pathway. *PLoS One*, 7, e42456.
- INCORVAIA, L., BADALAMENTI, G., RINI, G., ARCARA, C., FRICANO, S., SFERRAZZA, C., DI TRAPANI, D., GEBBIA, N. & LETO, G. 2007. MMP-2, MMP-9 and activin A blood levels in patients with breast cancer or prostate cancer metastatic to the bone. *Anticancer Res*, 27, 1519-25.
- INSTITUTE, T. W. T. S. 2018. The Catalogue of Somatic Mutations in Cancer (COSMIC).
- ISRAELI, R. S., POWELL, C. T., CORR, J. G., FAIR, W. R. & HESTON, W. D. 1994. Expression of the prostate-specific membrane antigen. *Cancer Res*, 54, 1807-11.
- ITO, K. 2014. Prostate cancer in Asian men. *Nat Rev Urol*, 11, 197-212.
- JAMASPISHVILI, T., BERMAN, D. M., ROSS, A. E., SCHER, H. I., DE MARZO, A. M., SQUIRE, J. A. & LOTAN, T. L. 2018. Clinical implications of PTEN loss in prostate cancer. *Nat Rev Urol*, 15, 222-234.
- JAMES, N. D., SPEARS, M. R., CLARKE, N. W., DEARNALEY, D. P., DE BONO, J. S., GALE, J., HETHERINGTON, J., HOSKIN, P. J., JONES, R. J., LAING, R., LESTER, J. F., MCLAREN, D.,

- PARKER, C. C., PARMAR, M. K. B., RITCHIE, A. W. S., RUSSELL, J. M., STREBEL, R. T., THALMANN, G. N., MASON, M. D. & SYDES, M. R. 2015. Survival with Newly Diagnosed Metastatic Prostate Cancer in the "Docetaxel Era": Data from 917 Patients in the Control Arm of the STAMPEDE Trial (MRC PR08, CRUK/06/019). *Eur Urol*, 67, 1028-1038.
- JAMUR, M. C. & OLIVER, C. 2010. Permeabilization of cell membranes. *Methods Mol Biol*, 588, 63-6.
- JANEAWAY, C. 2001. *Immunobiology*, Garland.
- JIANG, Y., PALMA, J. F., AGUS, D. B., WANG, Y. & GROSS, M. E. 2010. Detection of androgen receptor mutations in circulating tumor cells in castration-resistant prostate cancer. *Clin Chem*, 56, 1492-5.
- JOHNS, L. E. & HOULSTON, R. S. 2003. A systematic review and meta-analysis of familial prostate cancer risk. *BJU Int*, 91, 789-94.
- JUNTILLA, M. R. & DE SAUVAGE, F. J. 2013. Influence of tumour micro-environment heterogeneity on therapeutic response. *Nature*, 501, 346-54.
- KAGAN, M., HOWARD, D., BENDELE, T., MAYES, J., SILVIA, J., REPOLLET, M., DOYLE, J., ALLARD, J., TU, N., BUI, T., RUSSELL, T., RAO, C., HERMANN, M., RUTNER, H. & TERSTAPPEN, L. W. M. M. 2002. A sample preparation and analysis system for identification of circulating tumor cells. *Journal of Clinical Ligand Assay*, 25, 104-110.
- KAHNG, J., KIM, Y., KIM, M., OH, E. J., PARK, Y. J. & HAN, K. 2015. Flow cytometric white blood cell differential using CytoDiff is excellent for counting blasts. *Ann Lab Med*, 35, 28-34.
- KAITTANIS, C., ANDREOU, C., HIERONYMUS, H., MAO, N., FOSS, C. A., EIBER, M., WEIRICH, G., PANCHAL, P., GOPALAN, A., ZURITA, J., ACHILEFU, S., CHIOSIS, G., PONOMAREV, V., SCHWAIGER, M., CARVER, B. S., POMPER, M. G. & GRIMM, J. 2018. Correction: Prostate-specific membrane antigen cleavage of vitamin B9 stimulates oncogenic signaling through metabotropic glutamate receptors. *J Exp Med*, 215, 377.
- KAKINUMA, T. & HWANG, S. T. 2006. Chemokines, chemokine receptors, and cancer metastasis. *J Leukoc Biol*, 79, 639-51.
- KANG, Q., HENRY, N. L., PAOLETTI, C., JIANG, H., VATS, P., CHINNAIYAN, A. M., HAYES, D. F., MERAJVER, S. D., RAE, J. M. & TEWARI, M. 2016. Comparative analysis of circulating tumor DNA stability In K3EDTA, Streck, and CellSave blood collection tubes. *Clin Biochem*, 49, 1354-1360.
- KARTHAUS, W. R., IAQUINTA, P. J., DROST, J., GRACANIN, A., VAN BOXTEL, R., WONGVIPAT, J., DOWLING, C. M., GAO, D., BEGTHEL, H., SACHS, N., VRIES, R. G. J., CUPPEN, E., CHEN, Y., SAWYERS, C. L. & CLEVERS, H. C. 2014. Identification of multipotent luminal progenitor cells in human prostate organoid cultures. *Cell*, 159, 163-175.
- KASIVISVANATHAN, V., RANNIKKO, A. S., BORGHI, M., PANEBIANCO, V., MYNDERSE, L. A., VAARALA, M. H., BRIGANTI, A., BUDAUS, L., HELLAWELL, G., HINDLEY, R. G., ROOBOL, M. J., EGENER, S., GHEI, M., VILLERS, A., BLADOU, F., VILLEIRS, G. M., VIRDI, J., BOXLER, S., ROBERT, G., SINGH, P. B., VENDERINK, W., HADASCHIK, B. A., RUFFION, A., HU, J. C., MARGOLIS, D., CROUZET, S., KLOTZ, L., TANEJA, S. S., PINTO, P., GILL, I., ALLEN, C., GIGANTI, F., FREEMAN, A., MORRIS, S., PUNWANI, S., WILLIAMS, N. R., BREW-GRAVES, C., DEEKS, J., TAKWOINGI, Y., EMBERTON, M. & MOORE, C. M. 2018. MRI-Targeted or Standard Biopsy for Prostate-Cancer Diagnosis. *N Engl J Med*, 378, 1767-1777.
- KATOH, M., IGARASHI, M., FUKUDA, H., NAKAGAMA, H. & KATOH, M. 2013. Cancer genetics and genomics of human FOX family genes. *Cancer Lett*, 328, 198-206.

- KELLER, E. T., ERSHLER, W. B. & CHANG, C. 1996. The androgen receptor: a mediator of diverse responses. *Front Biosci*, 1, d59-71.
- KERR, B. A., MIOCINOVIC, R., SMITH, A. K., WEST, X. Z., WATTS, K. E., ALZAYED, A. W., KLINK, J. C., MIR, M. C., STUREY, T., HANSEL, D. E., HESTON, W. D., STEPHENSON, A. J., KLEIN, E. A. & BYZOVA, T. V. 2015. CD117(+) cells in the circulation are predictive of advanced prostate cancer. *Oncotarget*, 6, 1889-97.
- KHEIRANDISH, P. & CHINEGWUNDOH, F. 2011. Ethnic differences in prostate cancer. *Br J Cancer*, 105, 481-5.
- KIM, M. Y., OSKARSSON, T., ACHARYYA, S., NGUYEN, D. X., ZHANG, X. H., NORTON, L. & MASSAGUE, J. 2009. Tumor self-seeding by circulating cancer cells. *Cell*, 139, 1315-26.
- KITZ, J., LOWES, L. E., GOODALE, D. & ALLAN, A. L. 2018. Circulating Tumor Cell Analysis in Preclinical Mouse Models of Metastasis. *Diagnostics (Basel)*, 8.
- KLARMANN, G. J., HURT, E. M., MATHEWS, L. A., ZHANG, X., DUHAGON, M. A., MISTREE, T., THOMAS, S. B. & FARRAR, W. L. 2009. Invasive prostate cancer cells are tumor initiating cells that have a stem cell-like genomic signature. *Clin Exp Metastasis*, 26, 433-46.
- KLEIN, C. A. 2008. Cancer. The metastasis cascade. *Science*, 321, 1785-7.
- KLEIN, C. A. 2013. Selection and adaptation during metastatic cancer progression. *Nature*, 501, 365-72.
- KOLOSTOVA, K., CEGAN, M. & BOBEK, V. 2014. Circulating tumour cells in patients with urothelial tumours: Enrichment and in vitro culture. *Can Urol Assoc J*, 8, E715-20.
- KOLOSTOVA, K., SPICKA, J., MATKOWSKI, R. & BOBEK, V. 2015. Isolation, primary culture, morphological and molecular characterization of circulating tumor cells in gynecological cancers. *Am J Transl Res*, 7, 1203-13.
- KONG, D., LI, Y., WANG, Z. & SARKAR, F. H. 2011. Cancer Stem Cells and Epithelial-to-Mesenchymal Transition (EMT)-Phenotypic Cells: Are They Cousins or Twins? *Cancers (Basel)*, 3, 716-29.
- KRAL, M., ROSINSKA, V., STUDENT, V., GREPL, M., HRABEC, M. & BOUCHAL, J. 2011. Genetic determinants of prostate cancer: a review. *Biomed Pap Med Fac Univ Palacky Olomouc Czech Repub*, 155, 3-9.
- KULASINGHE, A., PERRY, C., WARKIANI, M. E., BLICK, T., DAVIES, A., O'BYRNE, K., THOMPSON, E. W., NELSON, C. C., VELA, I. & PUNYADEERA, C. 2016. Short term ex-vivo expansion of circulating head and neck tumour cells. *Oncotarget*, 7, 60101-60109.
- KUMAR, A., SHENDURE, J. & NELSON, P. S. 2011. Genome interrupted: sequencing of prostate cancer reveals the importance of chromosomal rearrangements. *Genome Med*, 3, 23.
- KUZNETSOVA, T. G., STARODUBTSEVA, M. N., YEGORENKOV, N. I., CHIZHIK, S. A. & ZHDANOV, R. I. 2007. Atomic force microscopy probing of cell elasticity. *Micron*, 38, 824-33.
- LANG, S. H., FRAME, F. M. & COLLINS, A. T. 2009. Prostate cancer stem cells. *J Pathol*, 217, 299-306.
- LARSEN, S. K., GAO, Y. & BASSE, P. H. 2014. NK cells in the tumor microenvironment. *Crit Rev Oncog*, 19, 91-105.
- LAWRENCE, M. S., STOJANOV, P., POLAK, P., KRYUKOV, G. V., CIBULSKIS, K., SIVACHENKO, A., CARTER, S. L., STEWART, C., MERMEL, C. H., ROBERTS, S. A., KIEZUN, A., HAMMERMAN, P. S., MCKENNA, A., DRIER, Y., ZOU, L., RAMOS, A. H., PUGH, T. J., STRANSKY, N., HELMAN, E., KIM, J., SOUGNEZ, C., AMBROGIO, L., NICKERSON, E.,

- SHEFLER, E., CORTES, M. L., AUCLAIR, D., SAKSENA, G., VOET, D., NOBLE, M., DICARA, D., LIN, P., LICHTENSTEIN, L., HEIMAN, D. I., FENNELL, T., IMIELINSKI, M., HERNANDEZ, B., HODIS, E., BACA, S., DULAK, A. M., LOHR, J., LANDAU, D. A., WU, C. J., MELENDEZ-ZAJGLA, J., HIDALGO-MIRANDA, A., KOREN, A., MCCARROLL, S. A., MORA, J., LEE, R. S., CROMPTON, B., ONOFRIO, R., PARKIN, M., WINCKLER, W., ARDLIE, K., GABRIEL, S. B., ROBERTS, C. W., BIEGEL, J. A., STEGMAIER, K., BASS, A. J., GARRAWAY, L. A., MEYERSON, M., GOLUB, T. R., GORDENIN, D. A., SUNYAEV, S., LANDER, E. S. & GETZ, G. 2013. Mutational heterogeneity in cancer and the search for new cancer-associated genes. *Nature*, 499, 214-8.
- LEIBOVICI, D., SPIESS, P. E., AGARWAL, P. K., TU, S. M., PETTAWAY, C. A., HITZHUSEN, K., MILLIKAN, R. E. & PISTERS, L. L. 2007. Prostate cancer progression in the presence of undetectable or low serum prostate-specific antigen level. *Cancer*, 109, 198-204.
- LEITZMANN, M. F. & ROHRMANN, S. 2012. Risk factors for the onset of prostatic cancer: age, location, and behavioral correlates. *Clin Epidemiol*, 4, 1-11.
- LEKKA, M. & LAIDLER, P. 2009. Applicability of AFM in cancer detection. *Nat Nanotechnol*, 4, 72; author reply 72-3.
- LEON-MATEOS, L., VIEITO, M., ANIDO, U., LOPEZ LOPEZ, R. & MUINELO ROMAY, L. 2016. Clinical Application of Circulating Tumour Cells in Prostate Cancer: From Bench to Bedside and Back. *Int J Mol Sci*, 17.
- LEVERSHA, M. A., HAN, J., ASGARI, Z., DANILA, D. C., LIN, O., GONZALEZ-ESPINOZA, R., ANAND, A., LILJA, H., HELLER, G., FLEISHER, M. & SCHER, H. I. 2009. Fluorescence in situ hybridization analysis of circulating tumor cells in metastatic prostate cancer. *Clin Cancer Res*, 15, 2091-7.
- LI, Q. S., LEE, G. Y., ONG, C. N. & LIM, C. T. 2008. AFM indentation study of breast cancer cells. *Biochem Biophys Res Commun*, 374, 609-13.
- LI, Y. M., XU, S. C., LI, J., HAN, K. Q., PI, H. F., ZHENG, L., ZUO, G. H., HUANG, X. B., LI, H. Y., ZHAO, H. Z., YU, Z. P., ZHOU, Z. & LIANG, P. 2013. Epithelial-mesenchymal transition markers expressed in circulating tumor cells in hepatocellular carcinoma patients with different stages of disease. *Cell Death Dis*, 4, e831.
- LIAO, D., CORLE, C., SEAGROVES, T. N. & JOHNSON, R. S. 2007. Hypoxia-inducible factor-1alpha is a key regulator of metastasis in a transgenic model of cancer initiation and progression. *Cancer Res*, 67, 563-72.
- LIGTHART, S. T., COUMANS, F. A., BIDARD, F. C., SIMKENS, L. H., PUNT, C. J., DE GROOT, M. R., ATTARD, G., DE BONO, J. S., PIERGA, J. Y. & TERSTAPPEN, L. W. 2013. Circulating Tumor Cells Count and Morphological Features in Breast, Colorectal and Prostate Cancer. *PLoS One*, 8, e67148.
- LILJA, H. 1988. Structure and function of prostatic- and seminal vesicle-secreted proteins involved in the gelation and liquefaction of human semen. *Scand J Clin Lab Invest Suppl*, 191, 13-20.
- LILJA, H. 1993. Structure, function, and regulation of the enzyme activity of prostate-specific antigen. *World J Urol*, 11, 188-91.
- LIM, K. B. 2017. Epidemiology of clinical benign prostatic hyperplasia. *Asian J Urol*, 4, 148-151.
- LIN, D. W., PORTER, M. & MONTGOMERY, B. 2009. Treatment and survival outcomes in young men diagnosed with prostate cancer: a Population-based Cohort Study. *Cancer*, 115, 2863-71.
- LINDLEY, L. E. & BRIEGEL, K. J. 2010. Molecular characterization of TGFbeta-induced epithelial-mesenchymal transition in normal finite lifespan human mammary epithelial cells. *Biochem Biophys Res Commun*, 399, 659-64.

- LITVINOV, S. V., VELDERS, M. P., BAKKER, H. A., FLEUREN, G. J. & WARNAAR, S. O. 1994. Ep-CAM: a human epithelial antigen is a homophilic cell-cell adhesion molecule. *J Cell Biol*, 125, 437-46.
- LO, U. G., LEE, C. F., LEE, M. S. & HSIEH, J. T. 2017. The Role and Mechanism of Epithelial-to-Mesenchymal Transition in Prostate Cancer Progression. *Int J Mol Sci*, 18.
- LOCKE, J. A., ZAFARANA, G., ISHKANIAN, A. S., MILOSEVIC, M., THOMS, J., HAVE, C. L., MALLOFF, C. A., LAM, W. L., SQUIRE, J. A., PINTILIE, M., SYKES, J., RAMNARINE, V. R., MENG, A., AHMED, O., JURISICA, I., VAN DER KWAST, T. & BRISTOW, R. G. 2012. NKX3.1 haploinsufficiency is prognostic for prostate cancer relapse following surgery or image-guided radiotherapy. *Clin Cancer Res*, 18, 308-16.
- LOPEZ-RIQUELME, N., MINGUELA, A., VILLAR-PERMUY, F., CIPRIAN, D., CASTILLEJO, A., ALVAREZ-LOPEZ, M. R. & SOTO, J. L. 2013. Imaging cytometry for counting circulating tumor cells: comparative analysis of the CellSearch vs ImageStream systems. *Apmis*, 121, 1139-43.
- LOPICCOLO, J., BLUMENTHAL, G. M., BERNSTEIN, W. B. & DENNIS, P. A. 2008. Targeting the PI3K/Akt/mTOR pathway: effective combinations and clinical considerations. *Drug Resist Updat*, 11, 32-50.
- LORENTE, D., OLMOS, D., MATEO, J., DOLLING, D., BIANCHINI, D., SEED, G., FLOHR, P., CRESPO, M., FIGUEIREDO, I., MIRANDA, S., SCHER, H. I., TERSTAPPEN, L. & DE BONO, J. S. 2018. Circulating tumour cell increase as a biomarker of disease progression in metastatic castration-resistant prostate cancer patients with low baseline CTC counts. *Ann Oncol*, 29, 1554-1560.
- LOWES, L. E. & ALLAN, A. L. 2014. Recent advances in the molecular characterization of circulating tumor cells. *Cancers*, 6, 595-624.
- LU, Y., LIANG, H., YU, T., XIE, J., CHEN, S., DONG, H., SINKO, P. J., LIAN, S., XU, J., WANG, J., YU, S., SHAO, J., YUAN, B., WANG, L. & JIA, L. 2015. Isolation and characterization of living circulating tumor cells in patients by immunomagnetic negative enrichment coupled with flow cytometry. *Cancer*, 121, 3036-45.
- LU, Y. T., ZHAO, L., SHEN, Q., GARCIA, M. A., WU, D., HOU, S., SONG, M., XU, X., OUYANG, W. H., OUYANG, W. W., LICHTERMAN, J., LUO, Z., XUAN, X., HUANG, J., CHUNG, L. W., RETTIG, M., TSENG, H. R., SHAO, C. & POSADAS, E. M. 2013. NanoVelcro Chip for CTC enumeration in prostate cancer patients. *Methods*, 64, 144-52.
- LUCIA, M. S., DARKE, A. K., GOODMAN, P. J., LA ROSA, F. G., PARNES, H. L., FORD, L. G., COLTMAN, C. A., JR. & THOMPSON, I. M. 2008. Pathologic characteristics of cancers detected in The Prostate Cancer Prevention Trial: implications for prostate cancer detection and chemoprevention. *Cancer Prev Res (Phila)*, 1, 167-73.
- LUO, Q., KUANG, D., ZHANG, B. & SONG, G. 2016. Cell stiffness determined by atomic force microscopy and its correlation with cell motility. *Biochim Biophys Acta*, 1860, 1953-60.
- LV, Q., GONG, L., ZHANG, T., YE, J., CHAI, L., NI, C. & MAO, Y. 2016. Prognostic value of circulating tumor cells in metastatic breast cancer: a systemic review and meta-analysis. *Clin Transl Oncol*, 18, 322-30.
- MA, Z., XIN, Z., HU, W., JIANG, S., YANG, Z., YAN, X., LI, X., YANG, Y. & CHEN, F. 2018. Forkhead box O proteins: Crucial regulators of cancer EMT. *Semin Cancer Biol*, 50, 21-31.
- MAGBANUA, M. J., SOSA, E. V., SCOTT, J. H., SIMKO, J., COLLINS, C., PINKEL, D., RYAN, C. J. & PARK, J. W. 2012. Isolation and genomic analysis of circulating tumor cells from castration resistant metastatic prostate cancer. *BMC Cancer*, 12, 78.

- MAHESWARAN, S. & HABER, D. A. 2010. Circulating tumor cells: a window into cancer biology and metastasis. *Curr Opin Genet Dev*, 20, 96-9.
- MAJUMDER, P. K. & SELLERS, W. R. 2005. Akt-regulated pathways in prostate cancer. *Oncogene*, 24, 7465-74.
- MALEKI, M., GHANBARVAND, F., REZA BEHVARZ, M., EJTEMAEI, M. & GHADIRKHOMI, E. 2014. Comparison of mesenchymal stem cell markers in multiple human adult stem cells. *Int J Stem Cells*, 7, 118-26.
- MANI, S. A., GUO, W., LIAO, M. J., EATON, E. N., AYYANAN, A., ZHOU, A. Y., BROOKS, M., REINHARD, F., ZHANG, C. C., SHIPITSIN, M., CAMPBELL, L. L., POLYAK, K., BRISKEN, C., YANG, J. & WEINBERG, R. A. 2008. The epithelial-mesenchymal transition generates cells with properties of stem cells. *Cell*, 133, 704-15.
- MAOLAKE, A., IZUMI, K., NATSAGDORJ, A., IWAMOTO, H., KADOMOTO, S., MAKINO, T., NAITO, R., SHIGEHARA, K., KADONO, Y., HIRATSUKA, K., WUFUER, G., NASTIUK, K. L. & MIZOKAMI, A. 2018. Tumor necrosis factor-alpha induces prostate cancer cell migration in lymphatic metastasis through CCR7 upregulation. *Cancer Sci*, 109, 1524-1531.
- MARRINUCCI, D., BETHEL, K., KOLATKAR, A., LUTTGEN, M. S., MALCHIODI, M., BAEHRING, F., VOIGT, K., LAZAR, D., NIEVA, J., BAZHENOVA, L., KO, A. H., KORN, W. M., SCHRAM, E., COWARD, M., YANG, X., METZNER, T., LAMY, R., HONNATTI, M., YOSHIOKA, C., KUNKEN, J., PETROVA, Y., SOK, D., NELSON, D. & KUHN, P. 2012. Fluid biopsy in patients with metastatic prostate, pancreatic and breast cancers. *Phys Biol*, 9, 016003.
- MATIN, F., JEET, V., MOYA, L., SELTH, L. A., CHAMBERS, S., CLEMENTS, J. A. & BATRA, J. 2018. A Plasma Biomarker Panel of Four MicroRNAs for the Diagnosis of Prostate Cancer. *Sci Rep*, 8, 6653.
- MATSIKA, A., SRINIVASAN, B., DAY, C., MADER, S. A., KIERNAN, D. M., BROOMFIELD, A., FU, J., HOOPER, J. D., KENCH, J. G. & SAMARATUNGA, H. 2015. Cancer stem cell markers in prostate cancer: an immunohistochemical study of ALDH1, SOX2 and EZH2. *Pathology*, 47, 622-8.
- MAY, C. D., SPHYRIS, N., EVANS, K. W., WERDEN, S. J., GUO, W. & MANI, S. A. 2011. Epithelial-mesenchymal transition and cancer stem cells: a dangerously dynamic duo in breast cancer progression. *Breast Cancer Res*, 13, 202.
- MCNEAL, J. E. 1968. Regional morphology and pathology of the prostate. *Am J Clin Pathol*, 49, 347-57.
- MCNEAL, J. E. 1988. Normal histology of the prostate. *Am J Surg Pathol*, 12, 619-33.
- MEACHAM, C. E. & MORRISON, S. J. 2013. Tumour heterogeneity and cancer cell plasticity. *Nature*, 501, 328-37.
- MEGO, M., GIORGI, U. D., DAWOOD, S., WANG, X., VALERO, V., ANDREOPOULOU, E., HANDY, B., UENO, N. T., REUBEN, J. M. & CRISTOFANILLI, M. 2011. Characterization of metastatic breast cancer patients with nondetectable circulating tumor cells. *International Journal of Cancer*, 129, 417-423.
- MEHRA, R., TOMLINS, S. A., YU, J., CAO, X., WANG, L., MENON, A., RUBIN, M. A., PIENTA, K. J., SHAH, R. B. & CHINNAIYAN, A. M. 2008. Characterization of TMPRSS2-ETS gene aberrations in androgen-independent metastatic prostate cancer. *Cancer Res*, 68, 3584-90.
- MEI, L., SMITH, S. C., FABER, A. C., TRENT, J., GROSSMAN, S. R., STRATAKIS, C. A. & BOIKOS, S. A. 2018. Gastrointestinal Stromal Tumors: The GIST of Precision Medicine. *Trends Cancer*, 4, 74-91.

- MELLER, B., BREMMER, F., SAHLMANN, C. O., HIJAZI, S., BOUTER, C., TROJAN, L., MELLER, J. & THELEN, P. 2015. Alterations in androgen deprivation enhanced prostate-specific membrane antigen (PSMA) expression in prostate cancer cells as a target for diagnostics and therapy. *EJNMMI Res*, 5, 66.
- METCALFE, C., PATEL, B., EVANS, S., IBRAHIM, F., ANSON, K., CHINEGWUNDOH, F., CORBISHLEY, C., DORLING, D., THOMAS, B., GILLATT, D., KIRBY, R., MUIR, G., NARGUND, V., POPERT, R., PERSAD, R. & BEN-SHLOMO, Y. 2008. The risk of prostate cancer amongst South Asian men in southern England: the PROCESS cohort study. *BJU Int*, 102, 1407-12.
- MILLER, M. C., ROBINSON, P. S., WAGNER, C. & O'SHANNESY, D. J. 2018. The Parsortix Cell Separation System-A versatile liquid biopsy platform. *Cytometry A*, 93, 1234-1239.
- MIYAMOTO, D. T., LEE, R. J., STOTT, S. L., TING, D. T., WITTNER, B. S., ULMAN, M., SMAS, M. E., LORD, J. B., BRANNIGAN, B. W., TRAUTWEIN, J., BANDER, N. H., WU, C. L., SEQUIST, L. V., SMITH, M. R., RAMASWAMY, S., TONER, M., MAHESWARAN, S. & HABER, D. A. 2012. Androgen receptor signaling in circulating tumor cells as a marker of hormonally responsive prostate cancer. *Cancer Discovery*, 2, 995-1003.
- MIYAMOTO, D. T., ZHENG, Y., WITTNER, B. S., LEE, R. J., ZHU, H., BRODERICK, K. T., DESAI, R., FOX, D. B., BRANNIGAN, B. W., TRAUTWEIN, J., ARORA, K. S., DESAI, N., DAHL, D. M., SEQUIST, L. V., SMITH, M. R., KAPUR, R., WU, C. L., SHIODA, T., RAMASWAMY, S., TING, D. T., TONER, M., MAHESWARAN, S. & HABER, D. A. 2015. RNA-Seq of single prostate CTCs implicates noncanonical Wnt signaling in antiandrogen resistance. *Science*, 349, 1351-6.
- MIYAZAWA, K., TANAKA, T., NAKAI, D., MORITA, N. & SUZUKI, K. 2014. Immunohistochemical expression of four different stem cell markers in prostate cancer: High expression of NANOG in conjunction with hypoxia-inducible factor-1alpha expression is involved in prostate epithelial malignancy. *Oncol Lett*, 8, 985-992.
- MOCHIZUKI, H., MATSUBARA, A., TEISHIMA, J., MUTAGUCHI, K., YASUMOTO, H., DAHIYA, R., USUI, T. & KAMIYA, K. 2004. Interaction of ligand-receptor system between stromal-cell-derived factor-1 and CXC chemokine receptor 4 in human prostate cancer: a possible predictor of metastasis. *Biochem Biophys Res Commun*, 320, 656-63.
- MOLECULES, H. C. D. 2019. *HCDM* [Online]. Available: <http://www.hcdm.org/index.php> [Accessed].
- MORROW, C. J., TRAPANI, F., METCALF, R. L., BERTOLINI, G., HODGKINSON, C. L., KHANDELWAL, G., KELLY, P., GALVIN, M., CARTER, L., SIMPSON, K. L., WILLIAMSON, S., WIRTH, C., SIMMS, N., FRANKLILN, L., FRESE, K. K., ROTHWELL, D. G., NONAKA, D., MILLER, C. J., BRADY, G., BLACKHALL, F. H. & DIVE, C. 2016. Tumourigenic non-small-cell lung cancer mesenchymal circulating tumour cells: a clinical case study. *Ann Oncol*, 27, 1155-60.
- MOZAFARI, M. R., REED, C. J., ROSTRON, C. & HASIRCI, V. 2005. A review of scanning probe microscopy investigations of liposome-DNA complexes. *J Liposome Res*, 15, 93-107.
- MULLER, V., STAHMANN, N., RIETHDORF, S., RAU, T., ZABEL, T., GOETZ, A., JANICKE, F. & PANTEL, K. 2005. Circulating tumor cells in breast cancer: correlation to bone marrow micrometastases, heterogeneous response to systemic therapy and low proliferative activity. *Clin Cancer Res*, 11, 3678-85.
- MURPHY, G. P., SNOW, P. B., BRANDT, J., ELGAMAL, A. & BRAWER, M. K. 2000. Evaluation of prostate cancer patients receiving multiple staging tests, including ProstaScint scintiscans. *Prostate*, 42, 145-9.
- MURPHY, M. F., LILLEY, F., LALOR, M. J., CROSBY, S. R., MADDEN, G., JOHNSTON, G. & BURTON, D. R. 2013. Evaluation of a nonlinear Hertzian-based model reveals prostate

- cancer cells respond differently to force than normal prostate cells. *Microsc Res Tech*, 76, 36-41.
- NAGRATH, S., SEQUIST, L. V., MAHESWARAN, S., BELL, D. W., IRIMIA, D., ULKUS, L., SMITH, M. R., KWAK, E. L., DIGUMARTHY, S., MUZIKANSKY, A., RYAN, P., BALIS, U. J., TOMPKINS, R. G., HABER, D. A. & TONER, M. 2007. Isolation of rare circulating tumour cells in cancer patients by microchip technology. *Nature*, 450, 1235-9.
- NAKANO, A., HARADA, T., MORIKAWA, S. & KATO, Y. 1990. Expression of leukocyte common antigen (CD45) on various human leukemia/lymphoma cell lines. *Acta Pathol Jpn*, 40, 107-15.
- NATHOO, N., CARIS, E. C., WIENER, J. A. & MENDEL, E. 2011. History of the vertebral venous plexus and the significant contributions of Breschet and Batson. *Neurosurgery*, 69, 1007-14; discussion 1014.
- NI, J., COZZI, P., HAO, J., BERETOV, J., CHANG, L., DUAN, W., SHIGDAR, S., DELPRADO, W., GRAHAM, P., BUCCI, J., KEARSLEY, J. & LI, Y. 2013. Epithelial cell adhesion molecule (EpCAM) is associated with prostate cancer metastasis and chemo/radioresistance via the PI3K/Akt/mTOR signaling pathway. *Int J Biochem Cell Biol*, 45, 2736-48.
- NIFOROU, K. M., ANAGNOSTOPOULOS, A. K., VOUGAS, K., KITTAS, C., GORGOLIS, V. G. & TSANGARIS, G. T. 2008. The proteome profile of the human osteosarcoma U2OS cell line. *Cancer Genomics Proteomics*, 5, 63-78.
- NISHIDA, C., KUSUBATA, K., TASHIRO, Y., GRITLI, I., SATO, A., OHKI-KOIZUMI, M., MORITA, Y., NAGANO, M., SAKAMOTO, T., KOSHIKAWA, N., KUCHIMARU, T., KIZAKA-KONDOH, S., SEIKI, M., NAKAUCHI, H., HEISSIG, B. & HATTORI, K. 2012. MT1-MMP plays a critical role in hematopoiesis by regulating HIF-mediated chemokine/cytokine gene transcription within niche cells. *Blood*, 119, 5405-16.
- NOWELL, P. C. 1976. The clonal evolution of tumor cell populations. *Science*, 194, 23-8.
- O'CONNOR, J. E., CALLAGHAN, R. C., ESCUDERO, M., HERRERA, G., MARTINEZ, A., MONTEIRO, M. D. & MONTOLIU, H. 2001. The relevance of flow cytometry for biochemical analysis. *IUBMB Life*, 51, 231-9.
- OAKLEY-GIRVAN, I., KOLONEL, L. N., GALLAGHER, R. P., WU, A. H., FELBERG, A. & WHITTEMORE, A. S. 2003. Stage at diagnosis and survival in a multiethnic cohort of prostate cancer patients. *Am J Public Health*, 93, 1753-9.
- ODERO-MARAH, V., HAWSAWI, O., HENDERSON, V. & SWEENEY, J. 2018. Epithelial-Mesenchymal Transition (EMT) and Prostate Cancer. *Adv Exp Med Biol*, 1095, 101-110.
- OKTEM, G., BILIR, A., USLU, R., INAN, S. V., DEMIRAY, S. B., ATMACA, H., AYLA, S., SERCAN, O. & UYSAL, A. 2014. Expression profiling of stem cell signaling alters with spheroid formation in CD133(high)/CD44(high) prostate cancer stem cells. *Oncol Lett*, 7, 2103-2109.
- OLMOS, D., BREWER, D., CLARK, J., DANILA, D. C., PARKER, C., ATTARD, G., FLEISHER, M., REID, A. H., CASTRO, E., SANDHU, S. K., BARWELL, L., OOMMEN, N. B., CARREIRA, S., DRAKE, C. G., JONES, R., COOPER, C. S., SCHER, H. I. & DE BONO, J. S. 2012. Prognostic value of blood mRNA expression signatures in castration-resistant prostate cancer: a prospective, two-stage study. *Lancet Oncol*, 13, 1114-24.
- OSMULSKI, P., MAHALINGAM, D., GACZYNSKA, M. E., LIU, J., HUANG, S., HORNING, A. M., WANG, C. M., THOMPSON, I. M., HUANG, T. H. & CHEN, C. L. 2014. Nanomechanical biomarkers of single circulating tumor cells for detection of castration resistant prostate cancer. *Prostate*, 74, 1297-307.

- OUSSET, M., VAN KEYMEULEN, A., BOUVENCOURT, G., SHARMA, N., ACHOURI, Y., SIMONS, B. D. & BLANPAIN, C. 2012. Multipotent and unipotent progenitors contribute to prostate postnatal development. *Nat Cell Biol*, 14, 1131-8.
- OZKUMUR, E., SHAH, A. M., CICILIANO, J. C., EMMINK, B. L., MIYAMOTO, D. T., BRACHTEL, E., YU, M., CHEN, P. I., MORGAN, B., TRAUTWEIN, J., KIMURA, A., SENGUPTA, S., STOTT, S. L., KARABACAK, N. M., BARBER, T. A., WALSH, J. R., SMITH, K., SPUHLER, P. S., SULLIVAN, J. P., LEE, R. J., TING, D. T., LUO, X., SHAW, A. T., BARDIA, A., SEQUIST, L. V., LOUIS, D. N., MAHESWARAN, S., KAPUR, R., HABER, D. A. & TONER, M. 2013. Inertial focusing for tumor antigen-dependent and -independent sorting of rare circulating tumor cells. *Sci Transl Med*, 5, 179ra47.
- PAGLIARULO, V., BRACARDA, S., EISENBERGER, M. A., MOTTET, N., SCHRODER, F. H., STERNBERG, C. N. & STUDER, U. E. 2012. Contemporary role of androgen deprivation therapy for prostate cancer. *Eur Urol*, 61, 11-25.
- PANTEL, K. & BRAKENHOFF, R. H. 2004. Dissecting the metastatic cascade. *Nat Rev Cancer*, 4, 448-56.
- PARK, S., ANG, R. R., DUFFY, S. P., BAZOV, J., CHI, K. N., BLACK, P. C. & MA, H. 2014. Morphological differences between circulating tumor cells from prostate cancer patients and cultured prostate cancer cells. *PLoS One*, 9, e85264.
- PATEL, A. R. & KLEIN, E. A. 2009. Risk factors for prostate cancer. *Nat Clin Pract Urol*, 6, 87-95.
- PAYNE, H. & CORNFORD, P. 2011. Prostate-specific antigen: an evolving role in diagnosis, monitoring, and treatment evaluation in prostate cancer. *Urol Oncol*, 29, 593-601.
- PEINADO, H., OLMEDA, D. & CANO, A. 2007. Snail, Zeb and bHLH factors in tumour progression: an alliance against the epithelial phenotype? *Nat Rev Cancer*, 7, 415-28.
- PERDOMO, H. A. G., ZAPATA-COPETE, J. A. & SANCHEZ, A. 2018. Molecular alterations associated with prostate cancer. *Cent European J Urol*, 71, 168-176.
- PETERS, M., KANTHABALAN, A., SHAH, T. T., MCCARTAN, N., MOORE, C. M., ARYA, M., VAN DER VOORT VAN ZYP, J. R., MOERLAND, M. A., HINDLEY, R. G., EMBERTON, M. & AHMED, H. U. 2018. Development and internal validation of prediction models for biochemical failure and composite failure after focal salvage high intensity focused ultrasound for local radiorecurrent prostate cancer: Presentation of risk scores for individual patient prognoses. *Urol Oncol*, 36, 13.e1-13.e10.
- PEZARO, C., OMLIN, A., LORENTE, D., RODRIGUES, D. N., FERRALDESCHI, R., BIANCHINI, D., MUKHERJI, D., RIISNAES, R., ALTAVILLA, A., CRESPO, M., TUNARIU, N., DE BONO, J. & ATTARD, G. 2014. Visceral disease in castration-resistant prostate cancer. *Eur Urol*, 65, 270-273.
- PINTO, L. A., TRIVETT, M. T., WALLACE, D., HIGGINS, J., BASELER, M., TERABE, M., BELYAKOV, I. M., BERZOFKY, J. A. & HILDESHEIM, A. 2005. Fixation and cryopreservation of whole blood and isolated mononuclear cells: Influence of different procedures on lymphocyte subset analysis by flow cytometry. *Cytometry B Clin Cytom*, 63, 47-55.
- PONOMARYOV, T., PELED, A., PETIT, I., TAICHMAN, R. S., HABLER, L., SANDBANK, J., ARENZANA-SEISDEDOS, F., MAGERUS, A., CARUZ, A., FUJII, N., NAGLER, A., LAHAV, M., SZYPER-KRAVITZ, M., ZIPORI, D. & LAPIDOT, T. 2000. Induction of the chemokine stromal-derived factor-1 following DNA damage improves human stem cell function. *J Clin Invest*, 106, 1331-9.
- POTOSKY, A. L., MILLER, B. A., ALBERTSEN, P. C. & KRAMER, B. S. 1995. The role of increasing detection in the rising incidence of prostate cancer. *Jama*, 273, 548-52.
- PUNNOOSE, E. A., FERRALDESCHI, R., SZAFER-GLUSMAN, E., TUCKER, E. K., MOHAN, S., FLOHR, P., RIISNAES, R., MIRANDA, S., FIGUEIREDO, I., RODRIGUES, D. N., OMLIN, A.,

- PEZARO, C., ZHU, J., AMLER, L., PATEL, P., YAN, Y., BALES, N., WERNER, S. L., LOUW, J., PANDITA, A., MARRINUCCI, D., ATTARD, G. & DE BONO, J. 2015. PTEN loss in circulating tumour cells correlates with PTEN loss in fresh tumour tissue from castration-resistant prostate cancer patients. *Br J Cancer*, 113, 1225-33.
- PURICELLI, L., GALLUZZI, M., SCHULTE, C., PODESTA, A. & MILANI, P. 2015. Nanomechanical and topographical imaging of living cells by atomic force microscopy with colloidal probes. *Rev Sci Instrum*, 86, 033705.
- QIN, J., ALT, J. R., HUNSLEY, B. A., WILLIAMS, T. L. & FERNANDO, M. R. 2014. Stabilization of circulating tumor cells in blood using a collection device with a preservative reagent. *Cancer Cell Int*, 14, 23.
- QIN, J., LIU, X., LAFFIN, B., CHEN, X., CHOY, G., JETER, C. R., CALHOUN-DAVIS, T., LI, H., PALAPATTU, G. S., PANG, S., LIN, K., HUANG, J., IVANOV, I., LI, W., SURANENI, M. V. & TANG, D. G. 2012. The PSA(-/lo) prostate cancer cell population harbors self-renewing long-term tumor-propagating cells that resist castration. *Cell Stem Cell*, 10, 556-69.
- QUALITY, A. F. H. R. A. 2018. Prostate-Specific Antigen-Based Screening for Prostate Cancer: A Systematic Evidence Review for the U.S. Preventative Services Task Force. US Preventative Services Task Force Website.
- RAIMONDI, C., GRADILONE, A., NASO, G., VINCENZI, B., PETRACCA, A., NICOLAZZO, C., PALAZZO, A., SALTARELLI, R., SPREMBERG, F., CORTESI, E. & GAZZANIGA, P. 2011. Epithelial-mesenchymal transition and stemness features in circulating tumor cells from breast cancer patients. *Breast Cancer Res Treat*, 130, 449-55.
- RAMIREZ, J. M., FEHM, T., ORSINI, M., CAYREFOURCQ, L., MAUDELONDE, T., PANTEL, K. & ALIX-PANABIERES, C. 2014. Prognostic relevance of viable circulating tumor cells detected by EPISPOT in metastatic breast cancer patients. *Clin Chem*, 60, 214-21.
- RASTI, A., MEHRAZMA, M., MADJD, Z., ABOLHASANI, M., SAEEDNEJAD ZANJANI, L. & ASGARI, M. 2018. Co-expression of Cancer Stem Cell Markers OCT4 and NANOG Predicts Poor Prognosis in Renal Cell Carcinomas. *Sci Rep*, 8, 11739.
- RATAJCZAK, M. Z., MAJKA, M., KUCIA, M., DRUKALA, J., PIETRZKOWSKI, Z., PEIPER, S. & JANOWSKA-WIECZOREK, A. 2003. Expression of functional CXCR4 by muscle satellite cells and secretion of SDF-1 by muscle-derived fibroblasts is associated with the presence of both muscle progenitors in bone marrow and hematopoietic stem/progenitor cells in muscles. *Stem Cells*, 21, 363-71.
- RAUDENSKA, M., KRATOCHVILOVA, M., VICAR, T., GUMULEC, J., BALVAN, J., POLANSKA, H., PRIBYL, J. & MASARIK, M. 2019. Cisplatin enhances cell stiffness and decreases invasiveness rate in prostate cancer cells by actin accumulation. *Sci Rep*, 9, 1660.
- REID, A. H., ATTARD, G., AMBROISINE, L., FISHER, G., KOVACS, G., BREWER, D., CLARK, J., FLOHR, P., EDWARDS, S., BERNEY, D. M., FOSTER, C. S., FLETCHER, A., GERALD, W. L., MOLLER, H., REUTER, V. E., SCARDINO, P. T., CUZICK, J., DE BONO, J. S. & COOPER, C. S. 2010. Molecular characterisation of ERG, ETV1 and PTEN gene loci identifies patients at low and high risk of death from prostate cancer. *Br J Cancer*, 102, 678-84.
- REN, J., HUANG, H., LIU, Y., ZHENG, X. & ZOU, Q. 2015. An Atomic Force Microscope Study Revealed Two Mechanisms in the Effect of Anticancer Drugs on Rate-Dependent Young's Modulus of Human Prostate Cancer Cells. *PLoS One*, 10, e0126107.
- RESEARCH, I. F. C. 2019. <https://cansar.icr.ac.uk/cansar/cell-lines/SJSA-1/>. [Accessed 2019].
- REYA, T., MORRISON, S. J., CLARKE, M. F. & WEISSMAN, I. L. 2001. Stem cells, cancer, and cancer stem cells. *Nature*, 414, 105-11.
- RICHARDSEN, E., ANDERSEN, S., MELBO-JORGENSEN, C., RAKAEE, M., NESS, N., AL-SAAD, S., NORDBY, Y., PEDERSEN, M. I., DONNEM, T., BREMNES, R. M. & BUSUND, L. T. 2019.

MicroRNA 141 is associated to outcome and aggressive tumor characteristics in prostate cancer. *Sci Rep*, 9, 386.

- RICHARDSEN, E., NESS, N., MELBO-JORGENSEN, C., JOHANNESSEN, C., GRINDSTAD, T., NORDBAKKEN, C., AL-SAAD, S., ANDERSEN, S., DONNEM, T., NORDBY, Y., BREMNES, R. M. & BUSUND, L. T. 2015. The prognostic significance of CXCL16 and its receptor C-X-C chemokine receptor 6 in prostate cancer. *Am J Pathol*, 185, 2722-30.
- RIETHDORF, S., FRITSCHKE, H., MÜLLER, V., RAU, T., SCHINDLBECK, C., RACK, B., JANNI, W., COITH, C., BECK, K., JÄNICKE, F., JACKSON, S., GORNET, T., CRISTOFANILLI, M. & PANTEL, K. 2007. Detection of circulating tumor cells in peripheral blood of patients with metastatic breast cancer: A validation study of the cell search system. *Clinical Cancer Research*, 13, 920-928.
- ROBBINS, C. M., TEMBE, W. A., BAKER, A., SINARI, S., MOSES, T. Y., BECKSTROM-STERMBERG, S., BECKSTROM-STERMBERG, J., BARRETT, M., LONG, J., CHINNAIYAN, A., LOWEY, J., SUH, E., PEARSON, J. V., CRAIG, D. W., AGUS, D. B., PIENTA, K. J. & CARPTEN, J. D. 2011. Copy number and targeted mutational analysis reveals novel somatic events in metastatic prostate tumors. *Genome Res*, 21, 47-55.
- ROBERTS, M. J., BENNETT, H. Y., HARRIS, P. N., HOLMES, M., GRUMMET, J., NABER, K. & WAGENLEHNER, F. M. E. 2017. Prostate Biopsy-related Infection: A Systematic Review of Risk Factors, Prevention Strategies, and Management Approaches. *Urology*, 104, 11-21.
- ROBERTSON-TESSI, M., GILLIES, R. J., GATENBY, R. A. & ANDERSON, A. R. 2015. Impact of metabolic heterogeneity on tumor growth, invasion, and treatment outcomes. *Cancer Res*, 75, 1567-79.
- ROBINSON, D., VAN ALLEN, E. M., WU, Y. M., SCHULTZ, N., LONIGRO, R. J., MOSQUERA, J. M., MONTGOMERY, B., TAPLIN, M. E., PRITCHARD, C. C., ATTARD, G., BELTRAN, H., ABIDA, W., BRADLEY, R. K., VINSON, J., CAO, X., VATS, P., KUNJU, L. P., HUSSAIN, M., FENG, F. Y., TOMLINS, S. A., COONEY, K. A., SMITH, D. C., BRENNAN, C., SIDDIQUI, J., MEHRA, R., CHEN, Y., RATHKOPF, D. E., MORRIS, M. J., SOLOMON, S. B., DURACK, J. C., REUTER, V. E., GOPALAN, A., GAO, J., LODA, M., LIS, R. T., BOWDEN, M., BALK, S. P., GAVIOLA, G., SOUGNEZ, C., GUPTA, M., YU, E. Y., MOSTAGHEL, E. A., CHENG, H. H., MULCAHY, H., TRUE, L. D., PLYMATE, S. R., DVINGE, H., FERRALDESCHI, R., FLOHR, P., MIRANDA, S., ZAFEIRIOU, Z., TUNARIU, N., MATEO, J., PEREZ-LOPEZ, R., DEMICHELIS, F., ROBINSON, B. D., SBONER, A., SCHIFFMAN, M., NANUS, D. M., TAGAWA, S. T., SIGARAS, A., ENG, K. W., ELEMENTO, O., SBONER, A., HEATH, E. I., SCHER, H. I., PIENTA, K. J., KANTOFF, P., DE BONO, J. S., RUBIN, M. A., NELSON, P. S., GARRAWAY, L. A., SAWYERS, C. L. & CHINNAIYAN, A. M. 2015. Integrative Clinical Genomics of Advanced Prostate Cancer. *Cell*, 162, 454.
- RODRIGUEZ, M. L., MCGARRY, P.J., SNIADECKI, N.J. 2013. Review on cell mechanics: experimental and modeling approaches. *Applied Mechanics Review*, 65.
- ROSENBERG, R., GERTLER, R., FRIEDERICHS, J., FUEHRER, K., DAHM, M., PHELPS, R., THORBAN, S., NEKARDA, H. & SIEWERT, J. R. 2002. Comparison of two density gradient centrifugation systems for the enrichment of disseminated tumor cells in blood. *Cytometry*, 49, 150-8.
- ROSS, A. A., COOPER, B. W., LAZARUS, H. M., MACKAY, W., MOSS, T. J., CIOBANU, N., TALLMAN, M. S., KENNEDY, M. J., DAVIDSON, N. E., SWEET, D. & ET AL. 1993. Detection and viability of tumor cells in peripheral blood stem cell collections from breast cancer patients using immunocytochemical and clonogenic assay techniques. *Blood*, 82, 2605-10.

- ROSS, R. W., GALSKEY, M. D., SCHER, H. I., MAGIDSON, J., WASSMANN, K., LEE, G. S., KATZ, L., SUBUDHI, S. K., ANAND, A., FLEISHER, M., KANTOFF, P. W. & OH, W. K. 2012. A whole-blood RNA transcript-based prognostic model in men with castration-resistant prostate cancer: a prospective study. *Lancet Oncol*, 13, 1105-13.
- RUSCETTI, M., QUACH, B., DADASHIAN, E. L., MULHOLLAND, D. J. & WU, H. 2015. Tracking and Functional Characterization of Epithelial-Mesenchymal Transition and Mesenchymal Tumor Cells during Prostate Cancer Metastasis. *Cancer Res*, 75, 2749-59.
- SALAZAR, N., CASTELLAN, M., SHIRODKAR, S. S. & LOKESHWAR, B. L. 2013. Chemokines and chemokine receptors as promoters of prostate cancer growth and progression. *Crit Rev Eukaryot Gene Expr*, 23, 77-91.
- SALINAS, C. A., TSODIKOV, A., ISHAK-HOWARD, M. & COONEY, K. A. 2014. Prostate cancer in young men: an important clinical entity. *Nat Rev Urol*, 11, 317-23.
- SALMINEN, E. K., KALLIOINEN, M. J., ALA-HOUHALA, M. A., VIHINEN, P. P., TIITINEN, S. L., VARPULA, M. & VAHLBERG, T. J. 2006. Survival markers related to bone metastases in prostate cancer. *Anticancer Res*, 26, 4879-84.
- SATELLI, A., BATTH, I., BROWNLEE, Z., MITRA, A., ZHOU, S., NOH, H., ROJAS, C. R., LI, H., MENG, Q. H. & LI, S. 2017. EMT circulating tumor cells detected by cell-surface vimentin are associated with prostate cancer progression. *Oncotarget*, 8, 49329-49337.
- SAUCEDO-ZENI, N., MEWES, S., NIESTROJ, R., GASIOROWSKI, L., MURAWA, D., NOWACZYK, P., TOMASI, T., WEBER, E., DWORACKI, G., MORGENTHALER, N. G., JANSEN, H., PROPPING, C., STERZYNSKA, K., DYSZKIEWICZ, W., ZABEL, M., KIECHLE, M., REUNING, U., SCHMITT, M. & LUCKE, K. 2012. A novel method for the in vivo isolation of circulating tumor cells from peripheral blood of cancer patients using a functionalized and structured medical wire. *Int J Oncol*, 41, 1241-50.
- SCATENA, R., BOTTONI, P. & GIARDINA, B. 2013. Circulating tumour cells and cancer stem cells: A role for proteomics in defining the interrelationships between function, phenotype and differentiation with potential clinical applications. *Biochimica et Biophysica Acta - Reviews on Cancer*, 1835, 129-143.
- SCHER, H. I., JIA, X., DE BONO, J. S., FLEISHER, M., PIENTA, K. J., RAGHAVAN, D. & HELLER, G. 2009. Circulating tumour cells as prognostic markers in progressive, castration-resistant prostate cancer: a reanalysis of IMMC38 trial data. *Lancet Oncol*, 10, 233-9.
- SCHILLING, D., TODENHOFER, T., HENNENLOTTER, J., SCHWENTNER, C., FEHM, T. & STENZL, A. 2012. Isolated, disseminated and circulating tumour cells in prostate cancer. *Nat Rev Urol*, 9, 448-63.
- SCHOENBORN, J. R., NELSON, P. & FANG, M. 2013. Genomic profiling defines subtypes of prostate cancer with the potential for therapeutic stratification. *Clin Cancer Res*, 19, 4058-66.
- SCOSYREV, E., MESSING, E. M., MOHILE, S., GOLIJANIN, D. & WU, G. 2012a. Prostate cancer in the elderly: frequency of advanced disease at presentation and disease-specific mortality. *Cancer*, 118, 3062-70.
- SCOSYREV, E., MESSING, E. M., MOHILE, S., GOLIJANIN, D. & WU, G. 2012b. Prostate cancer in the elderly: Frequency of advanced disease at presentation and disease-specific mortality. *Cancer*, 118, 3062-3070.
- SEIKI, M. 2003. Membrane-type 1 matrix metalloproteinase: a key enzyme for tumor invasion. *Cancer Lett*, 194, 1-11.

- SEIM, I., JEFFERY, P. L., THOMAS, P. B., NELSON, C. C. & CHOPIN, L. K. 2017. Whole-Genome Sequence of the Metastatic PC3 and LNCaP Human Prostate Cancer Cell Lines. *G3 (Bethesda)*, 7, 1731-1741.
- SEMENZA, G. L., JIANG, B. H., LEUNG, S. W., PASSANTINO, R., CONCORDET, J. P., MAIRE, P. & GIALLONGO, A. 1996. Hypoxia response elements in the aldolase A, enolase 1, and lactate dehydrogenase A gene promoters contain essential binding sites for hypoxia-inducible factor 1. *J Biol Chem*, 271, 32529-37.
- SHAFFER, D. R., LEVERSHA, M. A., DANILA, D. C., LIN, O., GONZALEZ-ESPINOZA, R., GU, B., ANAND, A., SMITH, K., MASLAK, P., DOYLE, G. V., TERSTAPPEN, L. W., LILJA, H., HELLER, G., FLEISHER, M. & SCHER, H. I. 2007. Circulating tumor cell analysis in patients with progressive castration-resistant prostate cancer. *Clin Cancer Res*, 13, 2023-9.
- SHARMA, U., PAL, D. & PRASAD, R. 2014. Alkaline phosphatase: an overview. *Indian J Clin Biochem*, 29, 269-78.
- SHEN, M. M. & ABATE-SHEN, C. 2010. Molecular genetics of prostate cancer: new prospects for old challenges. *Genes Dev*, 24, 1967-2000.
- SHTIVELMAN, E., BEER, T. M. & EVANS, C. P. 2014. Molecular pathways and targets in prostate cancer. *Oncotarget*, 5, 7217-59.
- SIEGEL, R., NAISHADHAM, D. & JEMAL, A. 2012. Cancer statistics, 2012. *CA Cancer Journal for Clinicians*, 62, 10-29.
- SINGH, R., KAPUR, N., MIR, H., SINGH, N., LILLARD, J. W., JR. & SINGH, S. 2016. CXCR6-CXCL16 axis promotes prostate cancer by mediating cytoskeleton rearrangement via Ezrin activation and alphavbeta3 integrin clustering. *Oncotarget*, 7, 7343-53.
- SINGH, R. K. & LOKESHWAR, B. L. 2011. The IL-8-regulated chemokine receptor CXCR7 stimulates EGFR signaling to promote prostate cancer growth. *Cancer Res*, 71, 3268-77.
- SINGH, S., SINGH, U. P., STILES, J. K., GRIZZLE, W. E. & LILLARD, J. W., JR. 2004. Expression and functional role of CCR9 in prostate cancer cell migration and invasion. *Clin Cancer Res*, 10, 8743-50.
- SMERAGE, J. B., BARLOW, W. E., HORTOBAGYI, G. N., WINER, E. P., LEYLAND-JONES, B., SRKALOVIC, G., TEJWANI, S., SCHOTT, A. F., O'ROURKE, M. A., LEW, D. L., DOYLE, G. V., GRALOW, J. R., LIVINGSTON, R. B. & HAYES, D. F. 2014. Circulating tumor cells and response to chemotherapy in metastatic breast cancer: SWOG S0500. *J Clin Oncol*, 32, 3483-9.
- SOUZA, M. F., KUASNE, H., BARROS-FILHO, M. C., CILIAO, H. L., MARCHI, F. A., FUGANTI, P. E., PASCHOAL, A. R., ROGATTO, S. R. & COLUS, I. M. S. 2017. Circulating mRNAs and miRNAs as candidate markers for the diagnosis and prognosis of prostate cancer. *PLoS One*, 12, e0184094.
- SOWTER, H. M., RATCLIFFE, P. J., WATSON, P., GREENBERG, A. H. & HARRIS, A. L. 2001. HIF-1-dependent regulation of hypoxic induction of the cell death factors BNIP3 and NIX in human tumors. *Cancer Res*, 61, 6669-73.
- SRAMKOSKI, R. M., PRETLOW, T. G., 2ND, GIACONIA, J. M., PRETLOW, T. P., SCHWARTZ, S., SY, M. S., MARENGO, S. R., RHIM, J. S., ZHANG, D. & JACOBBERGER, J. W. 1999. A new human prostate carcinoma cell line, 22Rv1. *In Vitro Cell Dev Biol Anim*, 35, 403-9.
- STANBROUGH, M., BUBLEY, G. J., ROSS, K., GOLUB, T. R., RUBIN, M. A., PENNING, T. M., FEBBO, P. G. & BALK, S. P. 2006. Increased expression of genes converting adrenal androgens to testosterone in androgen-independent prostate cancer. *Cancer Res*, 66, 2815-25.

- STATISTICS, O. F. N. 2016. *Cancer Registration statistics, England* [Online]. Available: <https://www.ons.gov.uk/peoplepopulationandcommunity/healthandsocialcare/conditionsanddiseases/datasets/cancerregistrationstatisticscancerregistrationstatisticsengland> [Accessed].
- STEINESTEL, J., LUEDEKE, M., ARNDT, A., SCHNOELLER, T. J., LENNERZ, J. K., WURM, C., MAIER, C., CRONAUER, M. V., STEINESTEL, K. & SCHRADER, A. J. 2019. Detecting predictive androgen receptor modifications in circulating prostate cancer cells. *Oncotarget*, 10, 4213-4223.
- STONE, R. C., PASTAR, I., OJEH, N., CHEN, V., LIU, S., GARZON, K. I. & TOMIC-CANIC, M. 2016. Epithelial-mesenchymal transition in tissue repair and fibrosis. *Cell Tissue Res*, 365, 495-506.
- STOTT, S. L., LEE, R. J., NAGRATH, S., YU, M., MIYAMOTO, D. T., ULKUS, L., INSERRA, E. J., ULMAN, M., SPRINGER, S., NAKAMURA, Z., MOORE, A. L., TSUKROV, D. I., KEMPNER, M. E., DAHL, D. M., WU, C. L., IAFRATE, A. J., SMITH, M. R., TOMPKINS, R. G., SEQUIST, L. V., TONER, M., HABER, D. A. & MAHESWARAN, S. 2010. Isolation and characterization of circulating tumor cells from patients with localized and metastatic prostate cancer. *Sci Transl Med*, 2, 25ra23.
- SUN, C., SHI, Y., XU, L. L., NAGESWARARAO, C., DAVIS, L. D., SEGAWA, T., DOBI, A., MCLEOD, D. G. & SRIVASTAVA, S. 2006. Androgen receptor mutation (T877A) promotes prostate cancer cell growth and cell survival. *Oncogene*, 25, 3905-13.
- SUN, Y. X., FANG, M., WANG, J., COOPER, C. R., PIENTA, K. J. & TAICHMAN, R. S. 2007. Expression and activation of alpha v beta 3 integrins by SDF-1/CXC12 increases the aggressiveness of prostate cancer cells. *Prostate*, 67, 61-73.
- SZARVAS, T., BECKER, M., VOM DORP, F., MESCHUDE, J., SCHERAG, A., BANKFALVI, A., REIS, H., SCHMID, K. W., ROMICS, I., RUBBEN, H. & ERGUN, S. 2011. Elevated serum matrix metalloproteinase 7 levels predict poor prognosis after radical prostatectomy. *Int J Cancer*, 128, 1486-92.
- TAKAHASHI, K., TANABE, K., OHNUKI, M., NARITA, M., ICHISAKA, T., TOMODA, K. & YAMANAKA, S. 2007. Induction of pluripotent stem cells from adult human fibroblasts by defined factors. *Cell*, 131, 861-72.
- TAKAHASHI, K. & YAMANAKA, S. 2006. Induction of pluripotent stem cells from mouse embryonic and adult fibroblast cultures by defined factors. *Cell*, 126, 663-76.
- TAM, W. L. & WEINBERG, R. A. 2013. The epigenetics of epithelial-mesenchymal plasticity in cancer. *Nat Med*, 19, 1438-49.
- TANGEN, C. M., HUSSAIN, M. H., HIGANO, C. S., EISENBERGER, M. A., SMALL, E. J., WILDING, G., DONNELLY, B. J., SCHELHAMMER, P. F., CRAWFORD, E. D., VOGELZANG, N. J., POWELL, I. J. & THOMPSON, I. M., JR. 2012. Improved overall survival trends of men with newly diagnosed M1 prostate cancer: a SWOG phase III trial experience (S8494, S8894 and S9346). *J Urol*, 188, 1164-9.
- TARIN, D., THOMPSON, E. W. & NEWGREEN, D. F. 2005. The fallacy of epithelial mesenchymal transition in neoplasia. *Cancer Res*, 65, 5996-6000; discussion 6000-1.
- TAYLOR, B. S., SCHULTZ, N., HIERONYMUS, H., GOPALAN, A., XIAO, Y., CARVER, B. S., ARORA, V. K., KAUSHIK, P., CERAMI, E., REVA, B., ANTIPIN, Y., MITSIADES, N., LANDERS, T., DOLGALEV, I., MAJOR, J. E., WILSON, M., SOCCI, N. D., LASH, A. E., HEGUY, A., EASTHAM, J. A., SCHER, H. I., REUTER, V. E., SCARDINO, P. T., SANDER, C., SAWYERS, C. L. & GERALD, W. L. 2010. Integrative genomic profiling of human prostate cancer. *Cancer Cell*, 18, 11-22.
- THALGOTT, M., RACK, B., MAURER, T., SOUVATZOGLOU, M., EIBER, M., KREß, V., HECK, M. M., ANDERGASSEN, U., NAWROTH, R., GSCHWEND, J. E. & RETZ, M. 2013. Detection

- of circulating tumor cells in different stages of prostate cancer. *Journal of Cancer Research and Clinical Oncology*, 139, 755-763.
- THIERY, J. P. & SLEEMAN, J. P. 2006. Complex networks orchestrate epithelial-mesenchymal transitions. *Nat Rev Mol Cell Biol*, 7, 131-42.
- THOMA, C. 2014. Prostate cancer: Analysis of circulating tumour DNA could guide therapy. *Nat Rev Urol*, 11, 659.
- THOMPSON, I. M., PAULER, D. K., GOODMAN, P. J., TANGEN, C. M., LUCIA, M. S., PARNES, H. L., MINASIAN, L. M., FORD, L. G., LIPPMAN, S. M., CRAWFORD, E. D., CROWLEY, J. J. & COLTMAN, C. A., JR. 2004. Prevalence of prostate cancer among men with a prostate-specific antigen level \leq 4.0 ng per milliliter. *N Engl J Med*, 350, 2239-46.
- TOMLINS, S. A., RHODES, D. R., PERNER, S., DHANASEKARAN, S. M., MEHRA, R., SUN, X. W., VARAMBALLY, S., CAO, X., TCHINDA, J., KUEFER, R., LEE, C., MONTIE, J. E., SHAH, R. B., PIENTA, K. J., RUBIN, M. A. & CHINNAIYAN, A. M. 2005. Recurrent fusion of TMPRSS2 and ETS transcription factor genes in prostate cancer. *Science*, 310, 644-8.
- TORQUATO, S., PALLAVAJJALA, A., GOLDSTEIN, A., TORO, P. V., SILBERSTEIN, J. L., LEE, J., NAKAZAWA, M., WATERS, I., CHU, D., SHINN, D., GROGINSKI, T., HUGHES, R. M., SIMONS, B. W., KHAN, H., FENG, Z., CARDUCCI, M. A., PALLER, C. J., DENMEADE, S. R., KRESSEL, B., EISENBERGER, M. A., ANTONARAKIS, E. S., TROCK, B. J., PARK, B. H. & HURLEY, P. J. 2019. Genetic Alterations Detected in Cell-Free DNA Are Associated With Enzalutamide and Abiraterone Resistance in Castration-Resistant Prostate Cancer. *JCO Precis Oncol*, 3.
- TRUDEL, D., FRADET, Y., MEYER, F., HAREL, F. & TETU, B. 2008. Membrane-type-1 matrix metalloproteinase, matrix metalloproteinase 2, and tissue inhibitor of matrix proteinase 2 in prostate cancer: identification of patients with poor prognosis by immunohistochemistry. *Hum Pathol*, 39, 731-9.
- UROLOGY, E. A. O. 2018. *EAU Guidelines for Prostate Cancer* [Online]. European Association of Urology website. Available: www.uroweb.org/guideline/prostate-cancer/ [Accessed 19th July 2018].
- VALDES, F., ALVAREZ, A. M., LOCASCIO, A., VEGA, S., HERRERA, B., FERNANDEZ, M., BENITO, M., NIETO, M. A. & FABREGAT, I. 2002. The epithelial mesenchymal transition confers resistance to the apoptotic effects of transforming growth factor Beta in fetal rat hepatocytes. *Mol Cancer Res*, 1, 68-78.
- VALENT, P., BONNET, D., DE MARIA, R., LAPIDOT, T., COPLAND, M., MELO, J. V., CHOMIENNE, C., ISHIKAWA, F., SCHURINGA, J. J., STASSI, G., HUNTLY, B., HERRMANN, H., SOULIER, J., ROESCH, A., SCHUURHUIS, G. J., WOHRER, S., AROCK, M., ZUBER, J., CERNY-REITERER, S., JOHNSEN, H. E., ANDREEFF, M. & EAVES, C. 2012. Cancer stem cell definitions and terminology: the devil is in the details. *Nat Rev Cancer*, 12, 767-75.
- VAN DENDEREN, B. J. & THOMPSON, E. W. 2013. Cancer: The to and fro of tumour spread. *Nature*, 493, 487-8.
- VAN DER TOOM, E. E., VERDONE, J. E., GORIN, M. A. & PIENTA, K. J. 2016. Technical challenges in the isolation and analysis of circulating tumor cells. *Oncotarget*, 7, 62754-62766.
- VERHAMME, K. M., DIELEMAN, J. P., BLEUMINK, G. S., VAN DER LEI, J., STURKENBOOM, M. C., ARTIBANI, W., BEGAUD, B., BERGES, R., BORKOWSKI, A., CHAPPEL, C. R., COSTELLO, A., DOBRONSKI, P., FARMER, R. D., JIMENEZ CRUZ, F., JONAS, U., MACRAE, K., PIENKA, L., RUTTEN, F. F., VAN SCHAYCK, C. P., SPEAKMAN, M. J., STURKENBOOM, M. C., TIELLAC, P., TUBARO, A., VALLENCIEN, G. & VELA NAVARRETE, R. 2002. Incidence and prevalence of lower urinary tract symptoms suggestive of

- benign prostatic hyperplasia in primary care--the Triumph project. *Eur Urol*, 42, 323-8.
- VIDAL, A. C., HOWARD, L. E., MOREIRA, D. M., CASTRO-SANTAMARIA, R., ANDRIOLE, G. L., JR. & FREEDLAND, S. J. 2014. Obesity increases the risk for high-grade prostate cancer: results from the REDUCE study. *Cancer Epidemiol Biomarkers Prev*, 23, 2936-42.
- VISAKORPI, T., HYYTINEN, E., KOIVISTO, P., TANNER, M., KEINANEN, R., PALMBERG, C., PALOTIE, A., TAMMELA, T., ISOLA, J. & KALLIONIEMI, O. P. 1995. In vivo amplification of the androgen receptor gene and progression of human prostate cancer. *Nat Genet*, 9, 401-6.
- VISHNOI, M., PEDDIBHOTLA, S., YIN, W., A, T. S., GEORGE, G. C., HONG, D. S. & MARCHETTI, D. 2015. The isolation and characterization of CTC subsets related to breast cancer dormancy. *Sci Rep*, 5, 17533.
- VOGELSTEIN, B., PAPADOPOULOS, N., VELCULESCU, V. E., ZHOU, S., DIAZ, L. A., JR. & KINZLER, K. W. 2013. Cancer genome landscapes. *Science*, 339, 1546-58.
- VONA, G., ESTEPA, L., BEROU, C., DAMOTTE, D., CAPRON, F., NALPAS, B., MINEUR, A., FRANCO, D., LACOUR, B., POL, S., BRECHOT, C. & PATERLINI-BRECHOT, P. 2004. Impact of cytomorphological detection of circulating tumor cells in patients with liver cancer. *Hepatology*, 39, 792-7.
- VOSS, M. J., MOLLER, M. F., POWE, D. G., NIGGEMANN, B., ZANKER, K. S. & ENTSCHLADEN, F. 2011. Luminal and basal-like breast cancer cells show increased migration induced by hypoxia, mediated by an autocrine mechanism. *BMC Cancer*, 11, 158.
- WANG, J., LOBERG, R. & TAICHMAN, R. S. 2006. The pivotal role of CXCL12 (SDF-1)/CXCR4 axis in bone metastasis. *Cancer Metastasis Rev*, 25, 573-87.
- WANG, J., LU, Y., WANG, J., KOCH, A. E., ZHANG, J. & TAICHMAN, R. S. 2008. CXCR6 induces prostate cancer progression by the AKT/mammalian target of rapamycin signaling pathway. *Cancer Res*, 68, 10367-76.
- WANG, S., LIU, K., LIU, J., YU, Z. T., XU, X., ZHAO, L., LEE, T., LEE, E. K., REISS, J., LEE, Y. K., CHUNG, L. W., HUANG, J., RETTIG, M., SELIGSON, D., DURAISWAMY, K. N., SHEN, C. K. & TSENG, H. R. 2011. Highly efficient capture of circulating tumor cells by using nanostructured silicon substrates with integrated chaotic micromixers. *Angew Chem Int Ed Engl*, 50, 3084-8.
- WANG, S., WANG, H., JIAO, J., CHEN, K. J., OWENS, G. E., KAMEI, K., SUN, J., SHERMAN, D. J., BEHRENBRUCH, C. P., WU, H. & TSENG, H. R. 2009. Three-dimensional nanostructured substrates toward efficient capture of circulating tumor cells. *Angew Chem Int Ed Engl*, 48, 8970-3.
- WANG, Y., HAYWARD, S., CAO, M., THAYER, K. & CUNHA, G. 2001. Cell differentiation lineage in the prostate. *Differentiation*, 68, 270-9.
- WATANABE, M., UEHARA, Y., YAMASHITA, N., FUJIMURA, Y., NISHIO, K., SAWADA, T., TAKEDA, K., KOIZUMI, F. & KOH, Y. 2014. Multicolor detection of rare tumor cells in blood using a novel flow cytometry-based system. *Cytometry A*, 85, 206-13.
- WEDGE, D. C., GUNDEM, G., MITCHELL, T., WOODCOCK, D. J., MARTINCORENA, I., GHORI, M., ZAMORA, J., BUTLER, A., WHITAKER, H., KOTE-JARAI, Z., ALEXANDROV, L. B., VAN LOO, P., MASSIE, C. E., DENTRO, S., WARREN, A. Y., VERRILL, C., BERNEY, D. M., DENNIS, N., MERSON, S., HAWKINS, S., HOWAT, W., LU, Y. J., LAMBERT, A., KAY, J., KREMEYER, B., KARASZI, K., LUXTON, H., CAMACHO, N., MARSDEN, L., EDWARDS, S., MATTHEWS, L., BO, V., LEONGAMORNLEERT, D., MCLAREN, S., NG, A., YU, Y., ZHANG, H., DADAEV, T., THOMAS, S., EASTON, D. F., AHMED, M., BANCROFT, E., FISHER, C., LIVNI, N., NICOL, D., TAVARE, S., GILL, P., GREENMAN, C., KHOO, V., VAN AS, N., KUMAR, P., OGDEN, C., CAHILL, D., THOMPSON, A., MAYER, E., ROWE, E.,

- DUDDERIDGE, T., GNANAPRAGASAM, V., SHAH, N. C., RAINE, K., JONES, D., MENZIES, A., STEBBINGS, L., TEAGUE, J., HAZELL, S., CORBISHLEY, C., DE BONO, J., ATTARD, G., ISAACS, W., VISAKORPI, T., FRASER, M., BOUTROS, P. C., BRISTOW, R. G., WORKMAN, P., SANDER, C., HAMDY, F. C., FUTREAL, A., MCDERMOTT, U., AL-LAZIKANI, B., LYNCH, A. G., BOVA, G. S., FOSTER, C. S., BREWER, D. S., NEAL, D. E., COOPER, C. S. & EELES, R. A. 2018. Sequencing of prostate cancers identifies new cancer genes, routes of progression and drug targets. *Nat Genet*, 50, 682-692.
- WEIGELT, B. & REIS-FILHO, J. S. 2009. Histological and molecular types of breast cancer: is there a unifying taxonomy? *Nat Rev Clin Oncol*, 6, 718-30.
- WEITZ, J., KIENLE, P., LACROIX, J., WILLEKE, F., BENNER, A., LEHNERT, T., HERFARTH, C. & VON KNEBEL DOEBERITZ, M. 1998. Dissemination of tumor cells in patients undergoing surgery for colorectal cancer. *Clin Cancer Res*, 4, 343-8.
- WERNER, S. L., GRAF, R. P., LANDERS, M., VALENTA, D. T., SCHROEDER, M., GREENE, S. B., BALES, N., DITTAMORE, R. & MARRINUCCI, D. 2015. Analytical Validation and Capabilities of the Epic CTC Platform: Enrichment-Free Circulating Tumour Cell Detection and Characterization. *J Circ Biomark*, 4, 3.
- WIESNER, C., NABHA, S. M., DOS SANTOS, E. B., YAMAMOTO, H., MENG, H., MELCHIOR, S. W., BITTINGER, F., THUROFF, J. W., VESSELLA, R. L., CHER, M. L. & BONFIL, R. D. 2008. C-kit and its ligand stem cell factor: potential contribution to prostate cancer bone metastasis. *Neoplasia*, 10, 996-1003.
- WONG, C. H., HEIT, B. & KUBES, P. 2010. Molecular regulators of leucocyte chemotaxis during inflammation. *Cardiovasc Res*, 86, 183-91.
- WOUTERS, B. G. & KORITZINSKY, M. 2008. Hypoxia signalling through mTOR and the unfolded protein response in cancer. *Nat Rev Cancer*, 8, 851-64.
- XUE, J., QIN, Z., CAI, H., ZHANG, C., LI, X., XU, W., WANG, J., XU, Z., YU, B., XU, T. & ZOU, Q. 2017. Comparison between transrectal and transperineal prostate biopsy for detection of prostate cancer: a meta-analysis and trial sequential analysis. *Oncotarget*, 8, 23322-23336.
- YANG, J., HUANG, Y., WANG, X. B., BECKER, F. F. & GASCOYNE, P. R. 1999. Cell separation on microfabricated electrodes using dielectrophoretic/gravitational field-flow fractionation. *Anal Chem*, 71, 911-8.
- YANG, J., MANI, S. A., DONAHER, J. L., RAMASWAMY, S., ITZYKSON, R. A., COME, C., SAVAGNER, P., GITELMAN, I., RICHARDSON, A. & WEINBERG, R. A. 2004. Twist, a master regulator of morphogenesis, plays an essential role in tumor metastasis. *Cell*, 117, 927-39.
- YAP, T. A., GARRETT, M. D., WALTON, M. I., RAYNAUD, F., DE BONO, J. S. & WORKMAN, P. 2008. Targeting the PI3K-AKT-mTOR pathway: progress, pitfalls, and promises. *Curr Opin Pharmacol*, 8, 393-412.
- YOSHIMOTO, M., CUNHA, I. W., COUDRY, R. A., FONSECA, F. P., TORRES, C. H., SOARES, F. A. & SQUIRE, J. A. 2007. FISH analysis of 107 prostate cancers shows that PTEN genomic deletion is associated with poor clinical outcome. *Br J Cancer*, 97, 678-85.
- YOU, L., GUO, X. & HUANG, Y. 2018. Correlation of Cancer Stem-Cell Markers OCT4, SOX2, and NANOG with Clinicopathological Features and Prognosis in Operative Patients with Rectal Cancer. *Yonsei Med J*, 59, 35-42.
- YU, M., BARDIA, A., ACETO, N., BERSANI, F., MADDEN, M. W., DONALDSON, M. C., DESAI, R., ZHU, H., COMAILLS, V., ZHENG, Z., WITTNER, B. S., STOJANOV, P., BRACHTEL, E., SGROI, D., KAPUR, R., SHIODA, T., TING, D. T., RAMASWAMY, S., GETZ, G., IAFRATE, A. J., BENES, C., TONER, M., MAHESWARAN, S. & HABER, D. A. 2014. Cancer therapy. Ex

- vivo culture of circulating breast tumor cells for individualized testing of drug susceptibility. *Science*, 345, 216-20.
- YU, M., STOTT, S., TONER, M., MAHESWARAN, S. & HABER, D. A. 2011. Circulating tumor cells: approaches to isolation and characterization. *J Cell Biol*, 192, 373-82.
- ZELEFSKY, M. J., PEI, X., CHOU, J. F., SCHECHTER, M., KOLLMEIER, M., COX, B., YAMADA, Y., FIDALEO, A., SPERLING, D., HAPPERSETT, L. & ZHANG, Z. 2011. Dose escalation for prostate cancer radiotherapy: predictors of long-term biochemical tumor control and distant metastases-free survival outcomes. *Eur Urol*, 60, 1133-9.
- ZHANG, D., WANG, H., SUN, M., YANG, J., ZHANG, W., HAN, S. & XU, B. 2014. Speckle-type POZ protein, SPOP, is involved in the DNA damage response. *Carcinogenesis*, 35, 1691-7.
- ZHANG, L., RIDGWAY, L. D., WETZEL, M. D., NGO, J., YIN, W., KUMAR, D., GOODMAN, J. C., GROVES, M. D. & MARCHETTI, D. 2013. The identification and characterization of breast cancer CTCs competent for brain metastasis. *Sci Transl Med*, 5, 180ra48.
- ZHENG, H. & KANG, Y. 2014. Multilayer control of the EMT master regulators. *Oncogene*, 33, 1755-63.
- ZHENG, S., LIN, H., LIU, J. Q., BALIC, M., DATAR, R., COTE, R. J. & TAI, Y. C. 2007. Membrane microfilter device for selective capture, electrolysis and genomic analysis of human circulating tumor cells. *J Chromatogr A*, 1162, 154-61.
- ZLOTNIK, A., BURKHARDT, A. M. & HOMEY, B. 2011. Homeostatic chemokine receptors and organ-specific metastasis. *Nat Rev Immunol*, 11, 597-606.
- ZUBA-SURMA, E. K., KUCIA, M., ABDEL-LATIF, A., LILLARD, J. W., JR. & RATAJCZAK, M. Z. 2007. The ImageStream System: a key step to a new era in imaging. *Folia Histochem Cytobiol*, 45, 279-90.
- ZUBA-SURMA, E. K. & RATAJCZAK, M. Z. 2011. Analytical capabilities of the ImageStream cytometer. *Methods Cell Biol*, 102, 207-30.